THE GEOLOGY, PETROLOGY AND PETROGENESIS OF THE WHITE HILLS PERIDOTITE, ST. ANTHONY COMPLEX, NORTHWESTERN NEWFOUNDLAND

CENTRE F STUDIES

PART 1

TOTAL OF 10 PAGES ONLY
MAY BE XEROXED

(Without Author's Permission)

RAYMOND WILLIS TALKINGTON

MEMORIAL UNIVERSITY
LIBRARY
AUG 17 1982
OF NEWFOUNDLAND

National Library of Canada
Collections Development Branch

Canadian Theses on
Microfiche Service

Bibliothèque nationale du Canada
Direction du développement des collections

Service des thèses canadiennes
sur microfiche

NOTICE

The quality of this microfiche is heavily dependent upon the quality of the original thesis submitted for microfilming. Every effort has been made to ensure the highest quality of reproduction possible.

If pages are missing, contact the university which granted the degree.

Some pages may have indistinct print especially if the original pages were typed with a poor typewriter ribbon or if the university sent us a poor photocopy.

Previously copyrighted materials (journal articles, published tests, etc.) are not filmed.

Reproduction in full or in part of this film is governed by the Canadian Copyright Act, R.S.C. 1970, c. C-30. Please read the authorization forms which accompany this thesis.

THIS DISSERTATION
HAS BEEN MICROFILMED
EXACTLY AS RECEIVED

AVIS

La qualité de cette microfiche dépend grandement de la qualité de la thèse soumise au microfilmage. Nous avons tout fait pour assurer une qualité supérieure de reproduction.

S'il manque des pages, veuillez communiquer avec l'université qui a conféré le grade.

La qualité d'impression de certaines pages peut laisser à désirer, surtout si les pages originales ont été dactylographiées à l'aide d'un ruban usé ou si l'université nous a fait parvenir une photocopie de mauvaise qualité.

Les documents qui font déjà l'objet d'un droit d'auteur (articles de revue, examens publiés, etc.) ne sont pas microfilmés.

La reproduction, même partielle, de ce microfilm est soumise à la Loi canadienne sur le droit d'auteur, SRC 1970, c. C-30. Veuillez prendre connaissance des formules d'autorisation qui accompagnent cette thèse.

LA THÈSE A ÉTÉ
MICROFILMÉE TELLE QUE
NOUS L'AVONS REÇUE

Ottawa, Canada
K1A 0N4

NL-339 (Rev. 8/80)

THE GEOLOGY, PETROLOGY AND PETROGENESIS OF THE WHITE HILLS PERIDOTITE, ST. ANTHONY COMPLEX, NORTHWESTERN NEWFOUNDLAND

by

© Raymond W. Talkington, B.Sc. (Massachusetts), M.Sc. (New Hampshire)

A Thesis submitted in partial fulfillment of the requirements for the degree of Doctor of Philosophy

Department of Geology
Memorial University of Newfoundland

February 1981

St. John's

Newfoundland



St. Anthony from the eastern margin of the White Hills Peridotite.

FRONTISPIECE

"We must remind ourselves that it is a long extrapolation to the upper mantle in most locations, and the method of multiple working hypotheses remains as useful in the earth sciences today as when it was first propounded. There is no single relationship between ultramafic rocks and the upper mantle."

P.J. Wyllie, 1970

ABSTRACT

The White Hills Peridotite is located at the northernmost tip of the Great Northern Peninsula of Newfoundland. The peridotite is the highest structural slice of the Hare Bay Allochthon and outcrops as three massifs (two large and one small) which may represent dissected parts of a once complete ophiolite complex tectonically emplaced during the Mid-Ordovician as a result of the closing of the Iapetus Ocean.

The peridotite is made up of an interlayered sequence (1 mm to ½ m) of spinel lherzolite and harzburgite (~ 85%), and dunite that occurs as layers, dikes and lenses which either parallel or are oblique to the lithological layering. High-alumina pyroxenite veins (orthopyroxenite, websterite, wehrlite, and clinopyroxenite) are ubiquitous, whereas gabbro veins are restricted to the eastern section of the eastern massif. Chromite-related lithologies (low-alumina orthopyroxenite, low-alumina "websterite", and chromitite) are common to the eastern massif. The vein material is concordant with or discordant to the lithological layering.

At least two major deformational events have affected the peridotite, F_1 and F_2. F_1 is tentatively interpreted to be the result of high temperature plastic flow of the peridotite during its ascent below an accreting ridge and during this event the orthopyroxene-foliation may have developed. F_2 is interpreted to have formed during the tectonic emplacement of the peridotite. An F_3 deformational event only slightly affects the peridotite and is post-emplacement, probably an Acadian feature.

The bulk rock chemistry for the White Hills Peridotite is similar to other ophiolites and subcontinental upper mantle material. There are, however, several internal geochemical differences which distinguish the various White Hills lithologies, especially the pyroxenite (all types) and gabbro veins. These differences are predominantly in the TiO_2 and Al_2O_3 contents of the constituent minerals. On the basis of mineral and bulk rock geochemical differences, at least two geochemical trends are inferred, and at least two distinct, yet genetically related, liquids are required to explain these differences. Most of the minerals of the peridotite show the effects of subsolidus mineral-bulk rock equilibration, although to various degrees.

The petrogenetic model proposed for the White Hills Peridotite envisages at least two major partial melting events one at moderate to high pressures, the other at low pressure. The first liquid, an olivine tholeiite (first-stage liquid), is derived by approximately 20 percent partial melting of the spinel lherzolite source at high pressure ($\sim$ 20 kb). The second liquid, a magnesian-quartz tholeiite (second-stage liquid), is derived by approximately 5 to 10 percent partial melting of the previously melted spinel lherzolite source at low pressure ($\lesssim$ 8 kb). The partial melting residua produced after the first- and second-stage melting are a clinopyroxene-poor lherzolite and a highly refractory harzburgite, respectively. Polybaric crystallization, from approximately 20 kilobars to approximately 10 kilobars, of

the first-stage liquid results in the formation of some dunite and high-alumina pyroxenite (orthopyroxenite, websterite, wehrlite, clinopyroxenite) and gabbro veins. Crystallization of the second-stage liquid at low pressure produces the chromite-related lithologies (low-alumina orthopyroxenite, low-alumina "websterite", chromitite).

The White Hills Peridotite represents a sample of upper mantle that preserves a variety of features and processes resulting from a hypothesized off-axis ascent trajectory.

TABLE OF CONTENTS

		Page
Frontispiece		
Quotation		
Abstract		(i)
List of Figures		(xii)
List of Tables		(xvi)
List of Plates		(xvii)
PART I		
Chapter 1		
Introduction		
I.1.A.	Location and Access	1
I.1.B.	Previous Geological Work	3
I.1.C.	Regional Setting	7
1.	The Newfoundland Appalachians	7
a.	The Humber Zone	10
b.	The Hare Bay Allochthon	15
I.1.D.	Purpose and Scope of Study	18
I.1.E.	Acknowledgements	19
Chapter 2		
The Geology of the St. Anthony Complex		
I.2.A.	Rocks Underlying the White Hills Peridotite	21
1.	General Statement	21
a.	Goose Tickle Formation	21
b.	Northwest Arm Formation	22

c. Maiden Point Formation 23

d. Goose Cove Schist 27

e. Green Ridge Amphibolite 27

(i) plagioclase amphibolite 28

(ii) biotite amphibolite 29

f. Alkali Pyroxenite, Jacupirangite, Hornblende Gneiss, and Syenite 30

I.2.B. The White Hills Peridotite 34

1. General Statement 34

2. Rock Classification and Textures 35

a. Classification 35

b. Textures 39

3. Distribution of Rock Textures in the White Hills Peridotite 39

4. Lithologies and Petrography 47

a. Spinel Lherzolite and Harzburgite 47

(i) field descriptions 47

(ii) petrography 51

(iii) silicate mineral alteration 53

(iv) clinopyroxene megacrysts 54

b. Dunite 54

(i) field description and petrography 54

(ii) silicate mineral alteration 59

c. Pyroxenite 59

(i) general statement 59

(ii) orthopyroxenite 62

(iii) websterite 62

(iv) clinopyroxenite 63

(v) wehrlite 64
d. Gabbro 65
(i) field description 65
(ii) petrography 69
e. Chromitite 70
(i) field description 70
5. Structural Features of the White Hills Peridotite. 71
a. Observations 71
b. Interpretation 76
6. Summary 80

PART II

CHEMISTRY AND PETROGENESIS

Chapter 3

Mineral Chemistry and Bulk Rock Chemistry

II.3.A. Mineral Chemistry 84
1. Olivine 84
a. Spinel Lherzolite, Harzburgite, Dunite 84
b. Pyroxenite Veins 87
c. Gabbro 88
d. Chromitite 88
2. Orthopyroxene 89
a. Spinel Lherzolite and Harzburgite 89
b. Pyroxenite Veins 97
c. Gabbro 97
d. Chromitite 97

3. Clinopyroxene 98

a. Spinel Lherzolite and Harzburgite 98

b. Pyroxenite Veins, Gabbro and Chromitite 99

(i) estimation of equilibration temperatures and pressures 104

4. Plagioclase 108

II.3.B. Bulk Rock Chemistry 108

1. Linear Variation Diagrams 109

2. AFM Diagrams 116

3. Rare Earth Elements 116

a. Discussion 122

II.3.C. Summary 125

Chapter 4

Spinel Group Minerals

II.4.A. General Statement 128

II.4.B. Textural Relationships 129

1. Spinel Lherzolite 129

2. Harzburgite 132

3. Dunite 133

4. Gabbro 133

5. Pyroxenite Veins 136

a. Orthopyroxenite 136

b. Websterite and Clinopyroxenite 137

c. Wehrlite 137

6. Chromitite 137

a. General Statement 137

b. Chromite in the Pod 138

c. Chromite-Orthopyroxene Seams 139

II.4.C. Spinel Chemistry 139

1. General Statement 139

2. Solid Solution in Spinels 142

3. Mineral Chemistry 144

II.4.D. Spinel Geothermometry 162

1. Fe^{2+} - Mg Partitioning Between Spinel and Olivine 162

2. Geothermometers 163

3. Application of Spinel - Olivine Geothermometers to the White Hills Peridotite 168

II.4.E. Summary 172

Chapter 5

Petrogenesis

II.5.A. CMAS Projections 174

1. General Statement 174

a. The Development of a Control Plane and Application of the CMAS System to Aid in the Development of the Petrogenetic Model for the White Hills Peridotite 174

b. Calculation of Percent Partial Melting 184

II.5.B. Origin of the Pyroxenite Veins and Other Cumulate Rocks 188

1. General Statement 188

2. Review of Origins for Pyroxenite, Gabbro and Dunite Veins and Bodies 189

a. Ophiolites and Alpine-type Peridotites 189

b. Ultramafic Xenoliths 196

3. Hypothesis of Origin of Pyroxenite, Gabbro and Dunite Veins and Bodies of the White Hills Peridotite 197

a. General Statement 197

b. Proposed Model for the Origin of the Pyroxenite, Gabbro and Dunite Veins and Bodies of the White Hills Peridotite 200

(i) systematics of the model 200

(ii) proposed model 202

(iii) discussion of the single liquid, polybaric crystallization model 205

(iv) comparisons and interpretations of the model 207

(v) do these veins represent mineral accumulation or the frozen liquid equivalent of the initial partial melt? 213

c. Variations of the Proposed Model 214

(i) hypothesis for origin of chromite-related lithologies 214

(ii) high-alumina orthopyroxenite and high-alumina websterite: an origin by mineral segregation during upper mantle deformation 217

II.5.C. Origin of Spinel Group Minerals 219

1. General Statement 219

2. Spinel Lherzolite 223

a. Mechanism for Spinel Formation and Interpretations 223

b. Discussion of the Variation in Spinel Composition 227

3. Harzburgite 236

a. Spinel Types and Origin and the Variation in the Spinel Cr/Al Ratio 236

4. Dunite 239

a. Origin, Compositional Variation and Equilibration 239

(i) partial melting 240

(ii) crystallization of spinel at elevated pressures 242

(iii) subsolidus equilibration 243

(iv) summary 244

5. Chromite 245

a. General Statement 245

b. Crystallization Model 246

(i) chromite-related lithologies - inferred crystallization order 246

(ii) mechanisms for initiating chromite crystallization and internal restrictions 246

(iii) systematics of the selected mechanisms 247

(iv) Irvine mechanisms: an example for the formation of chromitite layers in some layered intrusions 249

(v) model for the origin of the chromite-related lithologies of the White Hills Peridotite .. 251

(vi) discussion of the proposed model and the Irvine model 252

c. Summary 254

6. Gabbro and Pyroxenite Veins 254

a. General Statement 254

b. Mechanisms for Spinel Formation and Interpretation 255

(i) plagioclase + olivine reaction 255

(ii) application of reaction (5.3) to the White Hills Peridotite 256

(iii) spinel exsolved by silicates 258

(iv) spinel in websterite, wehrlite and clinopyroxenite 261

Chapter 6

Some Speculation on the Origin of the White Hills Peridotite

II.6.A. General Statement 263

a. Proposed Model for the Origin of the White Hills Peridotite 263

(i) the Duncan and Green (1980) model 263

(ii) proposed model for the White Hills Peridotite 264

References 271

Appendix I A1

Appendix II A10

Appendix III A96

Appendix IV A126

Appendix V A141

Endpiece

LIST OF FIGURES

			Page
Fig.	1.1.	The location and geology of the St. Anthony Complex	2
Fig.	1.2.	Tectonic lithostratigraphic zones of Newfoundland	9
Fig.	1.3.	The geology of the northern part of the Humber Zone	11
Fig.	1.4.	Stratigraphic sections of the northern part of the Humber Zone	12
Fig.	2.1.	The location of alkali pyroxenite, jacupirangite, hornblende gneiss, and syenite in the St. Anthony Complex	31
Fig.	2.2.	Schematic section through the jacupirangite-syenite assemblage	33
Fig.	2.3.	Idealized ophiolite stratigraphy	36
Fig.	2.4.	Modal plot of the ultramafic rocks	37
Fig.	2.5.	Modal plot of the mafic rocks	38
Fig.	2.6.	Distribution and locations of the various rock textures	43
Fig.	2.7.	Sketch of the oblique orientation of the dunite megalens to host harzburgite foliation	56
Fig.	2.8.	Sketch of the common pyroxenite vein outcrop configurations	61
Fig.	2,9.	Outcrop distribution of gabbro veins	66
Fig.	2.10.	Sketch of F_1 isoclinal fold	73
Fig.	2.11.	Comparison and relative location of the White Hills Peridotite stratigraphy to the ophiolites from the Bay of Islands Complex	83
Fig.	3.1.	Comparison of Fo vs. bulk rock concentrations of Al_2O_3 and CaO	86
Fig.	3.2.A.	Pyroxene compositions of rocks from the White Hills Peridotite	90

Fig. 3.2.B. Pyroxene compositions of rocks from the White Hills Peridotite 91

Fig. 3.2.C. Pyroxene compositions of rocks from the White Hills Peridotite 92

Fig. 3.3. Schematic drawing of two examples of clinopyroxene exsolution from orthopyroxene 95

Fig. 3.4. Plot of (Ti/Ti+Al) vs. (Mg/Mg+Fe*) for the clinopyroxenes from the White Hills Peridotite 100

Fig. 3.5. Plot of (Cr/Cr+Al) vs. (Mg/Mg+Fe*) for the clinopyroxenes from the White Hills Peridotite 101

Fig. 3.6. Clinopyroxene analyses from the White Hills Peridotite plotted according to the method of LeBas 103

Fig. 3.7. Major elements vs. MgO from the White Hills Peridotite 110

Fig. 3.8. Trace elements vs. MgO from the White Hills Peridotite 111

Fig. 3.9. Plot of Ni vs. FeO*/(FeO*+MgO) of probable cumulate rocks from the White Hills Peridotite 113

Fig. 3.10. Plot of CaO+ TiO_2 vs. FeO*/(FeO*+MgO) of probable cumulate rocks from the White Hills Peridotite 114

Fig. 3.11. Plot of Al_2O_3 vs. FeO*/(FeO*+MgO) of probable cumulate rocks from the White Hills Peridotite 115

Fig. 3.12. AF_tM diagram 117

Fig. 3.13. Chondrite normalized rare earth element patterns of gabbro veins from the White Hills Peridotite 119

Fig. 3.14. Chondrite normalized rare earth element patterns of gabbro veins from the White Hills Peridotite 120

Fig. 3.15. Chondrite normalized rare earth element patterns of gabbro veins from the White Hills Peridotite 121

Fig. 4.1. Conventional projections used for plotting spinel analyses 141

Fig. 4.2. Plot of the Cr x 100/(Cr+Al) vs. Mg x 100/($Mg+Fe^{2+}$) for spinels from various lithologies of the White Hills Peridotite..... 145

Fig. 4.3. Plot of Fe^{3+} x 100/($Cr+Al+Fe^{3+}$) vs. Mg x 100/($Mg+Fe^{2+}$) of spinels from various lithologies of the White Hills Peridotite . 146

Fig. 4.4. Spinel composition from various lithologies of the White Hills Peridotite plotted in the spinel prism 147

Fig. 4.5. Plot of Cr x 100/(Cr+Al) vs. Mg x 100/($Mg+Fe^{2+}$) of spinels from various lithologies of the White Hills Peridotite 149

Fig. 4.6. Al-Cr-Fe^{3+} triangular plot of spinels from various lithologies of the White Hills Peridotite 150

Fig. 4.7. TiO_2 vs. Mg x 100/($Mg+Fe^{2+}$) for spinels from various lithologies of the White Hills Peridotite 151

Fig. 4.8. Plot of Cr x 100/(Cr+Al) vs. Mg x 100/($Mg+Fe^{2+}$) for spinels from various lithologies of the White Hills Peridotite 153

Fig. 4.9. Plot of Cr x 100/(Cr+Al) vs. Mg x 100/($Mg+Fe^{2+}$) for spinels from various lithologies of the White Hills Peridotite 156

Fig. 4.10. Plot of Cr x 100/(Cr+Al) vs. Mg x 100/($Mg+Fe^{2+}$) for spinels from the chromite pod ... 157

Fig. 4.11. Plot of Cr x 100/(Cr+Al) vs. Mg x 100/($Mg+Fe^{2+}$) for spinels from websterite, clinopyroxenite, wehrlite, and gabbro 159

Fig. 4.12. Websterite, clinopyroxenite, wehrlite, and gabbro spinel compositions plotted in the spinel prism 160

Fig. 4.13. Al-Cr-Fe^{3+} plot of spinels from websterite clinopyroxenite, wehrlite, and gabbro 161

Fig. 5.1. Locations of the projection planes in the CMAS system used in this study 175

Fig. 5.2. Graphical development of a control plane .. 176

Fig. 5.3. Olivine projection onto the plane CS-MS-A . 180

Fig. 5.4. Enstatite projection onto the plane C_2S_3-M_2S-A_2S_3 181

Fig. 5.5. Diopside projection onto the plane C_3A-M-S. 182

Fig. 5.6. Melting curve of sample 1611 and $Fo_{55}En_{30}Di_{15}$ at 20 kb (from Mysen and Kushiro, 1977)..... 187

Fig. 5.7. Enlargement of the olivine projection to illustrate the proposed polybaric crystallization path for the origin of the pyroxenite, gabbro and dunite veins/bodies 201

Fig. 5.8. Chondrite normalized rare earth element patterns of gabbro and clinopyroxenite veins from the White Hills Peridotite 210

Fig. 5.9. Schematic representation of a clinopyroxenite pod with anastamosing gabbro veins emanating from the pod 212

Fig. 5.10. Range of spinel compositions in Alpine complexes and stratiform intrusions (after Irvine and Findlay, 1972) 220

Fig. 5.11. Generalized model for the petrological development of the White Hills Peridotite 222

Fig. 5.12. Flow chart detailing the petrological evolution of the White Hills Peridotite and proposed origins of the spinel phases of the White Hills Peridotite 224

Fig. 5.13. Mg-Fe^{2+} partitioning between coexisting spinel and olivine from ophiolitic ultramafic rocks 229

Fig. 5.14. Plot of Cr/Al spinel vs. Cr/Al bulk rock . 230

Fig. 5.15. Plot of Cr_2O_3 vs. Cr/(Cr+Al) spinel 231

Fig. 5.16. Plot of Al_2O_3 in orthopyroxene vs. Cr/(Cr+Al) in coexisting spinel 233

Fig. 5.17. Plot of Al_2O_3 in clinopyroxene vs. Cr/(Cr+Al) in coexisting spinel 234

Fig. 5.18. The system MgO-SiO_2-Cr_2O_3 (from Keith, 1954) 241

Fig. 5.19. Phase diagram models illustrating the possible paths of crystallization of the chromite-related lithologies 248

Fig. 6.1. Schematic representation of the proposed model for the White Hills Peridotite 266

LIST OF TABLES

		Page
Table 2.1.	Compilation of rock texture classification .	40
Table 3.1.	Chemical comparison of two types of clinopyroxene exsolution in orthopyroxene porphyroclasts in spinel lherzolite	96
Table 3.2.	Estimates of temperature for the equilibration of spinel lherzolite and harzburgite from the White Hills Peridotite	105
Table 4.1.	Textural variations of the spinel phases from the White Hills Peridotite	in pocket
Table 4.2.	Spinel equilibration temperatures of the White Hills Peridotite	169
Table 5.1.	Subtraction program compositional input data and estimations of upper mantle primary compositions	179
Table 5.2.	Calculated liquid and natural primitive liquid compositions	186
Table 5.3.	Proposed model for the origin of the pyroxenite, gabbro and dunite veins and bodies of the White Hills Peridotite	198

LIST OF PLATES

		Page
Plate 1.	The northern part of the Hare Bay Allochthon .	in pocket
Plate 2.	The geology of the White Hills Peridotite	in pocket
Plate 3.	Geological cross section of the western peridotite massif, White Hills Peridotite	in pocket
Plate 4.	Geological cross section of the eastern peridotite massif, White Hills Peridotite	in pocket
Plate 5A.	Quartz and feldspar grains in a matrix of quartz, feldspar and mica, Maiden Point Formation	25
Plate 5B.	Amphibole augen in mylonite texture, Green Ridge Amphibolite	25
Plate 5C.	Spongy textured amphibole, Green Ridge Amphibolite	25
Plate 5D.	Lens of massive alkaline pyroxenite within zone of interlayered syenite	25
Plate 5E.	Hornblendite at basal thrust fault containing peridotite fragment	25
Plate 6A.	Coarse-granular texture	41
Plate 6B.	Porphyroclastic texture	41
Plate 6C.	Granoblastic texture	41
Plate 6D.	Mylonitic texture	41
Plate 6E.	Allotriomorphic-granular texture	41
Plate 6F.	Cumulate texture	41
Plate 6G.	Resorbed euhedral spinels in euhedral orthopyroxene (bastite) phenocryst	42
Plate 7A.	Layered peridotite sequence	49
Plate 7B.	Layered peridotite sequence	49
Plate 7C.	Clinopyroxene and olivine grains in orthopyroxene porphyroclast	49
Plate 7D.	Clinopyroxene exsolution from orthopyroxene porphyroclast	49

Plate 7E. Mesh texture in olivine 49

Plate 7F. Clinopyroxene megacryst in spinel lherzolite .. 49

Plate 7G. Chromite seam in dunite layer 49

Plate 7H. Dunite lens in harzburgite 50

Plate 8A. Contact between dunite megalens and host rock . 58

Plate 8B. Anastamosing network of dunite dikes 58

Plate 8C. Dunite dike cutting layered sequence of harzburgite-dunite-orthopyroxene-rich dunite 58

Plate 8D. Anastamosing dunite dikes in harzburgite 58

Plate 8E. Composite dunite dike in harzburgite 58

Plate 8F. Close up of composite dunite dike in harzburgite 58

Plate 9A. Clinopyroxenite vein refolded by F_2 67

Plate 9B. Typical outcrop view of gabbro veins in harzburgite 67

Plate 9C. Network of gabbro veins with various orientations 67

Plate 9D. Zoned gabbro vein 67

Plate 9E. Clinopyroxenite pod 67

Plate 9F. Chromitite seam in the core of an orthopyroxenite vein 67

Plate 9G. Folded chromitite seam in slightly mylonitic orthopyroxene-rich dunite 67

Plate 9H. Typical field appearance of the peridotite deformed by F_2 68

Plate 9I. F_3 generation fold style 68

Plate 9J. Fault zone breccia which is developed within northeast-southwest fault set 68

Plate 10A. Exsolved vermicular spinel form in orthopyroxene in coarse-granular textured spinel lherzolite . 130

Plate 10B. Porphyroclast spinel form with "trail" in porphyroclastic textured spinel lherzolite 130

Plate 10C. Porphyroclast spinel form with occluded olivine in porphyroclastic textured harzburgite 130

Plate 10D. Pull apart texture in allotriomorphic-granular textured dunite 130

Plate 10E. Corroded "holly-leaf" spinel form in granoblastic textured dunite 130

Plate 10F. Spinel clusters in gabbro 130

Plate 11A. Vermicular spinel in olivine 135

Plate 11B. Plagioclase-(clinopyroxene + spinel)-olivine corona in gabbro 135

Plate 11C. Exsolved spinel droplets in clinopyroxene and plagioclase, and spinel interstitial to clinopyroxene and plagioclase 135

Plate 11D. Cumulus spinel in orthopyroxenite 135

Plate 11E. Exsolved spinel droplets in clinopyroxene, and spinel interstitial to clinopyroxene, orthopyroxene and olivine 135

Plate 11F. "Websterite" from the chromite pod 135

PART I

PART I

Chapter 1

INTRODUCTION

I.1.A. Location and Access

The White Hills Peridotite is composed of two large and one small dissected ultramafic massifs, which outcrop in a belt approximately 20 kilometers long and 9 kilometers wide trending approximately east-west on the northern tip of the Great Northern Peninsula, Newfoundland (Figure 1.1.). The three massifs have been mapped during the summers of 1977, 1978, and 1979 by the author using the town of St. Anthony as a base. St. Anthony can be reached by road, air or boat from all locations in Newfoundland.

Local access to the interior of the massifs can be accomplished by floatplane, helicopter, boat or on foot. The completion of the new Northern Peninsula Highway in 1979 now makes access into the western massif possible by foot. Otherwise travel into the massifs is difficult due to the thick overgrowth of trees and the numerous bog areas. The use of a boat for access into the western peridotite massif of the Howe Harbour area and coastal reconnaissance of the rocks underlying the peridotite is advised.

Figure 1.1. The location and geology of the St. Anthony Complex (after Williams, 1971; Williams et al., 1973; Jamieson, 1979).

ST. ANTHONY COMPLEX

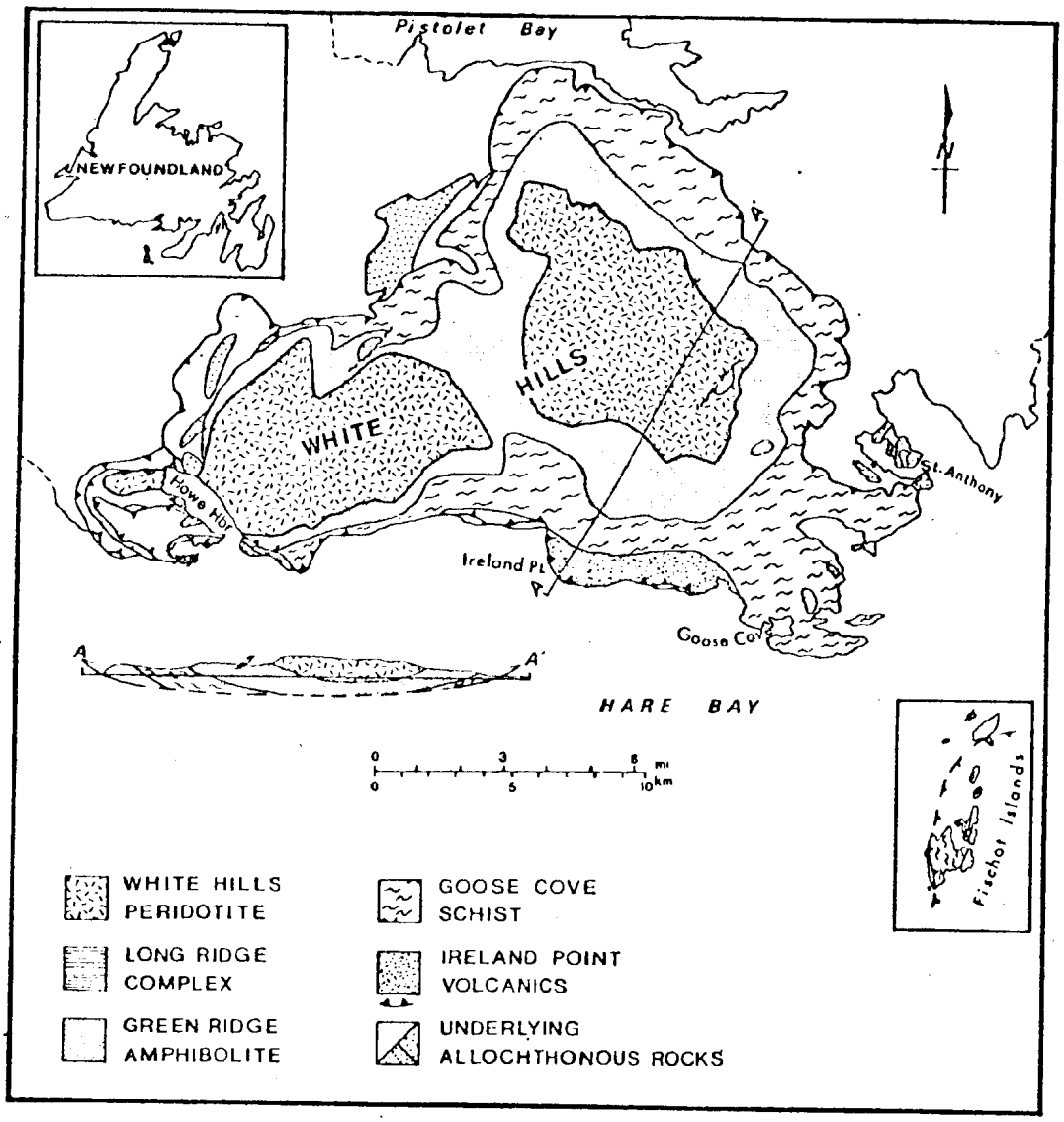

MM

I.1.B. Previous Geological Work

Detailed geological studies pertaining to the major ultramafic rock sequences of western Newfoundland* were carried out by Snelgrove (1934) and Snelgrove et al (1934). These authors described the economic potential of the chromite deposits of the mafic-ultramafic rocks of Newfoundland, and it was at this time that these authors interpreted the Bay of Islands Complex as a dismembered banded lopolith. However, Ingerson (1935, 1937) reinterpreted the Bay of Islands Complex mafic-ultramafic rocks and suggested that they represent individual laccoliths. Contrary to Ingerson's views (1935, 1937), Cooper (1936) and Buddington and Hess (1937) suggested that the 'massifs' or 'sheets' were remnants of a once possibly continuous lopolith. This hypothesis was extended by Cooper (1937) who suggested that the Bay of Islands Complex and the White Hills Peridotite sheet represented lopolith-shaped intrusions that had been thrust westwards and, in the case of the Bay of Islands Complex, segmented by tear faults. Cooper (1937) estimated a horizontal thrust displacement of approximately 7 kilometers for the White Hills Peridotite sheet.

* the White Hills Peridotite and the Bay of Islands Complex as a group are referred to as western Newfoundland mafic-ultramafic rock sequences (Williams, 1971). Both of these sequences are of ophiolitic affinity and probably because of accessibility and what is regarded as a nearly complete 'ideal' ophiolite stratigraphy, the Bay of Islands Complex has been more thoroughly studied than the White Hills Peridotite. Therefore, most of the following discussion has been taken from the geological history of the Bay of Islands Complex.

After detailed mapping and petrographic study of the Bay of Islands Complex Smith (1958) concluded that the isolated massifs represented individual intrusions surrounded in part by a metamorphic aureole.

Until 1963 then, the mafic-ultramafic rocks of western Newfoundland were considered intrusions which had crystallized in situ. However, in 1963 Rodgers and Neale interpreted the western Newfoundland mafic-ultramafic complexes as integral parts of a transported terrain, much like the Taconic Allochthon, because of their close association with the underlying clastics. Earlier, Johnson (1941) and Kay (1945) had suggested that the clastic sequence might be equivalent in age to the structurally underlying carbonates. Thus the working hypothesis as of 1963 required transport of both mafic and ultramafic rocks and the clastic sequence as a single entity, thus retaining the hypothesis that the igneous rocks crystallized in situ. Stevens (1970) was the first investigator to suggest that the mafic-ultramafic complexes of western Newfoundland (now termed ophiolites) represented transported 'slices' which had been thrust westward during the closing of the proto-Atlantic Ocean (Wilson, 1966). He based this interpretation on the presence of ophiolite detritus, mainly chromite grains, in an underlying arkose (Blow-Me-Down Brook Formation), its derivation believed to be from the advancing ophiolite. Since the initial recognition of the transported slices, additional allochthonous slices have been delineated and defined in the Bay of Islands area, mainly on the basis of lithology and fossil evidence (Williams,

1973, 1975). In total, five allochthonous slices have been recognized.

Although the mafic-ultramafic rocks represent material that had been transported, as earlier suggested by Cooper (1937), the mechanism that caused the metamorphism of the rocks immediately beneath the ophiolites was still in doubt. Previous investigators (e.g., Smith, 1958) suggested the metamorphism had been the result of cooling of the intrusion (i.e., contact metamorphism). The present interpretation, originally suggested by Church and Stevens (1971), propounds the metamorphism to be dynamothermal, and probably occurred as a result of and during obduction and emplacement transport of the hot ophiolite by convectional cooling and frictional heating (Williams and Smyth, 1973; Malpas, 1976, 1979; Jamieson, 1979, 1980a, b).

In the Hare Bay region, Tuke (1968) showed that superimposed sequences (structural slices) of similar lithology and age to the Bay of Islands region occurred in this region and from this he was able to delineate three allochthonous 'slices', of which the White Hills Peridotite is structurally the highest. The criteria used to delineate structural slices of the Humber Arm Allochthon were applied to the Hare Bay Allochthon by Smyth (1971, 1973), Williams et al (1973) and Williams and Smyth (in press). These investigators were able to define additional structural slices and their stacking order.

Until 1976, geological work on the White Hills Peridotite had been restricted mainly to reconnaissance mapping (Cooper, 1937; Shepperd, 1962a, b, c; Smyth, 1973; Williams and Smyth, in press). The first detailed work on the peridotite was done by Riccio (1976) who described some lithologies as part of his Ph.D. thesis. Riccio (1976) concluded that the White Hills Peridotite was relatively undepleted compared to that of the Bay of Islands upper mantle material, but compared to pyrolite (Ringwood, 1975), the White Hills was highly depleted in K, Na, and Ti. He also suggested that the dunites associated with the peridotite may represent a partial melt residuum or subsolidus metamorphic segregation, whereas the wehrlite (+ spinel) dikes were interpreted as early crystal cumulates derived from undersaturated picritic liquids. The lithological layering (i.e., spinel lherzolite, websterite (± spinel), harzburgite, dunite) was interpreted to have formed by solid state deformation.

More recently, Jamieson (1979) has completed a geochemical, petrological, and structural study of the White Hills Peridotite - metamorphic aureole contact and all of the associated lithologies of the metamorphic aureole; the results have been presented in her Ph.D. thesis (Memorial) and several publications (see references). In these works, Jamieson suggested that the metamorphic aureole did not form within a subduction zone, for if it had then the overriding peridotite would have come into contact first with continental margin sediments, rather than the gabbros and volcanics. Instead, she suggested that the White Hills Peridotite was derived

from the same piece of oceanic material as the metamorphic aureole and that the peridotite overrode the adjacent oceanic lithosphere. Although probably not formed in a subduction zone, the detachment of the peridotite may have been related to the initiation of an east-dipping subduction zone. Final emplacement of the allochthons was accomplished along high angle thrust faults that may have been related to isostatic rebound of the buried continental margin (Malpas and Stevens, 1977). Although it has generally been recognized that the metamorphic aureole formed as the result of the hot peridotite ($\sim 1000^{\circ}C$?) coming in contact with colder material and/or from frictional heating due to emplacement (Malpas, 1979), no combination of such mechanisms appear to provide a completely satisfactory result, and therefore, the answer to this problem must await further studies.

I.1.C. Regional Setting

1. The Newfoundland Appalachians

The St. Anthony Complex occurs at the northernmost limit of the Appalachian Orogen. The rocks of the Appalachians record the evolution of the Iapetus Ocean during late Precambrian and early Paleozoic times (Dewey, 1969; Stevens, 1970; Williams et al., 1972; Williams and Stevens, 1974, and others). In order to provide a convenient way of correlating the rocks of the Appalachian Orogen, the Middle Ordovician and older rocks of the Orogen have been subdivided on the basis of contrasts in thickness, facies, and structural-style

(Williams, 1979), mainly from examples in Newfoundland. The first zonal subdivision (Williams, 1964), divided the Newfoundland Appalachians into three zones (i.e., Western Platform, Central Volcanic Belt, and the Avalon Platform). A later subdivision into nine zones (Williams et al., 1974) proved too specialized and restricted in useage to the Northern latitudes. The recent synthesis of the Appalachian Orogen has resulted in fewer zones (Williams, 1976) and their extrapolation along the full length of the Appalachian Orogen (Williams, 1978a), as well as across to the British Caledonides (Williams, 1978b).

The five zones presently in use for the Appalachian Orogen are from west to east: Humber, Dunnage, Gander, Avalon, and Meguma* (Williams, 1976) (Figure 1.2.). The Humber Zone, which includes the St. Anthony Complex, records the development and destruction of an Atlantic-type continental margin (i.e., the ancient eastern continental margin of North America) (Williams, 1979), the Dunnage Zone represents the remains of an island arc sequence and melanges built upon oceanic crust (Williams, 1979), the Gander Zone records the development and destruction of a continental margin, the eastern margin of Iapetus Ocean (proto-Atlantic), the Avalon Zone during the Cambrian may have acted as a pre-Iapetus continental platform, whereas during the Precambrian it may have been the location of Iapetus related rifting or pre-Iapetus rift-related volcanism (Williams, 1979).

* The Meguma Zone does not occur on insular Newfoundland.

Figure 1.2. Tectonic lithostratigraphic zones of Newfoundland (after Williams, 1979). H - Humber zone; D - Dunnage zone; G - Gander zone; A - Avalon zone.

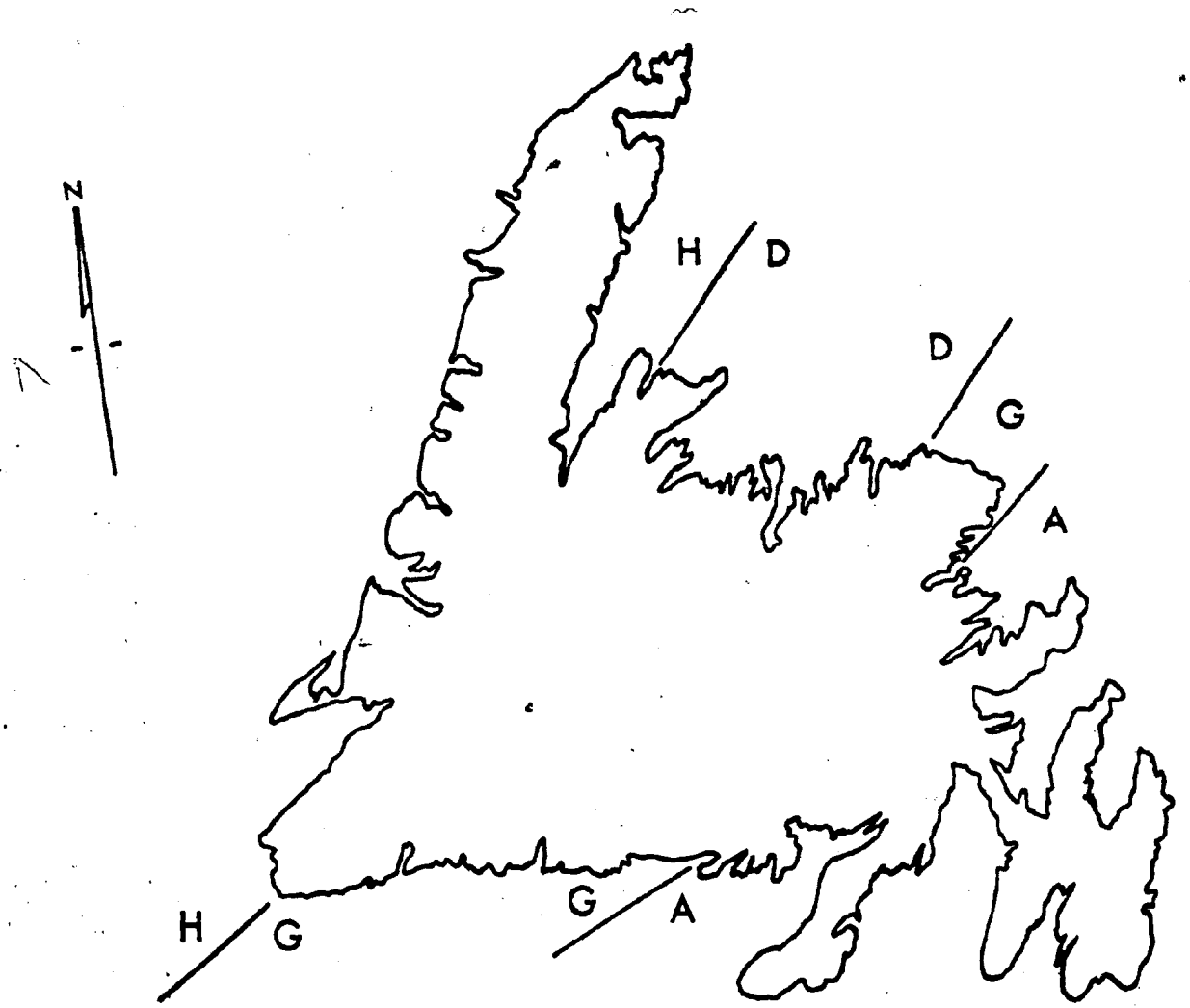
N
H
D
D
G
A
H
G
G
A

a. The Humber Zone

Within the Humber Zone the Middle Ordovician and older rocks of western Newfoundland (Figure 1.3.) are separated into three elements on the basis of tectonic similarities and lithology:

I. Precambrian crystalline basement (Long Range Mountains and Indian Head Range) of Grenville age (1130-840 Ma, Pringle et al., 1971).

II. Cambro-Ordovician autochthonous and neo-autochthonous sequences of predominantly carbonates, minor clastics and volcanics.

III. Cambro-Ordovician allochthonous sequence of clastic material, carbonate, and ophiolite sequences.

The Precambrian basement gneisses of the Long Range Mountains outcrop the total length of the Great Northern Peninsula. These rocks, radiometrically dated at 1130±90 Ma (Rb:Sr whole rock) to 840±20 Ma (K:Ar biotite) (Pringle et al., 1971), represent the eastern-most extension of Grenville basement in eastern North America (Williams and Stevens, 1974). The basement complex is unconformably overlain by a thin unit (∿ 120m) of tholeiitic rift facies volcanics and dikes (Lighthouse Cove Formation) (Strong and Williams, 1972) (Figure 1.4.). Stukas and Reynolds (1974) have determined an $^{40}Ar/^{39}Ar$ radiometric date of 621±6 Ma for these volcanics. This age contrasts sharply to the 850±35 Ma K:Ar date that has been determined for the same volcanics by Pringle et al (1971). Stukas and Reynolds (1974) suggest that the age determined by Pringle et al (1971) may be incorrect due to contamination of these rocks with significant quantities of radiogenic argon.

Figure 1.3. The geology of the northern part of the Humber zone (from Williams, 1971).

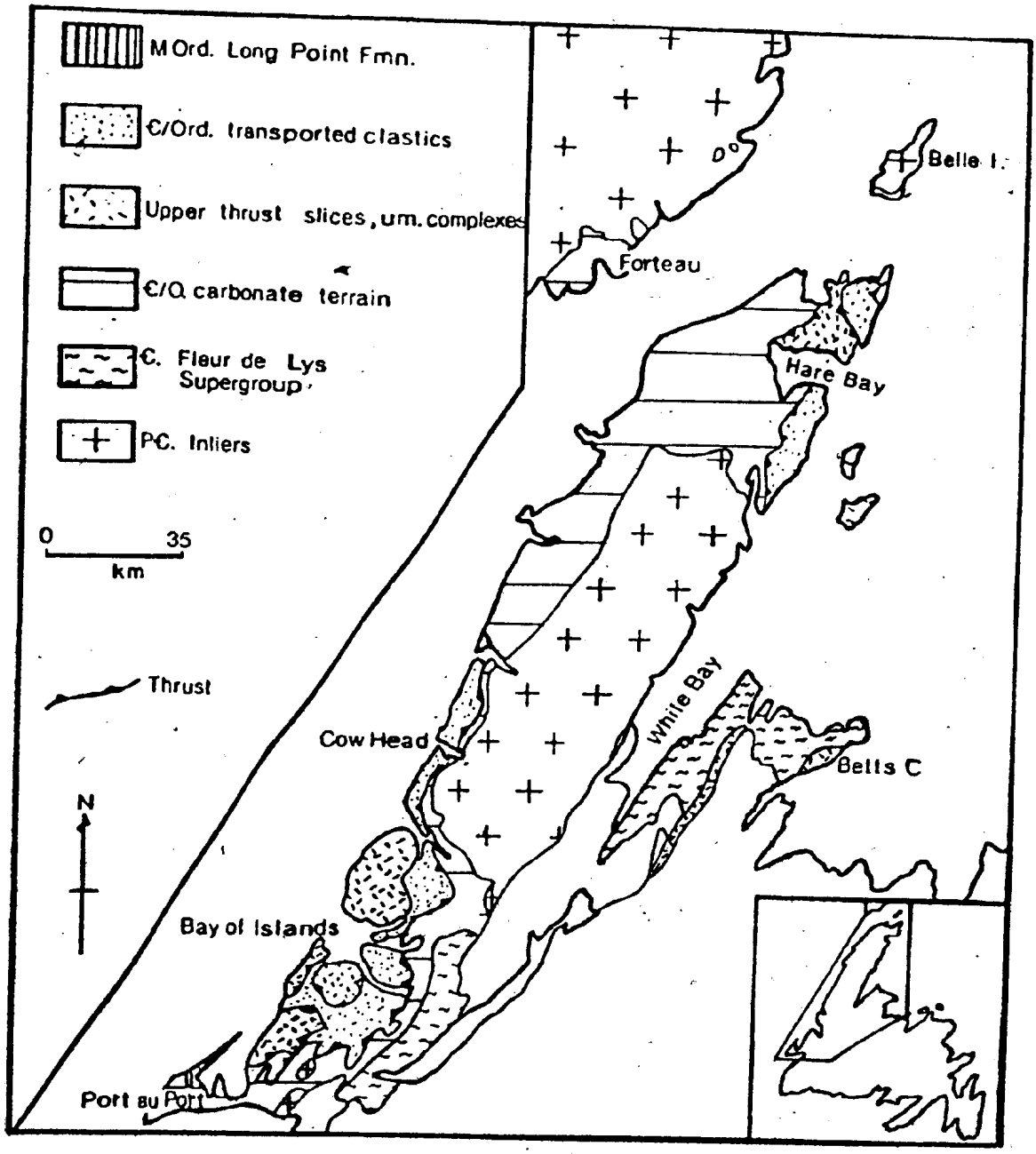
M Ord. Long Point Fmn.
€/Ord. transported clastics
Upper thrust slices, um. complexes
€/O. carbonate terrain
€. Fleur de Lys Supergroup
PC. Inliers
0
35
km
Thrust
N
Belle I.
Forteau
Hare Bay
White Bay
Cow Head
Belts C
Bay of Islands
Port au Port

Figure 1.4. Stratigraphic sections of the northern part of the Humber zone (from Williams, 1971).

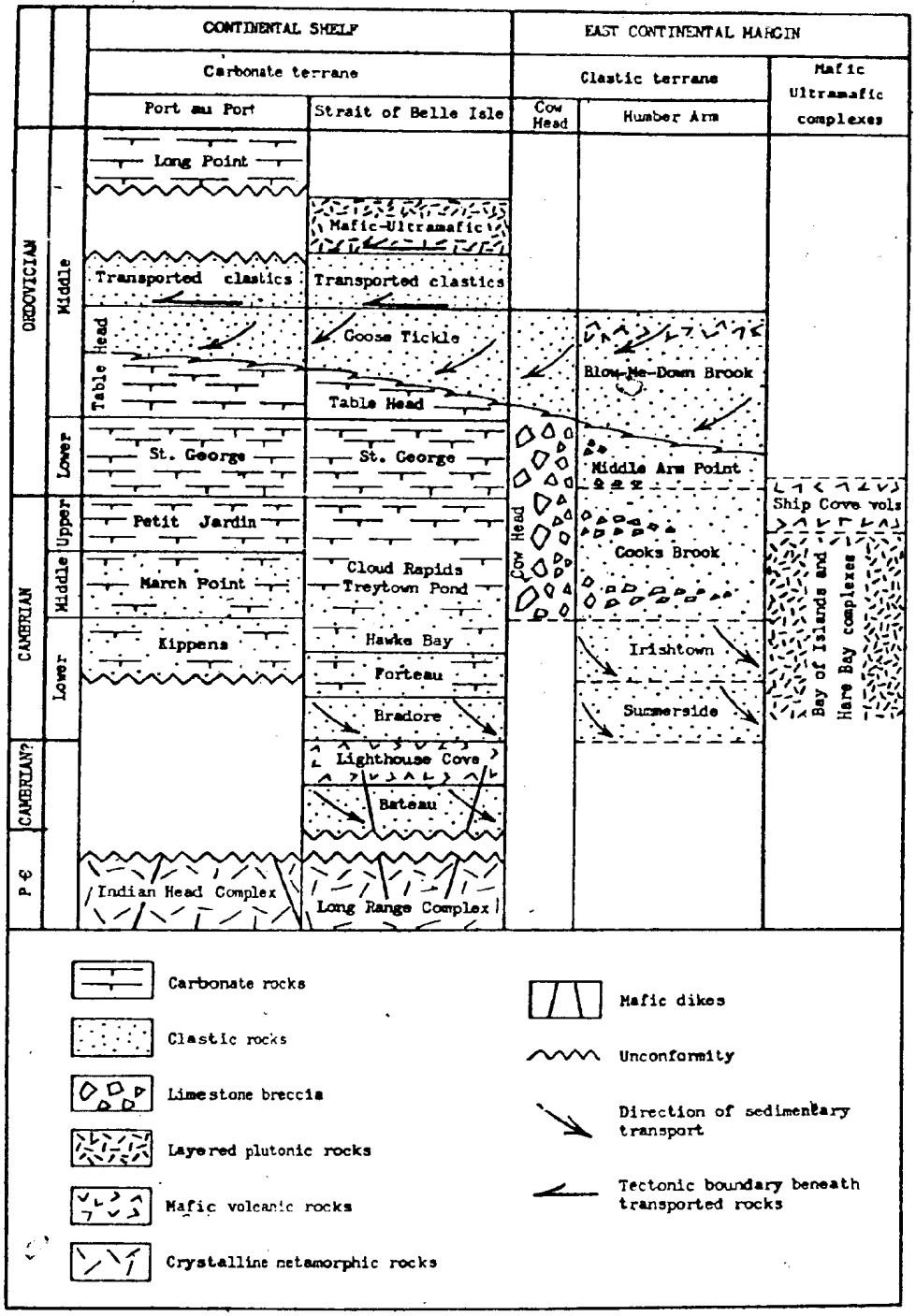

POOR COPY
COPIE DE QUALITÉE INFÉRIEURE

Locally, in the St. Anthony area, the Bateau Formation, a westerly-derived sandstone-conglomerate unit, occurs between the basement gneisses and the rift facies volcanics. Conformably overlying these volcanics is the autochthonous Cambro-Ordovician clastic succession (Humber Arm Supergroup, Maiden Point Formation, Fleur de Lys Formation) that has been derived from the craton to the west and subsequently deposited on the continental slope and rise areas (e.g., Stevens, 1970). Within the autochthonous sequences the rocks record the upward (landward) ocean transgression event, from immature sandstones to mature quartzites, and then limestones and dolomites (e.g., Bradore Formation to St. George Group; see Figure 1.4.) (Williams, 1979). The buildup of the autochthonous succession with the presence of rift facies volcanics is considered to represent the development of an Atlantic-type continental margin during late Hadrynian and early Paleozoic time (e.g., Stevens, 1970).

Destruction of this continental margin began in the early Ordovician, probably in response to the initiation of an east-dipping subduction zone, (Church and Stevens, 1971; Strong et al., 1974) and occurred diachronously from north to south (Dallmeyer and Williams, 1975; Dallmeyer, 1977). The formation of the subduction zone, which according to Jamieson (1979, 1980a, b) probably formed at some distance from the continental margin, marks the earliest recorded phase in the closing of the Iapetus Ocean. During this phase, detached fragments of oceanic lithosphere were obducted from their oceanic environment and thrust westward onto

oceanic lithosphere and the supracrustal rocks of the outer continental margin. The loading of the continental margin by the assembling allochthonous units (Humber Arm and Hare Bay) during continued closing of the Iapetus Ocean caused a subsidence of the continental shelf that resulted in a change from shallow water carbonate to deeper water carbonate sedimentation (Table Head Formation) and the deposition of Mid-Ordovician, graptolite-bearing black shales (upper Table Head Formation) (Stevens, 1970). As a result of the obduction of oceanic material onto the outer continental margin and subsidence of the continental shelf due to loading, a change in the predominant sediment transport direction from west to east occurred due to the erosion of the oceanic material (Stevens, 1970; Williams and Stevens, 1974).

The assembled allochthons overrode the autochthonous sequence of the continental shelf and emplacement was completed by the Middle Ordovician. Deposition of the neoautochthonous Long Point Formation (Stevens, 1970) on the southwestern part of the Humber Arm Allochthon (Rodgers, 1965; Stevens, 1970) provides an accurate means of dating these events.

Palinspastic reconstruction of the allochthons and continental margin indicates the highest structural slices were located farthest east as either an integral part of the continental margin sediment wedge (e.g., carbonate breccias – Cow Head Breccia, Cooks Brook Formation and continental rise-prism sediments – Summerside Formation, etc.) or as igneous rocks formed at an accreting ridge (Stevens, 1970). This reconstruction led Williams and Smyth (1973) to suggest the

highest structural slices travelled the farthest, originating at least 80-100 kilometers east of their present geographic location, most probably along or to the east of the Baie Verte-Brompton Line (Williams, 1976).

Post-emplacement deformation in the Humber Zone is represented by gentle upright folds and steep rock cleavages (Williams and Smyth, in press) that formed during the Acadian Orogeny. Siluro-Devonian red beds and Carboniferous sediments locally overlie the Cambro-Ordovician succession and Grenville basement (Williams et al., 1974).

b. The Hare Bay Allochthon

The Hare Bay Allochthon (Plate 1), like the Humber Arm Allochthon, is composed of a series of structurally interleaved slices (Williams, 1975) which are, from bottom to top: Northwest Arm Formation; Maiden Point Formation; Grandois Group; Milan Arm Melange; Cape Onion Formation; St. Anthony Complex.

The Northwest Arm Formation structurally overlies the autochthonous Goose Tickle Formation and consists of finely bedded shales, limy siltstones, limestones, limestone breccias, chert and siliceous argillite (Williams and Smyth, in press). A fairly abrupt but rubbly contact and a melange zone is observed between the Goose Tickle and Northwest Arm Formations (Williams and Smyth, in press). The thickness of the formation has been estimated by Cooper (1937) to be 150 meters, whereas Tuke (1968) and Williams and Smyth (in press) estimate it to be closer to 50 meters. Tuke (1968) has identified the early Ordovician graptolite Staurograptus dichotomus in the formation. The chaotic nature of the

formation has been suggested by Williams and Smyth (in press) to indicate emplacement while in a semi-consolidated state. The formation has been shown to be equivalent in age to the Middle Arm Point Formation in the Humber Arm Allochthon (Williams, 1975).

The Maiden Point Formation (Maiden Point Sandstone of Cooper, 1937) is the most widespread unit of the allochthon. It consists of greywackes, pebble conglomerates, mafic and felsic volcanics and a diorite-gabbro intrusive member (Cooper, 1937; Tuke, 1968; Smyth, 1973; Williams and Smyth, in press). Cooper (1937), Tuke (1968) and Williams and Smyth (in press) estimate the thickness of the unit to be in the order of about 2000 meters, and a stratigraphically determined Lower Cambrian or late Precambrian age has been assigned to this assemblage by Stevens (1970) and Williams (1971). Paleocurrent directions and sediment types indicate a westerly source region of Grenville basement gneisses (Williams and Stevens, 1974), whereas the volcanic member of the formation is believed to be associated with continental rifting during the opening of the proto-Atlantic Ocean (Williams and Stevens, 1974).

The Grandois Group is the least areally extensive slice of the allochthon. It is made up of the Irish Formation and the St. Julien Island Formation (Williams, 1975), which individually consist of a layered sequence of brecciated quartzites, siliceous limestone, slate and sandy limestone and about 60 meters of polymictic conglomerates with interbeds of red, green and purple greywacke (Smyth, 1971; Williams, 1975).

The age of this unit is not known but it may range from Middle Cambrian to Middle Ordovician (Williams, 1975).

The Milan Arm Melange is an example of an ophiolitic melange (Williams and Talkington, 1977). It consists of blocks of serpentinized peridotite, mafic volcanics, gabbro, diorite, pyroxenite, amphibolite, hornblendite, tonalite, hornblende-biotite schist, minor nephrite and some unidentified exotics (Williams, 1975), which range in size up to a kilometer or more across, contained in a green and black shale matrix. The thickness of the melange is not known. The presence of the exotics suggests a relative age for melange formation of upper Lower Ordovician to Middle Ordovician. This age thus coincides with that of the emplacement of the ophiolites (Tuke, 1968; Smyth, 1971).

The Cape Onion Formation consists of variolitic pillow lavas, local agglomerate and tuffaceous units, and mafic volcanic rocks interlayered with black shales some of which contain Lower Ordovician graptolites (Jamieson, 1979; Williams and Smyth, in press). Although this formation has been considered part of the Maiden Point Formation by Cooper (1937) and Tuke (1968), more recently, DeLong (1976) and Williams and Smyth (in press) suggest that it may be a large block within the Milan Arm Melange. Williams (1975) estimates the thickness of the unit to be about 1000 meters. The Cape Onion Formation lacks an obvious preemplacement deformation and Williams and Smyth (in press) have suggested that the pillow lavas resemble those which occur at the top of the Bay of Islands ophiolite Complex of the Humber Arm Allochthon.

In addition, Jamieson (1977a, 1979) indicates their lithological similarity with the Ireland Point Volcanics of the St. Anthony Complex.

The St. Anthony Complex, previously called the White Hills Slice (Williams et al., 1973) and St. Anthony Slice (Williams, 1975), is the highest structural slice of the Hare Bay Allochthon. It consists of a peridotite sheet and underlying metamorphic rocks. From bottom to top the units are: Ireland Point Volcanics; Goose Cove Schist; Green Ridge Amphibolite; White Hills Peridotite. The three lower units of the Complex are defined on the basis of metamorphic grade and structural style (Jamieson, 1979; Williams and Smyth, in press).

I.1.D. Purpose and Scope of Study

In the early stages of this study the objectives were to determine the stratigraphic position(s), chemistry, origin and structural features of the podiform chromite deposits located in the ultramafic zones of the western Newfoundland ophiolites. After examination of the podiform chromite deposits and host rocks during the first field season (1977), the objectives of the thesis had to be modified due principally to the lack of intact podiform deposits and the discovery that the White Hills Peridotite is an interlayered sequence of dominately spinel lherzolite and harzburgite. The study has been redesigned, therefore, to examine the White Hills Peridotite with the following objectives in mind:

(1) conduct a field mapping and geochemical study of the peridotite in an effort to determine the extent of the interlayering of spinel lherzolite and harzburgite and what may have caused the layering to form.

(2) to describe the various vein lithologies that are present in the peridotite and postulate an origin(s) for their formation.

(3) to describe spinel (s.l.)-silicate textural relationships, determine spinel chemistry and hypothesize an origin of the spinel phases in the peridotite.

I.1.E. Acknowledgements

The study of the western Newfoundland ophiolites was suggested by John Malpas, who provided supervision, guidance, patience, and financial support for my four years at Memorial. Thanks are expressed to Tom Calon and Bob Stevens who acted as members of my supervisory committee. Many discussions of the Hare Bay region with Hank Williams (Memorial), Chris Lynas (Memorial), Svend Stouge (Newfoundland Department of Mines and Energy), and especially Becky Jamieson (Dalhousie University) have been of enormous help. The writer thanks Dave Strong (Memorial), Brian Fryer (Memorial), John Dickey (National Science Foundation), John Reid (Hampshire College), John Smewing (Open University), Chris Neary (I.G.S.) and Jacques Girardeau (Universite de Nantes) for stimulating and thought provoking discussions concerning many aspects of ophiolite genesis.

Many thanks are extended to Fred Frey (Massachusetts Institute of Technology) for the opportunity to analyze for rare earth elements at his lab, and Steve Roy (M.I.T.) for providing valuable instruction and assistance in INAA techniques. Invaluable assistance in obtaining bulk rock

and mineral analyses has been provided by Gert Andrews, Dave Press, Jaan Vahtra, Alan Thompson, and Henry Longerich. Many diagrams in the thesis have been drafted by Mike MacIntyre and Bob Hiscock. Nat Noel and Wade Dunford provided capable field assistance.

The friendship of many people, especially Neville and Christine Higgins and Jim Hibbard (a.k.a. Ogden Tweeto), made the undertaking of this thesis memorable.

Finally, to Kathe, who patiently waited the completion of this study, I express my deepest gratitude.

Chapter 2

The Geology of the St. Anthony Complex

I.2.A. Rocks Underlying the White Hills Peridotite

1. General Statement

During the course of field study the rocks underlying the White Hills Peridotite have been briefly examined. Previous workers (i.e., Cooper, 1937; Tuke, 1968; Stevens, 1970; Smyth, 1971, 1973; Jamieson, 1977a, 1979; Talkington and Jamieson, 1979; Jamieson and Talkington, 1980; Lynas and Calon, 1980; Williams and Smyth, in press) have presented extensive descriptions of these lithologies and from these some of the following discussion has been taken. Most of the units described in this section outcrop in the Howe Harbour region (Plates 1 and 2) of the study area, where, because of limited outcrop, the delineated stacking order of the structural slices (Williams, 1975) cannot be fully appreciated, nor confidently determined.

a. Goose Tickle Formation (Unit 1, Plate 2)

The autochthonous Goose Tickle Formation outcrops on the west shore, near the head, of Howe Harbour (Plate 2). The unit consists of a finely laminated, medium- to fine-grained shale and siltstone. The laminae are commonly less than one centimeter thick.

The contact with the overlying allochthonous Northwest Arm Formation is not exposed, but Williams and Smyth (in press) indicate the contact in most other places is marked

by several meters of black shale melange.

A lower Middle Ordovician (Llanvirn) age has been determined from graptolites (Tuke, 1968).

b. Northwest Arm Formation (Unit 2, Plate 2)

The Northwest Arm Formation, the lowest unit in the Hare Bay Allochthon, outcrops on the west shore and at the head of Howe Harbour, where it occurs structurally above the Goose Tickle Formation and locally below the White Hills Peridotite and Maiden Point Formation (Plates 2 and 3) (Tuke, 1968; Williams and Smyth, in press).

Along the west shore of Howe Harbour, the unit consists of finely laminated, highly contorted limy sandstone, with laminae less than one centimeter thick, which transitionally grades into a black shale melange containing knockers of ultramafic rock toward the peridotite contact. At the head of Howe Harbour, the unit consists of an interbedded sequence of sandy conglomerates and conglomerate that may grade into a black shale melange approaching the peridotite contact. Whether the conglomerate is transitional into the black shale is not known due to a lack of rock exposure. Graded bedding within this unit indicates tops to the southeast. Bedding dips at a low angle (15-20°) to the southeast.

The contact with the peridotite on the west shore and at the head of the harbour is covered by glacial till and is nowhere exposed. At the head of Howe Harbour, the Northwest Arm Formation is believed to be in thrust contact with the Maiden Point Formation (Unit 3b, Plate 2; Plate 3). An

accurate thickness for the unit cannot be established.

c. Maiden Point Formation (Units 3a and 3b, Plate 2)

The Maiden Point Formation outcrops on the northeast side of Howe Harbour and along the north side of Three Brooks Pond (Plate 2). Locally, it is structurally above the Northwest Arm Formation and below the Green Ridge Amphibolite and the White Hills Peridotite.

The formation is divided into two units, a and b. Unit 3a consists of interlayered greywacke and red shale; the layering is generally less than one meter thick. Unit 3b consists of greywacke, gabbro and rhyolite. The relationship between these lithologies is not known.

Unit 3a is structurally overlain by the Green Ridge Amphibolite along the north shore of Three Brooks Pond, but the contact between the two units is not exposed. Between Three Brooks Pond and Howe Harbour the Green Ridge Amphibolite may have been faulted out so that the Maiden Point Formation at Howe Harbour is juxtaposed against the White Hills Peridotite. Only in the Howe Harbour region is this relationship observed, elsewhere the peridotite is dominantly in contact with the Green Ridge Amphibolite.

Unit 3b outcrops along the northeast shore of Howe Harbour near the peridotite contact as isolated exposures of greywacke and highly deformed rhyolite (Unit 16 of Williams and Smyth, in press). Away from the peridotite contact, gabbro and rhyolite blocks occur along the shore. The rocks have been included in unit 3b, (unit 17 of Williams and

and Smyth, in press), but it cannot be established whether these rocks are a part of unit 3b or glacial erratics. The contact between the peridotite and unit 3b has not been observed in this area, but judging from areas where it has been seen, a thrust contact is inferred (Williams and Smyth, in press). Outcropping a few meters from the deformed rhyolite exposure is peridotite that has a banded appearance. The banding is caused by the parallel alignment of serpentine veins (centimeter or less in width). This is a common feature of peridotitic rocks close to the basal contact.

In thin section, the greywacke of unit 3a, from Howe Harbour, consists of angular to rounded (dominantly subangular) grains of quartz and feldspar in a 'chloritic' matrix (Plate 5.A.). Rarely, recrystallized quartz neoblasts occur at quartz grain boundaries. Undulatory extinction is present in detrital quartz crystals which range in size from 0.1 millimeter to 3.5 millimeters. Detrital feldspar is unaltered, though occasionally clouded and is always smaller (<0.1 mm) than detrital quartz. The matrix consists of a white mica + quartz + carbonate assemblage. Pyrite (altered) appears to be the only opaque. Muscovite is rare and occurs in the matrix as small (<0.2 mm x 0.05mm) grains and is probably authigenic. Traces of detrital biotite are observed.

At Three Brooks Pond, the greywacke, which is identical to the Howe Harbour outcrops, is interlayered with red and green shale. The shale consists of a finer-grained mixture of greywacke components. A red- to black-colored opaque,

Plate 5

A. Maiden Point Formation. Quartz and feldspar grains in a matrix of quartz, feldspar and mica. Plane polarized light. Sample 7919. Western White Hills. Length of photograph is 1.9 millimeters.

B. Green Ridge Amphibolite. Amphibole augen in mylonite texture approximately 3 meters below basal thrust fault. Plane polarized light. Sample 7844. Western White Hills. Length of photograph is 1.9 millimeters.

C. Green Ridge Amphibolite. Spongy textured amphibole; inclusions include quartz, feldspar, magnetite. Long dimension of amphibole grain parallel to S_2. Plane polarized light. Sample 7912. Eastern White Hills. Length of photograph is 0.72 millimeters.

D. Lens of massive alkaline pyroxenite within zone of interlayered syenite (white) and hornblendite (black), locality A, Figure 2.1. (from Jamieson and Talkington, 1980). Lens 50 centimeters across.

E. Hornblendite at basal thrust fault containing peridotite fragment. S_2 parallel to long dimension of peridotite fragment. Plane polarized light. Sample 77WH67. Eastern White Hills. Length of photograph is 1.9 millimeters.


A


B

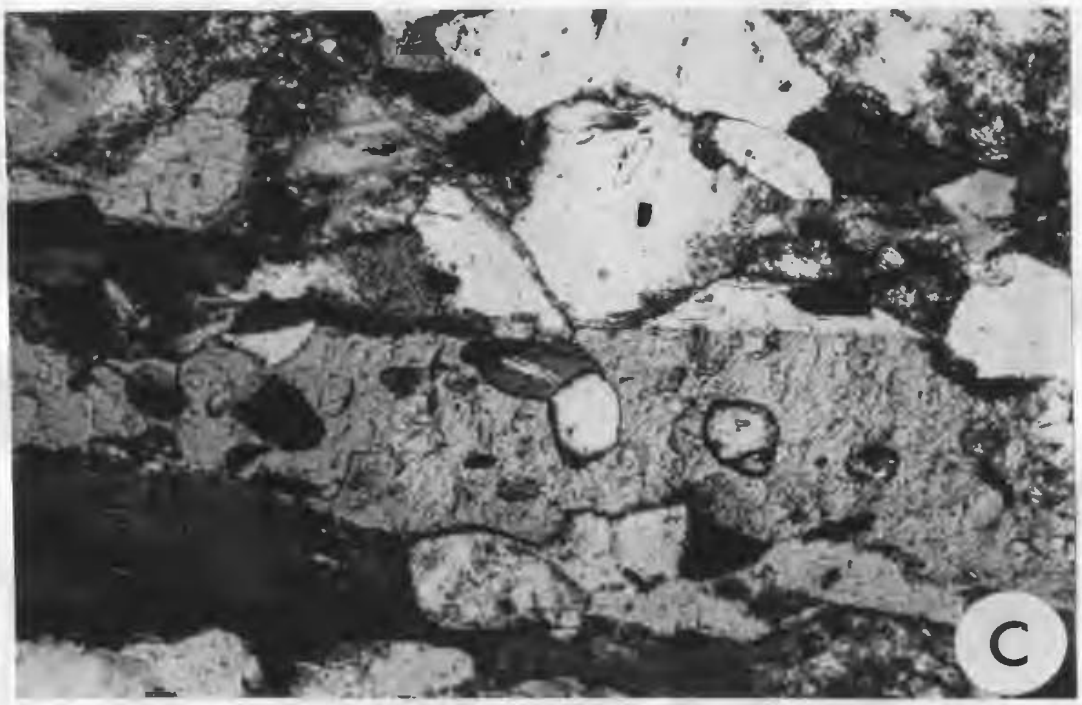
C


D

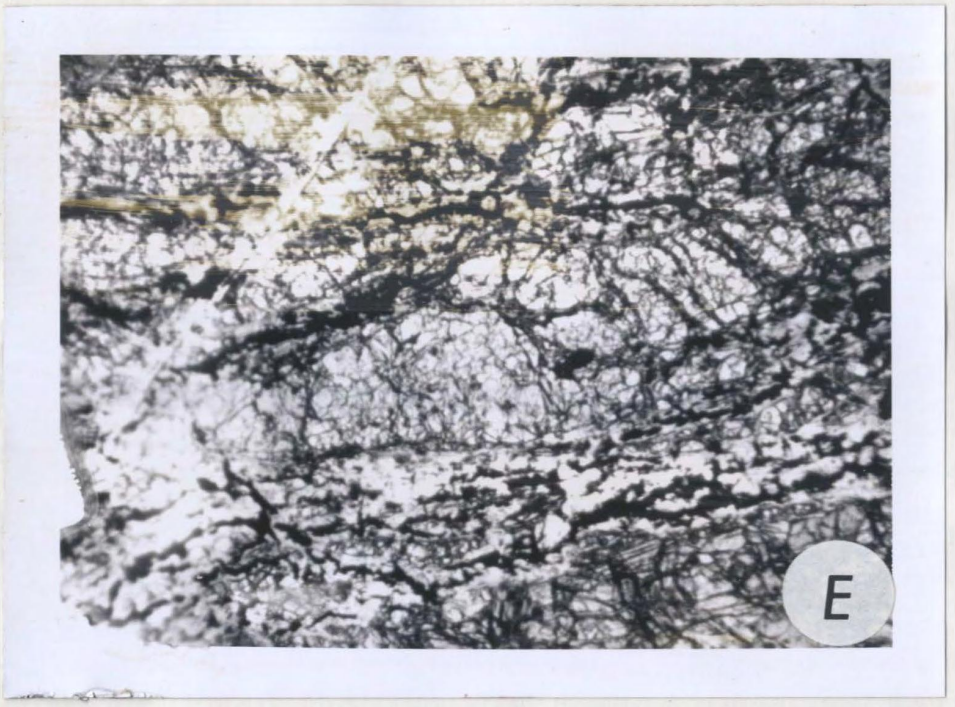
E

possibly altered chromite or magnetite, is an accessory phase. Grain size for all minerals is less than 0.1 millimeter.

Although a well-developed schistosity (S_1), defined by the alignment of the chloritic matrix material in both greywacke and shale, is parallel to bedding at the Three Brooks Pond locality, no folds have been observed in the area. Moreover, detrital quartz grains that are partially recrystallized are flattened into the schistosity plane. Thin veins of carbonate cut the schistosity at right angles.

In thin section, the gabbroic block of unit 3b consists of subhedral to euhedral, pink to purple Ti-rich augite that is commonly unaltered and exhibits undulatory extinction. Grain size is variable, but commonly less than 2 millimeters x 1 millimeter. Plagioclase grains are generally euhedral to subhedral, though laths longer than 1 millimeter tend to be idiomorphic. Approximately 50 percent of the plagioclase grains are altered to prehnite + sericite ± chlorite ± carbonate assemblage, though frequently plagioclase cores are altered only to sericite. Ilmenite is altered to a skeletal outline of leucoxene or sphene. The alkaline character of these minerals is typical of the gabbro that occurs in the Maiden Point Formation (Jamieson, 1977a).

The rhyolite member of unit 3b is highly altered with only ghosts of acicular feldspar laths (0.2 mm x 0.1 mm) (10-20%) preserved. Vesicles (?) are present and filled by carbonate and an unidentified mineral, possibly chlorite.

The genetic relationship to the gabbro is not known, but the bulk rock chemistry for both rocks indicates an alkaline lineage (Appendix IV, Table AIV. 8.).

d. Goose Cove Schist (Unit 4s, Plate 2)

The Goose Cove Schist outcrops in the study area along the southern side of the western massif, where it is exposed about 200 meters from the peridotite basal contact. In the field, the Goose Cove Schist (banded metavolcanic member of Jamieson, 1979) weathers a rusty brown color, is fine-grained and contains a well-developed amphibole schistosity (S_1).

The contact between the Goose Cove Schist and Green Ridge Amphibolite is transitional and defined by a change in metamorphic grade (Jamieson, 1979). In the present study area, this contact has not been located.

In thin section, green acicular amphibole needles exhibiting undulose extinction define the S_1 fabric. The amphibole sometimes shows incipient alteration to a chlorite + epidote assemblage. Plagioclase grains are untwinned, completely recrystallized and commonly dusted with inclusions of iron oxide. Otherwise, plagioclase is unaltered. The average grain size is less than 0.5 millimeters. Post tectonic chlorite veins cut the schist.

e. Green Ridge Amphibolite (Unit 4a, Plate 2)

The Green Ridge Amphibolite is the most extensive unit directly underlying the peridotite in the study area and is divided into two lithological units: plagioclase amphibolite

and biotite amphibolite.

(i) plagioclase amphibolite

The name plagioclase amphibolite is used in keeping with the terminology of Jamieson (1979).

At most localities, the plagioclase amphibolite weathers a dull grey and chalky white color (though black, brown and green are recognized), and contains a well-developed S_2 fabric defined by the preferred orientation of amphibole grains (Jamieson, 1979). The contact between the amphibolite and peridotite is sharp and no melange development has been observed. Locally, on the southern side of the western massif a strongly foliated amphibolite occurs at the thrust contact. In thin section, the foliation is defined by brown pleochroic amphibole augen in a mylonitic groundmass of dominantly amphibole and plagioclase (Plate 5.B.). Normally, this extreme textural development has either not developed or is not preserved in the amphibolite.

In thin section, primary, colorless to faint pink pleochroic clinopyroxene is incipiently altered to brown amphibole which in turn is overgrown by a green amphibole that, locally, is retrograded to chlorite + magnetite. Clinozoisite + sphene patches are present in some amphiboles, but in general alteration is minimal. Plagioclase is almost totally altered to a white felty-textured mica (sericite?) and a carbonate + epidote assemblage. Accessory minerals are sphene (leucoxene) and apatite. Grain size for all minerals is less than 1 millimeter, though the oxide phase is larger (up to 2 mm).

The formation of the brown and/or green amphibole from primary clinopyroxene may have occurred as a result of metamorphism during ophiolite emplacement, with post-emplacement retrogradation of the clinopyroxene and amphiboles.

(ii) biotite amphibolite*

At the northwestern boundary of the eastern massif, a biotite amphibolite occurs about 200 meters from the basal contact. The unit weathers a grey to black colour and is speckled with dark brown biotite. The amphibole and biotite define the S_2 schistosity.

In thin section, the amphibole is green and has a spongy texture with inclusions of an opaque mineral (magnetite?), sphene, quartz and apatite (Plate 5.C.). The plagioclase is fresh but may be altered in part to sericite. The grain boundaries are diffuse, scalloped and may show well-developed triple points. Polysynthetic twinning is present in the plagioclase. Quartz shows wavy extinction, is flattened in the schistosity plane and has curved to scalloped grain boundaries. Biotite is deep red-brown color and has a spongy texture with inclusions of plagioclase,

* Jamieson (1979) calls a red-brown weathered, mylonitic, biotite-rich rock, biotite amphibolite. It is part of the Green Ridge Amphibolite that outcrops on the Fishot Islands and Three Mountain Summit. Mineralogically, Jamieson's biotite amphibolite is quartz-free, whereas the one described here contains quartz. She suggests that the lithology may be a biotite-rich, metasomatized, synmetamorphic mylonite zone (ophiolite emplacement-related feature). An analogue to the biotite amphibolite described for the present study has not been observed by Jamieson (pers. comm., 1979).

opaque and quartz. Incipient alteration of the biotite to chlorite is rare. Commonly the (001) biotite cleavage is parallel to the (110) amphibole cleavage, an association which suggests that either the biotite forms an equilibrium microstructure with amphibole (T. Calon, pers. comm., 1980) or is a retrograde(?) overgrowth of amphibole.

The protoliths for the Green Ridge Amphibolite lithologies, as suggested by Jamieson (1979) on the basis of mineralogy, mineral chemistry, rock texture, and bulk rock chemistry are gabbros (tholeiitic to slightly alkaline) and possibly pelitic material for the biotite amphibolite, though metasomatized basalt is also a possibility.

f. Alkali Pyroxenite, Jacupirangite, Hornblende Gneiss, and Syenite (unit 4pj, Plates 2 and 4)

Along the eastern and northeastern margin of the eastern massif an assemblage of alkali pyroxenite, jacupirangite, hornblende gneiss and syenite occurs (Figure 2.1.) (Jamieson, 1979; Jamieson and Talkington, 1980). This assemblage has not been observed in any other location in the Hare Bay Allochthon nor elsewhere in the ophiolites of western Newfoundland.

The assemblage includes undeformed medium- to coarse-grained, dark purple to black jacupirangite and alkali pyroxenite (depending on the ratio of clinopyroxene to ilmenite + apatite) (Figure 2.2.). Below the basal contact of the peridotite, the degree of deformation increases, amphibole replaces pyroxene and feldspar-rich bands appear, forming the banded hornblende gneiss. The banding is parallel to the base of the peridotite. Below the hornblende

Figure 2.1. The locations (A-D) of alkali pyroxenite, jacupirangite, hornblende gneiss, and syenite in the St. Anthony Complex.


WESTERN NEWFOUNDLAND
ALLOCHTHONS
Hare Bay
Humber Arm
Pistolet Bay
ST. ANTHONY COMPLEX
N
WHITE HILLS
St. Anthony
HARE BAY
0 3 6
0 5 10

gneiss, occurring only at the northern-most locality (Figure 2.1., location A), is a finely banded black and white rock; these black bands consist of hornblende and the white bands are syenite (Jamieson, 1979). Enclosed in this lithology are undeformed alkali pyroxenite pockets and very coarse-grained hornblende crystals (Plate 5.D.). The base of the assemblage is marked by a white colored mylonitic syenite that contains pyroxene and amphibole smears that define the fabric (S_2?).

The alkali pyroxenite, jacupirangite, hornblende gneiss, syenite assemblage is found only at the northernmost exposure. Where this assemblage is not complete, the relative order of appearance of a specific lithology does not change (see Figure 2.2.).

The upper contact of the alkaline rocks and lower contact of the leucocratic mylonite have never been observed. However, along the southwest shore of Eastern Long Pond (Plate 2), hornblendite is in contact with the peridotite. No melange is developed at this contact or at any other location where the peridotite and alkali pyroxenite, jacupirangite, hornblende gneiss, syenite assemblage outcrop together; rather, all peridotite-alkali pyroxenite, jacupirangite, hornblende gneiss, syenite assemblage contacts are seemingly tectonic. Also, at locality D fragments and thin layers (<5 mm) of peridotite are interleaved with the hornblendite (Plate 5.E.). The peridotite fragments and layers are cut by serpentine + magnetite veins. The grain

Figure 2.2. Schematic section through the jacupirangite-syenite assemblage showing changes in lithology, fabric, and mineralogy and relative structural positions of the units. Diagram not to scale, but the relative proportions of the units (except peridotite) are approximately as shown (from Jamieson and Talkington, 1980).

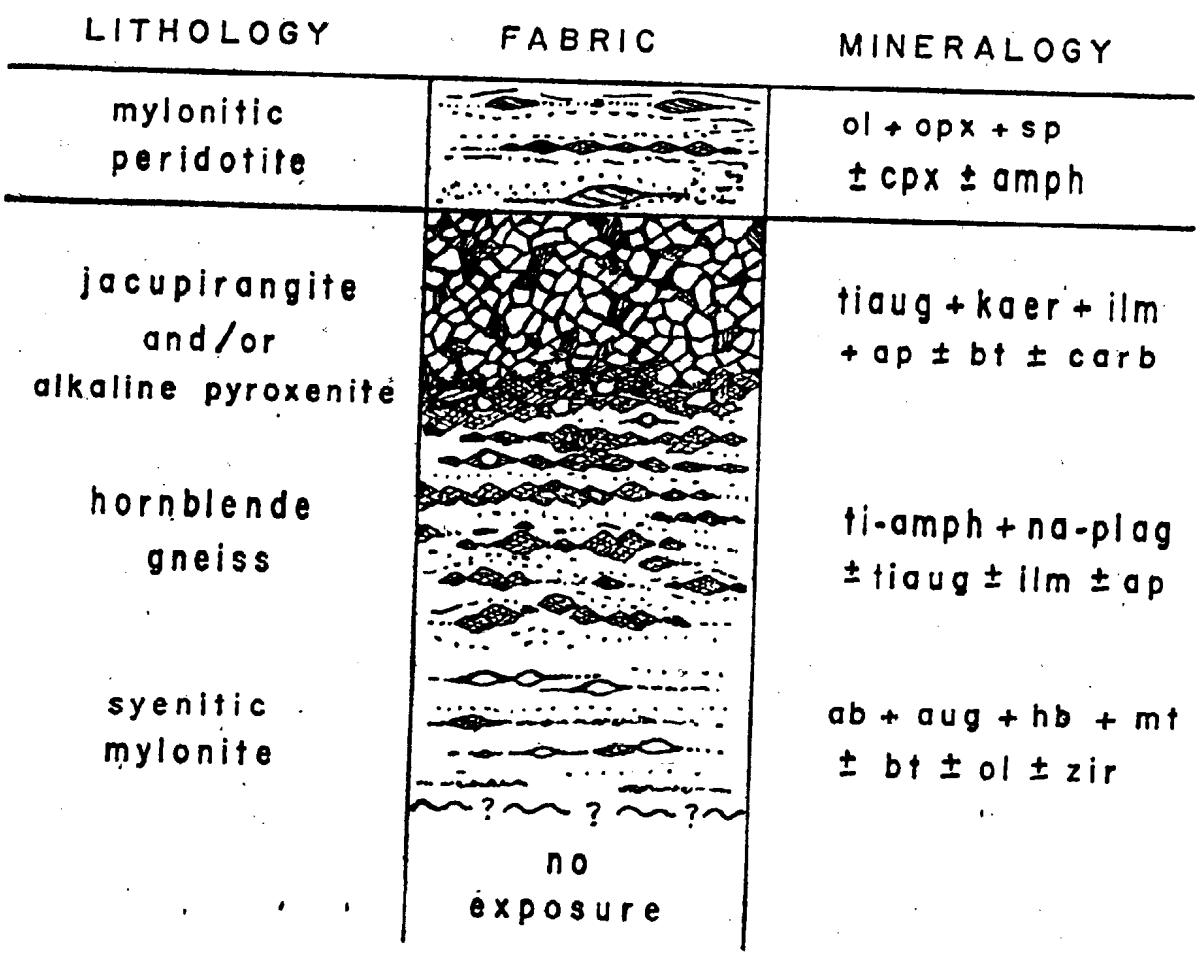
LITHOLOGY
FABRIC
MINERALOGY
mylonitic peridotite
ol + opx + sp ± cpx ± amph
jacupirangite and/or alkaline pyroxenite
tiaug + kaer + ilm + ap ± bt ± carb
hornblende gneiss
ti-amph + na-plag ± tiaug ± ilm ± ap
syenitic mylonite
ab + aug + hb + mt ± bt ± ol ± zir
? ? ?
no exposure

size of all minerals in the peridotite fragments and layers is less than 0.2 millimeters, and any peridotite fragment or layer may contain isolated grains of red-brown colored amphibole (pargasite?). This relationship disappears farther from the basal contact.

I.2.B. The White Hills Peridotite

1. General Statement

Since 1974, detailed studies, mainly petrological, of the peridotite and metamorphic aureole have been carried out (Riccio, 1976; Jamieson, 1979; Talkington, 1979; Talkington and Jamieson, 1979; Jamieson and Talkington, 1980; Talkington and Malpas, 1980a, d). This work has shown that the St. Anthony Complex and specifically the White Hills Peridotite has features which distinguish it from the general (reconstructed) appearance of most ophiolites of the world and more specifically from the Bay of Islands Complex: these are 1. only the ultramafic section of the ophiolite is preserved; 2. harzburgite interlayered with spinel lherzolite forms about 85 percent of the peridotite outcrop; 3. dunite occurs as layers, lenses and dikes throughout the peridotite; 4. gabbro veins are found only in the eastern massif and cut all rock types; 5. alkali pyroxenites are found between the peridotite and a well-developed metamorphic aureole.

In this section of the study the petrography and field relationships are described for the various lithologies of the peridotite. An attempt has been made to determine whether

a stratigraphy can be defined for the White Hills and how it compares with the idealized ophiolite stratigraphy (Figure 2.3.), which is similar to the stratigraphy for the Bay of Islands Complex (Malpas, 1976).

2. Rock Classification and Texture

a. Classification

The rock classification scheme of Streckeisen (1976) has been adopted for this study. Modal analyses have been made on rocks where the deformation of primary silicates and secondary alteration are minimal. Where secondary alteration of primary silicates is observed, the most logical anhydrous precursor mineral (e.g., serpentine + magnetite to olivine; bastite to orthopyroxene) has been counted. Accessory minerals, commonly spinel, have not been used in the recalculation because no provisions are made for them on the modal diagrams. Exsolution lamellae in pyroxene have been counted as part of the host phase unless noted to the contrary.[1] Dunites have not been plotted on the ol-opx-cpx[2] diagram because they are essentially monomineralic, containing only accessory spinel. The rock modes are shown in Figures 2.4. and 2.5.

1. in rare cases, clinopyroxene exsolution from orthopyroxene forms coarse lamellae or blebs and these have been counted as clinopyroxene. This total never amounts to more than 0.2 percent of the total rock mode.

2. ol - olivine; opx - orthopyroxene; cpx - clinopyroxene

Figure 2.3. Idealized ophiolite stratigraphy (from Malpas, 1976).

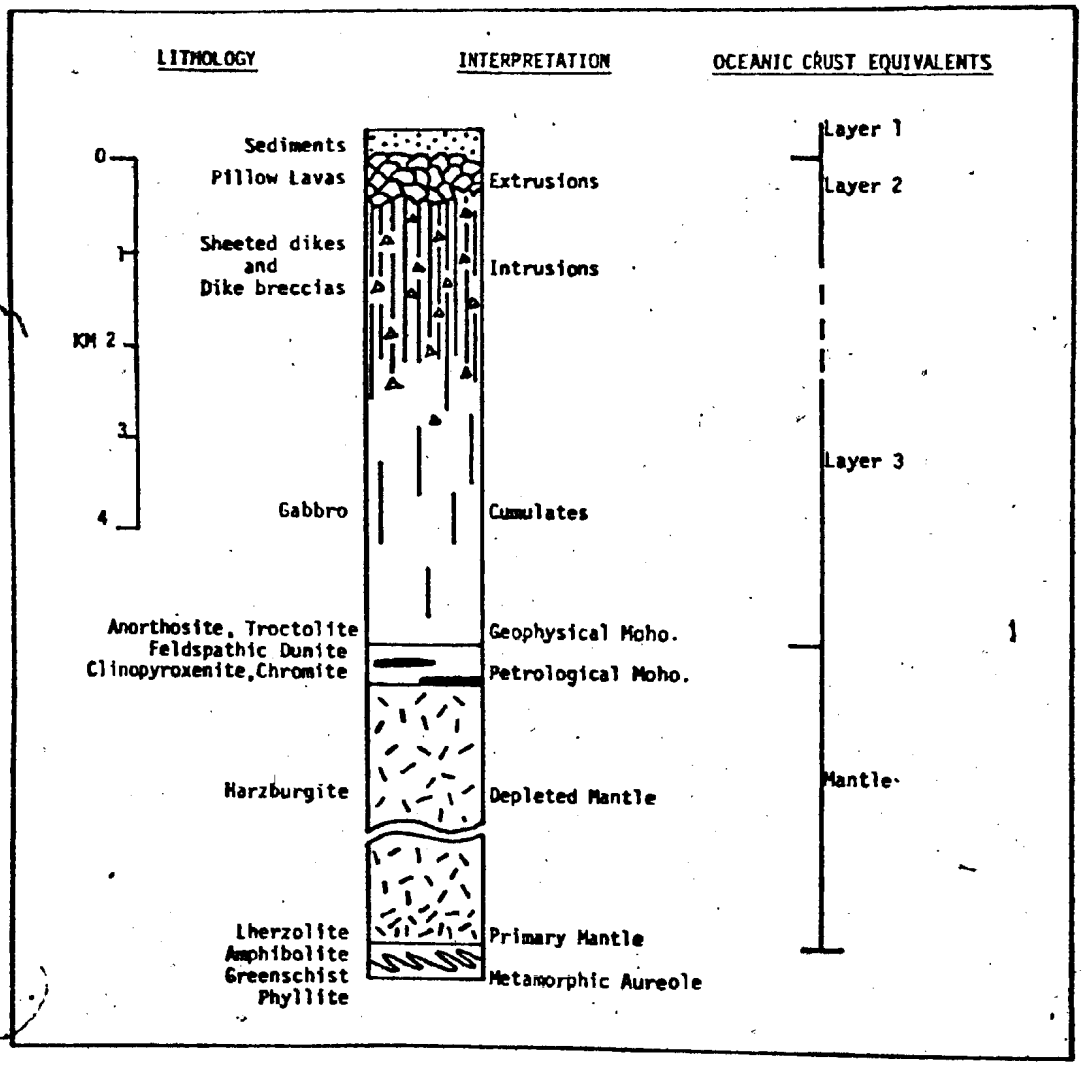
LITHOLOGY
INTERPRETATION
OCEANIC CRUST EQUIVALENTS
0
1
KM 2
3
4
Sediments
Pillow Lavas
Sheeted dikes and Dike breccias
Gabbro
Anorthosite, Troctolite Feldspathic Dunite Clinopyroxenite, Chromite
Harzburgite
Lherzolite Amphibolite Greenschist Phyllite
Extrusions
Intrusions
Cumulates
Geophysical Moho.
Petrological Moho.
Depleted Mantle
Primary Mantle
Metamorphic Aureole
Layer 1
Layer 2
Layer 3
Mantle

Figure 2.4. Modal plot of the ultramafic rocks. Solid circle-pyroxenite of the pod, all other pyroxenites are from veins.

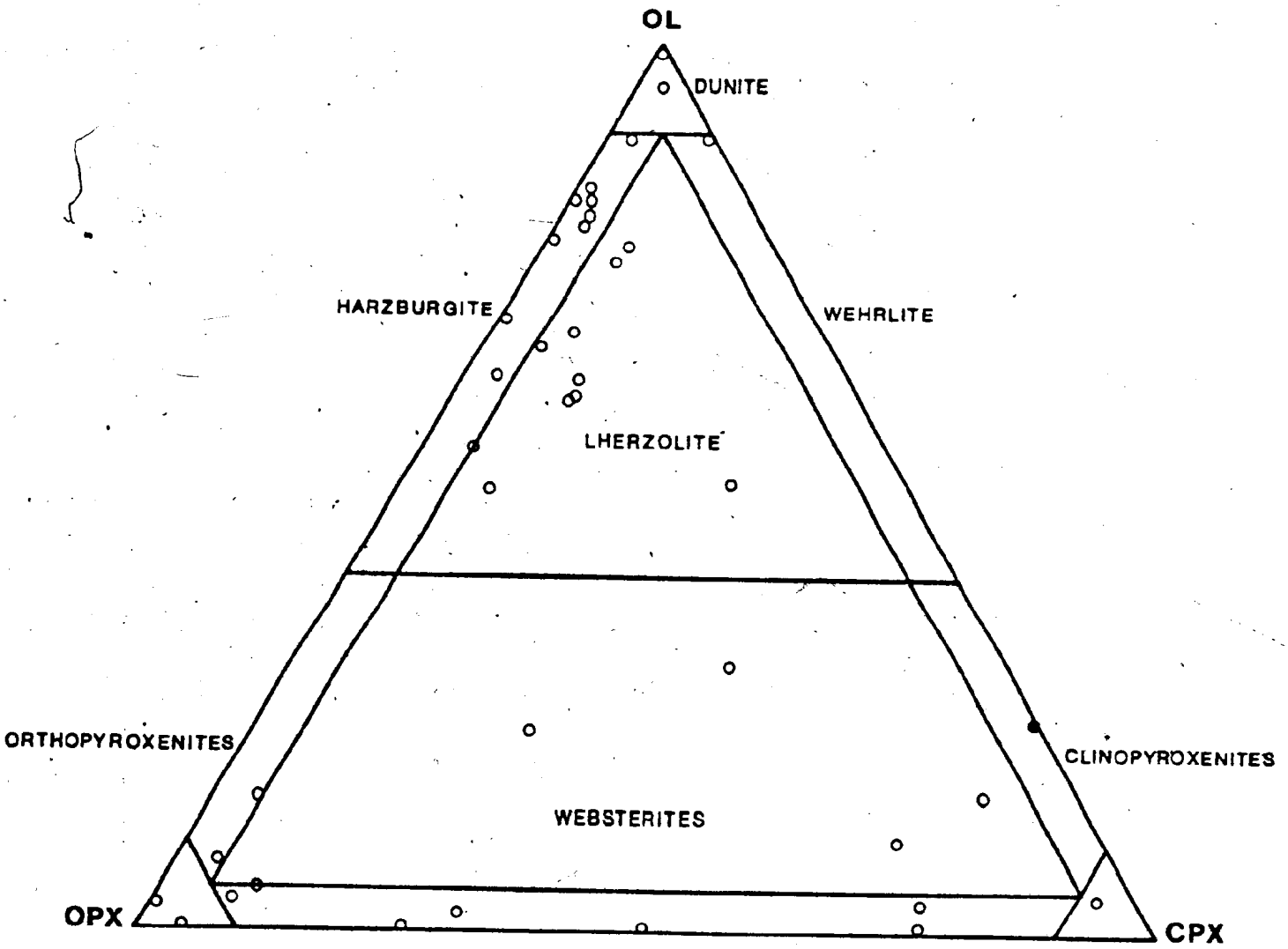
OL
DUNITE
HARZBURGITE
WEHRLITE
LHERZOLITE
ORTHOPYROXENITES
CLINOPYROXENITES
WEBSTERITES
OPX
CPX

Figure 2.5. Modal plot of the mafic rocks.

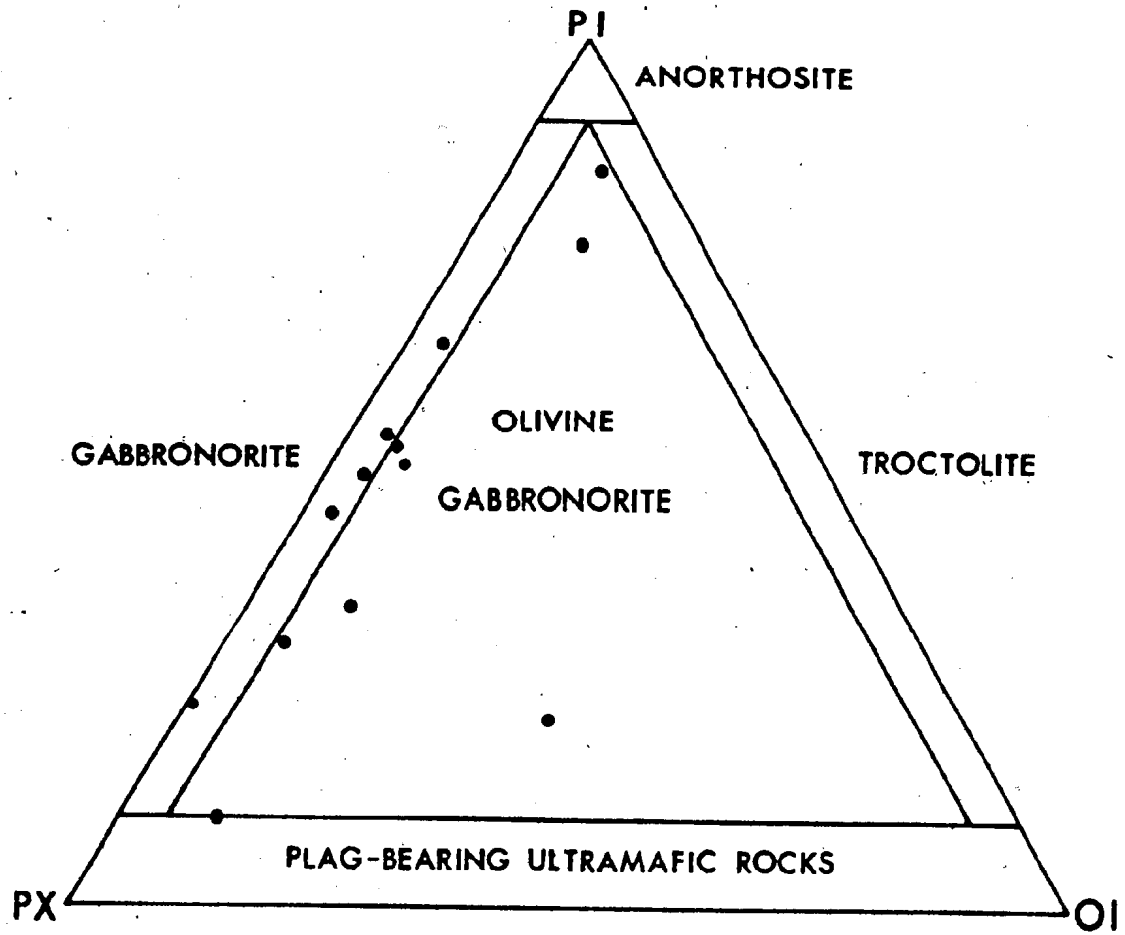
PI
ANORTHOSITE
GABBRONORITE
OLIVINE
GABBRONORITE
TROCTOLITE
PLAG-BEARING ULTRAMAFIC ROCKS
PX
OI

b. Textures

The textural terminology is presented in Table 2.1. It reflects a compilation of terminology from several authors (Wager et al., 1960; Jackson, 1961; Spry, 1969; Mercier and Nicolas, 1975; Basu, 1977; Pike and Schwarzman, 1977; Harte, 1977) and accomodates the wide range of textural variation, including aspects related to crystallization from melts, as well as to solid state physical/chemical processes observed in peridotitic rocks. Throughout this thesis the name listed under the heading 'TEXTURE' of Table 2.1. is used. For convenience the various nomenclatures as used by the aforementioned authors are mentioned in the table. Illustrations of the various textures are presented in Plate 6.

3. Distribution of Rock Textures in the White Hills Peridotite

The distribution of the various textures is shown in Figure 2.6. By far the most common texture is porphyroclastic. It appears evenly distributed throughout the massifs and does not seem to be restricted or controlled by local small-scale structures.

The coarse-granular texture is common in the western massif. The reason for this is not understood, but may be the result of sample collection, or if there is the local preservation of a 'primary' upper mantle texture (cf., Mercier and Nicolas, 1975) for the peridotite and a, as yet unrecognized, spatial distribution of this texture for the peridotite, then differences in the level of erosion of the massifs may account for this distribution.

Table 2.1. Compilation of rock texture classification

Texture*	Porphyroclasts	Grain Size	Mineral Deformation	Grain Boundaries	Nomenclature in the Literature	
Coarse-granular	absent	average grain size greater than 2 mm	rare; restricted to undulose extinction, olivine subgrain structure, development of kink bands in orthopyroxene and minor silicate recrystallization may be present	variable; commonly straight to curvilinear. grains may be interlocking	Protogranular Coarse-granular Coarse 'Allotriomorphic'	Mercier and Nicolas (1975) Basu (1977) Harte (1977) Pike and Schwarzman (1977)
Porphyroclastic	present(olivine orthopyroxene, clinopyroxene, spinel)	variable; in the range of .01 mm to 4mm	present; undulose extinction, olivine subgrain structure, kink bands developed in opx and cpx. Kink bands may be recrystallized, opx aspect ratio of 7:1(average) are present in some basal thrust zones. Neoblasts may show undulose extinction	two varieties: porphyroclasts irregular to curvilinear; neoblasts straight to curvilinear, triple point development	Porphyroclastic Porphyroclastic Porphyroclastic Porphyroclastic	Mercier and Nicolas (1975) Basu (1977) Harte (1977) Pike and Schwarzman (1977)
Granoblastic	absent or rare.	variable; but average about 0.2 mm	present; undulose extinction, olivine subgrain. Well-developed triple point junctions	variable; irregular to straight	Equigranular Mosaic Granuloblastic Mosaic Granoblastic	Mercier and Nicolas (1975) Basu (1977) Harte (1977) Pike and Schwarzman (1977) Spry (1969)
Mylonitic	absent or rare.	variable; but less than 0.05 mm	present; undulose extinction	variable; irregular to curvilinear	Mylonitic	Basu (1977)
Allotriomorphic-granular	absent or rare	average grain size 6 mm (max. 1.4 cm)	present; restricted to undulose extinction and subgrain structure, olivine grains appear elongate parallel to foliation plane	smooth to curvilinear	Similar to: Protogranular Coarse granular Allotriomorphic-granular	Mercier and Nicolas (1975) Basu (1977) Pike and Schwarzman (1977)
Cumulate	absent	average grain size greater than 2 mm	undulose extinction and minor kink banding	regular to interlocking	Cumulate (adcumulus) Cumulate	Wager et al. (1960) Jackson (1961)

* Preferred usage in thesis

POOR COPY
COPIE DE QUALITEE INFERIEURE

Plate 6

A. Coarse-granular texture. See Table 2.1. for details. Crossed polars. Sample 7822, spinel lherzolite. Western White Hills. Length of photograph is 8.5 millimeters.

B. Porphyroclastic texture. See Table 2.1. for details. Note zoning in partially extinct orthopyroxene porphyroclast. Crossed polars. Sample 78151, spinel lherzolite. Eastern White Hills. Length of photograph is 8.5 millimeters.

C. Granoblastic texture. See Table 2.1. for details. Note well-developed triple point junctions and oxide (magnetite?) inclusions in olivine. Plane polarized light. Sample 77WH55, dunite. Eastern White Hills. Length of photograph is 0.61 millimeters.

D. Mylonitic texture. See Table 2.1. for details. Crossed polars. Sample 78161, spinel lherzolite. Eastern White Hills. Length of photograph is 1.9 millimeters.

E. Allotriomorphic-granular texture. See Table 2.1. for details. Anhedral olivine grain is outlined by black line. Crossed polars. Sample 797, dunite. Eastern White Hills. Length of photograph is 1.9 millimeters.

F. Cumulate texture. See Table 2.1. for details. O-intercumulus olivine. Crossed polars. Sample 7898, orthopyroxenite vein containing disseminated spinel. Western White Hills. Length of photograph is 1.9 millimeters.

G. Resorbed euhedral spinels in euhedral orthopyroxene (bastite) phenocryst. Note hole in center of spinel grain to the lower right of the large spinel grain; the hole possibly formed due to resorption of the spinel grain or the hole may have been the site of a fluid/solid inclusion (see text). Plane polarized light. Sample 78122, Chromitite pod. Eastern White Hills. Length of photograph is 3.5 millimeters.


A


B

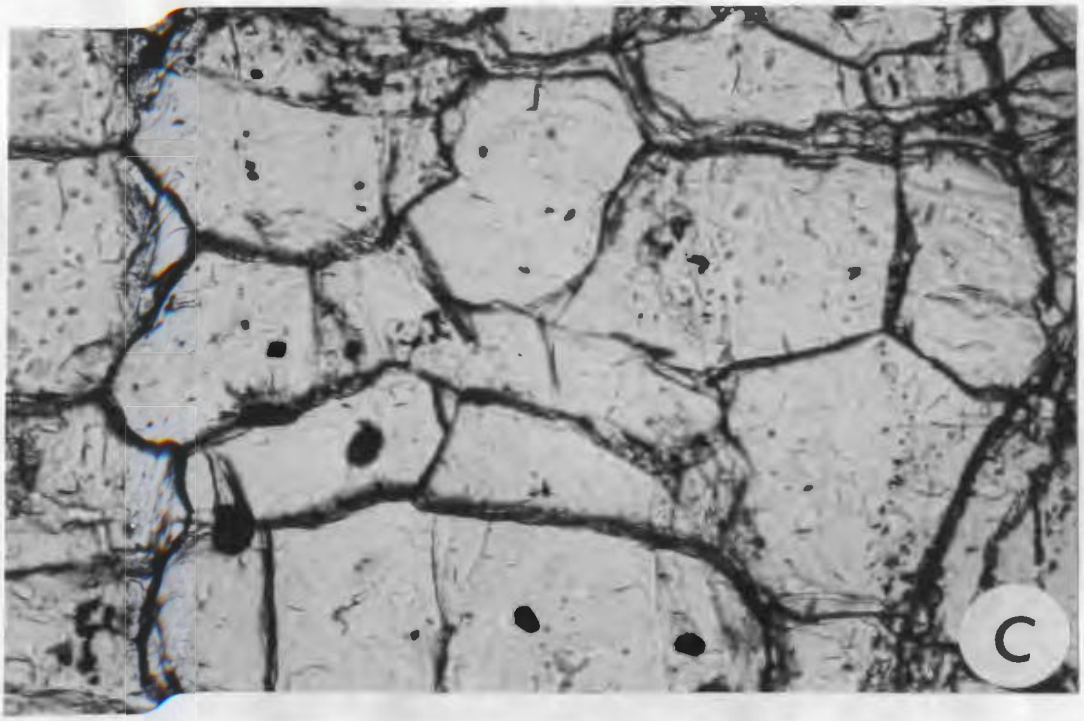
C


D


E

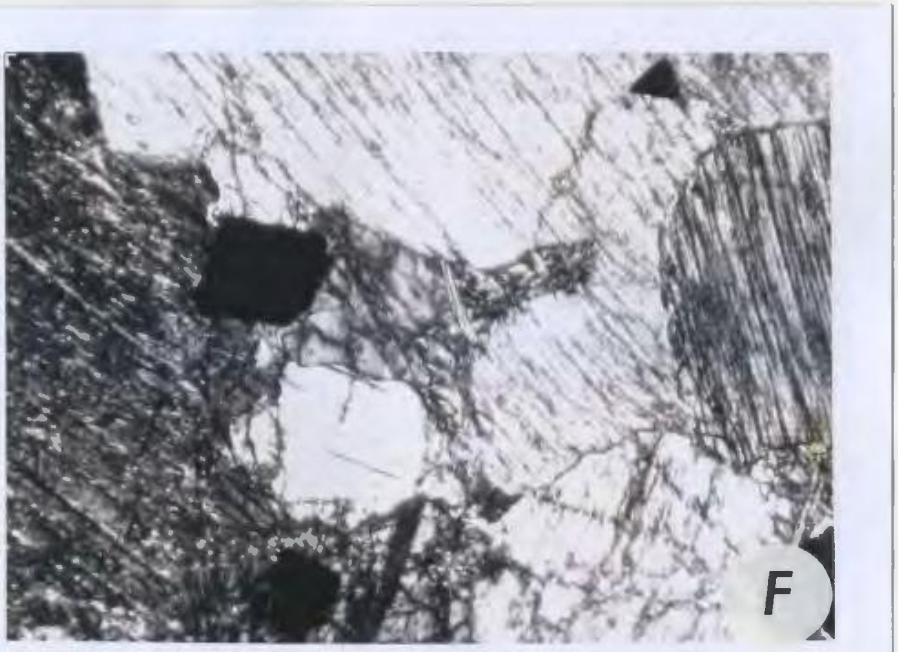
F


G

Figure 2.6. Distribution and locations of the various rock textures.

- ○ coarse-granular
- ● porphyroclastic
- ★ granoblastic
- △ mylonitic
- □ allotriomorphic-granular
- ■ cumulate

Hybrid textures:

- ⊙ coarse-granular and porphyroclastic
- ☆ porphyroclastic and granoblastic
- ▲ porphyroclastic with localized mylonitic zones

See Table 2.1. and section I.2.B.3. for full description of rock textures.

E – eastern massif
W – western massif
M – Mount Mer, Howe Harbour area

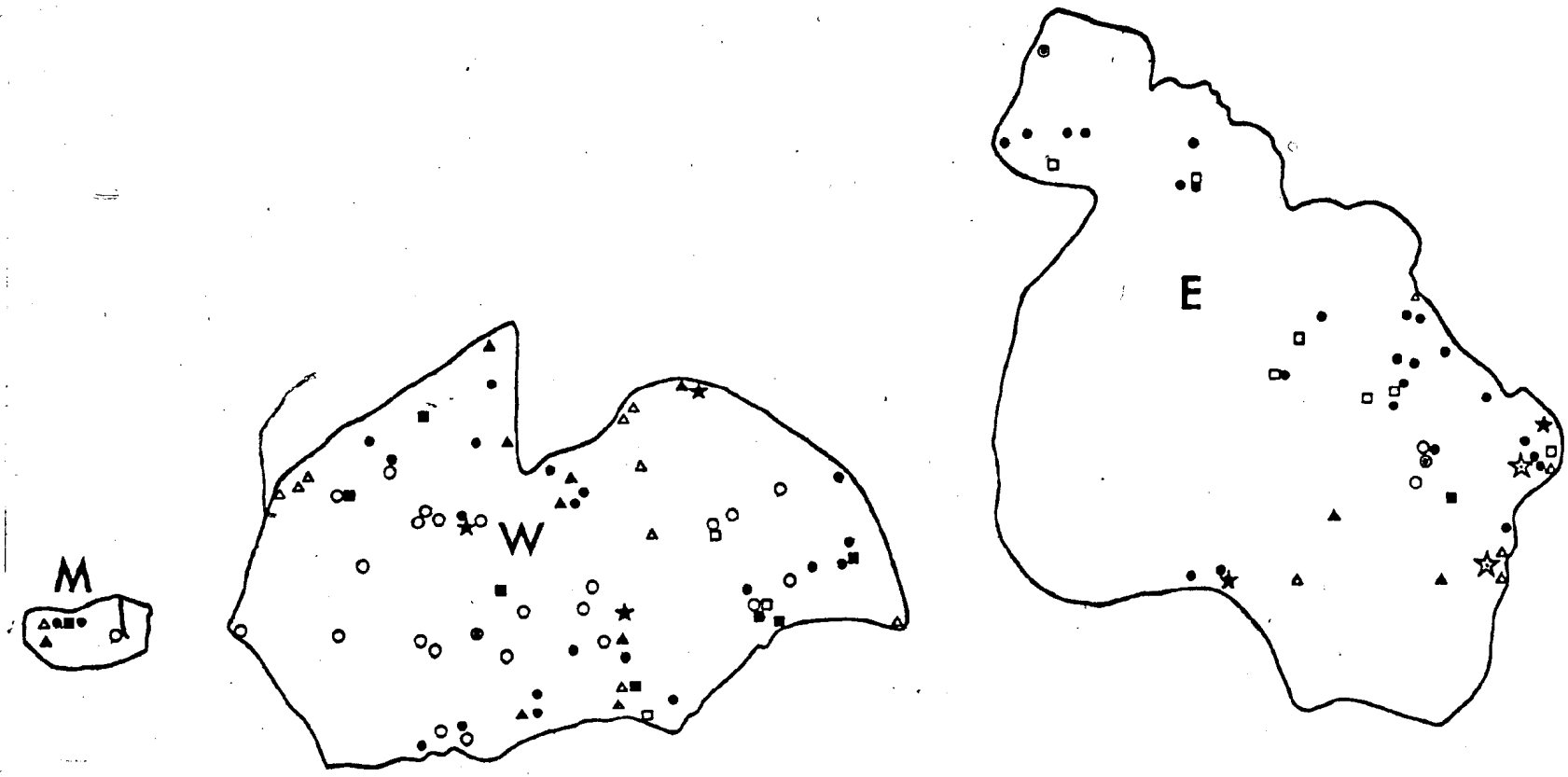
M
W
E

The mylonitic texture is dominant close to the basal thrust fault (< 25 m from the contact) and is exposed along internal thrust faults. This texture is believed to have formed during displacement of the ophiolite from its oceanic setting and/or its emplacement on the continental margin. Granoblastic texture occurs nearly exclusively in the dunite close to the basal thrust. The development of this type of texture is suggested to be the result of intense or complete recrystallization in a static or dynamic environment (Mercier and Nicolas, 1975; Calon, in preparation) under moderate to high strain rates (Ave'Lallemant and Carter, 1970; Calon, in preparation). Mercier and Nicolas (1975), Basu (1977), and Calon (in preparation) have suggested this type of texture may be the end member of a deformation cycle where the coarse-granular (protogranular of Mercier and Nicolas, 1975) texture is the least deformed member, the porphyroclastic the intermediate member and the granoblastic texture the most deformed member.

Two textures that suggest direct crystallization from a melt are the allotriomorphic-granular (found in dunite) and cumulate (found in orthopyroxenite, "websterite" and chromitite). In the allotriomorphic-granular texture, olivine grain size is large (average 6 mm, maximum 1.4 cm) and grain boundary and intracrystalline recrystallization are negligible. Olivine grain boundaries are smooth and rounded and some grains appear to be elongate parallel to the foliation plane, but the degree of plastic deformation and subgrain development in

response to recovery processes suffered by olivine is minimal (T. Calon, pers. comm., 1979). Spinel occurs at olivine grain boundaries, occluded in olivine, and occassionally may define a lineation. Spinel grains are euhedral to anhedral and commonly show a pull-apart texture (Thayer, 1964). Severely corroded spinel exhibits holly-leaf like forms, possibly due to resorption.

Spinel-silicate relationships, shape, lack of consistently pervasive deformational characteristics with respect to olivine and a strong resemblance to cumulus spinel-forms of stratiform intrusions (Jackson, 1961, see Fig. 59, p. 55) suggests this texture is probably of cumulus origin and has suffered only minor deformation. The possibility that this texture may represent the end product of complete annealing of a deformed dunite (secondary texture) cannot be disregarded; especially because, for the majority of cases, this texture is associated with the porphyroclastic type for which Mercier and Nicolas (1975) have shown that the characteristic spinel form is holly-leaf. Therefore, whether this texture represents an igneous or metamorphic event(s) cannot be determined solely by textural relationships (Vernon, 1970, see Plate 1) and as Hobbs et al (1976) state "Certainly the observation that the grains in a deformed rock show no obvious signs of deformation is not sufficient to show that the rock has recrystallized after the deformation ceased.". Even so, Vernon (1970) contends generally that adcumulates can be distinguished from granulites as they contain a higher proportion of elongate

grains (e.g., plagioclase) that tend toward a parallel alignment (igneous foliation), some rational grain boundaries, and minor intercumulus material. This argument is discussed further using petrological evidence in later sections (Chapter 4; Chapter 5, sections II.5.B. and II.5.C.), but definite statements of origin await a detailed study of these textures.

Orthopyroxenite veins and orthopyroxenite, "websterite", and chromitite of the chromite pod have cumulate textures directly comparable to those of stratiform intrusions. Cumulus orthopyroxene is euhedral to subhedral with a grain size of about 3.5 millimeters. Undulatory extinction and minor kink band development are observed. Cumulus clinopyroxene is subhedral to anhedral with a grain size of about 1 millimeter. Undulatory extinction is observed and grain boundaries are regular and interlocking, suggesting adcumulus growth (see Jackson, 1961, Fig. 62, p. 56). Olivine and clinopyroxene are anhedral, intercumulus phases in the orthopyroxenites. Spinel in these rock types is euhedral to anhedral and interstitial to occluded in orthopyroxene and clinopyroxene. The spinel in chromitite may show chain structure (Jackson, 1961) and pull-apart texture. Where associated with orthopyroxene phenocrysts (now altered to amphibole; Appendix IV, Table AIV.6.) the spinel shows resorption features (Plates 6.G.) possibly due to reaction with the orthopyroxene (cf., LeBlanc, 1980). Rarely spinel is elongate parallel or subparallel to (100) of the orthopyroxene.

When two microstructures occur in a rock sample, the names of the two rock textures are used to describe the overall texture of the sample. This composite textural description is termed the hybrid texture; no genetic connotation is implied. The textural combinations (hybrid textures) encountered are coarse-granular and porphyroclastic, porphyroclastic and granoblastic, and porphyroclastic with localized mylonite zones. The first combination occurs throughout the massifs, but generally not near the basal thrust zone. Here, the porphyroclastic-granoblastic and porphyroclastic-mylonite types are common (see Figure 2.6.). These are the predicted associations and distributions since the pairs are interrelated as initial and final stages (e.g., coarse-granular-initial, granoblastic-final) of a deformation/dynamic recrystallization event that occurs at high temperatures (Mercier and Nicolas, 1975; Calon, in preparation).

4. Lithologies and Petrography

a. Spinel Lherzolite and Harzburgite

(i) field descriptions

Throughout the peridotite, spinel lherzolite and harzburgite occur in layers. In outcrop, these layers range in thickness from less than 1 millimeter to ½ meter and may remain uniform or vary irregularly in thickness along strike. The lateral extent of these layers is highly variable, however thick layers have been traced for hundreds of meters, though because of outcrop size, passage into regions

of non-layered (massive) peridotite, and faulting or folding, many are lost after short distances. Thinner layers persist for only a few meters before they pinch out, end abruptly or pass transitionally into another lithology.

The contacts between adjacent layers are sharp, though sometimes as the dunite component increases, the persistence of the layering decreases and the contacts between layers become irregular and diffuse. Where this latter feature is present and dunite abundant, either individual crystals of orthopyroxene or peridotite rafts occur within the dunite matrix (discussed in next section). Within layers the grain size of a particular mineral phase may be uniform or size-graded (Dick and Sinton, 1979). Often the amount of each rock type is difficult to determine due to complex interlayering with dunite, transitional contacts between lithologies, difficulty in discerning clinopyroxene in spinel lherzolite and folding and faulting.

The layering is not evenly distributed throughout the peridotite, and although well-developed in some regions, in other regions a nearly massive peridotite containing a few pyroxenite segregations (i.e., veins) is found.

Various lithological sequences are found in the peridotite. The most commonly recognized types are (no order of abundance has been established): (a) spinel lherzolite – dunite – spinel lherzolite – harzburgite (Plate 7.F.); (b) spinel lherzolite – dunite – spinel lherzolite; (c) harzburgite – dunite – harzburgite; (d) dunite – harzburgite (Plate 7.D.); (e) dunite –

Plate 7

A. Layered peridotite sequence. See text section I.2.B.4.a. for details. Location of samples 794, dunite (d) and 795, spinel lherzolite (s). harzburgite - h. Eastern White Hills.

B. Layered peridotite sequence. See text section I.2.B.4.a. for details. Location of samples 7873, harzburgite and 7874, dunite. Western White Hills.

C. Clinopyroxene (c) and olivine (o) grains in orthopyroxene porphyroclast. Crossed polars. Sample 7834, harzburgite. Western White Hills. Length of photograph is 3.5 millimeters.

D. Clinopyroxene exsolution from orthopyroxene porphyroclast. See Figure 3.3. and Table 3.1 for details. Crossed polars. Sample 77WH94, spinel lherzolite. Eastern White Hills. Length of photograph is 1.7 millimeters.

E. Mesh texture in olivine. Crossed polars. Sample 7894, spinel lherzolite. Western White Hills. Length of photograph is 3.5 millimeters.

F. Clinopyroxene megacryst in spinel lherzolite. Eastern White Hills.

G. Chromite seam in dunite layer. Chromite elongate parallel to S_1(?). Eastern White Hills.

H. Dunite lens in harzburgite. Size approximately 50 meters wide x 400 meters long. See Figure 2.7. for lens configuration. Eastern White Hills.

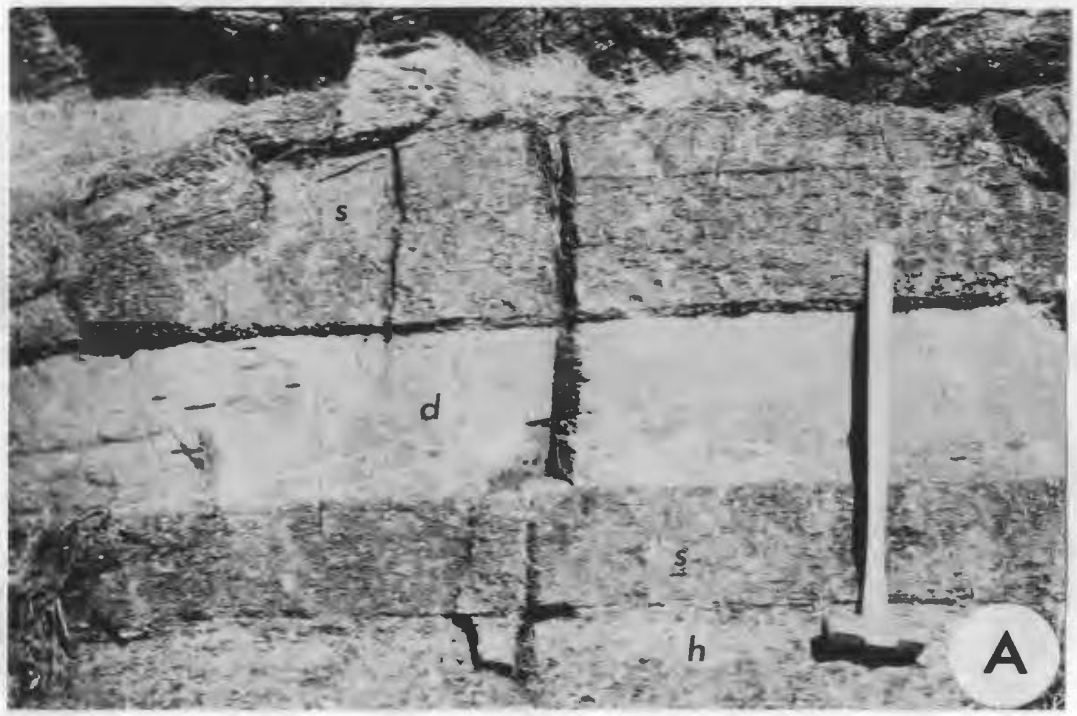
s
d
s
h
A


B


C
O
C

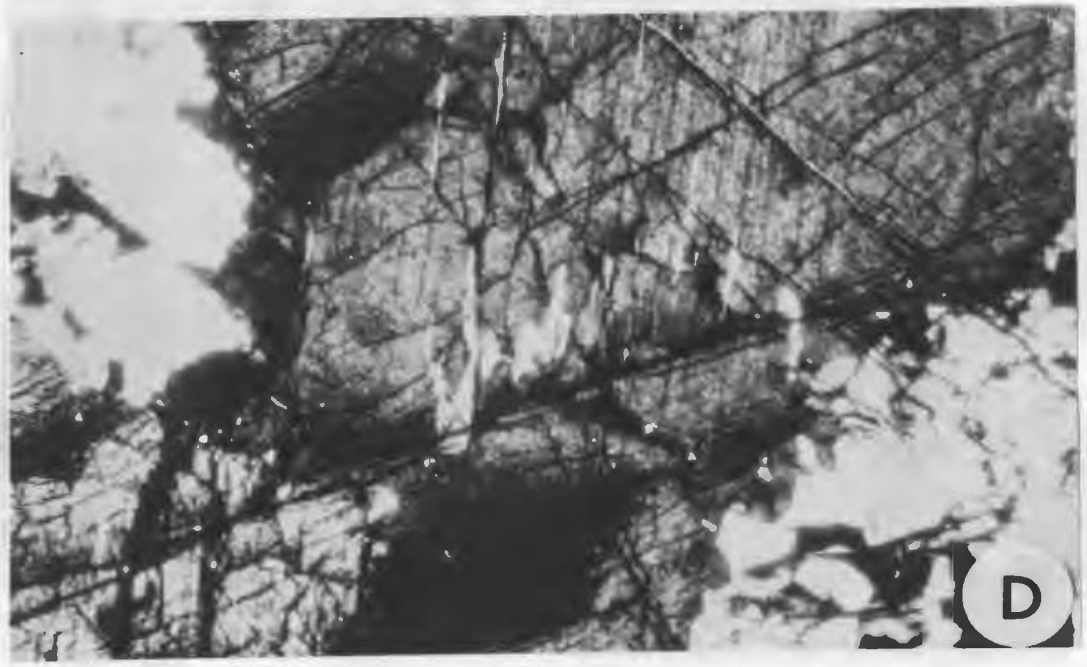
D


G


H

spinel lherzolite; (f) harzburgite - (harzburgite + dunite) - (dunite + orthopyroxene-rich dunite - dunite).

In addition to lithological layering an orthopyroxene foliation (S_1)* is present and appears to always parallel the lithological layering. S_1 is well-developed in most instances but as previously stated the peridotite may also have a massive appearance.

(ii) petrography

Spinel lherzolite is composed of (average amounts) olivine (63.1%), orthopyroxene (27.5%), clinopyroxene (8.3%), and spinel (1.1%) (Figure 2.4.). Olivine (77.3%) and orthopyroxene (20.0%) are the principal minerals of harzburgite, and clinopyroxene (1.5%) and spinel (1.2%) are subordinate (Figure 2.4.).

Olivine is commonly anhedral to subhedral and shows a wide range in grain size as a function of the degree of deformation (largest $\sim$ 3 mm in the coarse-granular texture). Undulatory extinction is ubiquitous with the development of subgrain structures and neoblasts restricted to the more deformed samples. Where developed, subgrain boundaries, particularly (100)(T. Calon, written comm., 1980), occur

* In light of the work of Dick and Sinton (1979) regarding the formation of compositional layers in Alpine-type peridotites by pressure solution during anatexis and ascent of the peridotite diapir through the upper mantle, the lithological (=compositional) layering may not represent a primary upper mantle feature (i.e., S_0); therefore S_1, though still of upper mantle origin, is the preferred useage in this text. S_1 of the peridotite is not equivalent to S_1 of the underlying metamorphic rocks, rather S_2 of the peridotite and S_1 and S_2 of the metamorphic rocks probably formed during the same deformational event (i.e., emplacement).

in primary olivine and are oriented either perpendicular or subparallel (up to 24°) to the foliation plane. Neoblasts may show undulatory extinction, while their grain boundaries are in various stages of adjustment. In both spinel lherzolite and harzburgite, subhedral to anhedral olivine grains are enclosed by orthopyroxene (Plate 7.A). Translucent, brown spinel droplets have been observed in olivine grains in one case (sample 7879).

Orthopyroxene is commonly colorless, but in some samples has a faint tan color. Undulatory extinction is again ubiquitous. Grain shape is frequently equant except in zones of intense deformation. Locally within these zones long lamellar orthopyroxenes, deformed by slip on the (100) plane (Darot and Boudier, 1975), have aspect ratios up to 17:1 (7 mm x 0.4 mm), but the average aspect ratio is 7:1. Retorted orthopyroxene (cornue of Etchecopar, 1977), porphyroclasts, identical to the ones described by Basu (1977), occur in several samples. In some of these, primary, secondary and tertiary kink bands are formed in the 'locked' (Etchecopar, 1977) portion of the deformed orthopyroxene porphyroclasts giving rise to a "tuning fork-like" geometry (see Basu, 1977, p. 222, Fig. 6). Kink bands showing no recrystallization and those containing neoblasts of orthopyroxene and small rounded blebs of spinel have also been found. Abundant clinopyroxene exsolution, parallel to the (100) plane of the orthopyroxene porphyroclasts, occurs as thin and often coalesced lamellae (Plate 7.B.). In the more deformed samples, the clinopyroxene lamellae do not extend

to the orthopyroxene grain margins. Clinopyroxene exsolution lamellae are found only in equant orthopyroxene grains. Neoblasts have undulatory extinction and are in various stages of grain boundary adjustment. Sometimes spinel has been exsolved parallel to the (100) plane of orthopyroxene, though commonly spinel occurs as rounded blebs or as a vermicular intergrowth with olivine and/or clinopyroxene at the orthopyroxene grain margins.

Clinopyroxene is colorless and may occur as isolated clusters or evenly distributed throughout the rock. Grain size in either mode of occurrence is not very different and not larger than 5 millimeters x 2 millimeters. Although undulatory extinction is ubiquitous, highly deformed grains are uncommon. In extreme cases, e.g., in the basal thrust zone, clinopyroxene is kinked. Some kink bands are completely recrystallized to aggregates of clinopyroxene that show undulatory extinction. No long lamellar clinopyroxene grains have been observed. Small, slightly rounded grains of clinopyroxene occur in orthopyroxene porphyroclasts (Plate 7.A.).

Spinel associations are discussed in Chapter 4.

(iii) silicate mineral alteration

Olivine is commonly altered to serpentine + magnetite and rarely to chlorite. Where olivine is highly serpentinized, a mesh texture is developed (Plate 7.C.), and in extreme cases of serpentinization, serpentine + magnetite completely replace olivine and only isolated olivine kernals remain. This texture is found in localized areas of

the basal thrust zone and along other faults in the peridotite.

Bastite alteration of orthopyroxene occurs along fractures and grain margins. Again, in the basal thrust zone and along faults, complete bastite pseudomorphs are found.

Most clinopyroxene is altered to uralite and an unidentified, highly birefringent clinoamphibole.

(iv) clinopyroxene megacrysts

Occurring exclusively in spinel lherzolite are clinopyroxene megacrysts (Plate 7.G.). These have been found in the northwest region of the eastern massif. Some megacrysts are intact, up to 6.5 centimeters in size, while others occur in aggregates of variously sized and oriented clinopyroxenes that could have been derived from large single crystals. No reaction features (e.g., halo) are apparent in hand specimen. One megacryst preserves an asymmetric bending of cleavage planes. Similar crystals have been observed in the cumulate sections of various ophiolites (i.e., Bay of Islands and Quebec; pers. observations) and tentatively have been suggested to be a result of high temperature- high strain-deformation (J. Malpas, pers. comm., 1980).

b. Dunite

(i) field description and petrography

Dunite is found throughout the peridotite and occurs in several forms: layers, lenses and dikes. Relatively large concentrations of all forms are found in the eastern

massif, whereas dunite layers are the predominant form for other parts of the peridotite.

Dunite layers range in thickness from less than 1 millimeter to tens of meters (Plate 7.D.), though commonly averaging 1 to 10 centimeters. Laterally the layers have been traced for a few centimeters to a few tens of meters, but only rarely can they be traced for longer distances; commonly they terminate abruptly. Contacts with adjacent lithologies are sharp and in some cases, not straight. Frequently peridotite rafts are surrounded by dunite (the reverse situation has also been observed). These two lithologies are separated by a sharp contact.

The percentage of dunite as layers in any locale and over the whole outcrop region is variable, ranging from less than 1 percent to 20 percent. Where larger volumes of dunite layers occur the other dunite types are more abundant as well (see below).

The dunite is nearly pure olivine except for 1 percent to 3 percent disseminated spinel. Spinel occurs rarely as seams in the dunite, not exceeding 3 to 4 millimeters in thickness. Flattening of spinel parallel to the host peridotite foliation is common (Plate 7.E.).

Dunite lenses range in size from centimeter size pockets to bodies 50 meters x 400 meters (Plate 7.F.; Figure 2.7.). The lenses are always oblique to the S_1 foliation and the contacts with the host rock are sharp for both small and large lenses, but in the latter the contacts are

Figure 2.7. Sketch (plan) of the oblique orientation of the dunite megalens to the host harzburgite (stippled). Structural symbols indicate strike and dip of S_1.

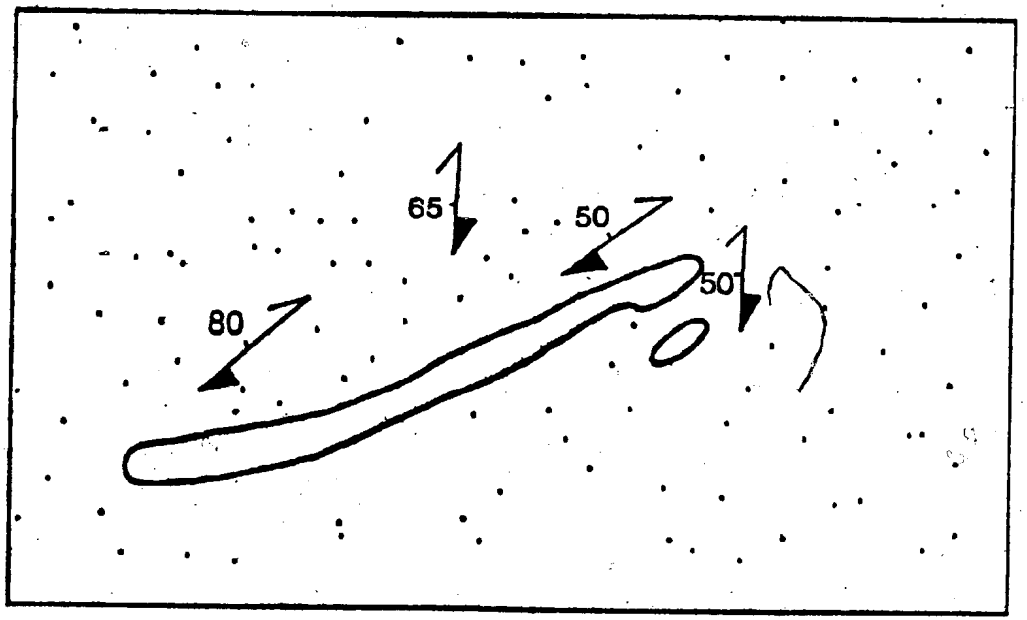
65
50
50
80

usually more irregular (Plate 8.A.). Occasionally, disrupted sections of spinel lherzolite and harzburgite layers are present in the dunite close to the contact and apophyses of dunite extend from the lenses a few meters into the host rock.

Within the lenses, spinel occurs as disseminated grains (1% to 4%) or as narrow discontinuous seams in some of the larger lenses. No evidence for crystal accumulation (e.g., graded beds, trough scours, etc.) has been observed in any of the lenses.

Dunite dikes range in size from a few centimeters to approximately ½ meter in width (Plates 8.B., 8.C., 8.D.). Laterally the dikes are not traceable for more than a few tens of meters, when they end either abruptly or taper out. No source region for the dunite dikes has been directly observed, but in regions where dunite lenses are common, dunite dikes are present in greater abundance. The relationship between dunite dikes and dunite lenses are equivocal, but at a few localities a dense network of anastamosing dunite dikes converge into small dunite lenses (Plate 8.B.). These lenses are oriented oblique to S_1 and the contact with the host rock irregular and, in most cases, sharp.

In one locality in the eastern massif a 'composite' dunite dike has been found (Plate 8.E.). The dike consists of an outer margin of dunite with a core of harzburgite (Plate 8.F.). The orthopyroxenes of the harzburgite core are not aligned parallel to the S_1 fabric of the host rock.

In some of the largest pure dunite dikes, spinel is concentrated as narrow (<4 mm) seams in the dike core. Any

Plate 8

A. Contact between dunite megalens (Plate 7.H., samples 78112 to 78117) and host rock (harzburgite, sample 78116). Eastern White Hills.

B. Anastamosing network of dunite dikes. Knife (top left of center) is parallel to S_1. Samples 78151, spinel lherzolite and 78152, dunite. Eastern White Hills.

C. Dunite dike cutting layered sequence of harzburgite-dunite-orthopyroxene-rich dunite. Spinel in the core of the dunite dike is parallel to the dunite-host rock contact. Samples 797, dunite; and 798, websterite vein cutting the dunite dike. Eastern White Hills.

D. Anastamosing dunite dikes in harzburgite. Field of view approximately 35 meters. Eastern White Hills.

E. Composite dunite dike in harzburgite. Knife parallel to S_1. Eastern White Hills.

F. Composite dunite dike, close up of Plate 8.E.; note that the orthopyroxene grains of the harzburgite core are oblique to S_1 (parallel to knife). Eastern White Hills.


A


B


C


D


E

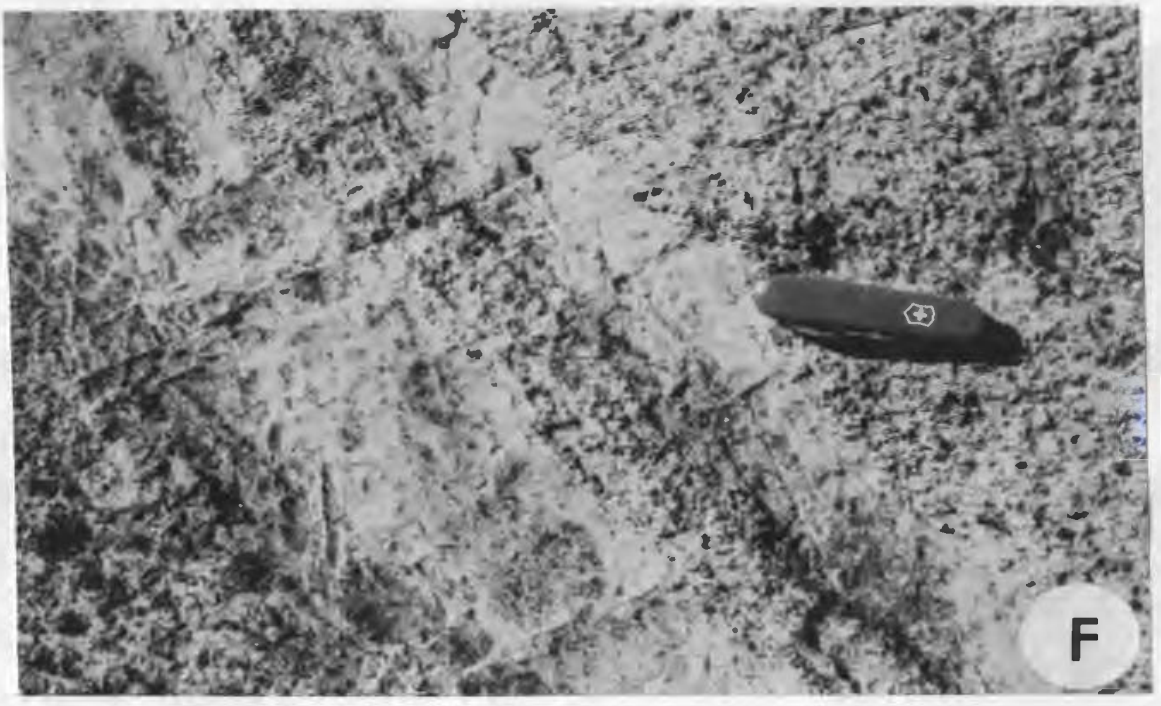
F

flattening of these spinels is commonly parallel to the dike margin, thus oblique to the host rock foliation (commonly S_1). The apparent non-coincidence of spinel alignment with S_1 is the main criterion used to identify dunite dikes and to distinguish them from dunite lenses. Otherwise this classification of dunite types seems unnecessary at this time until microstructural studies are completed.

In the dunites, olivine grains are euhedral to anhedral. In rocks outside the basal thrust zone the olivine grain size is uniform ($\sim$5 mm); within the basal thrust zone the olivine grain size is reduced and variable, dependent upon the severity of deformation and amount of recrystallization. Undulatory extinction is found in all olivine grains including neoblasts and those that are completely annealed and polygonized (i.e., Plate 6.C.). Subgrain structures are present in the more deformed samples.

Spinel assumes many forms and relationships with olivine and a full account is provided in Chapter 4.

(ii) silicate mineral alteration

Olivine is altered to serpentine + magnetite and rarely to chlorite. Serpentine mest texture preserving olivine kernals and serpentine pseudomorphs are present in the more hydrated samples.

c. Pyroxenite

(i) general statement

Pyroxenite veins are classified into four types: orthopyroxenite (± olivine, spinel); websterite (± second-

ary spinel)*; clinopyroxenite (± olivine, secondary spinel); and wehrlite (+ secondary spinel).

Each type occurs in varying proportions throughout the peridotite. The veins may either parallel or cross-cut the S_1 fabric (unless both S_1 and the veins have been overprinted by a subsequent deformation in the basal thrust zone) and range in width from 1 millimeter to 30 centimeters while laterally they can be traced up to, in rare cases, tens of meters. Contacts with the host rock are sharp. The pyroxenite veins outcrop as single veins, and as two or more parallel veins and branching networks (Figure 2.8.). Pyroxenite pods and boudins occur in the deformed rocks of the basal thrust zone and it is within this zone that the pyroxenite veins record folds that may be related to at least two periods of deformation (Plate 9.A.).

The orthopyroxenite vein lithology is the only pyroxenite vein type that is associated with chromite, and invariably these chromite concentrations are found in the orthopyroxenite veins with low-alumina orthopyroxenes and associated silicates with high Mg/Fe^{2+} ratios.

As a general rule, pyroxenite veins, especially websterite, increase in abundance locally where dunite is common.

* the rock name ariegite is used for a spinel websterite rock by Church (1972) and Riccio (1976). Websterite is used in this thesis in keeping with the Streckeisen (1976) classification.

Figure 2.8. Sketch of the common pyroxenite vein outcrop configurations. Cross-hatch--pyroxenite vein; long dash--peridotite; long dashes parallel to the prevailing peridotite foliation (S_1?). a. single vein; b. double, parallel veins; c. triple and double, parallel veins; d. branching network of veins parallel and oblique to foliation.

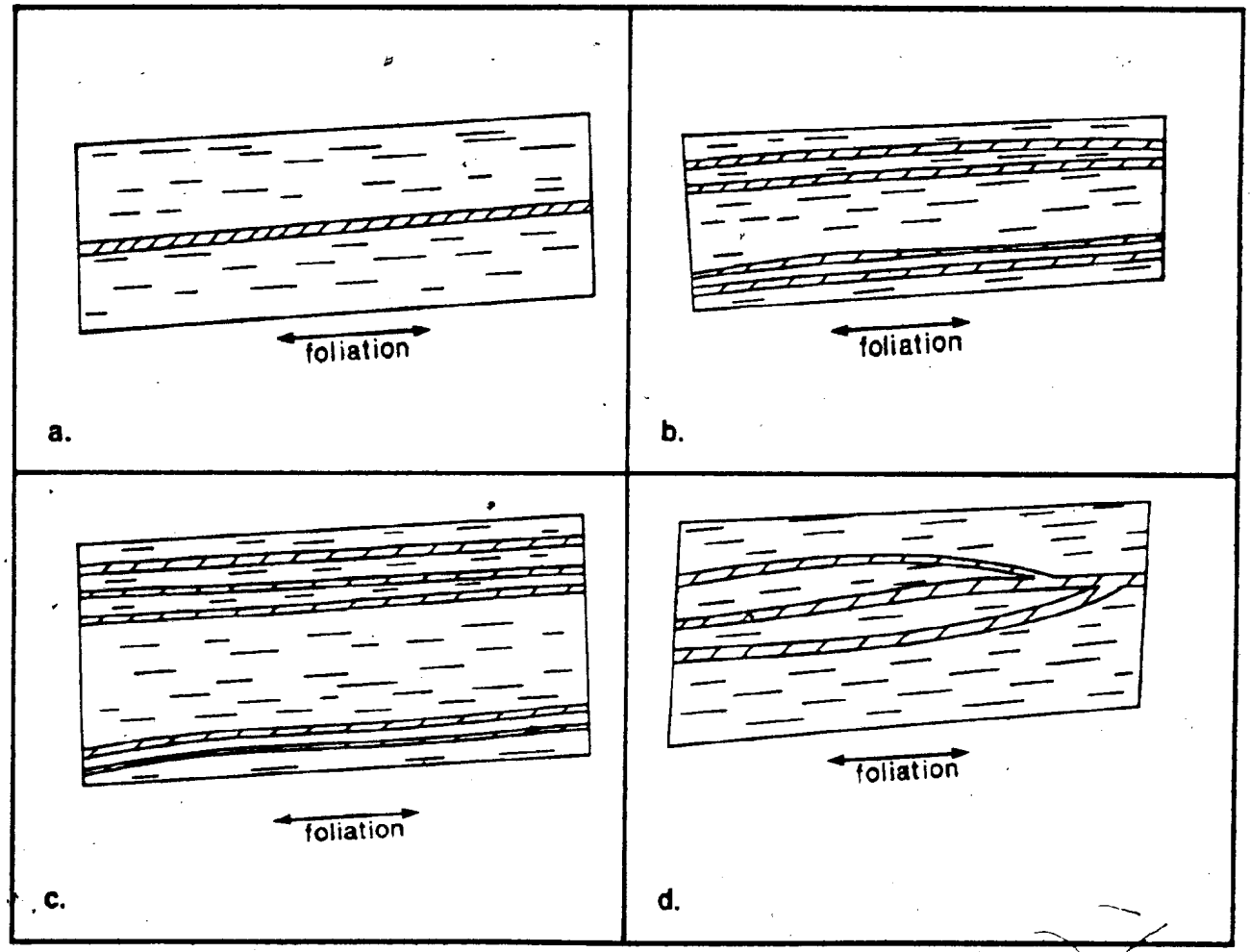
foliation
a.
foliation
b.
foliation
c.
foliation
d.

In Chapter 5, section II.5.B., pyroxenite vein origins are reviewed and proposed models for their origins based on the results of this study are presented.

(ii) orthopyroxenite

Orthopyroxenite veins occur parallel or oblique to the lithological layering and the S_1 foliation and are the only type of vein material that (see Plate 6.F.) may contain primary spinel and preserves a cumulate texture.

Orthopyroxene is euhedral to anhedral and colorless. Some grains contain exsolved clinopyroxene, but this is not a common feature. Grain boundaries are often interlocking, suggesting adcumulus growth (Wager et al., 1960), but may be ragged and sometimes adjacent cumulus orthopyroxenes are separated by a zone of orthopyroxene neoblasts. Undulatory extinction is present. Orthopyroxene neoblast aggregates are sometimes present along kink bands of some deformed cumulus grains.

Olivine and clinopyroxene are anhedral intercumulus phases. On occasion, rounded olivine grains (< 1 mm) may occur in orthopyroxene.

Spinel associations are discussed in Chapter 4.

Orthopyroxene is altered to bastite. Secondary sulphides are found in extremely altered samples.

(iii) websterite

Websterite veins are on average the widest (2 cm to 30 cm) pyroxenite vein type. They have been traced laterally for tens of meters and are either parallel to or cut S_1.

They also cross-cut most other lithologies except gabbro.

Clinopyroxene porphyroclasts are equant, approximately 4 millimeters in diameter, show undulatory extinction and are slightly bent. Porphyroclast grain boundaries are scalloped and clinopyroxene neoblasts with undulatory extinction occur along the grain boundaries of the larger grains. In a few samples orthopyroxene exsolution lamellae have been found.

Orthopyroxene porphyroclasts are colorless, approximately 2 millimeters x 1.5 millimeters in size, show undulatory extinction, and may show kink bands along which the material is partially recrystallized. Neoblasts are strained and are free of exsolution lamellae, whereas clinopyroxene exsolution lamellae are present in most orthopyroxene porphyroclasts.

Olivine grain size is small, approximately 1 millimeter x 0.5 millimeter, with undulatory extinction present in all grains. Olivine grains have been found in clinopyroxene porphyroclasts, but olivine mostly appears to be an intercumulus phase.

The clinopyroxene is altered to uralite and other amphiboles (mainly hornblende) and may contain magnetite grains where highly altered. Orthopyroxene is altered to serpentine + magnetite.

(iv) clinopyroxenite

Clinopyroxenite veins occur parallel to or oblique to S_1. Also, clinopyroxenite occurs as pods ($\sim$ 1 m x 3 m).

oriented with their long dimension approximately parallel to S_1 (Talkington, 1979). The clinopyroxenite veins cut most lithologies of the peridotite except gabbro. The clinopyroxenite pods are surrounded by spinel lherzolite and harzburgite, and have not been observed in the basal thrust zone.

Clinopyroxene grains sometimes show pink pleochroism and have a large, uniform grain size, 7 millimeters x 3 millimeters. Porphyroclasts show undulatory extinction, have been partially recrystallized and show scalloped grain boundaries. Some clinopyroxene grains have well-developed kink bands. The neoblasts have undulatory extinction and show various stages of grain boundary adjustment.

Olivine is anhedral and probably intercumulus, though this cannot be assessed with certainty due to the effects of recrystallization. Grains are frequently equant and small, 0.4 millimeters x 0.4 millimeters, in size. Subgrain structures are observed in large olivine grains, but not in the neoblasts, which show some undulatory extinction.

Clinopyroxene shows incipient alteration to uralite and chlorite. Olivine is altered to serpentine + magnetite.

(v) wehrlite

Wehrlite has been found in one location in the eastern massif. The vein is parallel to S_1 and about 5 centimeters in width. The lateral extent is not known and the contact with the host rock is sharp. Riccio (1976) has described spinel wehrlite veins that are oblique to the foliation (S_1?) and that cross-cut spinel websterite bands.

Olivine grains are anhedral and cut by numerous serpentine + magnetite veins that have resulted in the development of a mesh texture. Original grain size is difficult to determine optically. Measurements of the largest optically continuous grains average 2 millimeters x 1 millimeter. Undulatory extinction is ubiquitous and subgrain structures rarely observed. Primary anhedral olivine grains are present in clinopyroxene porphyroclasts.

Clinopyroxene porphyroclasts have a faint pink pleochroism and an average grain size of 2 millimeters x 1 millimeter. Undulatory extinction is common. Grain boundaries are generally uniform, but minor recrystallization is observed.

Olivine is altered to serpentine + magnetite. Clinopyroxene shows incipient alteration to amphibole.

d. Gabbro

(i) field description

Gabbro veins (± olivine, spinel) outcrop in a 200 to 300 meter wide zone on the eastern massif (Plate 2; Figure 2.9.). The veins occur within spinel lherzolite and harzburgite, and either parallel or cross-cut S_1 (Plate 9.B.), and range in width from 1 millimeter to 20 centimeters. Pockets (1 cm wide and < 1 m long) of gabbroic material (leucogabbro) are found in the zone only where gabbro veins are uncommon. Gabbro veins are commonly solitary and have been traced laterally for 20 meters, but other groupings such as two or more parallel veins or a branching network are not unusual (Plate 9.C.). Gabbro veins cut all other lithologies. The

Figure 2.9. Outcrop distribution of gabbro veins - stippled pattern

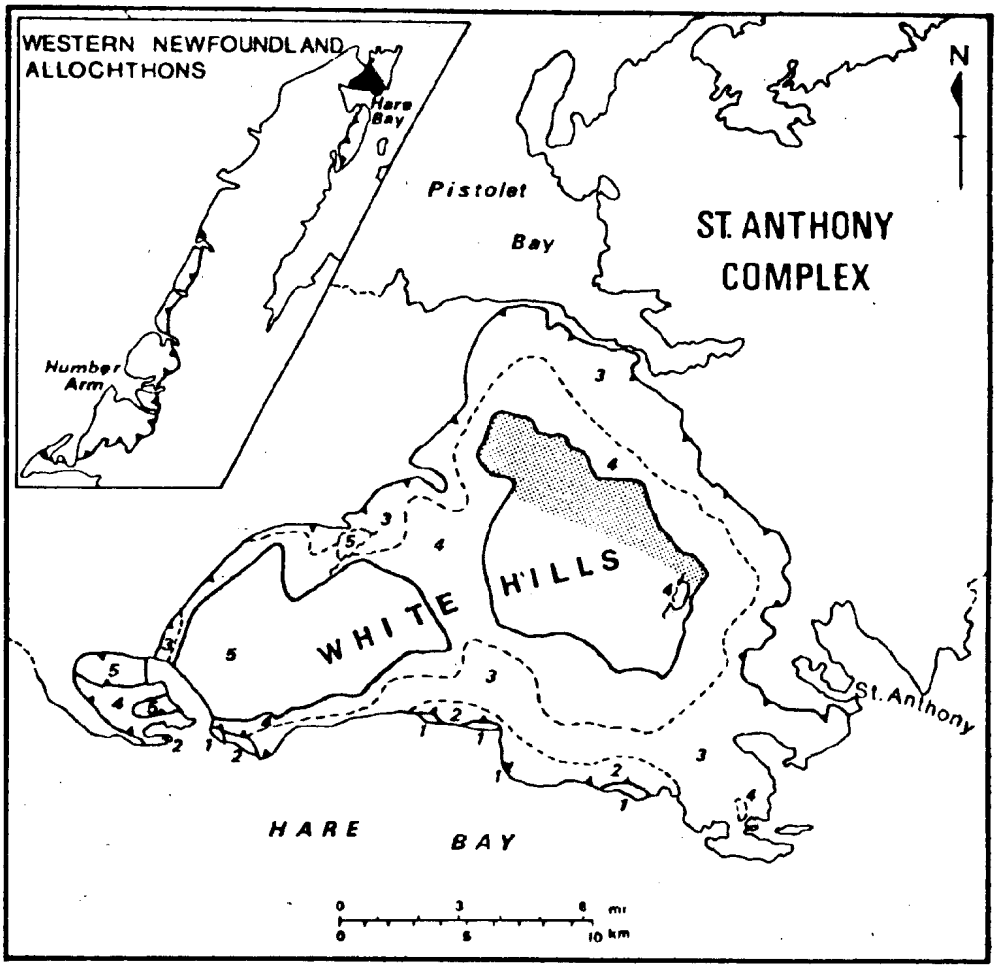
WESTERN NEWFOUNDLAND
ALLOCHTHONS
Hare Bay
Humber Arm
Pistolet Bay
ST. ANTHONY COMPLEX
N
WHITE HILLS
St. Anthony
HARE BAY
0 3 6 mi
0 5 10 km

Plate 9

A. Clinopyroxenite vein from near the basal thrust zone with an F_1 fold refolded by F_2. Western White Hills.

B. Typical outcrop view of gabbro veins in harzburgite. Scale bar is approximately 16 centimeters long and is approximately parallel to S_1. Orientation of wide gabbro veins, 038-30°N (~ parallel to S_1); narrow gabbro veins 080-35°N. Eastern White Hills.

C. Network of gabbro veins with various orientations. Eastern White Hills.

D. Zoned gabbro vein. Clinopyroxene-rich core; plagioclase-rich margins. Eastern White Hills.

E. Clinopyroxenite pod (grass area). Long dimension of pod is approximately 3 meters (~ parallel to S_1); short dimension is approximately 1 meter. Shape unknown. Eastern White Hills.

F. Chromitite seam in the core of an orthopyroxenite vein. Scale is 3 centimeters in diameter. Sample 78119. Eastern White Hills.

G. Folded chromitite seam (F_2?-fold) in slightly mylonitic orthopyroxene-rich dunite. Scale is 3 centimeters in diameter. Sample 78120. Eastern White Hills.

H. Typical field appearance of the peridotite deformed by F_2. See text section I.2.B.5.a. for further details. Scale is approximately 5 centimeters in length. Sample 283-20'. Eastern White Hills.

I. F_3 generation fold style. Dashed line is the approximate location of the fold axis. Eastern White Hills.

J. Fault zone breccia which is developed within northeast-southwest fault set. Deformed peridotite clasts in comminuted serpentine matrix. Scale is 6 centimeters long.


A


B


C

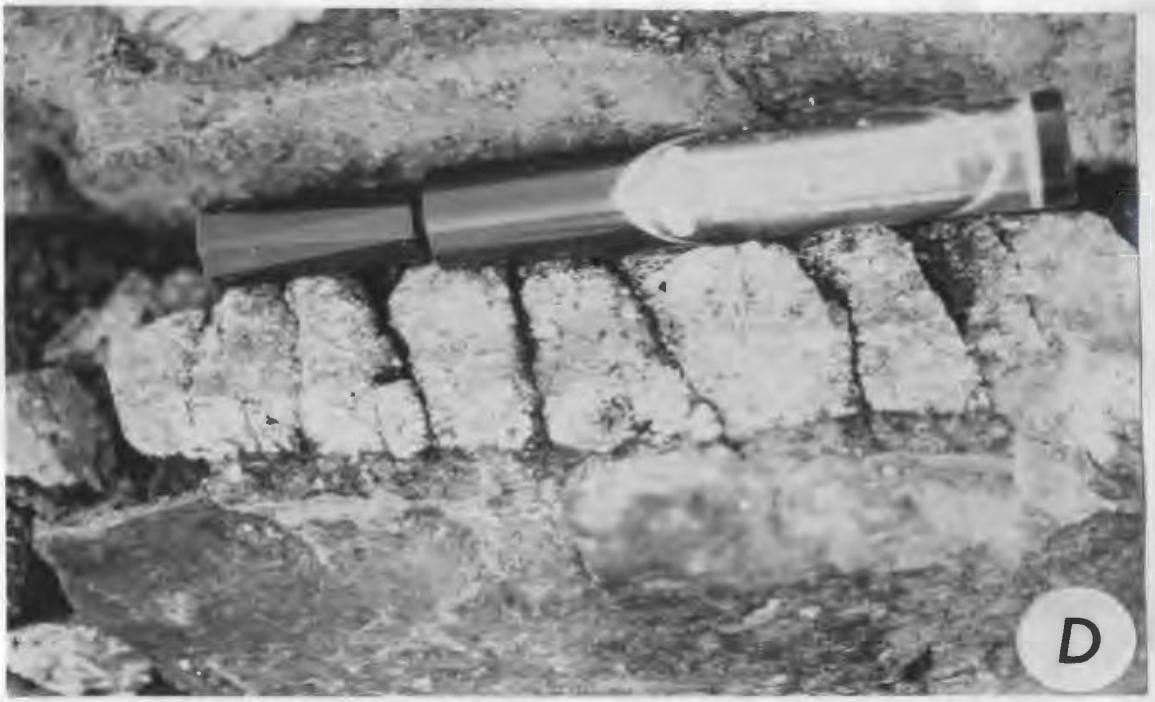
D


E


F


G


H


I


J

contacts with the host rock are sharp and the host rock foliation does not appear to be preserved in the veins. Mineralogical zoning has been found in one gabbro vein outcrop. Here, a plagioclase-rich margin encloses a clinopyroxene-rich core (Plate 9.D., Figure 5.9.).

In the east central part of the eastern massif, small olivine clinopyroxene pods have been mapped. Neither their size nor shape are readily discernible since the outcrop area is essentially felsenmeer, but they appear to be about 3 meters long and 1 to 2 meters wide (Plate 9.E.) oriented with their long dimension parallel to S_1. This is therefore possibly a structurally controlled orientation. Numerous gabbro veins are found in the area and are presumed to be connected to the pods, although there is no clear field evidence to prove this. Close to the pods, the volume of gabbro veins makes up as much as 40 percent of the outcrop. This decreases to about 1 percent at a distance of 40 meters. The thickness of the veins, likewise, decreases with distance from the pods. In one location, the gabbro veins cut a pyroxenite pod (Talkington, 1979) (Figure 5.9.) and within the pod isolated patches of plagioclase are found.

(ii) petrography

In the gabbro, clinopyroxene porphyroclasts show a pink pleochroism and are variable in size. In the least deformed samples, clinopyroxene porphyroclasts average approximately 2 millimeters in size. Twinning is common in both large and small grains, but has not been observed in clinopyroxene neoblasts. Undulatory extinction is always

observed in porphyroclasts and neoblasts and porphyroclasts are sometimes bent and have kink bands; some of the kink bands are recrystallized.

Olivine is anhedral and variable in size. Undulatory extinction is common and subgrain structures are present in the larger grains. Olivine grains sometimes are found in clinopyroxene porphyroclasts.

Plagioclase is always anhedral and polysynthetic twinning is ubiquitous. In most samples where recrystallization has not been intense, plagioclase is sausseritized. Where recrystallized, plagiclase forms either small neoblasts that have well-developed triple point junctions or larger grains with diffuse, sometimes lobate grain boundaries. In the latter type, polysynthetic twinning is less common. Clinopyroxene porphyroclasts are found in large non-recrystallized plagioclase grains.

Orthopyroxene is a very rare modal phase. When found, it is colorless and can be up to 2 millimeters in size. Clinopyroxene exsolution lamellae have been observed in the larger grains. Undulatory extinction is present in all grains.

Clinopyroxene is altered to uralite, hornblende and minor pyrite and/or magnetite or in rare cases to secondary biotite. Olivine is altered to serpentine + magnetite.

e. Chromitite

(i) field description

Only a field description of the chromite accumulations is provided in this section. A complete documentation of

all spinel phases of the White Hills Peridotite is provided in Chapter 4.

No podiform chromite deposits, common to many ophiolite cumulate dunite and/or uppermost tectonite peridotite zones, have been found in the White Hills Peridotite. Chromite in the White Hills is invariably associated with orthopyroxenite as disseminations, seams and pods of undefined shapes.

In the one area where massive chromite is found, large euhedral orthopyroxene crystals up to 4 centimeters long x 3 centimeters wide occur in a chromitite matrix and a chromite + clinopyroxene matrix. In the same area, a vein of chromitite with orthopyroxenite margins cross-cuts S_1 (Plate 9.F.) and locally where the peridotite is highly deformed (i.e., basal thrust zone) disrupted seams of chromitite have been folded by the F_2 event (Plate 9.G.).

5. Structural Features of the White Hills Peridotite

a. Observations

As well as observations made for the present work, results of structural studies of the White Hills Peridotite have been published by Girardeau (1979).

Two major planar fabrics of tectonic origin are present in the peridotite and are termed S_1 and S_2.

S_1 is the dominant planar fabric and is found throughout most of the peridotite especially in rocks outside the basal thrust zone (B.T.Z.). It is defined by the parallel alignment of slightly to moderately flattened and/or elongate orthopyroxene grains or aggregates and rarely spinel grains, and is always parallel to the lithological layering and vice versa* (see section 4.a. of this Chapter) and axial

* The chronological order for S_1 and the lithological layering has not yet been established, however, these features may have formed in the upper mantle during upwelling of the source diapir (see Chapter 5).

planar to F_1 folds. F_1 folds are isoclinal and sometimes symmetrical in form, have thickened fold hinges and thin or tapered fold limbs and are always rootless (Figure 2.10.).

No mineral lineations have been recorded.

Discontinuously developed in the lower 25 meters (B.T.Z.) of the peridotite and recognized up to 50 meters above the B.T.Z. are F_2 generation structures. F_2 structures overprint the S_1 foliation and refold F_1 folds. F_2 generation folds are reclined and asymmetric in form and the fold hinge and limbs are uniform in thickness or there may be slightly thickened fold hinges. This fold generation is best manifested by pyroxenite veins. The S_2 foliation is defined by the parallel alignment of flattened and/or elongate orthopyroxenes and amphiboles and elongate or slightly flattened (granulated?) spinels. The fabric trends parallel to the basal thrust contact and dips at shallow angles ($< 35^{o}$) into the peridotite massifs. S_2 foliation is distinguished from S_1, in most areas outside the B.T.Z., by the highly accentuated flattening and elongation of the orthopyroxene porphyroclasts. For example, for the S_2 foliation, orthopyroxene porphyroclasts maintain a size range of approximately 2 centimeters to 5 centimeters in length and spinel grain size averages approximately 5 millimeters (Plate 9.H.) in length.. This is in contrast to S_1 where the orthopyroxene porphyroclasts are generally less than 1 centimeter in length and spinel grains are approximately 2 millimeters in diameter and rarely elongate. In addition, the spinel grains that have been deformed by F_2 often have an

Figure 2.10. Sketch of F_1 isoclinal fold (recumbent) with thickened fold hinge and thin on tapered fold limbs. S_1 is axial planar.

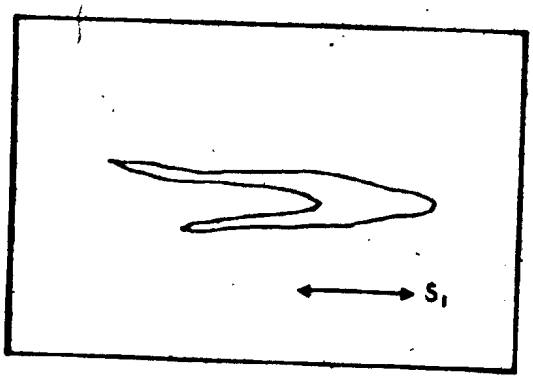
S_1

alteration rim of kämmererite(?). Other physical features that are interpreted to have been the result of the F_2 deformation event are: 1) dunite concentrations with a shaly cleavage(?) which on outcrop surfaces is approximately parallel to S_2; and 2) lithological layers that have been disrupted and thin (streak out) and thicken (boudinage, especially pyroxenite veins).

No mineral lineations have been recorded for the F_2 event.

F_3 generation folds are symmetrical with vertical axial planes (Plate 9.I.) and have wavelengths that average 30 meters and amplitudes as great or greater than the topographic thickness of the peridotite. The deformation associated with F_3 folding does not appear to have been intense (relative to F_2) having only slightly deformed F_1 (folded S_1) and F_2 generation structures. No S_3 fabric has been identified.

Four major sets of variously oriented thrusts and high angle faults are recognized in the peridotite. They are: northeast-southwest thrust faults, northwest-southeast high angle faults, north-south high angle faults, basal thrust fault.

Northeast-southwest trending thrust faults that dip at moderate angles to the southeast are recognized in the east and west massifs. The best developed examples of this fault type occurs in the southwest to central parts of the western massif (see Plates 2 and 3). In this region a series

of closely spaced fault planes can be traced for a total distance of approximately 4 kilometers and are marked by a discontinuous, chaotic zone of well-developed fault breccia (Plate 9.J.). The fault breccia contains peridotite fragments up to cobble size and of various shapes in a highly comminuted serpentine matrix. The width of an individual fault zone is up to 10 meters. The displacement on the fault set is not accurately known, but 150 meters is taken as a minimum distance (shortest displacement vector) because B.T.Z. rocks outcrop along the fault plane traces.

Northwest-southeast trending high angle faults are common to the western massif. The best developed example of this fault type occurs in the central part of the western massif where it nearly bifurcates the massif and separates two regions of radically different S_1 orientations (see Plate 2). On the east side of the fault, S_1 trends northwest-southeast, but to the west, northeast-southwest trends prevail. The lateral extent and displacement of this fault set is uncertain, but basal zone rocks are exposed along the fault trace and a crude minimum estimate for fault displacement of 75 meters may be in order.

A north-south trending high angle fault approximately 2 kilometers in length occurs in the central region of the western massif. The fault is clearly visible on air photos and on the ground forms a 50 meter high cliff. The fault plane is vertical and the relative sense of movement is east side up, but the displacement is not known, though, it possibly is no greater than approximately 100 meters (see

Plate 3) as no basal zone rocks have been found on either side of the fault or along the trace of the fault plane. The overall outcrop pattern of the peridotite massif in this region gives the impression that the fault continues 3 kilometers to 4 kilometers farther north (see Plate 2), but no field data support this theory. The fault is cut by a prominent northeast-southwest trending fault set near the southern peridotite-metamorphic aureole contact (see Plate 2).

The most prominent fault in the White Hills Peridotite is the basal thrust fault (B.T.F.). The B.T.F. separates, in most areas, the peridotite from the underlying Green Ridge Amphibolite. Locally, the B.T.F. overlaps other allochthonous (e.g., Maiden Point Formation in the Howe Harbour area) and autochthonous units (e.g., Goose Tickle Formation, Tuke, 1968). The B.T.F. plane appears to dip at shallow angles ($< 35^{o}$) beneath the massifs. Whether the fault plane is horizontal, saucer-shaped (with a flat bottom), concave up or rippled due to F_3 folding remains uncertain.

A chronology for the fault sets on the basis of field relationships appears to be (oldest to youngest): 1) basal thrust fault; 2) north-south high angle faults; 3) northwest-southeast high angle faults; 4) northeast-southwest thrust faults.

b. Interpretation

Nearly all of the structural elements that have been described for the White Hills Peridotite occur in most, if not all, ophiolite peridotite sections (e.g., Ligurian, Bezzi

and Piccardo, 1971; Coast Ranges, U.S.A., Loney et al., 1971; Dun Mountain, New Zealand, Coombs et al., 1976; Bay of Islands Complex, Malpas, 1976; Semail, Oman, Boudier and Coleman, in press), subcontinental lherzolite intrusions (e.g., Ivrea Zone, Nicolas, 1976; Shervais, 1979), and oceanic peridotites from spreading ridges and trenches (Nicolas et al., 1980). The deformational mechanisms responsible for developing many of these features may be determined largely from microstructural studies on the behaviors and interrelationships of minerals that have been deformed during mineral and rock (natural and synthetic) deformational experiments and experimental mineral deformational modelling (e.g., Ave'Lallemant and Carter, 1970; Nicolas et al., 1973; Etchecopar, 1977).

A microstructural study of the minerals in the various lithologies of the White Hills Peridotite has not been undertaken. Therefore, the interpretations made in this section must await such a study before they can be verified.

A uniform foliation in upper mantle ophiolite peridotites that is defined by the parallel alignment of orthopyroxene porphyroclasts, spinel grains, etc., such as the S_1 foliation of the White Hills Peridotite, is ubiquitous to many ophiolite upper mantle peridotite sections (Bezzi and Piccardo, 1971; Loney et al., 1971; Malpas, 1976; Juteau et al., 1977; and many others). The development of this type of fabric has been suggested to be the result of high temperature plastic flow of the peridotite during its ascent beneath an accreting ridge (Nicolas et al., 1973, Nicolas, 1976; Juteau et al., 1977;

Nicolas et al., 1980). During this event, olivine grains are deformed dominantly by slip parallel to (100) with a slight rotational component and concommitantly are flattened in the plane of foliation (Nicolas et al., 1973; Juteau et al., 1977), e.g., S_1, producing a lineation (Juteau et al., 1977). The microscopic rock textures commonly recognized in peridotites that have been subjected to only the upper mantle high temperature plastic flow deformation during ascent are coarse-granular (∿ protogranular) and/or coarse-grained porphyroclastic (see review in Nicolas et al., 1980). Also, during this upper mantle deformational event, F_1 folds may have developed in the pyroxenite veins probably by mechanical reorientation of the veins (Juteau et al., 1977).

The F_2 overprint on F_1 related structures within the B.T.Z. has resulted in: 1) pronounced elongation and flattening of mainly orthopyroxene porphyroclasts and spinel grains, 2) a reorientation of S_1 to an S_2 mineral foliation of the peridotite that is parellel to the B.T.F. and the underlying metamorphic aureole (Jamieson, 1979), and 3) the parallel alignment of F_2 generation fold axial planes in the peridotite with F_2 or F_3 generation fold axial planes in the metamorphic aureole (Jamieson, 1979). The microscopic rock textures of the B.T.Z. are porphyroclastic and granoblastic (foam texture of Calon, 1980) but hybrid combinations of the two textures are common. The deformation mechanism that produces these textures is probably a dynamic, syntectonic recrystallization (Calon, 1980; Nicolas et al., 1980) that

occurs during the early stages of the emplacement of the ophiolite onto outer continental margin supracrustal rocks or oceanic crust.

In the White Hills Peridotite, Calon (1980) recognizes a low-temperature, dynamic recrystallization (young mylonites) of F_2 microstructures (old mylonites) within the B.T.Z. The low-temperature, higher strain, recrystallization event produces a mortar structure with olivine grains in an L-plane that is nearly parallel to the S_2 foliation plane.

The F_3 fold generation may be Acadian age (Williams et al., 1973) and therefore not related to ophiolite emplacement.

The formation and distribution of the various rock textures can be correlated with specific deformation episodes and mechanisms, but it is not always easy to distinguish S_1 from S_2 in the field especially if the F_2 overprint has been locally less intensely developed. The development of the S_1 foliation and F_1 folds probably occurs by high temperature plastic flow during ascent of the peridotite diapir beneath an accreting ridge.[1] F_2 generation structures may have formed during emplacement of the peridotite while it still retained much of its heat. Locally, in the B.T.Z., S_{2c}[2] microstructures appear to have developed within nearly parallel L-planes as F_2 generation structures, but at lower temperatures and higher strain (Calon, 1980).

1. a discussion of the origin of the lithological layering is presented in Chapters 5 and 6.
2. structural designation according to the inferred deformational events of Calon (1980).

F_3 generation folds have long wavelengths and large amplitudes and may have formed after final emplacement of the peridotite (Llanvirn or slightly later, Tuke, 1968), possibly in response to the Acadian disturbance (Williams et al., 1973).

The fault sets are interpreted to have developed after displacement of the peridotite from its oceanic environment. The basal thrust fault is recognized as the oldest major fault and it records the emplacement history that affected the peridotite of the B.T.Z. The north-south and northwest-southeast fault sets are high angle faults that may have developed at approximately the same time. This is based solely on the similarity of fault type. The northeast-southwest fault set is a northwestward directed thrust fault, at least in the western massif, where it intersects the north-south fault set. The northeast-southwest fault set trends in the same direction as the Hare Island, Brent Island, and Little Arm Faults, all of which are westward directed thrust faults, that cut allochthonous and autochthonous rocks (Cooper, 1937; Tuke, 1966). If these faults are related to the same tectonic event, then they post-date the final emplacement of the Hare Bay Allochthon and must therefore be post-Llanvirn and may be as young as Carboniferous (Stancioff and Hill, 1979; Williams and Smyth, in press).

6. Summary

Field mapping of the White Hills Peridotite and a few lithologies directly underlying the peridotite indicates that

the peridotite is dominantly a layered sequence of spinel lherzolite, harzburgite, and dunite which contains various types of pyroxenite veins, a localized occurrence of gabbro veins and a chromitite pod. There does not appear to be a predominant order for the lithological layering nor for the distribution of the pyroxenite veins, though, the gabbro veins and chromitite pod are only found on the eastern massif. No quantitative estimate for the amount of a particular lithology has been made.

At least two major deformational events have affected the peridotite, F_1 and F_2. F_1 is tentatively interpreted to be the result of high temperature plastic flow of the peridotite during its ascent beneath an accreting ridge, whereas F_2 is interpreted to have formed during the emplacement of the peridotite. The F_3 deformation event (as recognized for this study) only slightly affects the peridotite (and allochthon) as upright symmetrical folds; F_3 is post-emplacement, possibly an Acadian feature.

Several rock microstructures of the peridotite are present in rocks that have been affected by F_2. These are mylonitic and granoblastic. The formation (or destruction) of the other microstructures of the peridotite can not accurately be determined, though on the basis of comparison with published descriptions of microstructures from other ophiolites, the coarse-granular and porphyroclastic textures may have been formed in the upper mantle; the cumulate and allotriomorphic-granular microstructures are the result of crystal fractionation from a liquid. The region of the upper mantle/lower crust

where these latter two textures form is not known ($\lesssim$ 8 kb for the cumulate texture of the chromite-related lithologies, but probably higher for the other lithologies which preserve these textures). Because the cumulate texture has only been slightly deformed, its formation may be a late feature in the evolution of this ophiolite.

During this study an attempt to construct a 'stratigraphy' for the White Hills Peridotite by studying mineral rhythmic variations, cryptic mineral and bulk rock variations, and rock textures produced no satisfactory result. Although an internal stratigraphy could not be determined, an estimate for a minimum stratigraphic thickness of approximately 2 kilometers* is suggested and is based on what is considered a nearly intact section of peridotite located on the east side of the western massif. Because no analog of the White Hills Peridotite has been recognized in Newfoundland, the Appalachians or elsewhere, principally because of the presence of lithological layering in the White Hills, the White Hills Peridotite has been placed for direct comparison, below the deepest exposed level of mantle peridotite (e.g., below the spinel lherzolite subsection of the Bay of Island Complex) (Figure 2.11.).

* the topographic thicknesses for the western and eastern massifs are 250 meters and 200 meters, respectively.

Figure 2.11. Comparison and relative location of the White Hills Peridotite stratigraphy to the ophiolites from the Bay of Islands Complex.

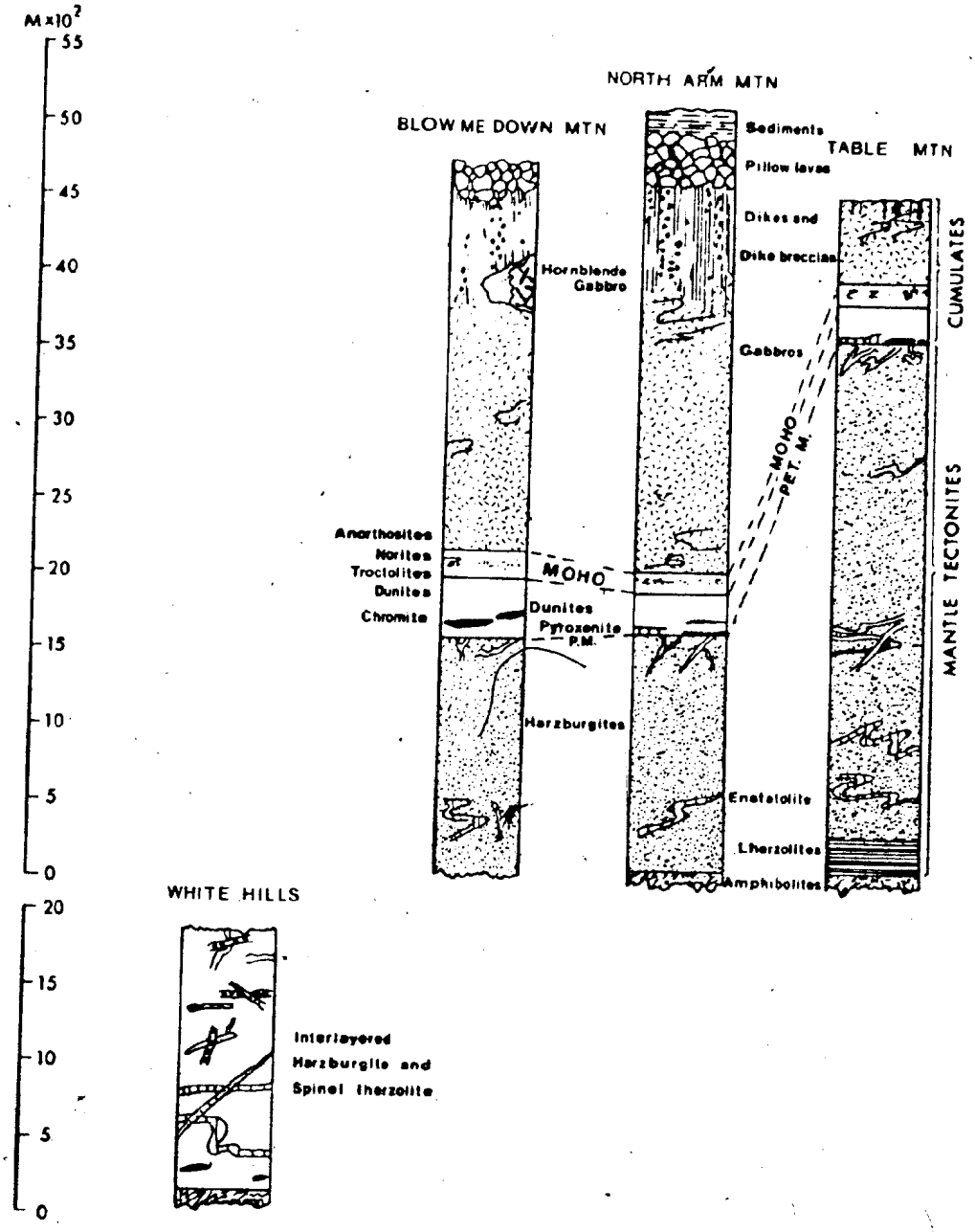
M x10²
55
50
45
40
35
30
25
20
15
10
5
0
NORTH ARM MTN
BLOW ME DOWN MTN
TABLE MTN
Sediments
Pillow lavas
Dikes and
Dike breccias
Hornblende
Gabbro
Gabbros
CUMULATES
MOHO
PET. M.
Anorthosites
Norites
Troctolites
Dunites
Chromite
MOHO
Dunites
Pyroxenite
P.M.
Harzburgites
MANTLE TECTONITES
Enstatolite
Lherzolites
Amphibolites
WHITE HILLS
20
15
10
5
0
Interlayered
Harzburgite and
Spinel lherzolite

Table 4.1. Summary of the textural variations of the spinel phases in the rocks of the White Hills Perido and Malpas, 1980[4].

Rock Type	Microstructure Rock Texture[1]	Color[2]	Grain Shapes and Sizes[3]
Spinel lherzolite:	a. coarse-granular	straw-yellow to light red-brown	porphyroclasts (.4mm x .2mm irregular interstitial to o cpx, ol (.2mm); vermicular, wormlike exsolu from opx (.1mm x .02mm); exsolved droplets from opx (.05mm)
	b. porphyroclastic	bronze to light red-brown	'Holly-Leaf' (.8mm); porphy clasts with spinel trails (.1mm); exsolved droplets a KBB[5] in opx and cpx (<.1mm) exsolved droplets in opx an (<.05mm)
	c. mylonitic	bronze to brown-green	'Holly-Leaf' (.4mm); porphy clasts (.3mm); linear trail spinel clusters (variable s
Harzburgite	a. coarse-granular	various shades of red-brown	porphyroclasts (ovoid shape (.2mm); vermicular exsolutio in opx (<.2mm); exsolved dro lets in opx (<.1mm)
	b. porphyroclastic	various shades of red-brown	'Holly-Leaf' (2mm x .2mm); porphyroclast (ovoid and tad forms with ol and opx, some porphyroclasts show pull-apa texture) (3mm)
	c. mylonitic	various shades of red-brown	'Holly-Leaf' (.4mm); porphyr clasts (.3mm); linear trails of spinel clusters (variable
Dunite[6]:	a. allotriomorphic-granular	green-brown to red-brown	porphyroclasts (ovoid, showi pull-apart texture; severely corroded to produce 'Holly-L like structure) (.5mm, range .2mm to 4mm)
	b. granoblastic (equigranular and elongate[7])	deep red-brown to black[8]	xenoblastic interstitial (various size ranges, .01mm to .2mm)
Gabbro:	porphyroclastic and granoblastic	green(translu-cent)	'Holly-Leaf' (.2mm); cluster interstitial (.15mm); vermi-cular in opx, cpx, pl, ol (<.1mm) and exsolved droplet in opx, cpx, pl, ol (.05mm)
Pyroxenite:			
1. orthopyroxenite (tol)	a. cumulate	red-brown	euhedral to anhedral intersi and occluded within opx (.2m rarely elongate parallel and parallel to (100) opx (<.1mm

1 of

es in the rocks of the White Hills Peridotite (modified from Talkington

lor[2]	Grain Shapes and Sizes[3]	Grain Boundary	Orientation
w-yellow light red-own	porphyroclasts (.4mm x .2mm); irregular interstitial to opx, cpx, ol (.2mm); vermicular, wormlike exsolution from opx (.1mm x .02mm); exsolved droplets from opx (.05mm)	irregular to curvilinear for porphyroclasts, exsolution and interstitial forms; smooth and rounded droplet form	random
nze to light d-brown	'Holly-Leaf' (.8mm); porphyroclasts with spinel trails (.1mm); exsolved droplets along KBB[5] in opx and cpx (<.1mm); exsolved droplets in opx and cpx (<.05mm)	scalloped to irregular for 'Holly-Leaf' and porphyroclast forms; rounded to subidioblastic for droplet form	'Holly-Leaf' and porphyroclast parallel to foliation; random for droplets
nze to wn-green	'Holly-Leaf' (.4mm); porphyroclasts (.3mm); linear trails of spinel clusters (variable sizes)	scalloped to irregular for all forms	all forms parallel to foliation
ious shades red-brown	porphyroclasts (ovoid shaped) (.2mm); vermicular exsolution in opx (<.2mm); exsolved droplets in opx (<.1mm)	scalloped to serrate for porphyroclast form; smooth, curvilinear for vermicular form; round to subidioblastic for droplets	porphyroclasts either random or to foliation; random for vermic droplet forms
ious shades red-brown	'Holly-Leaf' (2mm x .2mm); porphyroclast (ovoid and tadpole forms with ol and opx, some porphyroclasts show pull-apart texture) (3mm)	scalloped to irregular for 'Holly-Leaf' and porphyroclast forms	all forms parallel to foliation
ious shades red-brown	'Holly-Leaf' (.4mm); porphyroclasts (.3mm); linear trails of spinel clusters (variable sizes)	scalloped to irregular for all forms	random or defining a lineation
en-brown red-brown	porphyroclasts (ovoid, showing pull-apart texture; severely corroded to produce 'Holly-Leaf' like structure) (.5mm, range .2mm to 4mm)	regular, scalloped and curvilinear	all forms parallel to foliation
p red-brown black[8]	xenoblastic interstitial (various size ranges, .01mm to .2mm)	irregular	random or parallel to foliation
en(translu-t)	'Holly-Leaf' (.2mm); cluster interstitial (.15mm); vermicular in opx, cpx, pl, ol (<.1mm) and exsolved droplets in opx, cpx, pl, ol (.05mm)	scalloped to irregular for 'Holly-Leaf' and cluster forms; rounded for droplets in primary and recrystallized pl; commonly irregular for droplets in cpx and opx	random
brown	euhedral to anhedral interstitial and occluded within opx (.2mm); rarely elongate parallel and subparallel to (100) opx (<.1mm)	irregular to rounded	random

Hills Peridotite (modified from Talkington

nd Sizes[3]	Grain Boundary	Orientation
<.4mm x .2mm); rstitial to opx, ; rmlike exsolution x .02mm); ets from opx	irregular to curvilinear for porphyroclasts, exsolution and interstitial forms; smooth and rounded droplet form	random
.8mm); porphyro- inel trails d droplets along cpx (<.1mm); ts in opx and cpx	scalloped to irregular for 'Holly-Leaf' and porphyroclast forms; rounded to subidioblastic for droplet form	'Holly-Leaf' and porphyroclast forms parallel to foliation; random for droplets
.4mm); porphyro- linear trails of (variable sizes)	scalloped to irregular for all forms	all forms parallel to foliation
(ovoid shaped) lar exsolution exsolved drop- 1mm)	scalloped to serrate for porphyroclast form; smooth, curvilinear for vermicular form; round to subiodioblastic for droplets	porphyroclasts either random or parallel to foliation; random for vermicular and droplet forms
mm x .2mm); ovoid and tadpole nd opx, some show pull-apart	scalloped to irregular for 'Holly-Leaf' and porphyroclast forms	all forms parallel to foliation
4mm); porphyro- linear trails ers (variable sizes)	scalloped to irregular for all forms	random or defining a lineation
(ovoid, showing ure; severely duce 'Holly-Leaf' (.5mm, range	regular, scalloped and curvilinear	all forms parallel to foliation
erstitial nges, .01mm	irregular	random or parallel to foliation
mm); cluster .5mm); vermi- x, pl, ol lved droplets ol (.05mm)	scalloped to irregular for 'Holly-Leaf' and cluster forms; rounded for droplets in primary and recrystallized pl; commonly irregular for droplets in cpx and opx	random
dral intersitial hin opx (.2mm); parallel and sub-) opx (<.1mm)	irregular to rounded	random

Dunite[6]:	a. allotriomorphic-granular	green-brown to red-brown	porphyroclasts (ovoid, s pull-apart texture; seve corroded to produce 'Hol like structure) (.5mm, r .2mm to 4mm)
	b. granoblastic (equigranular and elongate[7])	deep red-brown to black[8]	xenoblastic interstitial (various size ranges, .0 to .2mm)
Gabbro:	porphyroclastic and granoblastic	green(translu-cent)	'Holly-Leaf' (.2mm); clu interstitial (.15mm); ve cular in opx, cpx, pl, o (<.1mm) and exsolved dro in opx, cpx, pl, ol (.05
Pyroxenite:			
i. orthopyroxenite (±ol)	a. cumulate	red-brown	euhedral to anhedral int and occluded within opx rarely elongate parallel parallel to (100) opx (<
		bronze	irregular interstitial t ol, cpx (.2mm); vermicul solution from opx (.2mm
ii. websterite (±ol)	b. porphyroclastic	various shades of green-brown	'Holly-Leaf' (1.5mm); cl interstitial (.4mm); exs droplets in opx (.1mm)
iii. clinopyroxenite (±ol)	c. porphyroclastic	various shades of green-brown	clusters interstitial to opx, ol (.15mm); exsolve lets along KBB cpx (<.1m
iv. wehrilite	d. porphyroclastic	green-brown	clusters (.1mm)
Chromitites	cumulus-massive	red-brown	euhedral to anhedral cum (.2mm to massive); anhed rounded when granulated formation (<.02mm)

1. microstructure nomenclature as defined in Table 2.1.
2. color as seen in transmitted light
3. size - average grain size
4. bronze color for higher modal amounts of cpx
5. KBB is acronym for kink band boundary
6. the disposition of spinel grains with respect to olivine is such to suggest a 'cumulus' origin, and phase
7. equigranular and elongate varieties of the granoblastic texture as defined by Spry (1969); the deve in only a trace of spinel, less than 1 modal percent, left in dunite
8. when a black color, the spinel has altered to magnetite - ferritchromite

green-brown to red-brown	porphyroclasts (ovoid, showing pull-apart texture; severely corroded to produce 'Holly-Leaf' like structure) (.5mm, range .2mm to 4mm)	regular, scalloped and curvilinear	all forms parallel to folia
deep red-brown to black	xenoblastic interstitial (various size ranges, .01mm to .2mm)	irregular	random or parallel to foliat
green(translucent)	'Holly-Leaf' (.2mm); cluster interstitial (.15mm); vermicular in opx, cpx, pl, ol (<.1mm) and exsolved droplets in opx, cpx, pl, ol (.05mm)	scalloped to irregular for 'Holly-Leaf' and cluster forms; rounded for droplets in primary and recrystallized pl; commonly irregular for droplets in cpx and opx	random
red-brown	euhedral to anhedral intersitial and occluded within opx (.2mm); rarely elongate parallel and subparallel to (100) opx (<.1mm)	irregular to rounded	random
bronze	irregular interstitial to opx, ol, cpx (.2mm); vermicular exsolution from opx (.2mm x <.01mm)	irregular to curvilinear for all forms	random
various shades of green-brown	'Holly-Leaf' (1.5mm); clusters interstitial (.4mm); exsolved droplets in opx (.1mm)	scalloped to irregular for cluster	'Holly-Leaf' defines a linea other forms random
various shades of green-brown	clusters interstitial to cpx, opx, ol (.15mm); exsolved droplets along KBB cpx (<.1mm)	scalloped to irregular for cluster form; irregular to curvilinear for droplet form	random
green-brown	clusters (.1mm)	scalloped to irregular	random
red-brown	euhedral to anhedral cumulus (.2mm to massive); anhedral to rounded when granulated due to deformation (<.02mm)	regular to rounded	random

such to suggest a 'cumulus' origin, and therefore a primary crystallization

ure as defined by Spry (1969); the development of this texture results
n dunite

rritchromite

ts (ovoid, showing exture; severely produce 'Holly-Leaf' re) (.5mm, range	regular, scalloped and curvilinear	all forms parallel to foliation
interstitial ranges, .01mm	irregular	random or parallel to foliation
(.2mm); cluster (.15mm); vermi- cpx, pl, ol exsolved droplets pl, ol (.05mm)	scalloped to irregular for 'Holly-Leaf' and cluster forms; rounded for droplets in primary and recrystallized pl; commonly irregular for droplets in cpx and opx	random
nhedral intersitial within opx (.2mm); te parallel and sub- 100) opx (<.1mm)	irregular to rounded	random
erstitial to opx,); vermicular ex- opx (.2mm x <.01mm)	irregular to curvilinear for all forms	random
(1.5mm); clusters (.4mm); exsolved px (.1mm)	scalloped to irregular for cluster	'Holly-Leaf' defines a lineation; for other forms random
rstitial to cpx, m); exsolved drop- cpx (<.1mm)	scalloped to irregular for cluster form; irregular to curvilinear for droplet form	random
a)	scalloped to irregular	random
hedral cumulus ive); anhedral to granulated due to de- 2mm)	regular to rounded	random

rigin, and therefore a primary crystallization

the development of this texture results

PLATE I THE NORTHERN

KEY

- ALLOCHTHON -

8 ST. ANTHONY COMPLEX
- 8e White Hills Peridotite
- 8d Long Ridge Metagabbro
- 8c Green Ridge Amphibolite
- 8b Goose Cove Schist
- 8a Ireland Point Volcanics

7 CAPE ONION FORMATION

6 MILAN ARM MELANGE

5 MAIDEN POINT FORMATION
- 5c Gabbro
- 5b Sediments
- 5a Volcanics

4 NORTHWEST ARM FORMATION

- AUTOCHTHON -

MIDDLE ORDOVICIAN

3 GOOSE TICKLE FORMATION

2 TABLE HEAD GROUP

LEGE

GEOLOGICAL BOU

defined

THRUST FAULT

defined

VERTICAL FAULT

(F) Fossil Loca

Melange

1 of

NORTHERN PART OF THE HARE

LEGEND

GEOLOGICAL BOUNDARY

defined — approximate

THRUST FAULT

defined — approximate

VERTICAL FAULT

Ⓕ Fossil Location

Melange

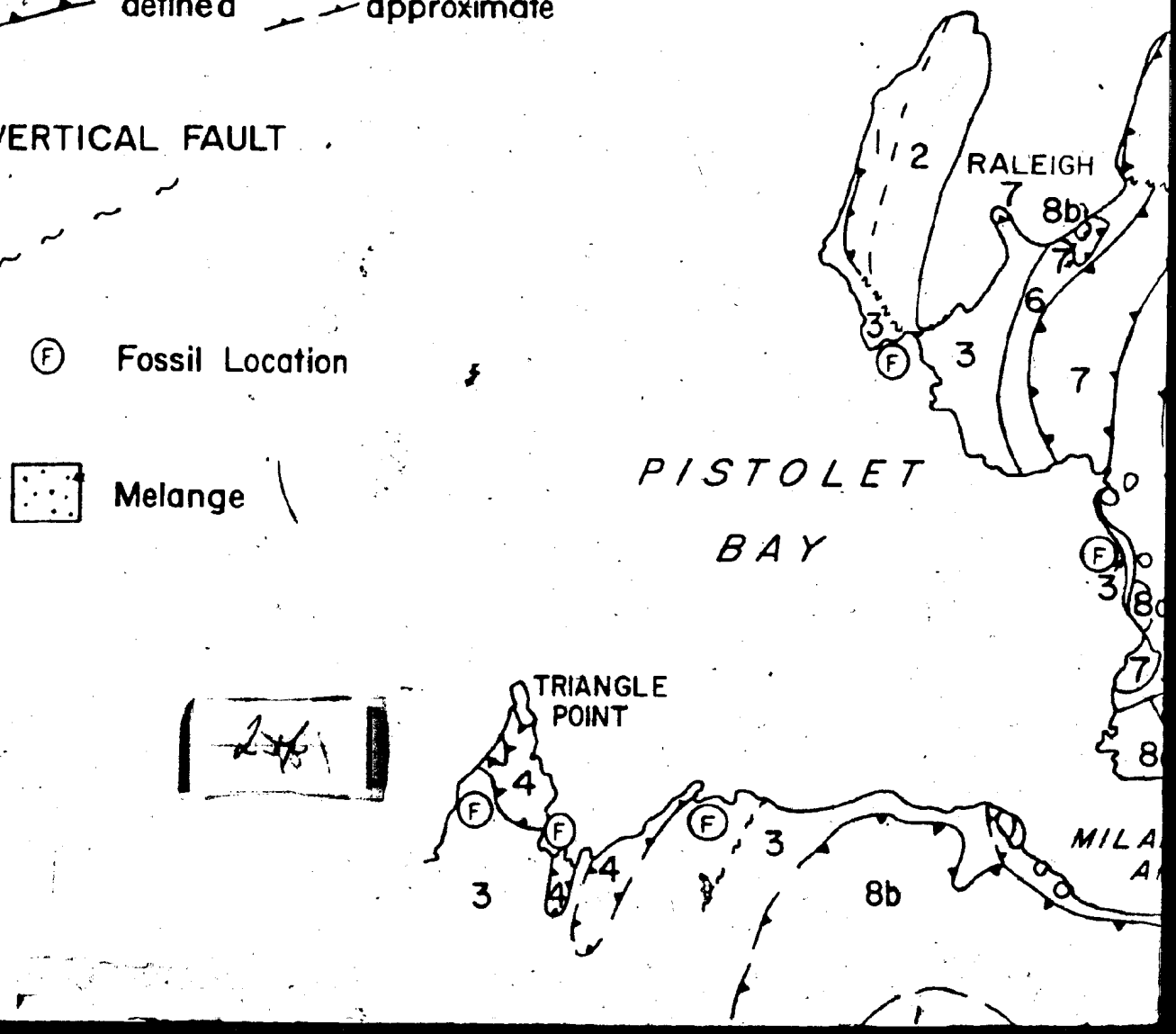

THE HARE BAY ALLOCHTHON

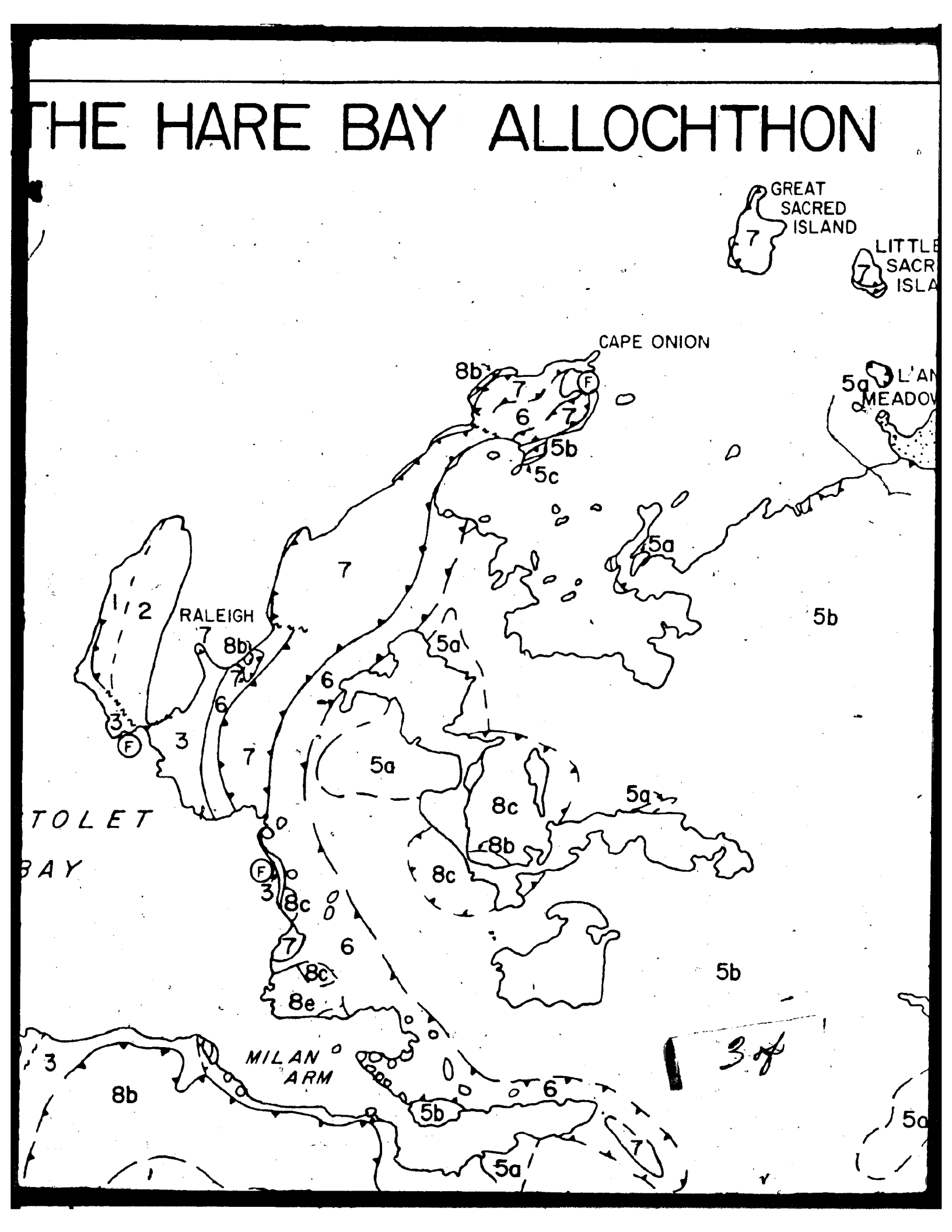

LLOCHTHON

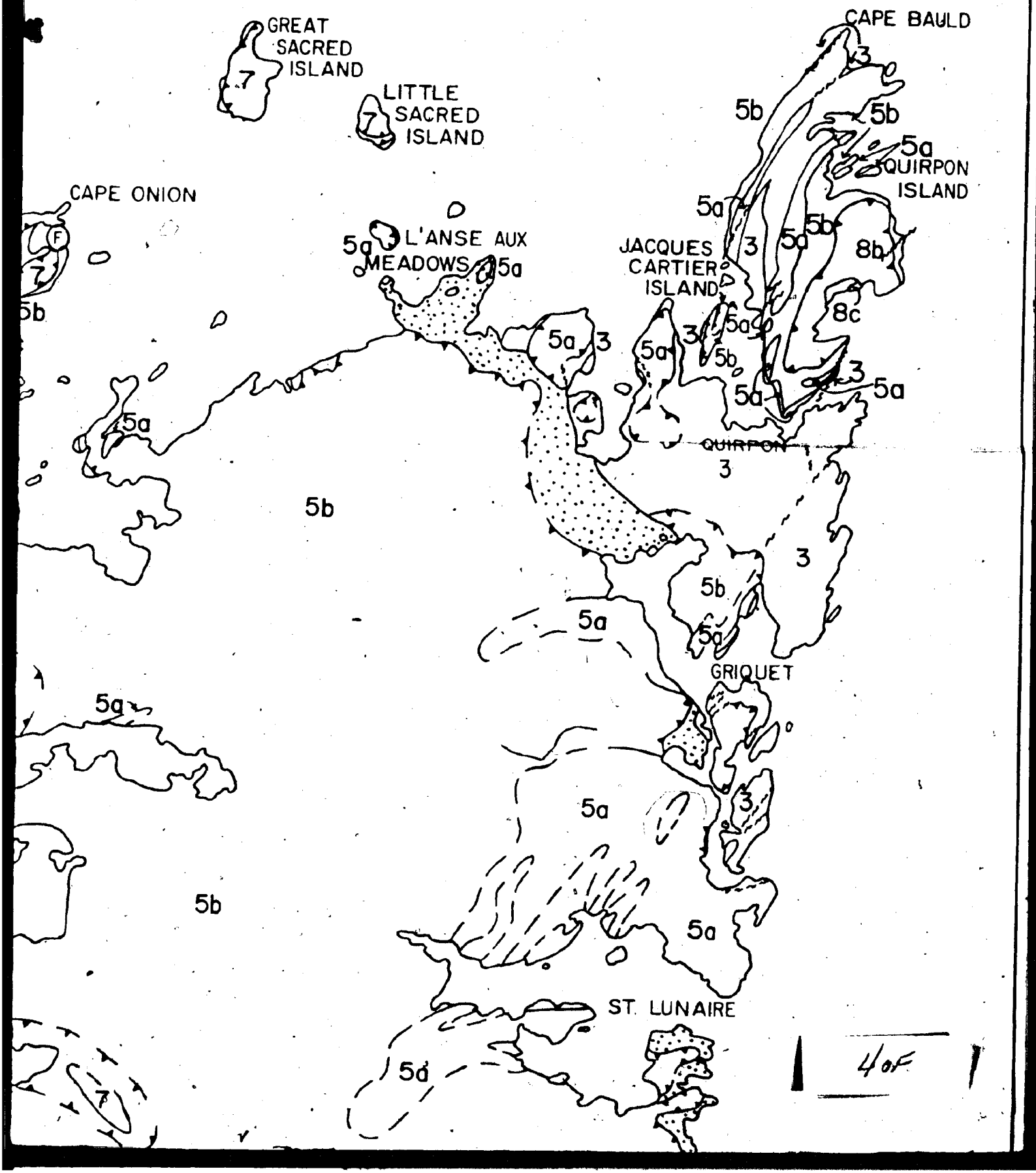
GREAT SACRED ISLAND
LITTLE SACRED ISLAND
CAPE BAULD
CAPE ONION
L'ANSE AUX MEADOWS
JACQUES CARTIER ISLAND
QUIRPON ISLAND
QUIRPON
GRIQUET
ST. LUNAIRE
5a
5b
3
7
8b
8c
4 of

3 GOOSE TICKLE FORMATION

2 TABLE HEAD GROUP

LOWER ORDOVICIAN

1 ST. GEORGE GROUP

Geology compiled from Williams *et al.* (1973), Jamieson (1979), Williams and Smyth (unpublished), DeLong (unpublished), Stouge (unpublished), Lynas (unpublished), Talkington (this work)

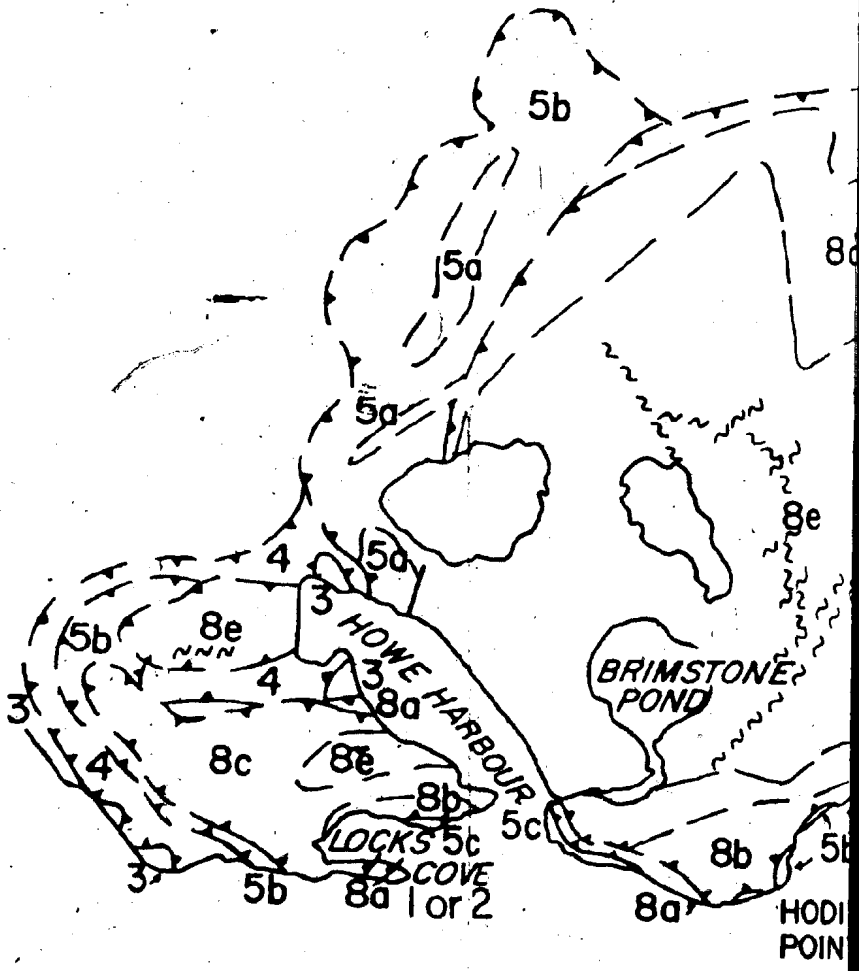

5 of

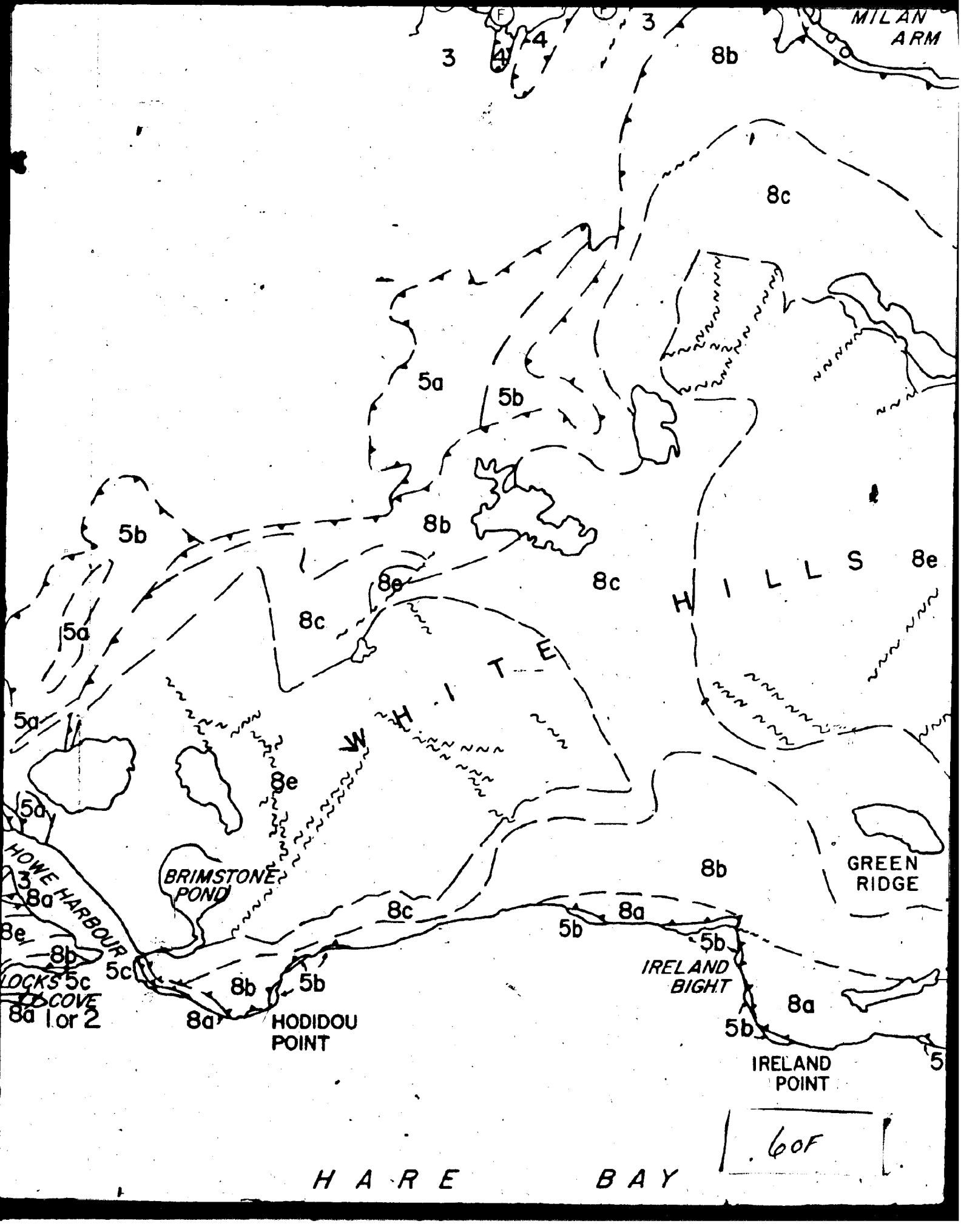
MILAN ARM
3
4
8b
8c
5a
5b
8e
HILLS
WHITE
BRIMSTONE POND
HOWE HARBOUR
LOCKS COVE
8a 1 or 2
HODIDOU POINT
GREEN RIDGE
IRELAND BIGHT
IRELAND POINT
6 OF
HARE BAY

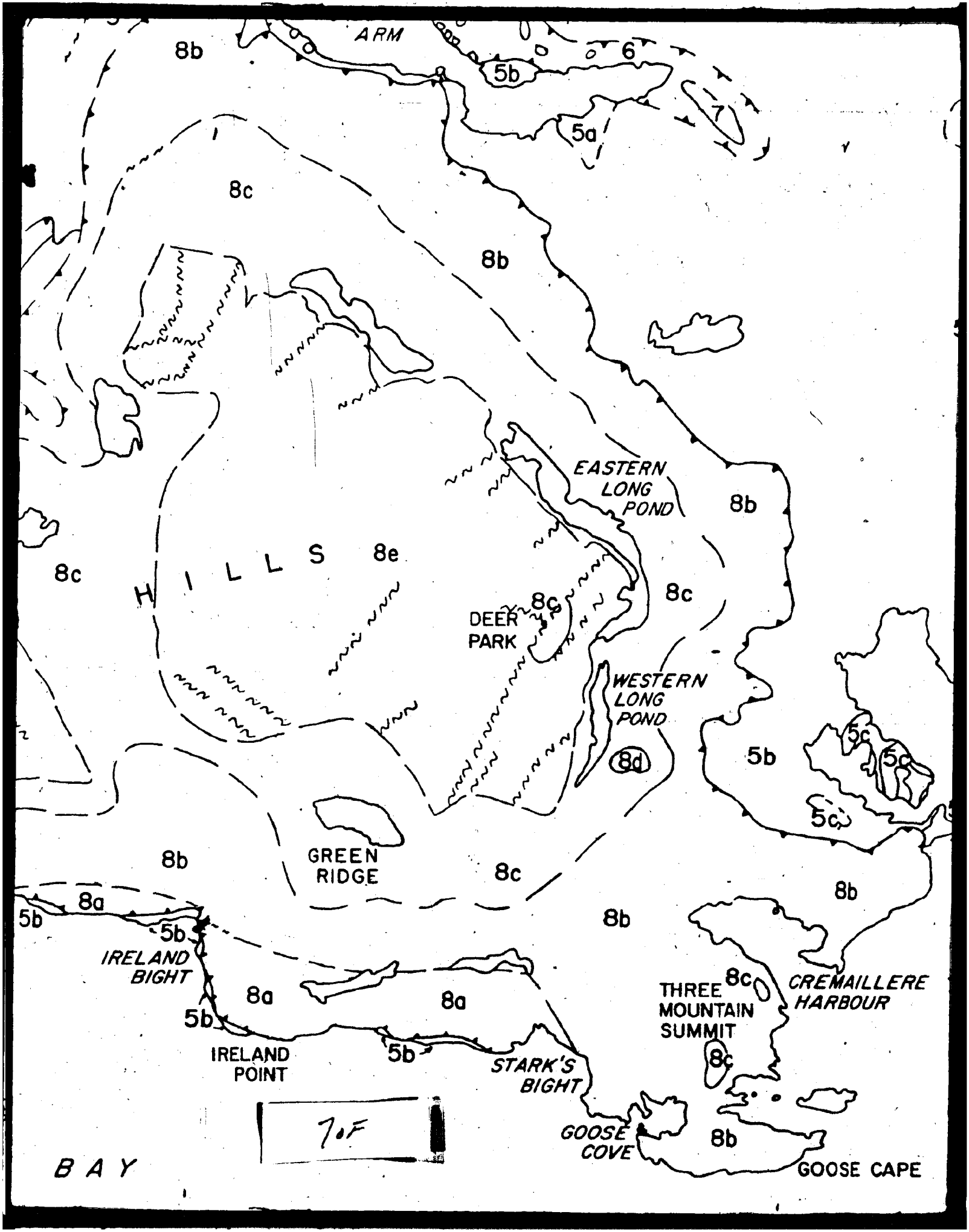
ARM
8b
5b
6
5a
8c
8b
EASTERN
LONG
POND
8b
8c
H I L L S
8e
8c
DEER
PARK
8c
8c
WESTERN
LONG
POND
8d
5b
5c
5c
5c
8b
GREEN
RIDGE
8c
8b
8a
5b
5b
8b
8b
IRELAND
BIGHT
8a
8a
8c
THREE
MOUNTAIN
SUMMIT
CREMAILLERE
HARBOUR
5b
5b
IRELAND
POINT
STARK'S
BIGHT
8c
7 of
GOOSE
COVE
8b
GOOSE CAPE
B A Y

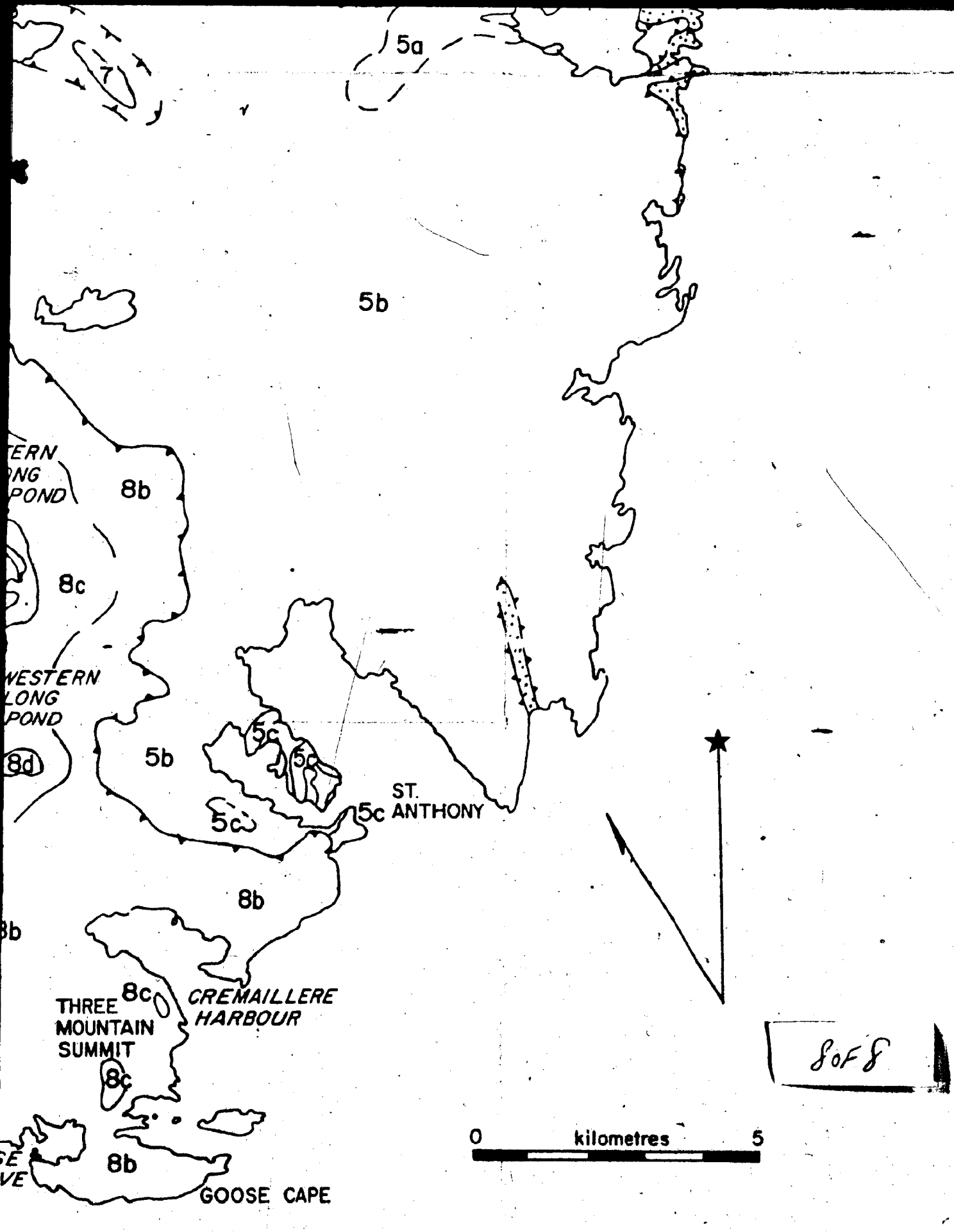
5a
5b
8b
8c
WESTERN
LONG
POND
8d
5b
5c
5c
5c
ST.
ANTHONY
8b
8b
8c
CREMAILLERE
HARBOUR
THREE
MOUNTAIN
SUMMIT
8c
8b
GOOSE CAPE
0
kilometres
5
8 OF 8

ALLOCHTHONOUS

ST. ANTHONY COMPLEX

White Hills Peridotite

4pu	undivided spinel lherzolite, harzburgite, dunite, gabbro, pyroxenite
4pd	dunite layers
4pj	jacupirangite, hornblende gneiss, syenite
4pdl	dunite lenses
4pg	region of gabbro vein exposure

Metamorphic Aureole

4a	Green Ridge Amphibolite dominantly plagioclase amphibolite
4s	Goose Cove Schist epidote - amphibolite facies

MAIDEN POINT FORMATION

3a 3b	a medium coarse greywacke and purple green slate b undivided gabbro and rhyolite

NORTHWEST ARM FORMATION

2	black shale with blocks of ultramafic rocks, finely laminated, highly contorted sandstone, sandstone - conglomerate

1 of

AUTOCHTHONOUS

LEGEND

Geological boundary(def

Thrust fault beneath

(defined, approx.)

High angle fault(define

Bedding(tops: known, un

Foliation in peridotite (

Schistosity in metamorp

Lineation(horizontal, inc
vertical)

Minor folds

a. F_1

b. F_2

c. F_3

Dike, Vein (horizontal, inc

(c-clinopyroxenite; co-
o-orthopyroxenite; w-

Mineral occurrence . .

Location of analyzed s

MINERALS: Chromite

Road (position known,

ed,

ND

Geological boundary(defined, approx., assumed)

Thrust fault beneath transported rocks
(defined, approx.)

High angle fault(defined, approx., assumed)

Bedding(tops: known, unknown, overturned)

Foliation in peridotite (horizontal , inclined, vertical) (S_1 & S_2)

Schistosity in metamorphic rocks (horizontal, inclined, vertical)

Lineation(horizontal, inclined, inclined but plunge unknown, vertical)

Minor folds

a. F_1

b. F_2

c. F_3

Dike, Vein (horizontal, inclined, vertical, unknown)

(c - clinopyroxenite; co - wehrlite; d - dunite; g - gabbro,
o - orthopyroxenite; w - websterite)

Mineral occurrence

Location of analyzed sample

MINERALS: Chromite

Road (position known, approximate)

(S$_1$ & S$_2$)

d, vertical)

unknown,

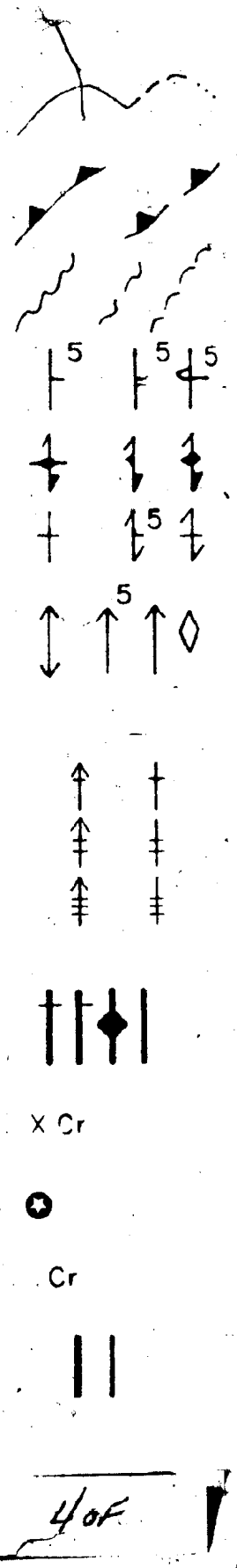

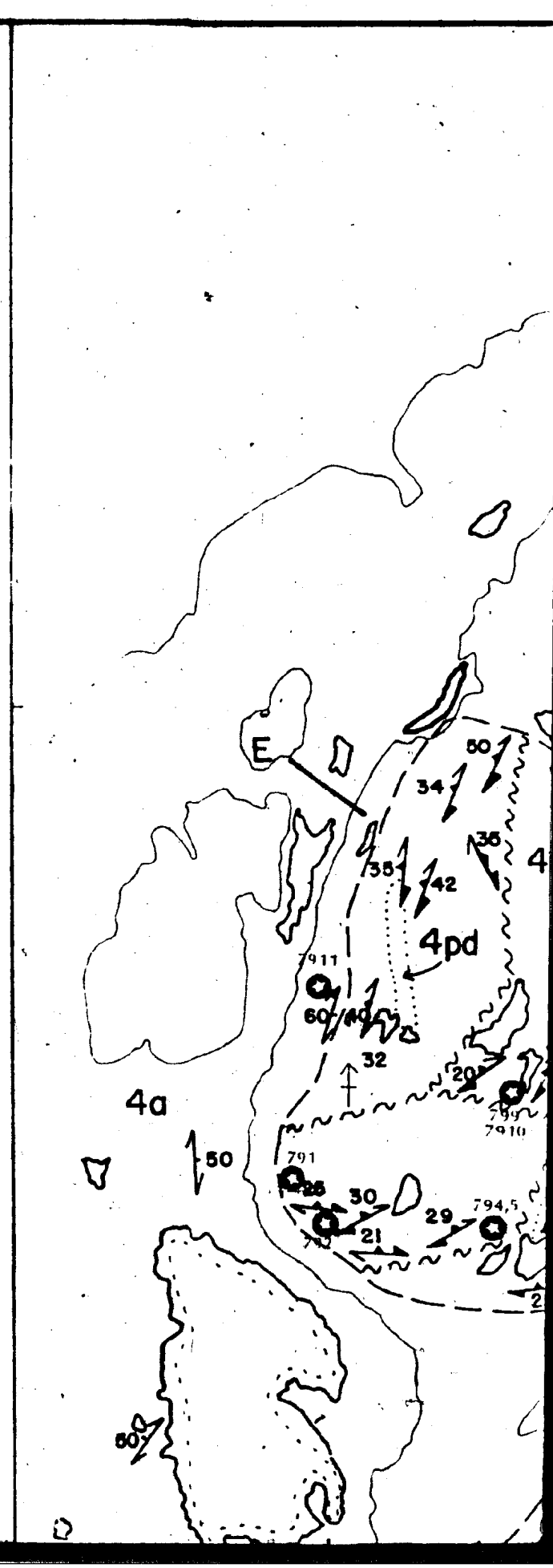

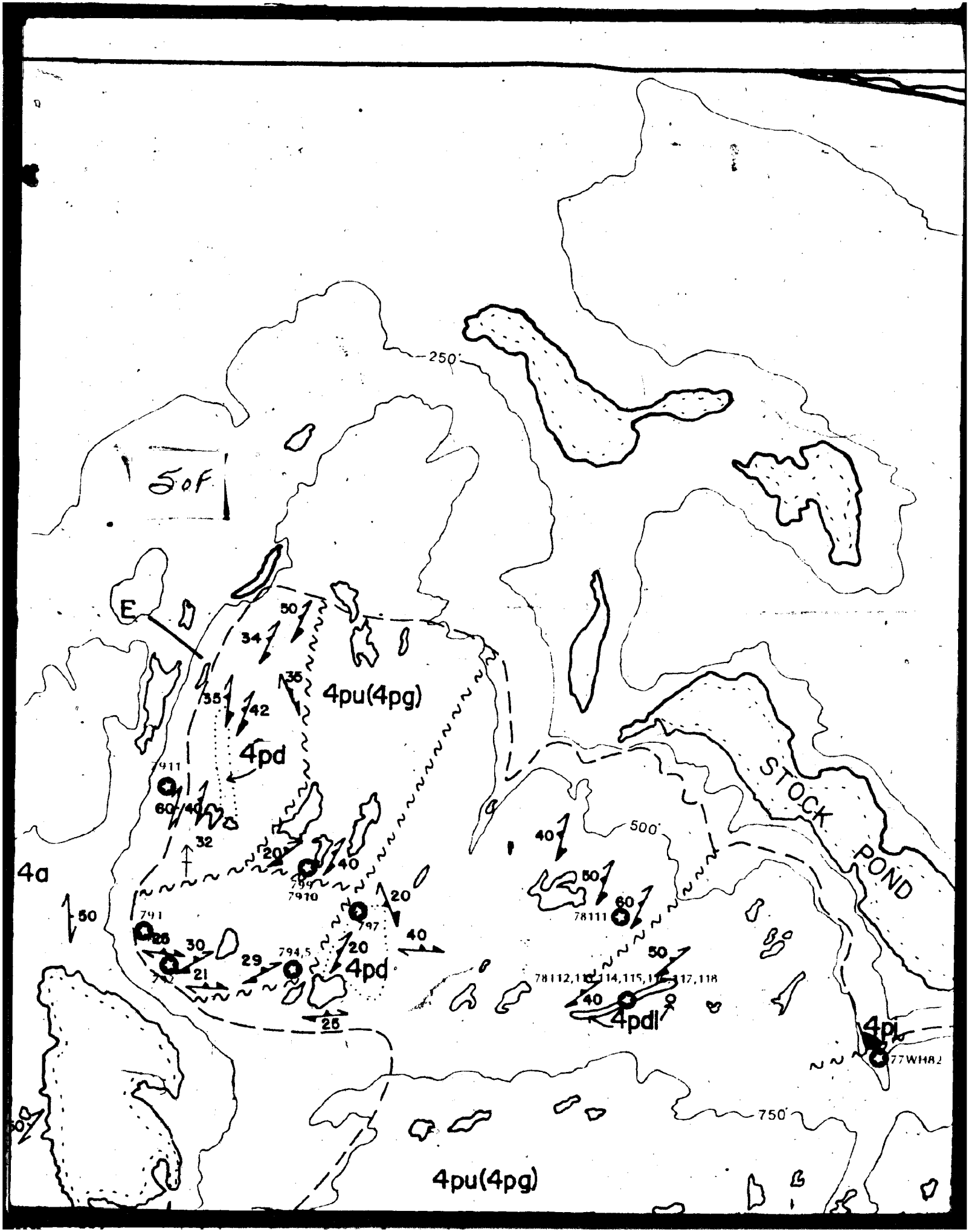

250
5 of
E
50
34
35
35
42
4pu(4pg)
4pd
7911
60
40
32
20
40
799
7910
4a
50
791
25
30
29
794,5
21
20
797
20
40
4pd
25
40
50
60
78111
50
78112,113,114,115,116,117,118
40
4pdl
500
STOCK POND
4pj
77WH82
750
4pu(4pg)

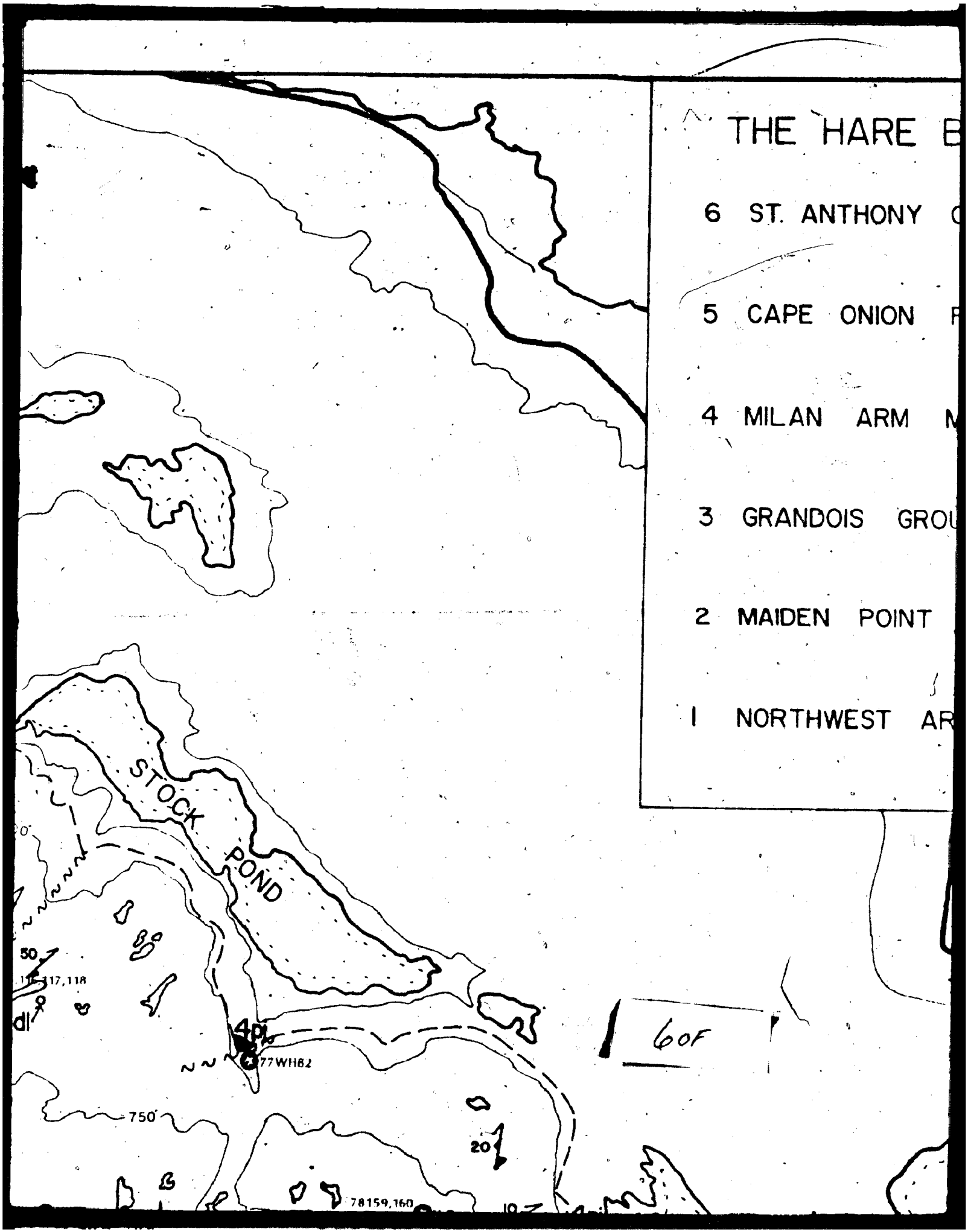
THE HARE B
6 ST. ANTHONY
5 CAPE ONION
4 MILAN ARM
3 GRANDOIS GROU
2 MAIDEN POINT
1 NORTHWEST AR
STOCK POND
50
117,118
4pl
77WH82
750
20
78159,160
10
6 OF

THE HARE BAY ALLOCHTHON

6 ST. ANTHONY COMPLEX

5 CAPE ONION FORMATION

4 MILAN ARM MELANGE

3 GRANDOIS GROUP

2 MAIDEN POINT FORMATION

1 NORTHWEST ARM FORMATION

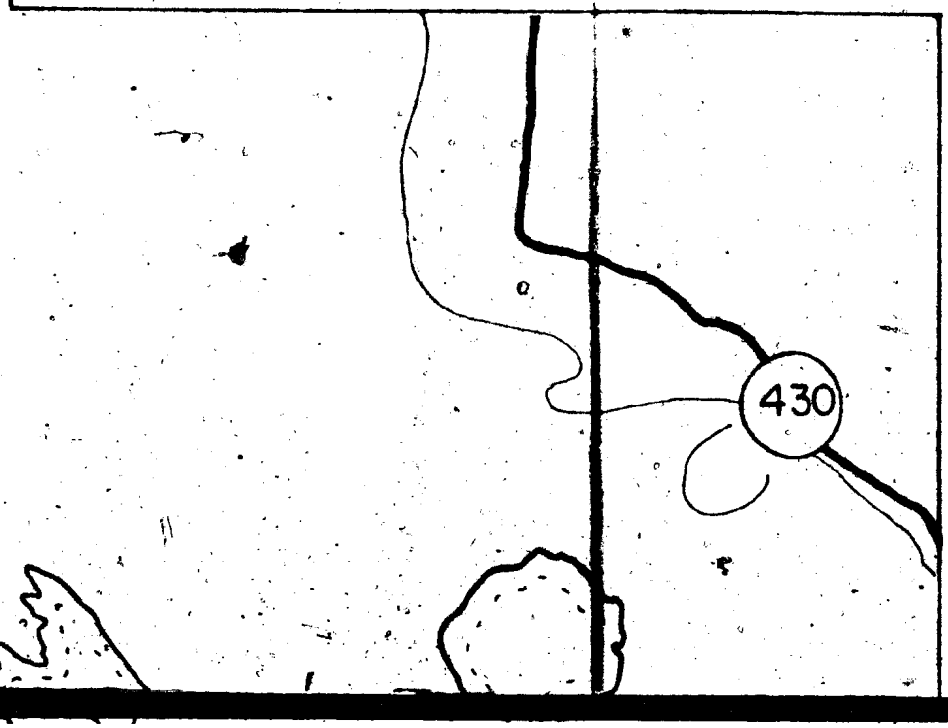

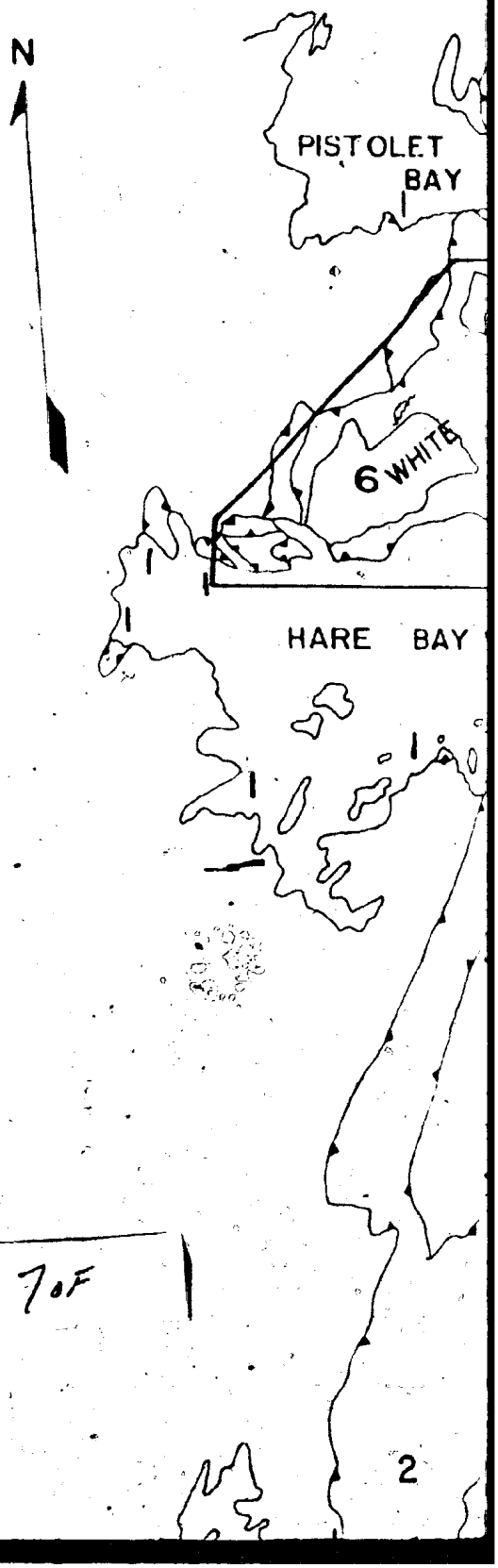

ALLOCHTHON

X

TION

E

TION

RMATION

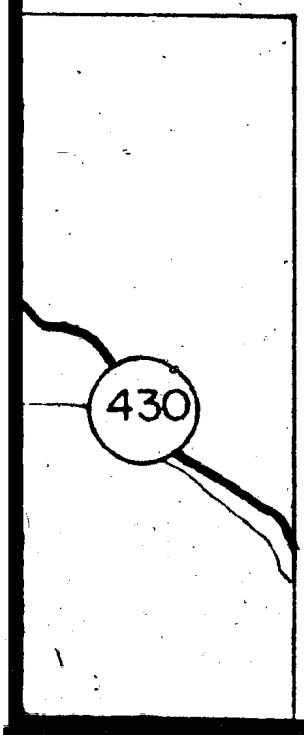

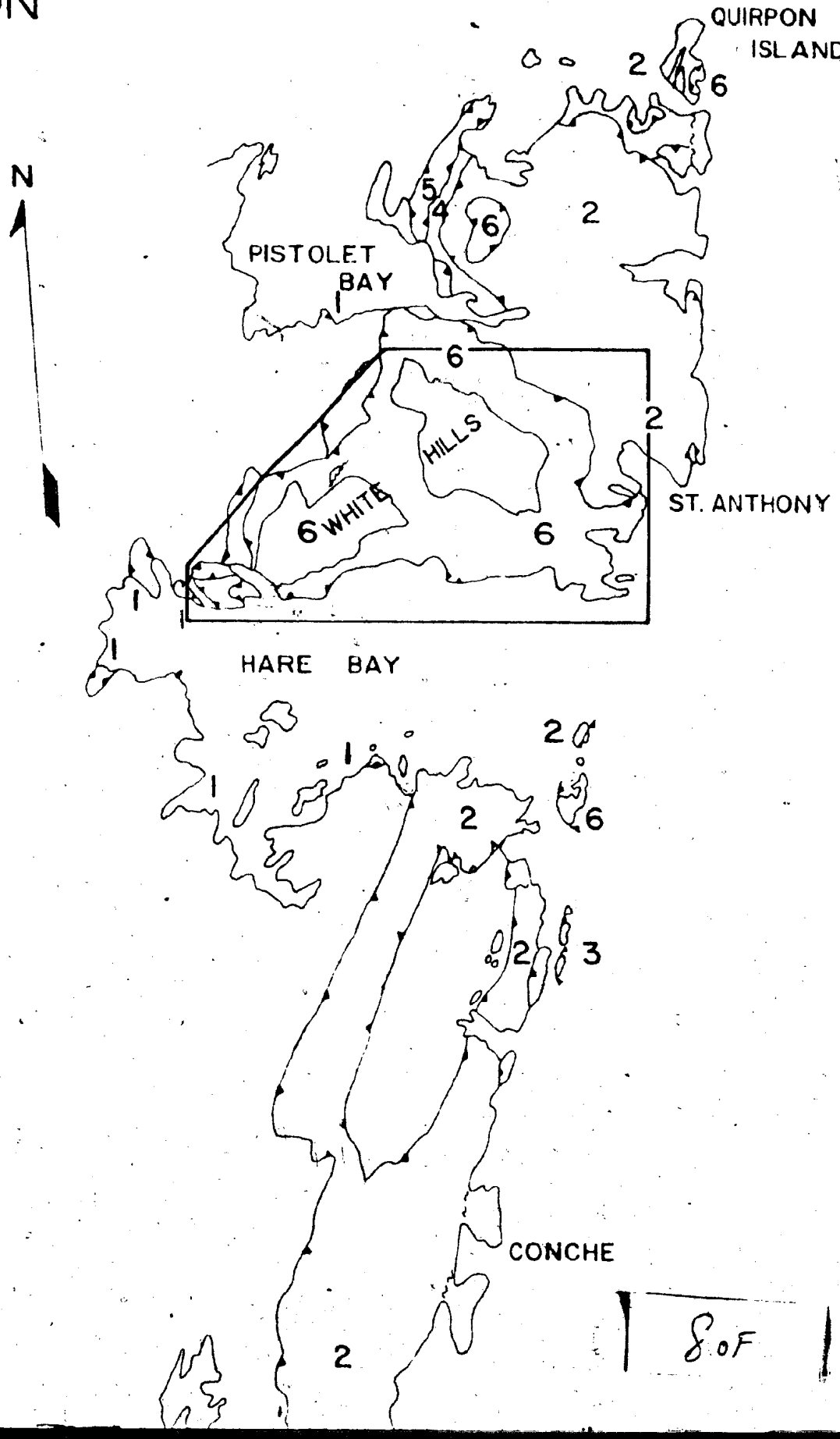

NORTHWEST ARM FORMATION

2 black shale with blocks of ultramafic rocks, finely laminated, highly contorted sandstone, sandstone - conglomerate

AUTOCHTHONOUS

GOOSE TICKLE FORMATION

1 finely laminated black to grey sandstone

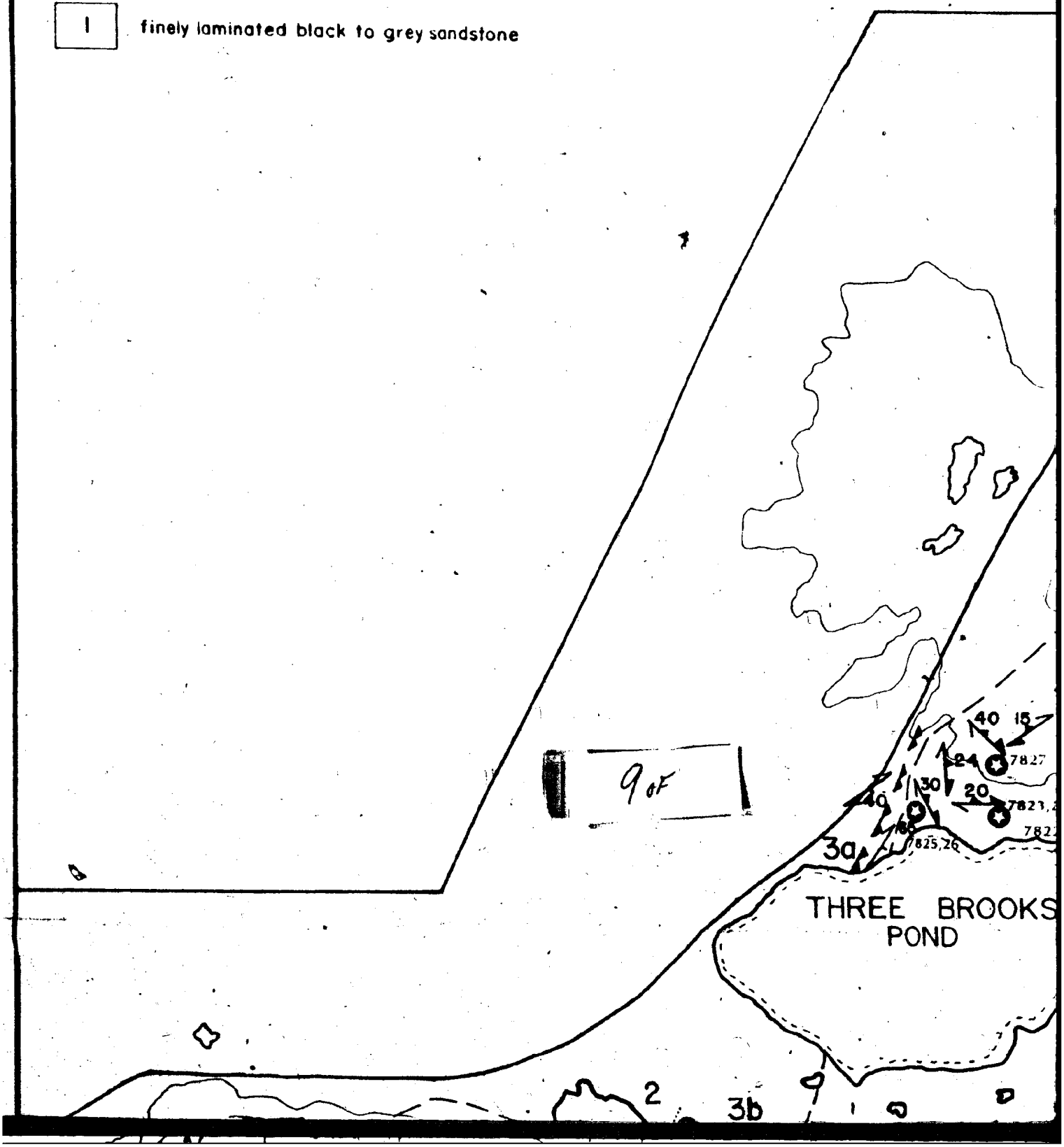

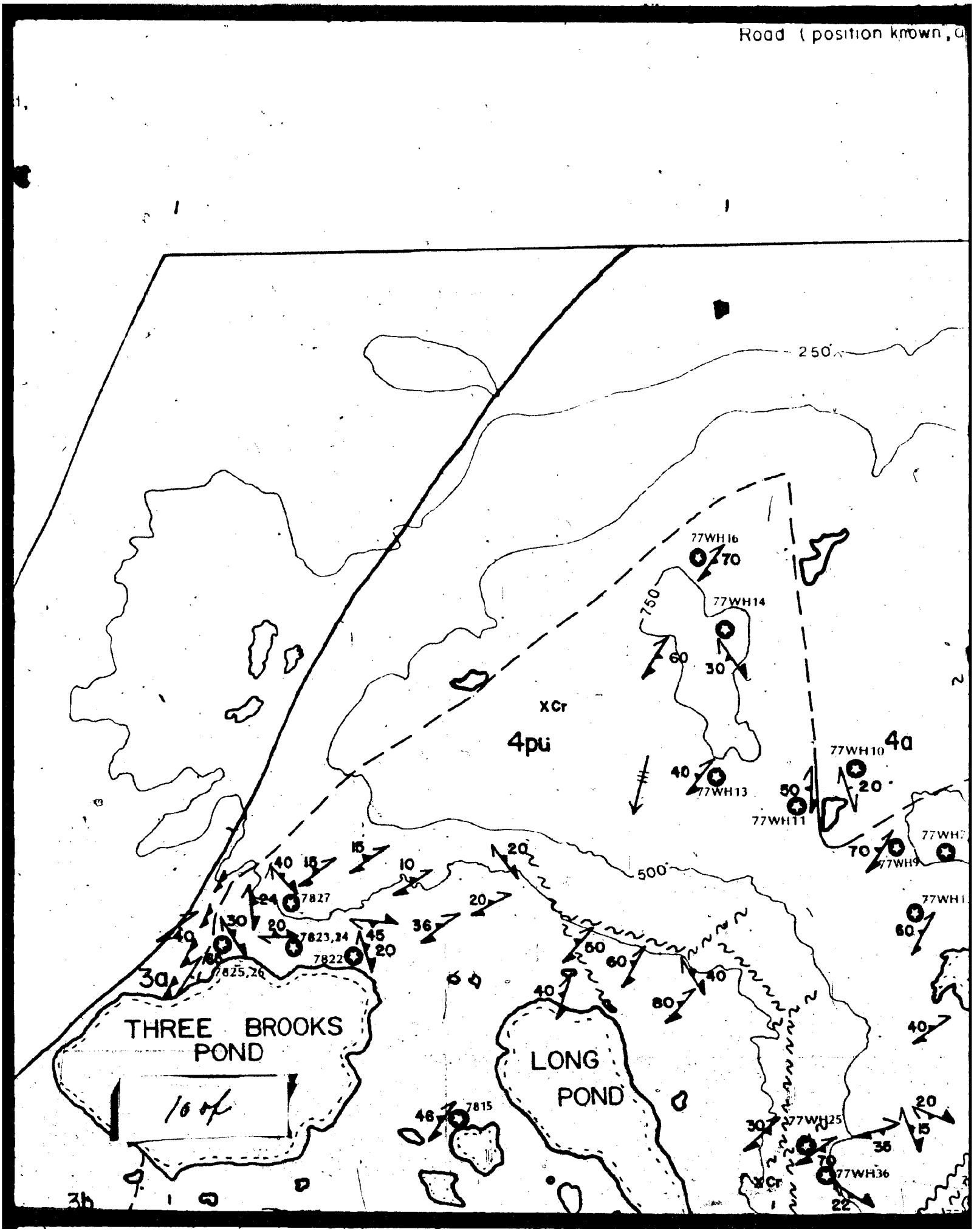
Road (position known, a
250
750
500
77WH16
70
77WH14
60
30
XCr
4pu
4a
77WH10
20
40
77WH13
50
77WH11
70
77WH9
77WH1
60
40
15
15
10
20
7827
24
20
30
20
7823,24
45
36
20
7822
7825,26
3a
50
60
40
80
40
THREE BROOKS POND
LONG POND
46
7815
30
77WH25
20
15
35
70
77WH36
XCr
22
3b

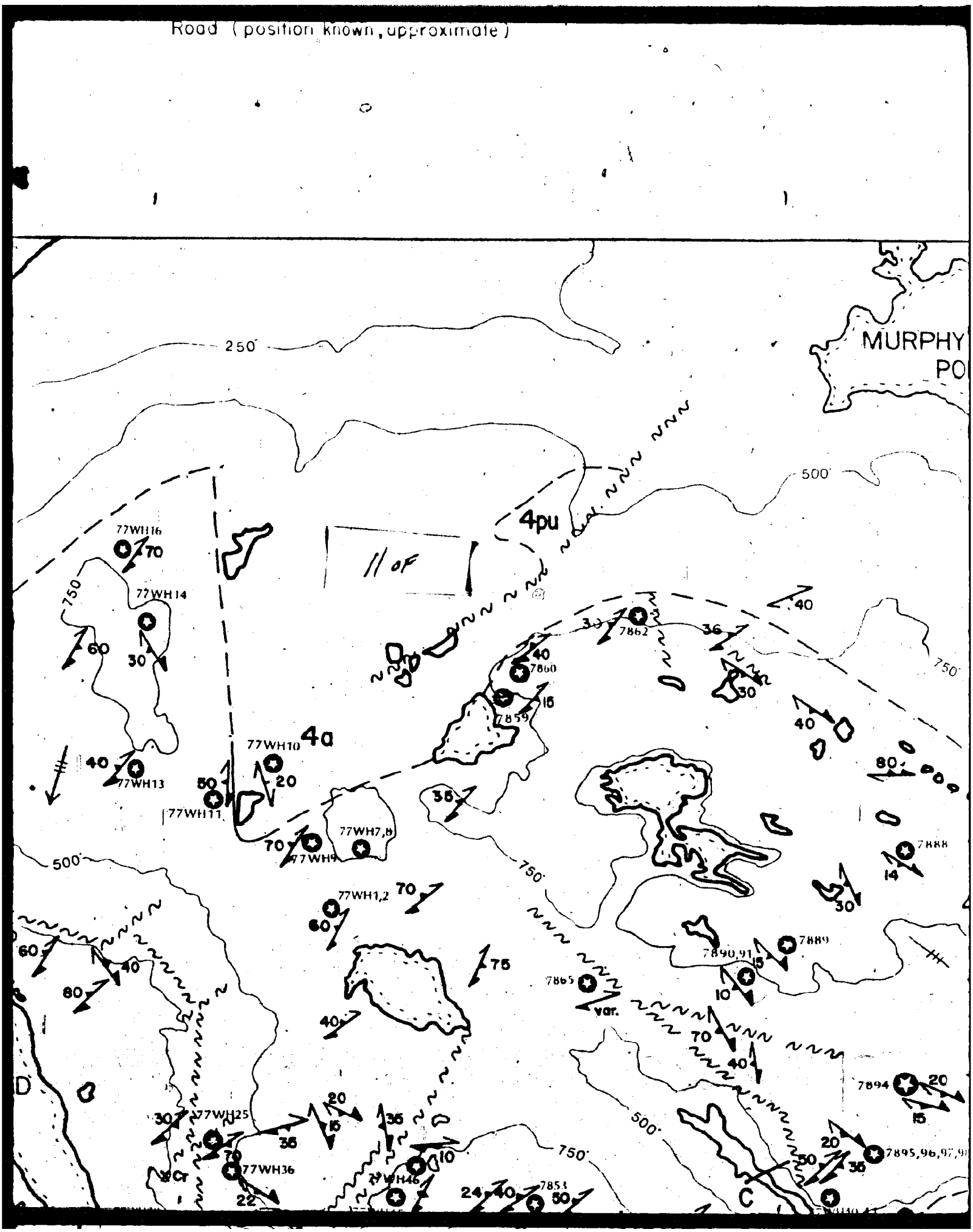
Road (position known, approximate)
MURPHY
PO
250
500
750
4pu
11 OF
4a
77WH16
77WH14
77WH13
77WH10
77WH11
77WH7,8
77WH9
77WH1,2
77WH25
77WH36
77WH46
7862
7860
7859
7888
7889
7890,91
7865
var.
7894
7895,96,97,98
7853
D
C

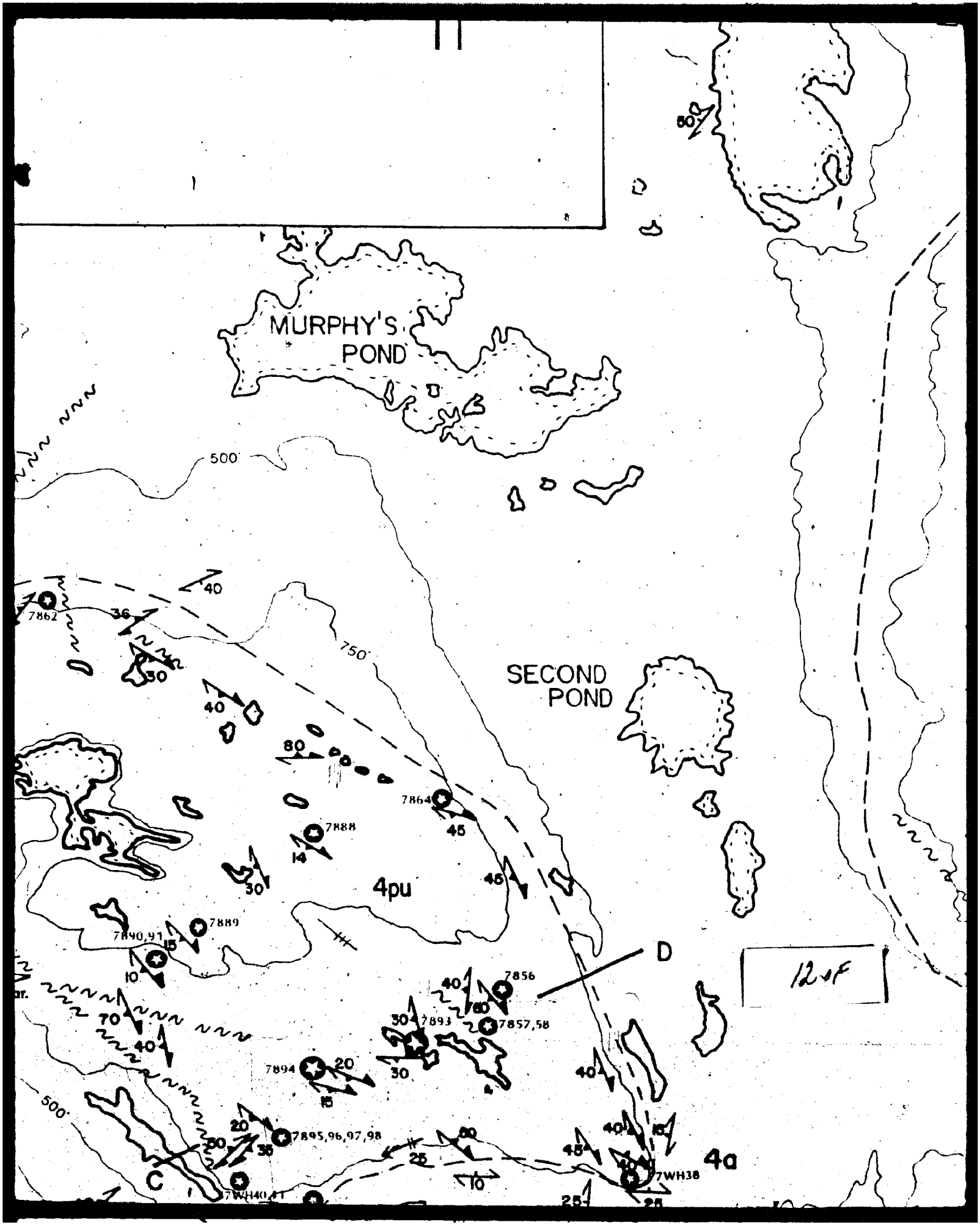
MURPHY'S POND
SECOND POND
500'
750'
7862
7864
7888
7889
7890,91
7856
7893
7857,58
7894
7895,96,97,98
7WH40,41
7WH38
4pu
4a
C
D
12 of F

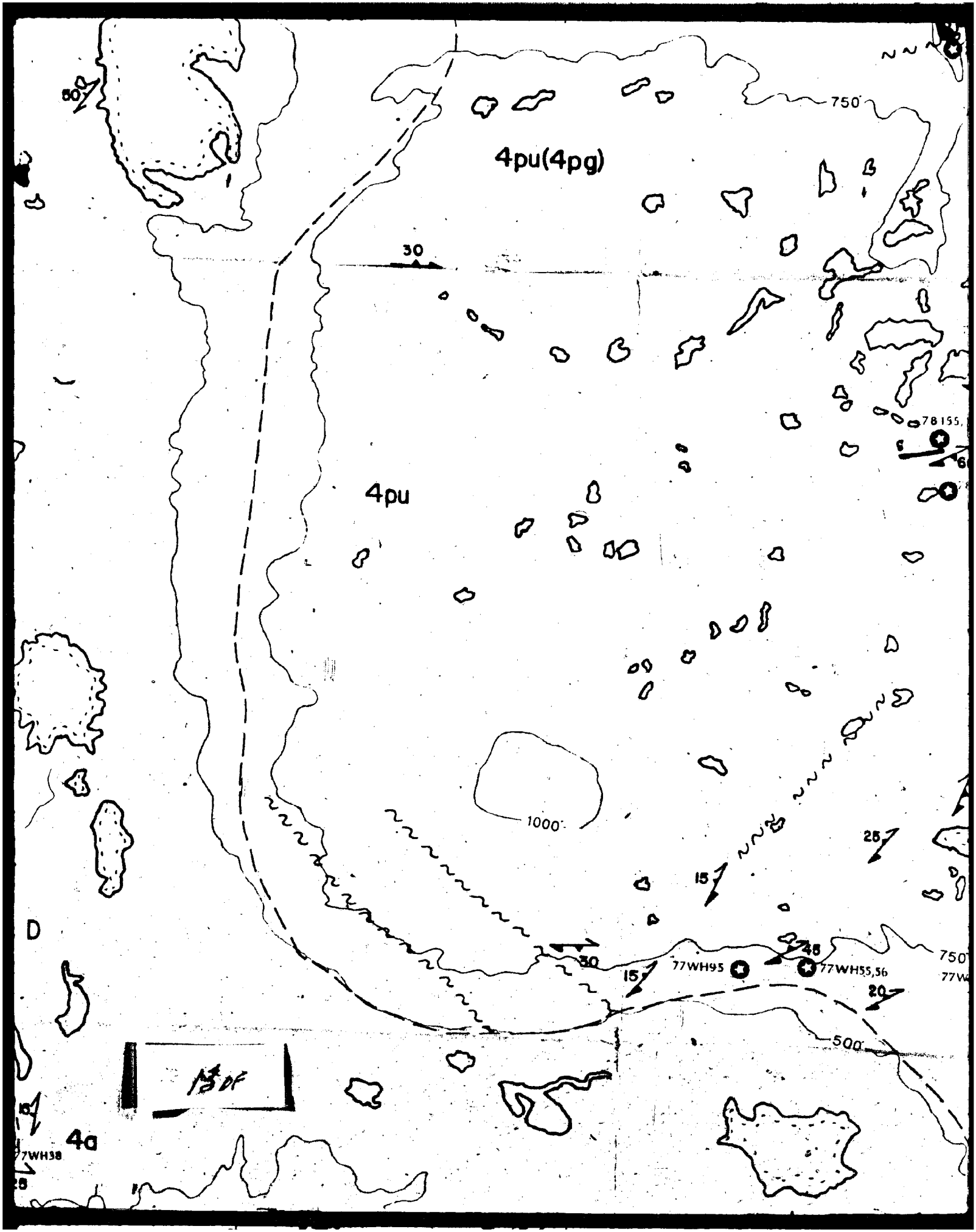

4pu(4pg)
4pu
750
30
1000
500
78155,
77WH95
77WH55,56
77WH38
4a
D

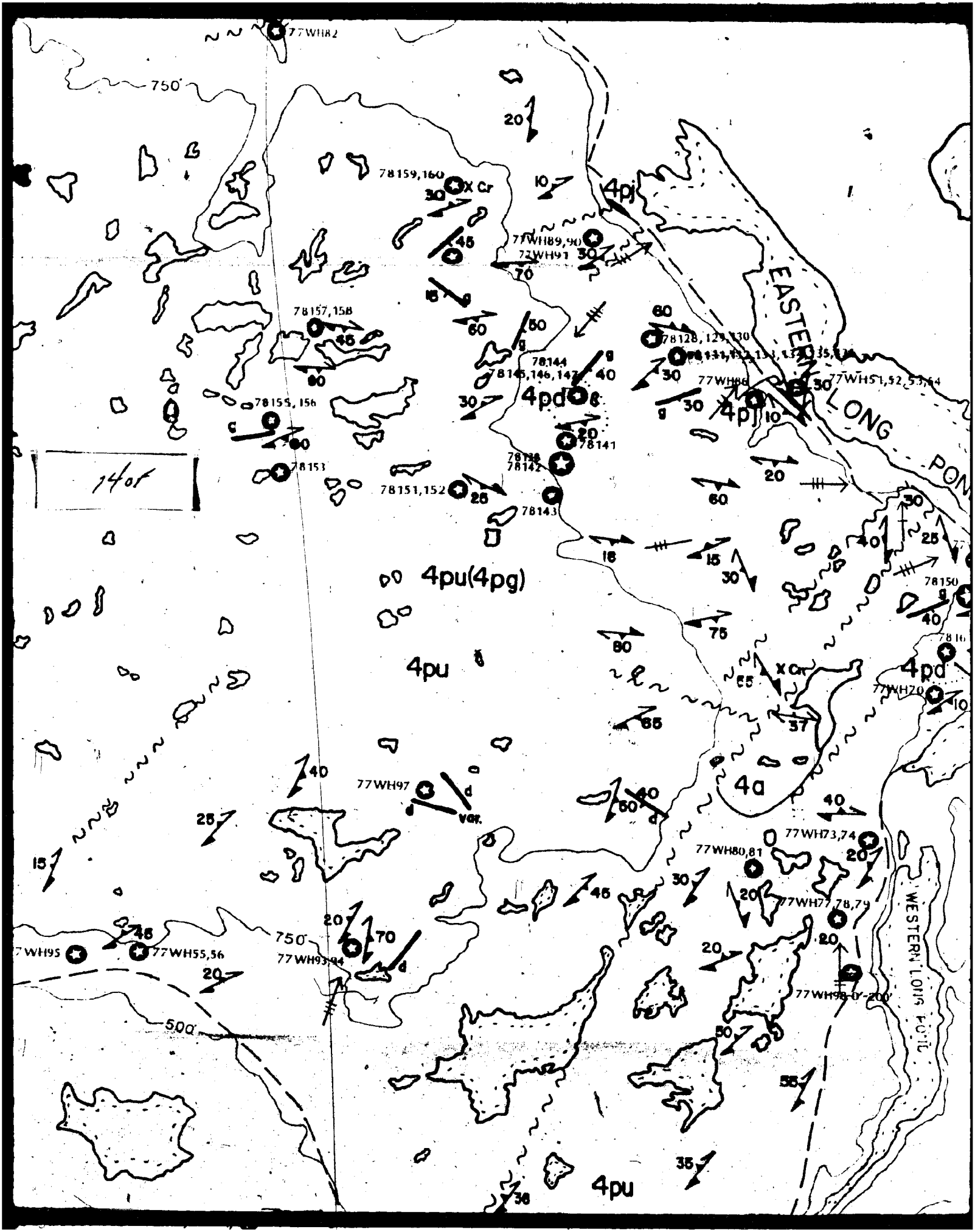

77WH82
750
78159,160
X Cr
4pj
77WH89,90
77WH91
78157,158
78128,129,130
78144
78145,146,147
4pd
77WH86
77WH51,52,53,54
78155,156
78141
78142
78153
78151,152
78143
14 of
4pu(4pg)
4pu
78150
78161
77WH70
4a
77WH97
var.
77WH73,74
77WH80,81
77WH77,78,79
77WH95
77WH55,56
77WH93,94
500
77WH98-0'-200'
EASTERN LONG POND
WESTERN LONG POND

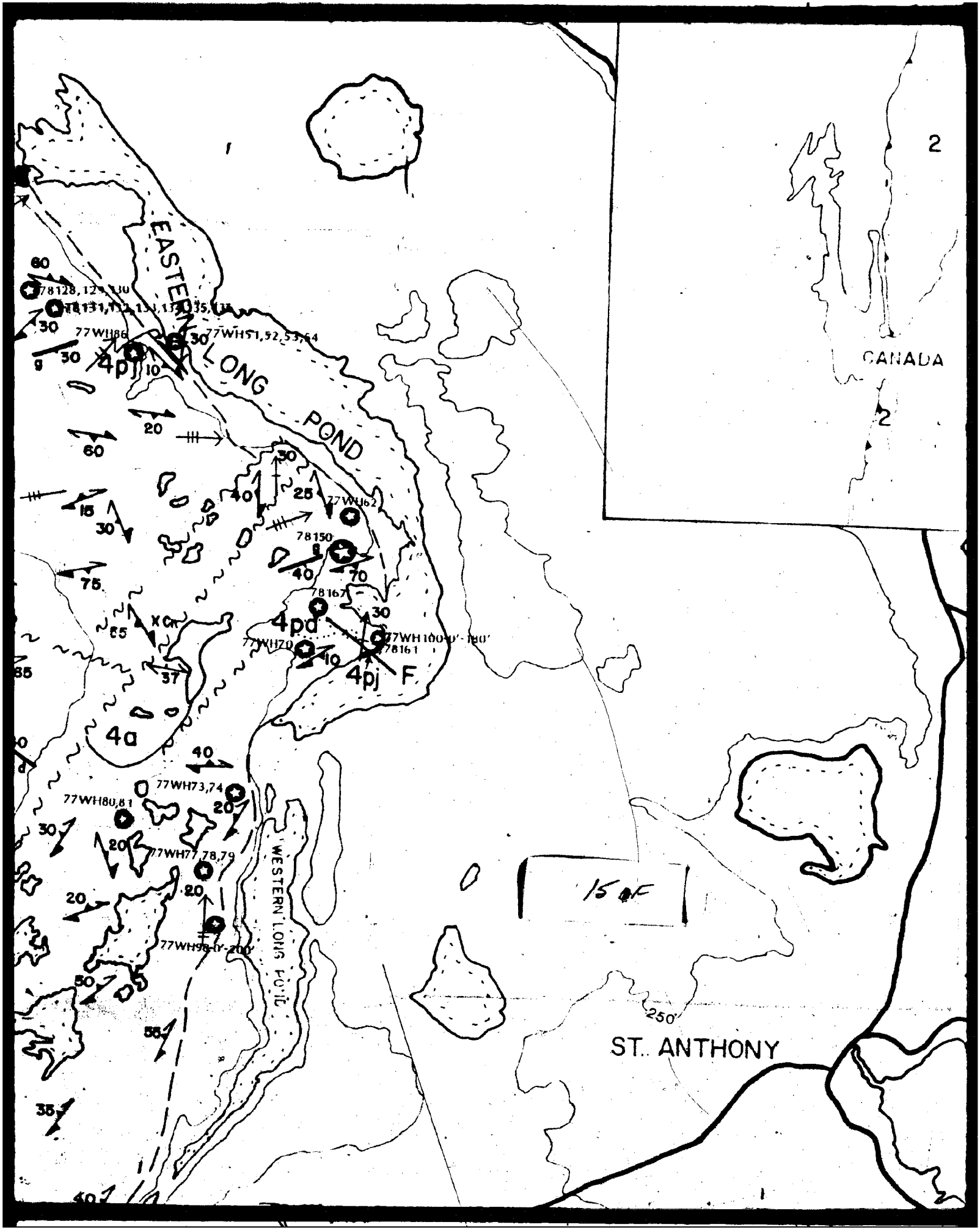
EASTERN LONG POND
WESTERN LONG POND
ST. ANTHONY
CANADA
4pj
4pd
4a
F
77WH86
77WH51,52,53,54
77WH62
78150
78167
77WH70
77WH100-0'-180'
78161
77WH73,74
77WH80,81
77WH77,78,79
77WH98-0'-200'
250'
15 OF

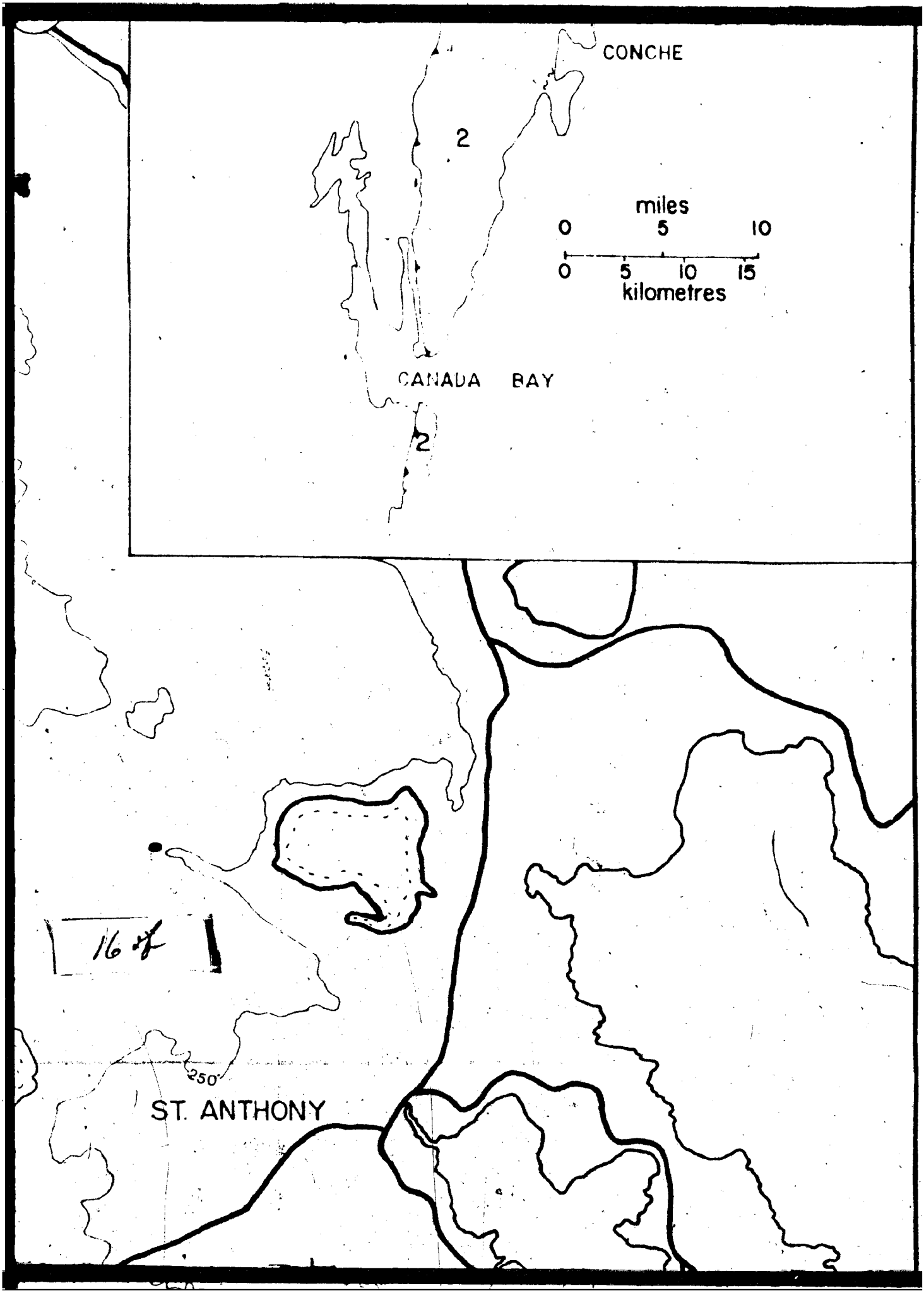
CONCHE
2
miles
0 5 10
0 5 10 15
kilometres
CANADA BAY
2
16 ft
250
ST. ANTHONY

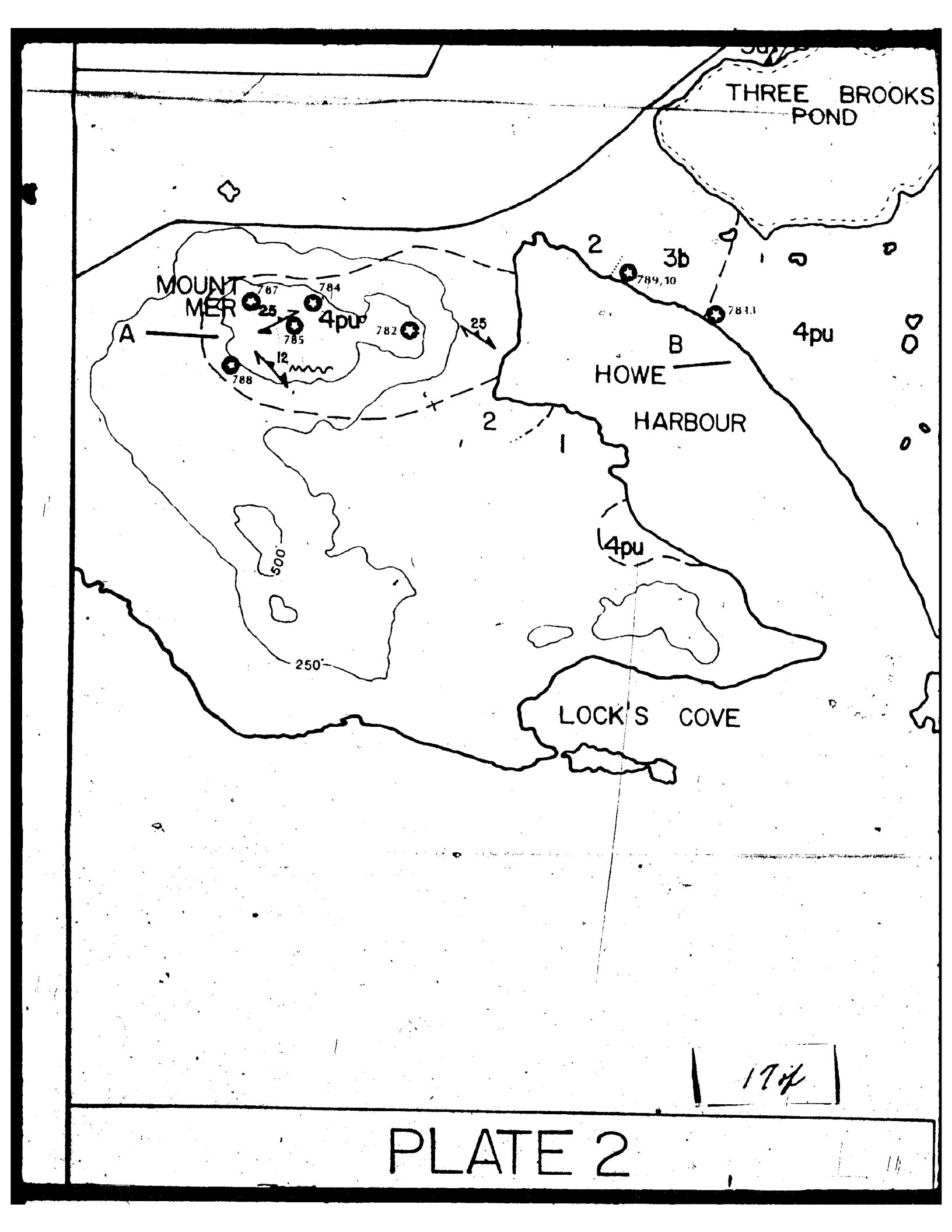
THREE BROOKS POND
MOUNT MER
787
784
25
4pu
785
782
25
A
12
788
2
3b
789,10
784.3
4pu
B
HOWE HARBOUR
2
1
4pu
500'
250'
LOCK'S COVE
17

PLATE 2

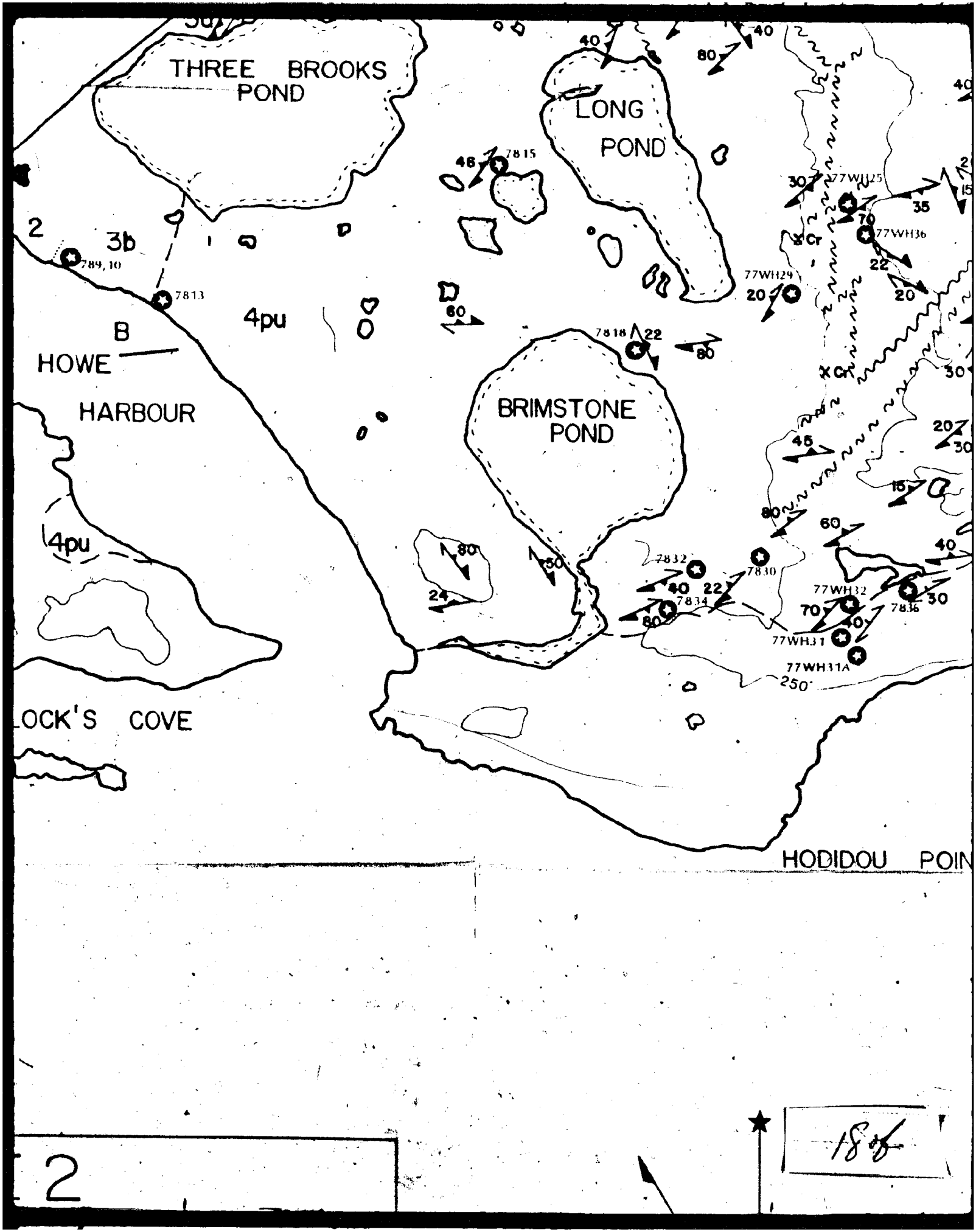
THREE BROOKS POND
LONG POND
BRIMSTONE POND
HOWE HARBOUR
LOCK'S COVE
HODIDOU POIN
2
3b
4pu
B
789,10
7813
7815
7818
7832
7830
7834
7836
77WH25
77WH36
77WH29
77WH32
77WH31
77WH31A
250
2
18 of

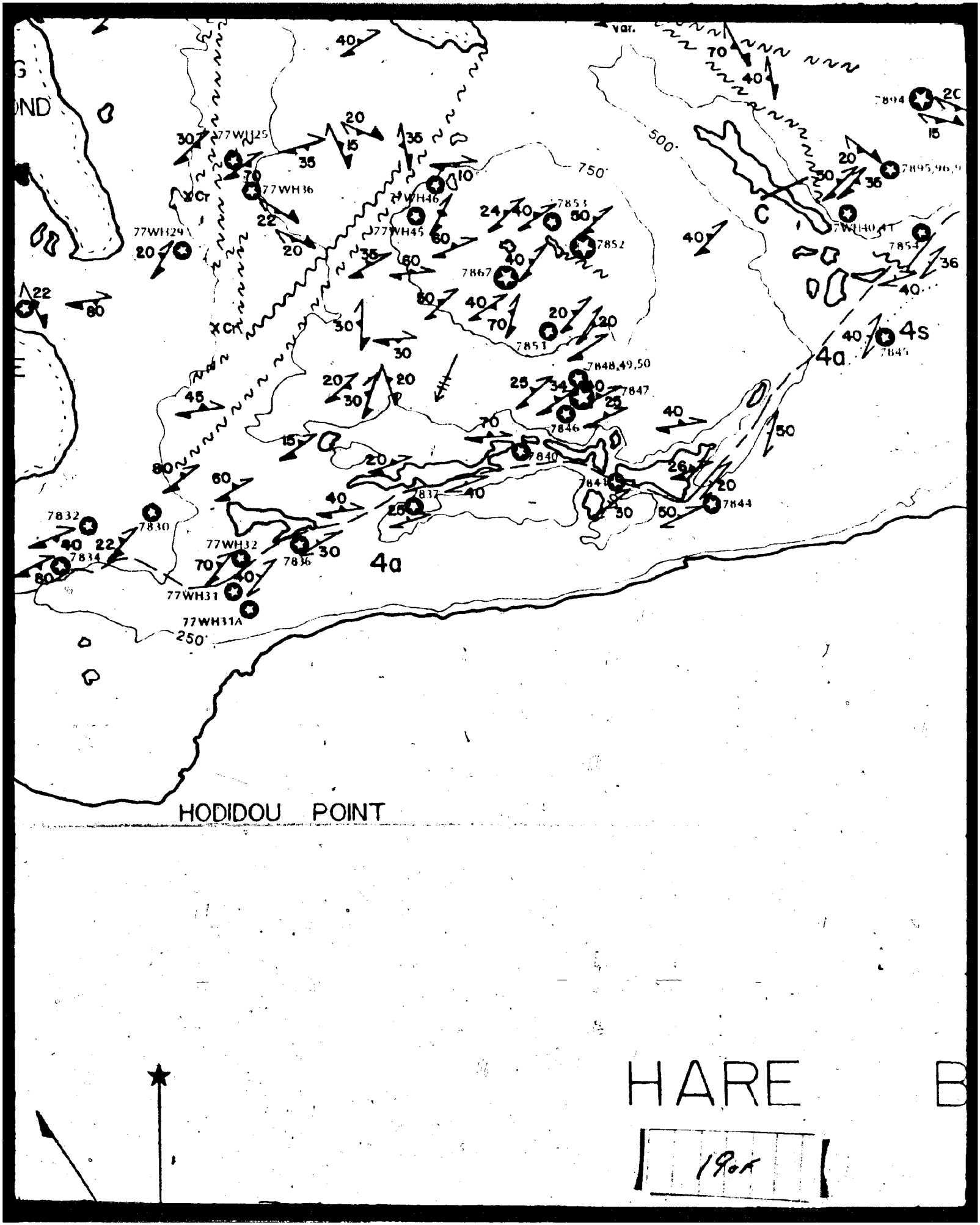

HODIDOU POINT
HARE B
77WH25
77WH36
77WH29
77WH46
77WH45
7853
7852
7867
7851
7848,49,50
7847
7846
7840
7841
7844
7837
7836
77WH32
77WH31
77WH31A
7832
7830
7834
7894
7895,96,9
7854
7845
4a
4s
C
750'
500'
250'

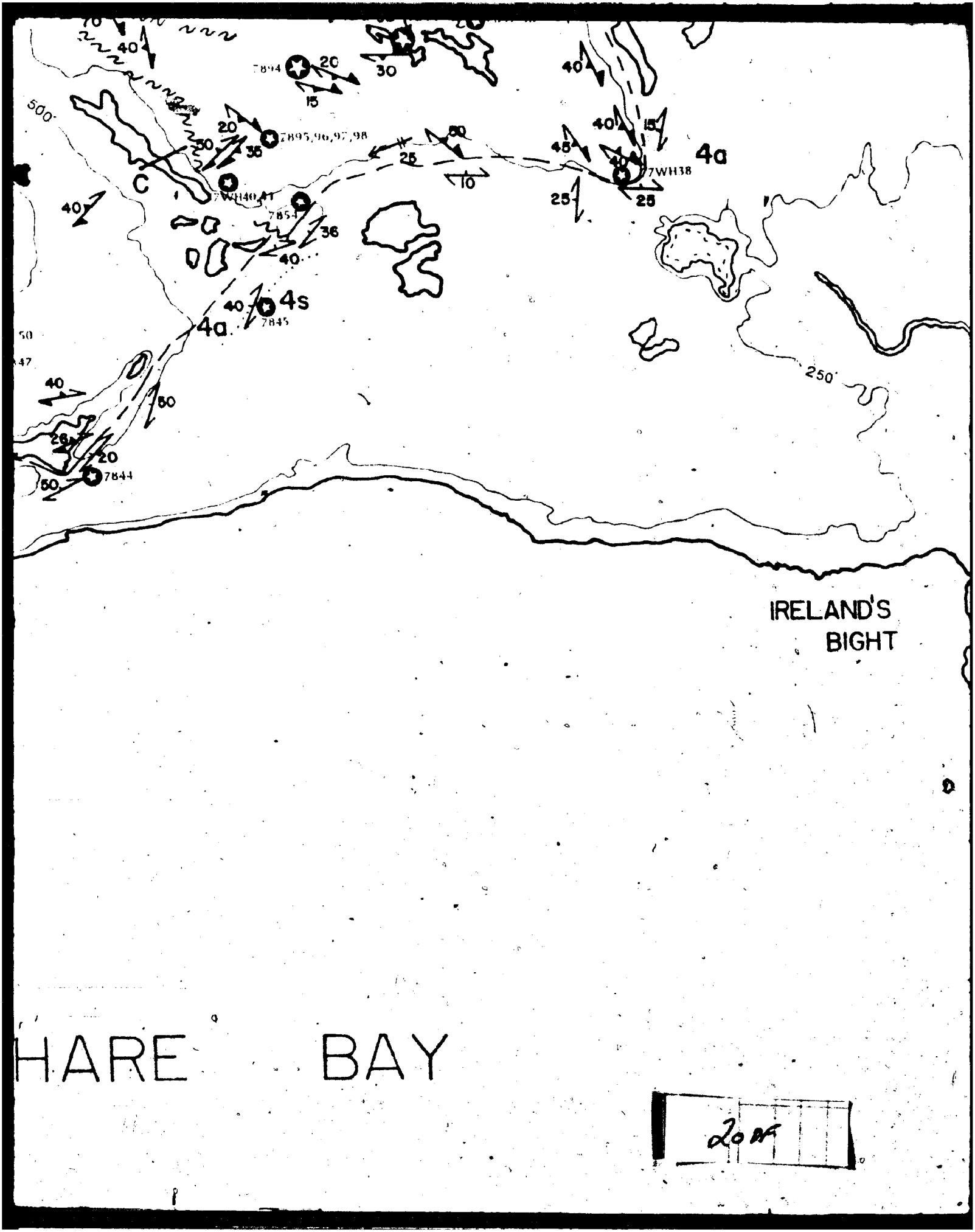

7894
7895,96,97,98
7WH40,41
7854
7845
7844
7WH38
4a
4s
C
500
250
IRELAND'S
BIGHT
HARE BAY
20 DF

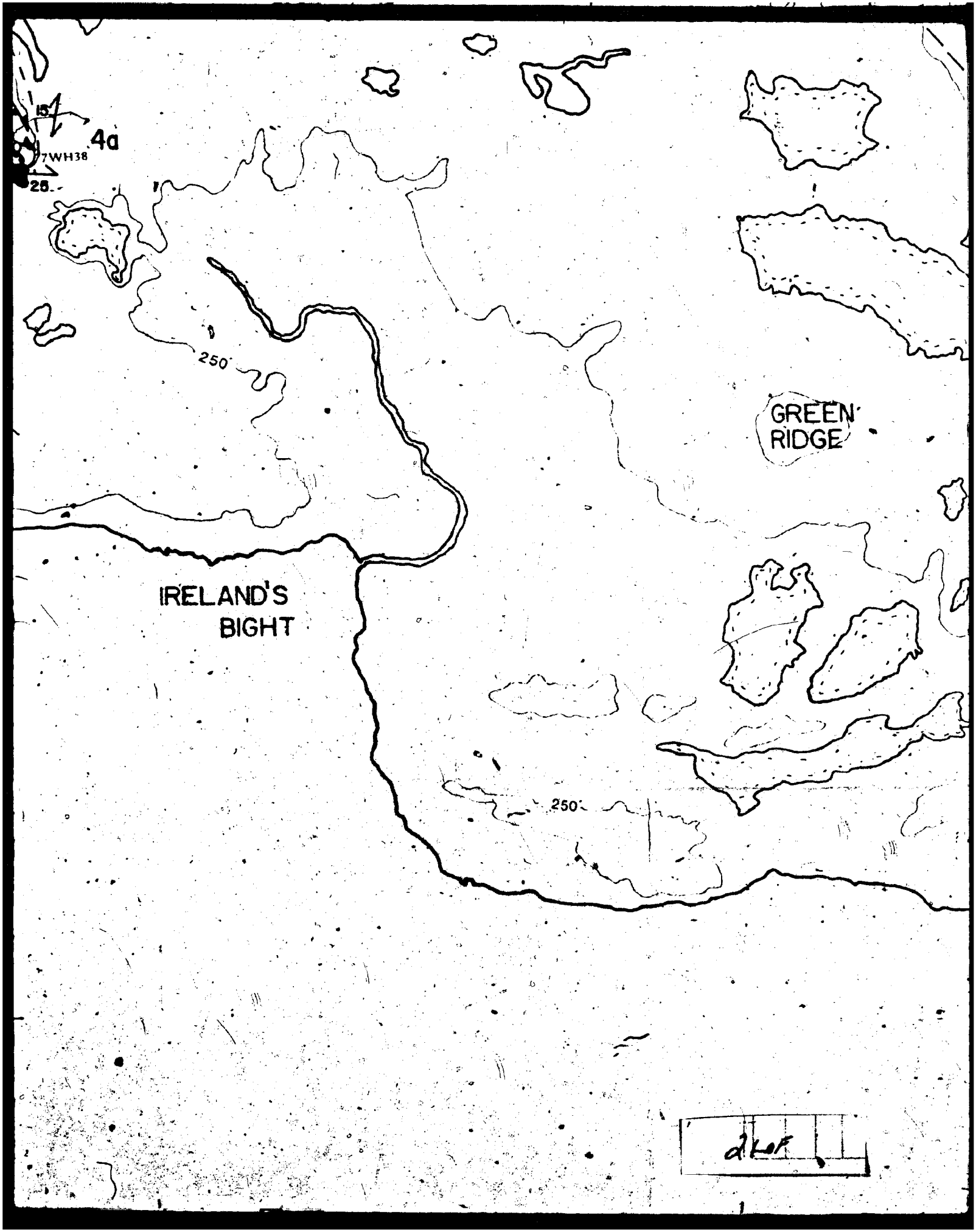
15
4a
7WH38
25
250
GREEN
RIDGE
IRELAND'S
BIGHT
250
2 KM

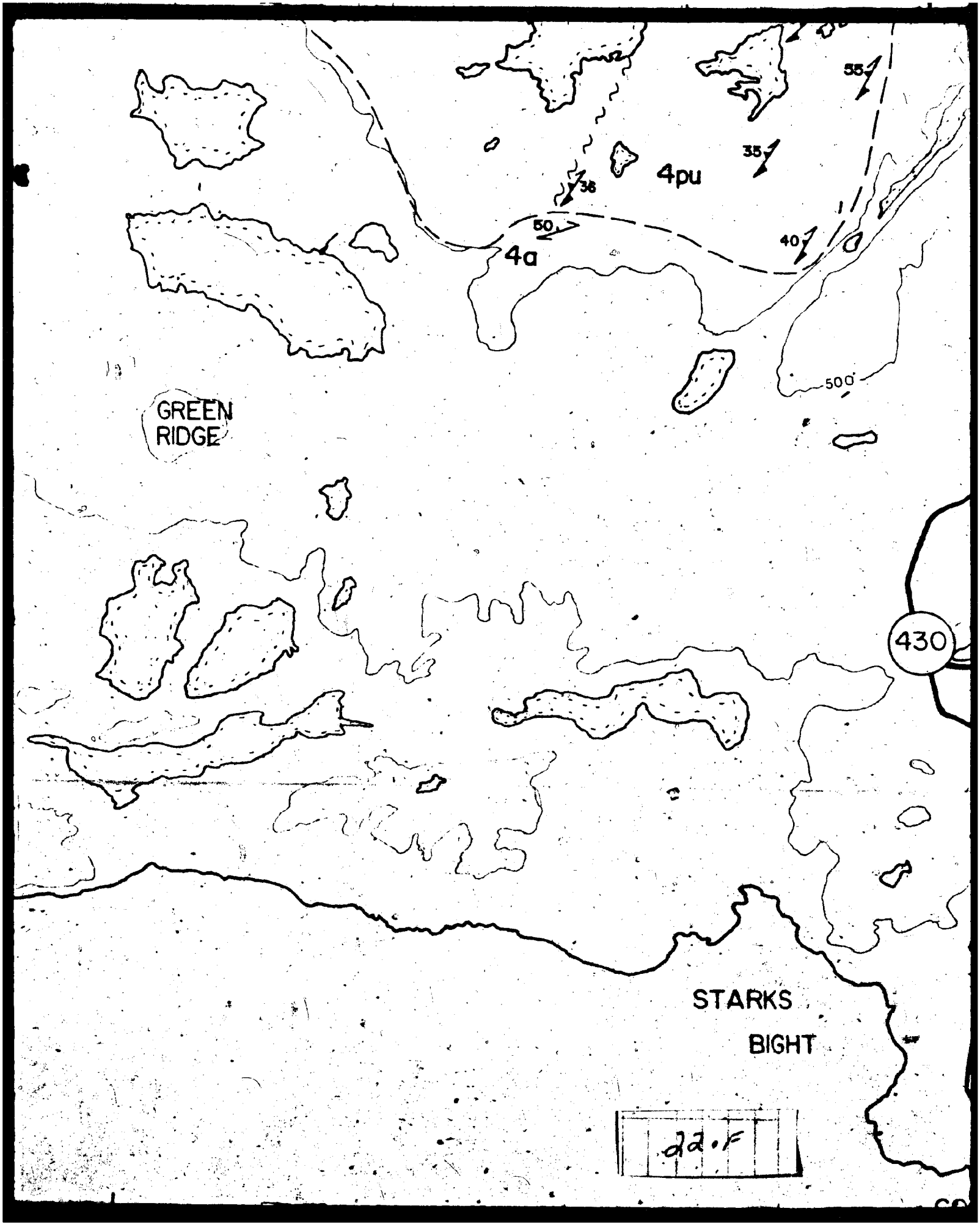
35
35
4pu
38
50
40
4a
500
GREEN
RIDGE
430
STARKS
BIGHT
22.F

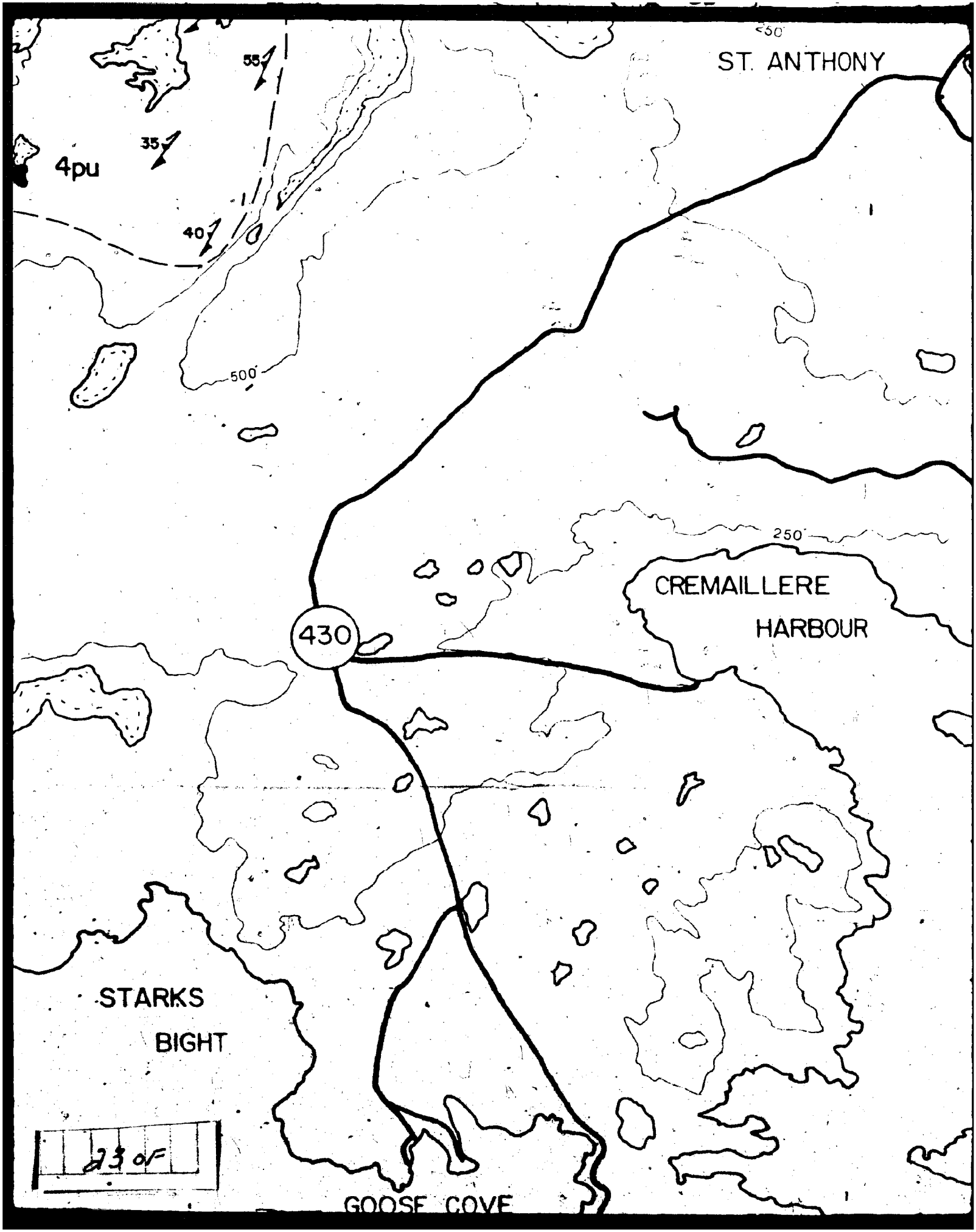
ST. ANTHONY
4pu
55
35
40
500
250
CREMAILLERE
HARBOUR
430
STARKS
BIGHT
GOOSE COVE

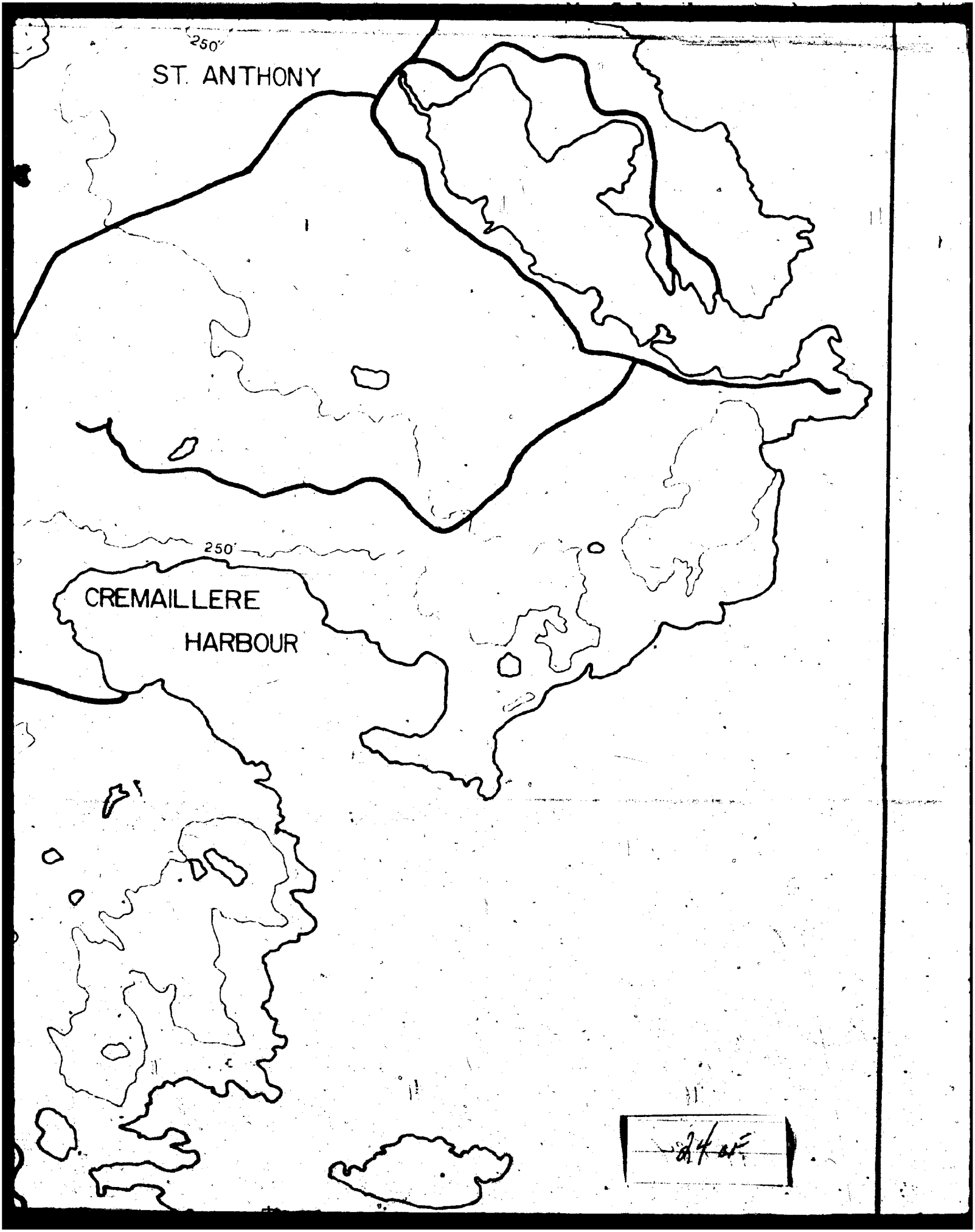
250'
ST. ANTHONY
250'
CREMAILLERE
HARBOUR
24 of

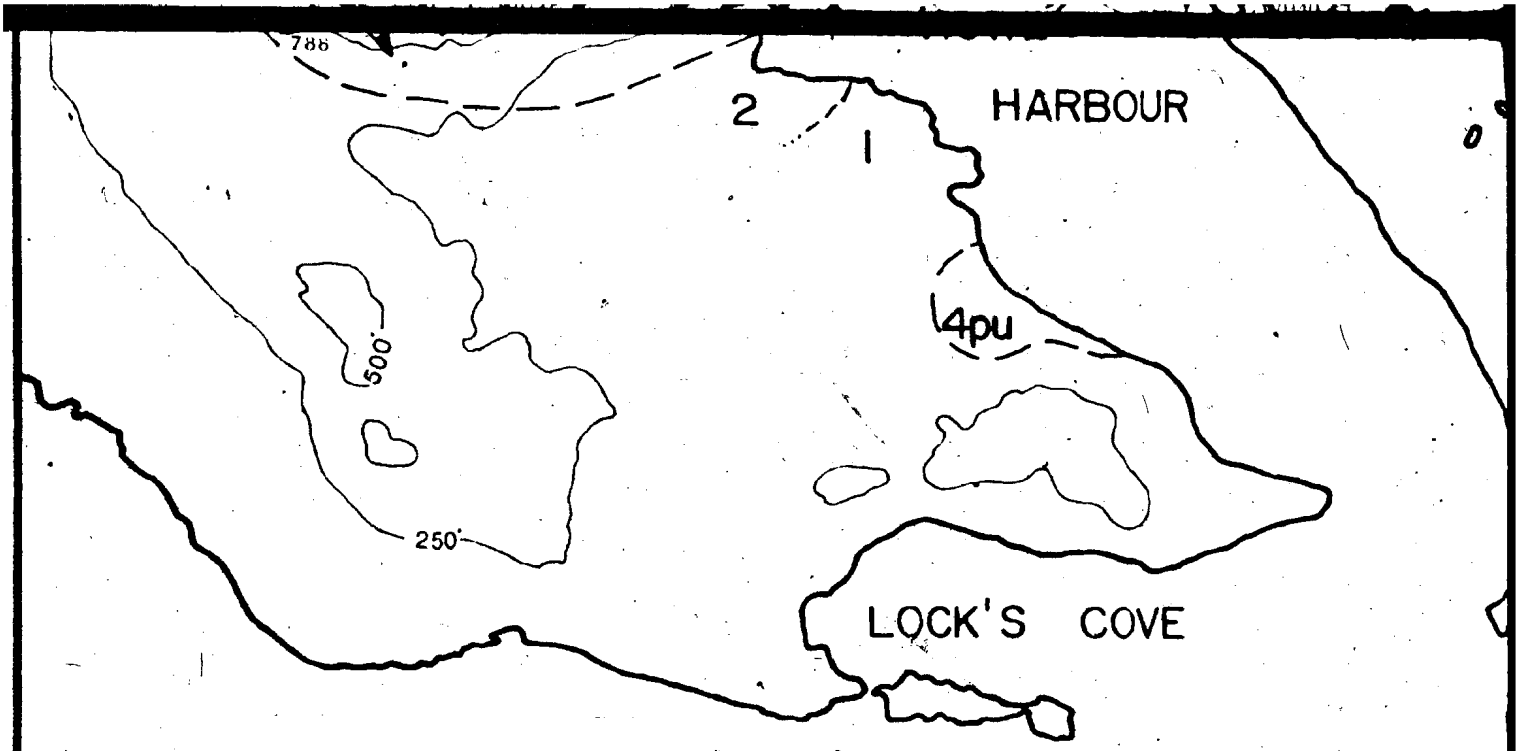

PLATE 2

THE SOUTHWESTERN PART OF THE ST. ANTHONY COMPLEX

25 of

GEOLOGY BY R.W. TALKINGTON 1977–1979

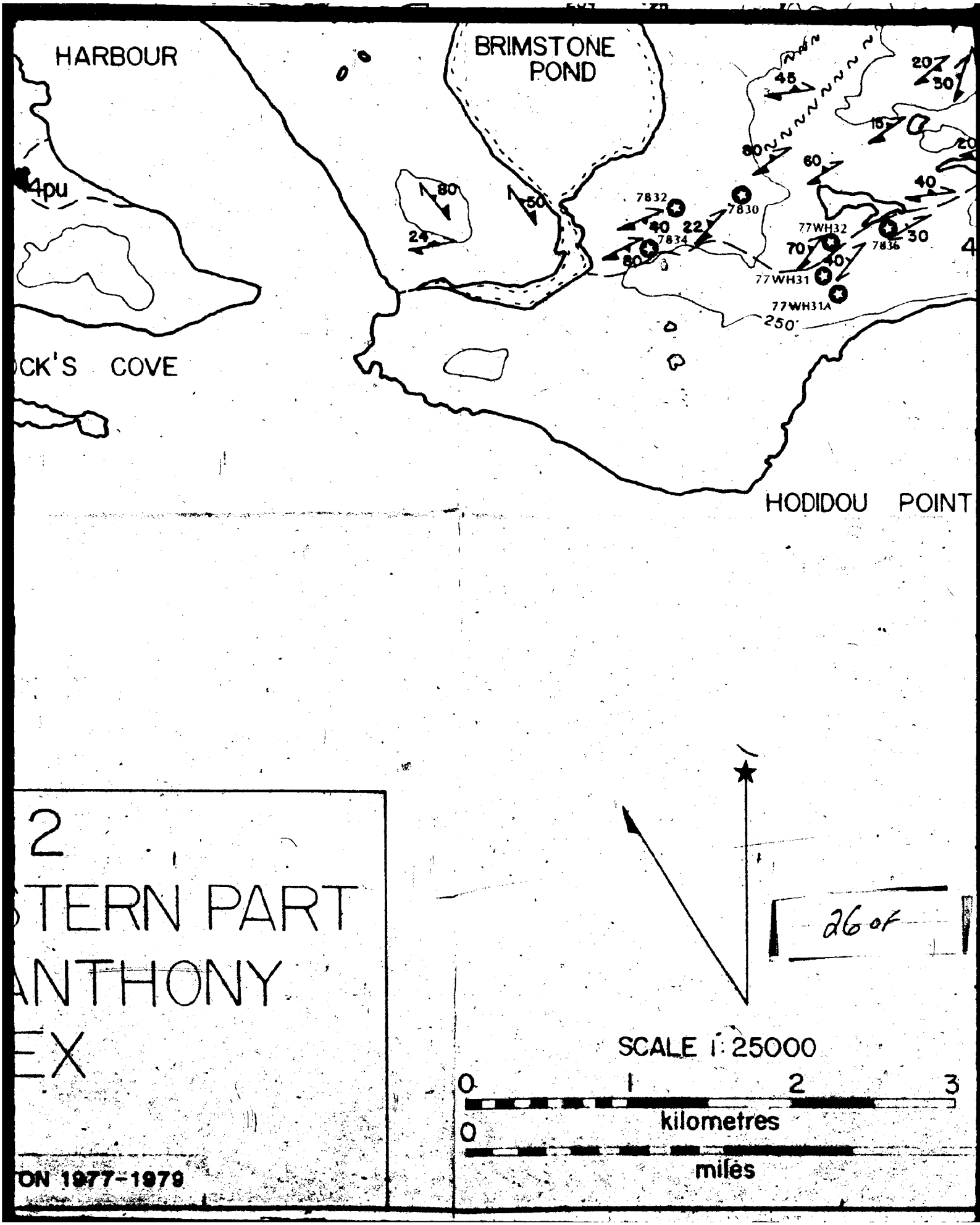

2

STERN PART

ANTHONY

EX

ON 1977-1979

26 of

SCALE 1:25000

0 1 2 3

kilometres

0

miles

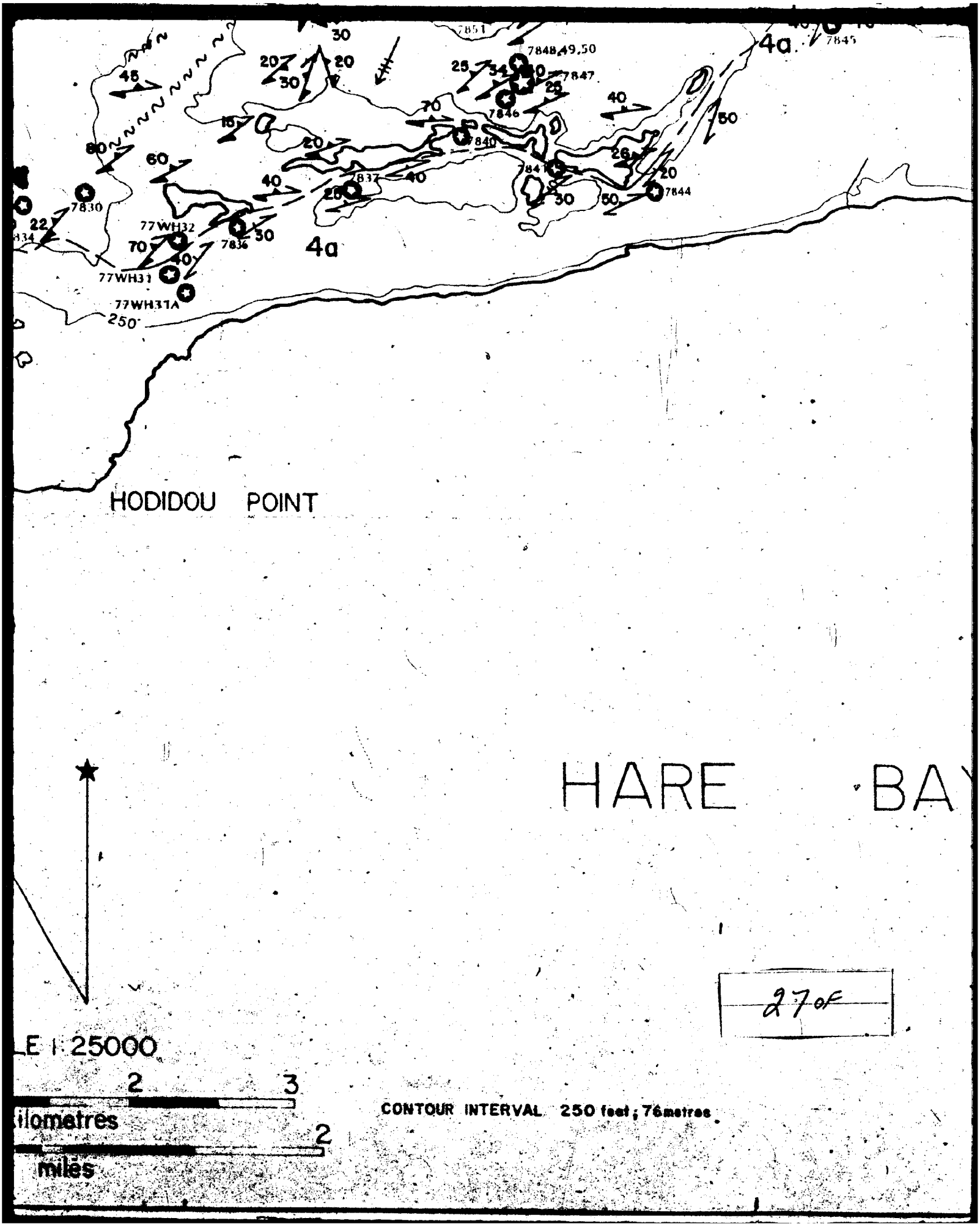
HODIDOU POINT
HARE BA
4a
4a
77WH31
77WH31A
77WH32
7830
7834
7837
7840
7841
7844
7845
7846
7847
7848,49,50
7851
250
27 of
LE 1:25000
2
3
ilometres
2
miles
CONTOUR INTERVAL 250 feet; 76metres

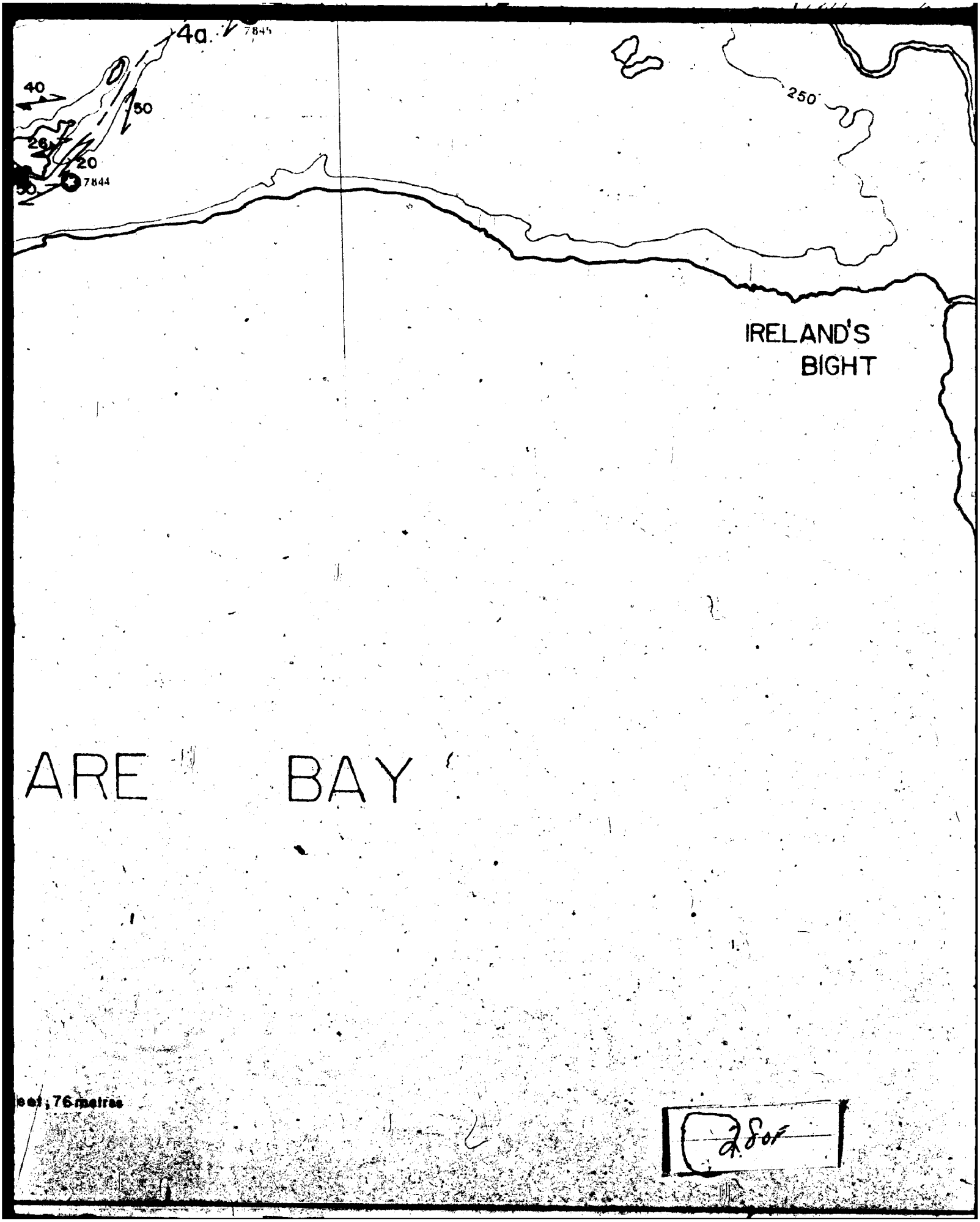
4a
7845
40
50
26
20
7844
250
IRELAND'S
BIGHT
ARE
BAY
eet; 76 metres
2 of

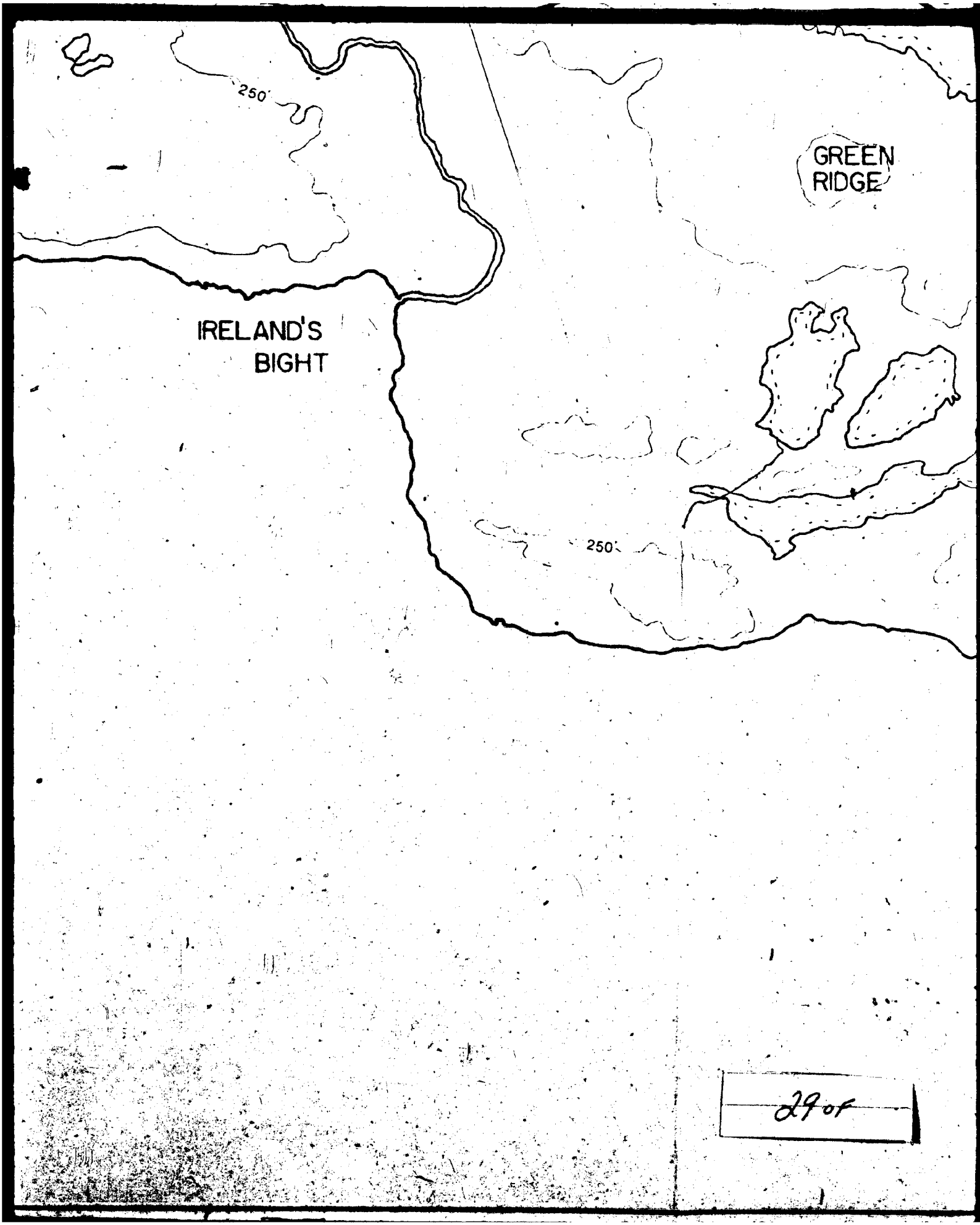
250'
GREEN
RIDGE
IRELAND'S
BIGHT
250'
29 of

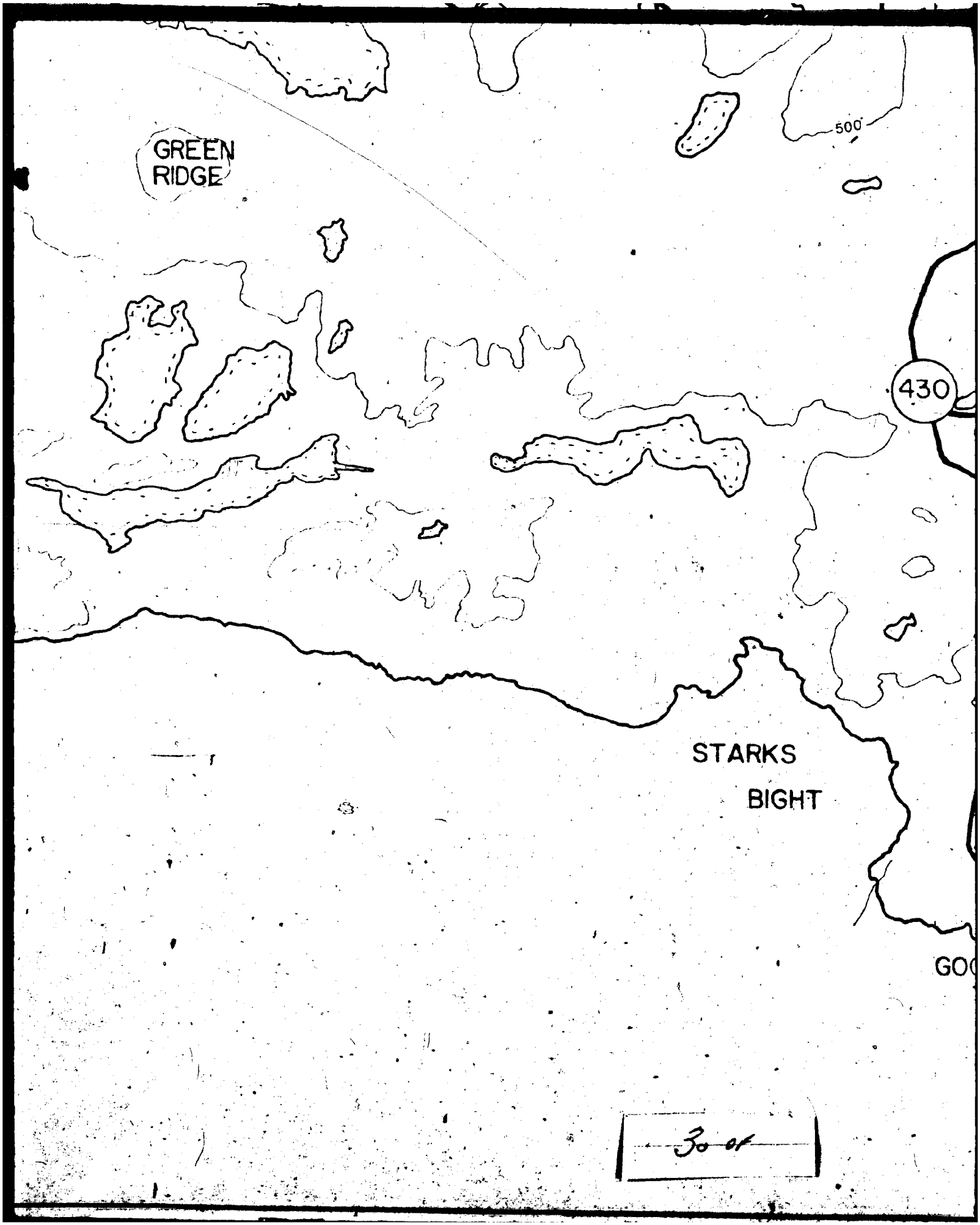
GREEN
RIDGE
500
430
STARKS
BIGHT
GO
30 of

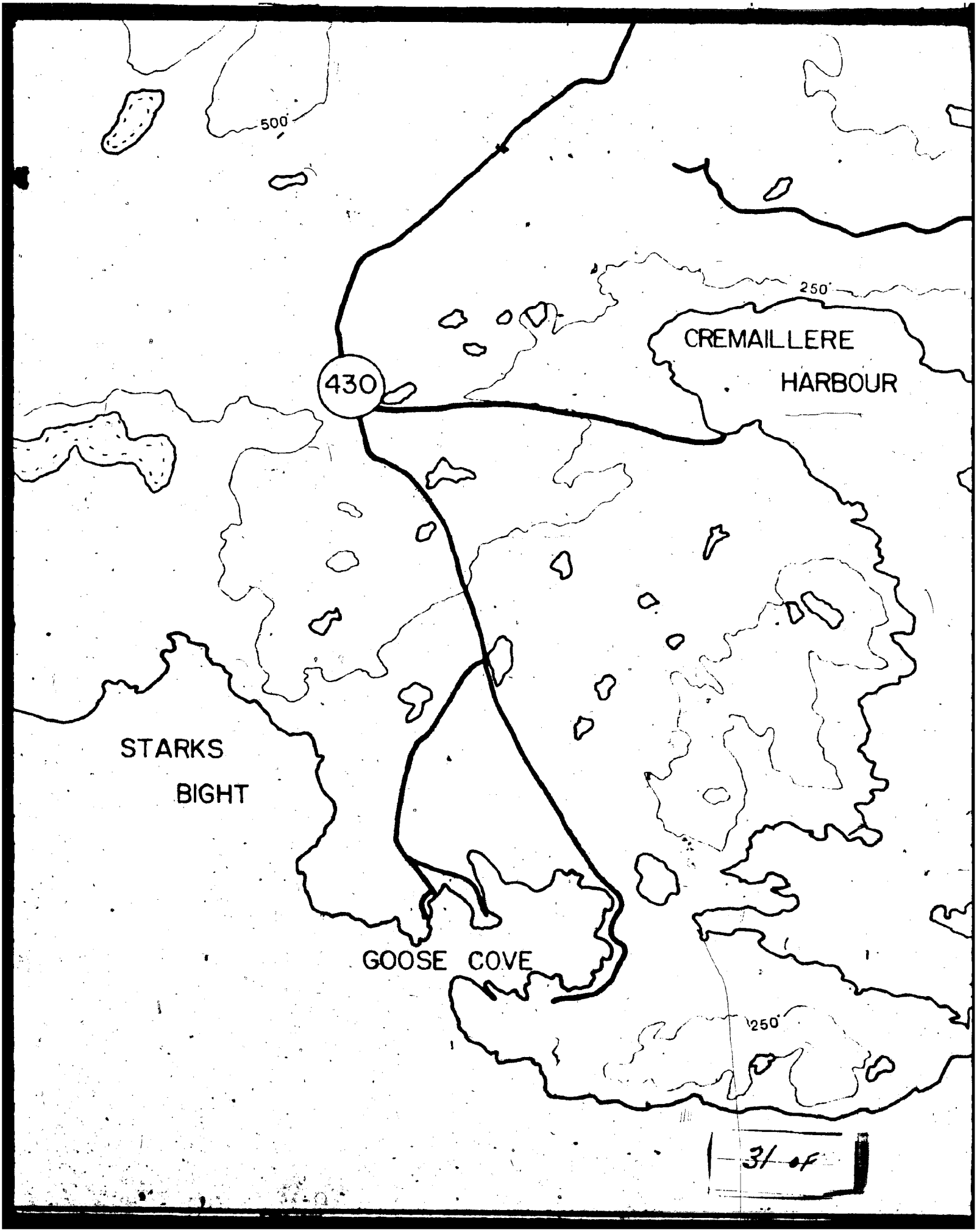
500
250
CREMAILLERE
HARBOUR
430
STARKS
BIGHT
GOOSE COVE
250
31 of

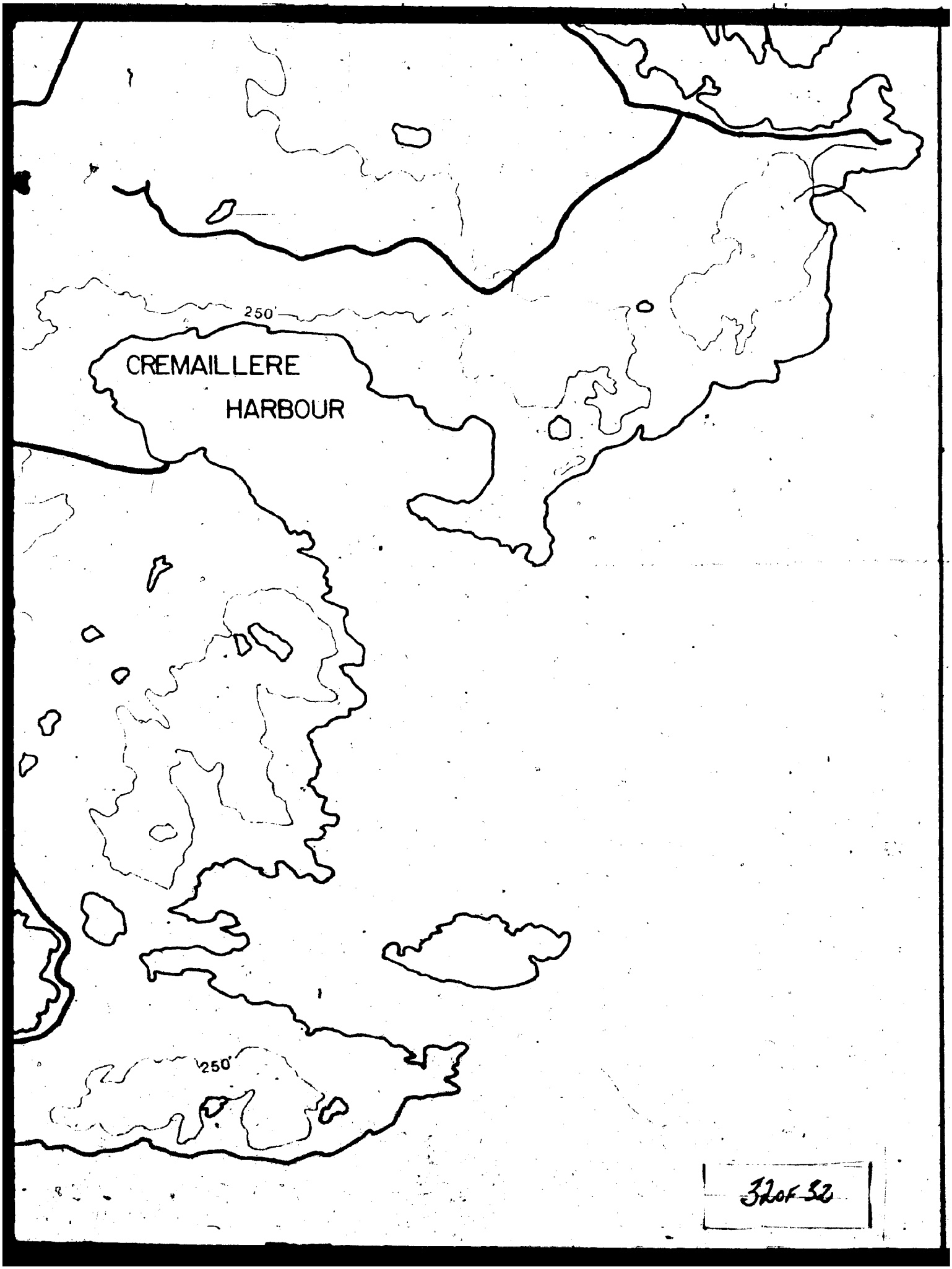
250'
CREMAILLERE
HARBOUR
250'

Geological

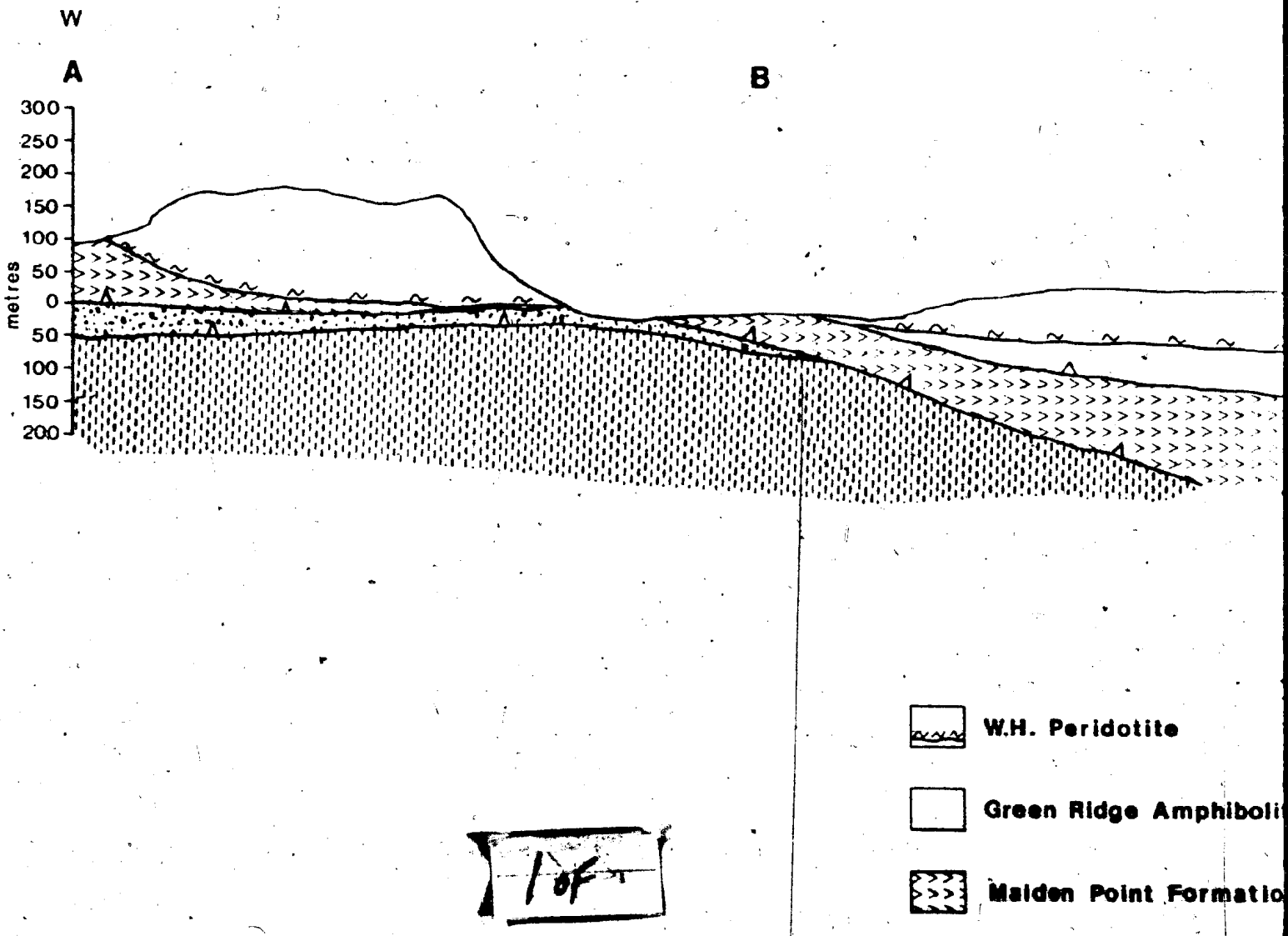

1 of 1

PLATE 3

Geological cross section of the western peridotite massifs(lineA-B-C-D of Pl

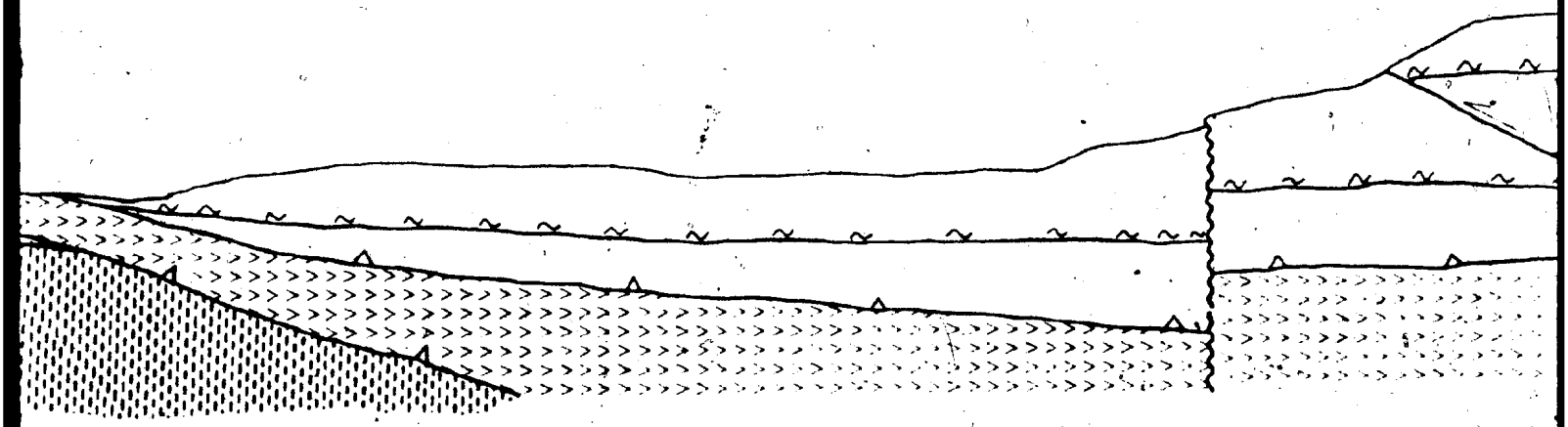

Vertical Exaggeration 3x

LEGEND

W.H. Peridotite

Green Ridge Amphibolite & Goose Cove Schist

Meiden Point Formation

Northwest Arm Format

Goose Tickle Formatio

Scale: 4cm = 1km

LATE 3

ern peridotite massifs(lineA-B-C-D of Plate 2).

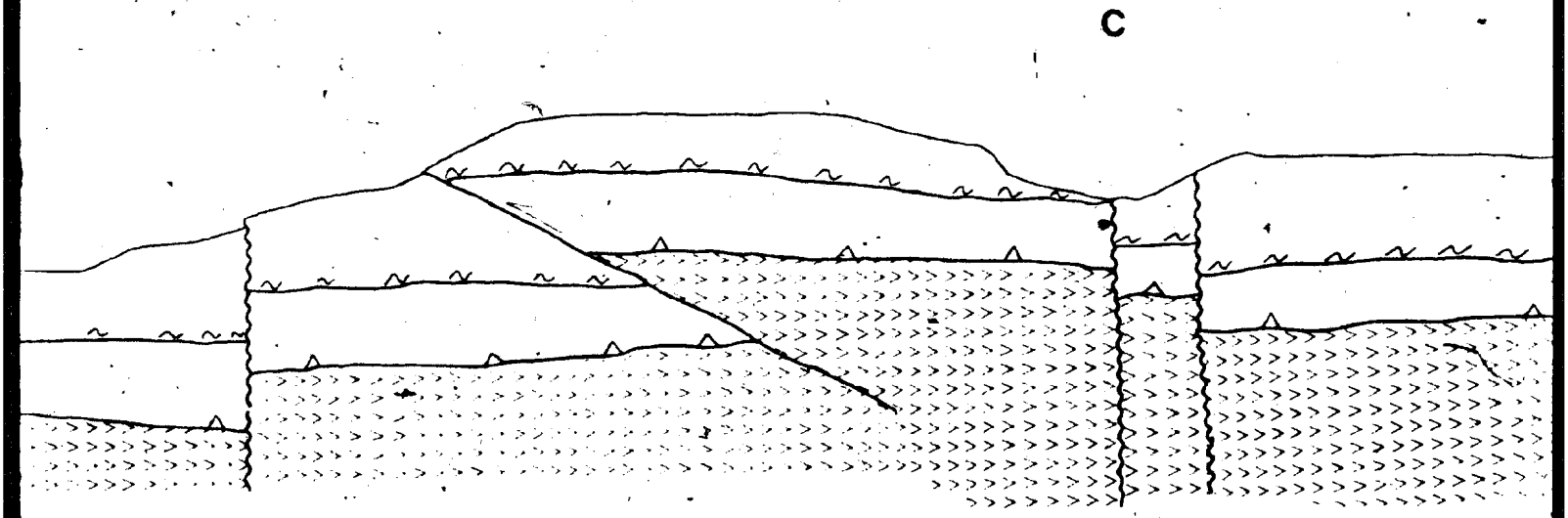

Exaggeration 3x

LEGEND

Northwest-Arm Formation

Goose Tickle Formation

Thrust Fault

a) separates allochthonous slices

b) interassemblage

High Angle Fault

Scale: 4cm = 1km

te 2).

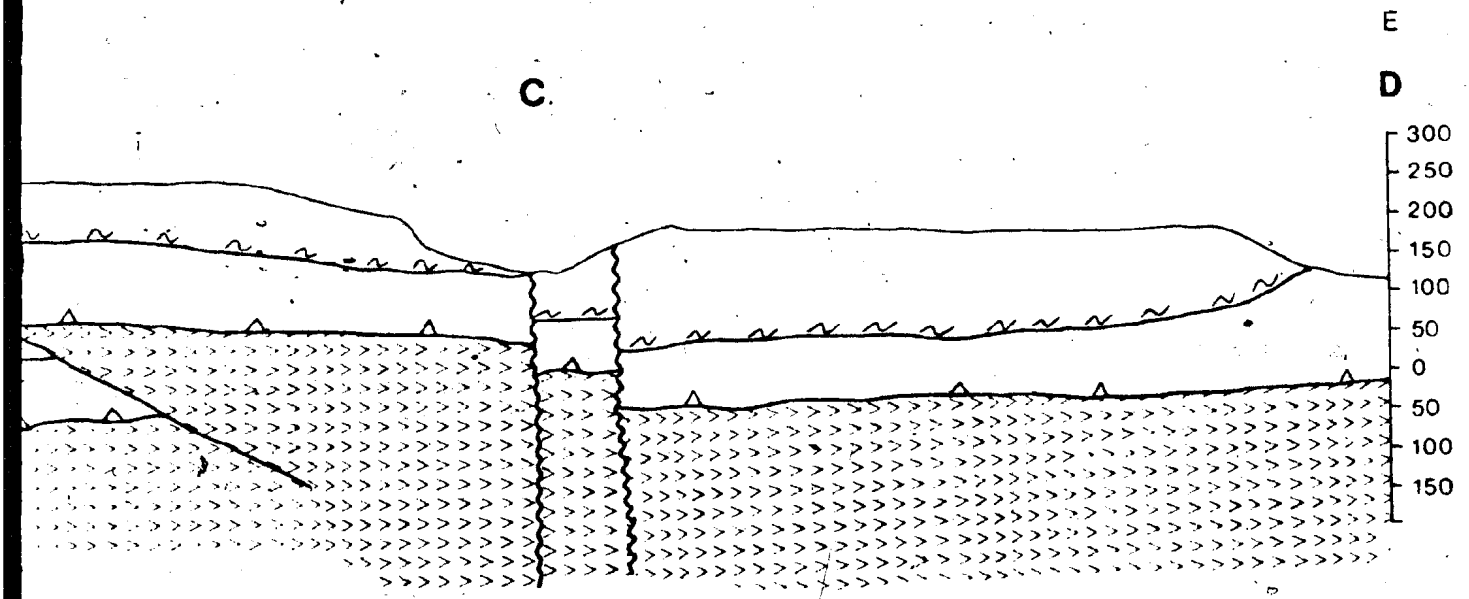

n

Thrust Fault

a) separates allochthonous slices

b) interassemblage

High Angle Fault

Geological cross section

C

NW

E

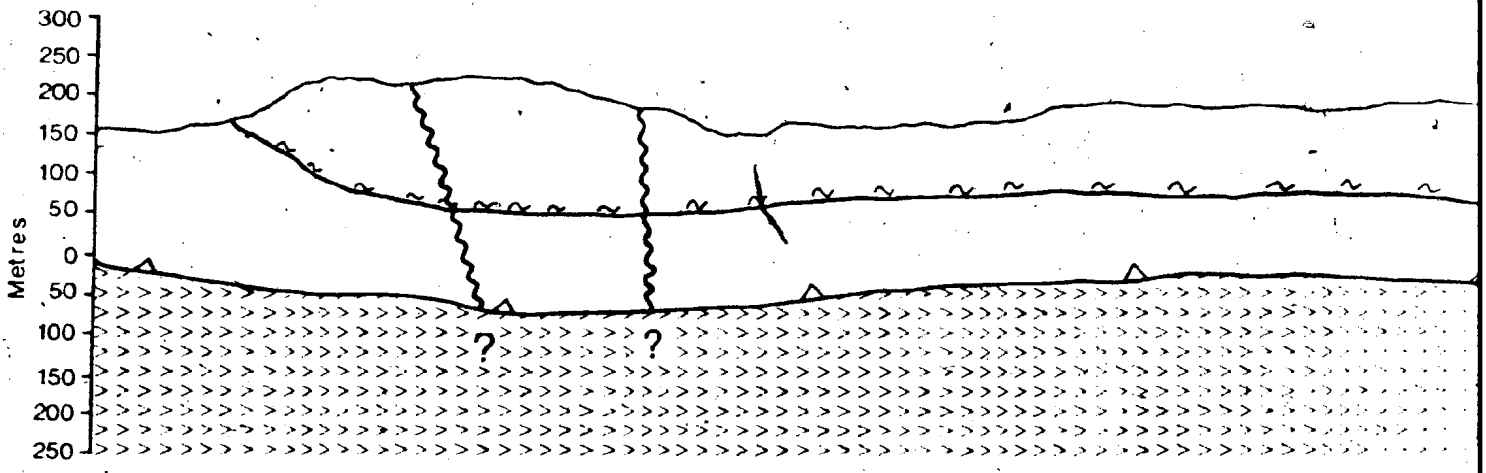

Vertic

W.H. Peridot

Alkaline Py

Green Ridge

Maiden Poin

1 of

PLATE 4

Geological cross section of the eastern peridotite massif(line E-F of Plate 2).

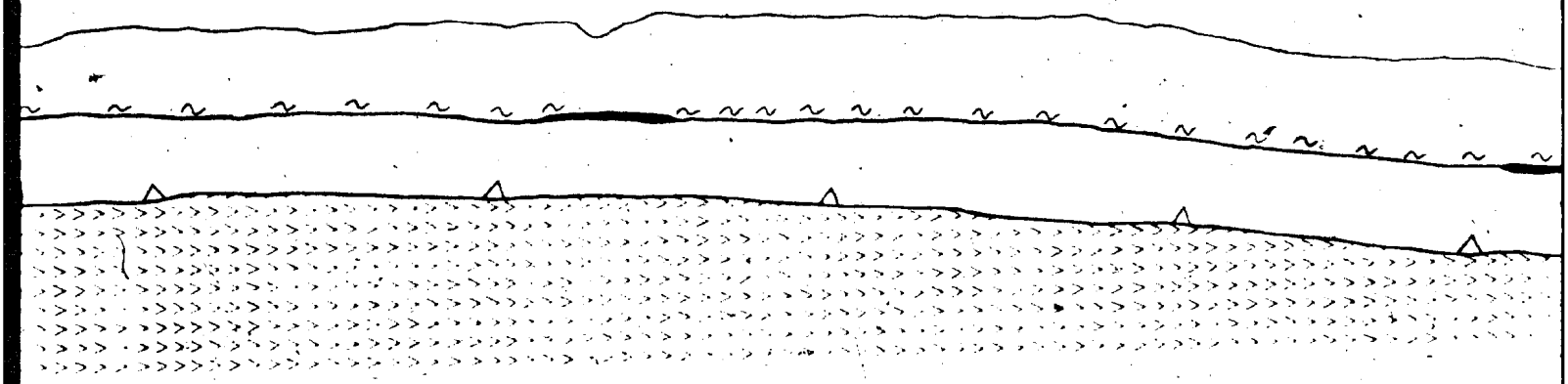

Vertical Exaggeration 3x

LEGEND

- W.H. Peridotite
- Alkaline Pyroxenite-Syenite
- Green Ridge Amphibolite & Goose Cove Schist
- Malden Point Fm.

- Thrust Fault
- High Angle Fault

Scale: 4cm = 1km

ne E-F of Plate 2).

SE

F

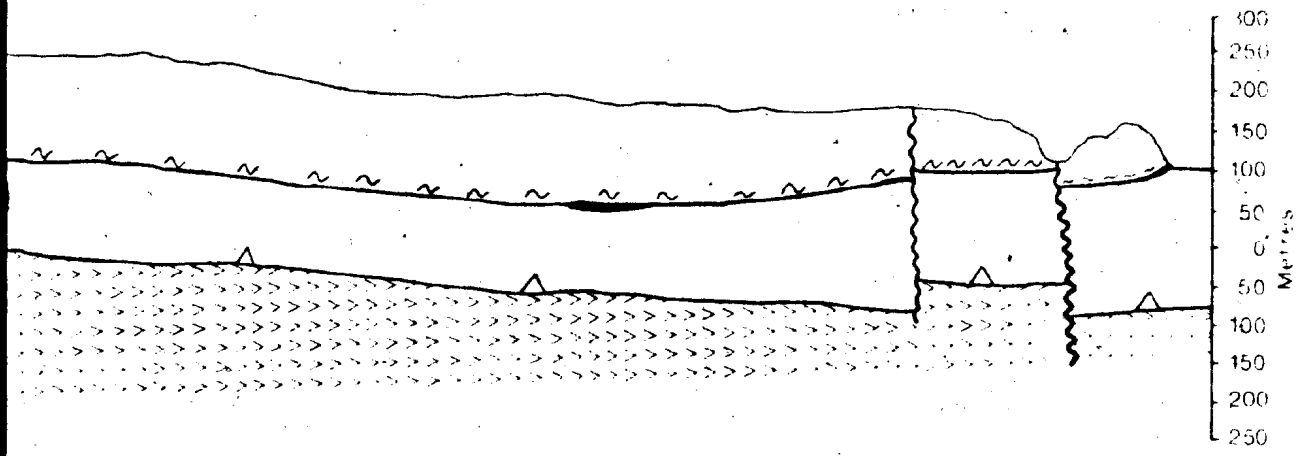

Thrust Fault

High Angle Fault

chist

3.F3

km



(2) 5016 83 Pocket

THE GEOLOGY, PETROLOGY AND PETROGENESIS OF THE WHITE HILLS PERIDOTITE, ST. ANTHONY COMPLEX, NORTHWESTERN NEWFOUNDLAND

CENTRE F PART 2 D STUDIES

TOTAL OF 10 PAGES ONLY
MAY BE XEROXED

(Without Author's Permission)

RAYMOND WILLIS TALKINGTON

000131

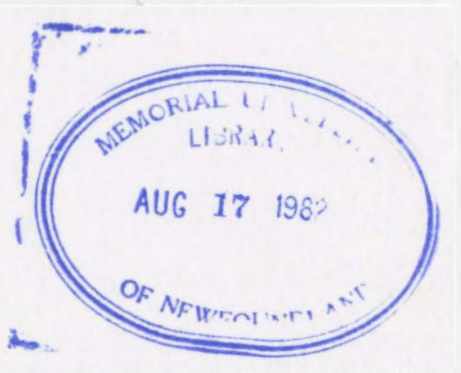

PART II



PART II

CHEMISTRY AND PETROGENESIS

Chapter 3

Mineral Chemistry and Bulk Rock Chemistry

II.3.A. Mineral Chemistry

Chemical compositions have been determined for the anhydrous minerals and some hydrous minerals from the White Hills Peridotite by electron microprobe. Analytical details are given in Appendix I. Mineral analyses from all lithologies of the peridotite and rocks associated with the St. Anthony Complex are compiled in Appendices II, III, and IV.

1. Olivine

a. Spinel lherzolite, Harzburgite, Dunite

Chemical analyses of olivine from spinel lherzolite, harzburgite and dunite are listed in Table AII.1. Fo contents (mole %) range from 89.5 - 91.6 (average 90.2) in spinel lherzolite, 90.4 - 91.3 (average 90.8) in harzburgite and 88.8 - 91.6 (average 90.5) in dunite. Olivine is homogeneous within any particular sample and no significant chemical differences exist (within analytical precision) whether grains are primary or secondary (neoblasts).

The range in Fo contents for spinel lherzolite given by Riccio (1976) for the White Hills Peridotite is increased to 2.1 mole percent Fo from the 0.7 mole percent Fo he reports. The Fo contents of olivines from the Bay of Islands Complex, S.W. Oregon Peridotites, and lherzolitic rocks from

the Western Alps (Medaris, 1972; Malpas, 1976, Ernst, 1978) are all included within the Fo range of those from the White Hills Peridotite.

The compositions of olivine from harzburgite from the White Hills Peridotite are comparable to olivine compositions from the Oman ophiolite (Gass et al., ms), Vulcan Peak Peridotite (Himmelberg and Loney, 1973), Red Mountain Peridotite (Sinton, 1977), Josephine Peridotite (Dick, 1976a), S.W. Oregon Peridotites (Medaris, 1972), Bay of Islands Complex (Malpas, 1976) and others.

Fo contents of olivine from dunite are similar to the values reported by Malpas (1976) for the Bay of Islands cumulate dunite (87.5 - 91.3 mole % Fo) and dunites within harzburgite of the Vulcan Peak Peridotite (89.9 - 91.9 mole % Fo) (Himmelberg and Loney, 1973).

In an attempt to provide evidence for the igneous origin of Group I xenoliths (lherzolite, harzburgite, spinel dunite) from San Carlos, Arizona, Frey and Prinz (1978) indicate that, as the Fo content (mole %) of olivines in the range 91 - 88 decreases, there is a systematic increase in bulk rock Al_2O_3 and CaO contents. They suggest that the trends defined in their diagrams provide evidence for an igneous origin for the xenoliths. This argument is applied to the spinel lherzolite, harzburgite and dunite lithologies from the White Hills Peridotite, where, for the same compositional range, similar trends are defined (Figure 3.1.). However, even though

Figure 3.1. Comparison of Fo (mole %) vs. bulk rock concentrations of Al_2O_3 and CaO for spinel lherzolite (●), harzburgite (o), and dunite (■) from the White Hills Peridotites. Trend lines visually estimated.

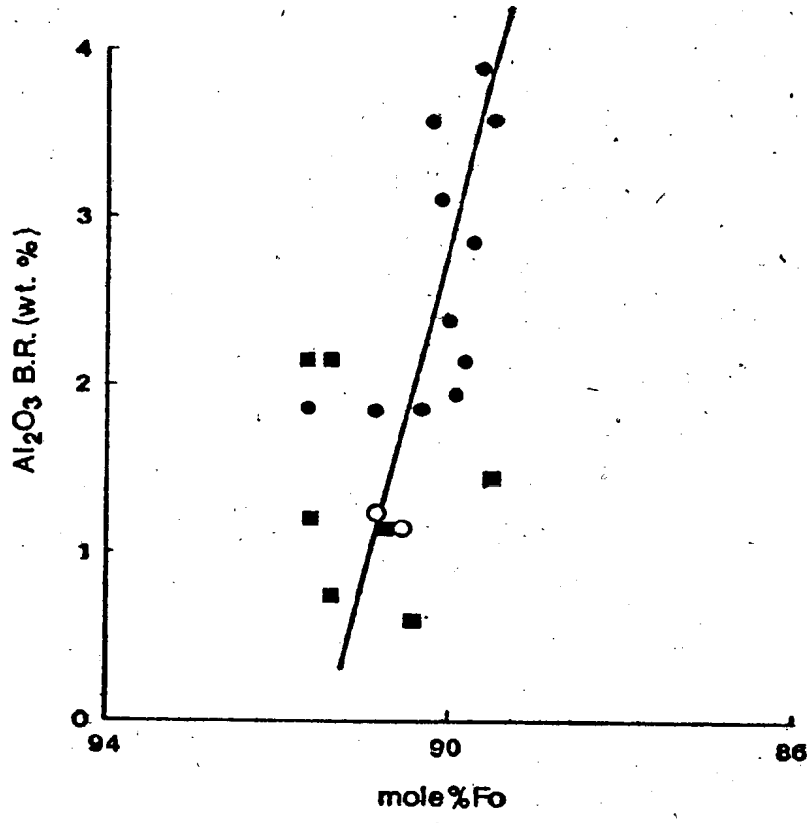
4
3
2
1
0
Al_2O_3 B.R. (wt. %)
94
90
86
mole%Fo

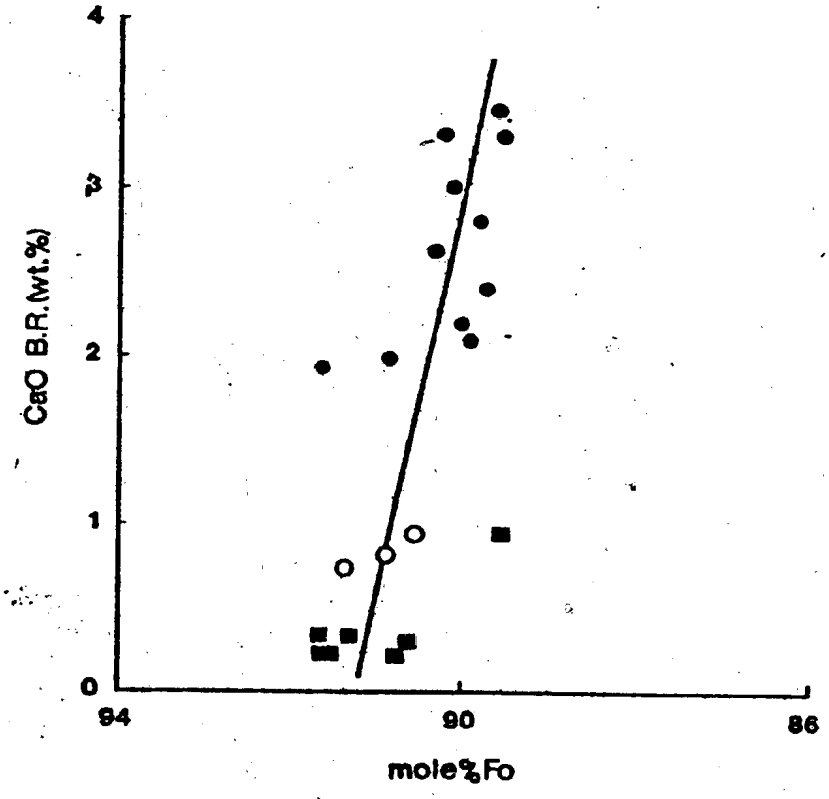
4
3
2
1
0
CaO B.R.(wt.%)
94
90
86
mole%Fo

these trends suggest an igneous origin, more specifically, the increase in Fo content with a decrease in the Al_2O_3 and CaO contents from spinel lherzolite and the rather high content of Al_2O_3 in dunite indicate that partial fusion processes and perhaps, subsolidus mineral-mineral (or rock-mineral) (e.g., spinel lherzolite-dunite) equilibration may have been responsible for these chemical trends (see Chapter 5 for discussion of this topic).

b. Pyroxenite Veins

The compositions of olivine from orthopyroxenite, websterite, clinopyroxenite and wehrlite veins are listed in Table AII.2. The Fo content of olivines for these rocks ranges from 82.1 to 93.2 (mole %). Olivines from the orthopyroxenites and websterites have the highest and most uniform Fo content amongst pyroxenite veins (∿ Fo 91) and are similar to the Fo values from the Red Mountain and Burro Mountain peridotites (Sinton, 1977; Loney et al., 1971) and for Group I xenoliths from San Carlos, Arizona (Frey and Prinz, 1978). Olivine from clinopyroxenite veins ranges in Fo content from 84.3 to 88.4 (mole %). The Fo content of olivine from the wehrlite veins is comparable to that of olivine from wehrlite of the transitional peridotite from the Red Mountain Peridotite.

The most striking difference in mineral chemistry between the pyroxenite veins other than the decrease in Fo content from orthopyroxenite and websterite to clinopyroxenite, is the similar NiO olivine content (∿ 0.35 wt.%) for orthopyroxenite

and websterite, which decreases to about 0.25 weight percent in olivine from clinopyroxenite. Due to the high octahedral site preference of nickel in olivine relative to the liquid (Burns, 1973), the early crystallization of olivine (i.e., in dunite, orthopyroxenite and websterite) takes up most of the available nickel from the liquid. Thus, only a relatively depleted nickel resevoir is left for olivines that crystallize late. Therefore, on the basis of only nickel data, most orthopyroxenite and possibly all websterite veins are probably "older" than clinopyroxenite and wehrlite veins, if all of the pyroxenites are produced from the same parent liquid.

c. Gabbro

The compositions of olivine from gabbro veins from the White Hills Peridotite are listed in Table AII.3. The Fo contents vary from 77.1 to 83.4 (mole %), i.e., within the olivine compositional range for cumulate gabbros from the Bay of Islands Complex (Irvine and Findlay, 1972; Malpas, 1976). NiO contents of these olivines average approximately 0.20 weight percent, slightly less than in the pyroxenites.

d. Chromitite

Olivine compositions from chromite-related lithologies are listed in Table AII.4. The Fo contents of olivines are rather uniform and the highest values found in the peridotite ($\sim$ 92.5). High Fo contents of olivine associated with chromite concentrations have been noted by many investigators (e.g., Himmelberg and Loney, 1973; Dick, 1976a). Ulmer (1969) and Snethlage and Klemm (1978) correlate the Fo increase and

corresponding increase in the $Mg/(Mg + Fe^{2+})$ ratio for all other silicates and chromite relative to a non-chromite bearing host rock of the same lithology to a higher oxygen fugacity of the liquid at the time of mineral crystallization. This Fo increase in olivine seems to be further enhanced during subsolidus cooling as shown by the experimental work of Roeder et al (1979).

Preliminary determinations of the fO_2 values for coexisting olivine and spinel from the White Hills Peridotite in spinel lherzolite, harzburgite, orthopyroxenite, websterite and gabbro using the fO_2 diagram of Irvine (Figure 11, p. 670, 1965) yield results for olivine associated with primary chromite from the orthopyroxenite veins of approximately 10^{-4} atm, whereas the more aluminum rich, exsolved and secondary spinels of the other lithologies give fO_2 values of approximately 10^{-11} atm. There is a considerable difference between the fO_2 values for cumulus spinel types and the fO_2 values for secondary (exsolved) spinel types, and neither value is believed to represent the fO_2 condition when they formed (cf., Hill and Roeder, 1974; Fisk and Bence, 1980), due to serpentinization and/or reequilibration of the host rocks during the post-crystallization history of the peridotite.

2. Orthopyroxene

a. Spinel Lherzolite and Harzburgite

The compositions of 25 orthopyroxenes from spinel lherzolite and harzburgite are listed in Table AII.5. and plotted in Figure 3.2. The orthopyroxenes from harzburgite differ from

Figure 3.2.A. Pyroxene compositions of rocks from the White Hills Peridotite.
Key:

- ▲ Spinel lherzolite, White Hills Peridotite
- ▬ Harzburgite, White Hills Peridotite
- ● Spinel lherzolite, Bay of Islands Complex (Malpas, 1976)
- ○ Spinel lherzolite, Lanzo Peridotite (Ernst, 1978)
- × Spinel lherzolite, Group I xenoliths, San Carlos, Arizona (Frey and Prinz, 1978)
- △ Harzburgite, Bay of Islands Complex (Malpas, 1976)
- ◆ Harzburgite, Group I xenoliths, San Carlos, Arizona (Frey and Prinz, 1978)

Tieline connects coexisting clinopyroxene and orthopyroxene. Ca:Mg:Fe_{total} values are in cation proportions.

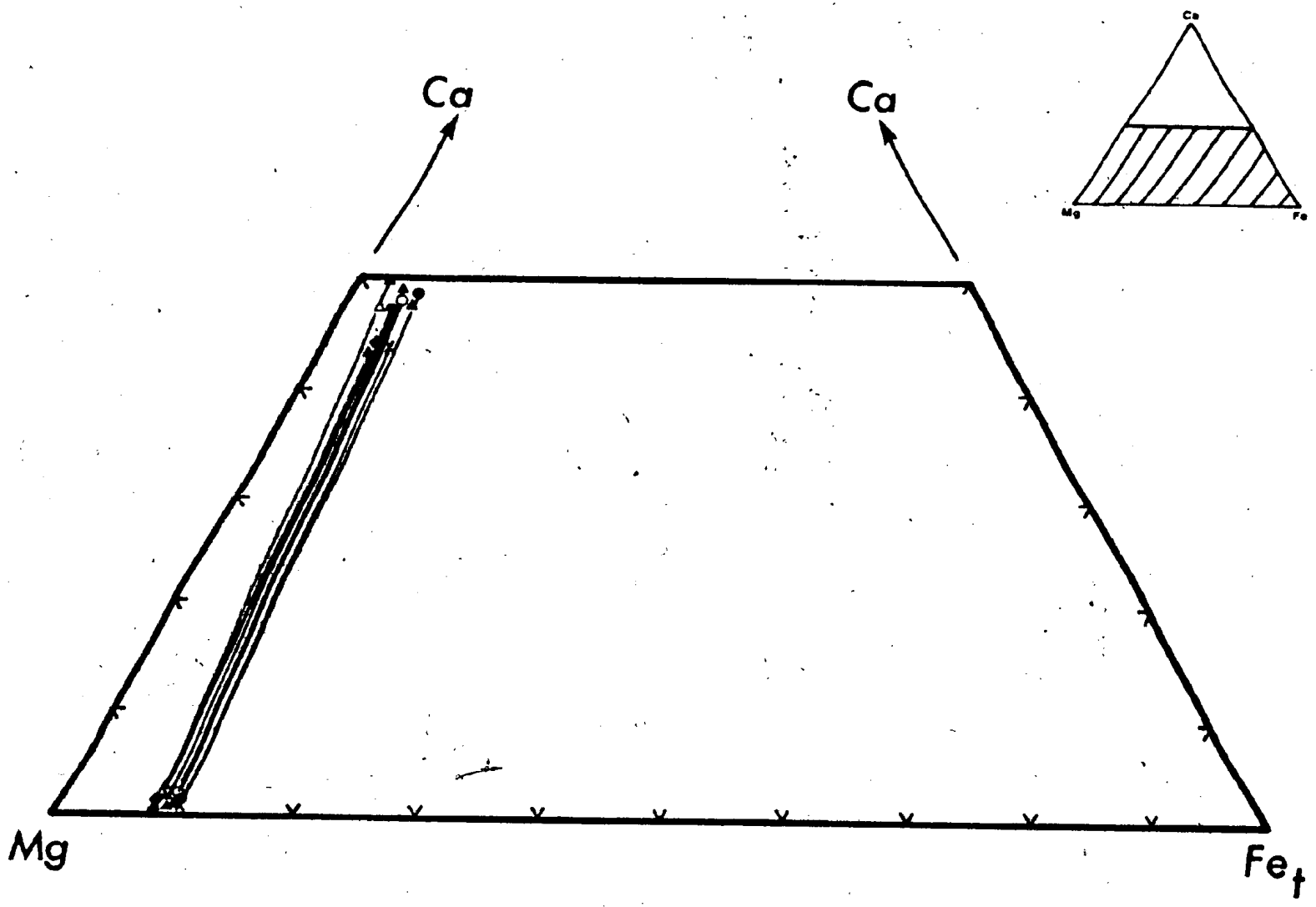
Ca
Ca
Mg
Fe$_t$

Figure 3.2.B. Pyroxene compositions of rocks from the White Hills Peridotite.
Key:

- ● Orthopyroxenite without disseminated chromite
- ▲ Websterite
- + Clinopyroxenite
- ◆ Chromite pod
- X Orthopyroxenite with disseminated chromite

Tieline connects coexisting clinopyroxene and orthopyroxene. Ca:Mg:Fe_{total} values are in cation proportions.

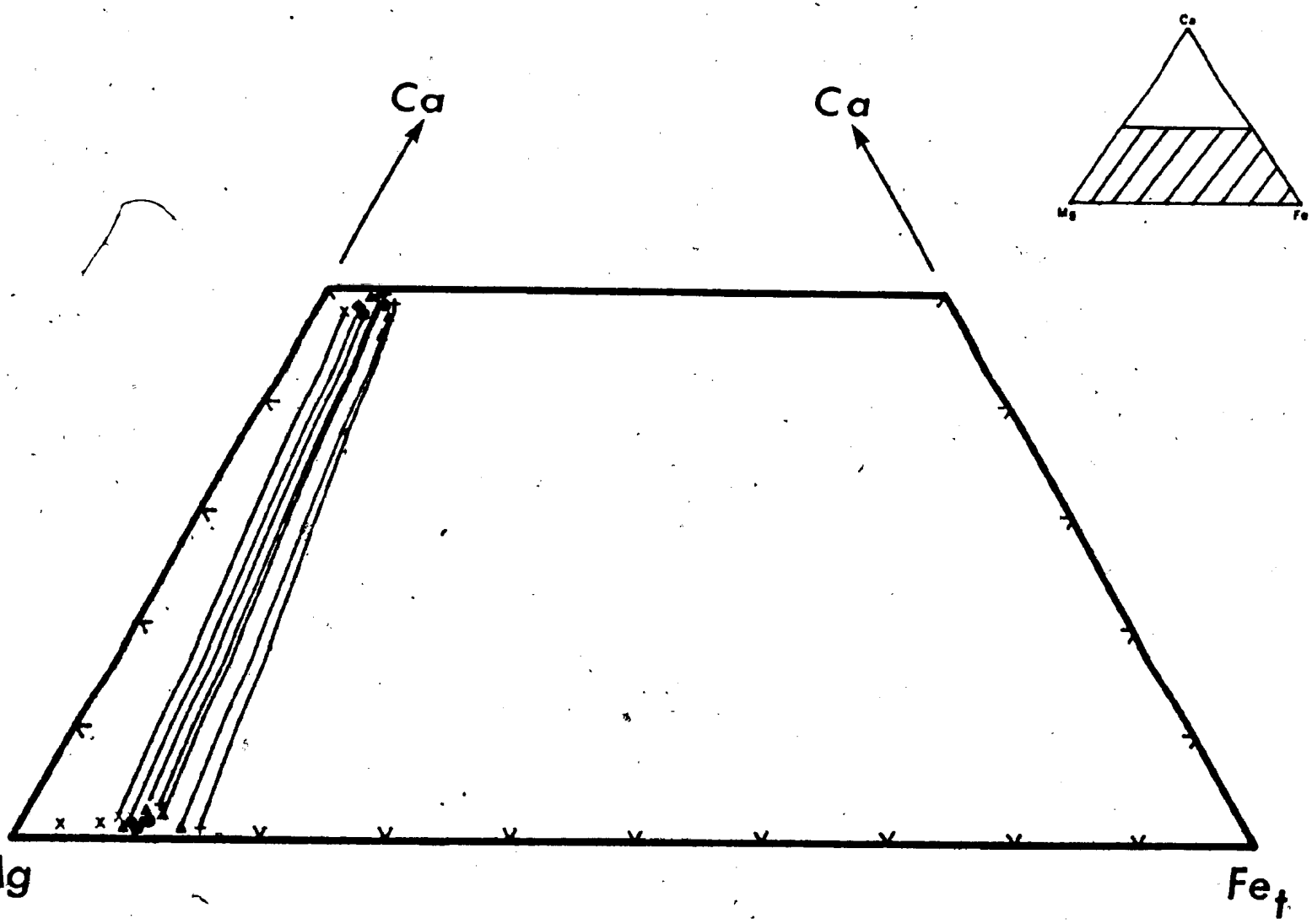
Ca
Ca
Mg
Fe$_t$

Ca
Mg
Fe

Figure 3.2.C. Pyroxene compositions of rocks from the White Hills Peridotite.
Key:

- ● Gabbro (coexisting orthopyroxene and clinopyroxene), White Hills Peridotite
- ▲ Gabbro (clinopyroxene), White Hills Peridotite
- X Cumulate gabbro, Bay of Islands Complex (Malpas, 1976)
- ◆ Gabbro I, Lanzo Peridotite (Boudier, 1976)
- + Gabbro II, Lanzo Peridotite (Boudier, 1976).
- ▬ Long Ridge Metagabbro, St. Anthony Complex (Jamieson, 1979)

Tieline connects coexisting clinopyroxene and orthopyroxene. Ca:Mg:Fe_{total} values are in cation proportions.

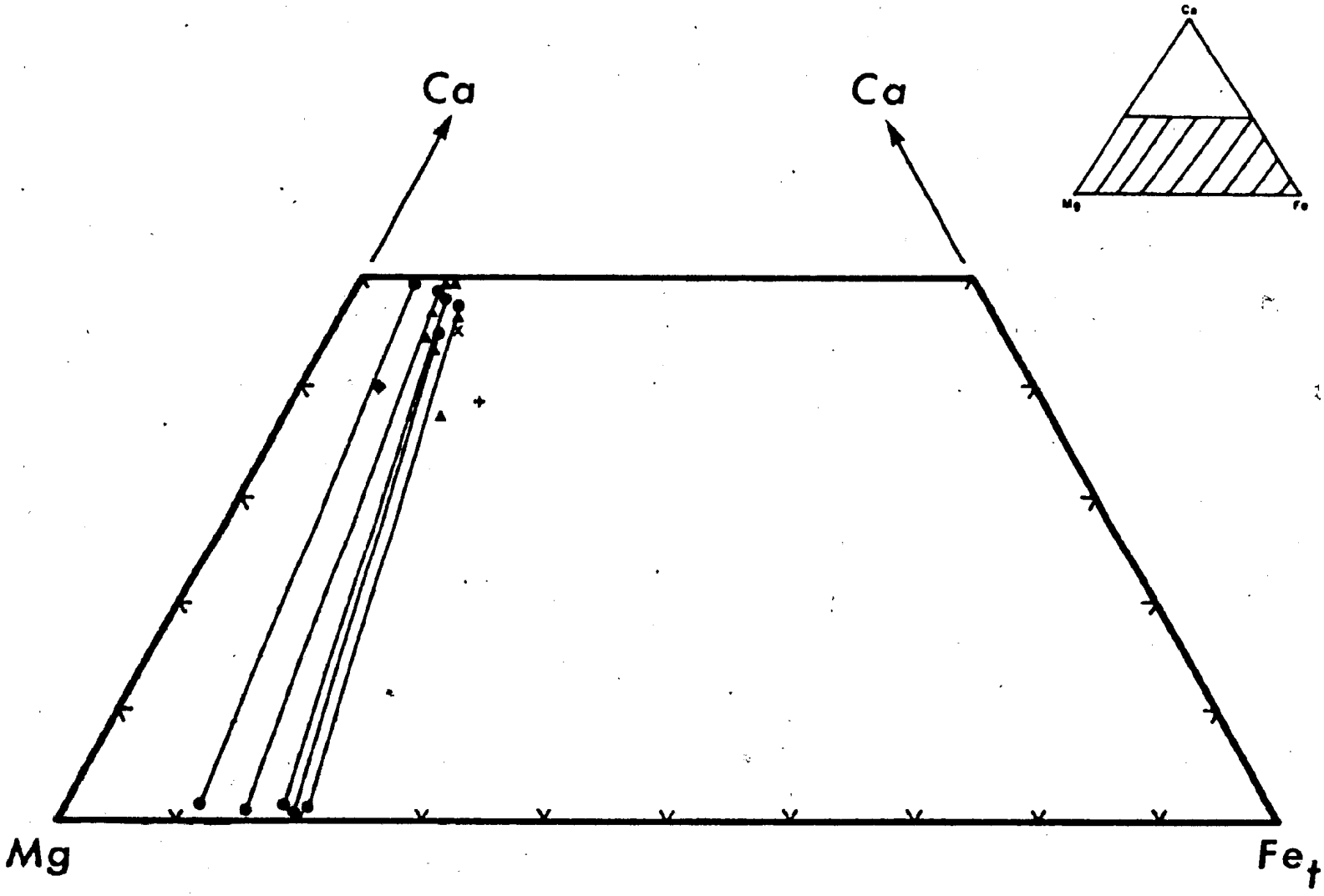
Ca
Ca
Mg
Fe$_t$

those in spinel lherzolite only in an overall lower Al_2O_3 content; the Ca:Mg:Fe* ratios are the same for both types (Figure 3.2.A.) and are indentical to values reported for the Bay of Islands Complex (Malpas, 1976), Lanzo Peridotite (Ernst, 1978), and Group I Xenoliths from San Carlos, Arizona (Frey and Prinz, 1978).

No differences in composition have been found between orthopyroxene porphyroclasts and orthopyroxene neoblasts. However, chemical zoning of CaO and Al_2O_3 is found in the orthopyroxene porphyroclasts of sample 78105 (Table AII.5.). Both CaO and Al_2O_3 decrease by approximately 1 weight percent from porphyroclast core to rim. This decrease in the $CaAl_2SiO_6$ molecule (Ca-Tschermak's) solubility in the orthopyroxene rims is in response to falling temperatures (Sinton, 1977); TiO_2 and Cr_2O_3 show a similar but more restricted chemical trend.

The chemical homogeneity of orthopyroxene porphyroclasts is difficult to assess due to the presence of clinopyroxene and spinel exsolution lamellae. In sample 78105, the rim region of the orthopyroxene porphyroclast is visually nearly free of clinopyroxene exsolution, whereas in the core region clinopyroxene lamellae are present. In an attempt to define the "homogeneity" for the orthopyroxene porphyroclasts from these rocks, the two most commonly observed types of orthopyroxene-clinopyroxene exsolution relationships have been studied. In one type, clinopyroxene is present as large,

* $Ca:Mg:Fe_{total}$ values are in cation proportions

coalesced exsolution blebs in a lamella-free orthopyroxene host (Figure 3.3., Type I); the second type consists of alternating well-defined exsolution lamellae with sharp mineralogical boundaries between the orthopyroxene and the clinopyroxene (Figure 3.3., Type II). For these two examples, the rock microstructures are porphyroclastic and mylonitic, and neoblasts of olivine, orthopyroxene and clinopyroxene occur at the orthopyroxene porphyroclast grain boundaries. The neoblasts are often indistinguishable because of their small size and similar interference colors. In all the samples examined for this study, the size of the orthopyroxene porphyroclast does not appear to be the determining factor as to whether the Type I or II exsolution develops. The chemical data for the two exsolution types are listed in Table 3.1. Although the bulk rock chemistries for samples 77WH94 (Type I) and 77WH1 (Type II) are similar (Appendix III), in the first type the host orthopyroxene has CaO and Al_2O_3 contents of 0.32 weight percent and 4.13 weight percent respectively; while for the second type the host orthopyroxene has CaO and Al_2O_3 contents of approximately 0.68 weight percent and 6.10 weight percent respectively. That is, for these two exsolution types, the orthopyroxene with the coalesced clinopyroxene exsolution lamellae has the lower CaO and Al_2O_3 contents. A comparison of the mineral chemistry data for exsolution Types I and II to the mineral chemistry data for sample 78105 (Table AII.5.) indicates a higher CaO content for the orthopyroxene from sample 78105. The higher

Figure 3.3. Schematic drawing of two examples of clinopyroxene exsolution blebs (Type I) and lamellae (Type II) in orthopyroxene porphyroclasts from the White Hills Peridotite (see text for explanation). Type I - orthopyroxene - opx; clinopyroxene - cpx; scale bar 0.1 millimeter; Type II - clinopyroxene - stippled; orthopyroxene - ruled; scale bar 0.2 millimeters; number locates the location of electron microprobe analysis (see Table 3.1. for analyses).

Type I

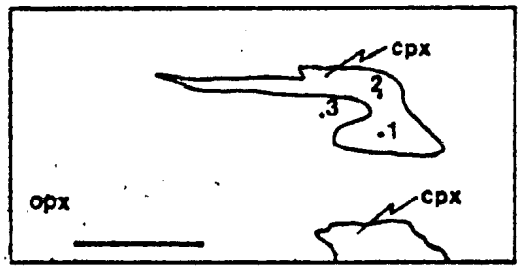

Type II

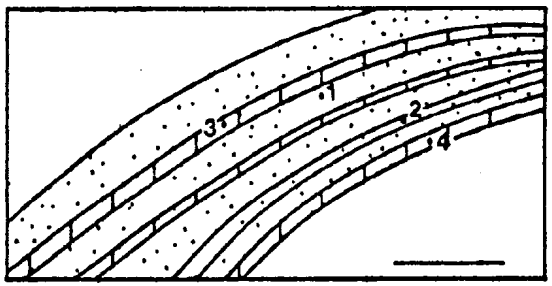

TABLE 3.1. Chemical comparison of two types of clinopyroxene exsolution in orthopyroxene porphyroclasts in spinel lherzolite

	Type I			Type II			
	clinopyroxene		orthopyroxene	clinopyroxene		orthopyroxene	
	1	2	3	1	2	3	4
SiO_2	51.53	51.55	54.89	48.67	50.21	53.48	54.43
TiO_2	0.27	0.25	0.03	0.12	0.12	0.05	0.01
Al_2O_3	5.36	4.93	4.13	6.86	6.98	6.14	6.04
Cr_2O_3	1.25	1.23	0.58	1.34	1.44	0.95	0.91
FeO*	2.12	1.98	6.51	2.86	2.55	6.63	6.64
MnO	0.07	0.07	0.10	0.07	0.07	0.16	0.05
MgO	15.23	15.93	34.02	15.70	15.11	31.83	31.26
CaO	23.32	23.50	0.32	22.22	22.10	0.68	0.67
Na_2O	0.88	0.96	—	0.77	0.70	—	—
NiO	0.06	0.05	0.05	0.13	—	0.05	0.10
TOTAL	100.09	100.45	100.63	98.74	99.28	99.97	100.11

Type I - sample 77WH94, see Figure 3.3. for location of analyzed points.

Type II - sample 77WH1, see Figure 3.3. for location of analyzed points.

* - total iron as FeO.

CaO content is probably caused by the presence of clinopyroxene exsolution lamellae or an orthopyroxene with a higher diopside component. Of these two alternatives, the former is favored since there is limited solubility of diopside in enstatite at subsolidus temperatures (Boyd and Schairer, 1964).

b. Pyroxenite Veins

Thirteen chemical analyses of orthopyroxenes from pyroxenite veins are listed in Table AII.6. and plotted in Figure 3.2.B. The Mg component of orthopyroxenes from orthopyroxenite and websterite veins is similar, but decreases in those from clinopyroxenite. The TiO_2 and Na_2O contents are similar for all types, but on average are higher in clinopyroxenite.

The compositions of orthopyroxene in orthopyroxenites from the Burro Mountain Peridotite (Loney et al., 1971) and and Red Mountain Peridotite (Sinton, 1977) are lower in Al_2O_3 but otherwise similar to the White Hills Peridotite orthopyroxenite veins.

c. Gabbro

Compositional data for orthopyroxenes in gabbro veins are listed in Table AII.7. and plotted in Figure 3.2.C. The Mg content ranges from 78.5 percent to 83.8 percent, nearly identical to the range for the Fo content of olivine in gabbro.

d. Chromitite

Orthopyroxene compositions from rocks associated with chromitite are listed in Table AII.8. and plotted in Figure 3.2.A. The Mg content of these orthopyroxenes is slightly higher than those from chromite free orthopyroxenite veins.

Also, the Al_2O_3 contents for orthopyroxenes associated with chromite is 2 to 3 weight percent lower than for orthopyroxenes in the chromite free type, and the lowest overall Al_2O_3 contents in orthopyroxene for all rocks of the peridotite. The compositions of the orthopyroxenes associated with chromitite are comparable to the orthopyroxene compositions reported by Loney et al (1971) and Sinton (1977), i.e., ~ En 92.

3. Clinopyroxene

a. Spinel Lherzolite and Harzburgite

Clinopyroxene compositions from spinel lherzolite and harzburgite are listed in Table AII.9. and diagramatically represented in Figure 3.2.A. The spinel lherzolite clinopyroxenes are richer in Al_2O_3, Na_2O and TiO_2 (Jadeite or $NaTiAlSiO_6$) than those from the harzburgite, however there is some overlap in these compositions. Clinopyroxene porphyroclast compositions are homogeneous and are remarkably similar to the compositions for clinopyroxene exsolution lamellae in orthopyroxene porphyroclasts (Table AII.8., analyses 77WH11, 77WH11-exs; 78105, 78104-1), and unlike the compositional differences between the primary and recrystallized clinopyroxenes of sample 78105.

The clinopyroxenes from the White Hills are similar in composition to those reported by Malpas (1976) and Ernst (1978), but are slightly more diopside-rich than clinopyroxenes of Group I xenoliths from San Carlos (Frey and Prinz, 1978).

b. Pyroxenite Veins, Gabbro and Chromitite

Clinopyroxene compositions from the various pyroxenite and gabbro veins and chromitite are listed in Tables AII.10., AII.11., and AII.12. and plotted in Figure 3.2. These clinopyroxene compositions differ mainly in the concentrations of the minor elements TiO_2, Cr_2O_3 and Al_2O_3 and the major elements MgO and FeO*, as illustrated in Figures 3.4. and 3.5. For the various White Hills Peridotite 'cumulate' lithologies (see Chapter 5), there is a linear increase in Ti/(Ti + Al) (cation proportions) of clinopyroxene with a decrease in Mg/(Mg + Fe*) (cation proportions); these lithologies also define distinct compositional fields. A similar, but antipathetic, trend results when the Cr/(Cr + Al) (cation proportions) ratio of clinopyroxene is plotted against the Mg/(Mg + Fe*) (cation proportions) ratio of clinopyroxene from these lithologies.

Clinopyroxene compositions have been used to indicate the chemistry of the liquid during their formation, e.g., LeBas (1962) suggests the $Al^{\frac{1}{4}}$ Si tetrahedral site substitution in clinopyroxene can be used to indicate magma types; such a plot containing White Hills Peridotite mineral data is shown in Figure 3.6. The clinopyroxene compositions of the rocks from White Hills plot in both the tholeiite and alkaline fields, but more specifically, clinopyroxene compositions from rocks associated with the chromite pod plot in only the tholeiite field and those from gabbro veins plot nearly

* total iron



Figure 3.4. Plot of (Ti/Ti+Al) vs. (Mg/Mg+Fe*) (cation proportions) for the clinopyroxene from the White Hills Peridotite. The dashed lines that separate the lithological fields are approximate (fit by eye) and may not be statistically meaningful or applicable to other complexes.
Symbols:

- △ orthopyroxenite
- ● websterite
- ○ clinopyroxenite
- ★ wehrlite
- ▲ gabbro

The clinopyroxenite symbol close to the gabbro symbols is for a clinopyroxene (sample 78128) from the clinopyroxenite pod and the clinopyroxenite symbol near the upper Ti/(Ti+Al) ratio limit is for a clinopyroxene from a clinopyroxene vein (sample 7917) in the gabbro outcrop region (see Figure 2.9.). The orthopyroxenite symbol in the clinopyroxenite field is for a clinopyroxene from an orthopyroxene boudin in the basal thrust zone. * - total iron.

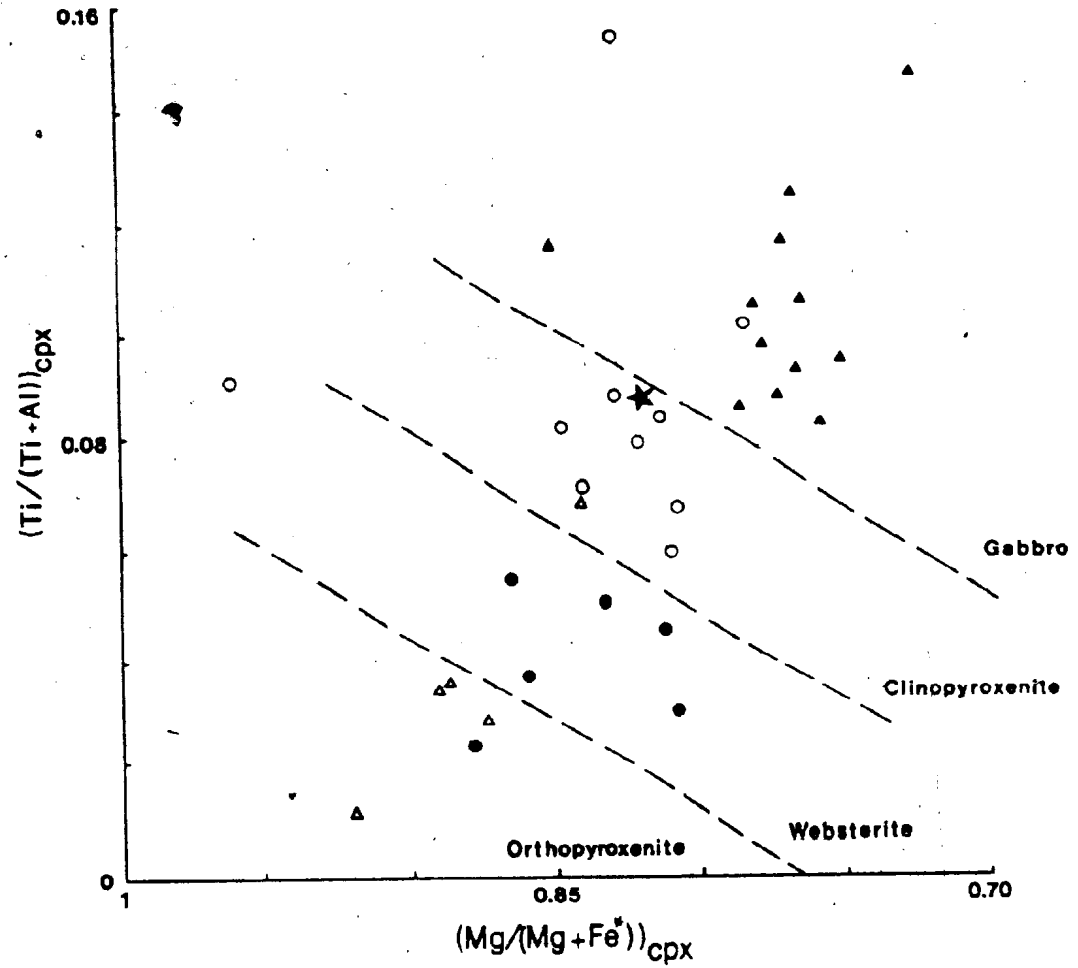
0.16
0.08
0
1
0.85
0.70
$(Ti/(Ti+Al))_{cpx}$
$(Mg/(Mg+Fe^*))_{cpx}$
Gabbro
Clinopyroxenite
Websterite
Orthopyroxenite

Figure 3.5. Plot of (Cr/Cr + Al) ratio vs. (Mg/Mg + Fe*) ratio (cation proportions) for clinopyroxenes from the White Hills Peridotite. Symbols as for Figure 3.4. Note: orthopyroxenite symbols near the upper Cr/(Cr + Al) ratio limit are for orthopyroxenes (samples 7898, 78123x) from the chromite-related litholgies. * - total iron.

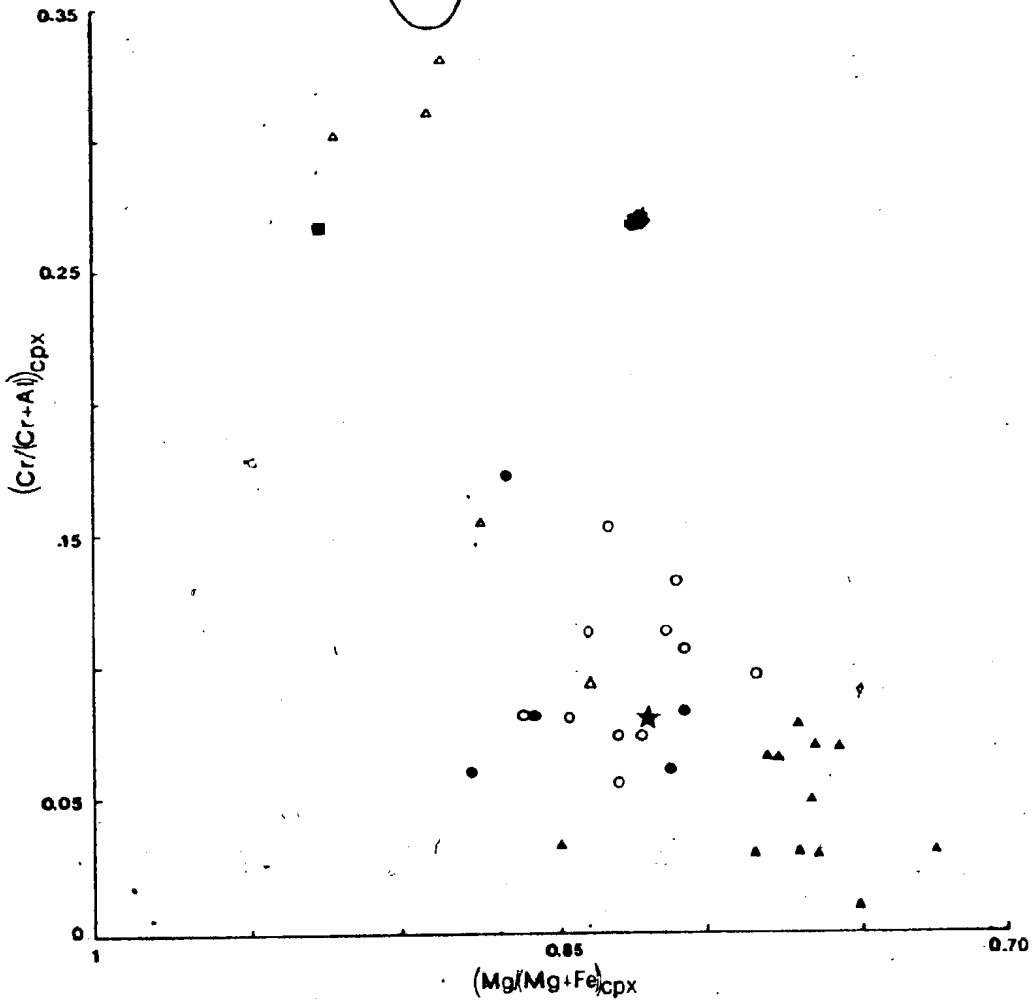
0.35
0.25
.15
0.05
0
1
0.85
0.70
(Cr/(Cr+Al))cpx
(Mg/Mg+Fe)cpx

exclusively in the alkaline field. A discussion of these chemical differences is presented in Chapter 5.

The quantity of TiO_2 in the clinopyroxenes from the various rock types is possibly a function of bulk rock composition (i.e., magma type), however the increase in TiO_2 content of the clinopyroxenes from orthopyroxenite veins to gabbro veins could probably be a result of falling temperature during crystallization (Thompson, 1974). Capedri and Venturelli (1979) describe the chemical variability of clinopyroxenes from ophiolite metabasalts and suggest that the chemical diversity of clinopyroxene compositions for the various Mediterranean ophiolites does not appear dependent on the physical conditions of crystallization, but on the bulk composition of the parent magma. Thompson's (1974) experimental results on high pressure crystallization of pyroxenes from natural lavas are in accord with the Capedri and Venturelli (1979) hypothesis. Thus the differences in the TiO_2, Al_2O_3 and perhaps Cr_2O_3 contents of clinopyroxene from the chromite associated setting relative to those of the pyroxenite and gabbro veins can be interpreted as a consequence of crystallization from distinct liquids of different compositions. Support for this type of evolution is present in the Troodos upper pillow lavas where the clinopyroxene phenocrysts have low abundances of Al_2O_3 and TiO_2 in contrast to clinopyroxene in the lower pillow lavas (Duncan and Green, 1980). The upper pillow lavas are thought to have been derived from an already depleted harzburgite (Smewing et al., 1975) and

Figure 3.6. Clinopyroxene analyses from the White Hills Peridotite plotted according to the method of LeBas (1962).
Symbols:

△ orthopyroxenite
▲ orthopyroxenite with disseminated chromite
◆ websterite
□ clinopyroxenite
⊘ wehrlite
● gabbro

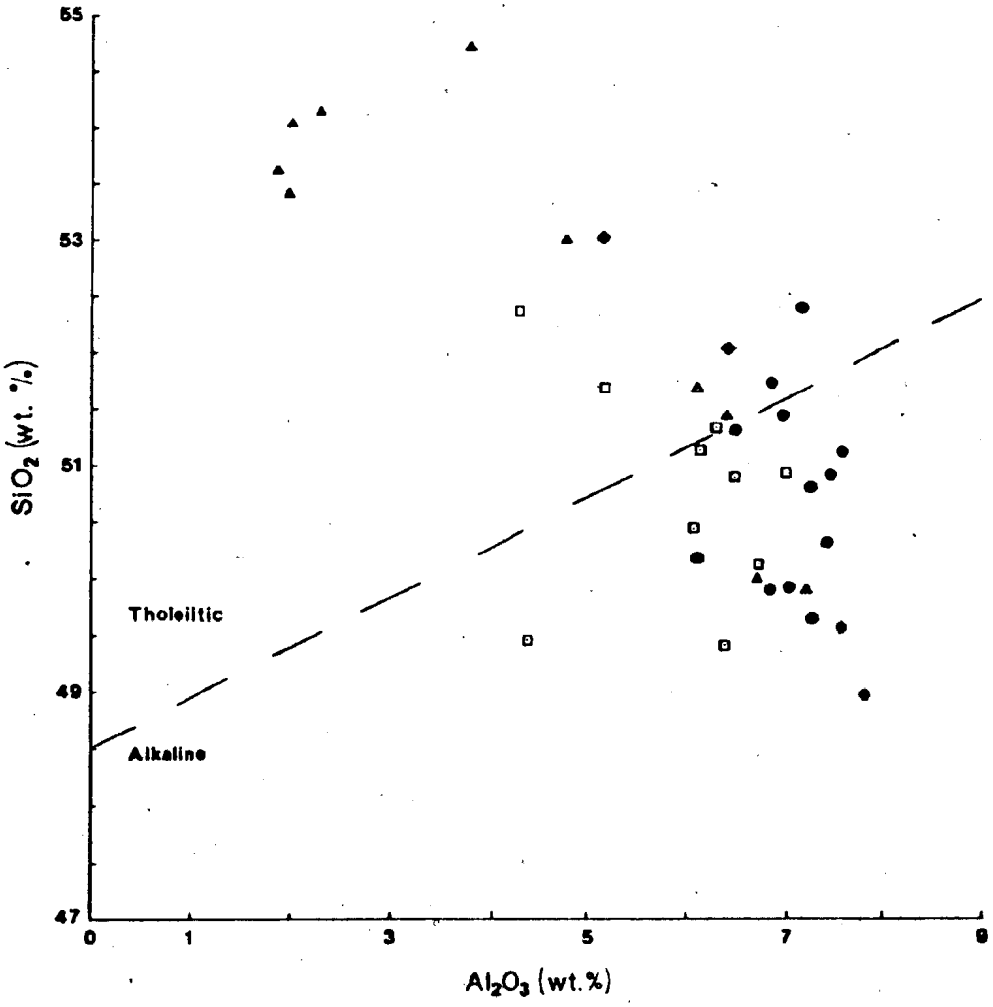
55
53
51
49
47
0
1
3
5
7
9
SiO2 (wt. %)
Al2O3 (wt.%)
Tholeiitic
Alkaline

recent experimental data support this hypothesis (Duncan and Green, 1980). On the other hand, the lower pillow lavas have probably been derived from a less-depleted source material (Smewing et al., 1975; Jaques and Green, 1980).

(i) estimation of equilibration temperatures and pressures

Three methods have been used to estimate equilibration temperatures for spinel lherzolite and harzburgite (Table 3. 2.). Two of the methods use the activity of $Mg_2Si_2O_6$ in orthopyroxene and clinopyroxene (Wood and Banno, 1973; Wells, 1977) and are calibrated using experimental data from natural and synthetic systems. The Wells (1977) method is an updated version, based on different thermodynamic values, of the Wood and Banno (1973) method. The third method is a two pyroxene method based on the partitioning of Al^{VI} and Cr between orthopyroxene and clinopyroxene and has been calibrated with natural rocks (Mysen, 1976). All three methods are based on the experimental data for the pyroxene solvus (Davis and Boyd, 1966) either directly (Wood and Banno, 1973; Wells, 1977) or indirectly (Mysen, 1976).

The calculated temperatures from the Wood and Banno (1973) and Wells (1977) methods range from 694°C to 1175°C, with the Wood and Banno (1973) method yielding temperatures up to approximately 100°C higher than for the Wells method. Wells (1977) has determined a similar discrepency for the two methods when applied to the mineral data of Wood and Banno (1973).

Table 3.2. Estimates of temperature for the equilibration of spinel lherzolite and harzburgite from the White Hills Peridotite.

Method	Reference	T^oC
activity of $Mg_2Si_2O_6$ in opx and cpx	Wood and Banno (1973)[1]	828-1175[a] (1011)[b]
activity of $Mg_2Si_2O_6$ in opx and cpx	Wells (1977)[2]	694-1099[a] (903)[b]
$K_D=(Al^{VI}/Cr)_{opx}/(Al^{VI}/Cr)_{cpx}$	Mysen (1976)[3]	975-1400[a] (1134)[b]

1. $$T^oK = \frac{-10202}{\ln \frac{a^{cpx}_{Mg_2Si_2O_6}}{a^{opx}_{Mg_2Si_2O_6}} - 7.65 \times x^{opx}_{Fe} + 3.88(x^{opx}_{Fe})^2 - 4.6}$$

2. $$T^oK = \frac{7341}{3.355 + 2.44 \times x^{opx}_{Fe} - \ln \frac{a^{cpx}_{Mg_2Si_2O_6}}{a^{opx}_{Mg_2Si_2O_6}}}$$

3. $$1/T = (0.26 \pm 0.01) \ln \frac{(Al^{VI}/Cr)_{opx}}{(Al^{VI}/Cr)_{cpx}} + (0.67 \pm 0.01)$$

a. range of equilibration temperatures for spinel lherzolite and harzburgite.

b. average temperature.

Mysen's (1976) method yields temperatures that range from 975°C to 1400°C for spinel lherzolite and harzburgite samples. The differences in the temperatures between the Mysen (1976) method and the two other methods is probably due to inaccuracies in determining the Al^{VI} content of the pyroxenes in the spinel lherzolites and harzburgites, and as stated by Mysen (1976) if the Cr_2O_3 and Al_2O_3 contents of the pyroxenes are high, greater than 1 weight percent and 6 weight percent, respectively, unreasonable temperatures result.

The equilibration temperatures for the White Hills Peridotite lithologies, using the Wood and Banno and the Wells method, are similar to temperatures calculated by Jamieson (1979) for rocks from the metamorphic aureole (Green Ridge Amphibolite) of the St. Anthony Complex.

Pressure estimates for the equilibration of the White Hills Peridotite spinel lherzolite using the Al_2O_3 content of enstatite (MacGregor, 1974) and CaO and Al_2O_3 contents for clinopyroxenes (O'Hara, 1967) range from a minimum pressure of approximately 2 kilobars to a maximum of approximately 40 kilobars, without regard for microstructure. Recently, both of these methods have received much criticism as to their usefullness as geobarometers (Wilshire and Jackson, 1975; Wood, 1975; Fujii, 1976; Herzberg and Chapman, 1976; Obata, 1976; Danckwerth and Newton, 1978), especially the former method. Fujii (1976), Obata (1976) and Danckwerth and Newton (1978) argue against applying the Al_2O_3 content

of enstatite for use as a geobarometer because the solubility of Al_2O_3 in orthopyroxene from spinel lherzolite compositions is insensitive to pressure, contrary to the experimental results of MacGregor (1974). Wood (1975) has shown that there are errors in MacGregor's (1974) experimental data (i.e., solubility of alumina in Mg-Al orthopyroxene co-existing with forsterite and spinel) which results in the steep positive slopes to the Al_2O_3 isopleths. In addition, the spinel-silicate textural and chemical data indicates that during subsolidus cooling Al_2O_3 is released by orthopyroxene to form spinel (Talkington and Malpas, 1980a). Similar results have been reported by Frey and Prinz (1978) for Group I xenoliths from San Carlos.

Herzberg and Chapman (1976) have experimentally shown that the $CaAl_2SiO_6$ molecule (calcium Tschermak) content of clinopyroxene varies sympathetically with the $MgSiO_3$ content of clinopyroxene with changes in temperature and pressure, and that these variations are predominantly temperature dependent in spinel lherzolite assemblages, therefore nullifying the O'Hara clinopyroxene geobarometer.

In lieu of using a specific thermodynamically determined geobarometer, a mineralogical geobarometer using modal mineralogy is preferred, i.e., olivine + orthopyroxene + clinopyroxene + spinel. If the theoretical calculations of Obata (1976) are accepted, then in the system CaO-MgO-Al_2O_3-SiO_2 in a pressure range from approximately 8 kilobars to approximately 20 kilobars at 1300°C, the spinel lherzolite mineralogy is a stable assemblage.

4. Plagioclase

Plagioclase compositions from the gabbro veins are listed in Table AII.13. The compositions of these plagioclases vary from An_{42} to An_{70}. The lower An content plagioclase occurs in the most deformed rocks which have been affected by metasomatic alteration during deformation. The higher An content plagioclase occurs in either the least deformed gabbros or in the more plagioclase-rich samples.

II.3.B. Bulk Rock Chemistry

Chemical analyses and CIPW norms for the rocks of the White Hills Peridotite are compiled in Appendix IV. Major elements have been determined by X-ray fluorescence spectrometry except for the gabbro vein samples and samples 782 and 78144 which have been determined by atomic absorption spectrophotometry. Na_2O has been determined by atomic absorption spectrophotometry for all samples and all trace elements have been determined by X-ray fluorescence spectrometry. Analytical procedures for X-ray fluorescence and atomic absorption methods, and precision and accuracy of determinations of major and trace element analyses are given in Appendix I. Rare earth elements (REE) have been determined by instrumental neutron activation analysis (INAA). REE analyses for rocks of the White Hills Peridotite and analytical procedures for this technique are listed in Appendix I.

1. Linear Variation Diagrams

All major and trace element data are plotted against MgO (Figures 3.7. and 3.8.) and for Ni, $CaO+TiO_2$ and Al_2O_3 against FeO*/(FeO*+MgO) ratio (Figures 3.9., 3.10., 3.11.). This latter ratio is an indicator of mafic mineral differentiation (Miyashiro, 1973).

Sympathetic increases in CaO, Al_2O_3, Na_2O, K_2O, TiO_2 and P_2O_5 reflect the increase in modal abundances of plagioclase and pyroxenes (mainly clinopyroxene). Some of the TiO_2 may be incorporated in ilmenite or spinel, but the lack of these phases as primary crystallization products (except chromite in dunite) suggests most titanium is in clinopyroxene. Fe_2O_3 and FeO decrease with decreasing MgO content as a consequence of magma differentiation, which is best recorded by the pyroxenite vein assemblages. MnO remains constant for rocks high in mafic mineral content but decreases in gabbro as plagioclase becomes a more important phase.

The trace element data trends show good separation into characteristic groupings on the basis of modal mineralogy and mineral accumulation. The most noticeable trends are for Ni, V, Cu, Sr, Zr, and Zn. Ni is concentrated in olivine and is usually nearly exhausted from the liquid phase during the initial stages of crystallization (Burns, 1973), thus producing a progressive decrease in nickel from dunite to gabbro. Vanadium is usually concentrated in pyroxene, with minor amounts in spinel (see Chapter 4). The increase in V

* total iron as FeO

Figure 3.7. Major elements vs. MgO (wt. %) from the White Hills Peridotite.
Symbols:

◆ spinel lherzolite
● harzburgite
△ dunite
○ orthopyroxenite
□ websterite
▲ clinopyroxenite
◇ wehrlite
■ gabbro
⌀ low alumina orthopyroxenite



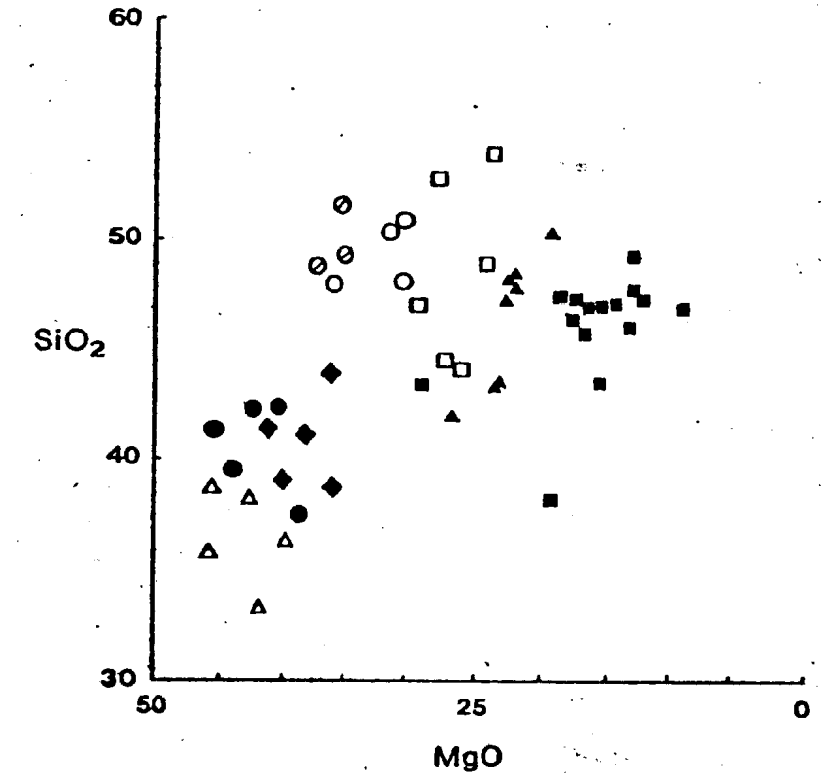
60
50
40
30
SiO_2
50
25
0
MgO

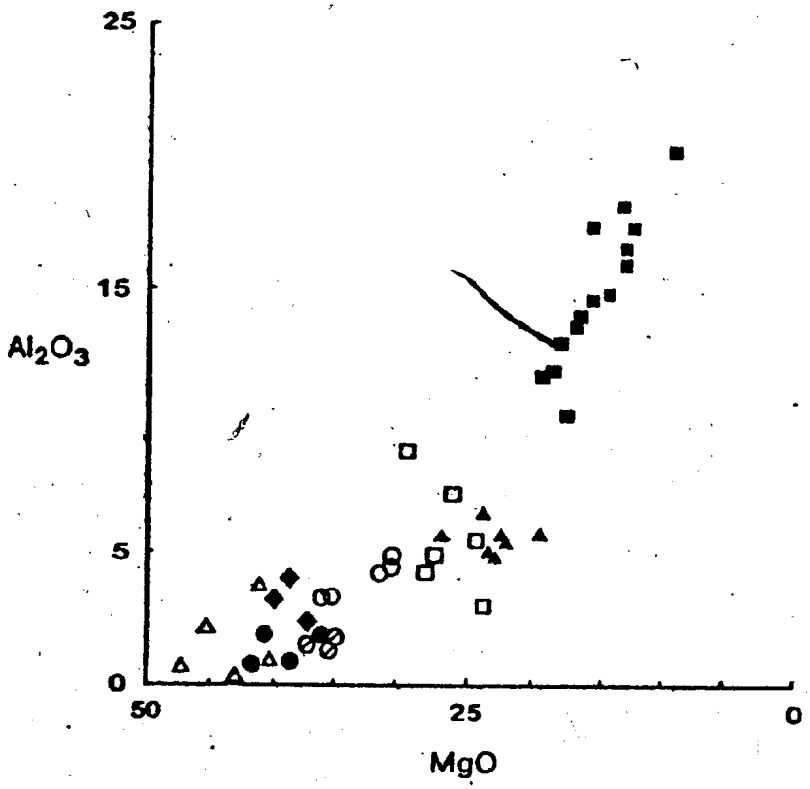
25
15
5
0
Al_2O_3
50
25
0
MgO

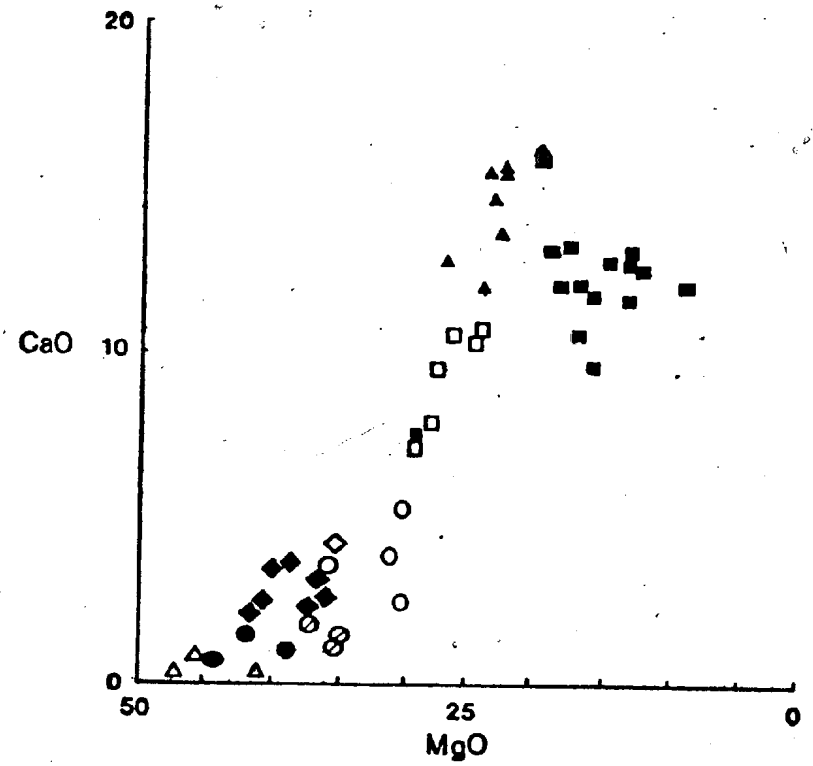
20
CaO
10
0
50
25
0
MgO

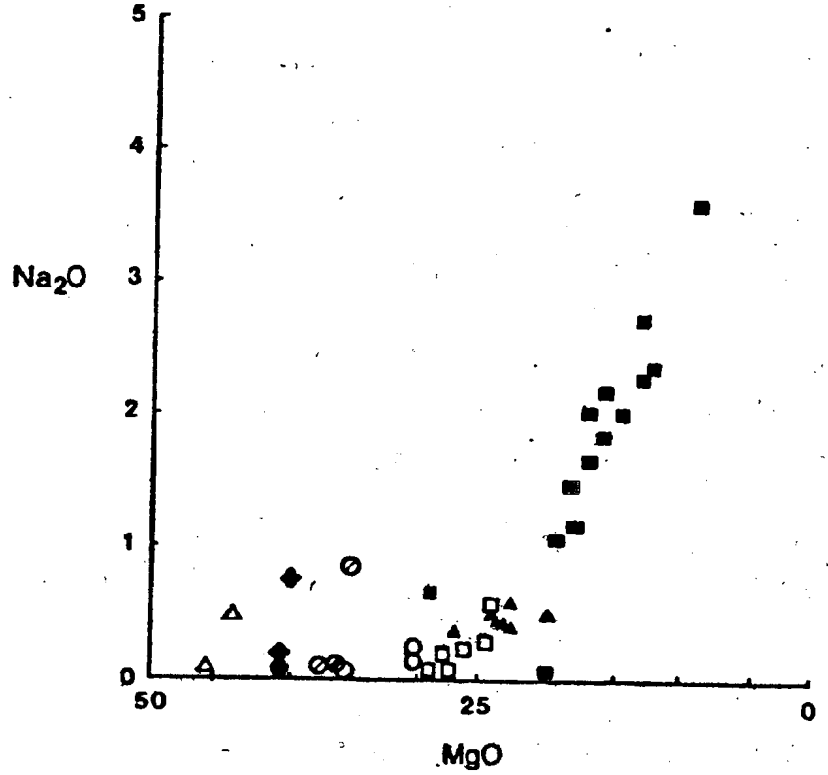
5
4
Na_2O
3
2
1
0
50
25
0
MgO

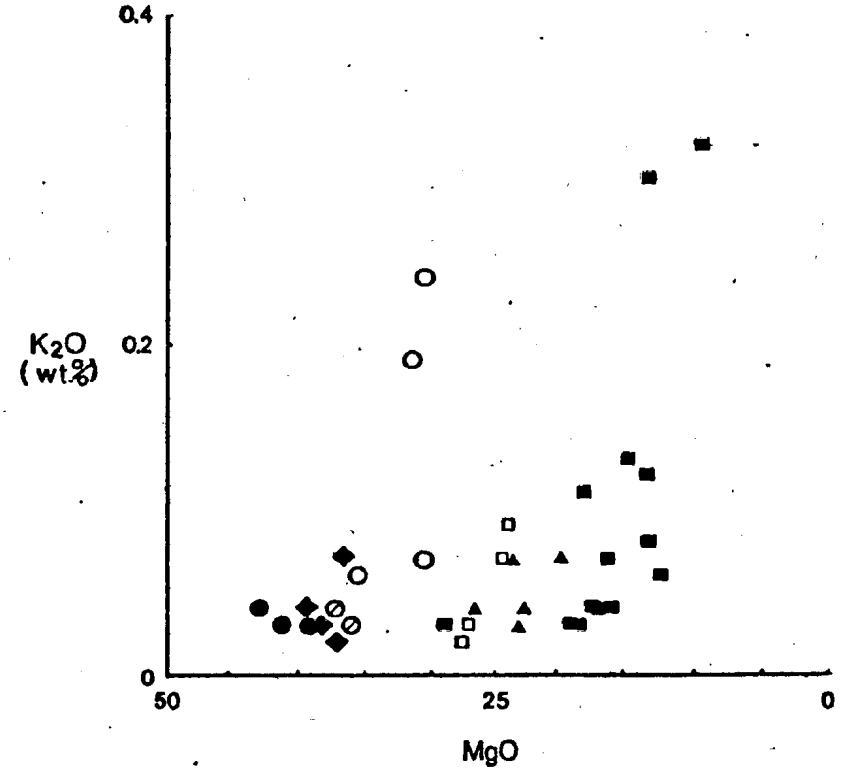
0.4
0.2
0
K_2O (wt.%)
50
25
0
MgO

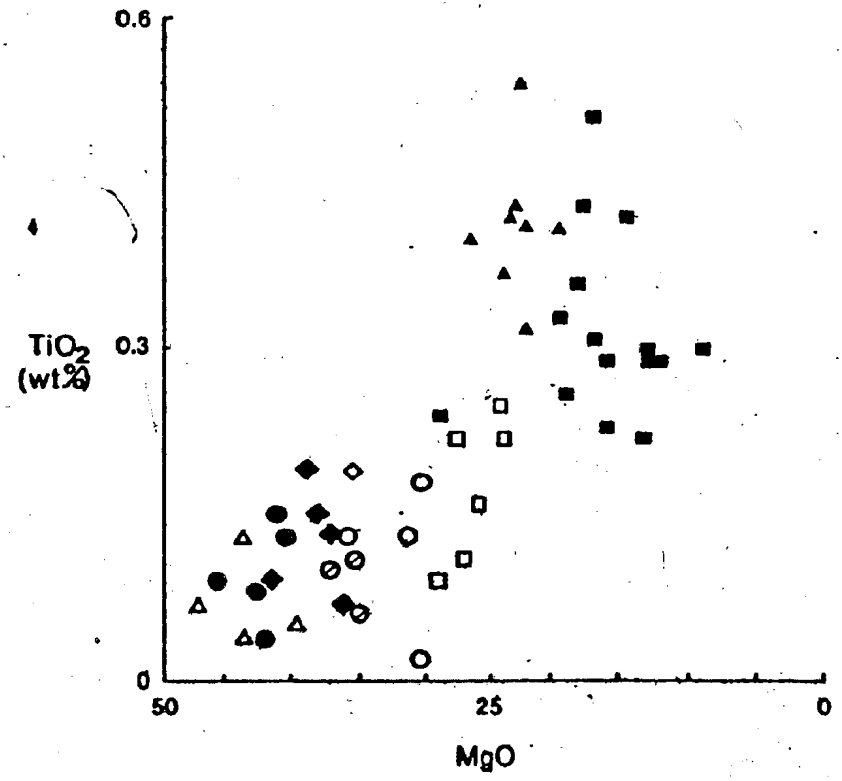
0.6
0.3
0
TiO_2 (wt.%)
50
25
0
MgO

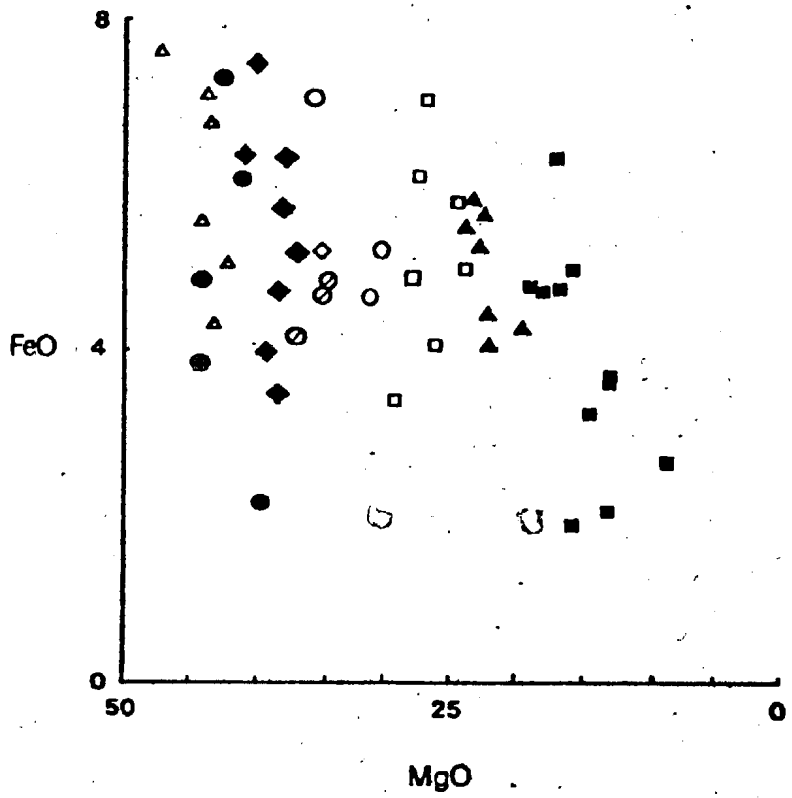
8
FeO
4
0
50
25
0
MgO

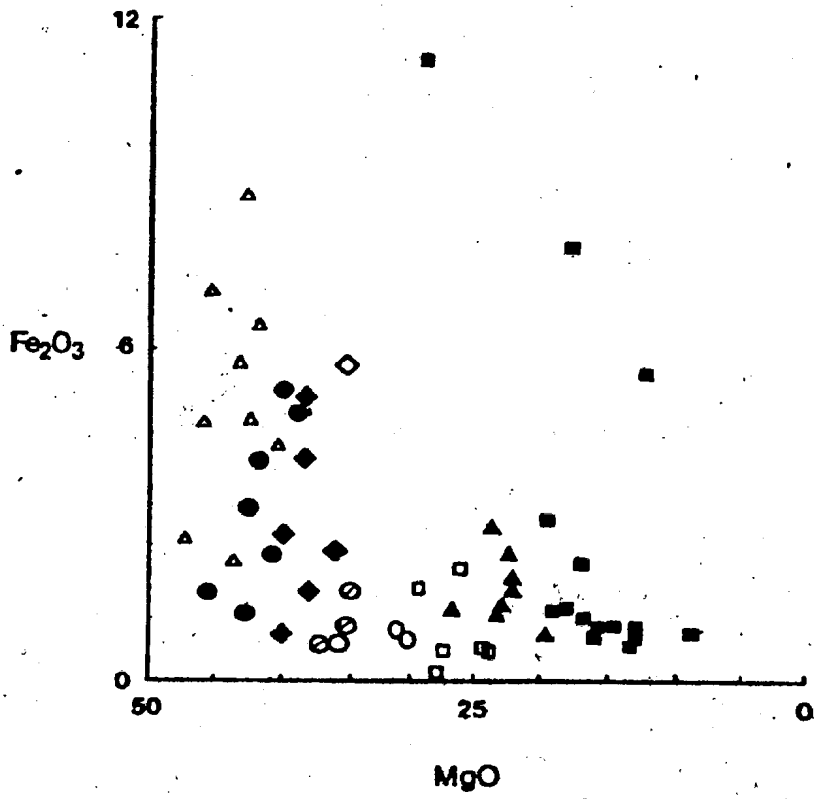
12
Fe_2O_3
6
0
50
25
0
MgO

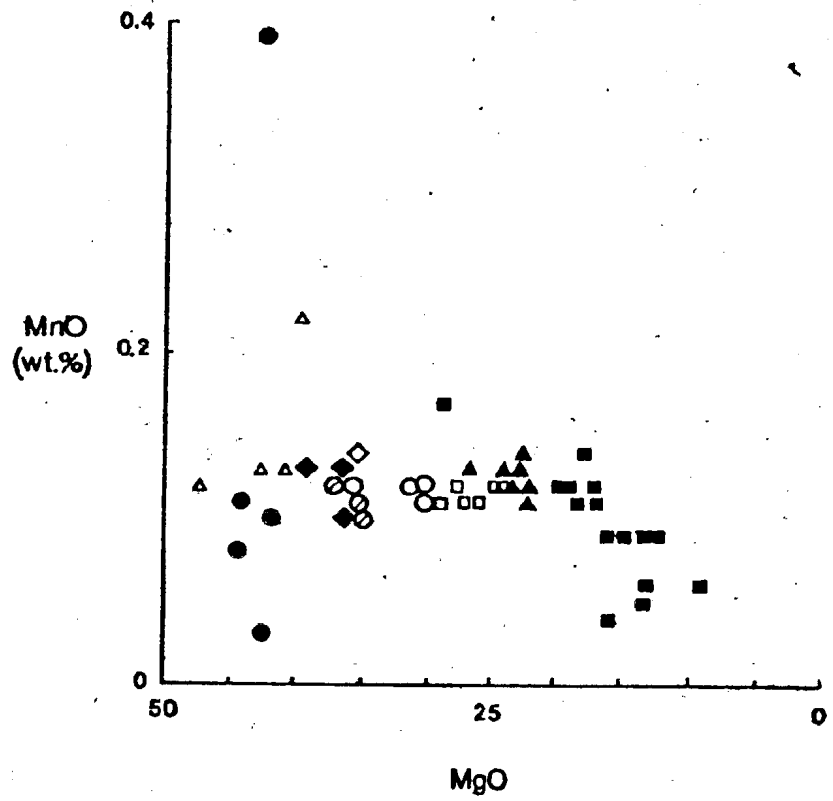
0.4
0.2
0
MnO
(wt.%)
50
25
0
MgO

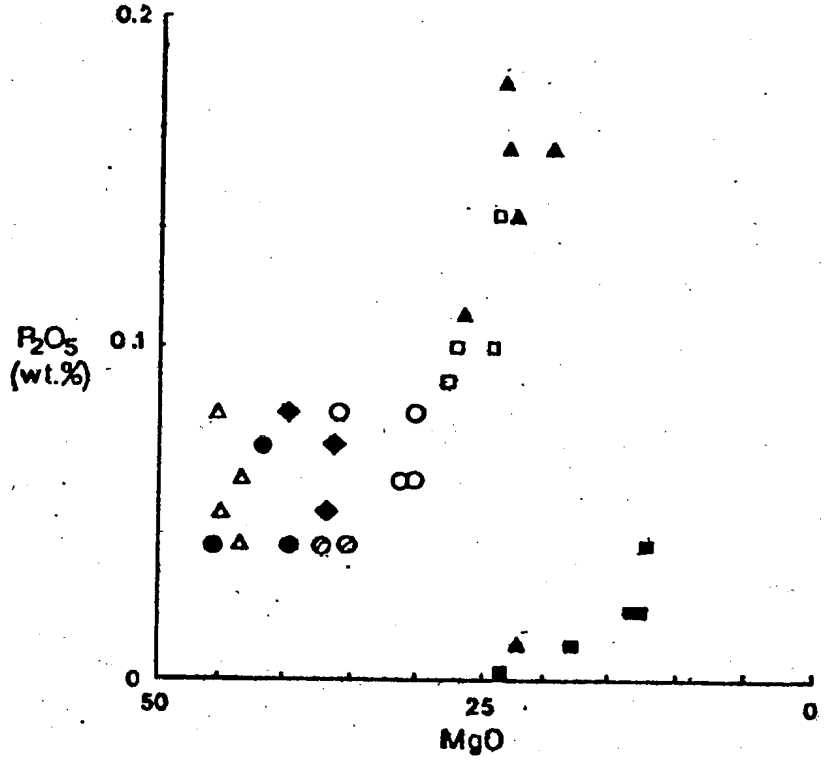
0.2
0.1
0
P_2O_5
(wt.%)
50
25
0
MgO

Figure 3.8. Trace elements (ppm) vs. MgO (wt. %) from the White Hills Peridotite. Symbols as for Figure 3.7.

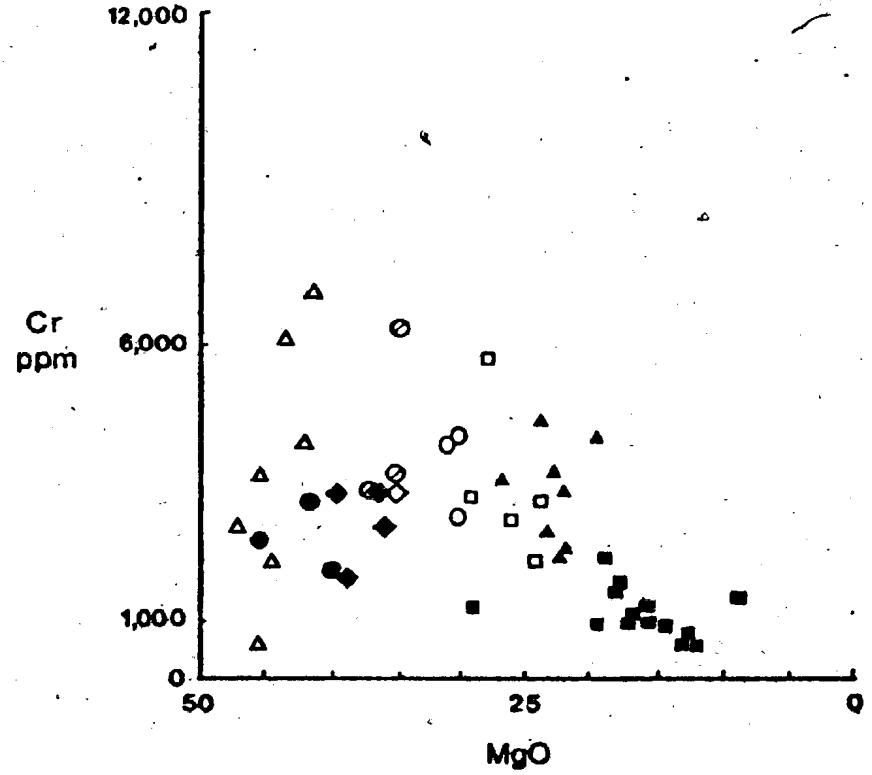
12,000
6,000
1,000
0
Cr
ppm
50
25
0
MgO

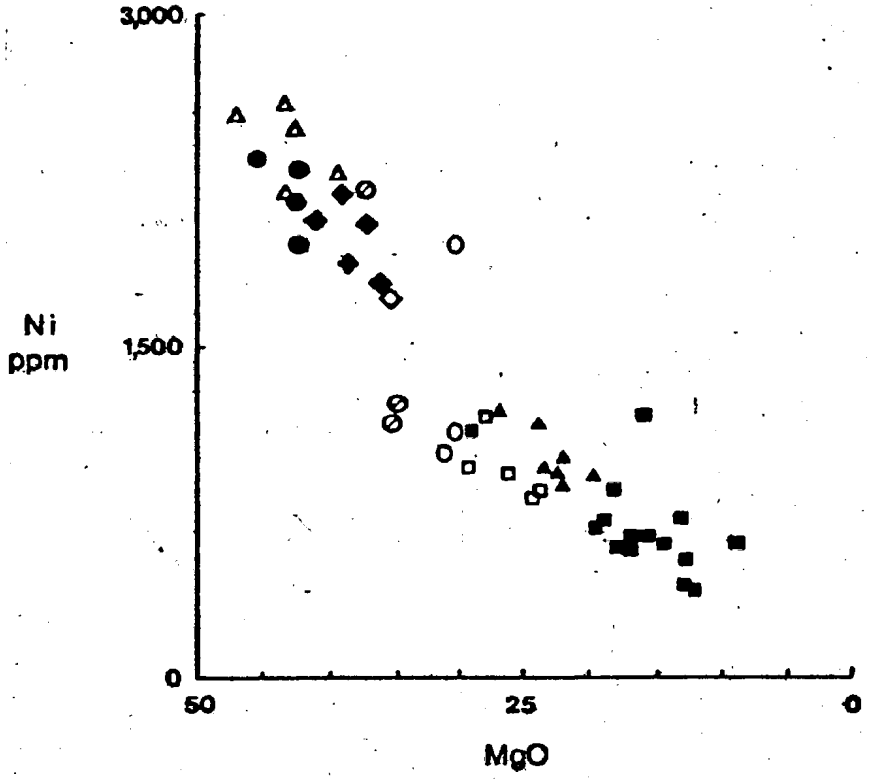
3,000
1,500
0
Ni
ppm
50
25
0
MgO

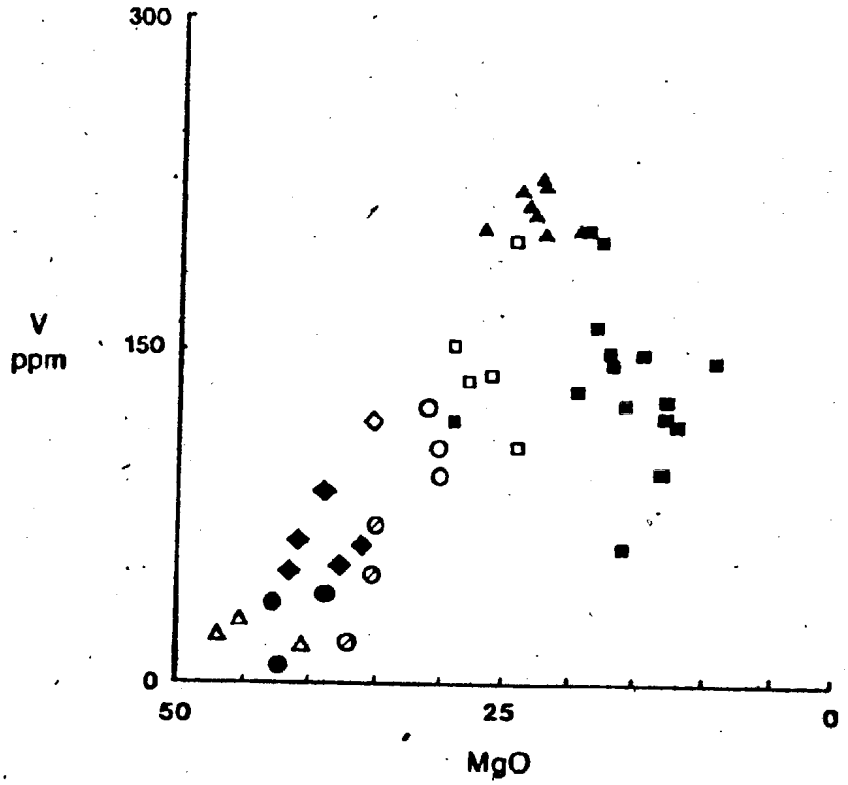
300
150
0
V
ppm
50
25
0
MgO

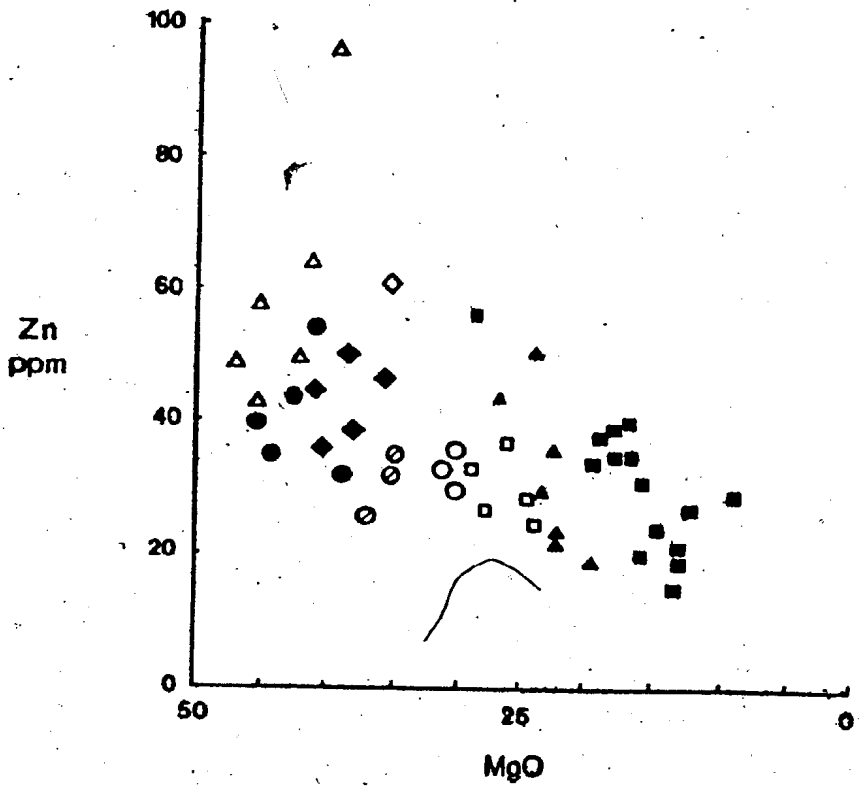
100
80
60
40
20
0
Zn
ppm
50
25
0
MgO

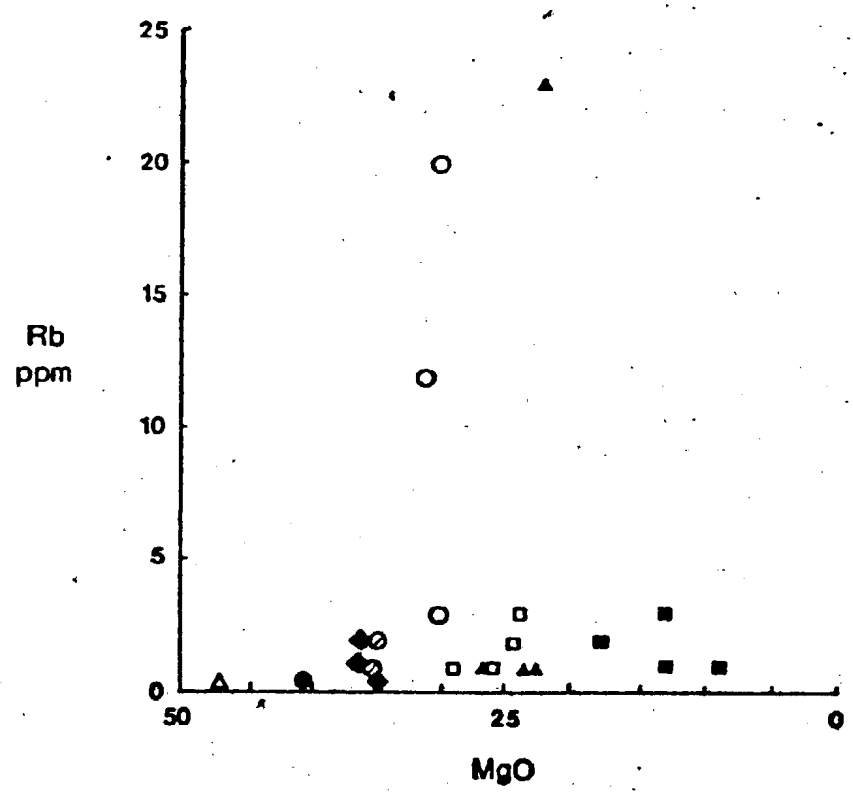
25
20
15
10
5
0
Rb
ppm
50
25
0
MgO

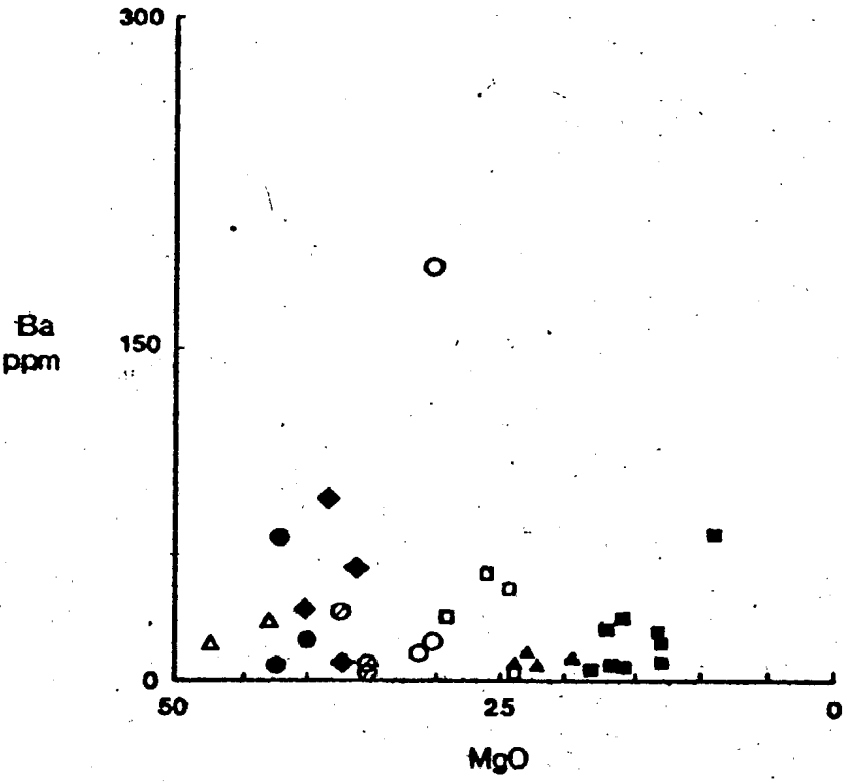
300
150
0
Ba
ppm
50
25
0
MgO

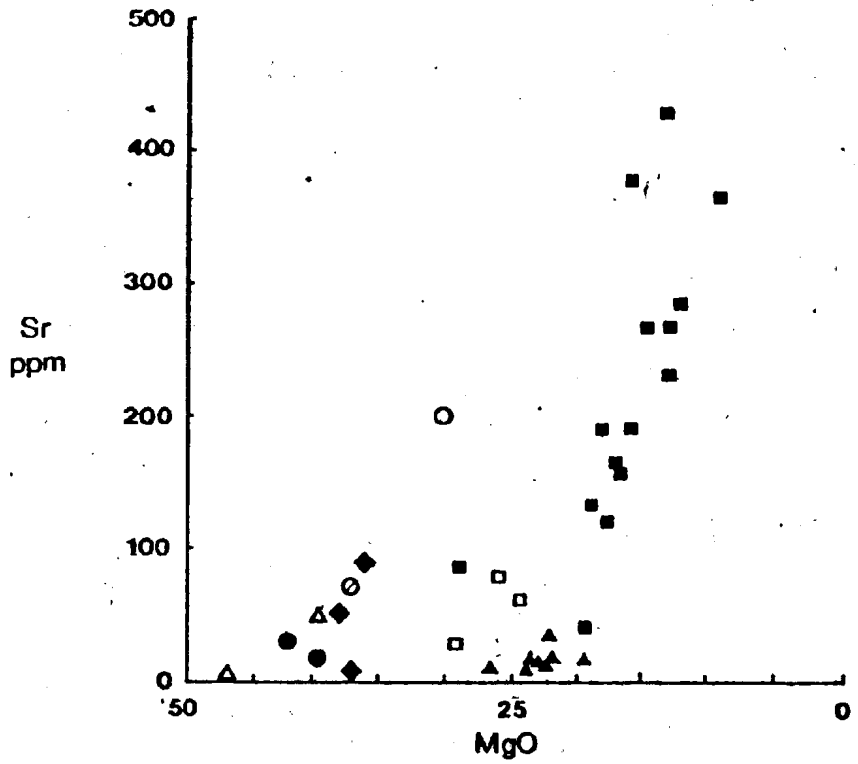
500
400
300
200
100
0
Sr
ppm
50
25
0
MgO

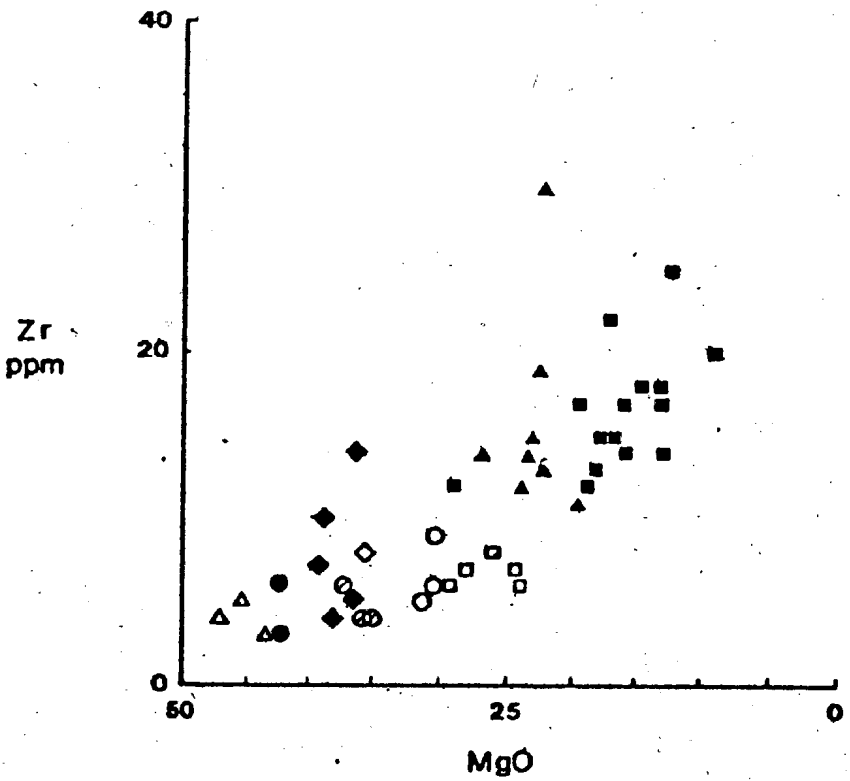
40
20
0
Zr
ppm
50
25
0
MgO

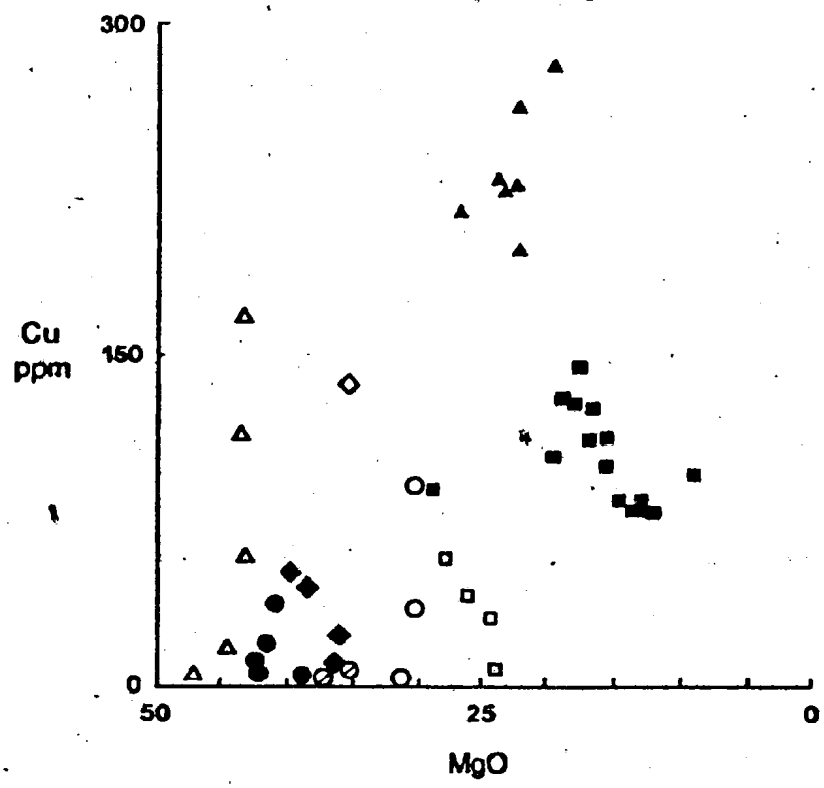
300
150
0
Cu
ppm
50
25
0
MgO

content from dunite to clinopyroxenite and its decrease in gabbro is caused by an increase in modal clinopyroxene and the appearance of plagioclase in gabbro, respectively. Cu behaves similiarly to V, but is more strongly partitioned into clinopyroxene. Zr is concentrated in the later rock types either substituting for Ti in ilmenite or in pyroxene (Taylor, 1965). Zn shows a relative depletion as MgO decreases and appears to be concentrated in cumulus spinel (gahnite molecule-$ZnAl_2O_4$); though it may also substitute for Fe^{3+} in magnetite (Wager and Brown, 1968). Sr freely substitutes for Ca, accounting for the high concentration in the gabbro. Ba and Rb occur in trace quantities in all rock types; anomalously high concentrations are attributed to metasomatism, since samples with high concentrations of these elements occur in the internal faults (within the peridotite) and at the basal thrust fault. Cr is concentrated in the chromite of the dunite accumulations and in the pyroxenes where it substitutes for Fe^{3+} (Taylor, 1965).

Ni, $CaO+TiO_2$ and Al_2O_3 of the bulk rock and various mineral phases of the White Hills Peridotite are plotted against $FeO^*/(FeO^*+MgO)_{B.R.}$[1] to illustrate the course of crystallization for the cumulate rocks (Figures 3.9., 3.10., 3.11.). Figure 3.11. clearly shows the effect of the accumulation of plagioclase. Similar mineral crystallization (accumulation) trends have been reported for the cumulate zone rocks from the Bay of Islands Complex (Malpas, 1976),

1 B.R. - bulk rock



Figure 3.9. Plot of Ni (ppm) vs. FeO*/(FeO* + Mg) (wt. %) ratio of probable cumulate rocks from the White Hills Peridotite.
* - total iron as FeO.
Symbols:

- ● Dunite
- ▲ Orthopyroxenite
- ▲ Orthopyroxenite with disseminated chromite
- ○ Websterite
- □ Clinopyroxenite
- ◎ Wehrlite
- ■ Gabbro

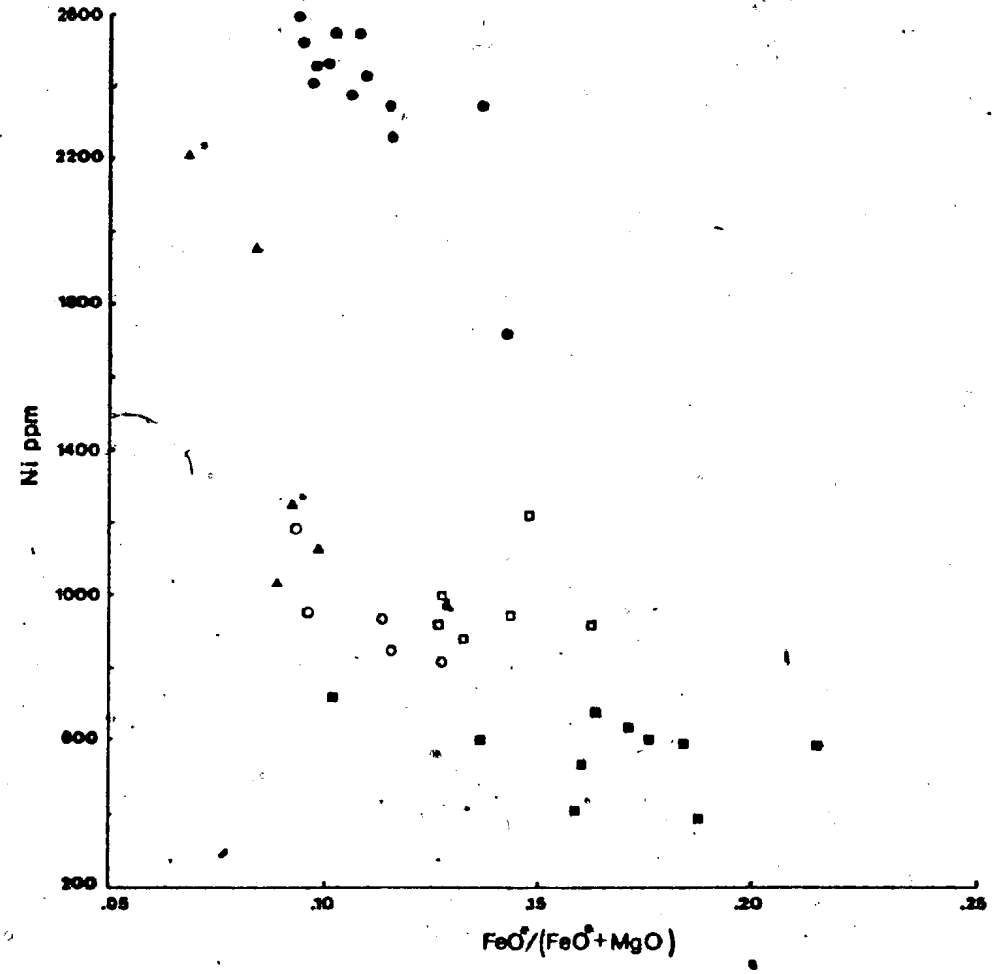
2600
2200
1800
1400
1000
600
200
Ni ppm
.05
.10
.15
.20
.25
FeO*/(FeO*+MgO)

Figure 3.10. Plot of CaO + TiO_2 (wt. %) vs. FeO*/(FeO* + MgO) (wt. %) ratio of probable cumulate rocks from the White Hills Peridotite. Symbols as for Figure 3.9. * - total iron as FeO.

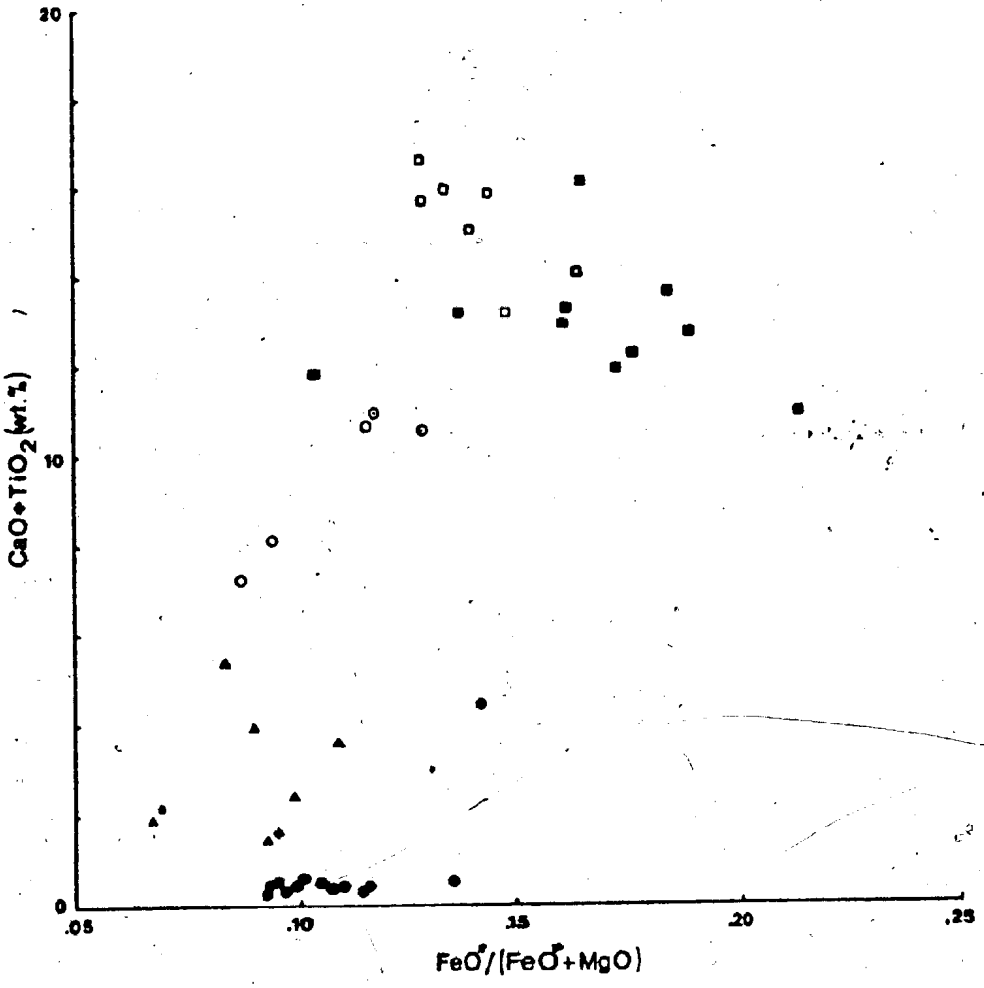
20
10
0
CaO+TiO2 (wt.%)
.05
.10
.15
.20
.25
FeO*/(FeO*+MgO)

Figure 3.11. Plot of Al_2O_3 (wt. %) vs. FeO*/(FeO* + MgO) (wt. %) ratio of probable cumulate rocks from the White Hills Peridotite. Dashed line approximates plagioclases accumulation (some Al_2O_3 is present in the pyroxenes and spinel). Symbols as for Figure 3.9. * - total iron as FeO.

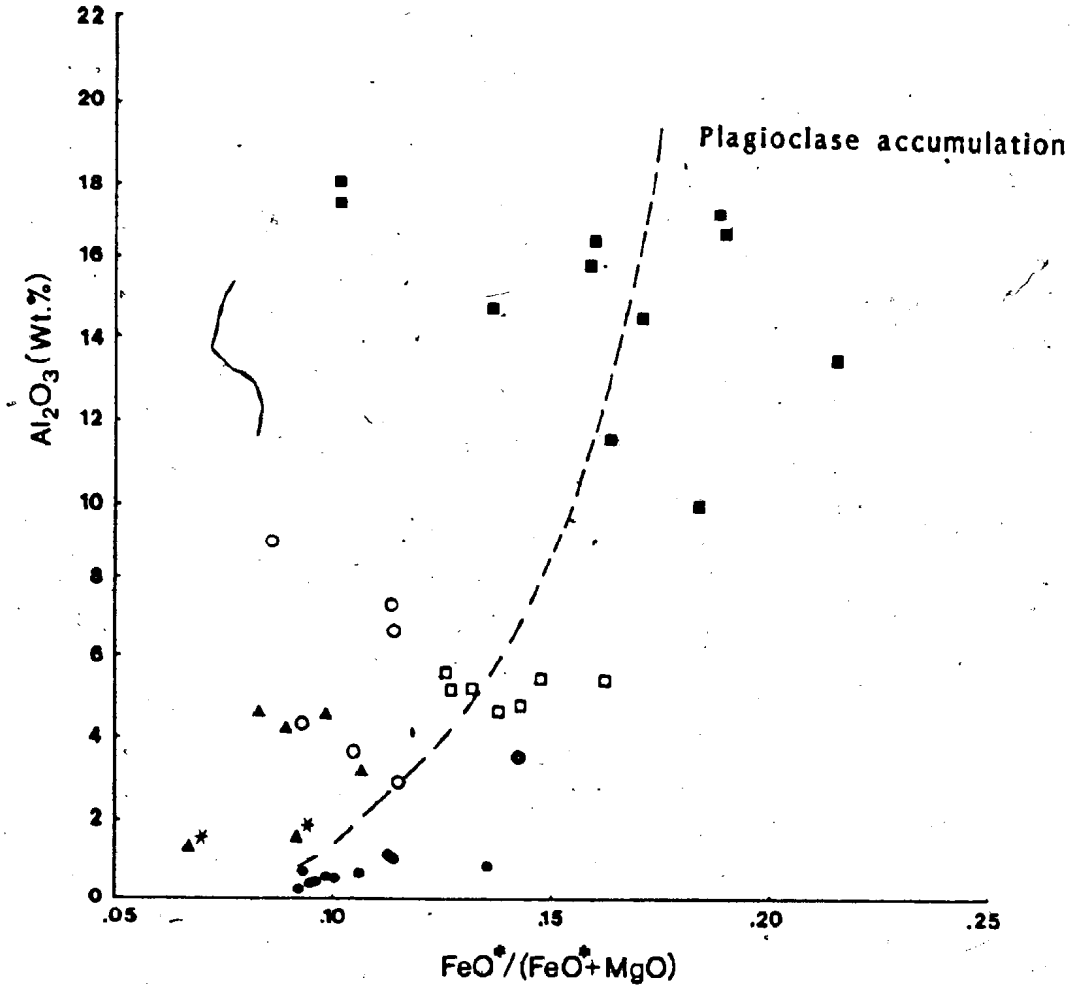
Plagioclase accumulation
Al_2O_3 (Wt.%)
22
20
18
16
14
12
10
8
6
4
2
0
.05
.10
.15
.20
.25
$FeO^*/(FeO^*+MgO)$

Betts Cove ophiolite (Church and Riccio, 1977) and for the Muskox Stratiform Intrusion (Irvine, 1970).

2. AFM Diagrams

The rock types of the White Hills Peridotite are compared with rocks from other ophiolites and rocks from present oceanic environments (Figure 3.12.). The standard Skaergaard and Hawaii differentiation trends are used for reference.

In Figure 3.12.A., the gabbro vein analyses plot at the lower portion of the Bay of Islands gabbro field. A few of the White Hills gabbro samples show a slight alkali enrichment, a result of plagioclase alteration; overall the gabbro compositions are similar to the Mg-rich gabbros from the Mid-Atlantic Ridge at 24°N (Thompson, 1973) and 26°N (Tiezzi, 1977), but are less iron rich than gabbro samples from the Romanche Trench (Thompson, 1973).

Pyroxenite vein samples (Figure 3.12.B.) plot on the AFM diagram in a similar position to cumulate zone pyroxenite samples reported by Bailey and Blake (1974) for worldwide ophiolite occurrences.

Spinel lherzolite, harzburgite and dunite analyses define a compositional field (Figure 3.12.B.) similar to other ophiolites.

3. Rare Earth Elements

Rare earth element (REE) data for three gabbro vein samples are plotted in Figures 3.13., 3.14., and 3.15. where they are compared to REE fields and patterns from various ophiolites (Menzies et al., 1977; Suen et al., 1979),

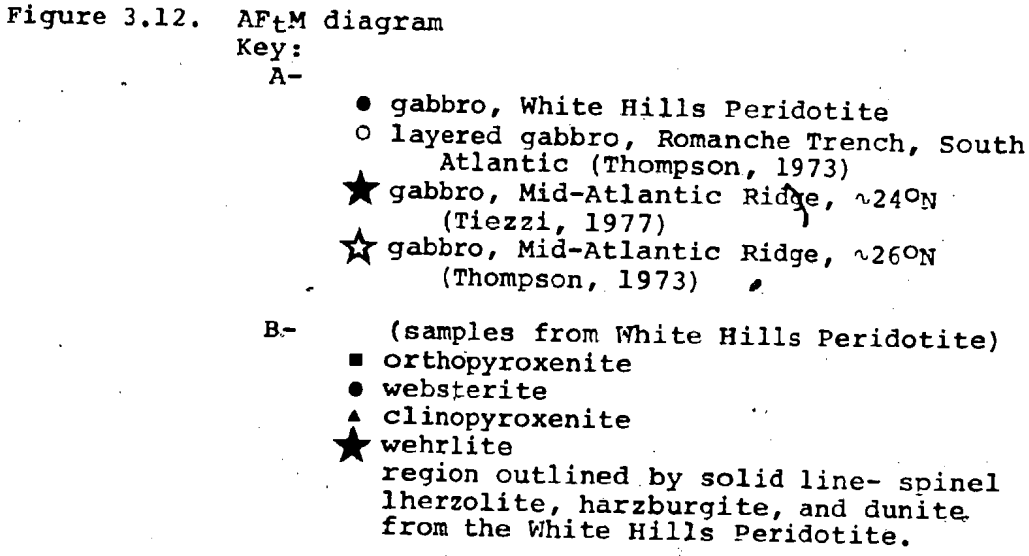

Figure 3.12. AF_tM diagram
Key:
A-
- ● gabbro, White Hills Peridotite
- o layered gabbro, Romanche Trench, South Atlantic (Thompson, 1973)
- ★ gabbro, Mid-Atlantic Ridge, ~24°N (Tiezzi, 1977)
- ☆ gabbro, Mid-Atlantic Ridge, ~26°N (Thompson, 1973)

B- (samples from White Hills Peridotite)
- ■ orthopyroxenite
- ● websterite
- ▲ clinopyroxenite
- ★ wehrlite

region outlined by solid line- spinel lherzolite, harzburgite, and dunite from the White Hills Peridotite.

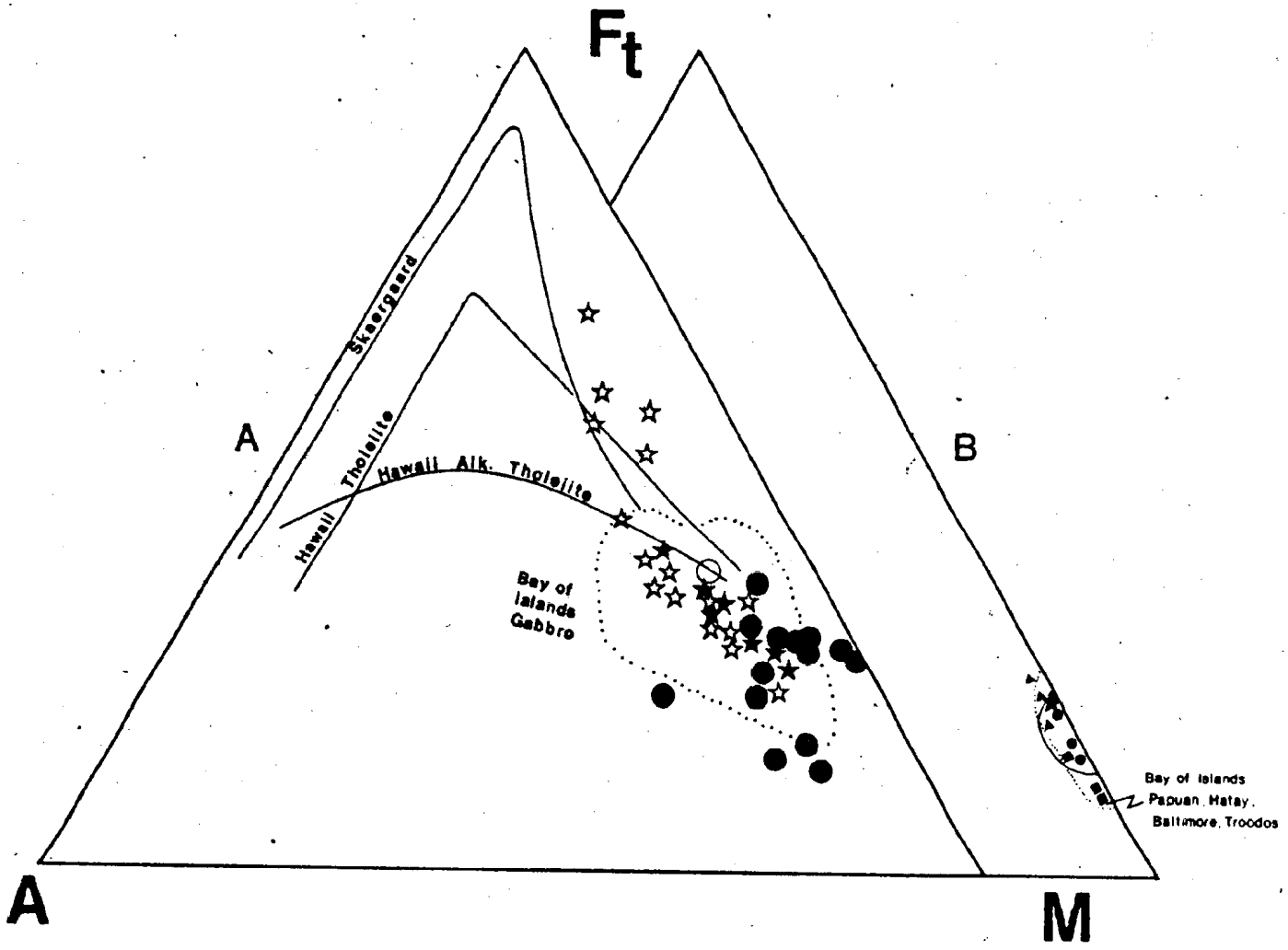
Ft
A
Skaergaard
Tholeiite
Hawaii Alk. Tholeiite
Hawaii
B
Bay of
Islands
Gabbro
Bay of Islands
Papuan, Hatay,
Baltimore, Troodos
A
M

a Proterozoic ophiolitic assemblage (Strong and Dostal, 1980) and oceanic gabbros (Frey et al., 1973, in Strong and Dostal, 1980). The rare earth element abundances have been normalized against chondritic abundances and are plotted against atomic number.

The three White Hills Peridotite gabbro samples have low REE abundances (Appendix I) and the chondrite normalized patterns are characterized by a relative light REE (LREE) depletion and moderate positive Eu anomalies that are characteristic of gabbros from ophiolites and the Mid-Atlantic Ridge (Suen et al., 1979). The chondrite normalized REE patterns of the White Hills gabbros are higher than the olivine-clinopyroxene gabbro (LK) from the Point Sal Ophiolite (Menzies et al., 1977) and gabbros from the Bay of Islands Complex (Suen et al., 1979) (Figure 3.13.), yet, the White Hills gabbros lie mainly within the oceanic gabbro field (Figure 3.14.) except for the sample 77WH89 which has slightly lower La and Eu contents. The low Eu content of sample 77WH89 may be due to the lack of plagioclase in the rock ($\sim$ 13.0 modal %); as Eu is strongly partitioned in to plagioclase (Menzies et al., 1977; Suen et al., 1979) or may reflect the extensive crystallization of plagioclase during an early stage of magma fractionation (Menzies et al., 1977; Shih and Gast, 1971). The lower La content may reflect a higher clinopyroxene content. The bulk rock chemistry for sample 77WH89 (MgO = 29.00 wt. %, Al_2O_3 = 5.90 wt. %; Ni = 119 ppm, Cr = 1263 ppm, V = 118 ppm) appears to support the low plagioclase/

Figure 3.13. Chondrite normalized rare earth element (REE) patterns of gabbro veins from the White Hills Peridotite. Absolute REE abundances for these gabbro veins are compiled in Appendix I.
Key:

- ▲ gabbro vein (77WH60)
- ■ gabbro vein (77WH89)
- ● gabbro vein (77WH90)
- □ gabbro, Point Sal Ophiolite (Menzies et al., 1977)

Stippled field-gabbro, Bay of Islands Complex (Suen et al., 1979)

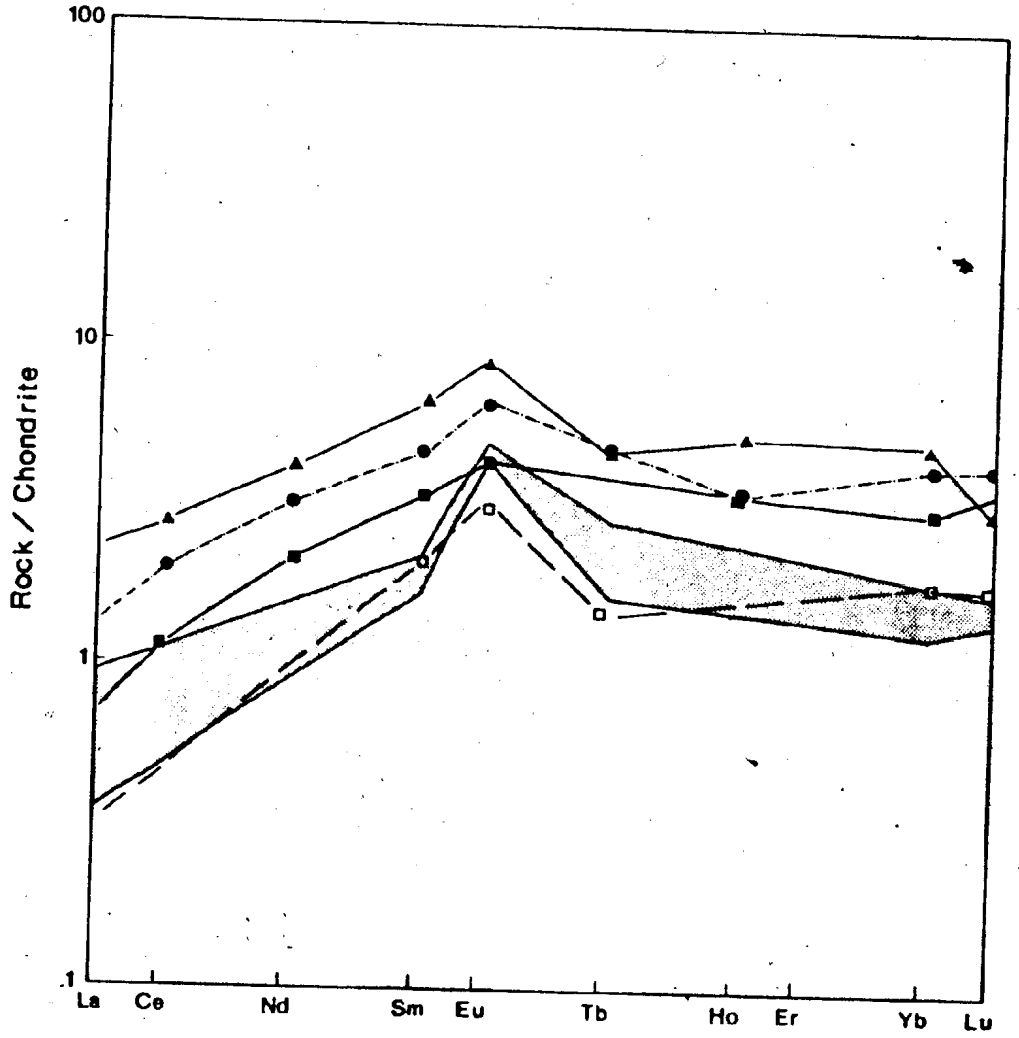
100
10
1
.1
Rock / Chondrite
La
Ce
Nd
Sm
Eu
Tb
Ho
Er
Yb
Lu

Figure 3.14. Chondrite normalized rare earth element (REE) patterns of gabbro veins from the White Hills Peridotite. Symbols as for Figure 3.13. Stippled field - Mid-Atlantic Ridge gabbros (in Strong and Dostal, 1980).

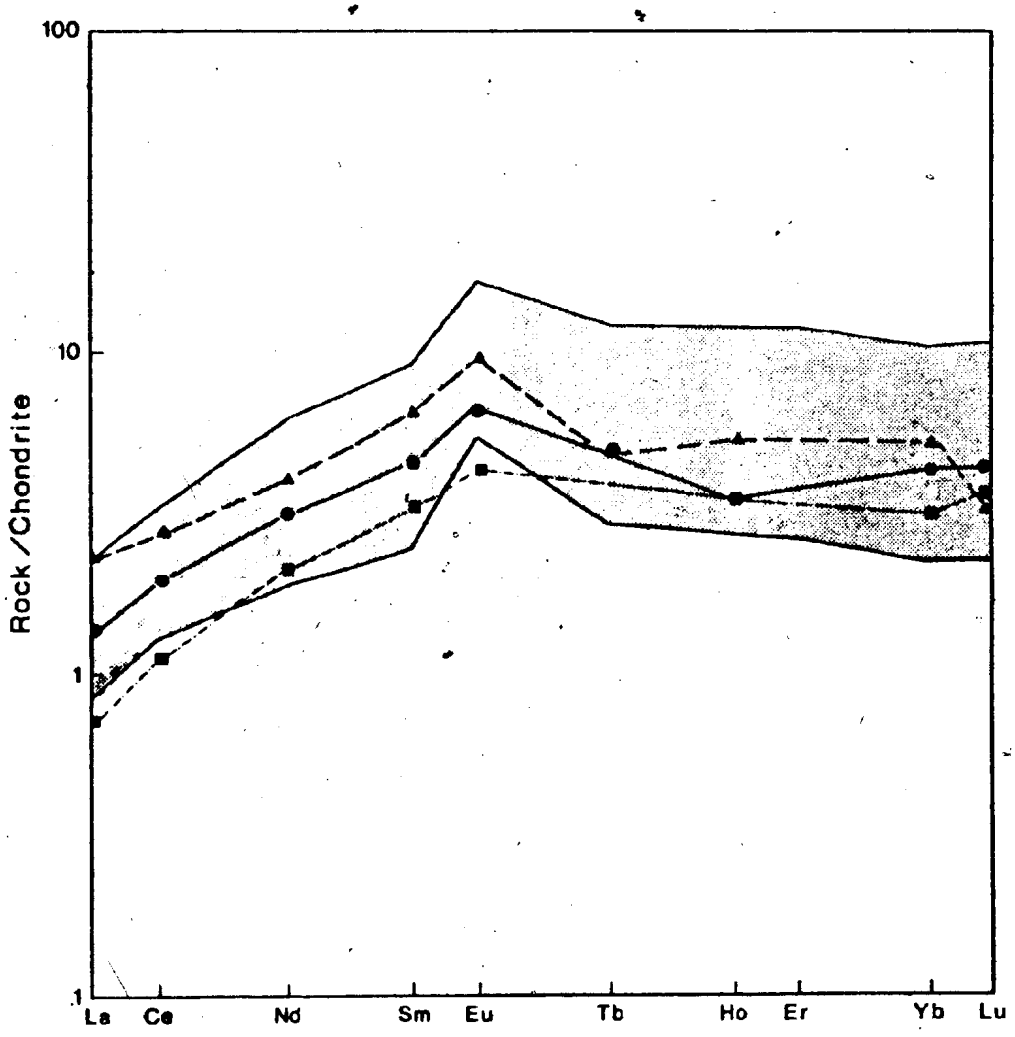
100
10
1
1
Rock /Chondrite
La
Ce
Nd
Sm
Eu
Tb
Ho
Er
Yb
Lu

Figure 3.15. Chondrite normalized rare earth element (REE) patterns of gabbro veins from the White Hills Peridotite. Symbols as for Figure 3.13. Stippled field - Wandsworth Gabbro (Strong and Dostal, 1980).

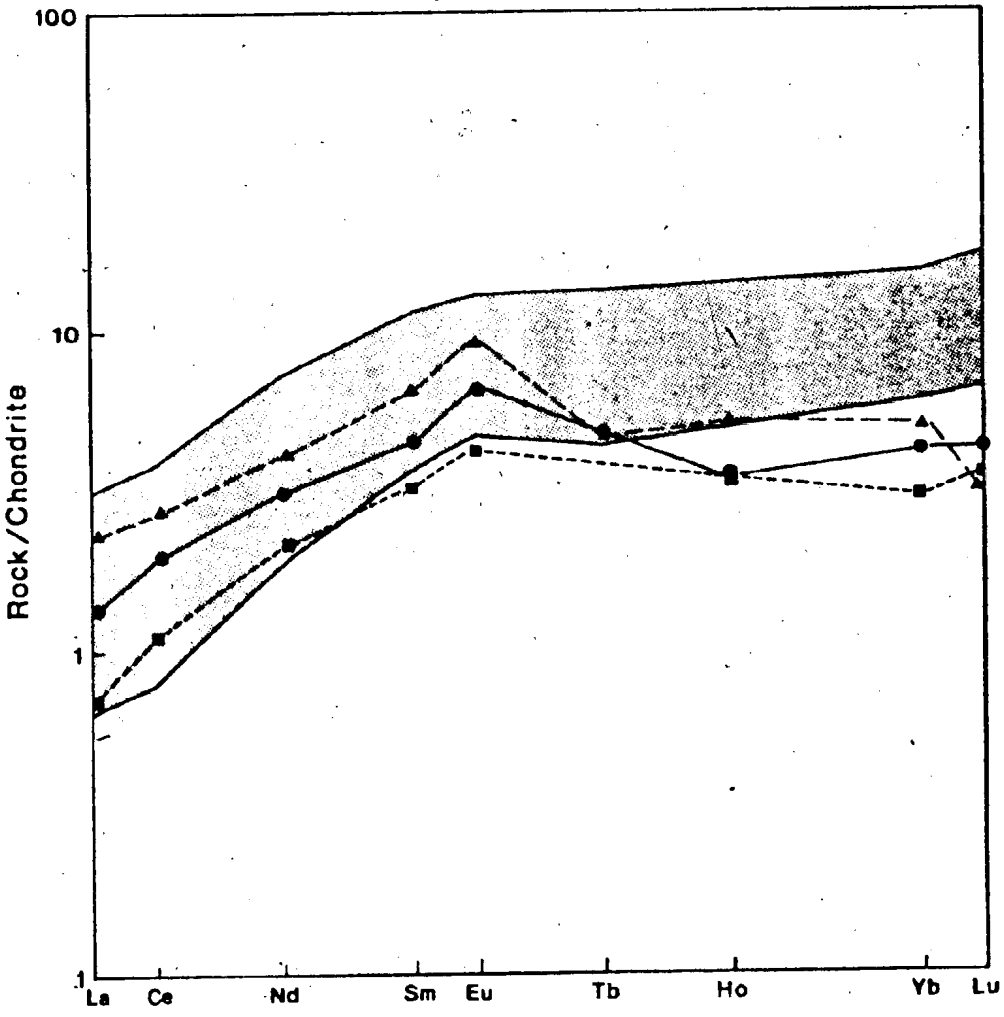
100
10
1
.1
Rock/Chondrite
La
Ce
Nd
Sm
Eu
Tb
Ho
Yb
Lu

high clinopyroxene case (plagioclase/clinopyroxene ratio for sample 77WH89 is about 0.3).

Comparison of the White Hills gabbros with the Proterozoic Wandsworth Gabbro (Strong and Dostal, 1980) (Figure 3.15.) shows a good correlation between the two groups except for a heavy REE (HREE) enrichment in the Wandsworth Gabbro. The cause of this deviation is not understood at present.

a. Discussion

Strong and Dostal (1980) propose a model for the evolution of the Burin Group rocks that assumes dynamic melting of the parent source material (Langmuir et al., 1977). The model assumes an upper mantle peridotite source, initially garnet bearing, with 2x chondrite REE abundances. Initially the garnet peridotite undergoes 3 percent partial melting, the liquid produced from the partial melting event has an overall enriched chondrite normalized REE pattern (La/Lu > 1) and is similar to the Pardy Island Formation chondrite normalized REE pattern. For their model no additional partial melting of the upper mantle diapir occurs during its ascent into higher parts of the asthenosphere until the source diapir is within the spinel lherzolite stability field. Subsequent partial melting of the spinel lherzolite diapir at specified melt increments can produce the chondrite normalized REE patterns determined analytically for the Burin Group rocks. For example, the Wandsworth Gabbro liquid is generated during the fifth 2 percent partial melt increment of the lherzolite residue (after the initial 3 percent melting

of the garnet lherzolite that is required to generate the initial Burin Group liquid i.e., Pardy Island Formation) (Strong and Dostal, 1980). Thus, with this type of petrogenetic model REE patterns similar to the White Hills gabbros can be generated. The residue that results from this dynamic partial melting model has a LREE-depleted chondrite normalized pattern that resembles the harzburgite residue as computed by Menzies (1976), but differs from natural ophiolite harzburgite residues which commonly have a convex downwards chondrite normalized REE pattern (Montigny et al., 1973; Menzies, 1976; Kay and Senechal, 1976; Suen et al., 1979).

Suen et al (1979) consider the convex downwards chondrite normalized REE pattern typical of tectonite peridotites in ophiolites, but also indicate that this is not the expected REE distributions for a residue that remains after the generation of basalts with relative LREE depletion. Rather the residue should be more LREE-depleted than both the source rock and co-existing liquids (Suen et al., 1979). The cause for the convex downwards chondrite normalized REE pattern is not known at present, however Menzies (1976), Suen et al (1979) and Suen and Frey (1979) suggest that late-stage metasomatic alteration of the harzburgite may cause an increase in the LREE, which, for low temperature alteration processes, i.e., spilitization and zeolitization is a viable transport mechanism, especially for La (Hellman and Henderson, 1977; Ludden and Thompson, 1979).

Many other partial melting calculations for derived liquids from spinel lherzolite material have been reported in the

literature (Menzies, 1976; Mysen and Holloway, 1977; Smewing and Potts, 1975; Frey et al., 1978). Results from these calculations range from about 10 percent to 30 percent partial melting of lherzolitic upper mantle material to produce REE liquid and residue patterns similar to the Burin Group rocks and White Hills gabbros.

An accurate estimate for the amount of partial melting of a lherzolite source material necessary to produce the White Hills gabbro REE contents cannot accurately be made because these rocks are crystal cumulates (B. Fryer, pers. comm., 1979). This drawback is accentuated if any intercumulus melt is trapped between the cumulus grains or if the cumulus minerals experience adcumulus growth (Kay and Senechal, 1976). The REE compositional data for the White Hills gabbros, nevertheless, indicate an evolutionary history and therefore liquid composition (olivine tholeiite), similar to oceanic and ophiolitic gabbros. The amount of partial melting of a spinel lherzolite source material necessary to form this liquid composition is in the order of 10-30 percent (Frey et al., 1974; Menzies, 1976; Strong and Dostal, 1980).

There are differences in the absolute abundances of the REE for the Bay of Islands gabbros (Suen et al., 1979) and the White Hills Peridotite gabbros. Although the reasons for these differences are not known, possible contributions are, perhaps, a source material for the Bay of Islands gabbros with lower REE abundances (Menzies, 1976; Frey et al., 1978), the percent partial melting of the source material (affects the

shape of the chondrite normalized REE pattern) or the absolute REE content of the clinopyroxene at various crystallization intervals. The more positive Eu anomaly of the White Hills Peridotite gabbros relative to the Bay of Islands gabbros does not appear to be the result of a higher plagioclase content because, to the contrary, the Bay of Islands gabbros have, on average, a higher plagioclase content, yet less positive Eu anomaly (Malpas, 1976; Suen et al., 1979).

At present, these questions must remain unanswered until additional REE mineral and bulk rock data become available for the White Hills samples.

II.3.C. Summary

Although examination of the mineral chemistries for the rocks from the White Hills Peridotite indicates that for all lithologies there is an overall geochemical similarity to other ophiolites and subcontinental upper mantle material, there are several internal geochemical differences which serve to distinguish, yet group, the various White Hills lithologies. These differences are preserved, primarily, in the pyroxenite and gabbro veins and the lithologies associated with the chromite pod and are:

(1) For the pyroxenite and gabbro veins

a. probable co-magmatic TiO_2 trend for clinopyroxenes that increases from high-alumina orthopyroxenite to gabbro
b. probable co-magmatic trend for the Fo content of olivines that decreases from high-alumina orthopyroxenite to gabbro
c. similar Al_2O_3 contents for high-alumina orthopyroxenite and gabbro, which may indicate

a co-magmatic origin, and does suggest formation during similar P-T conditions

d. on the basis of the aforementioned mineral chemical similarities and the variation in the Ni content of olivines from the pyroxenite veins, it is apparent that for the pyroxenite and gabbro veins the high-alumina orthopyroxenite and websterite lithologies formed prior to the clinopyroxenite, wehrlite and gabbro lithologies

(2) For the chromite-related lithologies

a. tholeiitic character of the silicate phases
b. high Mg/Fe ratios of the silicate phases
c. low TiO_2 and Al_2O_3 contents of the pyroxenes
d. chromium-rich cumulus spinel is associated with these lithologies

The differences between the two groups suggest the formation of the lithologies under different P-T conditions but, more importantly, formation from different parent liquids.

The bulk rock chemistries for the pyroxenite and gabbro veins and the limited bulk rock analyses for the chromite-related lithologies indicate that at least two geochemical trends exist for these lithologies. During one trend (high TiO_2, Al_2O_3 and slightly transitional parent liquid) the high-alumina pyroxenite and gabbro veins may have formed, whereas the chromite-related lithologies may have formed from a liquid tholeiitic in composition and low in TiO_2 and Al_2O_3. The spinel lherzolite, harzburgite, dunite and pyroxenite bulk rock chemistries are indistinguishable from other ophiolites. The gabbro vein bulk rock chemistry is similar to that of gabbros from ophiolites and oceanic gabbro from a variety of oceanic settings (e.g., trenches; Thompson, 1973).

REE data are available for the gabbro veins. The chondrite normalized patterns are nearly identical to the chondrite normalized patterns for gabbros from some ophiolites and the Mid-Atlantic Ridge.

The amount of partial melting of a spinel lherzolite source material believed necessary to yield the bulk rock and REE chemistries of the White Hills Peridotite gabbros is estimated to be in the range from 10 percent to 30 percent on the basis of experimental partial melting studies and theoretical modelling calculations.

Thus, for the White Hills Peridotite several important mineral and bulk rock chemistry relationships have been shown to exist which appear to suggest, for some of the lithologies, a co-magmatic evolution. Although all the rocks may not be co-magmatic (i.e., especially the pyroxenite and gabbro veins, and chromitite), they do appear to be genetically related, and hence are probably crystallization products (cumulates) from liquids derived by the partial melting of a common source material. As is suggested by most geological investigators and as discussed in Chapter 5, spinel lherzolite and harzburgite are the parent source material for the partial melting events and the residuum from the partial melting, respectively. Although the origin for the dunite cannot at this time be specifically linked to either a partial melting or crystallization event(s), in Chapter 2 it has been suggested on the basis of rock microstructure that the dunite is of cumulus origin.

Chapter 4

Spinel Group Minerals

II.4.A. General Statement*

Spinel Group minerals are a common accessory phase in the ultramafic and mafic portions of ophiolites. As an early- or late-forming phase (subsolidus) of these rocks, the spinels must preserve a geochemical and textural link between either the liquid phase or the solid phase from which they form, if the system operates under equilibrium, "closed" chemical conditions. Although textural and chemical relationships between spinel phases and their host rock have not been tabulated in any single publication, for an ophiolite suite, recent work on "ophiolitic" rocks and ultramafic xenoliths, e.g., Loney et al 1971; Malpas and Strong, 1975, Menzies, 1975; Basu, 1977; Sinton, 1977; Varne, 1977; Donaldson, 1978, has provided a partial compilation of these relationships.

Spinels are present in all rock types of the White Hills Peridotite (i.e., spinel lherzolite, harzburgite, dunite, pyroxenites, gabbro and chromitites), and as such provide

* The silicate-spinel textural relationships and spinel chemistry for most White Hills Peridotite lithologies have been described in the manuscript "Spinel Phases of the White Hills Peridotite, St. Anthony Complex, Newfoundland; Part I occurrence and chemistry". A copy of this manuscript is provided in Appendix V. In order to avoid undue repetition only the important points of silicate-spinel textural relationships are presented here. Spinel chemistry is discussed in its entirety.

good opportunity to determine the relationships between spinels and silicates.

II.4.B. Textural Relationships

The textural relationships between spinels and silicates from the White Hills Peridotite are discussed on a rock-type basis. A summary of the textural variations of the spinel phases from the White Hills Peridotite is presented in Table 4.1. (in pocket) and is based on data collected from about 300 thin sections. Rock texture terms which may imply specific deformational processes are avoided.

1. Spinel Lherzolite

In the coarse-granular textured samples, spinel occurs along the margins of the orthopyroxene porphyroclasts characteristically as exsolved vermicules (Plate 10.A.). Commonly, olivine-orthopyroxene-spinel (± clinopyroxene) are in contact but similar spinel textures with clinopyroxene have not been observed. The vermicules are small (0.1 mm x 0.02 mm, average size) and have a variety of colors ranging from straw-yellow to light red-brown. These colors for spinel usually do not vary in a single thin section, but frequently do from one rock sample to another. In one thin section (7815) exsolved spinel associated with only orthopyroxene and olivine has a yellow-brown color, whereas spinel associated with orthopyroxene-olivine-clinopyroxene has a light red-brown color. The percentage of exsolved spinel is higher in rocks where clinopyroxene exsolution in orthopyroxene is lowest.

Plate 10

A. Exsolved vermicular spinel form in orthopyroxene in coarse-granular textured spinel lherzolite. Plane polarized light. Sample 7815. Western White Hills. Length of photograph is 4.1 millimeters.

B. Porphyroclast spinel form with "trail" in porphyroclastic textured spinel lherzolite. Plane polarized light. Sample 7830. Western White Hills. Length of photograph is 4.1 millimeters.

C. Porphyroclast spinel form with occluded olivine in porphyroclastic textured harzburgite. Plane polarized light. Sample 78116. Eastern White Hills. Length of photograph is 5 millimeters.

D. Pull apart texture in allotriomorphic-granular textured dunite. Plane polarized light. Sample 7841. Western White Hills. Length of photograph is 5 millimeters.

E. Corroded "Holly-leaf" spinel form in granoblastic textured dunite. Plane polarized light. Sample 78152. Eastern White Hills. Length of photograph is 4.1 millimeters.

F. Spinel clusters in gabbro. Plane polarized light. Sample 78136. Eastern White Hills. Length of photograph is 4.1 millimeters.

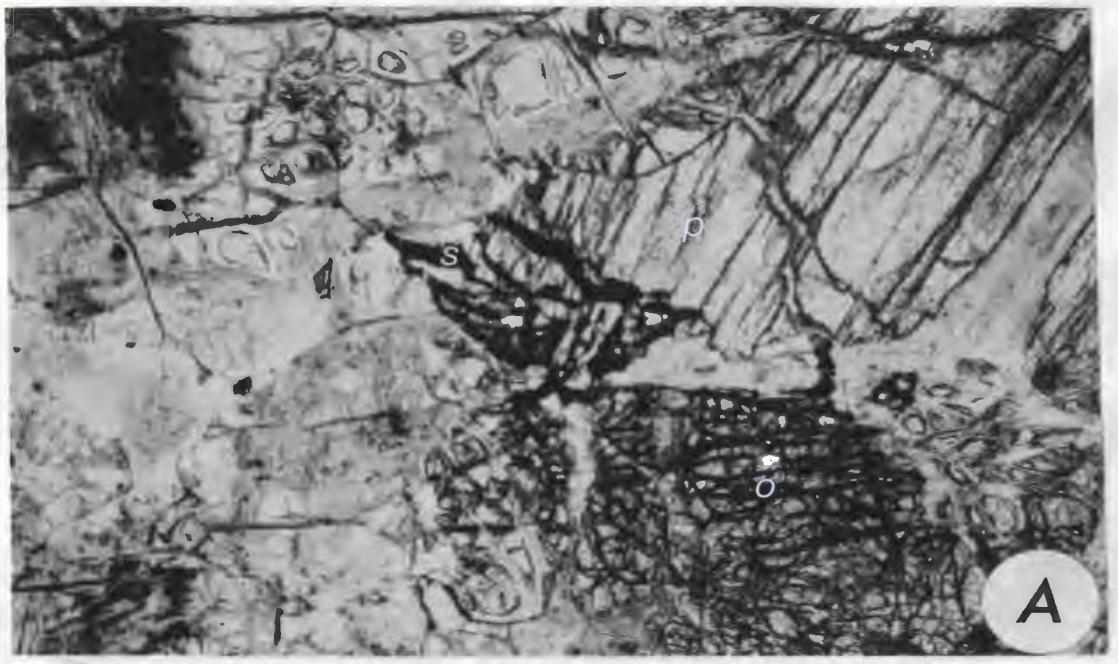
A

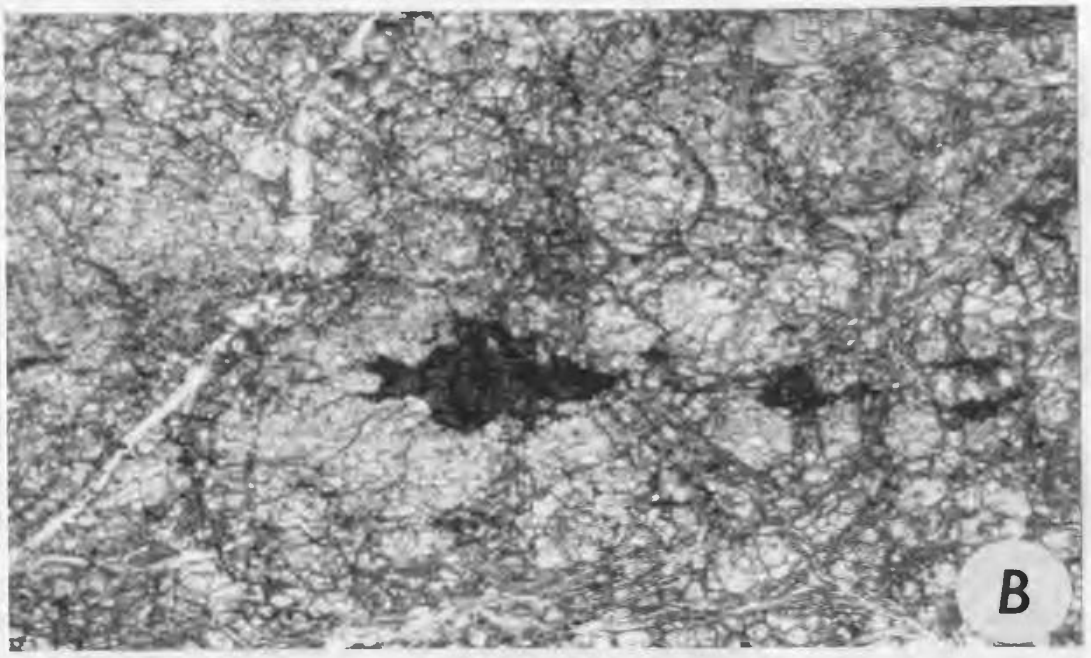
B

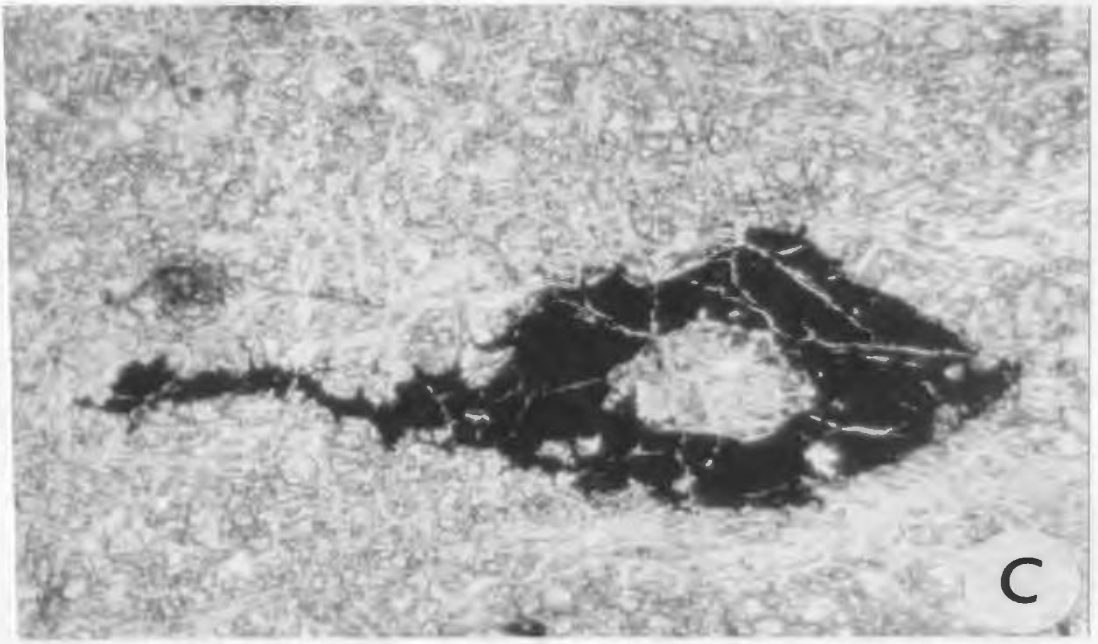
C

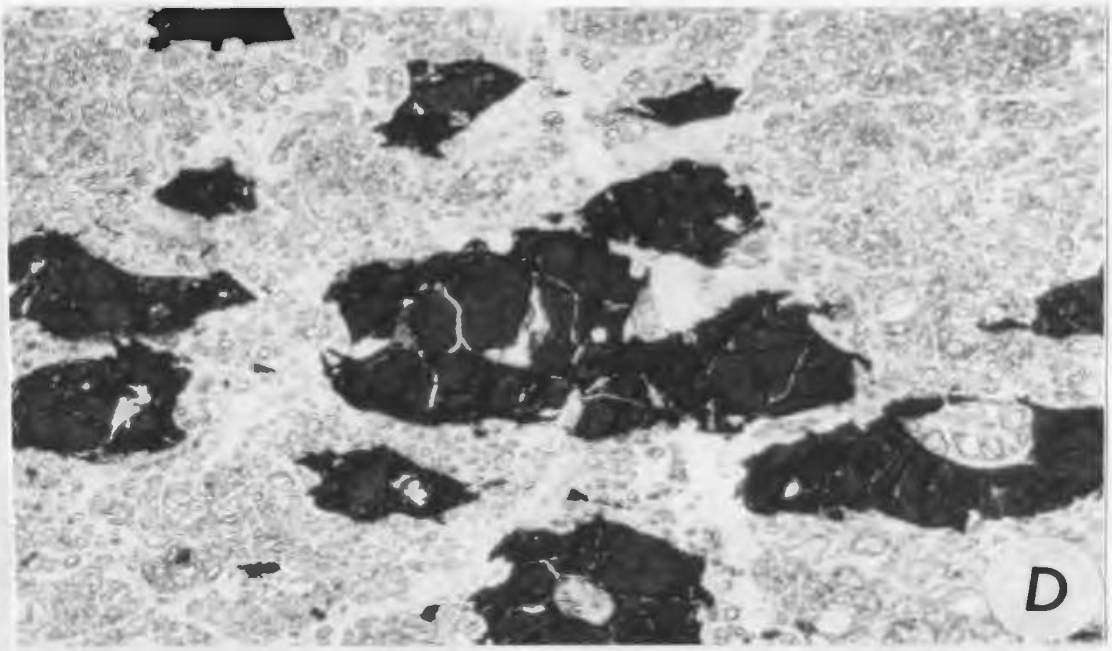
D

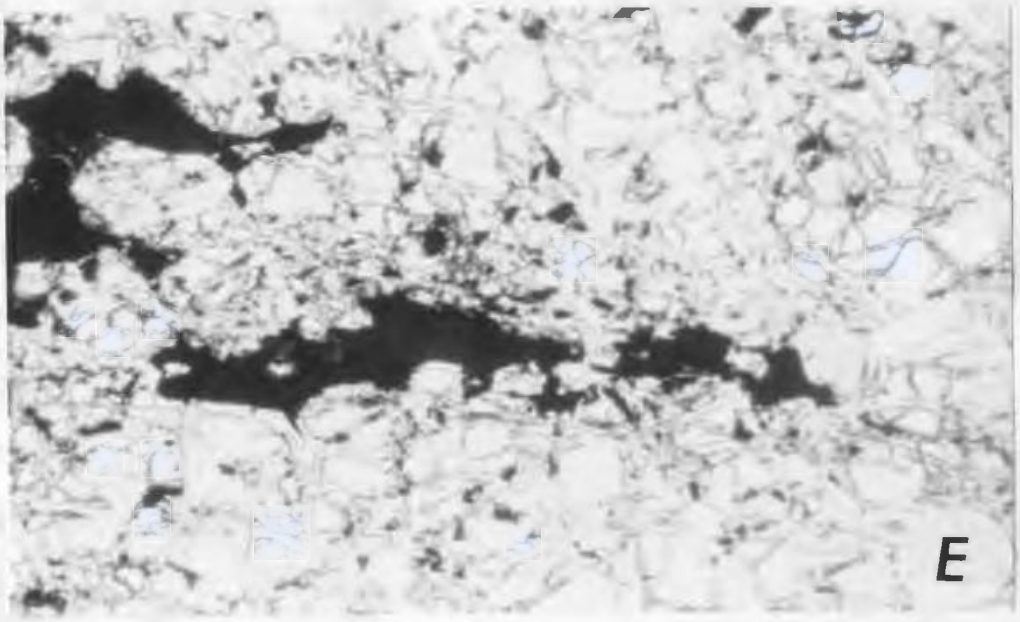
E


C
s
p
F

In slightly more deformed rocks, still classed as coarse-granular but where recrystallization and a decrease in grain size are observed, the spinel vermicules occur as either irregularly shaped, interstitial clusters or porphyroclasts (Plate 10.B.). The size of the clusters is highly variable and appears dependent upon the degree of deformation and original amount of exsolved spinel. The color of the spinel does not change during deformation, but if deformation is accompanied by serpentinization, rims of ferritchromite or magnetite are produced around the spinel. In extreme cases of hydration total alteration of the spinel to ferritchromite or magnetite may occur in addition to the formation of a serpentine or a chlorite selvage around the spinel.

The development of a porphyroclastic texture results in the destruction of the spinel vermicules along the orthopyroxene porphyroclast margins and the development of spinel clusters (Plate 10.B.), by the coalescence of the spinel vermicules. Ovoid spinel droplets are observed along recrystallized kink band boundaries in orthopyroxene porphyroclasts and in rare cases, clinopyroxene porphyroclasts. The spinel clusters are anhedral, commonly have holly-leaf form, sizes up to 7 millimeters. Due to the high-aluminum content of this spinel-type, "trails" of granulated spinel porphyroclasts (Basu, 1977) tend to develop interstitial to silicates (Plate 10.B.) upon plastic flow during deformation (Mercier and Nicolas, 1975). No color change of the spinel is noted when compared to the spinel form in the coarse-granular

textured rocks. Ovoid spinel droplets that form together with silicate neoblasts along recrystallized kink bands are always less than 0.1 millimeter in size and are interstitial to the neoblasts.

Elliptical to oblate shaped spinel droplets are observed within some deformed orthopyroxene porphyroclasts, dominantly in ones which contain few clinopyroxene exsolution lamellae. The spinel is small ($\sim$ 0.5 mm) and is commonly associated with either an isolated clinopyroxene exsolution lamella or an isolated patch of clinopyroxene, apparently derived by exsolution. The color of the spinel is light brown.

Spinel in more deformed rock textures may retain the anhedral cluster habit, or form narrow, elongate "trails" that parallel the rock fabric. From examination of the spinel lherzolite samples from the White Hills, it appears that the spinels which occur in the coarse-granular textures develop only in orthopyroxene and originate by exsolution processes. No residual (after partial melting) spinels are found in spinel lherzolite.

2. Harzburgite

The spinel forms and deformational mechanisms that have been described for the coarse-granular and the porphyroclastic rock textures from spinel lherzolite pertain also to harzburgite. The most striking difference between the spinels of these two rock types is color, i.e., in harzburgite the colors of spinel are various shades of red-brown, and as discussed below, are a function of bulk rock chemistry.

In addition to the exsolved spinel form, spinel in harzburgite occurs as porphyroclasts (Plate 10.C.). Spinel porphyroclasts are present in rocks of all microstructures, are anhedral to ovoid in shape, have scalloped to serrate grain boundaries and may contain occluded silicates, commonly olivine. The presence of spinel porphyroclasts in the coarse-granular texture suggests these may be residual spinels, identical to those commonly found in harzburgites of Alpine-type peridotites and ophiolites (e.g., Dickey and Yoder, 1972; Malpas and Strong, 1975).

3. Dunite

In the allotriomophic-granular texture, spinels vary from porphyroclasts (originally a cumulus phase) that are ovoid in shape (Plate 10.D.) to severely corroded grains having a holly-leaf form (Plate 10.E.). Pull apart texture commonly occurs in the ovoid form of spinel. The grain size is variable (0.2 mm to 4 mm) and colors range from green-brown to red-brown. Commonly, the ovoid spinel form is altered to ferritchromite-magnetite along fractures and grain margins, whereas complete alteration of spinel to ferritchromite-magnetite occurs in the corroded form. Both forms of spinel are commonly elongate parallel to the dominant foliation.

4. Gabbro

Spinels in the porphyroclastic and the granoblastic textures assume a variety of forms and associations with the silicate phases. The most common form for spinel is anhedral

(holly-leaf) (Plate 10.F.). Less common, but not rare, are the vermicular (Plates 11.A., 11.B.) and the ovoid droplet forms (Plate 11.C.). The color of the spinel for all forms and associations is green (translucent). Alteration of spinel to magnetite is restricted to grain margins and fractures and is abundant where olivine is associated.

The various spinel-silicate associations (and corresponding spinel forms) are listed below:

a. Spinel-plagioclase; ovoid droplets, vermicules; anhedral clusters.

b. Spinel-plagioclase-clinopyroxene; anhedral clusters along clinopyroxene-plagioclase grain boundary, symplectite intergrowth with clinopyroxene.

c. Spinel-plagioclase-clinopyroxene-olivine-orthopyroxene; anhedral interstitial; symplectite intergrowth with olivine and/or orthopyroxene.

d. Spinel-plagioclase-olivine; anhedral clusters along grain boundaries, symplectite intergrowth with olivine.

e. Spinel-plagioclase-olivine-orthopyroxene; anhedral interstitial.

f. Spinel-clinopyroxene; ovoid droplets, vermicules, anhedral clusters.

g. Spinel-clinopyroxene-olivine; anhedral clusters along grain boundaries.

h. Spinel-clinopyroxene-olivine-orthopyroxene; anhedral grains and clusters along grain boundaries.

i. Spinel-clinopyroxene-orthopyroxene; anhedral grains along grain boundaries.

j. Spinel-olivine-orthopyroxene; anhedral grains along grain boundaries.

Plate 11

A. Vermicular spinel in olivine. Plane polarized light. Sample 77WH90, gabbro vein. Eastern White Hills. Length of photograph is 0.83 millimeters.

B. Plagioclase-(clinopyroxene+spinel)-olivine corona in gabbro. Plane polarized light. Sample 78136. P-plagioclase; C+S-clinopyroxene and spinel; O-olivine. Eastern White Hills. Length of photograph is 0.78 millimeters.

C. Exsolved spinel droplets in clinopyroxene and plagioclase, and spinel interstitial to clinopyroxene (grey) and plagioclase (white). Plane polarized light. Sample 77WH60, gabbro Eastern White Hills. Length of photograph is 4.1 millimeters.

D. Cumulus spinel in orthopyroxenite. Plane polarized light. Sample 7898. Western White Hills. Length of photograph is 5 millimeters.

E. Exsolved spinel droplets in clinopyroxene, and spinel interstitial to clinopyroxene, orthopyroxene and olivine. Plane polarized light. Sample 78159, websterite. Eastern White Hills. Length of photograph is 3.1 millimeters.

F. "Websterite" from chromite pod. Cumulus orthopyroxene, spinel, and clinopyroxene. The large cumulus grains are orthopyroxene, the spinel and clinopyroxene are approximatel the same size. Sample 78123. Eastern White Hills. Sample length is 6.5 centimeters.

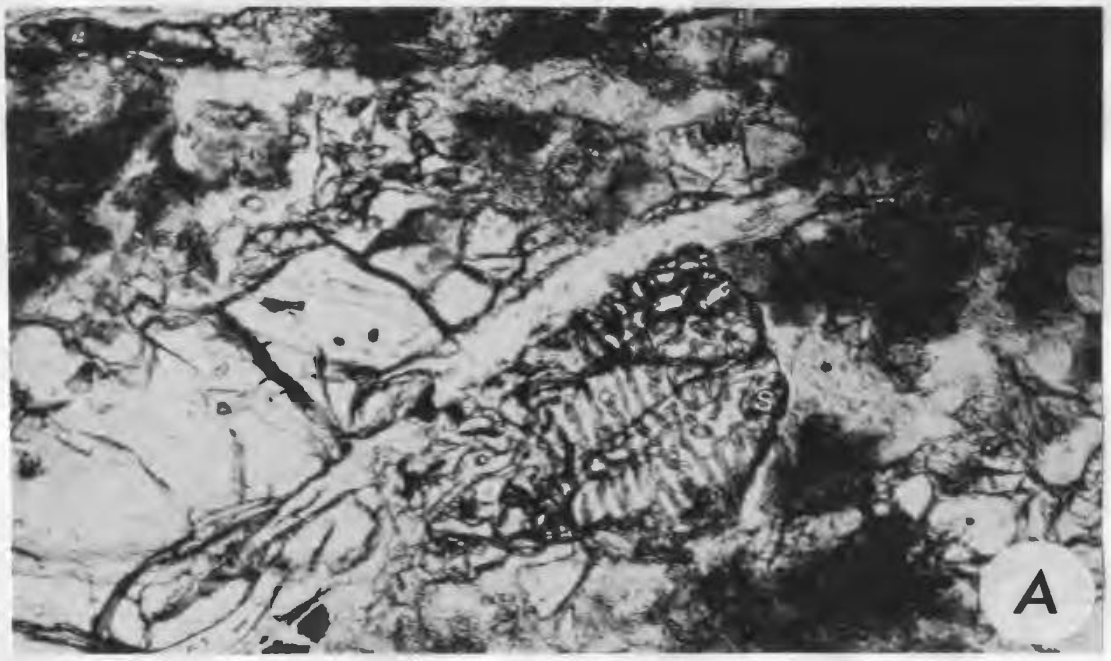
S
A

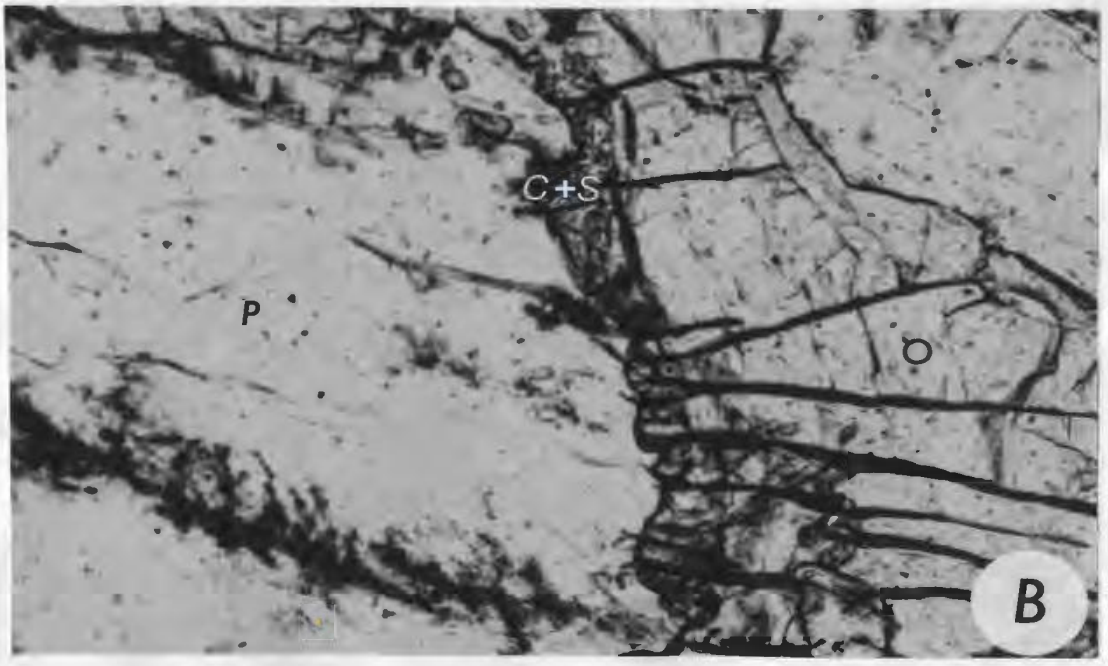
C+S
P
O
B

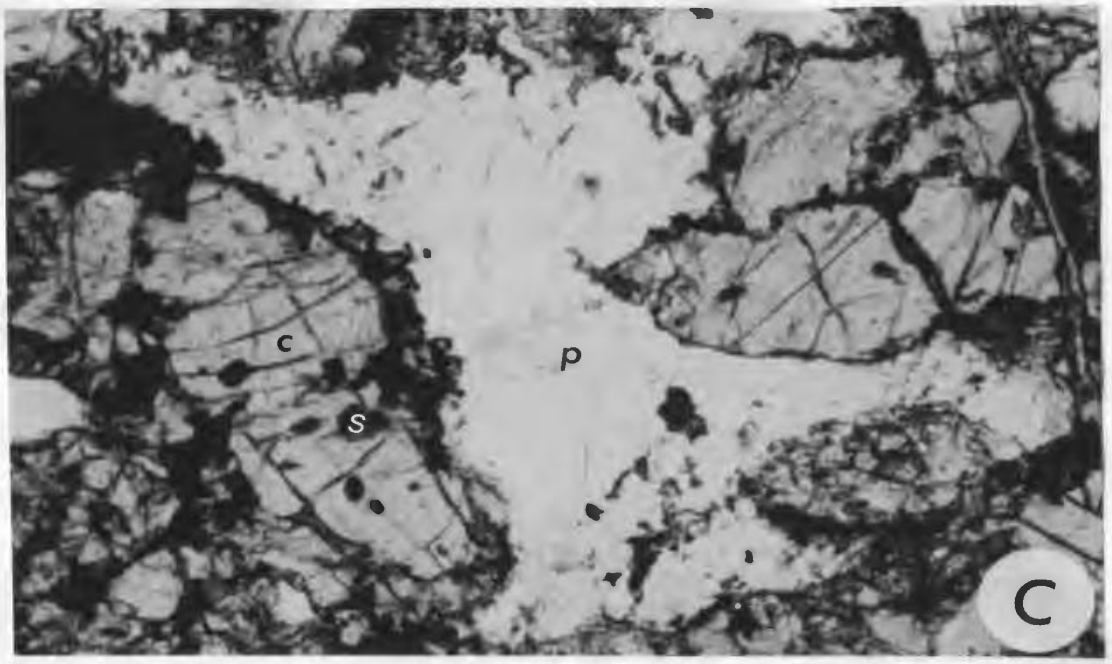
c
p
s
C

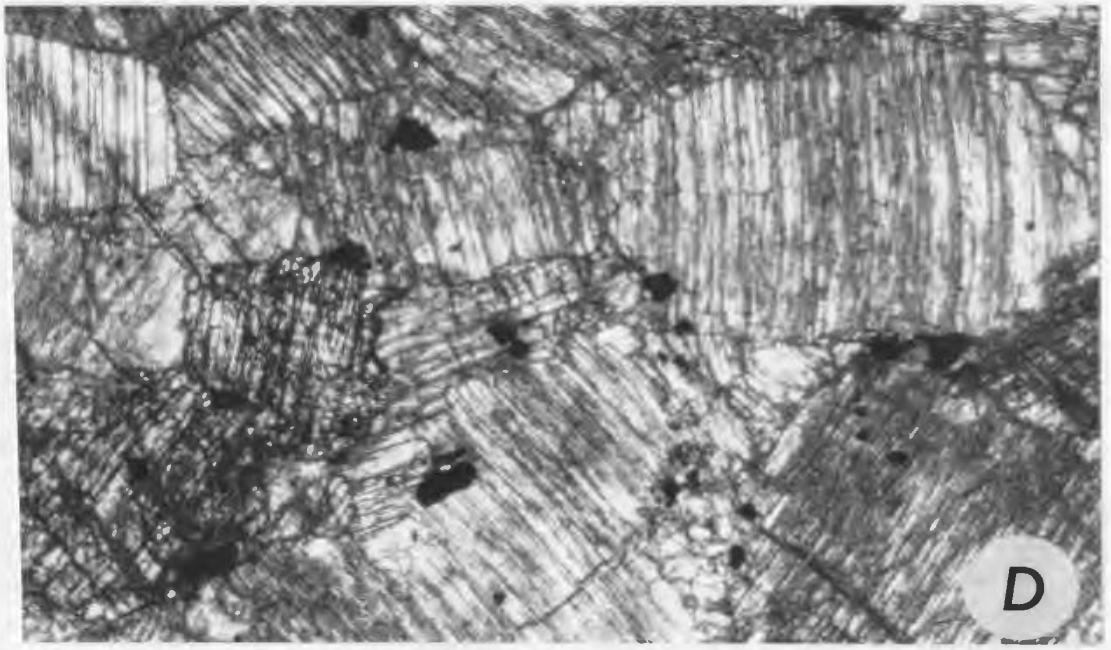
D

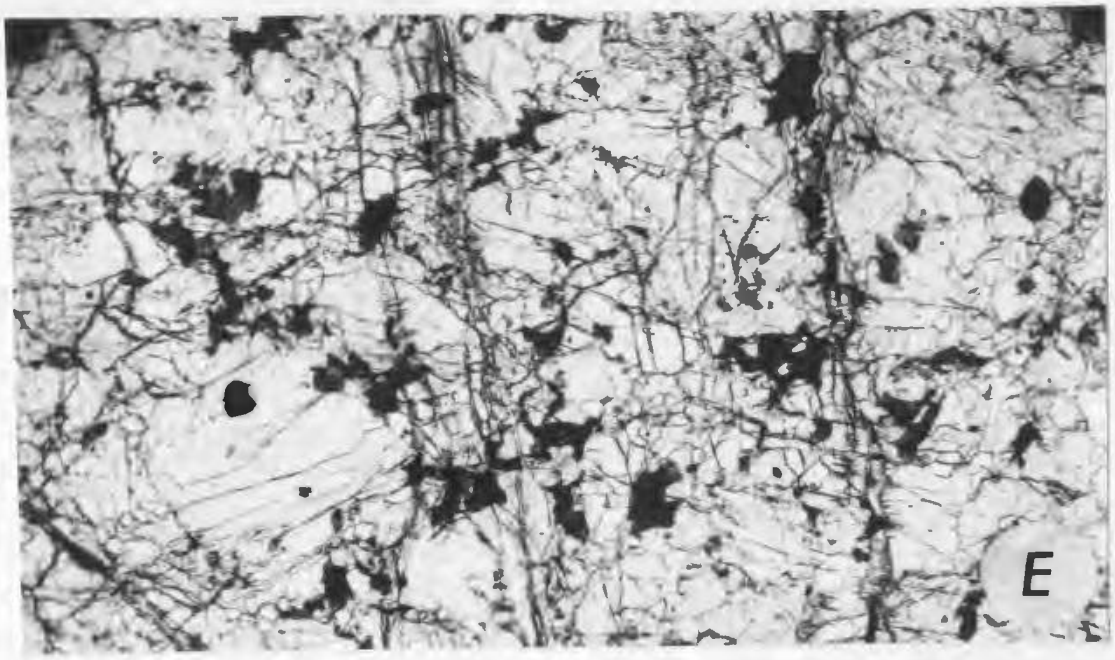
E

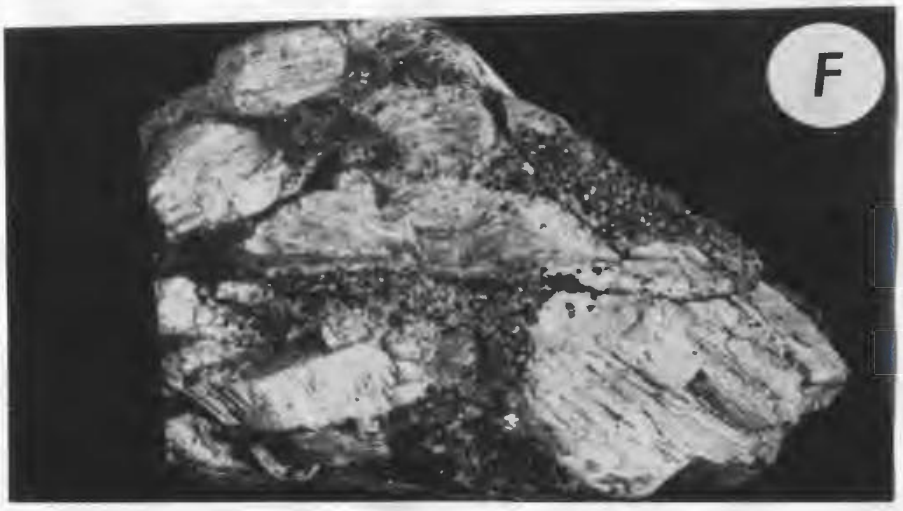
F

The associations are not listed in order of appearance or recurrence. The most common mineral associations are (c.) spinel-plagioclase-clinopyroxene-olivine-orthopyroxene and (h.) spinel-clinopyroxene-olivine-orthopyroxene, and mineral associations (b.)*, (e.), (g.), (i.), and (j.) are not commonly observed.

In the more deformed and hydrated samples where the granoblastic texture occurs, a brown pleochroic amphibole is formed as an incipient alteration of the pyroxenes. The development of this amphibole appears to post-date spinel formation.

5. Pyroxenite Veins

a. Orthopyroxenite

Accessory, disseminated, euhedral to anhedral spinel in the low-alumina orthopyroxenite is a cumulus phase that occurs interstitial to or occluded in orthopyroxene and rarely elongate parallel or subparallel to (100) of the orthopyroxene (Plate 11.D.). The color of this spinel is red-brown. Alteration of this spinel along grain margins has produced ferritchromite rims.

Spinel in orthopyroxenite assumes additional forms and associations. In a few low-alumina orthopyroxenite samples, but mostly in the high-alumina orthopyroxenite types, spinel is associated with cumulus orthopyroxene and intercumulus olivine and clinopyroxene as either an anhedral,

* The spinel-clinopyroxene symplectite and plagioclase is a rare association.

interstitial phase or a vermicular phase that occurs within orthopyroxene near the grain margins, similar in this respect to the exsolved spinel form that occurs in spinel lherzolite and harzburgite. Unlike the red color of the disseminated spinel, this spinel is a bronze color.

b. Websterite and Clinopyroxenite

Spinels in websterite and clinopyroxenite have similar forms, colors, and silicate associations.

The spinel form is anhedral interstitial for spinel associated with the silicate mineral assemblages clinopyroxene-olivine-orthopyroxene and orthopyroxene-clinopyroxene (Plate 11.E.). In contrast, ovoid to irregularly shaped droplets are found in clinopyroxene or rarely in orthopyroxene. Colors vary from shades of light translucent green through green-brown to light brown-bronze, and these color variations are observed within a single thin section even for identical spinel-silicate associations.

c. Wehrlite

Spinel in wehrlite is anhedral interstitial and olive-brown color. It is associated with either olivine or olivine plus clinopyroxene.

6. Chromitite

a. General Statement

One occurrence of a massive chromite pod, occurs in the east central region of the eastern massif. The size and shape of the pod are not definable due to localized faulting and a felsenmeer ground surface. The host rock surrounding the pod is harzburgite containing about 1 percent dunite dikes.

Veins of low-alumina orthopyroxenite with cores of chromitite extend from the pod into the harzburgite (Plate 9.F.). Within the pod, orthopyroxene phenocrysts, and/or colorless clinopyroxene phenocrysts and emerald green clinopyroxenes are surrounded by massive chromite (Plate 11.F.). Kämmererite alteration is developed on chromite cleavage surfaces. These silicate-chromite associations, as far as the writer knows, have not been described in any other ophiolite. However, Himmelberg and Loney (1973) in describing chromitite specimens from the Vulcan Peak Peridotite note the presence of intercumulus olivine, orthopyroxene and clinopyroxene. Also, Thayer (1969) describes the occurrence of spinel grains enclosed by a clinopyroxene matrix from the Celebration Mine, Oregon.

b. Chromite in the Pod

Chromite within the pod is euhedral to anhedral, red in color and variable in size ($\sim$ 0.1 mm), and although alteration is minimal, fracturing and pull apart texture are common to massive chromite concentrations. Chromite occluded in orthopyroxene (bastite) phenocrysts is partially resorbed (see Plate 6.G., section I.2.B.3.). Such resorption of the chromite results in various shapes of which a "doughnut" form, where the core of a chromite grain has been preferentially resorbed, is the most common*. The "doughnut" form is observed in

* The formation of a "doughnut" form may not be the result of resorption, but the site of a fluid or solid inclusion (D. Watkinson, pers. comm., 1980).

disseminated chromite associated with emerald green colored clinopyroxene and orthopyroxene phenocrysts. Fluid inclusions, now negative cavities, and sulphide inclusions (chalcopyrite and laurite) have been observed in a few chromite grains. These inclusions are small (< 0.01 mm) and, apparently due to the preparation technique for the polished thin sections, the fluid inclusions have been decrepitated.

c. Chromite-Orthopyroxene Seams

Chromite in orthopyroxenite seams is nearly identical to chromite from the pod, the major difference being the extent to which resorption of the chromite has developed. This process is not as far advanced as in the pod.

II.4.C. Spinel Chemistry

1. General Statement

The principal constituents of chromian spinel are MgO, FeO, Cr_2O_3, Al_2O_3, and Fe_2O_3. These oxides commonly total to more than 98 percent by weight. MnO, NiO, TiO_2, ZnO, and V_2O_3 are present in minor quantities.

The Spinel Group of minerals may be represented by the general formula, $R^{++}R_2^{+++}O_4$. Cations may occupy either of two structural positions, tetrahedral (A), and octahedral (B) sites. The distribution of cations between the A and B sites determines whether the spinel structure is normal or inverse. The cation distribution for the normal spinel structure is $8R^{++}$ in the A site and $16R^{+++}$ in the B site. For the inverse spinel structure the cation distribution is

$8R^{+++}$ in the A site and $8R^{++} + 8R^{+++}$ in the B site. Spinel, hercynite, chromite, and picrochromite have the normal spinel structure and magnetite and magnesioferrite the inverse, although many other spinels are probably intermediate between these two extremes (Wyckoff, 1965).

The Spinel Group is divided into three series, spinel, magnetite, chromite, depending on whether the R^{3+} cation is Al, Fe^{3+}, Cr, respectively. The principal end members derived from this grouping are:

$Fe^{2+}Al_2O_4$:	hercynite	$MgAl_2O_4$:	spinel (s.s.)
$Fe^{2+}Fe_2^{3+}O_4$:	magnetite	$MgFe_2^{3+}O_4$:	magnesio-ferrite
$Fe^{2+}Cr_2O_4$:	chromite	$MgCr_2O_4$:	picrochromite

In the recalculation of spinel analyses carried out during this investigation the procedures described by Irvine (1965) have been used. In addition to the recalculation of spinel analyses to the principal end members, the end member Fe_2TiO_4, ulvöspinel, has been determined. This end member has an inverse spinel structure of the type $R^{++}R^{+++}R^{++}O_4$.

A convenient means of representing chemical variations in spinels is by a triangular prism devised by Johnston and discussed by Stevens (1944) (Figure 4.1.). The prism axes represent the variations in the divalent oxides, MgO and FeO, and the three prism edges the variations in the trivalent oxides, Al_2O_3, Fe_2O_3, Cr_2O_3. Thus, at each of the six corners of the prism a spinel end member may be plotted. Plotting of chemical analyses is conveniently done on two planar projections (Stevens, 1944; Thayer, 1945; Irvine, 1965).

Figure 4.1. Conventional projections used for plotting spinel analyses.

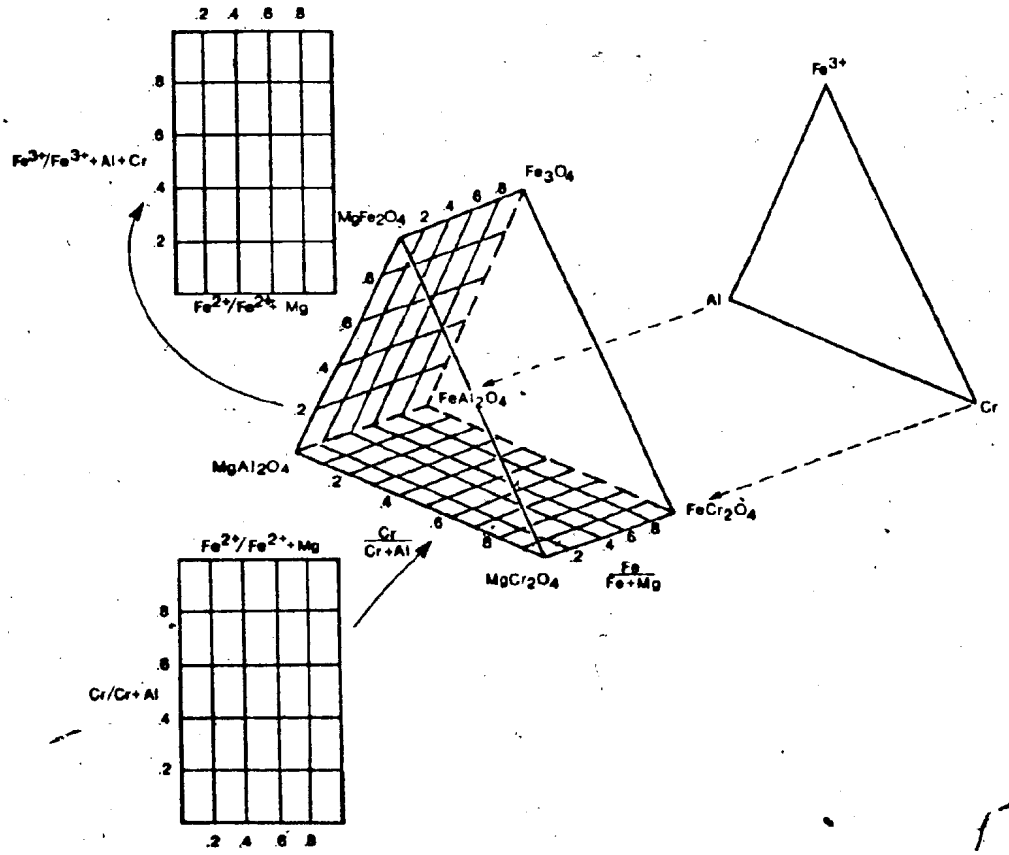
.2 .4 .6 .8
.8
.6
.4
.2
$Fe^{3+}/Fe^{3+}+Al+Cr$
$Fe^{2+}/Fe^{2+}+Mg$
Fe_3O_4
$MgFe_2O_4$
$FeAl_2O_4$
$MgAl_2O_4$
$FeCr_2O_4$
$MgCr_2O_4$
Fe^{3+}
Al
Cr
$\frac{Cr}{Cr+Al}$
$\frac{Fe}{Fe+Mg}$
$Fe^{2+}/Fe^{2+}+Mg$
$Cr/Cr+Al$

One projection (projection A of Irvine, 1965) is onto the plane picrochromite-chromite-hercynite-spinel (A in Figure 4.1.). With this projection the ratios $Cr/(Cr+Al)$ and $Mg/(Mg+Fe^{2+})$ can be viewed and compared simultaneously. The second projection (projection B of Irvine, 1965) is onto the plane picrochromite-chromite-magnesioferrite-magnetite (B in Figure 4.1.). For this projection, the ratios $Fe^{3+}/(Fe^{3+}+Cr+Al)$ and $Mg/(Mg+Fe^{2+})$ are plotted against each other; Irvine (1965) has used this projection to show variations in the oxygen partial pressures under which spinels form. The simultaneous projection of these prism faces into the triangular prism defines a three dimensional configuration depicting the chemical variations of the spinel in terms of the principal end members.

2. Solid Solution in Spinels

In the Spinel Group minerals, solid solution between the various end members exists to varying degrees. The extent of solid solution is strongly dependent upon temperature and in some cases oxygen fugacity (Ulmer, 1969). At 1300°C, the temperature at which many Spinel Group solid solution studies have been performed, complete solid solution has been achieved for the six end member spinels previously mentioned (Ulmer, 1969), although for some cases defect spinels with an excess of trivalent cations may be stable.

Chromite and magnetite show complete solid solution at or above 1300°C in the system $FeO-Fe_2O_3-Cr_2O_3$, although cation deficient (Katsura and Muan, 1964). Ulmer (1969, 1970) and Ulmer and Osborn (in Ulmer, 1969) report that solid solution in the series $MgAl_2O_4-FeAl_2O_4$ and $MgCr_2O_4-FeCr_2O_4$

cannot be attained because of the presence of a metallic iron phase. Complete solid solution between Fe_3O_4 and $FeAl_2O_4$ exists at temperatures in excess of 1000°C, but a miscibility gap appears at about 860°C; and exsolution is complete at about 500°C (Turnock and Eugster, 1962). Cremer (1969) arrives at results similar to Turnock and Eugster (1962), but his results show a less extensive miscibility gap. During the same experiments in the system $FeCr_2O_4$-Fe_3O_4-$FeAl_2O_4$, Cremer (1969) reports a miscibility gap between $FeCr_2O_4$ and $FeAl_2O_4$ but, Lindsley (1976) indicates Cremer's (1969) results are probably based on synthesis experiments, and thus it is unclear if equilibrium had been established. Muan et al (1972) have shown that along the join $MgAl_2O_4$-Mg_2TiO_4-$MgCr_2O_4$ complete solid solution exists between $MgAl_2O_4$-$MgCr_2O_4$ at all temperatures. Complete solid solution with cation deficient structures occurs between Fe_3O_4 and $MgFe_2O_4$ (Speidel, 1967), although Kwestroo (1959) documents the existence of a miscibility gap between $MgAl_2O_4$ and $MgFe_2O_4$ at 1250°C and 1400°C along with a complete series of cation deficient spinels. Complete solid solution exists at 1300°C between $MgCr_2O_4$ and $MgFe_2O_4$ (Ulmer and Smothers, 1968).

To summarize, it is probably a fair assumption to assume that solid solution exists between the six end members of the Spinel Group at magmatic temperatures. Comparison of the experimental findings with the chemistry of the spinels from the White Hills Peridotite suggests conformity and complete solid solution within these compositional ranges.

3. Mineral Chemistry

Compositions of spinels from spinel lherzolite cluster in a small field when projected onto the Cr/(Cr+Al) vs. $Mg/(Mg+Fe^{2+})$ diagram (Figure 4.2.). The Cr/(Cr+Al) ratio for the group is approximately 0.150 and the Fe^{3+} content is very low ($\sim$ 0.05 wt. %), which is consistent with results from other Alpine-type peridotites (Fabriès, 1979) (Figures 4.3. and 4.4.). The spinel lherzolite compositional field of the White Hills Peridotite overlaps the spinel lherzolite fields for the Bay of Islands Complex (Malpas and Strong, 1975) (Figure 4.2.), S.W. Oregon peridotites (Medaris, 1972), and Ligurian ophiolites (Bezzi and Piccardo, 1971). The composition of the exsolved spinel phase (Table AII.14.), when compared to the groundmass spinel phase from other White Hills Peridotite spinel lherzolite samples, has the higher Cr/Al ratio. Menzies (1975) notes a similar relationship for the Othris ophiolite.

Minor oxide concentrations, TiO_2, MnO, NiO, V_2O_3, where determined, are uniformly low and relatively constant for all samples independent of silicate association or spinel form.

Chemical zoning has not been detected in any samples although in one sample (Table AII.14., analyses 77WH76, 77WH76-1) the spinel has two colors, light brown and dark brown. The only chemical difference is a higher total iron content for the dark brown region and 1 weight percent lower MgO content for light brown region.

Figure 4.2. Plot of the Cr x 100/(Cr+Al) ratio vs. Mg x 100/($Mg+Fe^{2+}$) ratio for spinels from various lithologies of the White Hills Peridotite.

Symbols:

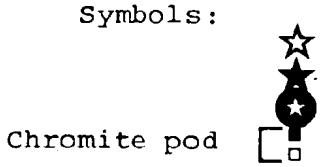

☆ Spinel lherzolite
★ Harzburgite
● Dunite
Chromite pod ■ Massive chromite
□ Cumulus chromite in "websterite"
○ Cumulus chromite in orthopyroxenite

Dashed line- spinel from spinel lherzolite, Bay of Islands Complex (Malpas and Strong, 1975).

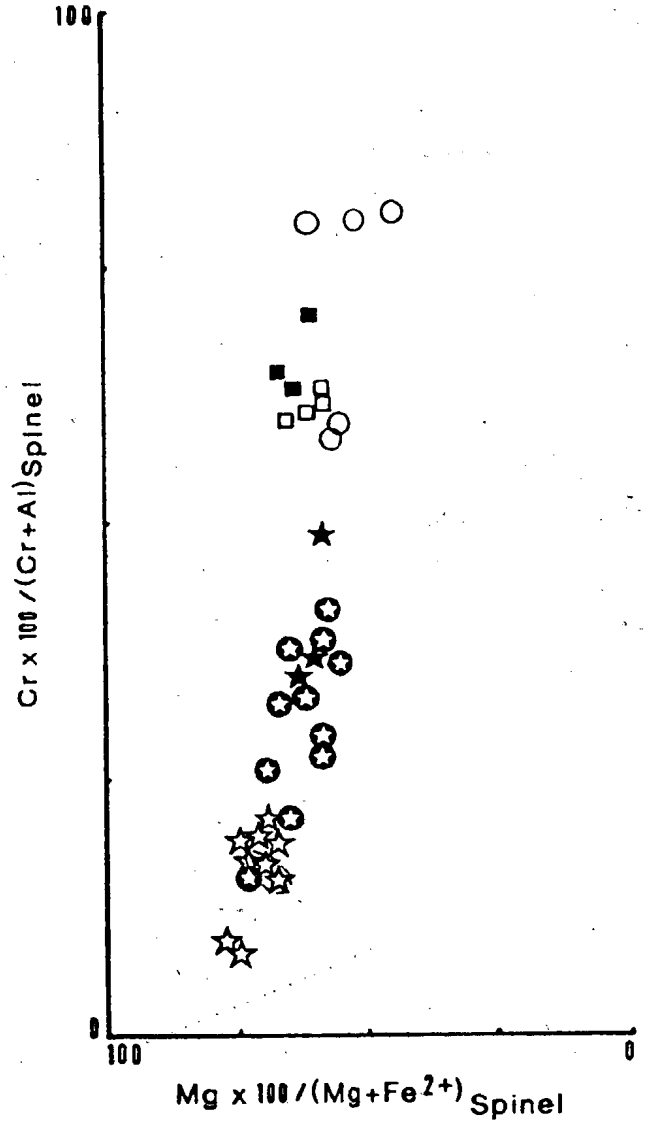
100
0
100
0
Cr x 100 /(Cr+Al)Spinel
Mg x 100 /(Mg+Fe2+)Spinel

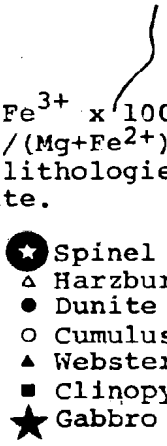

Figure 4.3. Plot of $Fe^{3+} \times 100/(Cr+Al+Fe^{3+})$ ratio vs. $Mg \times 100/(Mg+Fe^{2+})$ ratio of spinels from various lithologies of the White Hills Peridotite.

Symbols:

- ★ Spinel lherzolite
- △ Harzburgite
- ● Dunite
- ○ Cumulus chromite in orthopyroxenite
- ▲ Websterite
- ■ Clinopyroxenite
- ★ Gabbro

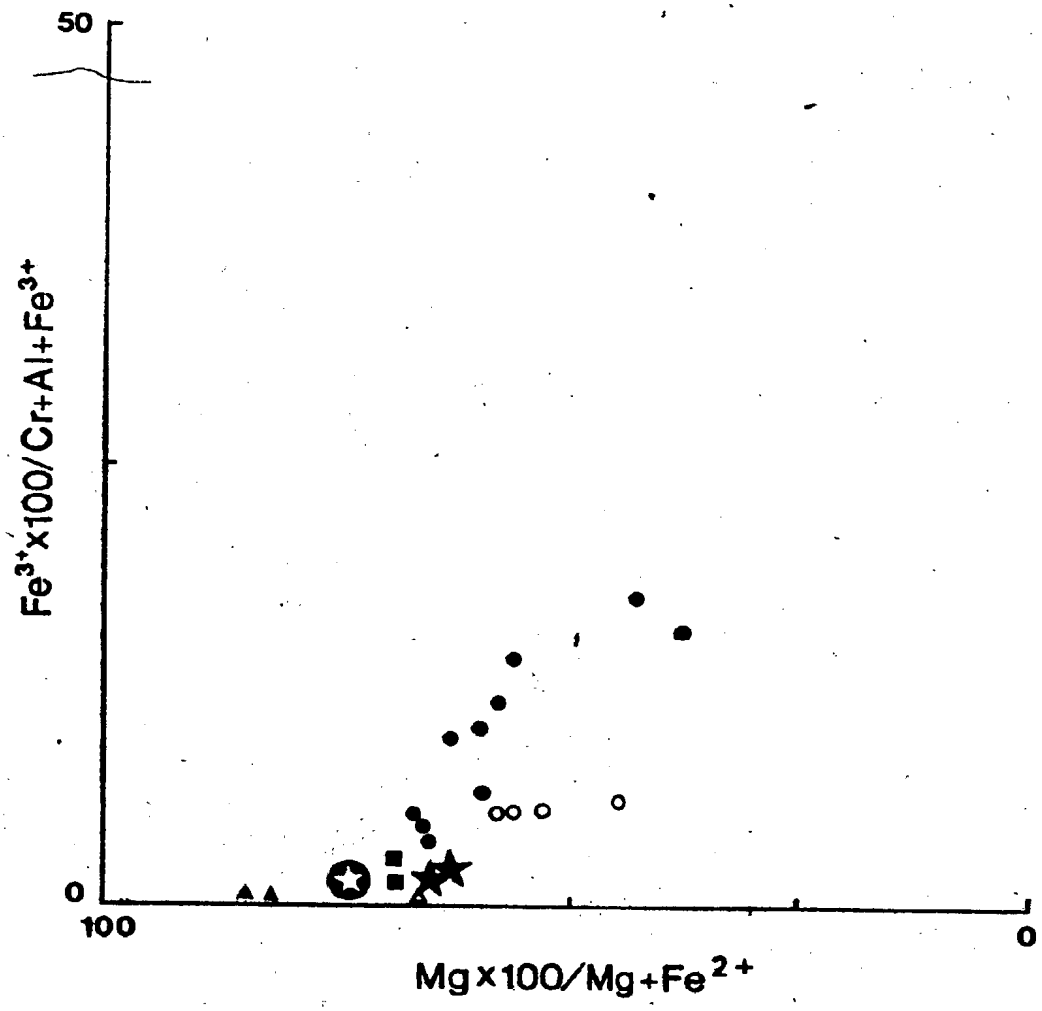
50
0
100
0
$Fe^{3+}x100/Cr+Al+Fe^{3+}$
$Mg x 100/Mg+Fe^{2+}$

Figure 4.4. Spinel compositions from various lithologies of the White Hills Peridotite plotted in the spinel prism. Symbols as for Figure 4.2. The solid lines connecting the symbols to the base of the prism represent the amount of $MgFe_2O_4$-Fe_3O_4 in the spinel. Note that the spinels in dunite, on average, contain the highest Fe^{3+}, see Figure 4.6. for comparison of Fe^{3+} contents of these spinels.

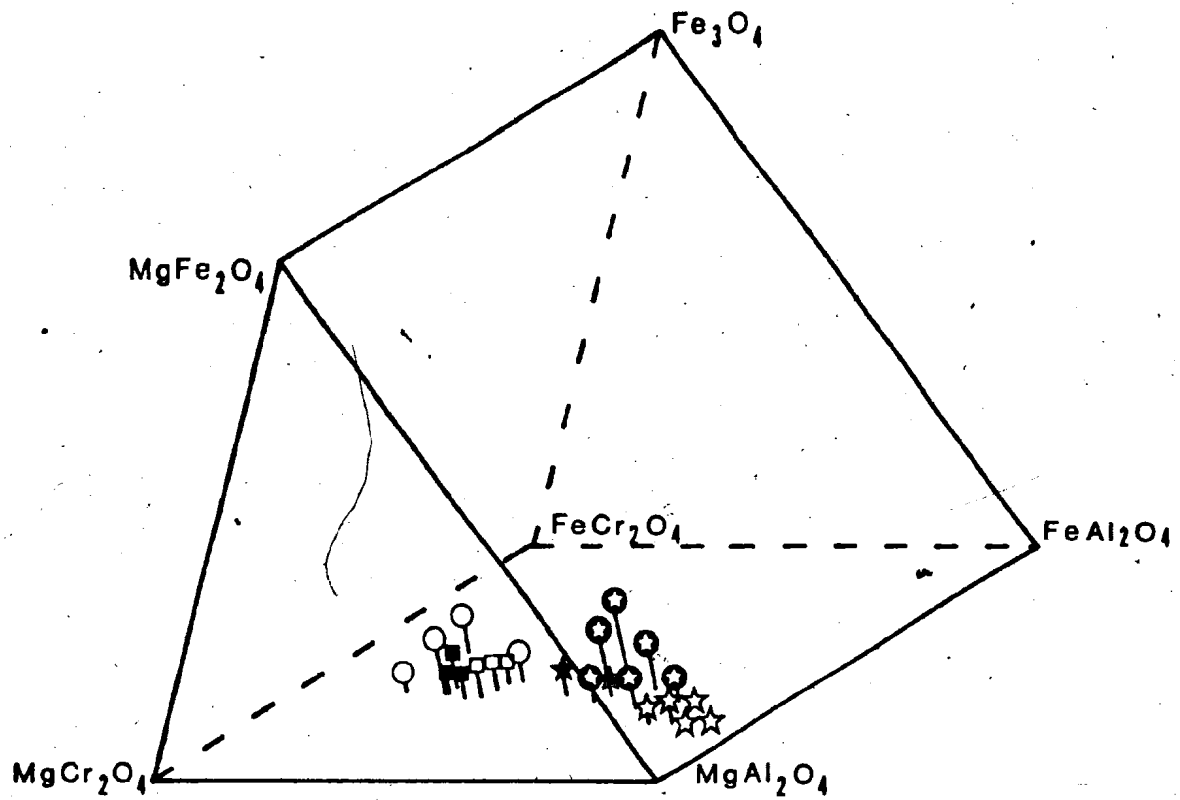
Fe_3O_4
$MgFe_2O_4$
$FeCr_2O_4$
$FeAl_2O_4$
$MgCr_2O_4$
$MgAl_2O_4$

Three spinel lherzolite samples (Table AII.14., analyses 77WH11, 796, 795) have high Al/Cr ratios. Samples 77WH11 and 795 have spinel forms and silicate associations similar to other spinel lherzolite samples, and the spinel in sample 796 is adjacent to a clinopyroxene megacryst. The reason for these high ratios is not known.

Harzburgite spinels are compositionally distinct from spinel in spinel lherzolite (Figures 4.5. and 4.6.). This appears as an increase in the Cr/(Cr+Al) ratio and a slight increase in the $Mg/(Mg+Fe^{2+})$ ratio. Fe^{3+} is low, but slightly higher than for spinel lherzolite. One harzburgite spinel composition lies within the harzburgite spinel field defined for the Bay of Islands Complex (Figure 4.5.). This spinel (Table AII.14., analysis 7818) contains the highest Cr_2O_3 and lowest Al_2O_3 content thus far found in harzburgite from the White Hills Peridotite. The remainder of the harzburgite spinel compositions lie outside the defined Bay of Islands field toward lower Cr/(Cr+Al) ratios.

No compositional differences between spinels of the different textural types are recorded.

TiO_2, MnO, NiO, and V_2O_3 contents are uniformly low, although a comparative plot of TiO_2 vs. $Mg/(Mg+Fe^{2+})$ (Figure 4.7.) shows that the TiO_2 abundances in harzburgite are commonly greater than for the spinel lherzolite.

Color and chemical variations of spinels in lherzolite and harzburgite appear to be dependent on the modal amount of clinopyroxene in the rock, i.e., modal amounts greater than

Figure 4.5. Plot of Cr x 100/(Cr+Al) ratio vs. Mg x 100/ ($Mg+Fe^{2+}$) ratio of spinels from various lithologies of the White Hills Peridotite. Symbols as for Figure 4.2. Dashed line - spinels from harzburgite, Bay of Islands Complex (Malpas and Strong, 1975).

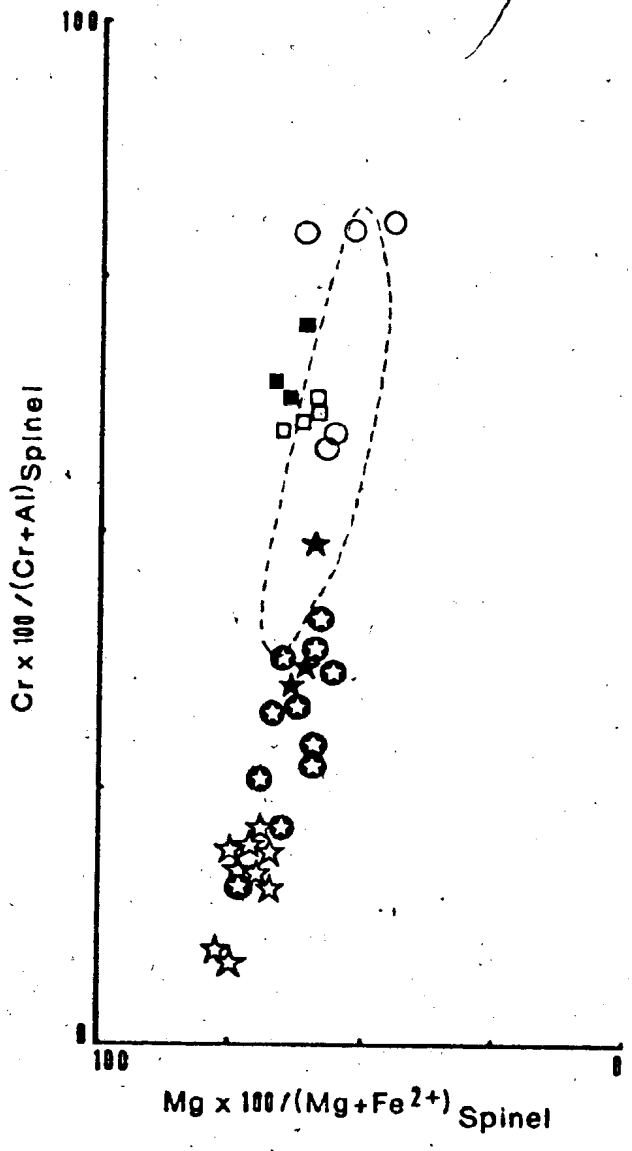
100
0
100
0
Cr x 100 /(Cr+Al)Spinel
Mg x 100/(Mg+Fe2+) Spinel

Figure 4.6. Al - Cr - Fe^{3+} plot (cation proportions) of spinels from various lithologies of the White Hills Peridotite. Symbols as for Figure 4.2.

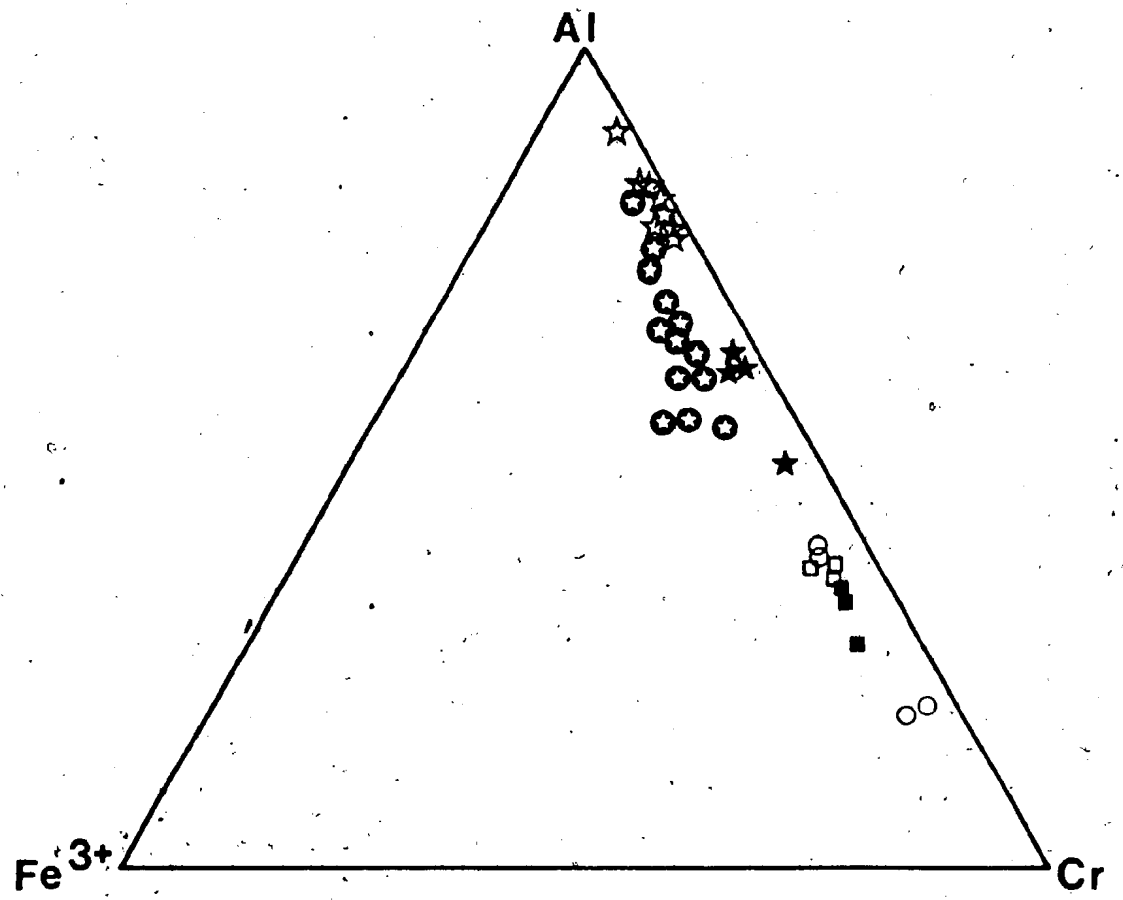
Al
Fe3+
Cr

Figure 4.7. TiO_2(wt. %) vs. Mg x 100/(Mg+Fe^{2+}) ratio for spinels from various lithologies of the White Hills Peridotite.
Symbols:

- Spinel lherzolite
- Harzburgite
- Dunite
- Chromite pod

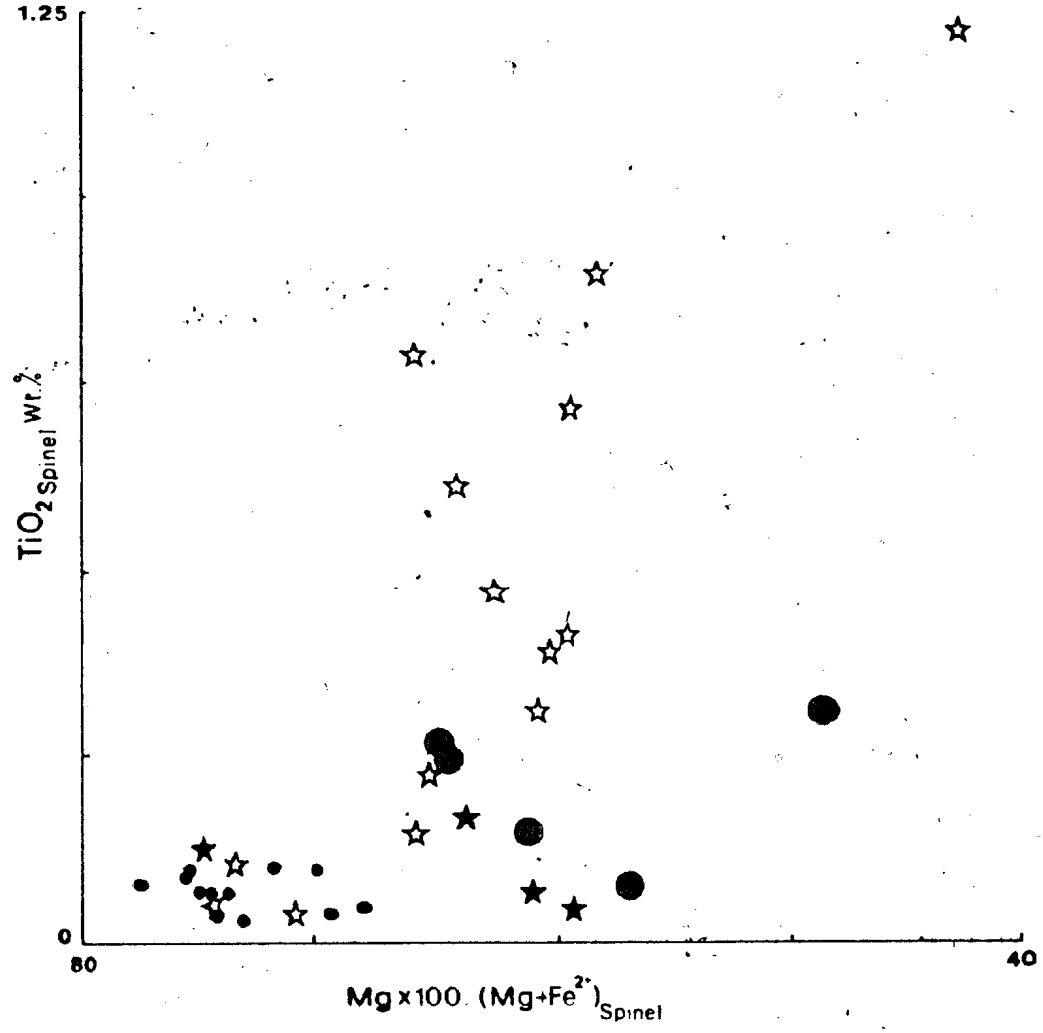
1.25
0
80
40
$TiO_{2\,Spinel}$ wt.%
$Mg \times 100 . (Mg+Fe^{2+})_{Spinel}$

5 to 7 percent result in bronze to straw-yellow colors; with less than this amount the spinel is varying colors of red-brown.

Spinel in dunite is divided into three groups based on rock associations:

1) disseminated spinel in dunite layers intercalated with harzburgite and disseminated spinel in dunite lenses.

2) disseminated spinel in dunite dikes.

3) disseminated spinel in dunite layers intercalated with spinel lherzolite.

In group 1, the spinels have the highest Cr/(Cr+Al) ratio of all the dunite spinel types ($\sim$ 0.400) (Figure 4.8.). The compositional field for this group is contained within the White Hills Peridotite harzburgite spinel field. Talkington and Malpas (1980a) report distinct groups for the two spinel associations of this group, but further sampling of these rocks proves this division unfounded.

Spinel in dunite dikes (group 2) has Cr/(Cr+Al) ratios ($\sim$ 0.250) intermediate between groups 1 and 3 (Figure 4.8.).

The spinel in dunite intercalated with spinel lherzolite has the lowest Cr/(Cr+Al) ratio of the dunite types ($\sim$ 0.160) (Figure 4.8.) and lies within the defined field for spinel lherzolite from the White Hills.

Spinel in dunite therefore shows a range in Cr/(Cr+Al) ratio from approximately 0.160 to 0.400 and compared to the White Hills Peridotite, spinels in the cumulate dunite from the Bay of Islands Complex (Malpas and Strong, 1975 and Figure 4.8.) have a higher and more restricted range for

Figure 4.8. Plot of Cr x 100/(Cr+Al) ratio vs. Mg x 100/ ($Mg+Fe^{2+}$) ratio for spinels from various lithologies of the White Hills Peridotite. Symbols as for Figure 4.2.
Dashed line - Spinels from cumulate dunite, Bay of Island Complex (Malpas and Strong, 1975).
Solid line - Group 1 dunite
Square bracket - Groups 2 and 3 dunite

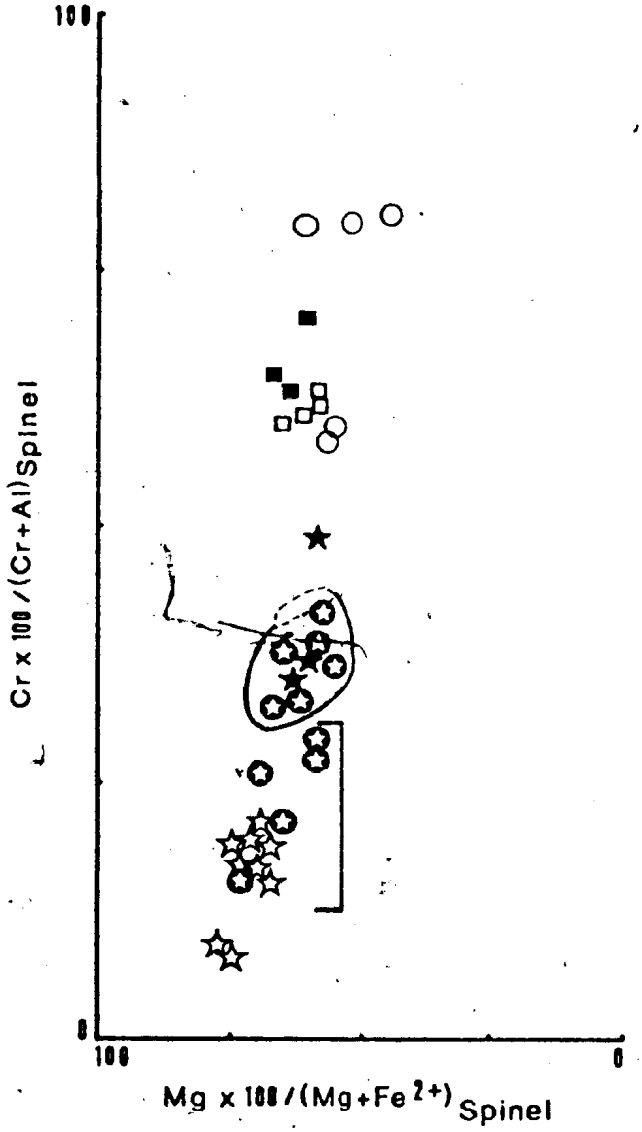
100
0
100
0
Cr x 100 / (Cr+Al) Spinel
Mg x 100 / (Mg+Fe 2+) Spinel

spinel Cr/(Cr+Al) ratios. Spinel in dunite from the Burro Mountain Peridotite (Loney et al., 1971, Table 8, p. 292) shows a large range in Cr/(Cr+Al) ratios (0.30 to 0.75) which has been correlated with dunite occurrence (lens, dike, sill). For nearly every dunite sample where spinel data are available, the chemistry of the spinel from dunite (mainly the Cr/(Cr+Al) ratio) mimics that for spinel of the host rock, e.g., a higher Cr/(Cr+Al) ratio for spinels from dunite associated with harzburgite, a lower Cr/(Cr+Al) ratio for spinels from dunite associated with spinel lherzolite.

The Fe^{3+} contents for all dunite spinels is higher relative to harzburgite and spinel lherzolite (compare the Fe_2O_3, $MgFe_2O_4$ and $FeFe_2O_4$ values).

MnO contents remain nearly constant for the dunite spinels and are similar to spinel lherzolite and harzburgite abundances. TiO_2 is moderately higher for the dunite spinels (Figure 4.7.). Evans and Wright (1972) indicate that with an increase in TiO_2, FeO and Fe_2O_3 there is a corresponding decrease in the Cr_2O_3 content of spinels in some Hawaiian basalts. For the spinels in dunite from the White Hills Peridotite, there is an increase in TiO_2 (reflected in spinel as Fe_2TiO_4, ulvöspinel) but a corresponding decrease in Cr_2O_3 or total iron is not recognized. Justification for this TiO_2 increase cannot be made if the spinel compositions from dunite are compared with spinels from spinel lherzolite and harzburgite. However this TiO_2 increase can be rationalized if the processes by which the spinels form are examined. For

example, spinel from spinel lherzolite and harzburgite, as is shown later, form in general by exsolution processes with subsequent modification of their chemistries by partial fusion processes, whereas spinels in dunite form by crystallization from a melt, later to have their chemistries modified during in situ reequilibration.

Spinel disseminated in orthopyroxenite (low-alumina) and spinel accumulations in seams or lenses have the highest Cr/(Cr+Al) ratios for spinels from the White Hills Peridotite (Figure 4.9; Table AII.15.). Spinel seams associated with deformed orthopyroxenite veins have the highest Cr/(Cr+Al) ratio for all White Hills Peridotite lithologies ($\sim$ 0.750), whereas disseminated cumulus spinels in orthopyroxenite veins and spinels associated with "websterite" and the massive spinel of the pod have a slightly lower Cr/(Cr+Al) ratio ($\sim$ 0.600). Loney et al (1971) report a similar Cr/(Cr+Al) ratio ($\sim$ 0.630) for spinels associated with orthopyroxenite of the Burro Mountain Peridotite.

No chemical zoning is detected for spinels associated with "websterite" or orthopyroxenite.

Resorbed spinels in orthopyroxene (bastite) phenocrysts and disseminated spinel in the emerald green clinopyroxene have a higher Cr/(Cr+Al) ratio and a lower $Mg/(Mg+Fe^{2+})$ ratio than the surrounding massive spinel (Figures 4.9. and 4.10.). The Cr/(Cr+Al) and $Mg/(Mg+Fe^{2+})$ ratios for these spinel-silicate associations are similar to those reported for podiform chromites of Alpine-type peridotites (Irvine , 1967;

Figure 4.9. Plot of Cr x 100/(Cr+Al) ratio vs. Mg x 100/ ($Mg+Fe^{2+}$) ratio for spinels from various lithologies of the White Hills Peridotite. Symbols as for Figure 4.2. Dashed line - spinels from podiform chromite deposits, Bay of Islands Complex (Talkington, unpublished data).

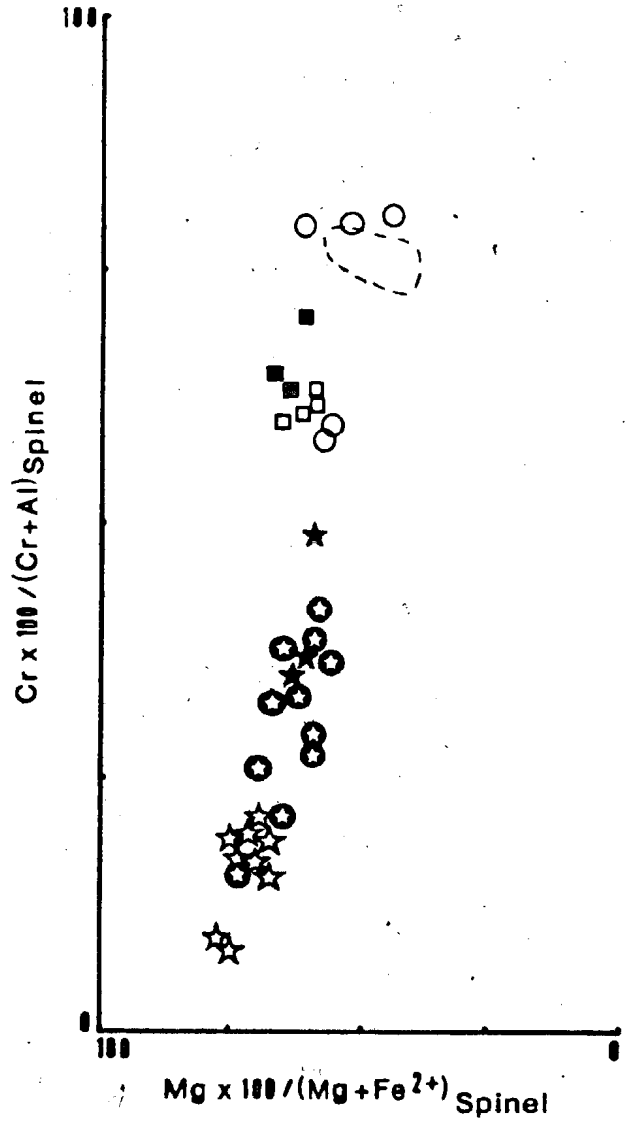
100
0
100
0
Cr x 100 /(Cr+Al)Spinel
Mg x 100 /(Mg+Fe2+)Spinel

Figure 4.10. Plot of Cr x 100/(Cr+Al) ratio vs. Mg x 100/ ($Mg+Fe^{2+}$) ratio for spinels from the chromite pod.
Symbols:

- ■ Massive chromite, sample 78122Y
- ▲ Resorbed chromite, sample 78122Y
- ● Massive and resorbed chromite, sample 78123X

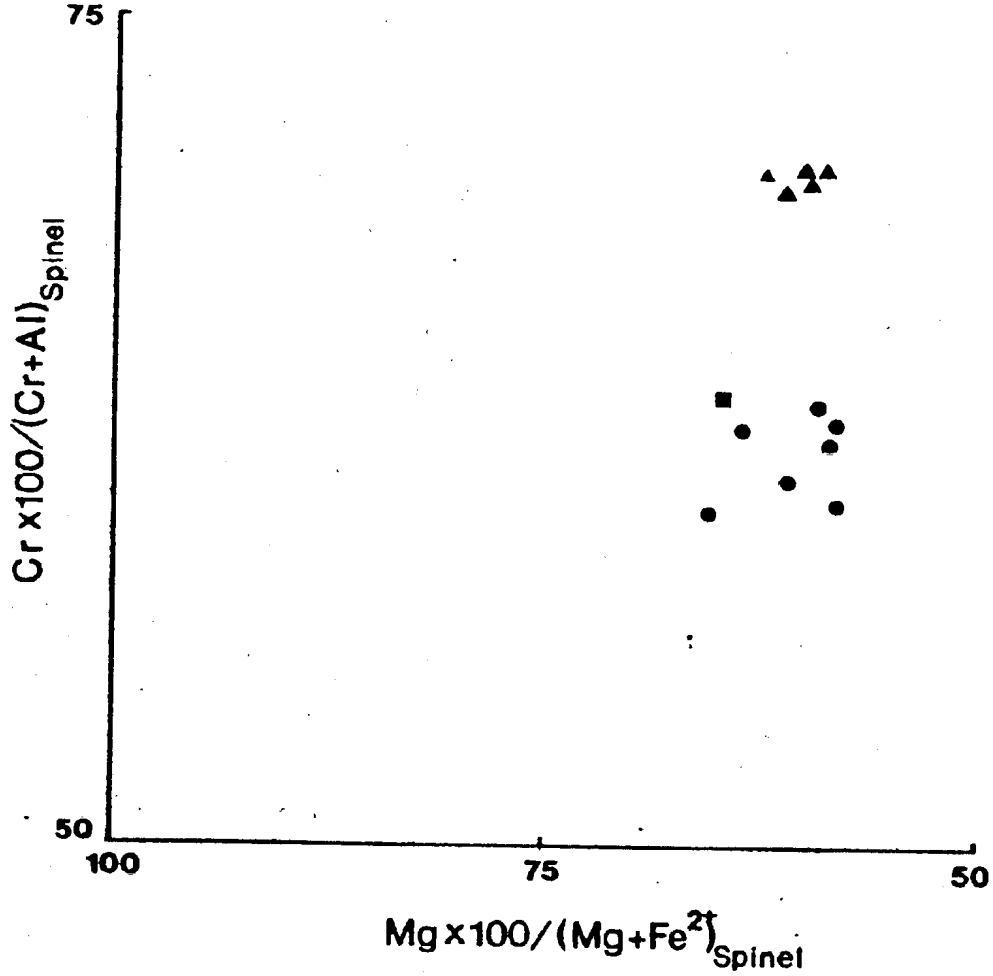
75
50
100
75
50
Cr x100/(Cr+Al)Spinel
Mg x100/(Mg+Fe2+)Spinel

Thayer, 1970; Dickey, 1975; Greenbaum, 1977; Panayiotou, 1978).

MnO, NiO and V_2O_3 concentrations are similar to the other ultramafic rocks of the White Hills Peridotite. The TiO_2 concentration is less than 0.31 weight percent and significantly lower than for spinels in dunite (Figure 4.7.). Dickey (1975) has compared spinel compositions from podiform deposits in Alpine-type peridotites with spinel compositions from stratiform layered intrusions and finds that for the podiform deposits the TiO_2 content is generally less than 0.3 weight percent, but for stratiform intrusions generally higher. Similar results are reported by Bird and Clark (1978) for spinels in dunite ($\sim$ 1 wt. % TiO_2) for the Alaskan-type ultramafic complex at Goodnews Bay, Alaska.

Spinel compositions in websterite, clinopyroxenite and wehrlite are similar (Table AII.16. Figures 4.11., 4.12., and 4.13.). All have Cr/(Cr+Al) ratios of about 0.100, but the $Mg/(Mg+Fe^{2+})$ ratios for spinels in clinopyroxenite and wehrlite are less than in websterite.

MnO, and NiO are comparable to all rock types of the White Hills. The spinel TiO_2 contents are similar to the other rock types of the peridotite but lower than the TiO_2 contents for spinels in dunite.

Spinel in gabbro has the lowest Cr/(Cr+Al) ratio for spinels of the White Hills ($\sim$ 0.010) (Table AII.17., Figures 4.11., 4.12., and 4.13.). The $Mg/(Mg+Fe^{2+})$ ratio shows a greater range than in spinels from the other rock types.

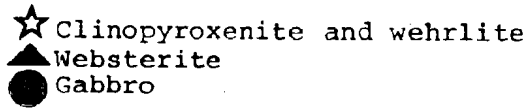

Figure 4.11. Plot of Cr x 100/(Cr+Al) ratio vs. Mg x 100/ ($Mg+Fe^{2+}$) ratio for spinels from websterite, clinopyroxenite, wehrlite, and gabbro.
Symbols:

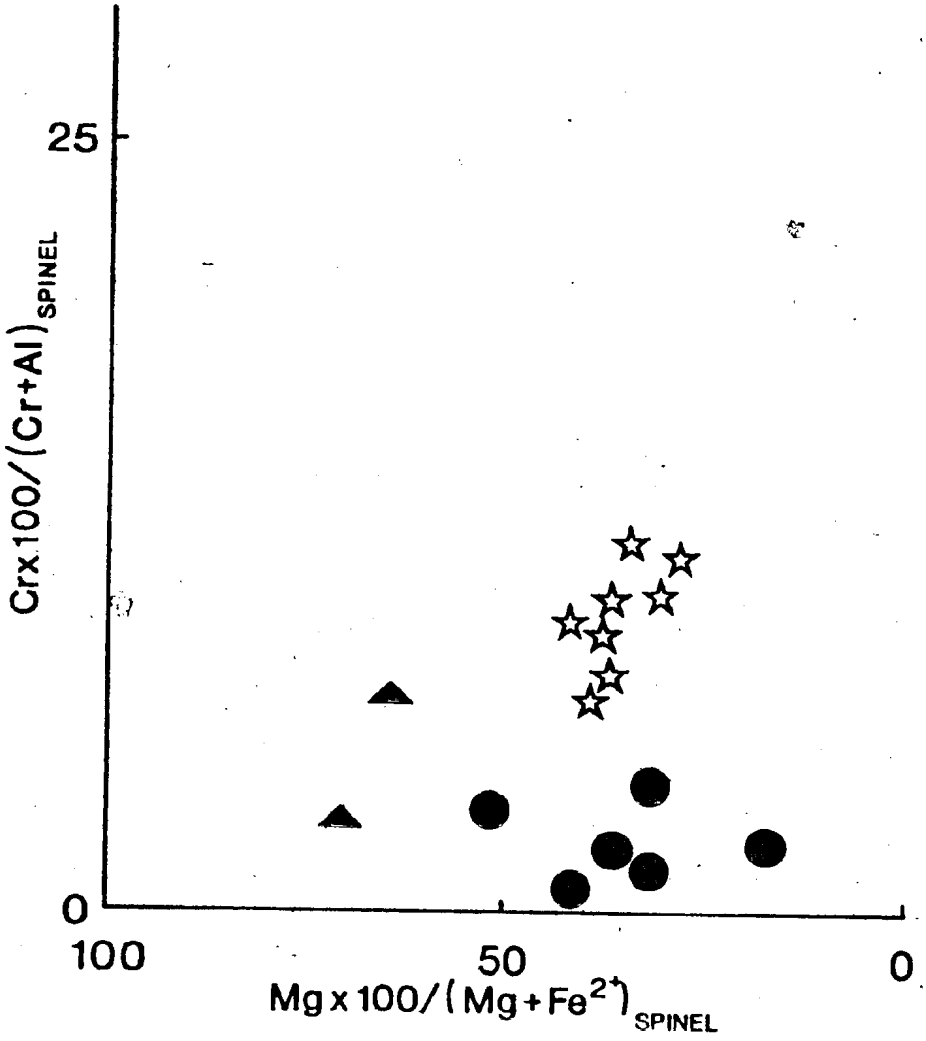
25
0
100
50
0
Crx100/(Cr+Al)SPINEL
Mgx100/(Mg+Fe2+)SPINEL

Figure 4.12. Websterite, clinopyroxenite, wehrlite, and gabbro spinel compositions plotted in the spinel prism. Symbols as for Figure 4.11. See Figure 4.4. for explanation of solid lines connecting symbols to prism base.

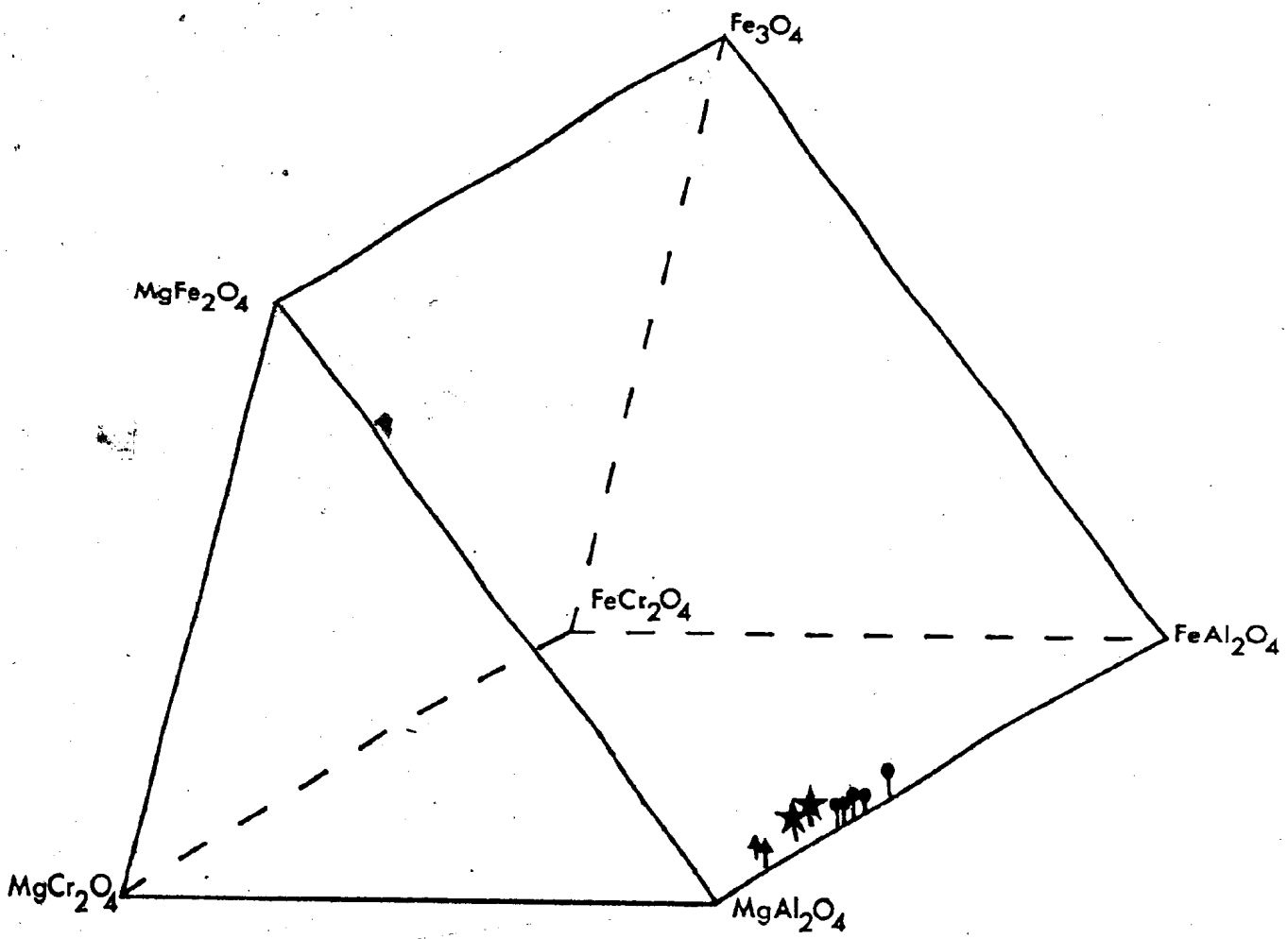
Fe_3O_4
$MgFe_2O_4$
$FeCr_2O_4$
$FeAl_2O_4$
$MgCr_2O_4$
$MgAl_2O_4$

Figure 4.13. Al - Cr - Fe^{3+} plot (cation proportion) of spinels from websterite, clinopyroxenite, wehrlite, and gabbro. Symbols as for Figure 4.11.

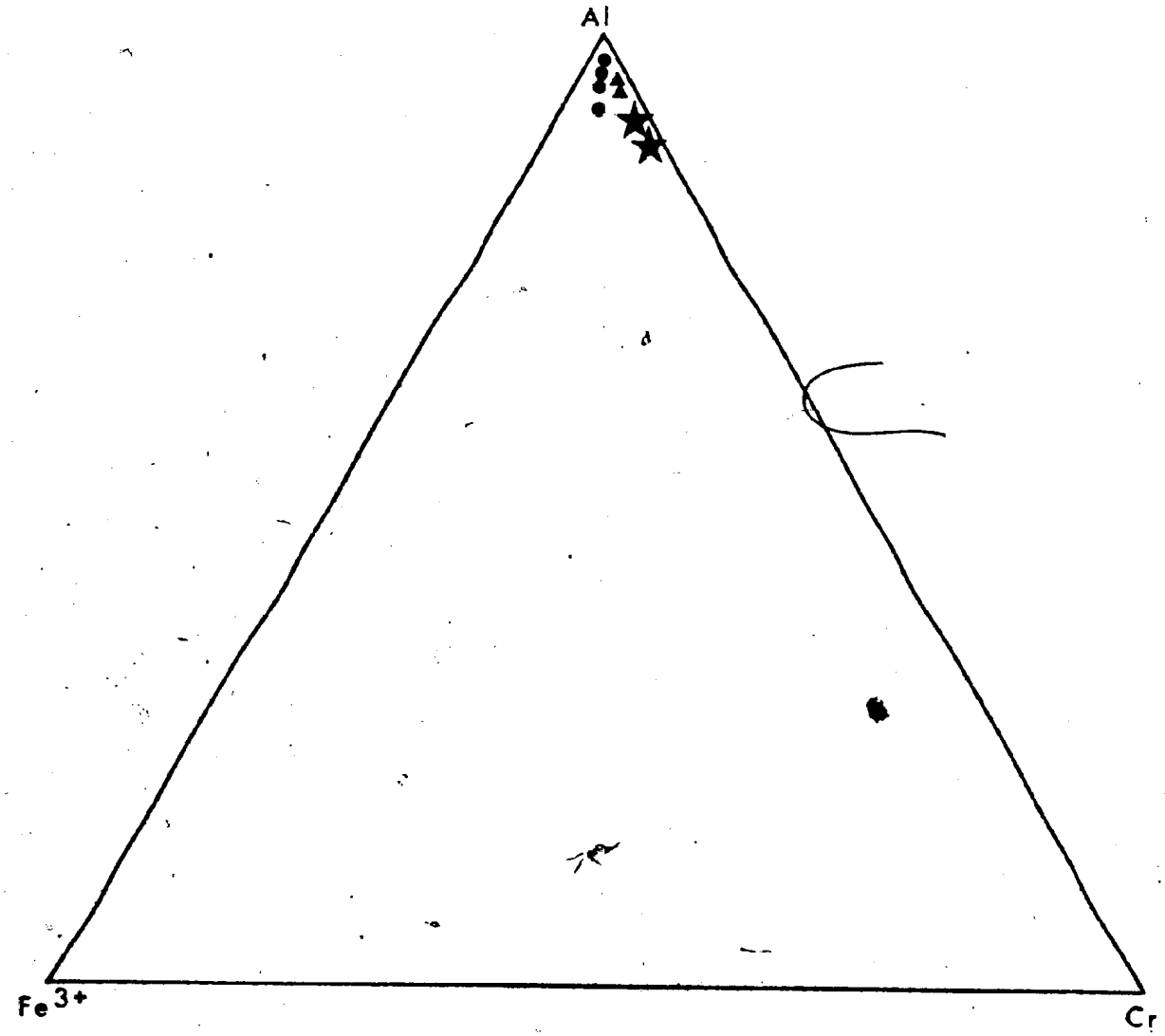
Al
Fe3+
Cr

II.4.D. Spinel Geothermometry

1. Fe^{2+} - Mg Partitioning Between Spinel and Olivine

Irvine (1965) has derived a series of three reactions expressing the Fe^{2+} - Mg exchange between coexisting spinel and olivine for the simple olivine components Fe_2SiO_4 and Mg_2SiO_4 and the complex spinel components $Fe(Cr_x,Al_y,Fe^{3+}_z)_2O_4$ and $Mg(Cr_x,Al_y,Fe^{3+}_z)_2O_4$. These are:

$$\tfrac{1}{2}Fe_2SiO_4 + MgCr_2O_4 \rightleftarrows \tfrac{1}{2}Mg_2SiO_4 + FeCr_2O_4 \qquad (4.1)$$

$$\tfrac{1}{2}Fe_2SiO_4 + MgAl_2O_4 \rightleftarrows \tfrac{1}{2}Mg_2SiO_4 + FeAl_2O_4 \qquad (4.2)$$

$$\tfrac{1}{2}Fe_2SiO_4 + MgFe_2O_4 \rightleftarrows \tfrac{1}{2}Mg_2SiO_4 + FeFe_2O_4 \qquad (4.3)$$

These reactions, when combined, give the following reaction which expresses the mutual solid solution between the six end member spinels and olivine:

$$\underset{\text{Olivine}}{\tfrac{1}{2}Fe_2SiO_4} + \underset{\text{Spinel}}{Mg(Cr_x,Al_y,Fe^{3+}_z)_2O_4} \rightleftarrows \underset{\text{Olivine}}{\tfrac{1}{2}Mg_2SiO_4} + \underset{\text{Spinel}}{Fe(Cr_x,Al_y,Fe^{3+}_z)_2O_4} \qquad (4.4)$$

Where,

$$x = \frac{Cr}{Al + Cr + Fe^{3+}}$$

$$y = \frac{Al}{Al + Cr + Fe^{3+}}$$

$$z = \frac{Fe^{3+}}{Al + Cr + Fe^{3+}}$$

x, y and z are the trivalent cations in the spinel

octahedral site and

$$x + y + z = 1$$

The empirical equilibrium distribution coefficient for exchange reaction (4.4) is

$$K_D = \frac{x_{Mg}^{Ol} \cdot x_{Fe^{2+}}^{Sp}}{x_{Fe^{2+}}^{Ol} \cdot x_{Mg}^{Sp}} \qquad (4.5)$$

Where,

$$x_{Mg}^{Ol} = \frac{Mg}{(Mg + Fe^{2+})\text{olivine}}$$

$$x_{Fe^{2+}}^{Sp} = \frac{Fe^{2+}}{(Mg + Fe^{2+})\ \text{spinel}}$$

2. Geothermometers

Jackson (1969) has used the Irvine (1965) data to calculate an olivine-spinel geothermometer. In his calculations, Jackson assumes that ideal mixing of Fe^{2+} and Mg between spinel and olivine is complete at high temperatures. He then relates the distribution coefficient for Fe^{2+} and Mg in equation (4.4) to the standard Gibbs free energies of the products and reactants so that:

$$K_D = \exp\{(-\Delta G^{\circ}_{\frac{1}{2}Mg_2SiO_4} - x\Delta G^{\circ}_{FeCr_2O_4} + y\Delta G^{\circ}_{FeAl_2O_4} - z\Delta G^{\circ}_{FeFe_2O_4} + \Delta G^{\circ}_{\frac{1}{2}Fe_2SiO_4} + x\Delta G^{\circ}_{MgCr_2O_4} + y\Delta G^{\circ}_{MgAl_2O_4} + z\Delta G^{\circ}_{MgFe_2O_4})/RT\} \quad (4.6)$$

Where $\Delta G^{\circ}_{\frac{1}{2}Mg_2SiO_4}$ and $\Delta G^{\circ}_{\frac{1}{2}Fe_2SiO_4}$ are the standard Gibbs free energies of formation of the olivine end members. $\Delta G^{\circ}_{FeCr_2O_4}$, $\Delta G^{\circ}_{MgCr_2O_4}$, $\Delta G^{\circ}_{FeAl_2O_4}$, $\Delta G^{\circ}_{MgAl_2O_4}$, $\Delta G^{\circ}_{FeFe_2O_4}$, and $\Delta G^{\circ}_{MgFe_2O_4}$ are the standard Gibbs free energies for the spinel end members. R is the gas constant, T the temperature in degrees Kelvin, x, y, and z are as described previously. To derive an equation that is expressed in terms of T, Jackson (1969) combines equations (4.5) and (4.6) and solves for T. The resulting equation has the form:

$$T = \{(-\Delta G^{\circ}_{\frac{1}{2}Mg_2SiO_4} - x\Delta G^{\circ}_{FeCr_2O_4} - y\Delta G^{\circ}_{FeAl_2O_4} - z\Delta G^{\circ}_{FeFe_2O_4} + \Delta G^{\circ}_{\frac{1}{2}Fe_2SiO_4} + x\Delta G^{\circ}_{MgCr_2O_4} + y\Delta G^{\circ}_{MgAl_2O_4} + z\Delta G^{\circ}_{MgFe_2O_4})/R\ln\left(\frac{x^{Ol}_{Mg} \cdot x^{Sp}_{Fe^{2+}}}{x^{Ol}_{Fe^{2+}} \cdot x^{Sp}_{Mg}}\right)\} \quad (4.7)$$

Substituting the available Gibbs free energy data into equation (4.7) and using R = 1.987 calories/degree mole, the equation that expresses the temperature relationship

between spinel and olivine assuming ideal mixing is:

$$T(^{o}K) = \frac{5580x + 1018y - 1702z + 2400}{.90x + 2.56y - 3.08z - 1.47 + 1.987 \ln K_{D\ Mg\text{-}Fe^{2+}}} \quad (4.8)$$

Uncertainties in the free energy values alone may affect the equilibration temperatures ± 300°C! Additional uncertainties probably result if there is non-ideal mixing of the mineral phases, which may be the case at low temperatures (Obata et al., 1974). However, Fujii's (1977) experiments on Fe^{2+}-Mg partitioning between olivine and spinel at 1 atm and 15 kilobars at temperatures from 1200°C to 1350°C suggest that, at these temperatures, either the two minerals are ideal or that nonidealities of both minerals cancel out.

Although most users of the Jackson geothermometer have adopted the view that the derived temperature represents equilibration from magmatic temperatures, this now appears not to be the case. Roeder et al (1979) have performed heating experiments on natural peridotite samples and find that at about 1200°C, considerable redistribution of Fe^{2+}-Mg occurs between spinel and olivine, whereas no appreciable redistribution in Fe^{2+}-Mg occurs below this temperature. During this same study, Roeder et al (1979) revise the Jackson (1969) geothermometer by using a different Gibbs free energy value for chromite ($FeCr_2O_4$). This results in a modified temperature equation:

$$T(^{o}K) = \frac{3480x + 1018y - 1720z + 2400}{2.23x + 2.56y - 3.08z - 1.47 + 1.987 \ln K_{D_{Fe^{2+}\text{-}Mg}}} \quad (4.9)$$

Temperatures calculated by Roeder et al (1979) for the experimentally heated samples using this form of the Jackson equation are consistent with the temperatures used during their melting experiments. Also, the temperatures calculated for the unheated experimental samples using equation (4.9) are subsolidus (cf., Roeder et al., 1979, Table 3). Therefore, the assumption made by Jackson (1969) of magmatic equilibration is unfounded.

Al-rich spinels heated to 1200°C during the experiments of Roeder et al (1979) yield temperatures, using the modified Jackson geothermometer, of about 1400°C, 200°C higher than the experimental runs. This temperature difference may be because the Gibbs free energy values for the aluminum-rich spinels are poorly known (Roeder et al., 1979), or because of non-ideal mixing of spinels and olivine or complications with the experimental procedure (e.g., Fe-loss to the Pt-crucible).

Spinels in Alpine-type peridotites often span a complete range of spinel compositions from chromium-rich to aluminum-rich and therefore application of a geothermometer to all spinel types is unadvisable. To this end, Fabriès (1979) has recalibrated the empirically derived, graphical spinel-olivine geothermometer of Evans and Frost (1975), which is also based on the Fe-Mg ion exchange equilibria equations of Irvine (1965), so that it may be applied to rocks from lherzolitic

complexes. Fabries (1979) assumes that in spinel peridotites the spinel compositions can be approximated by the composition, $(Mg,Fe^{2+})\ (Al,Cr)_2O_4$, thus neglecting the effect of ferric iron. After evaluating the various thermodynamic equations he arrives at the temperature equation:

$$T^{o}K = \frac{4250Y_{Cr}^{Sp} + 1343}{\ln K_D o = 1.825Y_{Cr}^{Sp} + 0.571} \qquad (4.10)$$

Where,

$$Y_{Cr}^{Sp} = \frac{Cr}{Al + Cr + Fe^{3+}}$$

and, $$K_D o = \frac{X_{Mg}^{Ol} \cdot X_{Fe^{2+}}^{Sp}}{X_{Fe^{2+}}^{Ol} \cdot X_{Mg}^{Sp}}$$

normalized to an Fe^{3+}-free basis.

Application of equation (4.10) to spinels from peridotitic rocks yields results consistent with the spinel heating experiments of Roeder et al (1979) and other studies(cf., Fabries, 1979, Table 2).

Factors which affect and therefore limit the usefulness of the spinel-olivine geothermometer are:

(1) non-ideal mixing of Fe^{2+}-Mg in spinel and olivine at high and low temperatures.

(2) incomplete solid solution between spinel end members.

(3) errors due to incomplete thermodynamic data.

(4) accuracy in determination of Fe^{2+} and Fe^{3+}.

(5) effect of minor elements on spinel-olivine and spinel-spinel equilibria.

3. Application of Spinel-Olivine Geothermometers to the White Hills Peridotite

If the drawbacks of the spinel-olivine geothermometers are accepted, "reequilibration" temperatures (or equilibration temperatures if olivine and spinel are not initially in equilibrium) for various rock types of the White Hills Peridotite can be calculated and compared using the Jackson (1969) equation, the modified Jackson equation (Roeder et al., 1979), and the Fabriès (1979) equation. The results are listed in Table 4.2. As is suggested by Roeder et al (1979), relative to the 1969 Jackson geothermometer, the modified Jackson version yields significantly lower temperature estimates for spinel-olivine "reequilibration". The Fabriès (1979) version shows how the high-aluminum content of spinel affects the temperature calculation. The high-aluminum spinels yield, overall, higher temperatures than the chromium-rich spinels, but for high chromium spinels the temperature estimates calculated using both the Roeder et al (1979) and the Fabriès (1979) equations are comparable. Both refined geothermometers yield temperature estimates significantly lower than the earlier version of Jackson (1969) which suggests that exchange equilibria between spinel and olivine operates at subsolidus temperatures.

It is not possible to correlate the temperatures from the spinel-olivine geothermometers with the development of

TABLE 4.2: Spinel equilibration temperatures (°C) using various spinel-olivine geothermometers

Samples Number	Rock Type	Jackson (1969)	Roeder et al (1979)	Febries (1979
77WH1	Spinel lherzolite	921	763	645
77WH11	Spinel lherzolite	1174	1039	782
77WH15A	Spinel lherzolite	958	783	658
77WH76	Spinel lherzolite	954	786	658
77WH94	Spinel lherzolite	953	775	656
7815	Spinel lherzolite	960	757	664
7862	Spinel lherzolite	1180	975	791
78105	Spinel lherzolite	1044	874	706
78151	Spinel lherzolite	873	719	613
795	Spinel lherzolite	976	881	678
796	Spinel lherzolite	1069	944	726
77WH56	Harzburgite	1030	714	699
7818	Harzburgite	1086	691	723
7910	Harzburgite	979	674	671
77WH37	Dunite	1020	770	675
77WH55	Dunite layers interlayered with harzburgite	967	661	651
77WH77	Dunite layer interlayered with spinel lherzolite	877	653	599
77WH80	Dunite layer interlayered with harzburgite	937	666	634
77WH93	Dunite layer interlayered with spinel lherzolite	979	795	663
7841	Dunite	1078	887	712
78114	Dunite megalens	1060	740	703
78117	Dunite megalens	868	687	602
78117	Dunite megalens	1194	816	765
78141	Dunite dike	1117	876	717
78147	Dunite layer interlayered with harzburgite	1067	753	701
78152	Dunite dike cutting spinel lherzolite	932	679	637
78160	Dunite layer (?)	962	617	654
797	Dunite dike cutting harzburgite	686	612	481
77WH19	Sheared massive spinel seam in orthopyroxentie	1199	648	766
77WH30	Massive spinel seam in ortho-pyroxenite	1551	820	880
7898	Disseminated spinel in ortho-pyroxentie	1194	715	764

specific rock textures and thus to spinel form, because these temperatures have been effected by subsolidus chemical equilibration which may have occurred after the development of a particular microstructure. As such, an attempt to correlate specific deformational events (e.g., displacement, emplacement) by using spinel-olivine geothermometry is not suggested and should be avoided until additional refinement of the various geothermometers is complete.

As has often been reported in the literature where a comparison is made between geothermometers (e.g., based on Fe-Mg ion exchange, Al-partitioning between coexisting minerals, Ca- contents of clinopyroxene) the equilibration(?) temperatures calculated for the olivine-spinel pair, in peridotite, are lower than for silicate-silicate geothermometers by, in some cases, several hundred degrees (Evans and Frost, 1975; Fabriès, 1979). Notwithstanding this, similar results have been calculated for this study; the average equilibration temperature is 686°C for the olivine-spinel pairs using equation (4.10), whereas the average equilibration temperature is 903°C using equation 3 (Wells (1977) method, Table 3.2) for coexisting pyroxenes, a difference of slightly more than 200°C.

The possible cause for this discrepency is suggested to be the result of different rates of equilibration (re)adjustment during cooling (Evans and Frost, 1975; Herzberg and Chapman, 1976; Wood and Fraser, 1976; Fabries, 1979), which are controlled by certain thermodynamic properties of the mineral equilibria (especially ΔH°) and probably the unknown

dependence on the thermodynamic values for the presence of elements which "contaminate" the mineral equilibria (Mercier, 1980).

Wood and Fraser (1976) have suggested that due to the large ΔH^{O} value for the Fe-Mg ion exchange equilibria for the olivine-spinel pair, these minerals are appropriate for use as a geothermometer. It is the large ΔH^{O} value for the Fe-Mg ion exchange equilibria for olivine and spinel (and apparently small ΔV^{O} value) that gives a steep slope to the equilibrium curve (i.e., change in $P >> T$), and hence allows the olivine-spinel geothermometer to be useful to much lower subsolidus temperatures (cf., Roeder et al., 1979) than the Wells (1977) geothermometer.

Thus, the differences in temperatures for the olivine-spinel and pyroxene geothermometers indicate that the pyroxene geothermometer is less sensitive to cooling and in effect calculated temperatures represent 'quenched' (Herzberg and Chapman, 1976) or 'blocked' (Fabries, 1979) temperatures of exchange reactions. The olivine-spinel geothermometer is apparently more sensitive to subsolidus cooling and yields temperatures approaching steady thermal state conditions (Fabries, 1979).

II.4.E. Summary

The transition from coarse-granular texture (most "primitive") to mylonitic texture in spinel lherzolite and in some cases harzburgite is recognized by a change from exsolved vermicular spinel in orthopyroxene porphyroclasts to irregularly shaped spinel interstitial to slightly deformed silicates, ultimately coalescing into porphyroclasts which, in the more deformed textures, flatten and elongate in the foliation plane. Where this gradation is observable for a single rock type, it appears possible to distinguish between a residual spinel and one exsolved from orthopyroxene.

There is a compositional difference between exsolved spinels in orthopyroxene and spinel porphyroclasts, at least in spinel lherzolite.

Spinel textures and microstructures in dunite and chromite suggest a cumulus origin for these rocks. Cumulus and exsolved spinel textures are recognized in orthopyroxenite. Progressive deformation of spinels in these rocks results in an apparent granulation of spinel grains in chromitites and most orthopyroxenites and the development of holly leaf shapes in dunites.

The Cr/(Cr+Al) ratios for chromitite and orthopyroxenite are the highest recorded for the White Hills whereas the dunite Cr/(Cr+Al) ratio spans nearly the entire range for the peridotite. This ratio in dunite is dependent upon host rock association.

Spinel phases in websterite, clinopyroxenite, wehrlite, and gabbro are all green in color and show relationships to

silicates that are similar to those in the porphyroclastic texture of spinel lherzolite and harzburgite. The Cr/(Cr+Al) ratios for spinels in these pyroxenite veins are low and do not lie within the Alpine-type field as outlined by Irvine and Findlay (1972). The $Mg/(Mg+Fe^{2+})$ ratio for gabbro spinels spans a larger range than the Cr/(Cr+Al) ratio.

In general, the Cr/(Cr+Al) ratio for the analyzed spinels of the White Hills Peridotite is the most notable chemical variation. Comparison of spinel compositional trends from the Bay of Islands Complex with the White Hills Peridotite shows good agreement with the spinel lherzolite field, but not with the harzburgite or dunite fields.

Various spinel-olivine geothermometers have been applied to some of the White Hills Peridotite rock types. It is concluded that the most useful geothermometer for peridotitic rocks is that proposed by Fabries (1979). There are two reasons for favoring it: (1) the spinel-olivine heating experiments of Roeder et al (1979) indicate spinel-olivine elemental exchange continues to subsolidus temperatures, and (2) the near conformity of 'equilibration' temperatures for all rock types. It is suggested that these values be used with caution and thus they will not be applied when formulating an hypothesis for the origin of the White Hills Peridotite.

The origins of the various spinel phases from rocks of the White Hills Peridotite are discussed in Chapter 5, section II.5.C.

Chapter 5

Petrogenesis

II.5.A. CMAS Projections

1. General Statement

Nearly 90 percent of the chemical constituents of the upper mantle are contained within the system CaO-MgO-Al_2O_3-SiO_2 (CMAS) (MacGregor, 1965; Kushiro, 1968; Wyllie, 1971; Presnall et al., 1978); and almost all of the anhydrous upper mantle silicate minerals can be produced from these four oxides. Unlike the normative basalt tetrahedron which displays near surface, low pressure processes, the CMAS system adequately portrays upper mantle, high pressure processes. Various projection planes (subprojections of O'Hara, 1968) are possible within the system of which three are used in the following discussion (Figure 5.1.). The projection rules for this tetrahedron have been given by O'Hara (1968).

a. The Development of a Control Plane and Application of the CMAS System to Aid in the Development of a Petrogenetic Model for the White Hills Peridotite

The development of a hypothetical control plane for the advanced partial melting in ophiolites has been discussed by Malpas (1976) with particular reference to the Bay of Islands Complex and serves here as a useful guide. In Figure 5.2. source rocks 1 and 2 upon melting produce a melt of composition E at the quaternary eutectic. For fractional melting, the liquid remains at E until the aluminous phase or clinopyroxene is consumed. If the bulk composition of the source rock is 1,

Figure 5.1. Schematic drawing of the pseudo-quaternary system CaO-MgO-Al_2O_3-SiO_2 (CMAS) and the locations of the projection planes used in this study (after Clarke, 1970; Morse, 1973).

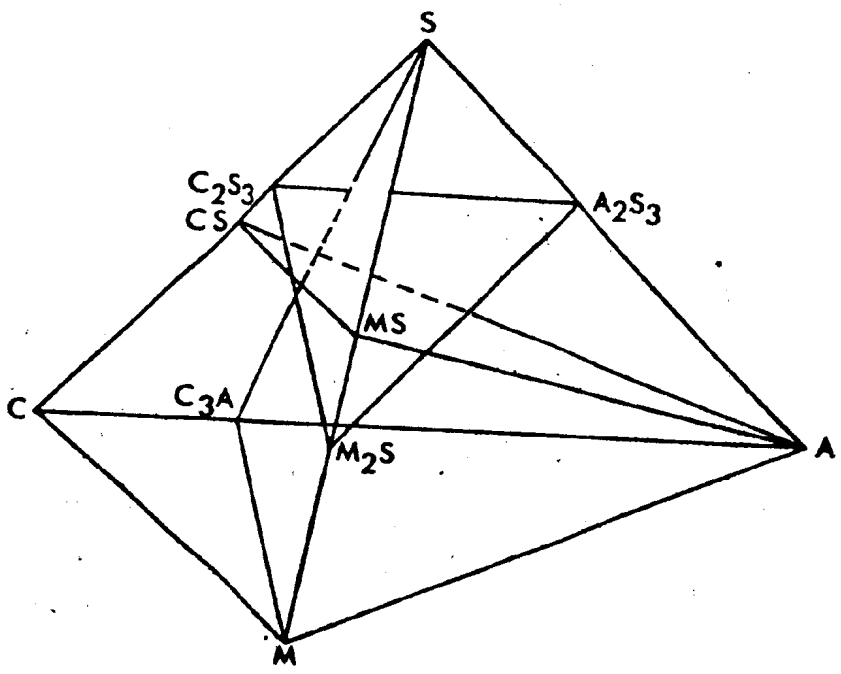
S
C_2S_3
CS
A_2S_3
MS
C
C_3A
M_2S
A
M

Figure 5.2. Graphical development of a control plane (olivine projection), see text for explanation (from Malpas, 1976).

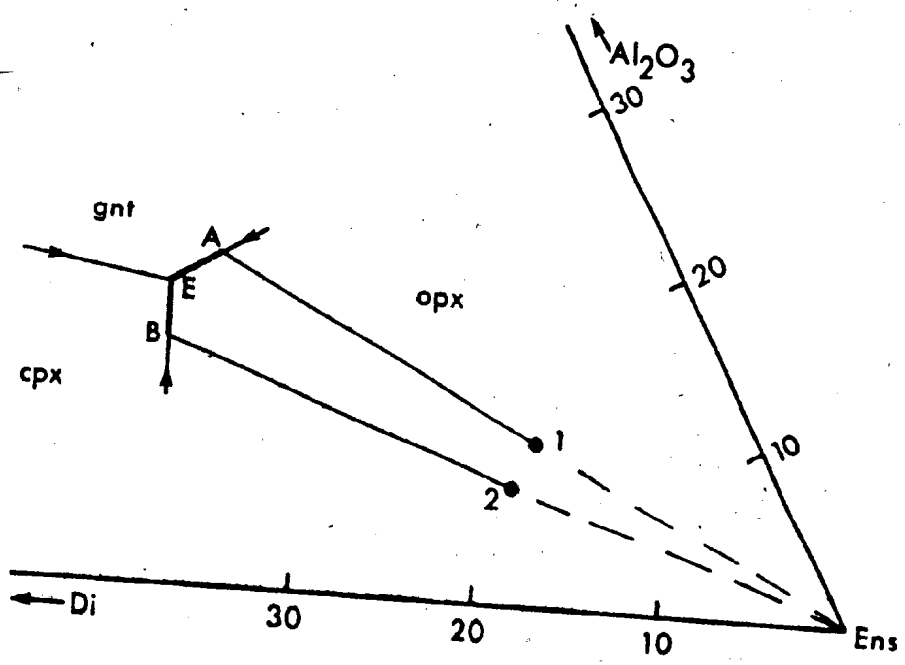
Al_2O_3
30
20
10
gnt
A
E
B
cpx
opx
1
2
Di
30
20
10
Ens

the aluminous phase will be consumed; if source rock 2, the clinopyroxene will be consumed. Subsequently, the liquid will migrate along either path EA1 or EB2 until the aluminous phase or clinopyroxene is completely melted, respectively; then along the path A1 or B2. Movement along paths A1 and B2 toward 1 or 2 causes the liquid composition to become progressively enriched in the enstatite molecule. The residue, therefore, produced from partial melting along control lines A1 and B2 is harzburgitic (olivine + enstatite). Thus, the control plane includes the composition of the source rock plus the residual harzburgite composition at advanced partial melting (Malpas, 1976).

The control plane for the White Hills Peridotite has been constructed using the average of 41 White Hills Peridotite spinel lherzolite compositions and the most refractory White Hills Peridotite harzburgite sample (77WH14) (Table 5.1.) and can best be seen on the olivine and enstatite projections. The Fe_2O_3 content for the average spinel lherzolite and the single harzburgite bulk rock compositions used to define the control plane have been adjusted to 2.00 weight percent for calculation purposes* (see section II.5.A.2.). As has been

* The value of 2.00 weight percent Fe_2O_3 has been used for three reasons: (1) most of the coarse-granular textured spinel lherzolite samples with low L.O.I. values have Fe_2O_3 contents of about 2.00 weight percent; (2) some published bulk rock chemical analyses for upper mantle spinel lherzolites or estimates of upper mantle spinel lherzolite compositions contain about 2.00 weight percent Fe_2O_3 (Table 5.1.); and (3) when uncorrected bulk rock Fe_2O_3 contents are used for the calculations in the subtraction program (next section), negative residuals (deficits) for Fe_2O_3 or other oxides are calculated for the residual material or unrealistically high $Mg/(Mg+Fe^{2+})$ ratios for the resultant liquid results after a moderate degree of partial melting (e.g., 20% partial melting, $Mg/(Mg+Fe^{2+})$

shown by Malpas (1976), the bulk chemical composition of the final liquid (first-stage) produced during partial melting of the source rock (spinel lherzolite) must lie on the control plane and if a small quantity of clinopyroxene remains in equilibrium in the harzburgite residue, the final liquid composition must plot on the olivine-orthopyroxene-clinopyroxene cotectic.

On the basis of pressure estimates determined from the modal mineralogy of the White Hills Peridotite spinel lherzolite (Chapter 3, II.3.A.3.i., which are not conclusive), the initial partial melt liquid (first-stage liquid) composition of the White Hills Peridotite is placed on the 20 kilobars cotectic. This pressure is chosen since it is thought to represent the pressure at which partial melting of the spinel lherzolite commenced during its ascent through the upper mantle (cf., Forsyth, 1977).

In the three CMAS projections (Figures 5.3., 5.4., 5.5.), spinel lherzolite and harzburgite bulk rock compositions plot in separate, yet slightly overlapping fields, and within the olivine or orthopyroxene phase volumes. The slight scatter of the plotted points on either side of the control plane is the result of the projection method (apices are not orthogonal to the projection plane). Also, as a result of adjusting the Fe_2O_3 contents for only the average White Hills spinel lherzolite

---

ratio of the resultant liquid is 0.814).

$Mg/(Mg+Fe^{2+})$ ratio in this section of the study is a weight percent ratio.

Table 5.1. Subtraction program compositional input data and estimations of upper mantle primary compositions

	1	2	3	4	5	6
SiO_2	44.40	43.57	47.50	44.40	45.10	45.10
TiO_2	0.13	0.11	0.20	0.13	0.50	0.20
Al_2O_3	2.63	0.94	8.97	2.38	4.10	4.60
Cr_2O_3	0.39	0.38	0.42	0.64	0.30	0.30
Fe_2O_3	2.00[a]	2.00[a]	1.97	8.31	2.00	0.30
FeO	6.22	5.35	9.48	--	7.90	7.60
MnO	0.13	0.12	0.17	0.17	0.20	0.10
MgO	41.30	46.79	20.64	42.06	36.70	38.10
CaO	2.64	0.60	10.30	1.34	2.30	3.10
Na_2O	0.10	0.05	0.29	0.27	0.60	0.40
K_2O	0.02	0.02	0.02	0.09	0.0(2)	0.02
P_2O_5	0.02	0.05	0.05	0.06	0.01	0.02
MgO/(MgO+FeO)	.869 (.823)[b]	.897	.685	(.835)[b]	.823	.834

1 - average bulk rock composition of 41 White Hills Peridotite spinel lherzolites.

2 - most refractory White Hills Peridotite harzburgite (77WH14).

3 - resultant liquid composition after 21 percent partial melting of the average White Hills Peridotite spinel lherzolite (column 1).

4 - average of 81 oceanic spinel lherzolites (Maaløe and Aoki, 1977).

5 - estimated upper mantle material (Nicholls, 1967, analysis 1, Table 9).

6 - average mantle pyrolite (Ringwood, 1975, column 8, Table 5.2).

a - Fe_2O_3 adjusted to 2.00 weight percent. Excess Fe^{3+} recalculated to FeO.

b - MgO/(MgO+IFe as Fe_2O_3).

Figure 5.3. Olivine projection onto the plane CS- MS- A.

Symbols:

- ✪ average spinel lherzolite
- ⊗ average harzburgite
- ◆ spinel lherzolite
- ● harzburgite
- △ dunite
- ○ orthopyroxenite
- □ websterite
- ▲ clinopyroxenite
- ◇ wehrlite
- ■ gabbro
- A' bulk composition of first-stage partial melt liquid

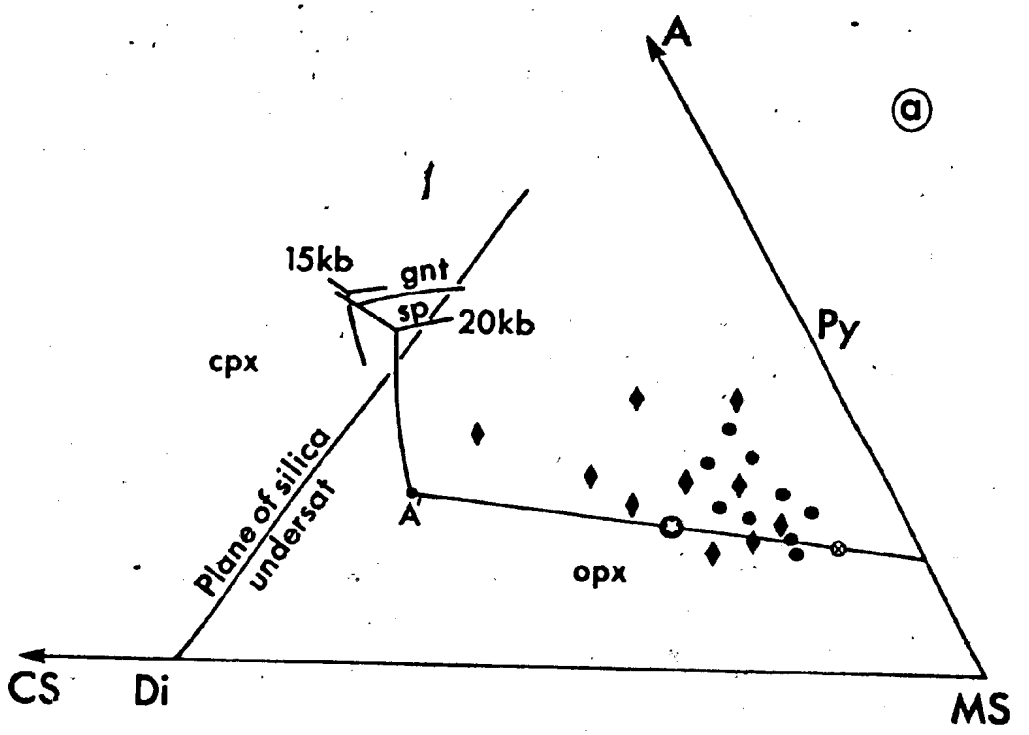
A
Py
CS
Di
MS
cpx
opx
15kb
gnt
sp
20kb
Plane of silica undersat
A'

(a)

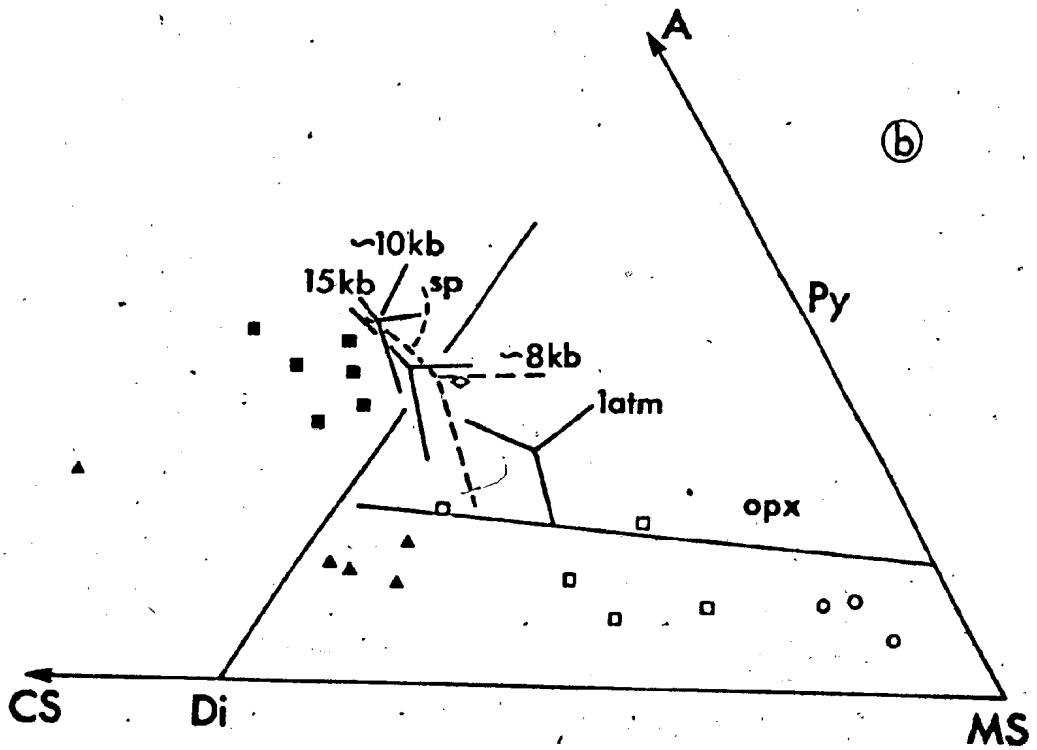
A
Py
CS
Di
MS
~10kb
15kb
sp
~8kb
1atm
opx

(b)

Figure 5.4. Enstatite projection onto the plane C_2S_3-M_2S-A_2S_3. Symbols as for Figure 5.3.

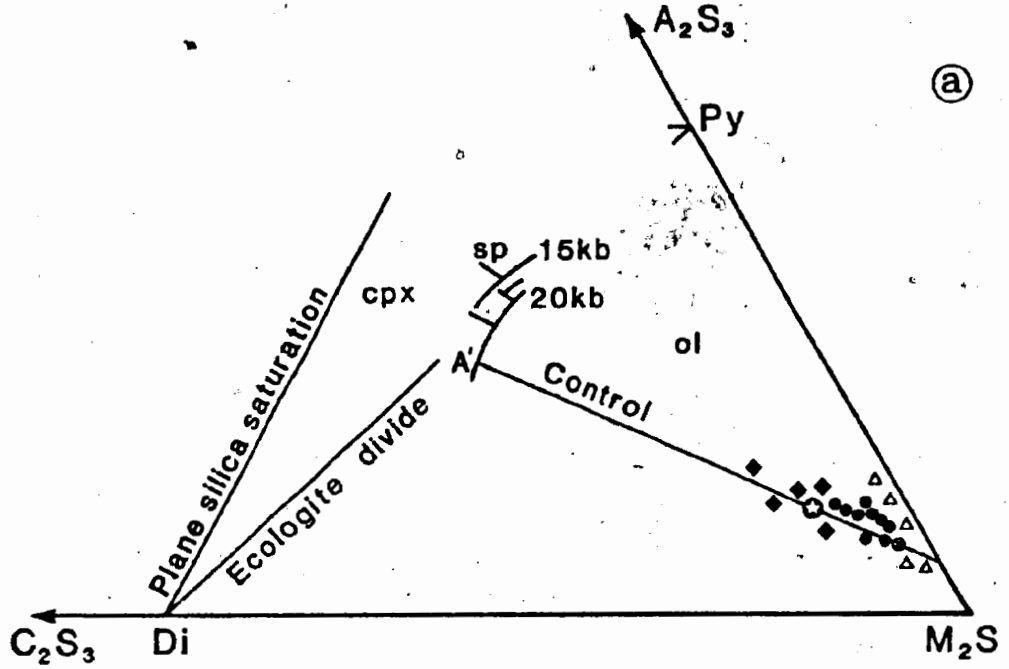
A_2S_3
Py
sp
15kb
20kb
cpx
ol
A'
Control
Plane silica saturation
Ecologite divide
C_2S_3
Di
M_2S

ⓐ

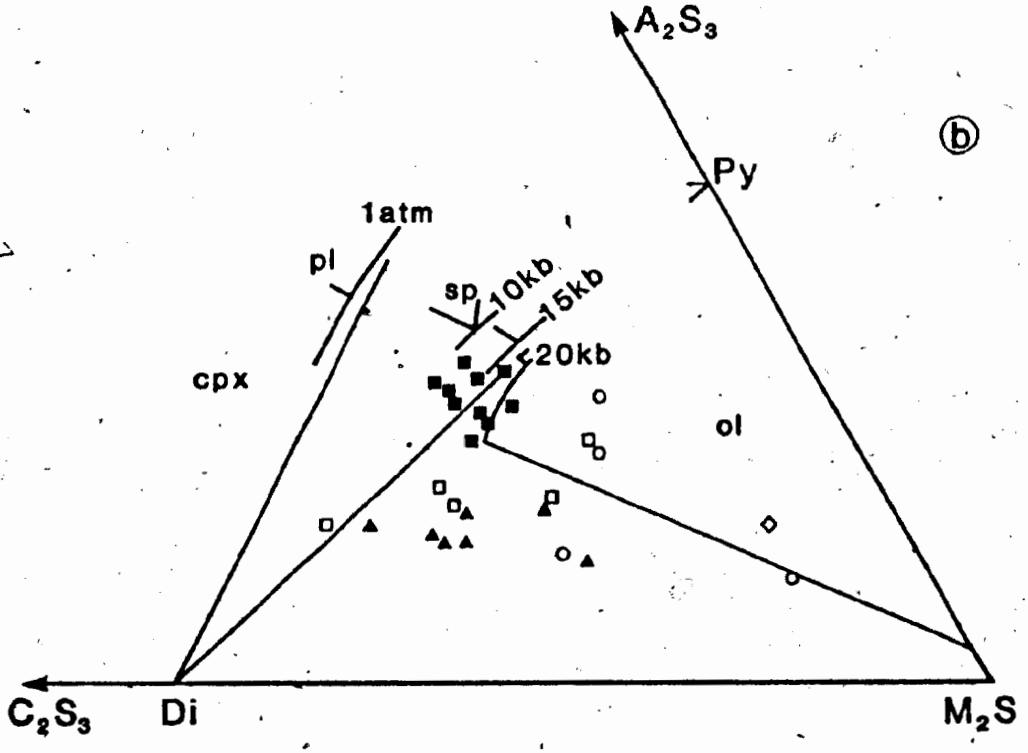
A_2S_3
Py
1atm
pl
sp
10kb
15kb
20kb
cpx
ol
C_2S_3
Di
M_2S

ⓑ

Figure 5.5. Diopside projection onto the plane C_3A-M-S. Symbols as for Figure 5.3.

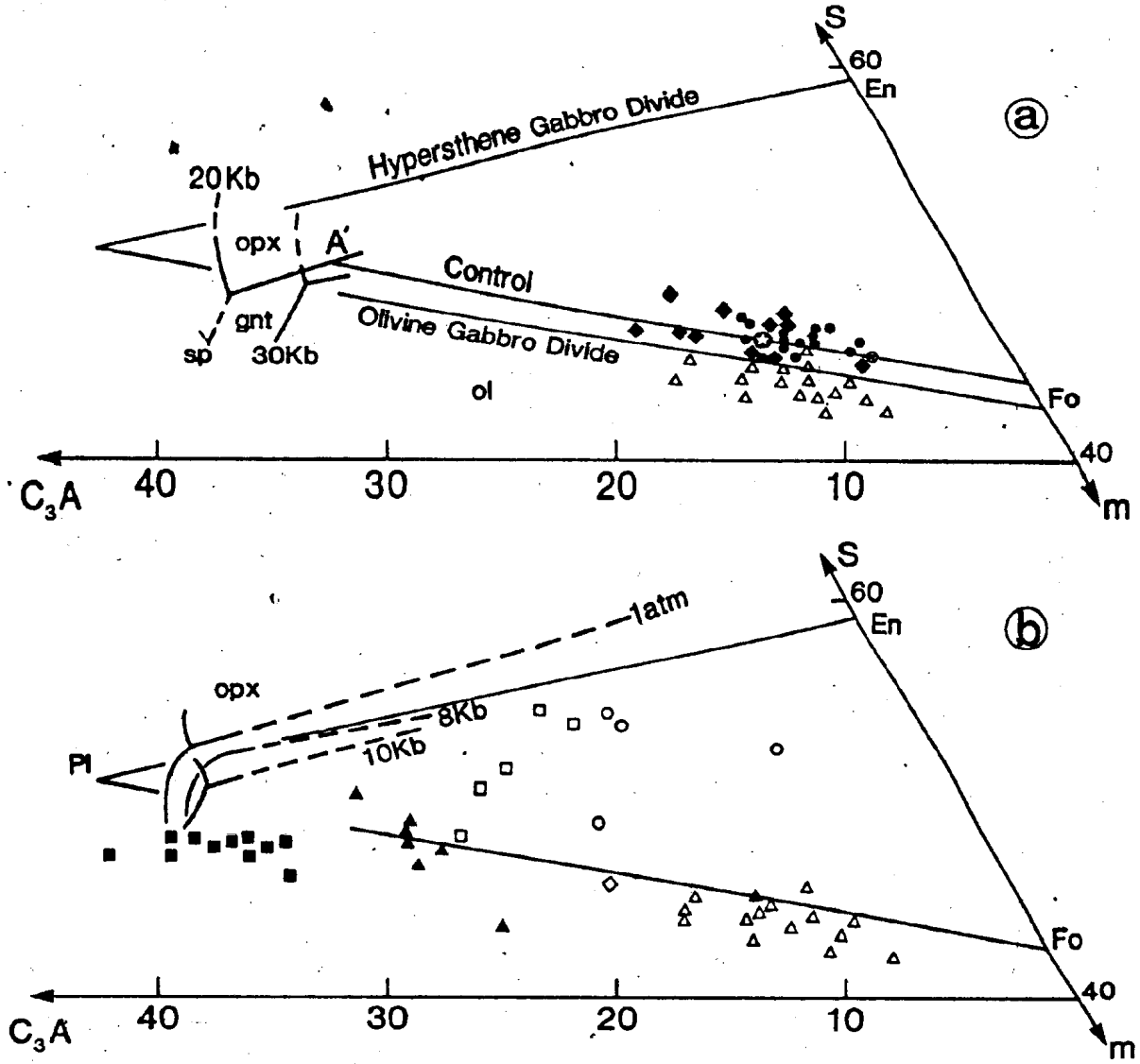
S
60
En
Hypersthene Gabbro Divide
20Kb
opx
A'
Control
gnt
sp
30Kb
Olivine Gabbro Divide
ol
Fo
40
C_3A
40
30
20
10
m
S
60
En
1atm
opx
8Kb
10Kb
Pl
Fo
40
C_3A
40
30
20
10
m

and refractory harzburgite samples to 2.00 weight percent and not all of the White Hills bulk rock chemical analyses, the control plane for each CMAS projection is shifted to higher values of M for projections that contain the M- and A-components. The reasons for the shift of the M- and A-components are that FeO is included in the M-component and Fe_2O_3 is included in the A-component for the CMAS projection calculations (O'Hara, 1968). Thus, the non-adjusted control plane is displaced toward the A-apex for the olivine projection; toward A_2S_3 for the enstatite projection; and toward C_3A for the diopside projection. The maximum error in the placement of the control plane resulting from Fe_2O_3 adjustment is 13 percent for the olivine and diopside projections, and 12 percent for the enstatite projection. Dunite, pyroxenite veins and gabbro bulk rock compositions plot away from the control plane and within a phase volume indicating mineral accumulation and possibly inefficient crystal fractionation (Jamieson, 1966; Malpas, 1976; Irvine, 1979).

Mineral crystallization orders for the proposed cumulate rocks are defined by the various projections based on the position of calculated first-stage partial melt liquid composition and the directions of change of the cotectics with pressure change. For gabbro the mineral sequence appears to be olivine, clinopyroxene, plagioclase; for clinopyroxenite - olivine, clinopyroxene; for wehrlite - olivine, clinopyroxene; for websterite - olivine, orthopyroxene, clinopyroxene; for orthopyroxenite - olivine, orthopyroxene; and for dunite - olivine.

b. Calculation of Percent Partial Melting

The percent of partial melting necessary to produce a melt of composition A' (Figures 5.3., 5.4., 5.5.) has been determined using an "extraction program", best suited for major element calculations, developed by R.G. Cawthorn (1975). The data input consist of (1) the Fe_2O_3-adjusted White Hills Peridotite average spinel lherzolite (Table 5.1.); (2) the Fe_2O_3-adjusted most refractory harzburgite bulk rock composition (Table 5.1.), and (3) melt extraction increments. The program subtracts the refractory harzburgite composition from the spinel lherzolite composition at the pre-defined extraction increments (percent extraction). The output is the resultant bulk rock liquid composition. For an acceptable solution, the resultant liquid composition is required to plot at A' in all CMAS projections and have an $Mg/(Mg+Fe^{2+})$ ratio in equilibrium with the refractory harzburgite (i.e., 0.68-0.69). Such a composition is obtained from 21 percent partial melting of the average spinel lherzolite composition (Table 5.1.). This liquid composition (21% normative olivine) is similar* to the calculated liquid compositions reported by Malpas (1976) for the Bay of Islands Complex and Reid and Woods (1977) for ultramafic xenoliths from Salt Lake Crater, Hawaii. A similar

* The Al_2O_3 and Na_2O contents of the resultant liquid are very low as compared to other calculated and natural primitive liquid compositions. The low Al_2O_3 content may be attributable to the calculation procedure for the "extraction program" because the composition of the starting materials for this study are similar to those used by Malpas (1976) (Table XXVI, p. 350). The low sodium content of the resultant liquid may represent a Na_2O depleted source material.

primary liquid composition has been reported by Clarke (1970) for Group II basalts from Baffin Island (Table 5.2.).

Recent partial melting experiments at 20 kilobars pressure on a natural garnet lherzolite sample (1611) (Mysen and Kushiro, 1977) and a natural spinel lherzolite sample (66PAL-3) (Scarfe et al., 1979) indicate that, at 21 percent partial melting, a harzburgite residue containing a small quantity of clinopyroxene is produced (Figure 5.6.). A clinopyroxene-free harzburgite residue (highly refractory) is produced only after at least 25 percent partial melting of these samples (Mysen and Kushiro, 1977; Scarfe et al., 1979); although at 35 kilobars, clinopyroxene coexists with olivine and orthopyroxene up to 40 percent partial melting in sample 66PAL-3 (Scarfe et al., 1979) and at 10 kilobars (anhydrous), clinopyroxene is consumed after 19 percent partial melting of the Tinaquillo lherzolite (Jaques and Green, 1980).

The field data and petrogenetic modelling for the White Hills Peridotite rocks support the experimental work of Mysen and Kushiro (1977) and Scarfe et al (1979),

Table 5.2. Calculated liquid and natural primitive liquid compositions.

	1	2	3
SiO_2	45.90	47.04	46.10
TiO_2	0.65	0.24	0.78
Al_2O_3	11.05	12.13	11.04
Cr_2O_3	0.42	0.66	0.28
Fe_2O_3	4.21	9.79*	2.45
FeO	6.72	--	8.28
MnO	0.07	0.08	0.18
MgO	19.11	17.52	20.13
CaO	10.42	11.20	9.40
Na_2O	0.49	1.34	1.06
K_2O	0.51	n.d.	0.08
P_2O_5	0.13	n.d.	0.09
NiO	0.31	n.d.	0.12
$Mg/(Mg+Fe^{2+})$	.740	(.642)	.709

1 - calculated liquid composition after 25 percent partial melting of average Bay of Islands spinel lherzolite (Malpas, 1976).

2 - calculated liquid composition after 24 percent partial melting of spinel lherzolite inclusion from Salt Lake Crater, Hawaii (Reid and Woods, 1977).

3 - Group II olivine basalt, Baffin Island (Clarke, 1970).

* - Total iron

n.d. - not determined

Figure 5.6. Melting curve of sample 1611 and $Fo_{55}En_{30}Di_{15}$ at 20 kb (anhydrous) (from Mysen and Kushiro, 1977).

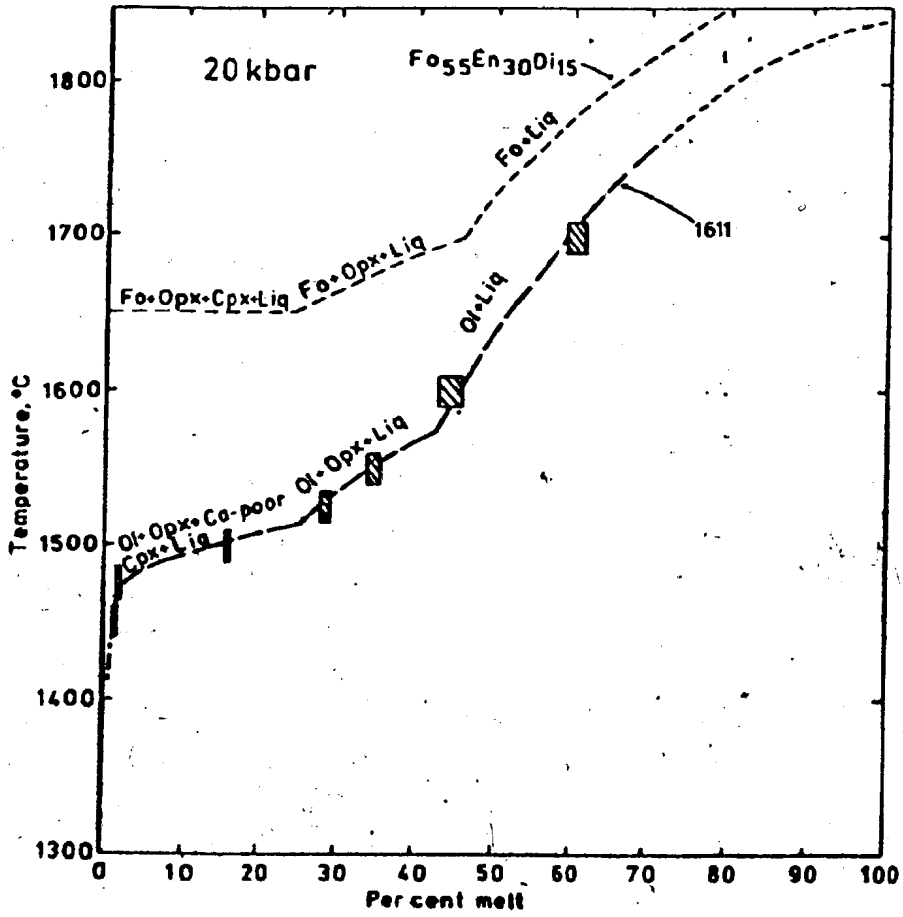
20 kbar
$Fo_{55}En_{30}Di_{15}$
Fo+Liq
Fo+Opx+Liq
Fo+Opx+Cpx+Liq
Ol+Liq
1611
Ol+Opx+Liq
Ol+Opx+Ca-poor Cpx+Liq
Temperature, °C
1800
1700
1600
1500
1400
1300
0
10
20
30
40
50
60
70
80
90
100
Per cent melt

II.5.B. Origin of the Pyroxenite Veins* and Other Cumulate Rocks

1. General Statement

During the past few decades and more recently within the past five years studies to define the origin of the various types of pyroxenite veins and cumulate rocks (i.e., dunite and gabbro) occurring in upper mantle spinel lherzolite (dominantly) xenoliths, ophiolites and Alpine-type peridotites have been the interest of many investigators (Dickey, 1970; Wilkinson, 1975; Wilshire and Pike, 1975; Wilshire and Shervais, 1975; Loubet et al., 1976; Malpas, 1976; Smith and Levy, 1976; Dick, 1977; Dickey et al., 1977; Frey and Prinz, 1978; Boudier and Coleman, in press; and others). In these occurrences, the pyroxenite vein assemblages (i.e., websterite, orthopyroxenite, clinopyroxenite; ± olivine, spinel, garnet) and cross-cutting relationships are similar, whereas the proposed origins for the veins and cumulate rocks are varied. The proposed modes of origin for these rocks range from the streaming of silica saturated and undersaturated vapors through the peridotite (Bowen and Tuttle, 1949) to episodic polybaric partial melting of a spinel or garnet lherzolite source material and polybaric fractional crystallization of these same partial melt liquids (e.g., Wilshire and Pike, 1975; Loubet et al., 1976; Malpas, 1976; Boudier and Coleman, in press).

* The term "bands" and "dikes" have been used by some authors. Layer is not preferred because it implies cumulate processes as applied to cumulate layer formation in stratiform-type intrusions. However, the use of the term layer is retained where found in referenced publications.

The general lack of complete mineralogical, chemical, structural, and field data for a suite of pyroxenite vein rocks from any one of these upper mantle occurrences is probably responsible for the variety of proposed origins. Other factors which have had and continue to have a pronounced affect on the proposed modes of origin for these rocks are subsolidus mineral equilibration, and the destruction of primary crystallization textures and mineralogy due to deformation. These factors have increased the difficulty of defining the parent liquid composition required for theoretical geochemical modelling. In addition, many investigators have neglected the widespread occurrence of dunite bodies (discordant to and concordant with the major structural trend) and gabbro veins (± olivine, spinel) in an aid to understand the origin(s) of these veins.

Under the subsequent headings of this section, hypotheses of origins for pyroxenite, gabbro, and dunite veins and bodies of ophiolites, Alpine-type peridotites and ultramafic xenoliths are reviewed. In light of this review and the available geological data for the White Hills Peridotite rocks, a discussion of the possible origins of the pyroxenite, gabbro and dunite veins and bodies of the White Hills Peridotite is presented.

2. Review of Origins for Pyroxenite, Gabbro and Dunite Veins and Bodies

a. Ophiolites and Alpine-type Peridotites

Bowen and Tuttle (1949) suggest that crosscutting dunite and pyroxenite veins in peridotite may have been formed by

the streaming of silica undersaturated and silica saturated hydrous vapors, respectively, through the peridotite along zones of weakness (e.g., cracks, faults). Silica saturated vapor streaming through olivine-rich rock (dunite) results in the replacement of olivine by enstatite to produce enstatolite veins, whereas silica undersaturated vapor streaming through the peridotite results in the replacement of enstatite by olivine.

The difficulties arising with such a mechanism are firstly, fully defining the origin of hydrous vapors in the quantity envisaged for vein formation when peridotites are regarded as being nearly volatile-free ($\leq$ 0.1 wt. % total volatiles; Wyllie, 1971); secondly, CaO is present in the orthopyroxene in addition to a minor amount of clinopyroxene as a modal phase. Although calcium is obviously required for this conversion, Malpas (1976) suggests the transport of calcium by a vapor phase is unlikely.

Unlike the Bowen and Tuttle (1949) model, Raleigh (1965) advocates a magmatic origin for pyroxenite vein formation by the filter-pressing of late stage liquids into the solidified intrusion. Although this mechanism for pyroxenite vein formation is similar to the hypotheses advocated in recent publications (e.g., Wilshire and Pike, 1975; Malpas, 1976; Frey and Prinz, 1978; Boudier and Coleman, in press) the process by which the liquid is generated and its composition are debatable. The Raleigh hypothesis assumes (1) that the peridotite is the result of crystal accumulation processes; and (2) the evolved liquid crystallized to form the pyroxenite

veins. For ophiolites, the upper mantle tectonite peridotite (harzburgite) has been shown to be a residue from the partial melting of upper mantle spinel or garnet lherzolite (e.g., O'Hara, 1968; Mysen and Kushiro, 1977). Secondly, the composition of the evolved liquid remaining after the formation of the cumulus peridotite will probably have an $Mg/(Mg+Fe^{2+})$ ratio that is unable to crystallize pyroxenite veins with bulk rock $Mg/(Mg+Fe^{2+})$ ratios of 0.793 to 0.870 ($Mg/(Mg+Fe^{2+})$ ratio for the pyroxenite veins of the White Hills Peridotite).

In the Ronda Peridotite, Spain, two types of layers are recognized: tectonic mafic layers and magmatic layers (Dickey, 1970). Dickey (1970) suggests that the tectonic mafic layers may have formed during deformation of the peridotite by mineralogical segregation of olivine from orthopyroxene, clinopyroxene, and spinel, whereas the magmatic layers represent the actual partial melt liquid composition (i.e., frozen liquid equivalent) from the partial melting of the peridotite. Also, Dickey (1970) suggests that the websterite layers of the Ronda Peridotite may have been magmatic in origin and probably crystallized at pressures less than 10 kilobars (on the basis of the Al_2O_3 content of the pyroxenes). Some objection to the mode of formation of the mafic layers on the basis of high pressure-temperature experiments on mafic layer R127 (plagioclase-garnet clinopyroxenite) has been discussed by Obata and Dickey (1976). In a subsequent paper, Dickey et al (1977) argue that a simple partial melting event involving the peridotite cannot adequately explain mafic layer formation;

rather a more plausible origin by multistage partial melting that may involve the repeated partial melting of the source peridotite and/or the resulting crystal cumulates is likely (cf., Dickey et al., 1977, Fig. 5, p. 86).

Pyroxenite dikes located near the top of the lherzolitic unit of the Pindos Ophiolite are thought to represent crystal cumulates derived from the final partial melt liquid of the peridotite (Montigny et al., 1973). According to Montigny et al (1973) this (these) liquid may have been derived from a second- or third-stage partial melting event. They support their suggestion by citing the very low Ti (∿ 200 ppm) and V (∿ 40 ppm) concentrations for the pyroxenite veins (orthopyroxenite, sample All). Menzies and Allen (1974) have suggested a similar origin for orthopyroxenite veins of the Othris and Troodos Ophiolites.

Similarly, Dick (1977) and Dick and Sinton (1979) suggest that the dunite bodies and orthopyroxenite veins of the Josephine Peridotite have formed in situ possibly during or immediately after the partial melting of the source material, whereas olivine websterite layers may have formed by metamorphic differentiation (i.e., mineral segregation) during the partial melting of the peridotite where diopside persisted locally during partial melting.

Loubet et al (1976) suggest that the pyroxenite layers of Alpine-type peridotites may represent crystal cumulates or residue derived from an undepleted peridotite during at least two stages of partial melting. During the first partial melting of the undepleted peridotite, pyroxenite layers form

by crystal accumulation processes from the primitive liquid. Subsequent partial melting of the peridotite affects only the pyroxenite layers probably because the solidus temperature for the layers is lower than for the peridotite (i.e., the pyroxenite layers have lower bulk rock $Mg/(Mg+Fe^{2+})$ ratios and a higher quantity of alkali metals). According to Loubet et al (1976), the partial melting of the pyroxenite layers results in a variety of chondrite normalized REE patterns and isotopic ratios.

The objections arising from their hypothesis are: (1) the uncertainty as to whether the pyroxenite layers represent crystal cumulates or a partial melt residue; and (2) if the layers are cumulates and have the same modal mineralogy, then unless the second partial melting event is non-uniform, only two chondrite normalized REE patterns should have been found for these layers.

Boudier and Coleman (in press) advocate multistage partial melting of an undepleted peridotite to explain the formation of discordant and deformed dunite bodies, and deformed and undeformed websterite and gabbro veins in the Semail Ophiolite. The discordant and deformed dunite may have been the product of olivine accumulation, beneath the accreting ridge, from the primitive picritic tholeiite magma (first-stage partial melt) or the residue after second-stage partial melting, whereas undeformed and deformed websterite veins and undeformed gabbro veins are produced from the crystallization and accumulation of clinopyroxene, plagioclase and olivine from a second

generation, off-axis, olivine-poor tholeiite magma as it passes through the peridotite. This second-stage melt is the product of the advanced partial melting of a slightly depleted lherzolite which is the residue after the first-stage partial melting of the undepleted lherzolite. Boudier and Coleman (in press) emphasize that the veins and dunite bodies which have bulk rock $Mg/(Mg+Fe^{2+})$ ratios of 0.820 to 0.930 do not represent the frozen liquid equivalents of the derived liquids. They support their point by showing that a liquid with an $Mg/(Mg+Fe^{2+})$ ratio of approximately 0.70 must, if the liquid crystallizes completely without loss of any material, crystallize with an $Mg/(Mg+Fe^{2+})$ ratio of 0.70 (Roeder and Emslie, 1970). Therefore, the veins and dunite bodies must preserve mineral accumulation processes or be a residue from a partial melting event.

According to Boudier and Nicolas (1977) the gabbro (indigenous and intrusive) and the dunite veins of the Lanzo Peridotite form in the following way. An extraneous magma (~ 5% liquid), probably derived from the partial melting of the host peridotite, is injected into the peridotite. Because the extraneous liquid is overheated (higher temperature) relative to the 'solid' peridotite, extensive localized partial melting of the peridotite occurs (~ 30%) leaving a dunitic residue. If the composite melt is to crystallize in situ an indigenous gabbro vein with a dunite selvage would form, but if the composite melt is removed from the site of formation, possibly by forceful injection into undepleted lherzolite, then, an intrusive gabbro vein would form, leaving a dunite

'vein' at the site of the peridotite partial melting. The gabbro veins for both situations are compositionally similar.

Unlike the multistage liquid evolution models suggested in the previous accounts, Malpas (1976, 1978) has adopted a polybaric crystallization mechanism that requires only a single stage partial melting event. In his approach all vein material, i.e., dunite, orthopyroxenite, websterite, clinopyroxenite, and gabbro, may form by cotectic and non-cotectic crystallization. The beauty of this mechanism, other than that only a single liquid is required, which may or may not be subsequently modified by other partial melting events, is that it explains the evolving chemical change of the liquid (i.e., change in $Mg/(Mg+Fe^{2+})$ ratio, etc.) (cf., Irvine, 1970 and many others), even though Malpas (1976) did not have much chemical data for the different vein types to show this evolution. Likewise, Herzberg (1979) has utilized a polybaric evolution model to explain the origin of garnet websterites from the Freychinede Lherzolite in the French Pyrenees. For his model, non-cotectic crystal fractionation from a picritic liquid of aluminous orthopyroxene + olivine (high ratio of modal orthopyroxene: olivine, due to the protracted olivine phase volume at high pressures) at high pressures (arbitrarily chosen between 50 and 40 kilobars by Herzberg) results in the formation of orthopyroxenite layers. Upon decreasing pressure, at approximately 40 kilobars, the clinopyroxene phase volume is intersected by the liquid composition, causing aluminous, subcalcic clinopyroxene fractionation, thereby decreasing the amount of modal orthopyroxene and olivine that is crystal-

lizing from the picritic liquid. Crystallization of these three phases between 40 kilobars and 35 kilobars results in the formation of websterite layers. Again, Herzberg does not totally support his model with chemical data.

Dungan and Ave'Lallement (1977, p. 109-110) review hypotheses for the origin of the dunite in Alpine-type peridotite and ophiolite complexes. The four origins are: (1) metasomatic; (2) metamorphic or tectonic differentiation; (3) crystal cumulates from primary magmas; and (4) partial melt residue. These hypotheses are identical to the hypotheses presented above for the origin of the pyroxenite veins.

b. Ultramafic Xenoliths

The pyroxenite, gabbro and dunite veins and bodies in ultramafic xenoliths in basalt show similar chronological relationships and geochemistry (bulk rock,mineral) to those described from ophiolites (cf., Wilshire and Pike, 1975). Although the ultramafic xenoliths are only small fragments of upper mantle material, these lithologies and various lithologic assemblages have received more detailed inspection than those from intact peridotite occurrences (e.g., White, 1966; Frey and Green, 1974; Wilshire and Pike, 1975; Wilshire and Shervais, 1975; Frey and Prinz, 1978). The reasons for this are not known. Interestingly, similar arguments to the ones presented for ophiolites and Alpine-type peridotites have been used to explain the formation of these vein lithologies in ultramafic xenoliths (cf., Frey and Prinz, 1978 vs. Dickey et al., 1977; Wilshire and Pike, 1975 vs. Malpas,

1976). Briefly, Frey and Prinz (1978) suggest Group I orthopyroxenite xenoliths from San Carlos, Arizona, may be fragments of tectonic layers formed in lherzolite or may represent early cumulates (now metamorphosed) that crystallized from the partial melt liquid in equilibrium with component A (partial melt residue of Frey and Prinz, 1978), whereas Group I clinopyroxenite xenoliths may represent early cumulates from a magma or the frozen magma composition.

Wilshire and Pike (1975) envisage ongoing partial melting of peridotitic material over a range of P-T conditions during diapiric rise of upper mantle material. The crystallization of these derived liquids occurs during all stages of diapir ascent with cumulus phase mineralogy controlled by mineral stability limits. The veins, therefore, would evolve sequentially from the liquids, e.g., dunite, pyroxenite, gabbro.

3. Hypothesis of Origin of Pyroxenite, Gabbro and Dunite Veins and Bodies in the White Hills Peridotite

a. General Statement

A proposed model of origin that requires two periods of crystallization from distinct liquids and a deformation related variation defined on the basis of the existing field relationships and geochemical data (i.e., mineral, major, trace, REE) is probable for the origin of pyroxenite, gabbro and dunite veins and bodies of the White Hills Peridotite. The proposed model and variation are outlined in Table 5.3.

The hypothesis envisages an upper mantle diapir of spinel lherzolite bulk composition which rises convectively directly

Table 5.3. Proposed model for the origin of the pyroxenite, gabbro and dunite veins and bodies of the White Hills Peridotite. See text for specific details.

1. Polybaric crystallization, cotectic and non-cotectic, of an olivine tholeiitic liquid (first-stage), at moderate pressures (< 18 to 20 kb), derived from the partial melting of the spinel lherzolite source material yields the lithologies:

   dunite
   high-alumina orthopyroxenite
   high-alumina websterite
   wehrlite
   clinopyroxenite
   gabbro

2. Renewed, localized partial melting of the nearly depleted spinel lherzolite source material at low pressures (< 8 kb) produces a liquid of magnesian-quartz tholeiite composition which crystallizes to yield the lithologies:

   chromitite
   orthopyroxenite
   "websterite"

3. Variation - alternative mechanism to form the high-alumina orthopyroxenite, high-alumina websterite and dunite by mechanical mineral segregation due to deformation is probable.

beneath or slightly away from an active spreading ridge. Partial melting of the spinel lherzolite source material is initiated at approximately 60 kilometers (~ 20 kb) depth, approximate depth where the anhydrous spinel lherzolite solidus is intersected (Forsyth, 1977; Jaques and Green, 1980). The liquid or liquids formed during partial melting (due to decompression, Yoder, 1976) are the parent liquids to the pyroxenite, gabbro and dunite material.

The formation of dunite, high-alumina orthopyroxenite, high-alumina websterite*, wehrlite, clinopyroxenite, and gabbro can be explained by well-established crystal fractionation processes, such as those applied to the formation of cumulate layers of layered intrusions (cf., Irvine, 1970; Jackson, 1970) and although these crystal fractionation processes in layered intrusions occur at low pressures (< 8 kb), preserve a particular geochemical signature (e.g., decreasing Mg/Fe ratio; increasing TiO_2, etc.), and mineralogical evolution (mafic to felsic), similar petrogenetic crystallization processes at moderate pressures can be developed (O'Hara, 1968; Malpas, 1976, 1978; and many others).

The petrogenetic model for this study envisages, initially, high pressure (≤ 18-20 kb) crystal fractionation of an olivine tholeiitic magma (such as primary melt composition A', Table 5.1.), and subsequent polybaric crystal fractionation at successively lower pressures to derive most of the vein/body

* The prefix high-alumina is used in this section only to distinguish this websterite from the chromite-related "websterite".

lithologies of the White Hills Peridotite.

The polybaric crystallization of an olivine tholeiitic liquid cannot fully explain the formation of all vein/body lithologies, but all of the lithologies can be accounted for if this process is complemented by the crystallization of a second liquid (~ magnesian-quartz tholeiite) and possibly, high pressure mineral segregation.

b. Proposed Model for the Origin of the Pyroxenite, Gabbro and Dunite Veins and Bodies of the White Hills Peridotite

(i) systematics of the model

An enlargement of Figure 5.3., (Figure 5.7.), olivine projection in the synthetic system CMAS, is used to illustrate the proposed crystallization model. Reference primary melt composition A' ($Mg/(Mg+Fe^{2+}$) ratio 0.68-0.69, 21% normative olivine) is selected as the starting liquid composition. The positions of the cotectics at the various pressures are taken from O'Hara (1968) and Malpas (1976) and have been slightly modified to include the experimental data of Presnall et al (1978). It should be emphasized that in this diagram (Figure 5.7.) from a pressure of approximately 12 kilobars (anhydrous) (Presnall et al., 1978) up to 20 kilobars (anhydrous), the highest pressure used in these diagrams, an initially tholeiitic liquid (e.g., primary melt composition A') eventually would become alkaline as it crosses the low pressure thermal divide and would remain alkaline if the liquid crystallizes to the eutectic at high pressures (> 12 kb) or if erupted directly to the surface from such pressures.

Figure 5.7. Enlargement of the olivine projection (CS-MS-A) to illustrate the proposed polybaric crystallization path for the origin of the pyroxenite, gabbro and dunite veins/bodies. See text for explanation.

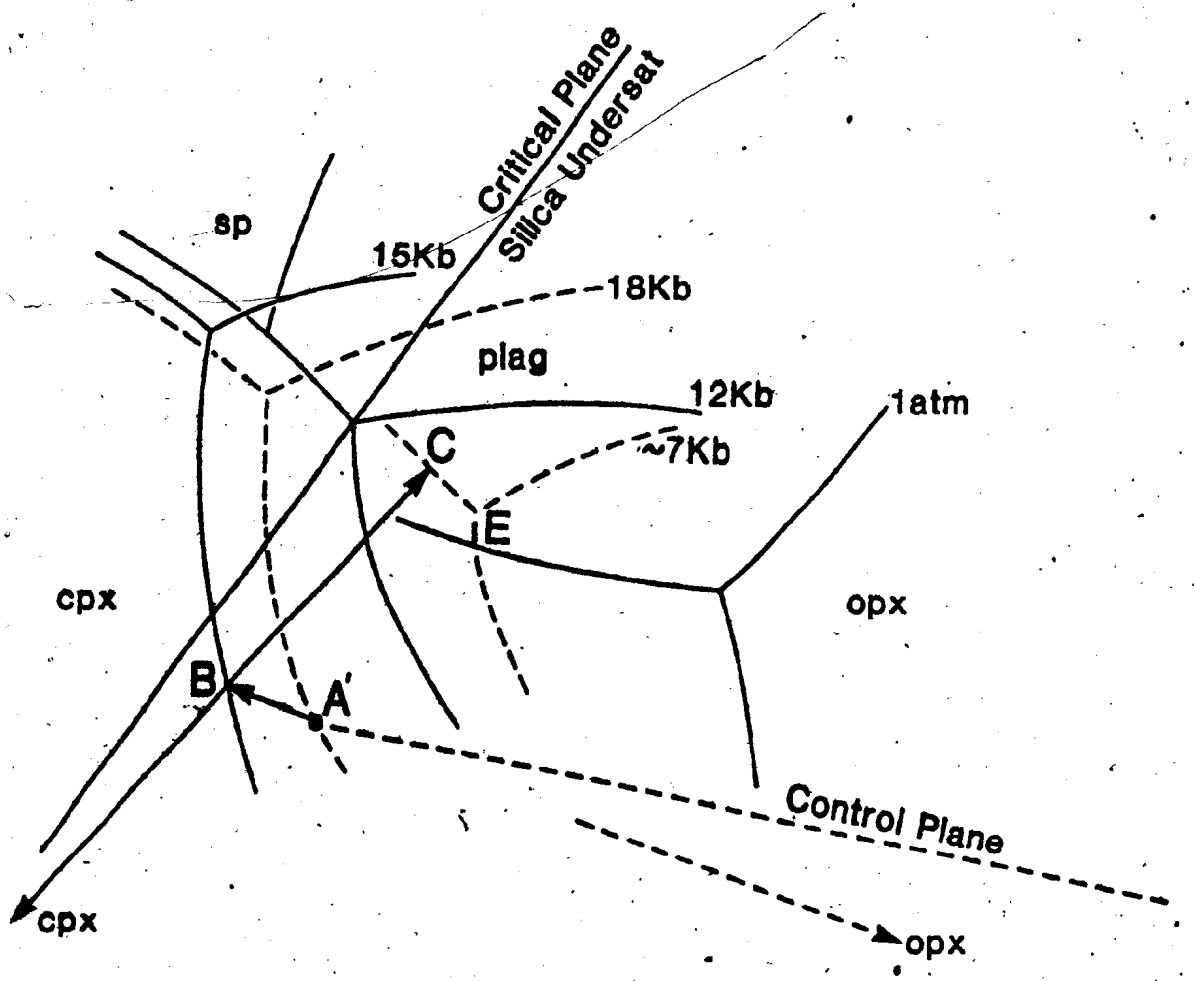
Critical Plane
Silica Undersat
sp
15Kb
18Kb
plag
12Kb
1atm
C
~7Kb
E
cpx
opx
B
A
Control Plane
cpx
opx

At pressures less than approximately 12 kilobars (anhydrous) an initially tholeiitic melt would remain tholeiitic if crystallization proceeds with decreasing pressure.

The convective rise of the spinel lherzolite source material to pressure regions of less than 20 kilobars causes the crystallization of liquids produced at greater depths (Malpas, 1978). Thus, the ascending diapir may consist of a solid/liquid mixture. The percentage of a modal phase (e.g., olivine, orthopyroxene, etc.) that crystallizes from the partial melt liquid of the diapir is related to the rate of pressure reduction. For instance, if the pressure reduction occurs slowly, then the rate of crystallization can maintain a liquid path along a cotectic. Accordingly, two to four mineral phases may crystallize together. However, if pressure reduction occurs rapidly, such that the instantaneous liquid composition (not bulk composition which remains as a fixed point; Morse, 1976) is unable to remain on a cotectic, non-cotectic crystallization takes place allowing only one or two mineral phases to crystallize until a cotectic is intersected. If cotectic intersection is not accomplished, because the change in pressure is more rapid than mineral crystallization, then monomineralic or two-phase cumulate layers are produced.

(ii) proposed model

Assuming primary melt composition A' lies within the olivine phase volume* at the start of mineral crystallization,

* This may not have been the initial starting location for mineral fractional crystallization for the pyroxenite, gabbro and dunite veins/bodies because the olivine composi-

upon crystallization, which is non-cotectic, olivine is the only phase (± spinel) to crystallize from bulk composition A'. If a pressure reduction due to the upwelling of the diapir occurs at a slow rate, then olivine may be joined by orthopyroxene if the olivine-orthopyroxene cotectic is intersected (Figure 5.7., point A'). The coprecipitation of olivine + orthopyroxene occurs to approximately 15 kilobars (path A' → B, Figure 5.7.), where by the repositioning of the cotectic due to the pressure decrease leaves the liquid composition in the olivine + clinopyroxene phase volume (point B). At point B, orthopyroxene is no longer a model phase and cotectic crystallization proceeds with the crystallization of olivine + clinopyroxene (path B → C). At point C, the two phase cumulate is joined by plagioclase as a modal phase. The continued cotectic crystallization of olivine + clinopyroxene + plagioclase may occur along path C → E, but the eutectic composition E is

---

tions, (olivine is thought to be a cumulus phase) are similar, ~Fo_{90}. The similarity of the olivine compositions may have been the result of a change in the $Mg/(Mg+Fe^{2+})$ ratio of olivine during deformation, or, indeed, may represent the initial cumulus olivine composition. If the latter situation is correct, then it may be necessary to adopt a petrogenetic model that involves several periods of fractional crystallization (episodic?) from a single liquid or several liquids. An alternative to this model, and the one preferred here, involves an initial period of olivine crystallization followed by orthopyroxene, clinopyroxene, plagioclase. This crystallization sequence is consistent with theoretically and experimentally predicted models (e.g., Irvine, 1970; 1979; Jackson, 1970; Morse, 1973). Although an estimate cannot be made for the amount of rock material these veins and bodies represent in the peridotite nor what fraction of the total liquid volume these veins represent, a qualitative estimate for the amount of crystallization required for a change in olivine Fo content from 91-77, dunite to gabbro range, neglecting the affect of coexisting minerals, can be made. This value is approximately 22 percent (cf., Irvine, 1979, p. 256, Fig. 9.2A.).

never reached (no cumulus orthopyroxene in gabbro). At any point during mineral crystallization the residual liquid composition is tholeiitic, although during crystallization along path C → E, the liquid composition tracks close to the low pressure thermal divide.

If this polybaric, high pressure fractionation sequence does occur during the ascent of the diapir, then the crystallization of various proportions of the modal phases olivine, orthopyroxene, clinopyroxene, plagioclase can account for the various pyroxenite, gabbro and dunite veins and bodies for example:

non-cotectic crystallization of olivine	- dunite
cotectic crystallization: olivine + orthopyroxene	- orthopyroxenite (high-alumina)
olivine + clinopyroxene + minor orthopyroxene	- websterite (high-alumina)
olivine + clinopyroxene	- wehrlite, clinopyroxenite
olivine + clinopyroxene + plagioclase	- gabbro

A similar mineral crystallization order and rock sequence have been reported by Irvine (1979, p. 272, Table 9-3, Class III) for the layered series of the Muskox Intrusion.

Of course, variations in the crystallization order and modal amount of these phases are possible depending upon the rate of pressure reduction. No estimate has been made for the rate of pressure reduction nor for the amount of each vein assemblage for the White Hills Peridotite. It is suggested, solely on the basis of the apparently ordered crystallization

sequence for the lithologies of the model, and with no evidence of one lithology predominanting over the others, that no drastic pressure reduction or pressure fluctuations have occurred during the convective upwelling of the White Hills Peridotite source material.

(iii) discussion of the single liquid, polybaric crystallization model

Although the proposed polybaric crystallization mechanism is simplistic and difficult to prove on the basis of modal mineralogy and modal mineral proportions for an individual vein lithology or suite, most of the geochemical data (although some inconsistencies do exist) and field relationships for the White Hills Peridotite (Chapters 2 and 3) support the fundamental model. Integrating this model with the models proposed by other workers may aid in not only understanding the origin of these vein assemblages but, also, the kinematics of ascending liquids and mineralogical differentiation beneath or slightly away from an accreting ridge and, in a less direct way, the variability of primary spinel compositions from ophiolitic rocks.

Geochemically if a primary melt of olivine tholeiitic composition, such as liquid A', is the starting bulk composition for the crystallization model, then a liquid with this $Mg/(Mg+Fe^{2+})$ ratio, ~ 0.685 (21% normative olivine), must initially crystallize olivine of composition Fo_{90-91}, under equilibrium conditions (Roeder and Emslie, 1970). This is the composition of the olivine from the dunite bodies. Succeeding olivines should have lower forsterite contents than the initial

Fo_{90-91} due to the decrease in the bulk liquid $Mg/(Mg+Fe^{2+})$ ratio. The two next lithologies predicted by the model are orthopyroxenite and websterite (high-alumina type for this study). These lithologies have average bulk rock $Mg/(Mg+Fe^{2+})$ ratios[1] of 0.853 (0.836-0.871, range) for high-alumina orthopyroxenite and 0.848 (0.801-0.896, range) for the high-alumina websterite. There is a slight discrepency with the bulk rock $Mg/(Mg+Fe^{2+})$ ratios for the high-alumina orthopyroxenite and high-alumina websterite and wehrlite, the fourth rock type of proposed crystallization model. The $Mg/(Mg+Fe^{2+})$ ratio for wehrlite is 0.872; clearly greater than for the second and third lithologies of the model. Whether this reversal is real or a result of sampling bias, since only one wehrlite sample has been collected, is not known. Riccio (1976) reports that a spinel-bearing wehrlite dike (HB-72-46) from the White Hills Peridotite has an $Mg/(Mg+Fe^{2+})$ ratio of 0.821 (Riccio, 1976, Appendix II, p. 215, analysis 9), therefore providing limited support for sample bias. Clinopyroxenite and gabbro veins with $Mg/(Mg+Fe^{2+})$ ratios of 0.814 (0.792-0.845, range) and 0.793 (0.729-0.839[2], range), complete the crystallization model.

1 There is a slight inconsistency between the $Mg/(Mg+Fe^{2+})$ ratios (wt.%) for the bulk rock and silicate phases which may be due to recrystallization of olivine during deformation, low modal abundance of olivine, olivine as an intercumulus phase (which it often is in the orthopyroxenite), difficulty with determining Fe^{2+}-Fe^{3+} during reduction of the microprobe data or the gravimetric determination of FeO for bulk rock analyses.

2 The $Mg/(Mg+Fe^{2+})$ ratio for gabbro sample 78156 is 0.893. However, the oxide total is low and may be caused by a low total iron concentration. No mineral data are available to use an as internal check. Therefore, this sample has not been used to develop the model.

In addition to applying the variation in $Mg/(Mg+Fe^{2+})$ ratio to develop the model, the variation of TiO_2 in clinopyroxene, increasing from high-alumina orthopyroxenite to gabbro (~ 0.15 to ~ 1.25 wt.%), and the constancy of Al_2O_3 in clinopyroxene (~ 6.4 wt.%) and orthopyroxene (~ 4.5 wt.%) for all vein lithologies, have been used to support this model. The implications of these data have been discussed in Chapter 3.

(iv) comparisons and interpretations of the model

Olivine compositions in dunite within a host rock of tectonite peridotite from the Oman Ophiolite (Boudier and Coleman, in press; Gass et al., ms) are similar to those for the dunite from the White Hills. As discussed in section 2.a. of this chapter, Boudier and Coleman (in press) recognize at least two types of dunite. One type (dunite body) is discordant to the predominant structural trend and is hypothesized to represent an olivine (± spinel) cumulate that crystallized from a primary olivine tholeiitic liquid ($Mg/(Mg+Fe^{2+})$ = 0.64-0.71) as the liquid passed through the depleted peridotite. The second type of dunite body, recognized as in situ in origin, is formed as a partial melt residue of high temperature second-stage partial melting of the peridotite. Although the mechanism for the formation of the in situ dunite is theoretically possible, the results of partial melting experiments of complex natural and synthetic spinel and garnet peridotites indicate that for a dunite residue to be produced from these source materials, partial melting must advance to 40 percent or greater, depending upon bulk composition, fluid content and pressure (cf., O'Hara, 1968; Mysen and Kushiro,

1977; Scarfe et al., 1979; Jaques and Green, 1980).

Gass et al (ms) suggest a nearly identical origin to Boudier and Coleman (in press) for the generation of dunite bodies of the Oman and Troodos ophiolites. Their interpretation of origin differs from that of Boudier and Coleman (in press) only in that the primary tholeiitic melt may have remained passive and crystallized in situ, in addition to crystallization as the liquid rose through the peridotite.

An interesting point intimated by Gass et al (ms) that comments on the final location of associated massive chromitite associated with these dunite bodies is that if the initial partial melt and peridotite diapir ascend at approximately the same rate then, the melt and crystallized dunite component rise en masse (i.e., no separation) until at some level of the uppermost mantle/lower crust the melt is fed into overlying magma chambers. Thus the chromite-bearing dunite must occur near the base of the cumulate sequence. However, if the melt ascends at a rate that is greater than that for the peridotite diapir then, the melt (or a percentage of the melt?) would have to separate from the crystallized dunite. The consequences for the latter situation are: (1) the crystallized dunite is susceptible to all deformations that affect the peridotite; and (2) dunite + minor chromitite bodies would be scattered throughout the peridotite, not just near the base of the cumulate sequence. In addition, if the degree of partial melting of the spinel lherzolite source material is small ($< 20\%$?), then because the solid/liquid partition coefficient for chromium is greater than 1 (Kurat et al., 1980), the

melt should contain a low concentration of chromium. As a consequence, less chromium is available to enter the crystallizing chromite. This would result in a chromite with a higher (relative) Al/Cr ratio (the origin of the spinels are discussed in the next section of this chapter).

Dispersed and partly deformed dunite bodies and chromite with a high Al/Cr ratio occur in the White Hills Peridotite, substantiating a dissimilar rate of ascent for the partial melt liquid and peridotite diapir and in support of the White Hills Peridotite partial melting calculation.

The REE data for the gabbro veins have been presented in Chapter 3 where they are compared with REE data for gabbroic rocks from a variety of geological ages and settings. During the gabbro REE discussion it has been suggested that the White Hills gabbro chondrite normalized REE patterns may have been produced by crystal fractionation from the first-stage partial melt liquid of the spinel lherzolite source material. In Figure 5.8., the White Hills gabbro chondrite normalized REE patterns are compared to Group E (R181) and Group F (R120, R322) mafic layer chondrite normalized REE patterns of the Ronda Peridotite (Suen, 1978). The relative REE abundances and shapes (LREE<HREE) to the chondrite normalized REE curves are similar for the gabbros of these peridotites. Suen (1978) has suggested that Groups E and F mafic layers may have been produced by crystal accumulation from liquids derived by 15 to 20 percent partial melting of a mantle source (garnet peridotite) that has 2x chondrite absolute REE

Figure 5.8. Chondrite normalized rare earth element patterns of gabbro and clinopyroxenite veins from the White Hills Peridotite. Absolute REE abundances for these veins are compiled in Appendix I.

Key:

● clinopyroxenite vein 77WH70

cross hatched - range of mafic layers Group E (R181) and Group F (R120, R322) (Suen, 1978)

vertically ruled - range of gabbro veins, White Hills Peridotite (this study)

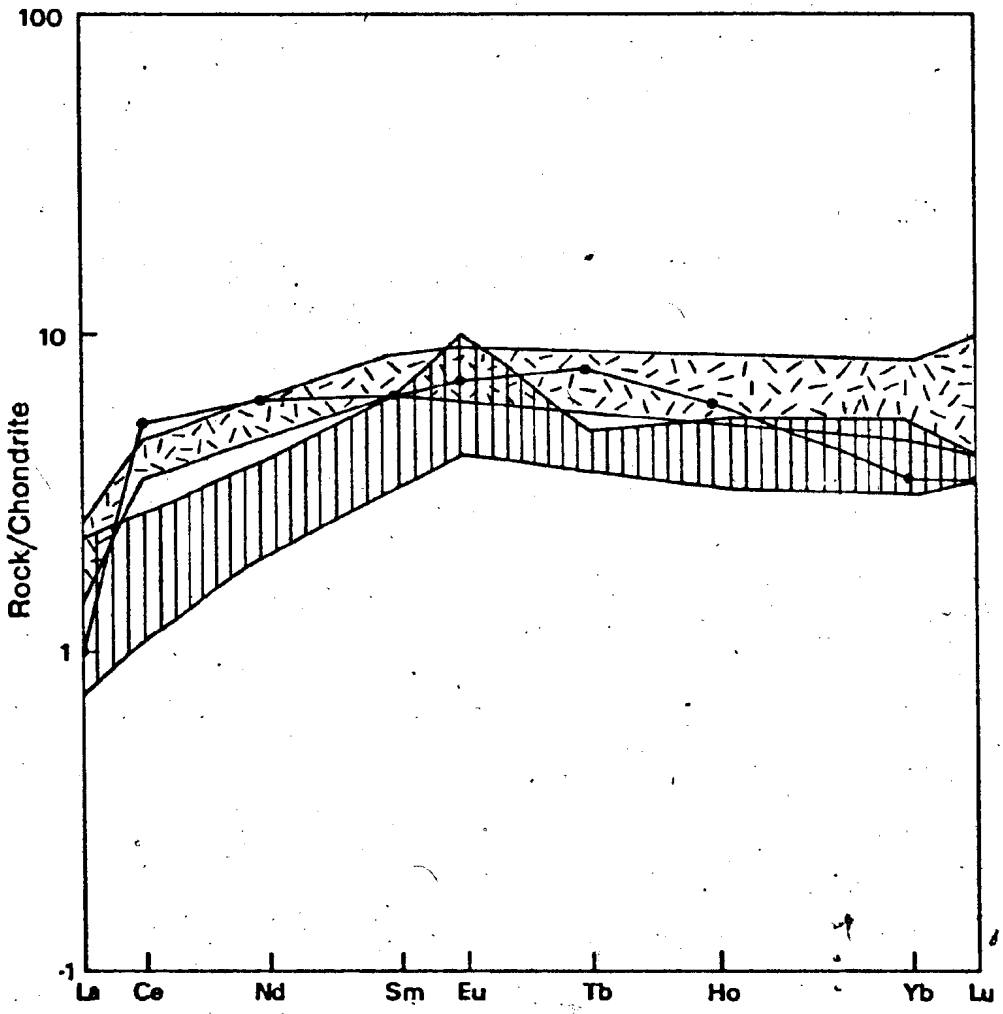
100
10
1
-1
Rock/Chondrite
La
Ce
Nd
Sm
Eu
Tb
Ho
Yb
Lu

abundances. Although the mafic layers have been metamorphosed (up to garnet lherzolite facies, Obata, 1977), the original REE patterns appear to have been retained (a similar argument has been used by Frey and Prinz, 1978, p. 155, to determine a possible origin of orthopyroxenite xenoliths from San Carlos, Arizona). The chondrite normalized REE pattern of a White Hills Peridotite clinopyroxenite vein (sample 77WH70) is also shown in Figure 5.8. It is used here only to show the close similarity to the White Hills gabbro REE patterns and, tentatively, on the basis of this comparison it appears likely that the White Hills clinopyroxenite and gabbros crystallized from the same parent liquid. Accordingly, the often close, though highly localized association of clinopyroxenite pods with gabbro veins (Figure 5.9.) supports a near contemporaneous crystallization for these two lithologies.

Whereas the White Hills Peridotite gabbro chondrite normalized REE patterns indicate fractionation from a liquid of olivine tholeiitic composition, Boudier and Coleman (in press) have suggested that the undeformed gabbro and websterite veins of the Semail Ophiolite crystallized at low pressures ($\sim$ 3 kb) from second-stage partial melt liquids. These liquids have been derived from advanced partial melting of the nearly depleted spinel lherzolite source material. They also indicate that the websterite and gabbro vein chondrite normalized REE patterns are U-shaped and are LREE enriched. If the nearly depleted spinel lherzolite source initially had chondritic

Figure 5.9. Schematic representation of a clinopyroxenite pod (oval shape) with anastamosing gabbro veins (heavy solid lines) apparently emanating from the pod. The long axis of the pod is believed oriented parallel to the orthopyroxene-defined foliation (horizontally dashed lines) of the host peridotite. Not to scale. Enlargement 1 - zoned gabbro vein (partially stippled pattern) oblique to foliation (dashed lines) of host harzburgite (see Plate 9.D.); 2 - olivine clinopyroxenite (ol cpxite) pod cut by gabbro vein, wavy solid lines represent fractures in the rock.

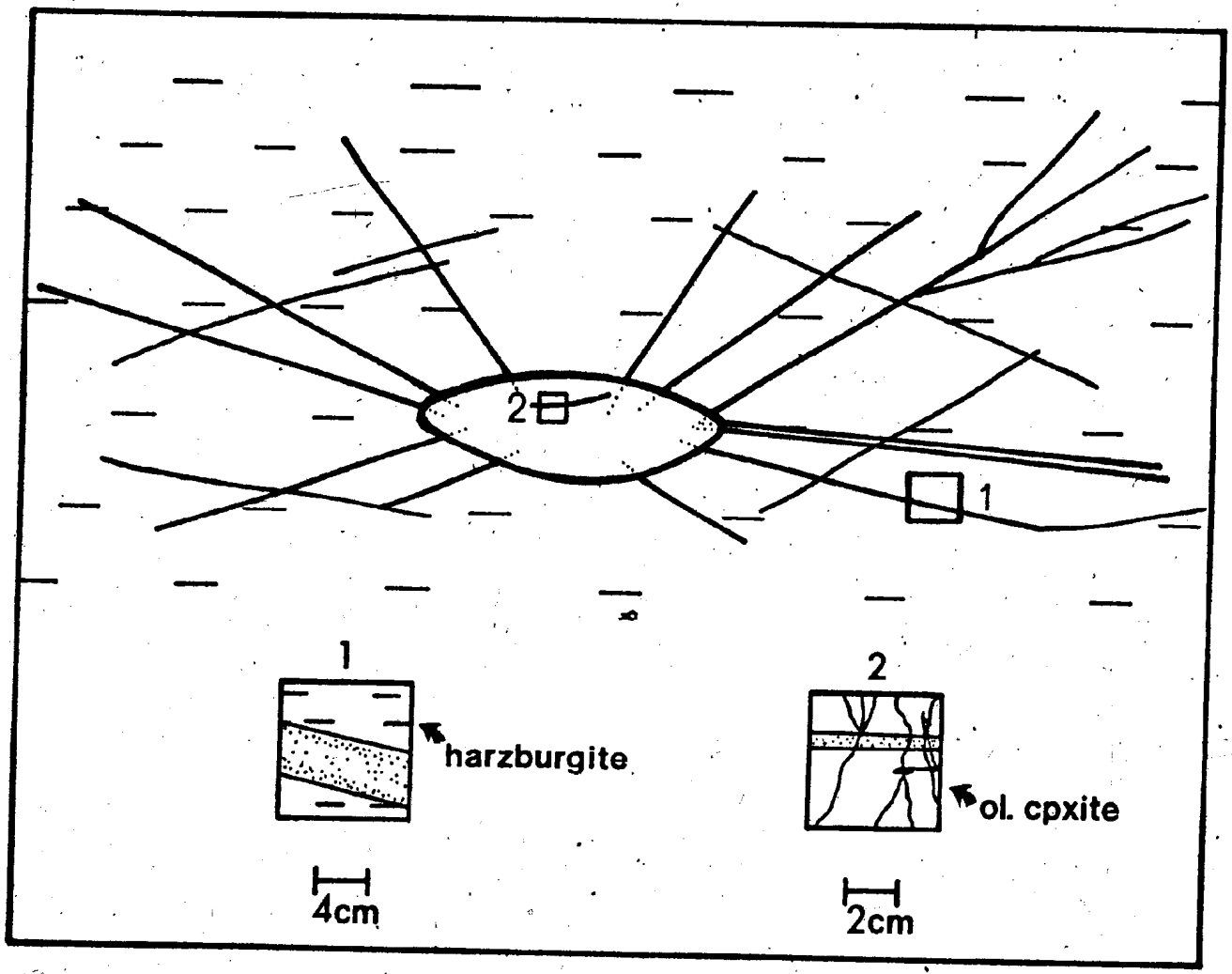
2
1
1
harzburgite
4cm
2
ol. cpxite
2cm

REE abundances, then multistage melting of the source would have preferentially depleted the source material in LREE (Gast, 1968; Smewing and Potts, 1976; Frey and Prinz, 1978; Thompson et al., 1980), thus producing a convex downwards or LREE-depleted chondrite normalized pattern and not a U-shaped chondrite normalized pattern. It must be pointed out that it is possible to produce a U-shaped pattern by the selective uptake of LREE during metamorphism (Hellman and Henderson, 1977; Ludden and Thompson, 1979) and by the blending or addition of an LREE-enriched component (i.e., component B of Frey and Green, 1974), but for the Semail Ophiolite, Boudier and Coleman (in press) make no reference to the extent of metamorphism of these rocks nor present field evidence of a LREE-enriched component (cf., Coish and Church, 1979 who present a similar case for the lower basalts of the Betts Cove Ophiolite).

(v) do these veins represent mineral accumulation or the frozen liquid equivalent of the initial partial melt?

The proposed model and the available bulk rock and trace element geochemistry for these rocks support an accumulative origin and not an origin where the veins are the frozen partial melt liquids. For these veins to be frozen equivalents of primary liquids requires that the bulk rock $Mg/(Mg+Fe^{2+})$ ratios be approximately 0.700 (or 0.680 to 0.690 if they are the frozen equivalent of the first-stage partial melt A'). Clearly, this is therefore not the case for any vein type that has a bulk rock $Mg/(Mg+Fe^{2+})$ ratio in the range 0.900 to 0.793 according to the experimental work of Roeder and Emslie

(1970)*. It is also difficult to envisage, if these veins are frozen primary liquid equivalents, how subsequent partial melting events could produce an orderly rock sequence (i.e., orthopyroxenite to gabbro) and corresponding bulk rock and mineral chemistries.

c. Variations of the Proposed Model

Although the single liquid polybaric crystallization model is able to explain the change of modal mineralogy, bulk rock and mineral chemistry changes for the majority of the vein types, the proposed model cannot explain the chemistry nor account for the crystallization of the chromite-related rock types (i.e., low-alumina orthopyroxenite, low-alumina "websterite", and chromite) due to the differences in mineral chemistries (bulk rock analyses are not available). Therefore additional factors must be considered as variations of the proposed model.

(i) hypothesis for origin of chromite-related lithologies

The mineral chemistry data for these lithologies have been presented and discussed in Chapter 3 where the writer suggests, mainly on the basis of differences in the TiO_2, Al_2O_3 and Cr_2O_3 content of the pyroxenes and the Mg/Fe ratio of the constituent minerals from the values reported for the high-alumina pyroxenites and gabbro, that the chromite-related

* Jaques and Green (1980) suggest, however, that K_DOl/liquid may be pressure dependent above 5 kilobars, where the K_D increases with increasing pressure resulting in olivine of a particular Fo content to be in equilibrium with a more magnesian liquid above 5 kilobars.

lithologies may not have crystallized from the first-stage partial melt liquid (i.e., not a liquid of olivine tholeiitic composition), but from a liquid derived from the partial melting of a nearly depleted source material.

Multistage partial melting of a single source material has been advocated by many workers to explain the differences (and changes) in the geochemistry (bulk rock, mineral, REE) of interlayered ophiolitic lavas (e.g., Smewing and Potts, 1976; Coish and Church, 1979; Laurent et al., 1979; Duncan and Green, 1980; Jaques and Green, 1980; Thompson et al., 1980). In general, most of these workers have found that the predominant lava within the bedded lava pile is olivine tholeiitic, whereas the less abundant lava has a composition approximating magnesian-quartz tholeiite.

The magnesian-quartz tholeiite partial melt liquid is hypothesized to have been derived by second-stage partial melting of a spinel lherzolite source material already nearly depleted of Na_2O, TiO_2, and LREE by first-stage partial melting (~ 20 to 25 percent) (Duncan and Green, 1980). A liquid with these geochemical characteristics has been suggested by Duncan and Green (1980) to result from approximately 5 to 10 percent partial melting of a nearly depleted spinel lherzolite source material at shallow depths (5 to 25 km). The bulk rock composition of the second-stage liquid compares favorably to the chemical composition of the Troodos upper pillow lavas (Duncan and Green, 1980; G. Langdon, pers. comm., 1980) and is similar to the depleted basalt (lower lavas) of the Betts Cove Ophiolite (Coish and Church, 1979) and the

olivine meta-tholeiite volcanics of the Quebec Ophiolites (Laurent et al., 1979). Jaques and Green (1980) indicate that the second-stage magnesian-quartz tholeiite liquid is similar in bulk composition to partial melt liquids produced at low pressures (2 and 5 kb) from the Tinaquillo Peridotite (relatively refractory lherzolite, $Mg/(Mg+Fe^{2+}) = 0.903$). The partial melt liquids produced at low pressures from the Tinaquillo Peridotite are Ti-poor magnesian-quartz tholeiites with high Al_2O_3/TiO_2 ratios and a bulk rock $Mg/(Mg+Fe^{2+})$ ratio of approximately 0.770 (see Duncan and Green, 1980, p. 23, Table 1, analysis 4; and Jaques and Green, 1980, p. 299, Table 5, column 16). Partial melting of the Tinaquillo Peridotite at high pressures (≥ 10 kb) produces less silica-rich, olivine normative liquid compositions (∿ olivine tholeiitic). The compositions of minerals produced from the partial melting of the Tinaquillo Peridotite are markedly different at low (2 and 5 kb) and high (10 and 15 kb) pressures. At low pressures the Al_2O_3 and Cr_2O_3 contents of the coexisting pyroxenes are lower than at high pressures (no data are provided by Jaques and Green, 1980) and spinel compositions are chrome-rich. These data imply a dependence on pressure for Al_2O_3 solubility in the pyroxenes (see Chapter 3) and Cr-Al exchange between coexisting pyroxenes and spinel.

A liquid such as the magnesian-quartz tholeiite with a bulk rock $Mg/(Mg+Fe^{2+})$ ratio of 0.770 is capable of crystallizing olivine of composition Fo_{93-94} (Roeder and Emslie, 1970), highly magnesian (∿ En_{93}) orthopyroxene and spinel with high

Cr/(Cr+Al) ratio ($\sim$ 0.700) (Duncan and Green, 1980; Jaques and Green, 1980). Minerals with similar compositions occur in the chromite-related lithologies (Chapter 3 and Appendix II). In addition, the residual material produced from this second-stage partial melting of the nearly depleted spinel lherzolite is a highly refractory harzburgite with a bulk rock $Mg/(Mg+Fe^{2+})$ ratio of approximately 0.900 (Duncan and Green, 1980) (e.g., sample 77WH14, most refractory harzburgite thus far found in the White Hills Peridotite, Table 5.1.).

The proposed mineral crystallization order and rock sequence and processes that produce the chromite-related lithologies are presented in section 5.C. of this chapter.

(ii) high-alumina orthopyroxenite and high-alumina websterite: an origin by mineral segregation during upper mantle deformation?

Although the pyroxenite, gabbro and dunite veins/bodies are considered cumulates in this work, other authors have described the origin of pyroxenite veins of similar compositions and mineralogies from ophiolites-Alpine-type peridotites by alternate hypothesis (e.g., Dickey, 1970 and Dick and Sinton, 1979). A most appealing mode of origin for the formation of pyroxenite and dunite veins by mechanical segregation of minerals during deformation in the upper mantle has been proposed by Dickey (1970) and Dick and Sinton (1979). This mechanical segregation process is based on the premise that, in a heterogeneous mixture of minerals, when an external force is applied, segregation occurs due to differences in mechanical properties of the modal phases (i.e., differences in strain rate). For example, minerals having similar

mechanical properties will collect in a separate locality from those having different mechanical properties (cf., Robin, 1979).

Dickey (1970) describes the formation of tectonic layers (chromian-pyroxenite layers of Obata, 1977) of websterite lithology by the above process where the more easily deformed olivine segregates from the pyroxenes and spinel during deformation of the Ronda Peridotite. An analogous application of this process, but on a larger scale, has been used by Dick and Sinton (1979) to explain the formation of layering (olivine-rich and olivine-poor layers) in Alpine-type peridotites. They envisage that the layering is the result of pressure solution creep due to the development of high strain (pyroxene-rich) and low strain (olivine) zones and the dissolution and reprecipitation of the pyroxenes, predominantly, in the high strain zones (cf., Dick and Sinton, 1979, p. 410-411, Figs. 9 and 10).

This variation to the proposed model is offered not as a replacement but as a possible supplement to the original model. The basis for suggesting this alternative is the similar mineral chemistries for the high-alumina orthopyroxenite and websterite veins to the host rock spinel lherzolite and, in some examples, harzburgite (see Chapter 3 and Appendix II). Although the formation of compositional layering by mechanical segregation may not be entirely applicable to the formation of the high-alumina orthopyroxenite and websterite veins, the mechanism does offer an explantion for the frequently observed association of dunite layers and patches adjacent to all of

the pyroxenite vein types.

II.5.C. Origin of Spinel Minerals

1. General Statement

Irvine and Findlay (1972) have shown that, in general, spinels from Alpine-type peridotites exhibit a large range in Cr/(Cr+Al) (cation proportion) ratio (∿ 0.80) and a less extensive range, although nearly as large, in the $Mg/(Mg+Fe^{2+})$ (cation proportion) ratio (∿ 0.60) (Figure 5.10.). In contrast, spinels from stratiform layered intrusions exhibit a more restricted range in Cr/(Cr+Al) ratio (∿ 0.20), but a similar range for $Mg/(Mg+Fe^{2+})$ ratio (∿ 0.60) to the Alpine-type peridotite spinel varieties.

Two questions require resolution, firstly why is there such a vast difference in the chemical compositions of spinels between the Alpine-type peridotite and the stratiform layered intrusion groups and secondly, and perhaps more important for this discussion, why is there such a large compositional variation for spinels from Alpine-type peridotites (and therefore ophiolites)?

For each spinel form (Chapter 4) and rock microstructure (Chapter 2) of the White Hills Peridotite, the spinel phase has a particular compositional range (Chapter 4) that as a group spans a large variation in Cr/(Cr+Al) ratios. This compositional range for spinel is not unique to the White Hills, but similar to other ophiolites (e.g., Loney et al., 1971; Malpas and Strong, 1975; Menzies, 1975; Sinton, 1977).

Figure 5.10. Range of spinel compositions in Alpine complexes and stratiform intrusions (after Irvine and Findlay, 1972).

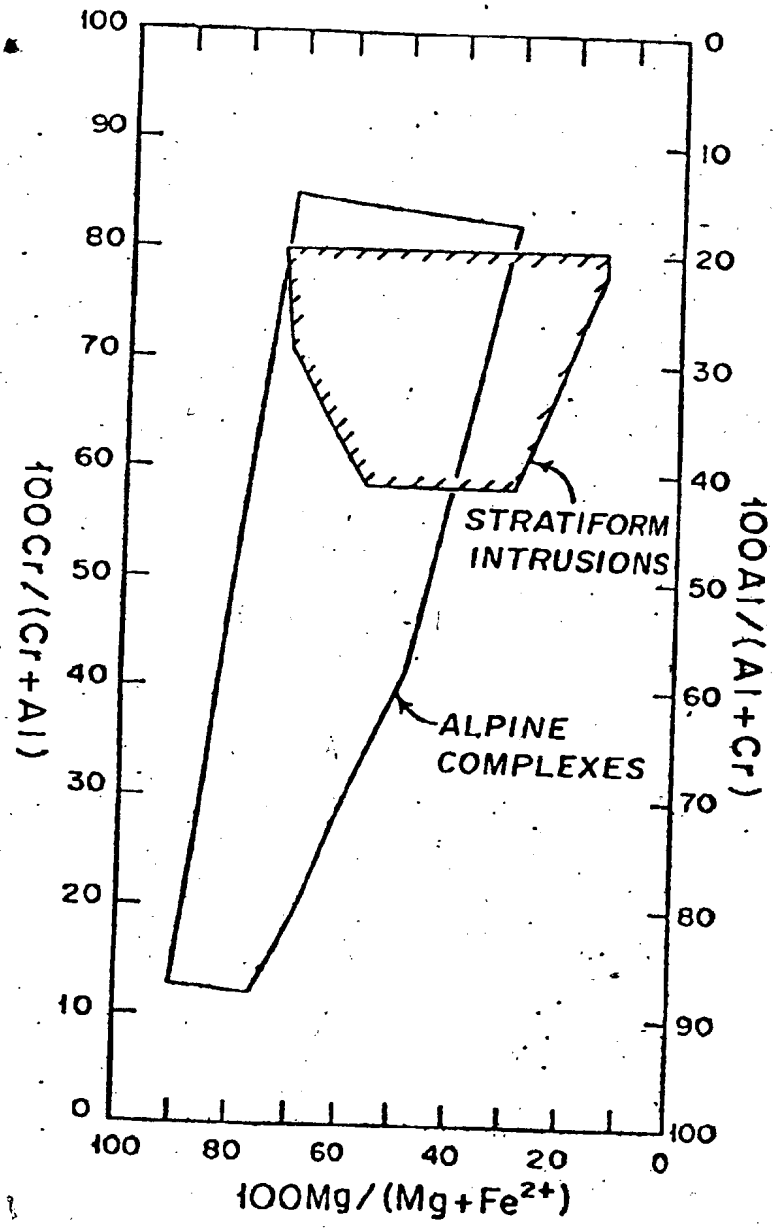
100
90
80
70
60
50
40
30
20
10
0
100Cr/(Cr+Al)
0
10
20
30
40
50
60
70
80
90
100
100Al/(Al+Cr)
STRATIFORM
INTRUSIONS
ALPINE
COMPLEXES
100
80
60
40
20
0
100Mg/(Mg+Fe2+)

Bearing this in mind and that temporal significance can be assigned to the various spinel-silicate relationships, whether primary or secondary (Chapter 4), and that a model for the petrological evolution of the White Hills Peridotite has been presented in the earlier sections of this chapter (II.5.A. and II.5.B.), then a basis exists to explain: (1) the origins for the various spinel phases of the White Hills Peridotite, and (2) the large compositional range of spinels from ophiolites (Alpine-type peridotites).

A discussion of the formation of the spinel phases from the least-deformed microstructures (i.e., coarse-granular, cumulate and allotriomorphic granular textures) for a specified peridotite lithology (e.g., spinel lherzolite, harzburgite, etc.) is presented. This is followed by a discussion of the chemical compositions and chemical variations of the spinel phase from the particular lithology. Where a primary microstructure has not been preserved, discussions of the possible timing and mechanisms for spinel formation and the factors governing the spinel chemical compositions are presented.

Thus, the major goals are to establish the role that partial melting plays, if any, in the genesis and the diversity of the chemical compositions of the spinels, and how subsolidus chemical equilibration influences spinel compositions. From these discussions, the range in the Cr/(Cr+Al) and the Mg/(Mg+Fe^{2+}) ratios of spinels from ophiolites (Alpine-type peridotites) may be explained.

The above discussions are structured around the petrological model for the White Hills Peridotite which is shown in Figure 5.11.,

Figure 5.11. Generalized model for the petrological development of the White Hills Peridotite. (see Figure 5.12. for full description).

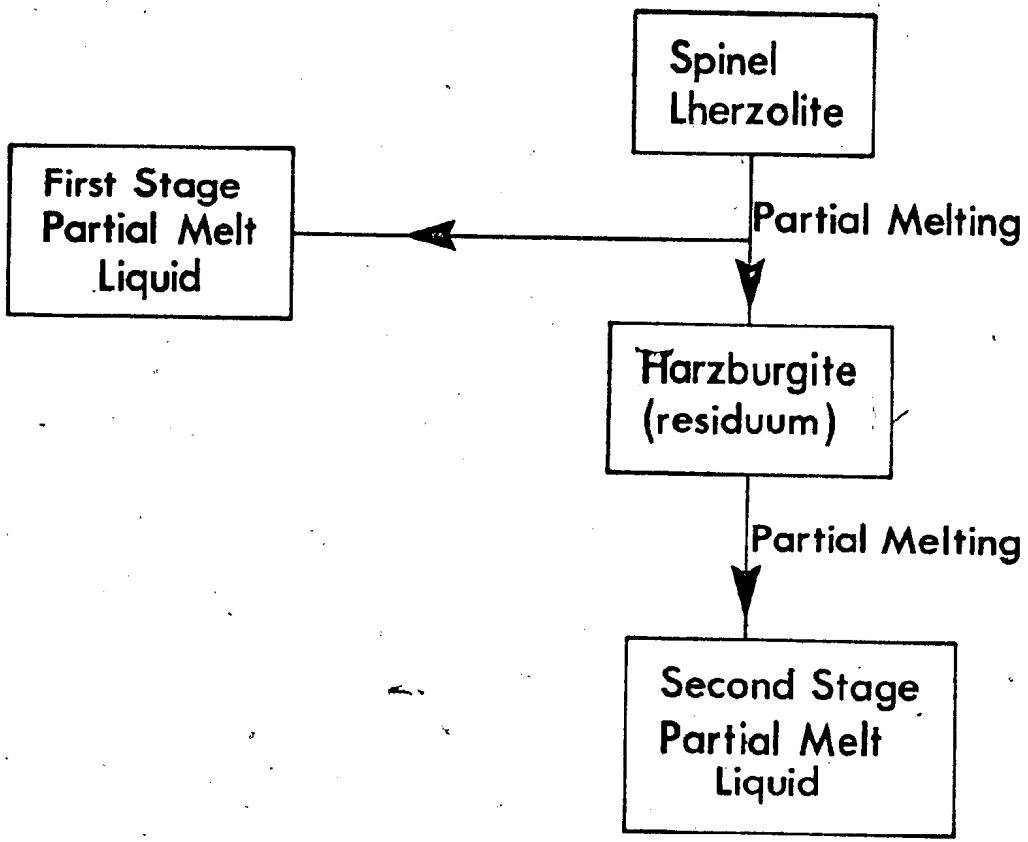
Spinel
Lherzolite
First Stage
Partial Melt
Liquid
Partial Melting
Harzburgite
(residuum)
Partial Melting
Second Stage
Partial Melt
Liquid

and more fully explained, especially with regards to spinel origins, in the flow chart in Figure 5.12. The model has been developed from the results in Chapters 2, 3, 4 and the initial sections of Chapter 5.

2. Spinel Lherzolite

a. Mechanisms for Spinel Formation and Interpretation

In the three component system $MgO-Al_2O_3-SiO_2$, MacGregor (1974) uses the divariant reaction:

$$\underset{\text{spinel}}{xMgAl_2O_4} + (1+x)\underset{\text{enstatite}}{MgSiO_3} \rightleftharpoons \underset{\text{Al-enstatite}}{MgSiO_3 \cdot xAl_2O_3} + \underset{\text{forsterite}}{xMg_2SiO_4} \quad (5.1)$$

to define the subsolidus chemical change in the solubility of Al_2O_3 in enstatite coexisting in equilibrium with olivine and spinel. The experimental results of Boyd and England (1964), Anastasiou and Seifert (1972) and MacGregor (1974) for equation (5.1) indicate that the Al_2O_3 solubility in enstatite increases with rising temperature at constant pressure and decreases with increasing pressure (at high temperatures, $\gtrsim 1000^{\circ}C$, Obata, 1976) at constant temperature. Thus, equation (5.1) will proceed to the right with either increasing temperature or decreasing pressure. Conversely, equation (5.1) will proceed to the left as the temperature decreases or if there is a pressure increase (up to approximately 10 kb, Anastasiou and Seifert, 1972). Hence, this reaction leads to the lowering of the Al_2O_3 content of enstatite by exsolution and the formation of spinel.

Similar theoretical results for equation (5.1) have been obtained by Obata (1976) in the system $CaO-MgO-Al_2O_3-SiO_2$. Obata's (1976) theoretical calculations indicate that the

Figure 5.12. Flow chart detailing the petrological evolution of the White Hills Peridotite and the proposed origins of the spinel phases from the various lithologies of the peridotite. See text for discussion.

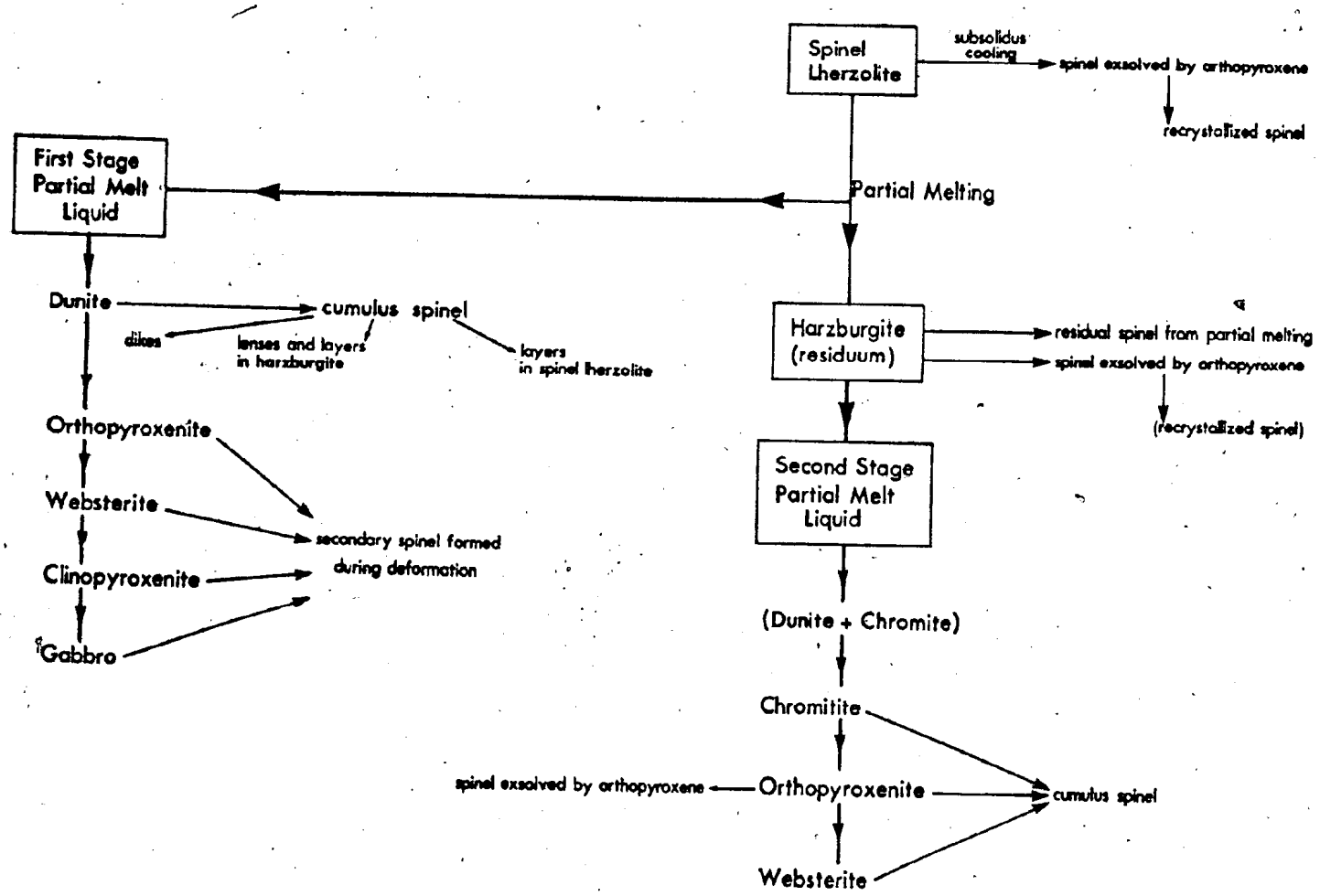
Spinel Lherzolite
subsolidus cooling
spinel exsolved by orthopyroxene
recrystallized spinel
Partial Melting
First Stage Partial Melt Liquid
Dunite
cumulus spinel
dikes
lenses and layers in harzburgite
layers in spinel lherzolite
Orthopyroxenite
Websterite
Clinopyroxenite
Gabbro
secondary spinel formed during deformation
Harzburgite (residuum)
residual spinel from partial melting
spinel exsolved by orthopyroxene
(recrystallized spinel)
Second Stage Partial Melt Liquid
(Dunite + Chromite)
Chromitite
spinel exsolved by orthopyroxene
Orthopyroxenite
cumulus spinel
Websterite

Al_2O_3 solubility in enstatite is relatively insensitive to pressure, but sensitive to temperature, only in the spinel lherzolite stability field (cf., Obata, 1976, p. 810, Fig. 6) (see page 106).

In contrast to the above results, Green (1964), in the four component system $CaO-MgO-Al_2O_3-SiO_2$, uses the reaction:

aluminous pyroxenes + olivine ⇌ less alumina-rich pyroxenes + spinel (5.2)

to explain the change in the high-alumina content of the pyroxenes in the primary mineral assemblage of the Lizard Peridotite to the low-alumina content of the pyroxenes in the recrystallized anhydrous mineral assemblages. Green (1964) indicates that the change in pyroxene mineral chemistry is brought about by a decrease in pressure during emplacement and deformation of the peridotite.

There is, therefore, a difference in the reaction initiating mechanism between equation (5.1) and (5.2) (i.e., decreasing temperature or decreasing pressure) to obtain the same product. It is apparent that in light of the recent experimental and theoretical work for equation (5.1), that the decrease in Al_2O_3 content of pyroxene of the recrystallized anhydrous mineral assemblage has probably been in response to a temperature decrease during deformation and emplacement of the Lizard Peridotite. However, it is quite probable that the combined effect of a pressure and temperature change (Anastasiou and Seifert, 1972) rather than solely a decrease of pressure would cause a decrease in the Al_2O_3 solubility

in enstatite and therefore, promote the formation of spinel.

Equation (5.1) has been used by Allen (1975) to explain the exsolution of spinel from orthopyroxene in harzburgite of the Troodos Ophiolite and similarly, Varne (1977) and Donaldson (1978) apply this reaction to explain spinel exsolution from pyroxenes in upper mantle spinel lherzolite xenoliths.

With regard to rock microstructure and as mentioned in Chapter 2, Mercier and Nicolas (1975) have used spinel-silicate textural relations to interpret the metamorphic recrystallization history of upper mantle ultramafic rocks. They suggest that spherical spinel inclusions in minerals, especially in olivine, form only when the starting rock microstructure has been completely recrystallized to an equigranular texture as a result of annealing. In addition, if a secondary texture similar or equivalent to the starting rock microstructure forms from the equigranular texture the spherical spinel inclusion may be preserved and appear in the 'new' rock microstructure. Therefore, at any one time, it is possible that two deformation cycles (i.e., primary and secondary, in the relative sense) may be recognized in a single rock suite. Even though the rocks may have undergone more deformational cycles, only the <u>last two</u> can be distinguished.

Spinel droplets (anhedral clot 0.1 mm) in olivine occur in only one coarse-granular textured spinel lherzolite sample from the White Hills and thus this texture may represent the protogranular II texture (or an equivalent) of the Mercier and Nicolas (1975) classification cycle. If so, then this sample reveals the following textural cycle: protogranular I →

porphyroclastic I → equigranular I → protogranular II. The protogranular II (?) texture has not been recognized in any other coarse-granular textured spinel lherzolite samples from the White Hills Peridotite and therefore may only be a localized feature. Quite possibly then, the coarse-granular textured spinel lherzolite samples from the White Hills Peridotite represent an 'initial' (first generation) upper mantle texture that has escaped the textural recrystallization cycle proposed by Mercier and Nicolas (1975), but this cannot be unequivocally proven.

b. Discussion of the Variation in Spinel Composition

Spinel compositions from spinel lherzolite of the White Hills have a low Cr/(Cr+Al) ratio and a relatively high $Mg/(Mg+Fe^{2+})$ ratio (Figure 4.2.). These compositional features are not unique to ophiolite complexes and are similar to spinel compositions reported for spinel lherzolite xenoliths (Aoki and Prinz, 1974; Varne, 1977; Donaldson, 1978; Frey and Prinz, 1978; Reid and Woods, 1978) and lherzolite massifs (Boudier, 1976; Ernst, 1978; Ernst and Piccardo, 1979). Bulk rock and coexisting silicate chemistries have been suggested by some authors to control spinel compositions (e.g., Irvine, 1965; 1967; Jackson, 1969; Loney et al., 1971; Sigurdsson and Schilling, 1976; Sinton, 1977; Frey and Prinz, 1978; Fisk and Bence, 1980; Talkington and Malpas, 1980a,b). Several reasons for suggesting these controls are (1) spinel is often the initial phase to crystallize from a liquid where crystal accumulation processes are operative and as such

may preserve some of the chemical characteristics of the liquid from which it crystallized; (2) if the spinel is exsolved from a silicate phase, during for example subsolidus cooling, then the spinel may inherit some chemical characteristics of the exsolving host phase; and (3) if a cognate inclusion and host rock undergo recrystallization during deformation, the chemical composition of the spinel phase and other mineral phases of the inclusion may be modified by the chemical composition of the host rock or surrounding lithologies.

Unlike the compositions of spinels from stratiform intrusions, the compositions of spinels from ophiolites do not show a dependence on the $Mg/(Mg+Fe^{2+})$ ratio of olivine (Figure 5.13.), which Roeder and Emslie (1970) have shown to be an accurate approximation of the liquid $Mg/(Mg+Fe^{2+})$ ratio. However, Irvine (1967) suggests that the Mg/Fe^{2+} ratio of coexisting spinel and silicate phases in equilibrium are closely linked and that the only large independent major element variable is the Cr/Al ratio. The Irvine (1967) hypothesis is supported by the White Hills Peridotite data which show a reasonable relationship between the spinel and bulk rock Cr/Al ratios (Figure 5.14.). There is a good correlation between the two especially at low Cr/Al ratios where a near 1:1 linear relationship exists, but this becomes poorer with increasing Cr/Al values. Less chemical dependence is found when the spinel Cr/Al ratios are compared to the bulk rock Cr_2O_3 contents (Figure 5.15.).

The spinel of coarse-granular textured rocks is always associated with orthopyroxene, less often with olivine and

Figure 5.13. $Mg-Fe^{2+}$ partitioning between coexisting spinel and olivine from ophiolitic ultramafic rocks. Solid lines G-zone and H-zone from the Stillwater Complex (Jackson, 1969). Plotted data from Burro Mountain Peridotite (Loney et al., 1971; ○); S.W. Oregon Peridotites (Medaris, 1975; x); Troodos Ophiolite (Allen, 1975; △); Bay of Islands Ophiolites (Malpas, 1976; □); Red Mountain Peridotite (Sinton, 1977; ◇); Oman Ophiolite (Smewing, unpub. data; ☆); White Hills Peridotite (this study; ▽).

Symbols:

Spinel lherzolite	○	X	△	□	◇	☆	▽
Harzburgite	◐		▲	◧	◆	☆	▼
Dunite	●		▲	■	◆	★	▼
Orthopyroxenite	◐		▲	◧	◆	☆	▼

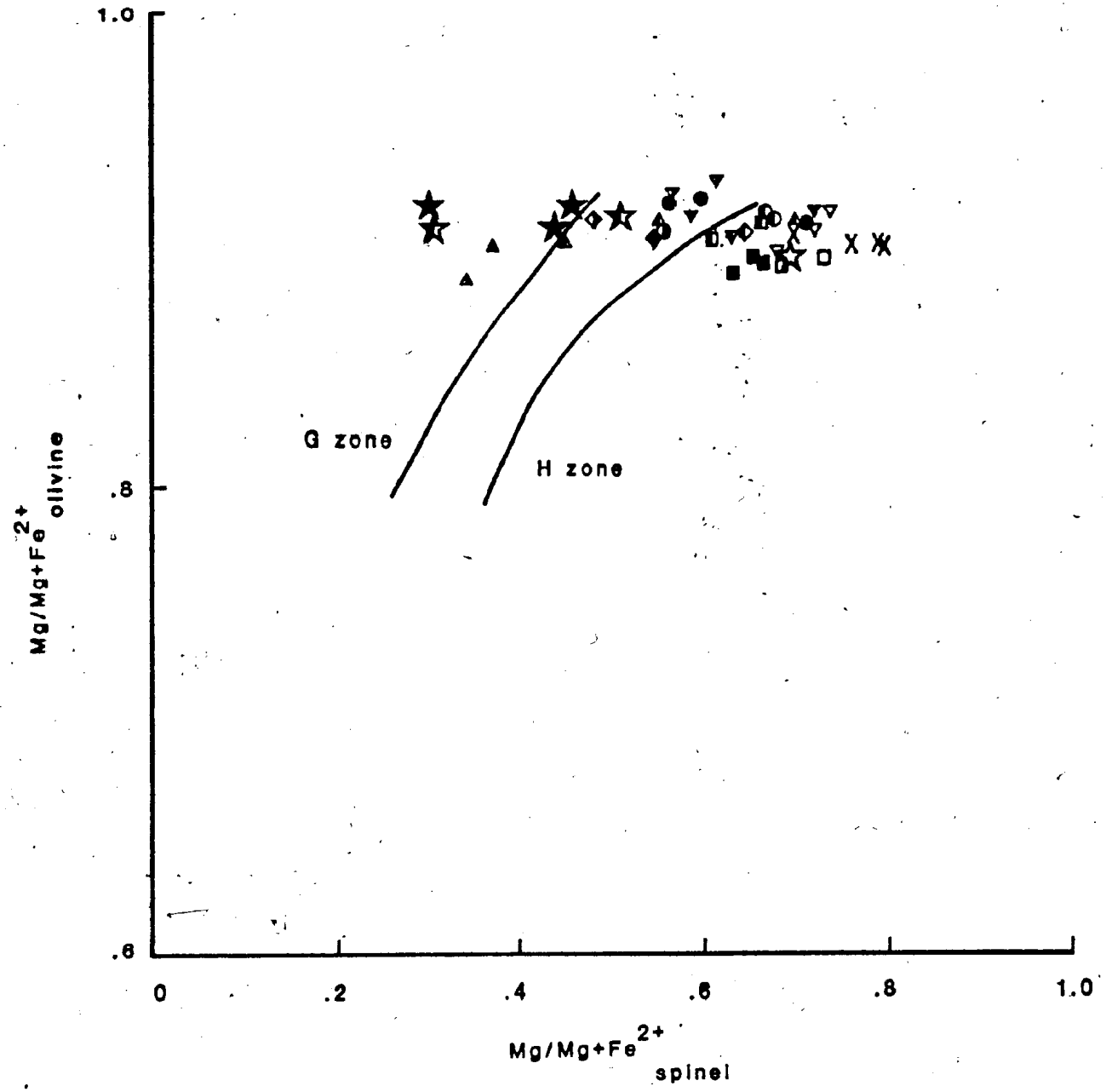
1.0
.8
.6
0
.2
.4
.6
.8
1.0
G zone
H zone
Mg/Mg+Fe2+ olivine
Mg/Mg+Fe2+ spinel

Figure 5.14. Plot of Cr/Al spinel against Cr/Al bulk rock (B.R.).
Symbols:



Spinel lherzolite
Harzburgite
Dunite
Low-alumina orthopyroxenite

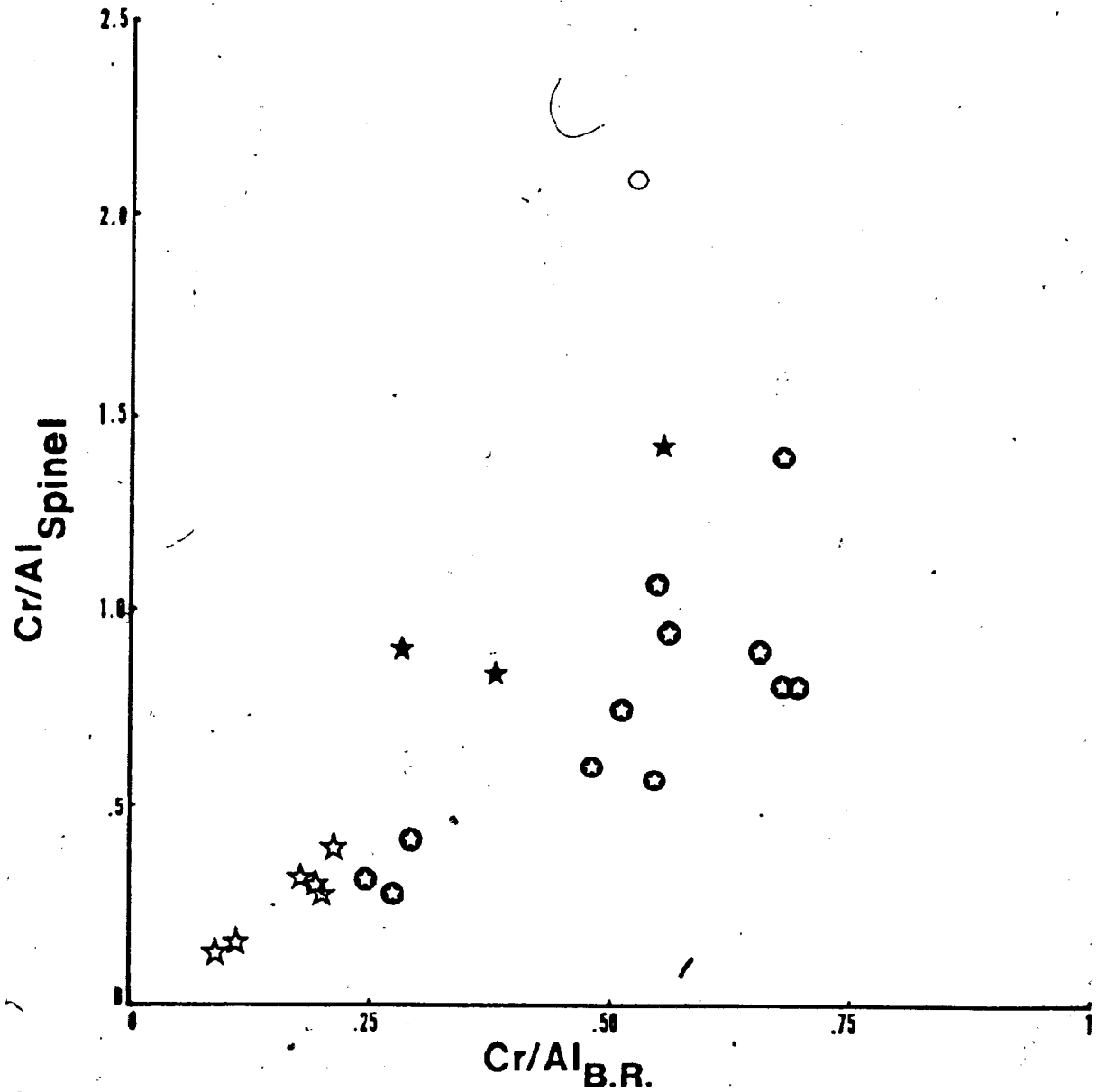
2.5
2.0
1.5
1.0
.5
0
0
.25
.50
.75
1
Cr/Al Spinel
Cr/Al B.R.

Figure 5.15. Plot of weight percent (wt.%) Cr_2O_3 bulk rock (B.R.) against Cr/(Cr+Al) spinel. Symbols as for Figure 5.14. Solid line connects discrete, coexisting spinels in dunite (sample 78117).

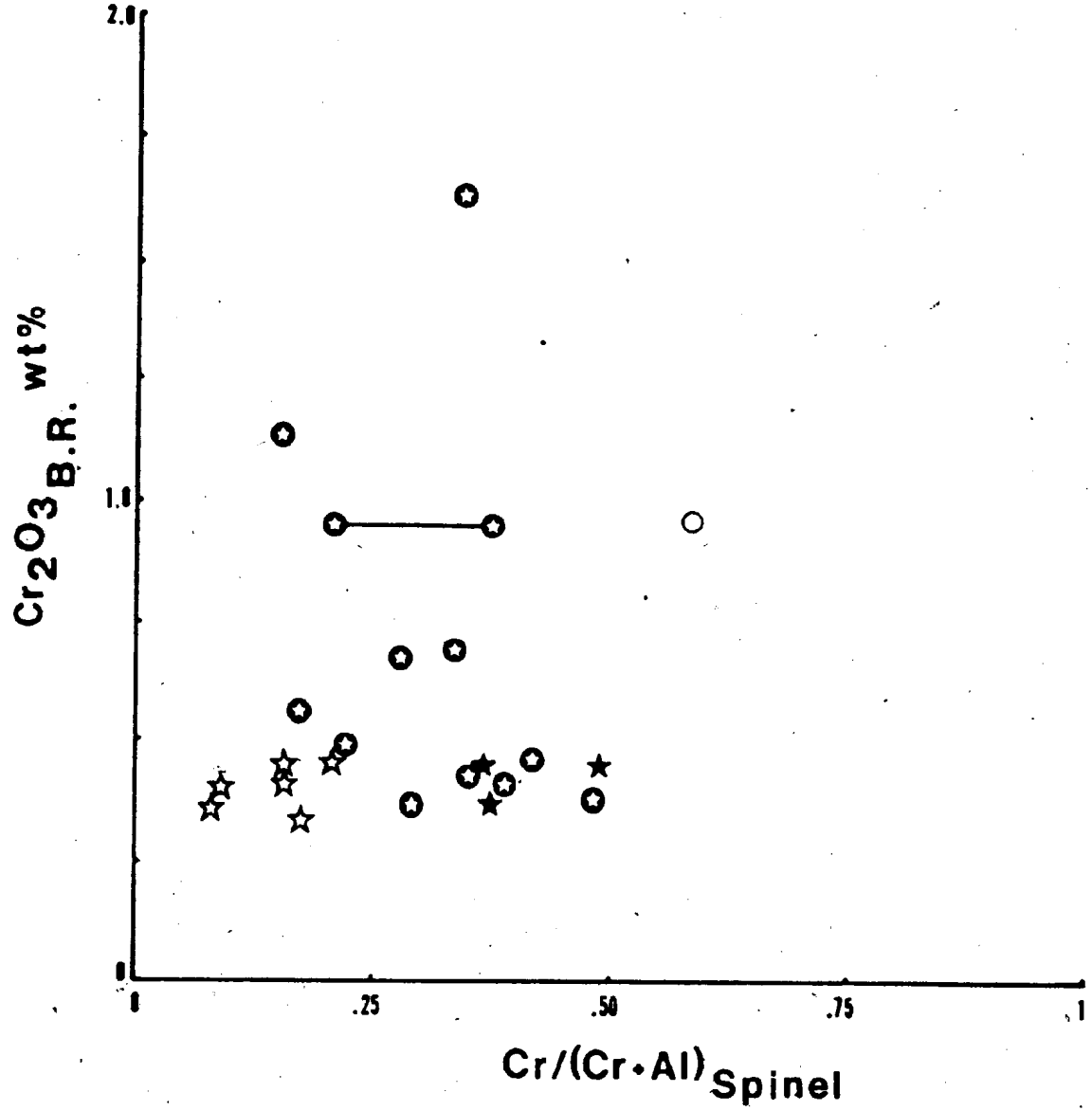
2.0
1.0
0
0
.25
.50
.75
1
Cr_2O_3 B.R. wt%
Cr/(Cr+Al) Spinel

rarely with clinopyroxene. Therefore, because of these associations, the spinel compositions might be influenced by pyroxene compositions as indicated by equations (5.1) and (5.2). The chemical data in Figures 5.16. and 5.17. show the variations in the Al_2O_3 content of orthopyroxene and clinopyroxene as a function of the Cr/(Cr+Al) ratio of the coexisting spinel. With a decrease in the Al_2O_3 content of the pyroxenes there is a smooth increase in the Cr/(Cr+Al) ratio of spinel. Similar chemical trends for ultramafic xenoliths are described by Basu and MacGregor (1975), Frey and Prinz (1978) and Reid and Woods (1978), by Sinton (1977) for the Red Mountian Peridotite and by Allen (1975) for the Troodos Ophiolite.

Two spinel forms occur in the porphyroclastic spinel lherzolite samples, an exsolved form and an anhedral interstitial form. In Chapter 4, section II.4.C.3. it has been shown that a compositional difference exists between the two spinel forms, the exsolved spinel having the higher Cr/Al ratio. To explain this chemical change two arguments may be used: (1) partial melting, and (2) subsolidus equilibration.

The initial formation of the exsolved spinel occurs during subsolidus cooling of the spinel lherzolite according to the relationships given by equations (5.1) and (5.2). If during the development of the porphyroclastic texture partial melting takes place, then because of the relationship $D^{Al}_{liquid\text{-}rock} > D^{Cr}_{liquid\text{-}rock}$ (Kurat et al., 1980), more aluminum than chromium would be removed from the solid and partitioned into the liquid. Spinel, being the least abundant modal phase

Figure 5.16. Plot of weight percent Al_2O_3 in orthopyroxene (opx) against Cr/(Cr+Al) ratio in coexisting spinel. Symbols as for Figure 5.14. Additional symbol:

■ "websterite"

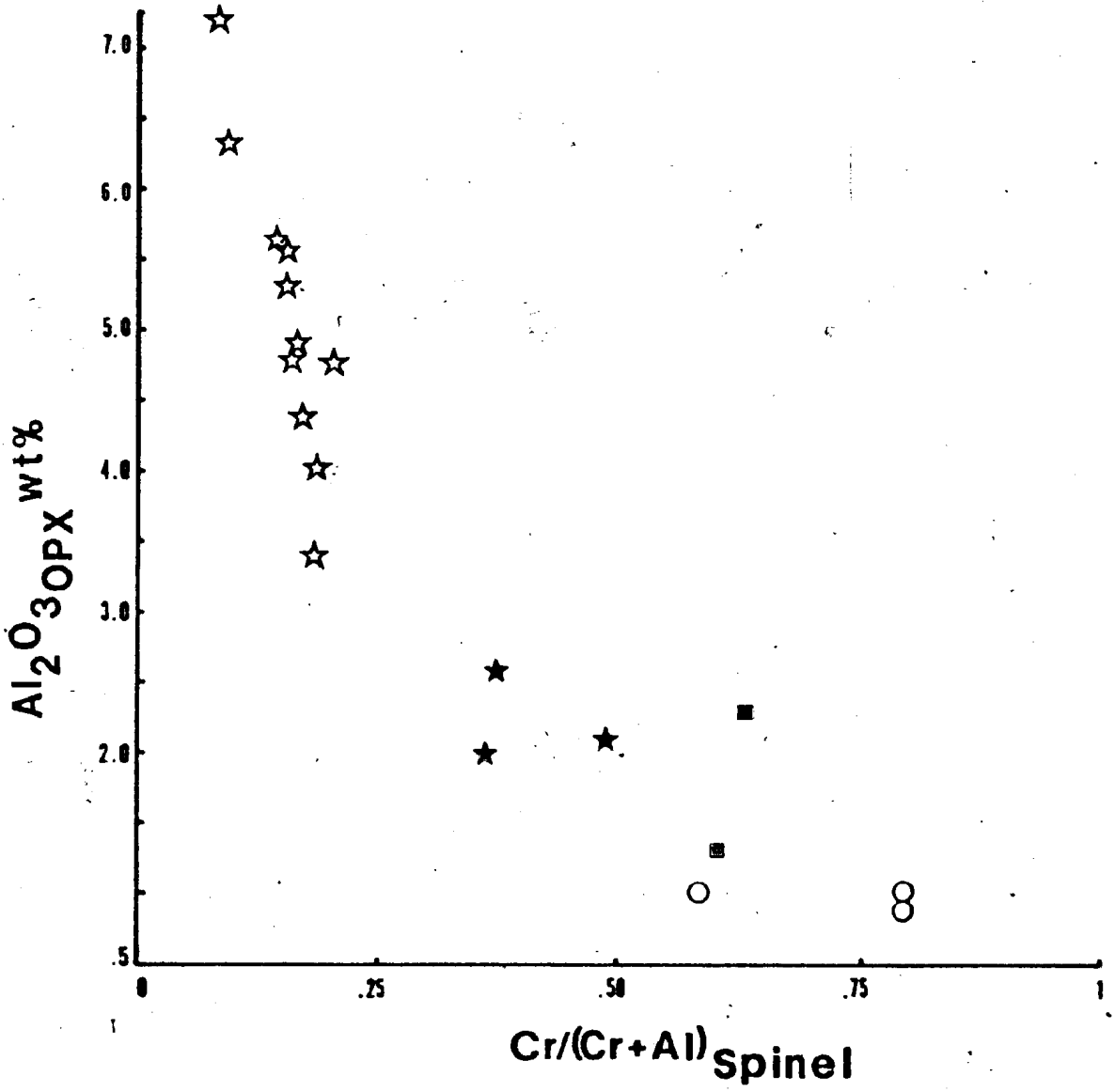
7.0
6.0
5.0
4.0
3.0
2.0
.5
0
.25
.50
.75
1
Al_2O_{3OPX} wt%
Cr/(Cr+Al)$_{spinel}$

Figure 5.17. Plot of weight percent Al_2O_3 in clinopyroxene (cpx) against Cr/(Cr+Al) ratio in coexisting spinel. Symbols as for Figures 5.14. and 5.16.

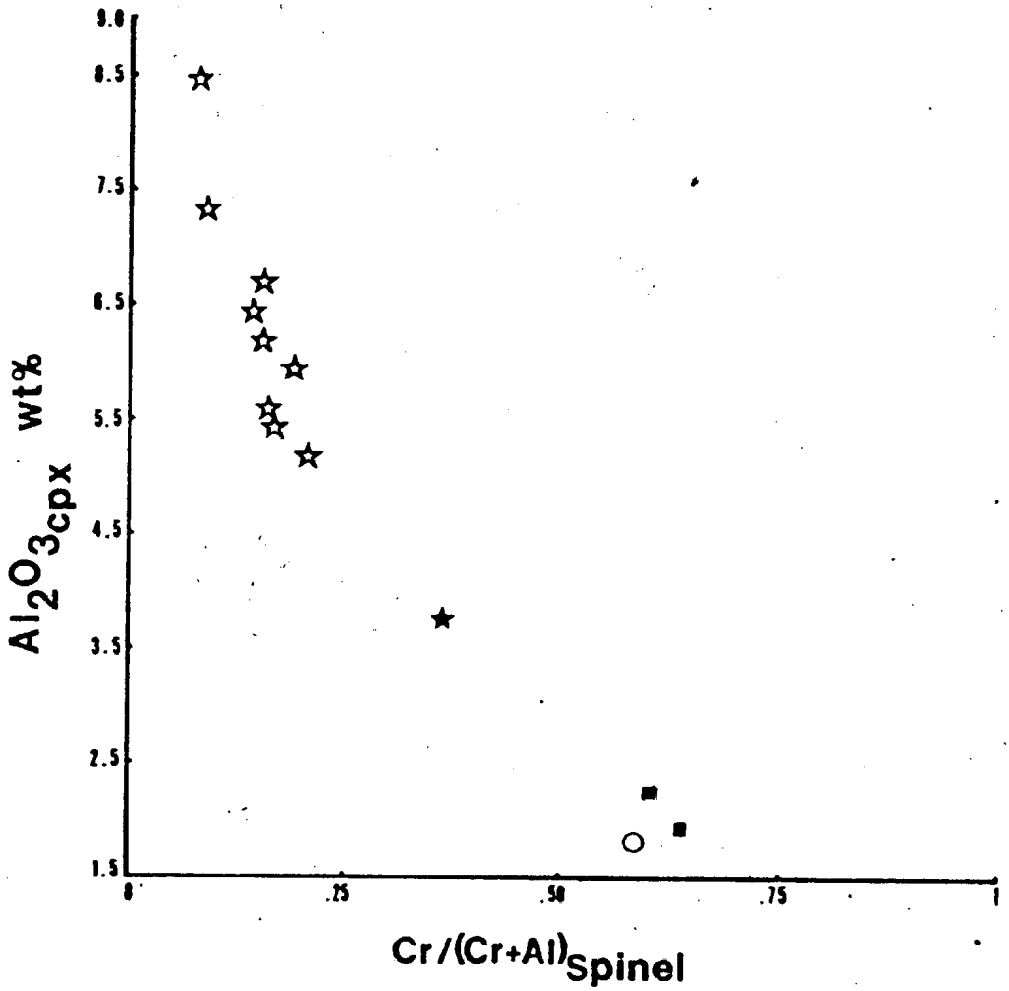
9.0
8.5
7.5
6.5
5.5
4.5
3.5
2.5
1.5
0
.25
.50
.75
1
Al_2O_{3cpx} wt%
Cr/(Cr+Al)Spinel

and the most sensitive to any physiochemical changes, becomes more residual (Cr-rich) with partial melting (Dickey and Yoder, 1972; Arai, 1980).

Alternatively, the compositional changes in spinel may be governed by diffusion controlled processes during a solid-state recrystallization-equilibration event. During this event, varying quantities of Tschermak's molecules ($MgAl_2SiO_6$ and $CaAl_2SiO_6$) are released by pyroxenes and partially incorporated in the spinel, thus lowering the spinel Cr/Al ratio (Aoki and Prinz, 1974). The subsolidus cooling and recrystallization-equilibration processes generate spinel and increase its volume in the rocks.

It is apparent that these two processes produce opposite chemical results with respect to spinel compositions. However as noted above, the recrystallized spinels of the porphyroclastic textured lherzolites have lower Cr/Al ratios than the exsolved spinels of the coarse-granular textured lherzolites. Thus it is suggested that the change in the Cr/Al ratio and Mg/Fe^{2+} ratio (Roeder et al., 1979) is controlled by mineral equilibration at subsolidus temperatures and does not involve nor require the presence of a partial melt liquid. If a partial melt liquid is present, then the recrystallized spinel would probably preserve a spinel with a higher Cr/Al ratio.

An interesting and rather important aspect of this discussion is that because of this chemical relationship between exsolved and recrystallized spinel and equation (5.1) the possibility exists that spinel may not be a modal phase during

supersolidus cooling, but a modal phase only at subsolidus P-T conditions.

3. Harzburgite

a. Spinel Types and Origin and the Variation in the Spinel Cr/Al Ratio

Two spinel types are recognized in coarse-granular textured harzburgite samples, exsolved and porphyroclastic. The exsolved spinel phase in orthopyroxene has an identical evolutionary history to that in the spinel lherzolite samples, i.e., subsolidus exsolution during cooling of the peridotite (cf., equation 5.1). The porphyroclastic spinel, on the other hand, may be a product of the spinel lherzolite partial melting process. The flow charts (Figures 5.11. and 5.12.) illustrate these processes.

In a series of experiments at 1 atmosphere on the join diopside ($CaMgSi_2O_6$)-Cr-Ca Tschermak's molecule ($CaCrAlSi_2O_6$) in the five component system CaO-MgO-Al_2O_3-SiO_2-Cr_2O_3, Dickey et al (1971) have shown that diopside containing more than 0.9 weight percent Cr_2O_3 ($\sim$ 1.6 wt. % CrCats) melts incongruently to chromian spinel plus liquid, whereas at 10 kilobars$_{H_2O}$ chromian diopside melts congruently (Dickey, 1975). This implies, therefore, that the incongruent melting of chromian diopside in spinel lherzolite at low pressures ($\leq$ 10 kb) may produce chrome-rich spinel in residual harzburgite. In addition, during this partial melting event the residual character of the harzburgite increases (Mg/Fe^{2+} increases), and the spinel Cr/Al ratio increases because of $D^{Al}_{liquid\text{-}rock} > D^{Cr}_{liquid\text{-}rock}$ increases with temperature at constant pressure

(Dickey and Yoder, 1972)($D^{Cr}_{Spinel\text{-}liquid}$ increases from approximately 20 for Al-rich spinels, Kurat et al., 1980, to approximately 1000 for Cr-rich spinels, Hill and Roeder, 1974). Thus, the compositions of the spinels in harzburgites at supersolidus temperatures are not controlled by the Cr/Al ratio of the bulk rock, supporting the results of many studies (e.g., Irvine, 1967; Loney et al., 1971; Dickey and Yoder, 1972; Dick, 1976a; Sinton, 1977; Talkington and Malpas, 1980a). Although this statement appears as a direct contradiction with the data presented in the spinel lherzolite section, the writer suggests that during subsolidus cooling of the host peridotite the spinel Cr/Al ratios may equilibrate to values approaching those of the bulk rock especially for pyroxene-bearing lithologies (Figure 5.14.).

The different Cr/Al ratios for spinels in harzburgite of the White Hills Peridotite and the Bay of Islands Complex (and other ophiolites with well-developed ultramafic sections) can be explained by differences in the degree of partial melting of the spinel lherzolite source material (cf., Arai, 1980). For example, the ultramafic zone of the Bay of Islands Complex contains a thin (~ 200 m) unit of spinel lherzolite overlain by a homogeneous harzburgite unit (~ 3 km) and a cumulate dunite zone (~ 300 m), respectively (Malpas, 1976). Whereas in the White Hills Peridotite spinel lherzolite and harzburgite are interlayered with varying amounts of dunite. Malpas (1976, 1978) has suggested that values ranging from 23 to 25 percent partial melting of spinel lherzolite will produce a

highly refractory harzburgite residuum (clinopyroxene-free), which agrees favorably with the results of experimental melting and modelling studies (O'Hara, 1968; Mysen and Kushiro, 1977; Reid and Woods, 1978). Earlier in this chapter it has been suggested that approximately 21 percent partial melting of the White Hills Peridotite spinel lherzolite would produce a harzburgite containing a small modal amount of chromian diopside. It is apparently this slight increase of "unused" clinopyroxene during partial melting of the spinel lherzolite that has a strong affect in decreasing the Cr/Al ratio of the spinel in harzburgite (see Figure 4.5.).

The chronological order for the spinel formation in harzburgite, therefore, appears to be (1) porphyroclastic (residual); (2) exsolved. The residual spinel, as stated above, forms as a consequence of the incongruent melting of chromian diopside during the partial melting of the spinel lherzolite source material. During this partial melting event the Al_2O_3 content of the pyroxenes is lowered (see Appendix II), leaving, apparently, an equilibrium situation for that particular P-T regime. However, the rare occurrence of exsolved spinel in orthopyroxene implies an attempt by the minerals in harzburgite during subsolidus cooling, to reequilibrate to the local P-T conditions.

Although a difference in composition between residual and exsolved spinels should exist as a result of their distinct origins, no microprobe analyses have yet been made to show this. In addition, a decrease in the Cr/Al ratio for both

spinel types should occur during the recrystallization of these spinels, but again no chemical data are available.

4. Dunite

a. Origin, Compositional Variation and Equilibration

Chrome-rich spinels may be either a residual product from partial melting or the product of fractional crystallization (Dickey and Yoder, 1972). On the basis of textural evidence (Chapter 2, section I.2.B.3., Table 2.1. and Chapter 4, section II.4.B.3., Table 4.1.) and petrogenetic modelling (Chapter 5, sections II.5.A. and II.5.B.) the dunites, and therefore the chrome-rich spinel, of the White Hills Peridotite have been shown to be products of fractional crystallization. This hypothesis is adhered to in this section (Figure 5.12.).

Although the initial compositions of the cumulus spinels in dunite of the White Hills cannot be determined due to extensive subsolidus mineral - host rock equilibration, some idea of their initial composition can be obtained by examining the present composition of spinels from the larger dunite bodies. Within these bodies the Cr/Al ratio is approximately 0.800 (Table AII.14.), which, as has been shown in Chapter 4, is lower than the Cr/Al ratio for spinels in dunite of the cumulate dunite zone from the Bay of Islands Complex and for most spinels in harzburgite from the White Hills. The composition of spinel in dunite of the White Hills Peridotite and the differences in spinel composition in dunite between the White Hills and most other ophiolites (e.g., Bay of Islands, Troodos, Oman, etc.) may be explained, in part or total, by differences in (1) the degree of partial melting of the spinel

lherzolite source material, (2) crystallization pressures of spinel formation, and (3) subsolidus mineral - host rock equilibration.

(i) partial melting

Recalling the discussion on harzburgite spinel origins, the experimental results of Dickey et al (1971) and Dickey and Yoder (1972) indicate that at moderate pressures (< 10 kb) in the system $CaO-MgO-Al_2O_3-SiO_2-Cr_2O_3$, chromian diopside melts incongruently to chrome-rich spinel plus liquid. In addition, at supersolidus temperatures the Cr/Al ratio of spinel increases because of the relationships $D^{Cr}_{spinel-liquid} > 1$ and $D^{Al}_{liquid-rock} > D^{Cr}_{spinel-liquid}$ (Dickey and Yoder, 1972). On the basis of these relationships and the results of Chapter 5, section II.5.A., which show that the partial melting of the spinel lherzolite source material of the White Hills did not advance far enough to eliminate clinopyroxene from the residuum, it is suggested that these processes may have a bearing on the initial Cr/Al ratios of the spinels that crystallize, during olivine fractionation, from the first-stage partial melt (olivine tholeiitic).

Although these relationships may apply only to the White Hills, it must be pointed out that only small amounts of chromium in the melt are needed to promote the crystallization of chrome-rich spinel at low pressures (Keith, 1954) (Figure 5.18.).

Figure 5.18. The system $MgO-SiO_2-Cr_2O_3$ at atmospheric pressure (from Keith, 1954).

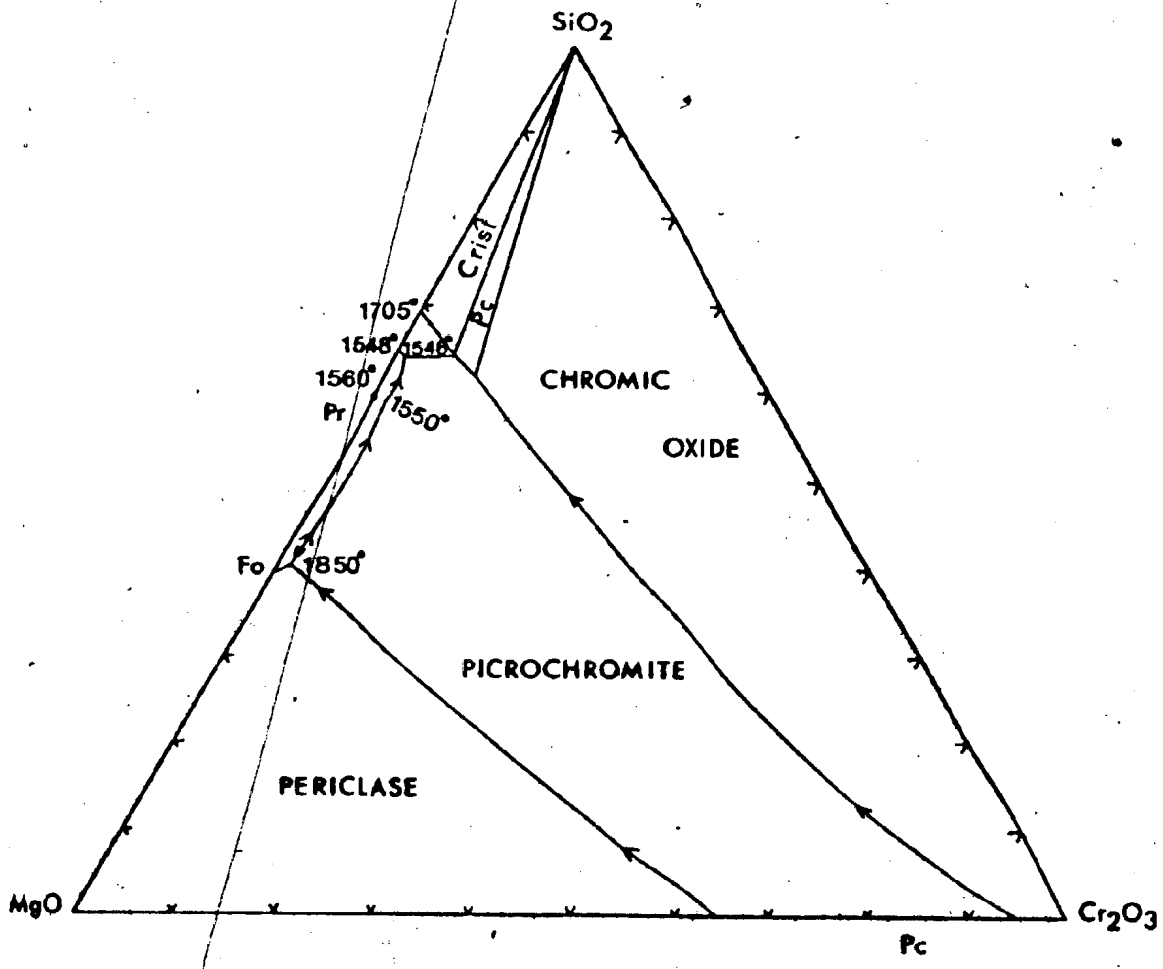
SiO2
Crist
Pc
1705°
1548°
1546°
1560°
Pr
1550°
CHROMIC
OXIDE
Fo
1850°
PICROCHROMITE
PERICLASE
MgO
Cr2O3
Pc

Clearly, however, even with these apparent restrictions, the partial melting hypothesis appears to be supported in part by the spinel and associated rock compositions (i.e., nearly clinopyroxene-free harzburgite) from the Bay of Islands (Malpas and Strong, 1975; Malpas, 1976) and Troodos (Greenbaum, 1977) ophiolites where, for each occurrence, the spinels in dunite have similar or higher Cr/Al ratios than in harzburgite and dunite from the White Hills. Thus the total elimination of clinopyroxene from the harzburgite residuum seems necessary in order to produce spinels, from the first-stage partial melt, with Cr/Al ratios higher than the spinels in dunite from the White Hills Peridotite. Clearly, if the assumption that the presence of clinopyroxene in the harzburgite residuum does affect the Cr-content of the liquid by lowering its absolute abundance is correct, then this change may cause the bulk composition of the liquid to lie closer to the MgO-SiO_2 join of the MgO-SiO_2-Cr_2O_3 triangle (see Figure 5.18.), thereby negating the opportunity for large-scale chromite crystallization from the liquid.

(ii) crystallization of spinel at elevated pressures

The Cr/Al ratio of spinel in dunite may not initially be controlled by the presence or removal of clinopyroxene from the source material during partial melting, but may be dependent on the pressure at which the spinel crystallizes.

Experimental studies by Green et al (1971), and Green et al (1972) on lunar basalts of various compositions (Apollo 12: samples 12009, 12021, 12022, 12040, 12065 and Apollo 14: sample 14310) at pressures from 1 atmosphere to 30 kilobars have established that the composition of the liquidus or near liquidus spinel is sensitive to pressure. The experimentally crystallized spinels from sample 14310 (plagioclase-rich basalt) at 5 and 7 kilobars show a marked change in Cr/(Cr+Al) ratio (wt.%) from 0.238 to 0.148, respectively.

Spinel phenocrysts in oceanic basalts of various bulk compositions have a wide range in Cr/(Cr+Al) ratios ($\sim$ 0.2 to 0.6) (Dick, 1976b; Sigurdsson and Schilling, 1976; Fisk and Bence, 1980). Extreme Cr/(Cr+Al) ratio variations also occur within individual pillow basalts (Fisk and Bence, 1980). These workers attribute the high relative Al_2O_3 content of spinel phenocrysts, regardless of bulk rock composition, to crystallization at high pressures.

Additional statements regarding the partitioning of Al_2O_3 and Cr_2O_3 into spinel as a function of pressure must await further experimental studies.

(iii) subsolidus equilibration

Although the compositions of spinels in dunite appear to initially reflect either differences in the extent of partial melting of the spinel lherzolite source material or the pressure at which the spinels crystallize, the present spinel compositional variation in dunite can be explained by subsolidus equilibration with the host rock. For example, spinel in

dunite interlayered with, or as dikes intruding spinel lherzolite and harzburgite (i.e., groups 1 and 3, Chapter 4, section II.4.C.3.) have similar compositions (Figure 4.8.). The spinels from these dunite bodies are suggested to have undergone subsolidus equilibration of their spinel chemistry to that of the dominant rock type that either surrounds or that is adjacent to these dunites by lowering their spinel Cr/Al ratio (see page 235).

Judging from the various spinel compositions in the dunite bodies, the extent of subsolidus equilibration is then apparently dependent on the size of the dunite body and bulk composition of the host rock. For example, in the larger dunite bodies, the spinels appear to show limited subsolidus equilibration with the surrounding or adjacent host rock.* Clearly then, limited subsolidus equilibration of these spinels with the adjacent lithologies occurs because the spinels are sealed off from extensive equilibration with the adjacent lithologies by the large volume of olivine. No compositional zoning in spinel has yet been found in dunite layers which support the above statements.

(iv) summary

In summary, the spinels in dunite are suggested to have crystallized from the first-stage partial melt liquid derived

* Spinel in dunite sample 78117 (Table AII.14.), does show zoning. This sample has been collected from near the center of the dunite body but it is not known whether the surface outcrop center of the body is the core of the body.

from the spinel lherzolite. The low Cr/Al ratios of these spinels are either a direct consequence of the incomplete melting of spinel lherzolite that left a small modal volume of clinopyroxene in the harzburgite residuum or crystallization at moderate to high pressures ($\geq$ 10 kb?). The Cr/Al ratios of most spinels in dunite have been further lowered to values of the surrounding or adjacent lithologies during subsolidus equilibration.

5. Chromite

a. General Statement

Information regarding the various aspects of the chromite-related lithologies has been presented in Chapters 2, 3, and 4. Briefly, these discussions have pointed out that (1) the chromite-related lithologies are chromitite, low-alumina orthopyroxenite and "websterite", (2) the compositions of the minerals of these lithologies are distinct from all other lithologies of the White Hills Peridotite, and (3) it is principally on contrasting mineral compositions that the chromite-related lithologies are suggested to have crystallized at low pressure from a second-stage partial melt liquid (with limited or no mixing with the first-stage partial melt liquid) derived from the advanced partial melting of the nearly depleted spinel lherzolite.

In the following discussion a crystallization model based on these lithological and geochemical restrictions is proposed.

b. Crystallization Model

(i) chromite-related lithologies - inferred crystallization order

The inferred mineral crystallization order, determined solely by petrography for the chromite pod is: (olivine + chromite), chromite or orthopyroxene, orthopyroxene or chromite, clinopyroxene (+ orthopyroxene). The corresponding rock sequence is (dunite), chromitite, orthopyroxenite, "websterite", respectively. The presence or absence of a dunite component in this sequence cannot be established but it has been included strictly to simplify and to accomodate the phase relationships for the system $MgO-SiO_2-Cr_2O_3$ (Figure 5.18.) used in the proposed crystallization model. There may have been reversals in the proposed crystallization order. For example, one orthopyroxenite vein emanating, and apparently originating, from the pod is zoned (Plate 9.F.). Its central region is massive cumulus chromite in an orthopyroxene (+ minor clinopyroxene) matrix; the margins are predominantly cumulus orthopyroxene with a trace of cumulus clinopyroxene. The intercumulus minerals are olivine and clinopyroxene throughout. Cumulus chromite in contact with cumulus orthopyroxene has been partially resorbed. The inferred crystallization order is: orthopyroxene, clinopyroxene, chromite.

(ii) mechanisms for initiating chromite crystallization and internal restrictions

There are several possible mechanisms for initiating chromite crystallization from a liquid of basaltic composition during fractionation. In general, the mechanisms are

(1) changes in oxygen fugacity (f_{O_2}) (Ulmer, 1969), (2) large influxes of new (undifferentiated) magma (Bichan, 1969), (3) blending or contaminating of liquids (Irvine, 1975; 1977), and (4) fluctuating total pressure of the crystallizing system to cause a change in the position of the silicate-chromite cotectic (Cameron, 1978; 1980).

Due to the lack of <u>initial</u> f_{O_2} data for the spinel phases and evidence for large influxes of magma in the White Hills, mechanisms (1) and (2) are not considered in this discussion. Rather the Irvine and Cameron mechanisms have been selected because they appear to better suit the data at hand (e.g., two generations of liquids) at this time.

(iii) systematics of the selected mechanisms

The mechanism for chromite crystallization as described by Irvine (1977) involves the mixing or blending of an undifferentiated liquid of, for example, picritic tholeiite composition with a relatively differentiated liquid (i.e., more siliceous). The mixing of these two liquids produces a hybrid liquid bulk composition which due to the mixing and mutual solution should be forced from the silicate-chromite cotectic to a position in the picrochromite phase volume (Figures 5.18. and 5.19.A.). Chromite must therefore crystallize from the liquid in order to return the liquid composition to a position on the silicate-chromite cotectic. Hence, the liquid mixing process initiates periods of chromite crystallization that result in the formation of chromitite seams.

Figure 5.19. Phase diagram models illustrating the possible paths of crystallization of the chromite-related lithologies. See text for explanation.

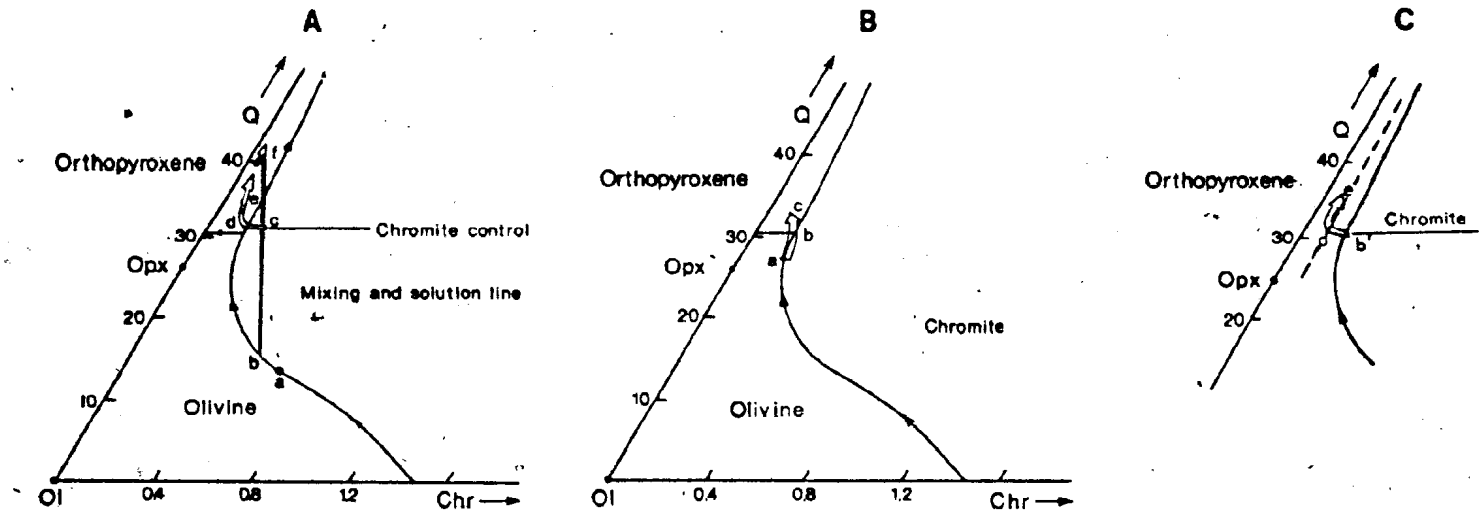
A
Q
Orthopyroxene
40
30
20
10
Opx
Olivine
Chromite control
Mixing and solution line
f
e
d
c
b
a
Ol
0.4
0.8
1.2
Chr
B
Q
Orthopyroxene
40
30
20
10
Opx
Olivine
Chromite
c
b
a
Ol
0.4
0.8
1.2
Chr
C
Q
Orthopyroxene
40
30
20
Opx
Chromite
b'

The chromite crystallization initiating mechanism proposed by Cameron (1978; 1980) envisages the change in position of the silicate-chromite cotectic by fluctuating total pressure on the system due to the escape of volatiles through fractures in the magma chamber roof.

Although these aforementioned mechanisms appear appropriate for the White Hills there are initially several key areas for which data are not yet available. These are (1) the lack of bulk rock chemistries for these lithologies, (2) the lack of evidence in the geological record of the White Hills supporting total pressure fluctuation, and (3) most important, the likely existence of a second-stage partial melt liquid.

(iv) Irvine mechanisms: an example for the formation of chromitite layers in some layered intrusions

Irvine (1977, p. 276) has described the formation of chromitite layers in some layered intrusions (e.g., Muskox, Stillwater, Great Dyke, Bushveld) using his magma mixing mechanism. This procedure is fully described in Irvine (1975; 1977) and, therefore, only the important points are discussed here. Figure 5.19.A. has been taken directly from Irvine (1977, p. 276, Fig. 2) to facilitate this discussion.

To begin, the initial primitive liquid (∿ picritic tholeiite) of Irvine (1977) has already differentiated to position f from a (Figure 5.19.A.) without massive chromite crystallization and at f orthopyroxene is the liquidus phase (the liquid is now silica-rich). At this stage of differentiation in the Irvine model, a new primitive liquid of similar original composition to the initial liquid (i.e., ∿ point a) mixes

with the evolved liquid (i.e., liquid at point f). Several options are possible depending upon the volume of new liquid: (1) if the volume of the two liquids are similar; (2) if the volume of original liquid exceeds that for the new liquid; and (3) if the volume of original liquid is relatively small compared with the new liquid. Only option (1) is detailed in this discussion in order to avoid undue repetition of Irvine's (1977) work. The reader is referred to Irvine's paper for an explanation of options (2) and (3).

According to Irvine, before the effects of the liquid mixing are observed, the new primitive liquid, a, may differentiate along the olivine-chromite cotectic, as from a to b, crystallizing olivine and chromite, thereby producing a peridotite (dunite + chromite) layer. However at b, as a consequence of the mutual solution of these two liquids the hybrid liquid should evolve along the schematic mixing and solution line, b-c-f, toward some bulk composition such as c. At point c, the precipitation of chromite would then drive the liquid composition toward the orthopyroxene-chromite cotectic at d, where because of the orthopyroxene-chromite reaction relationship, chromite ceases to crystallize and orthopyroxene is again the liquidus phase. Thus by this magma mixing and crystallization scheme the cumulate rock sequence is:

d-f	orthopyroxenite
c-d	chromitite
a-b	dunite + chromite (peridotite)

A similar rock sequence exists for Muskox Intrusion chromite-rich layers (Irvine, 1975; 1977).

(iv) model for the origin of the chromite-related lithologies of the White Hills Peridotite

At the outset it must be pointed out that this proposed model is schematic and appears to best fit the data at hand. Clearly, more field and geochemical data would be necessary to confirm or reject this model. The phase diagrams that have been used to graphically illustrate the proposed origins of the chromite-related lithologies of the White Hills Peridotite are illustrated in Figures 5.19.B. and 5.19.C.

The primitive partial melt liquid (second-stage?) with high SiO_2 content (Figure 5.19.B., point a suggested bulk composition of second-stage partial melt liquid) is allowed to differentiate with very limited or no magma mixing with the evolved initial liquid (i.e., liquid A' of Figure 5.3.). By restricting or limiting magma mixing no unnecessary manipulation of the model is required. Differentiation of the second-stage liquid along the olivine-chromite cotectic, as from a to b, results in olivine and chromite crystallization. At b, there is both an olivine-orthopyroxene and chromite-orthopyroxene reaction relationship (Irvine, 1965; 1967) that results in no further crystallization of olivine and chromite. Thus at b orthopyroxene becomes the liquidus phase. To allow for only the crystallization of chromite from this second-stage liquid, P_{total} fluctuations are necessary to cause a shift in the position of the orthopyroxene-chromite cotectic to a position closer to the MgO-SiO_2 side of the MgO-SiO_2-Cr_2O_3 triangle (Figure 5.19.C.) (cf., Irvine and

Smith, 1969; Cameron, 1978)*. The change in the position of cotectic does several things: (1) leaves the liquid composition in the chromite field (point b'); (2) ceases the crystallization of orthopyroxene; and (3) initiates chromite crystallization. Chromite crystallizes until the orthopyroxene-chromite cotectic is intersected, point d, as a result of either chromite crystallization or another change in P_{total}, and then orthopyroxene crystallization is resumed. The addition or buildup of CaO as a component to the system, possibly as a result of differentiation (or unknown phase relationships) may promote the crystallization of clinopyroxene at some stage in this model (cf., Irvine and Smith, 1967). The rock sequence for this differentiation model is:

d* - e	orthopyroxenite (± "websterite")
b'- d	chromitite
c - ?	orthopyroxenite (± "websterite")
a - b	dunite + chromite

The fluctuation of P_{total} at different times during differentiation can change the order of appearance of any phase. In addition, periodic fluctuations of P_{total} can repeat parts of the aforementioned crystallized rock sequence.

(v) discussion of the proposed model and the Irvine model

Although these schematic crystallization models appear to satisfy the inferred pod crystallization order, both models have their drawbacks and neither is totally satisfactory. For example, with case A (Figure 5.19.A.) the principal

* The amount of change in P_{total} required to cause a movement in the position of the cotectic necessary to initaae chromite crystallization is presently not known.

drawback is proving if and when magma mixing occurs. The questions raised in this respect are: where in the differentiation sequence of the initial primitive liquid does the mixing with the second liquid occur? If the mixing has occurred before the crystallization of the gabbro components (i.e., clinopyroxene, olivine, plagioclase), why do the pyroxenes of the pod silicate minerals have a low Al_2O_3 and TiO_2 contents and the spinel low in TiO_2? If the magma post-dates the crystallization of the gabbro veins why has no evidence for this unmixed, differentiated liquid been found in the peridotite? Other unanswered questions are: How would the high Fo and En contents of the pod silicate minerals be produced from the mixing of these distinct liquids? What would the composition of the hybrid liquid resemble if it reaches the surface (this depends upon when during differentiation of the initial liquid the second liquid mixes with it and how much differentiation of the hybrid liquid takes place)?

It is apparent, that although the magma mixing mechanism shows promise when applied to layered intrusions for the formation of chromitite layers as part of a cyclic sequence, the definite lack of knowledge regarding the relationships among the pod lithologies and the paucity of this type of chromitite-silicate occurrence in ophiolite upper mantle sections severly limits the application of a magma mixing mechanism to ophiolite peridotite sections at this time.

The chromite crystallization model described in Figures 5.19.B. and 5.19.C. appears more attractive an explanation for the mineral crystallization order of the pod, the zoned orthopyroxenite vein, and for the mineral chemistries, than case A. The principal drawback to this mechanism is, as mentioned earlier, the existence of a second-stage partial melt liquid. If this liquid does exist, then the inferred cumulate rock sequence can be produced by fluctuating changes in P_{total}.

c. Summary

In summary, whatever argument is used, the chromite-related lithologies are suggested to have crystallized from a second-stage partial melt liquid derived by advanced partial melting of the clinopyroxene-bearing harzburgite residuum. The mechanism that initiated chromite crystallization may have been a fluctuation in P_{total} for reasons that at present are not known, possibly during the ascent of the peridotite diapir. The mixing of the evolved initial liquid (first-stage liquid) and the new liquid (second-stage liquid) may have contributed to the chromite crystallization process.

6. Gabbro and Pyroxenite Veins

a. General Statement

The most common mineral assemblages in the gabbro veins are:

olivine + clinopyroxene + orthopyroxene + plagioclase + spinel (c)

olivine + clinopyroxene + orthopyroxene ± spinel (h)

Mineral assemblage (h) (± orthopyroxene) is also the most common spinel-silicate association in the websterite, wehrlite

and clinopyroxenite veins.

The spinels of these mineral assemblages are anhedral and interstitial to the recrystallized and non-recrystallized silicates. Commonly all minerals are in contact or in relative close proximity with each other. In addition, spinel exsolution lamellae and droplets occur more commonly in recrystallized plagioclase, clinopyroxene and olivine than in the non-recrystallized silicates.

The origin and petrogenetic history for spinel in these rocks are illustrated in Figure 5.12.

b. Mechanisms for Spinel Formation and Interpretation

(i) plagioclase + olivine reaction

A possible simplified reaction, based on the instability of olivine and plagioclase at elevated pressures (Kushiro and Yoder, 1966), is suggested to explain the formation of spinel in the gabbro veins

$$\text{plagioclase} + \text{olivine} \pm \text{alumina-rich clinopyroxene} + \text{alumina-rich orthopyroxene} + \text{spinel} (\pm \text{olivine}) \qquad (5.3)$$

In addition, this reaction can produce mineral assemblages (c) and (h) depending upon the initial quantities of the reactants and whether equilibrium is achieved.

Reaction (5.3), which marks the boundary between plagioclase lherzolite and spinel lherzolite, has been studied experimentally in simple and complex natural systems by Kushiro and Yoder (1966), Green and Hibberson (1970), Emslie (1970) and Herzberg (1976a, b). The experimental results of these studies indicate that the slopes ($^{dp}/_{dt}$) of the

equilibrium curves fall into two groups, those with slightly positive slopes (Kushiro and Yoder, 1966; Herzberg, 1976b) and those with zero slope (Emslie, 1970; Green and Hibberson, 1970; Herzberg, 1976a). In addition, these experimental results indicate that the reaction can be initiated over a large range in pressure and temperature from approximately 6 kilobars to 10 kilobars and 900°C to 1300°C.* Clearly, then, for the former case, and as has been suggested by Gardner and Robins (1974), there are a great number of possible P-T paths along which plagioclase and olivine can be made to react, but for the zero slope equilibrium curves a pressure increase is required for the olivine + plagioclase reaction to proceed.

(ii) application of reaction (5.3) to the White Hills Peridotite gabbros

There is one limiting fact which clearly restricts the application of the zero slope equilibrium curves to the White Hills gabbro, i.e., no event involving a pressure increase has been preserved in the petrological history of the White Hills. Then, if the selection of reaction (5.3) is valid for these rocks, either isobaric cooling or cooling accompanied by decreasing pressure must have initiated the reaction.

To recall from previous chapters, the gabbro veins are thought to have crystallized at pressures of approximately 7 kilobars to 10 kilobars and the porphyroclastic texture is

* The ranges in temperature and pressure are mainly due to seeding and technical problems and whether the reactants are pure end members or complex natural minerals.

suggested to have formed in the uppermost mantle. Therefore, an upper pressure limit of approximately 10 kilobars or less is assumed, but the temperature at which reaction (5.3) commenced cannot be determined due to the overprinting of the original cumulate texture by the porphyroclastic texture. However, a maximum temperature of approximately 1050°C (Wyllie, 1971) is estimated assuming an upper pressure limit of 10 kilobars and anhydrous cooling (i.e., solidus for basaltic composition at 10 kb anhydrous).

The pressures at constant temperatures at which reaction (5.3) may occur have been further refined by Frost (1976). He has thermodynamically evaluated the Kushiro and Yoder (1966) experimental results for reaction (5.3) and has obtained pressure and temperature values of 6.4 kilobars and 715°C* to initiate the reaction. Surprisingly, this pressure is within 0.2 kilobars of the value obtained when the Kushiro and Yoder (1966) equilibrium curve is extrapolated to 715°C. However, the pressure at which the reaction occurs is dependent on the amount of alumina in the spinel (Y_{Al}^{Sp}). The pressure estimates for reaction (5.3) to commence using the geochemical data of the White Hills is 6 kilobars (± 0.5 kb) (Frost, 1976, p. 745, Fig. 9) at a fixed temperature of 715°C. However, even if the 715°C for initiating reaction (5.3) for the White Hills gabbros is incorrect, the steep

* The temperature 715°C is the calculated chlorite breakdown temperature (between 2 kb and 4 kb) for the reaction
chlorite = forsterite + enstatite + spinel + H_2O
in the metaperidotite of the Ingalls Complex (Frost, 1976).

positive slope ($^{dp}/_{dt}$) for the Kushiro and Yoder (1966) equilibrium curve indicate that the error in estimating the pressure for reaction (5.3) is not very different between 700°C and 1000°C, i.e., approximately 1 kilobar.

To summarize, it is suggested, although with reservations, that for the White Hills gabbro, spinel forms due to the instability of coexisting olivine and plagioclase as a result of cooling from magmatic temperatures. The influence of recrystallization of the primary igneous textures cannot, however, at this time be evaluated.

(iii) spinel exsolved by silicates.

Spinel exsolution from plagioclase, olivine, and clinopyroxene has been reported from mafic and ultramafic xenoliths (Talbot et al., 1966; Lovering and White, 1969; Wass, 1973; Wilkinson, 1975), mafic cumulates (Talkington and Gaudette, in prep.), and lherzolite intrusions (Dickey, 1970).

Wass (1973) suggests spinel exsolved by plagioclase is a result of the plagioclase reacting with Mg and Fe^{2+} ions trapped in the plagioclase. She bases her theory on the results from a study of cumulate aggregates of plagioclase and spinel in alkali basalt flows from New South Wales, Australia. In her samples, she has found a compositional difference between plagioclase surrounding exsolved spinel (halo region) and the host plagioclase; within the halo region, the plagioclase is An_{40}, outside the halo region the plagioclase is An_{59}. In addition, FeO and MgO are low in the halo region, approximately 0.08 weight percent and 0.05 weight percent,

respectively, and relatively high in the host plagioclase, approximately 0.80 weight percent and 0.45 weight percent, respectively. From her calculations, based on the modal proportions of spinel in plagioclase (∿ 2% ± 50%), the minimum values for FeO and MgO needed to form the spinel are 0.60 weight percent and 0.35 weight percent, respectively. Although no quantitative estimate for the amount of spinel in plagioclase has yet been made nor have halos around spinel and high MgO and FeO amounts been noted for the White Hills Peridotite gabbros, the 2 percent spinel in plagioclase estimated by Wass from her calculations seems high for the White Hills, and also, the amounts of FeO and MgO in plagioclase of the White Hills Peridotite (Table AII.13.) are commonly less than the values within the halo region she decribes. Therefore, if spinel is to form in plagioclase of the White Hills Peridotite, MgO and FeO must be supplied to the system. In this respect, Whitney (1972) and Wilkinson (1975) propose a reaction whereby spinel results from the diffusion of Mg and Fe^{2+} ions into plagioclase:

$$\text{calcic plagioclase} + (Mg, Fe^{2+}) \rightleftharpoons \text{spinel} + \text{less calcic plagioclase} + Ca^{2+} \qquad (5.4)$$

Spinel and more soda-rich plagioclase are produced during the recrystallization of the original igneous assemblage. In this way, high MgO and FeO contents of plagioclase are not required, only the presence of Mg-Fe silicates. Even though no systematic study has been undertaken to test for Mg-Fe diffusion or to check chemical zoning of the plagioclase

surrounding spinel, recent work by Talkington and Gaudette (in preparation) has assessed the feasibility of defining the distance over which elemental diffusion can be detected by the electron microprobe (JOEL Model JXA-50A). The results of their study indicate that for the operating conditions used for the electron microprobe analyses of this thesis (Appendix I), a 5 to 6 micron or wider region of maximum analytical resolution is present on either side of adjacent mineral phases; for an overall $\geq$ 10 micron "region of uncertainity" (Talkington and Gaudette, in preparation). Within this region no accurate assessment for the extent of elemental diffusion can be determined. These results indicate that if elemental diffusion occurs across mineral grain boundaries, the chemical zoning near the grain boundaries, if it is present, cannot be identified by the electron microprobe. In addition, the frequently small size ($\leq$ 0.05 mm) of the exsolved spinel in plagioclase of the gabbro veins makes the determination of elemental diffusion unrealistic on this scale.

The formation of spinel intergrown with clinopyroxene has been discussed by Dawson and Smith (1975). They list five possible ways in which the intergrowths may form:

(1) reaction between pre-existing phases as a result of changes in P-T conditions
(2) metasomatic replacement of the silicate by chromite
(3) subsolidus exsolution from a higher temperature solid solution
(4) simultaneous (cotectic) crystallization
(5) pressure induced subsolidus recrystallization

Dawson and Smith (1975) discount mechanisms 1 through 4 on chemical and microstructural grounds and suggest mechanism 5

is the best solution to the problem but offer no other supporting evidence for their choice other than that mechanism 5 best fits the data at hand. In comparison to Dawson and Smith's (1975) interpretation, either the breakdown of a complex pyroxene (Lovering and White, 1969; Mercier and Nicolas, 1975) or the breakdown of a highly aluminous clinopyroxene (Wilkinson, 1975) have been suggested for the intergrowth of spinel with pyroxenes.

Spinel exsolution by olivine might have been caused by the diffusion of aluminum into the olivine at high pressures in a silica-undersaturated environment (Lovering and White, 1969).

All of the above reactions to form spinel require initially high pressures ($\sim$ 7 kb) and probably a high bulk rock Al/Si ratio. Whether the aluminum diffusion mechanism for the olivine-spinel symplectite can be justified theoretically is not known to the writer, but in view of the low Al_2O_3 content for the olivine of these rocks and the high Al_2O_3 contents of the surrounding minerals (providing a large compositional gradient) the diffusion mechanism appears feasible.

(iv) spinel in websterite, wehrlite and clinopyroxenite

Similar arguments to those presented above for the formation of spinel in gabbro can be used for the formation of spinel in the websterite, wehrlite and clinopyroxenite veins. Unlike the chromium-deficient spinels of the gabbro veins, the spinels of the pyroxenites are higher in chromium probably because of the higher chromium content of the parent

pyroxenes. No evidence for the presence of plagioclase has been found in the pyroxenites and therefore the formation of spinel using reaction (5.3) is unsuitable. However, the mineral assemblages of the pyroxenite veins (cpx + opx + ol + sp) are the same as for reaction (5.2). Therefore reaction (5.2) may have been operative for these assemblages. If so, then the reaction initiating mechanism defined for reaction (5.3) may be applicable for reaction (5.2).

Chapter 6

Some Speculation on the Origin of the White Hills Peridotite

II.6.A. General Statement

During the preceding chapters of this study some of the geological and geochemical aspects of the White Hills Peridotite have been discussed. The conclusions from these discussions indicate that the White Hills Peridotite is (1) a sample of upper mantle material, (2) dominantly an interlayered sequence of spinel lherzolite and harzburgite, and (3) contains a suite of pyroxenitic, gabbroic and dunitic material in the form of veins, dikes and lenses. These results are based on field evidence and commonly accepted geological interpretations. In addition, a number of conclusions are speculative (e.g., multistage partial melting, development of various microstructures, mineral crystallization orders) although supported by experimental and theoretical results. From these conclusions a model is proposed to explain most of the geological features and history of the White Hills Peridotite. Parts of this model have already been presented (Figure 5.11.) and discussed in Chapter 5. The proposed model also takes into account the three objectives of this study (Chapter 1, section I.1.D.).

a. Proposed Model for the Origin of the White Hills Peridotite

(i) the Duncan and Green (1980) model

The proposed model for the origin of the White Hills Peridotite is similar to the proposed multistage partial melting

model of pyrolite material for the formation of oceanic crust and upper mantle material (Duncan and Green, 1980, p. 25, Fig. 2). In their model, Duncan and Green envisage an upper mantle diapir of pyrolite material rising beneath a mid-ocean ridge spreading center. At 60 kilometers to 70 kilometers depth, picritic liquids, which are termed first-stage liquids, are derived by approximately 20 percent to 30 percent partial melting of the pyrolite diapir. Olivine crystallizes from these liquids as they rise to crustal magma chambers where they then crystallize to form the majority of oceanic crustal material. The continued upwelling of the diapir, now a clinopyroxene-poor lherzolite, results in small degrees of partial melting (5% to 10%) at shallow depths (5 km to 25 km). The liquids produced from this partial melting event are referred to as second-stage liquids and are magnesian-quartz tholeiites (i.e., olivine-poor tholeiites). These liquids may rise to the surface, remain in the diapir (which is now highly refractory harzburgite), or interfinger with rocks which crystallized from first-stage liquids. Therefore, if this partial melting model proceeds to completion, which it can (Jaques and Green, 1980), an 'idealized' ophiolite stratigraphy (Figure 2.3.) may result.

(ii) proposed model for the White Hills Peridotite

The Duncan and Green (1980) model has been slightly modified and developed further and, in addition combined with the idealized ridge structure model of Ahern and Turcotte (1979) to fit the requirements of the White Hills Peridotite.

The proposed model is schematically represented in Figure 6.1. and partially illustrated in Figure 5.11. The model is first presented then the various parts of the model which have not been treated in previous chapters are discussed.

In the proposed model (Figure 6.1.) an upper mantle diapir of lherzolitic material is thought to convectively rise through the upper mantle either directly below the spreading ridge axis or slightly off-axis. At a depth of approximately 60 kilometers (~ 20 kb) the anhydrous peridotite solidus is intersected and partial melting of the diapir commences. From this depth to approximately 25 kilometers first-stage partial melt liquids of olivine tholeiitic composition are produced by approximately 20 percent partial melting of the lherzolitic diapir. As a result of this partial melting event, most of the basaltic components (especially Na, K, Ti, LREE, etc.) are removed leaving a residuum which is barren of most of these components. However, this partial melting event has not advanced far enough to remove all of the clinopyroxene from the lherzolitic source diapir. Therefore, the residuum after first-stage partial melting is a clinopyroxene-poor lherzolite (nearly depleted lherzolite). During the upwelling of the diapir, which consists at any one time of a solid/liquid mixture, polybaric mineral crystallization of the first-stage liquid produces the suite of pyroxenite (high-alumina), gabbro, and most dunite veins and bodies. These veins may represent an interconnecting network of magma conduits.

Figure 6.1. Schematic representation of the proposed model for the White Hills Peridotite. The model is a slightly modified version of the Duncan and Green (1980) multistage partial melting of upper mantle diapirs for the origin of oceanic lithosphere. The currently proposed model also uses the theoretical modelling results for an idealized ridge structure (Ahern and Turcotte, 1979). Solidus and degrees of partial melting (15% and 25%) lines from Ahern and Turcotte (1979). Solid lines with arrows indicate direction of movement of asthenosphere away from the accreting ridge. Trapped region is the hypothesized location where the ascent of the White Hills Peridotite source diapir may have ceased (see text for explanation).

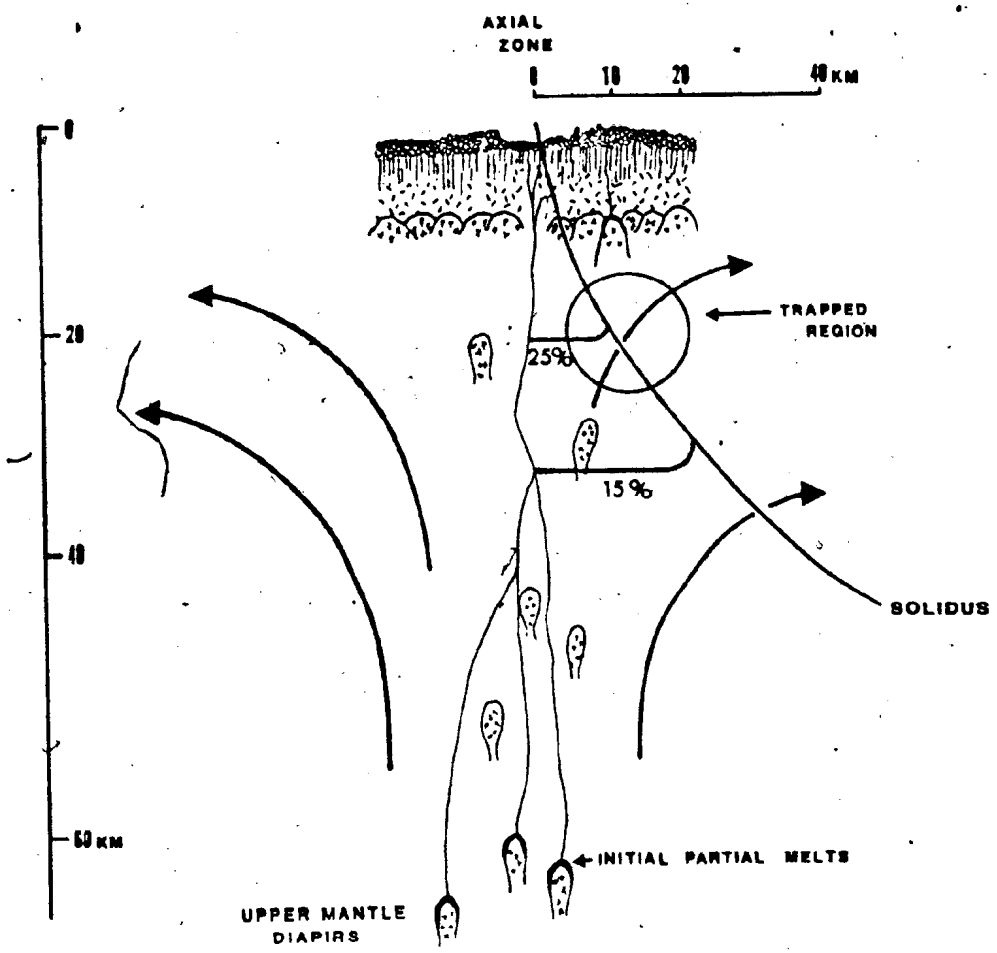
AXIAL
ZONE
0
10
20
40 KM
0
20
40
60 KM
TRAPPED
REGION
25%
15%
SOLIDUS
INITIAL PARTIAL MELTS
UPPER MANTLE
DIAPIRS

At a later stage in the upwelling of the diapir above 25 kilometers and possibly within the 'trapped region' (Figure 6.1.) (i.e., slightly off-axis), localized partial melting (~ 5% to 10%) of the clinopyroxene-poor lherzolite produces a volumetrically insignificant amount of magnesian-quartz tholeiite (olivine-poor tholeiite) second-stage liquid. Low pressure crystallization of the localized second-stage liquid produces the chromite-related lithologies (low-alumina orthopyroxenite, "websterite", and chromitite). The residual material produced from second-stage partial melting is a highly refractory harzburgite.

Although speculative, it is suggested that within the 'trapped region' the upwelling of the diapir may have been arrested due to the intersection with the solidus as a result of the off-axis ascent of diapir. Accordingly, the closer the ascent trajectory of the diapir to the center of the ridge axis, the greater the opportunity for extensive (i.e., advanced) partial melting. Clearly, this implies that the basaltic components of the diapir are more likely to be completely removed when the ascent trajectory is near the center of the ridge axis and this also suggests that the residuum produced in this region as a result of partial melting is devoid of basaltic components and therefore should be highly refractory (i.e., harzburgitic).

Thus, to this point in the model two of the three objectives for this study, i.e., origins of vein material and spinel phases, have been accounted for. Part of the

third objective, the origin of the lithological layering is problematic for a couple of reasons. For example, the timing of the formation of the majority of the vein material can be determined by crosscutting relationships, except in a few instances (Chapter 2, section I.2.B.). In most of these examples, the formation of the layering apparently predates the formation of most, if not all, vein material. Accordingly, this relationship limits the number of options available for the timing of formation of the lithological layering, but not the mechanisms (e.g., pressure solution, metamorphic differentiation). At this time no explanation for the formation of the lithological layering is offered in the context of the proposed model of origin of the White Hills Peridotite. However, utilizing some aspects of the White Hills Peridotite model and integrating these with the Dick and Sinton (1979) hypothesis for the origin of lithological layering by pressure solution-metamorphic differentiation (see Chapters 2 and 5) may offer some explanation to the type of layered sequence that can be expected in peridotites. For example, if the White Hills Peridotite source diapir did have an off-axis ascent trajectory, then extensive partial melting of the diapir, which most likely occurs during upwelling directly beneath the ridge axis (see Figure 6.1.) (cf., Sleep, 1974; Bottinga and Allegre, 1978; Ahern and Turcotte, 1979), may not occur. Therefore, a mid-axis ascent would remove nearly all of the basaltic components from the rising diapir resulting in a highly refractory residuum and possibly, according to Dick and Sinton (1979), a peridotite with harzburgite and

dunite layers compared with layers of spinel lherzolite, harzburgite and dunite produced during an off-axis ascent history. Although this difference in the location of the ascent trajectory may make a difference in the lithologies of the layered sequence, this argument cannot be used to explain the crosscutting relationships of the vein material and the lithological layering. Even though no alternative mechanism is offered, by far the most important fact for not applying the Dick and Sinton (1979) sequence of events and mechanisms for the formation of vein material and lithological layering of the White Hills Peridotite is the range of modal varieties of pyroxenite vein material. Because of this range, the rather simple high temperature and pressure solution-metamorphic differentiation model is therefore probably applicable only to peridotites which contain a restricted variety of pyroxenite vein types (e.g., dunite, orthopyroxenite, and websterite).

In summary, the White Hills Peridotite is thought to represent the residuum from at least two partial melting events. The first partial melting of the lherzolitic source occurred at high pressures ($\sim$ 20 kb) and produced olivine tholeiitic liquids (first-stage liquids) which crystallized at moderate to high pressures to form most of the pyroxenite, gabbro and dunite veins and bodies. The second partial melting event occurred at low pressures and produced a magnesian-quartz tholeiite liquid (second-stage liquid) which crystallized also at low pressures to form the chromite-related lithologies.

The residual material from the first-stage partial melting event is a clinopyroxene-poor lherzolite and from the second partial melting event, a highly refractory harzburgite.

The presence of clinopyroxene in the residuum after first-stage partial melting is suggested to be the result of limited partial melting of the diapir due to the off-axis ascent trajectory. The formation of the lithological layering may have been the result of an ongoing pressure solution-metamorphic differentiation event during upwelling of the diapir, however the timing for the formation of the layering must predate the pyroxenite vein formation, thereby placing petrological and time constraints on the formation of the lithological layering.

REFERENCES

REFERENCES

Ahern, J.L.,and Turcotte, D.L., 1979. Magma migration beneath an ocean ridge. Earth Planet. Sci. Lett., 45, 115-122.

Allen, C.R., 1975. The petrology of a portion of the Troodos plutonic complex, Cyprus. Unpubl. Ph.D. thesis, Cambridge University.

Anastasiou, P., and Seifert, F., 1972. Solid solubility of Al_2O_3 in enstatite at high temperatures and 1-5 kb water pressure. Contr. Mineral. Petrol., 34, 272-287.

Aoki, K.,and Prinz, M., 1974. Chromian spinels in lherzolite inclusions from Itinome-gata, Japan. Contr. Mineral. Petrol., 46, 249-256.

Arai, S., 1980. Dunite-harzburgite-chromitite complexes as refractory residue in the Sangun-Yamaguchi Zone, Western Japan. J. Petrol., 21, 141-165.

Ave'Lallemant, H.G.,and Carter, N.L., 1970. Syntectonic recrystallization of olivine and modes of flow in the upper mantle. Bull. Geol. Soc. America, 81, 2203-2220.

Bailey, E.H.,and Blake, M.C.,Jr. 1974. Major chemical characteristics of Mesozoic coast range ophiolites in California. J. Res. U.S. Geol. Surv., 2, 637-656.

Basu, A.R., 1977. Textures, microstructures and deformation of ultramafic xenoliths from San Quinton, Baja California. Tectonophysics, 43, 213-246.

Basu, A.R., and MacGregor, I.D., 1975. Chromite spinels from ultramafic xenoliths. Geochim. Cosmochim. Acta, 39, 937-945.

Bezzi, A., and Piccardo, G.B., 1971. Structural features of the Ligurian ophiolites: petrologic evidence for the "oceanic" floor of the northern Apennines geosyncline; a contribution to the problem of the Alpinetype gabbro-peridotite associations. Mem. Soc. Geol. It., 10, 55-63.

Bichan, R., 1969. Origin of chromite seams in the Hartley Complex of the Great Dyke. in H.D.B. Wilson (ed.), Magmatic Ore Deposits. Econ. Geol., Mono., 4, 95-113.

Bird, M.L., and Clark, A.L., 1976. Microprobe study of olivine chromitites of the Goodnews Bay Ultramafic Complex, Alaska, and the occurrence of platinum. J. Research U.S. Geol. Survey, 4, 6, Nov-Dec, 717-725.

Bottinga, Y., and Allègre, C.J., 1978. Partial melting under spreading ridges. Phil. Trans. R. Soc. London, A. 288, 501-525.

Boudier, F., 1976. Le Massif Lherzolitique de Lanzo (Alpes Piemontaises) etude structurale et petrologique. Le titre de docteur d'etat, Universite de Nantes.

Boudier, F., and Nicolas, A., 1977. Structural controls on partial melting in the Lanzo Peridotites. in Magma Genesis, H.J.B. Dick (ed.), Oregon Department of Geology and Mineral Industries, Bull., 96, 63-78.

Boudier, F., and Coleman, R.G., in press. Cross section through the peridotite in the Samail ophiolite, southeastern Oman Mountains, J. Geophys. Res.

Bowen, N.L., and Tuttle, O.F., 1949. The system MgO-SiO_2-H_2O. Bull. Geol. Soc. Amer., 60, 439-460.

Boyd, F.R., and England, J.L., 1964. The system enstatite-pyrope. Carnegie Inst. Wash. Yb., 63, 157-161.

Boyd, F.R., and Schairer, J.F., 1964. The system $MgSiO_3$-$CaMgSi_2O_6$. J. Petrol., 5, 275-309.

Buddington. A.F., and Hess; H.H., 1937. Layered peridotite laccoliths in the Trout River area, Newfoundland. Am. J. Sci., 33, 380-388.

Burns, R.G., 1973. The partitioning of trace elements in crystal structures: a provocative review with applications to mantle geochemistry. Geochim. Cosmochim. Acta, 37, 2395-2403.

Calon, T., 1980. Mylonites at the base of the ophiolitic White Hills Peridotite, Northern Newfoundland (abstr.). Geol. Soc. Amer., Abstracts with Programs, 12, 2, 27.

Capedri, S., and Venturelli, G., 1979. Clinopyroxene composition of ophiolitic metabasalts in the Mediterranean area. Earth Planet. Sci. Lett., 43, 61-73.

Cameron, E.N., 1978. The lower zone of the Eastern Bushveld Complex in the Olifants River Trough. J. Petrol., 19, 3, 437-462.

Cameron, E.N., 1980. Evolution of the lower critical zone, central sector, Eastern Bushveld Complex, and its chromite deposits. Econ. Geol., 75, 845-871.

Cawthorn, R.G., 1975. Petrochemical subtraction calculation (program F). Department of Geology, Memorial University of Newfoundland, unpubl. computer program.

Church, W.R., 1972. Ophiolite: its definition, origin as oceanic crust, and mode of emplacement in orogenic belts, with special reference to the Appalachians. Pub. Earth Phys. Branch, Dept. Energy, Mines and Res., Canada, 42, 71-86.

Church, W.R., and Stevens, R.K., 1971. Early Paleozoic ophiolite complexes of the Newfoundland Appalachians as mantle-oceanic crust sequences. J. Geophys. Res., 76, 1460-1466.

Church, W.R., and Riccio, L., 1977. Fractionation trends in the Bay of Islands ophiolites of Newfoundland: polycyclic cumulate sequences in ophiolites and their classification. Can. J. Earth Sci., 14, 1156-1165.

Clarke, D.B., 1970. Tertiary basalts of Baffin Bay: Possible primary magma from the mantle. Contr. Mineral. Petrol., 25, 203-224.

Coish, R.A., and Church, W.R., 1979. Igneous geochemistry of mafic rocks in the Betts Cove Ophiolite, Newfoundland. Contr. Mineral. Petrol., 70, 29-39.

Coombs, D.S., C.A. Landis, R.J. Norris, J.M. Sinton, D.J. Borns, and D. Craw, 1976. The Dun Mountain ophiolite belt, New Zealand, its tectonic setting, constitution, and origin, with special reference to the southern portion. Am. J. Sci., 276, 561-603.

Cooper, J.R., 1936. Geology of the southern half of the Bay of Islands igneous complex. Nfld. Dept. Nat. Res. Geol. Sec. Bull., 4, 62p.

Cooper, J.R., 1937. Geology and mineral deposits of the Hare Bay area. Geol. Surv. Nfld., Bull., 9, 28p.

Cremer, V., 1969. Die Mischkristallbildung im system chromit-magnetit-hercynit zwischen 1000°C und 500°C. Neues. Jahrb. Mineral. Abh., III, 184-205.

Dallmeyer, R.D., 1977. Diachronous ophiolite obduction in western Newfoundland: evidence from $^{40}Ar/^{39}Ar$ ages of the Hare Bay metamorphic aureole. Am. J. Sci., 277, 61-72.

Dallmeyer, R.D., and Williams, H., 1975. $^{40}Ar/^{39}Ar$ release spectra of hornblende from the Bay of Islands metamorphic aureole, western Newfoundland: their bearing on the timing of ophiolite obduction at the Ordovician continental margin of Eastern North America. Can. J. Earth Sci., 12, 1685-1690.

Danckwerth, P.A., and Newton, R.C., 1978. Experimental determination of spinel peridotite to garnet peridotite reaction in the system $MgO-Al_2O_3-SiO_2$ in the range 900°C-1,100°C and Al_2O_3 isopleths of enstatite in the spinel field. Contr. Mineral. Petrol., 66, 189-201.

Darot, M., and Boudier, F., 1975. Mineral lineations in deformed peridotites: kinematic meaning. Pétrologie, 1, 225-236.

Davis, B.T.C., and Boyd, F.R., 1966. The join $Mg_2Si_2O_6-CaMgSi_2O_6$ at 30 kilobars pressure and its application to pyroxenes from kimberlites. J. Geophys. Res., 71, 3567-3576.

Dawson, J.B., and Smith, J.V., 1975. Chromite-silicate intergrowths in upper mantle peridotites. Phys. Chem. Earth, 9, 339-350.

DeLong, C., 1976. Geology, petrography, and possible petrogenesis of the Cape Onion Formation. unpub., MSc. thesis, Memorial University of Newfoundland, 72 p.

Dewey, J.F., 1969. Evolution of the Appalachian/Caledonian Orogen. Nature, 222, 124-129.

Dick, H.J.B., 1976a. The origin and emplacement of the Josephine Peridotite of Southwestern Oregon. unpubl. Ph.D. thesis, Yale University, 409p.

Dick, H.J.B., 1976b. Spinel in fracture zone "B" and median valley basalts, FAMOUS area, Mid-Atlantic Ridge. EOS Trans. Am. Geophys. Union, 57, 341.

Dick, H.J.B., 1977. Partial Melting in the Josephine Peridotite I. The effect on mineral composition and its consequence for geobarometry and geothemometry. Am. J. Sci., 277, 801-832.

Dick, H.J.B., and Sinton, J.M., 1979. Compositional layering in alpine peridotites: evidence for pressure solution creep in the mantle. J. Geology, 87, 403-416.

Dickey, J.S.,Jr., 1970. Partial fusion products in alpine-type peridotites: Serrania de la Ronda and other examples. Mineral. Soc. Amer. Spec. Pap., 3, 33-50.

Dickey, J.S.,Jr., 1975. A hypothesis of origin for podiform chromite deposits. Geochim. Cosmochim. Acta, 39, 1061-1074.

Dickey, J.S., H.S. Yoder, J.F. Schairer, 1971. Chromium in silicate-oxide systems. Carnegie Inst. Wash. Yb., 70, 118-122.

Dickey, J.S., and Yoder, H.S., 1972. Partitioning of chromium and aluminum between clinopyroxene and spinel. Carnegie Inst. Wash. Yb., 71, 384-392.

Dickey, J.S. Jr., M. Obata, C.J. Suen, 1977, Partial fusion versus fractional crystallization: ypotheses for the differentiation of the Ronda ultramafic massif of Southern Spain. in Magma Genesis, H.J.B. Dick (ed.), Oregon Department of Geology and Mineral Industries, Bull., 96, 79-89.

Donaldson, C.H., 1978. Petrology of the uppermost upper mantle deduced from spinel-lherzolite and harzburgite nodules at Calton Hill, Derbyshire. Contr. Mineral. Petrol., 65, 363-377.

Duncan, R.A., and Green, D.H., 1980. Role of multistage melting in the formation of oceanic crust. Geology, 8, 22-26.

Dungan, M.A., and Avé Lallemant, H.G., 1977. Formation of small dunite bodies by metasomatic transformation of harzburgite in the Canyon Mountain ophiolite, Northeast Oregon. in Magma Genesis, H.J.B. Dick (ed.), Oregon Department of Geology and Mineral Industries, Bull., 96, 109-128.

Emslie, R.F., 1970. Liquidus relations and subsolidus reactions in some plagioclase bearing systems. Carnegie Inst. Wash. Yb., 69, 148-155.

Ernst, W.G., 1978. Petrochemical study of lherzolitic rocks from the Western Alps. J. Petrol., 19, 341-392.

Ernst, W.G., and Piccardo, G.B., 1979. Petrogenesis of some Ligurian peridotites -1 mineral and bulk-rock chemistry. Geochim. Cosmochim. Acta, 43, 219-237.

Etchecopar, A., 1977. A plane kinematic model of progressive deformation in a polycrystalline aggregate. Tectonophysics, 39, 121-139.

Evans, B.W., and Wright, T.L., 1972. Compositions of liquidus chromite from the 1959 and 1965 eruptions of Kilauea volcano, Hawaii. Am. Mineral., 57, 217-230.

Evans, B.W., and Frost, B.R., 1975. Chrome-spinel in progressive metamorphism-a preliminary analysis. Geochim. Cosmochim. Acta, 39, 959-972.

Fabries, J., 1979. Spinel-olivine geothermometry in peridotites from ultramafic complexes. Contr. Mineral. Petrol., 69, 329-336.

Finger, L.W., and Hadidiacos, C.G., 1972. Electron microprobe automation. Carnegie Inst. Wash. Yb., 71, 598-600.

Fisk, M.R., and Bence, A.E., 1980. Experimental crystallization of chrome spinel in FAMOUS basalt 527-1-1. Earth Plant. Sci. Lett., 48, 111-123.

Flanagan, F.J., compiler, 1976. Descriptions and analyses of eight new USGS rock standards. U.S. Geol. Surv. Prof. Paper 840, 192p.

Forsyth, D.W., 1977. The evolution of the upper mantle beneath Mid-ocean ridges. Tectonophysics, 38, 89-118.

Frey, F.A., W.B. Bryan, G. Thompson, 1974. Atlantic Ocean floor: geochemistry and petrology of basalts from Legs 2 and 3 of the Deep Sea Drilling Project. J. Geophys. Res., 79, 5507-5527.

Frey, F.A., and Green, D.H., 1974. The mineralogy, geochemistry and origin of lherzolite inclusions in Victorian basanites. Geochim. Cosmochim. Acta, 38, 1023-1059.

Frey, F.A., D.H. Green, S.D. Roy, 1978. Integrated models of basalt petrogenesis: a study of quartz tholeiites to olivine melilitites from South Eastern Australia utilizing geochemical and experimental petrological data. J. Petrol., 19, 463-513.

Frey, F.A., and Prinz, M., 1978. Ultramafic inclusions from San Carlos, Arizona: petrologic and geochemical data bearing on their petrogenesis. Earth Planet. Sci. Lett., 38, 129-176.

Frost, B.R., 1976. Limits to the assemblage forsterite-anorthite as inferred from peridotite hornfelses, Icicle Creek, Washington. Am. Mineral., 61, 732-750.

Fujii, T., 1976. Solubility of Al_2O_3 in enstatite coexisting with forsterite and spinel. Carnegie Inst. Wash. Yb., 75, 566-571.

Fujii, T., 1977. Fe-Mg partitioning between olivine and spinel. Carnegie Inst. Wash. Yb., 76, 563-569.

Gardner, P.M., and Robins, B., 1974. The olivine-plagioclase reaction: geological evidence from the Seiland petrographic province, Northern Norway. Contr. Mineral. Petrol., 44, 149-156.

Gass, I.G., C.R. Neary, M.A. Brown, ms. Nature and composition of ophiolite harzburgite sequences.

Gast. P.W., 1968. Trace element fractionation and the origin of tholeiitic and alkaline magma types. Geochim. Cosmochim. Acta, 32, 1057-1086.

Girardeau, J., 1979. Structure des ophiolites de l'ouest de Terre Neuve et modele de croute oceanique. These Docteur 3e Cycle. Universite de Nante, 154p.

Green, D.H., 1964. The petrogenesis of the high-temperature peridotite intrusion in Lizard Area, Cornwall. J. Petrol., 5, 134-188.

Green, D.H., and Hibberson, W., 1970. The instability of plagioclase in peridotite at high pressure. Lithos, 3, 209-221.

Green, D.H., A.E. Ringwood, N.G. Ware, W.O. Hibberson, A. Major, E. Kiss, 1971. Experimental petrology and petrogenesis of Apollo 12 basalts. Proc. Second. Lunar Sci. Conf., 1, M.I.T. Press, 601-615.

Green, D.H., A.E. Ringwood, N.G. Ware, W.O. Hibberson, 1972. Experimental petrology and petrogenesis of Apollo 14 basalts. Proc. Third Lunar Sci. Conf., Geochim. Cosmochim. Acta, Suppl. 3, 1, 197-206.

Greenbaum, D., 1977. The chromitiferous rocks of the Troodos Ophiolite Complex, Cyprus. Econ. Geol., 72, 1175-1194.

Harte, B., 1977. Rock nomenclature with particular relation to deformation and recrystallization textures in olivine-bearing xenoliths. J. Geology, 85, 279-288.

Hellman, P.L., and Henderson, P., 1977. Are rare earth elements mobile during spilitisation? Nature, 267, 38-40.

Herzberg, C.T., 1976a. The plagioclase lherzolite to spinel lherzolite facies boundary; its bearing on corona structure formation and tectonic history in the Norwegian Caledonides. Natural Environment Res. Council Ser. D. No. 6, 233-235.

Herzberg, C.T., 1976b. Influence of normative albite to anorthite ratio on mineral parageneses in peridotites. Natural Environment Res. Council Ser. D., No. 6, 249-251.

Herzberg, C.T., 1979. The bearing of phase equilibria in simple and complex systems on the origin and evolution of some well documented garnet websterites. - A Reply. Contr. Mineral. Petrol., 70, 223-229.

Herzberg, C.T., and Chapman, N.A., 1976. Clinopyroxene geothermometry of spinel-lherzolite. Am. Mineral., 61, 626-637.

Hill, R., and Roeder, P., 1974. The crystallization of spinel from basaltic liquid as a function of oxygen fugacity. J. Geology, 82, 709-729.

Himmelberg, G.R., and Loney, R.A., 1973. Petrology of the Vulcan Peak Alpine-type peridotite, southwestern Oregon. Bull. Geol. Soc. America, 84, 1585-1600.

Hobbs, B.E., W.D. Means, P.F. Williams, 1976. An Outline of Structural Geology. Wiley-Interscience, New York, 571p.

Ingerson, F.E., 1935. Layered peridotitic laccoliths of the Trout River, Area, Newfoundland. Am. J. Sci., Series 5, 29, 173, 422-440.

Ingerson, F.E., 1937. Layered peridotitic laccoliths of the Trout River Area, Newfoundland: a reply. Am. J. Sci., 33, 197, 389-392.

Irvine, T.N., 1965. Chromian spinel as a petrogenetic indicator Part I. theory. Can. J. Earth. Sci., 2, 648-672.

Irvine, T.N., 1967. Chromian spinel as a petrogenetic indicator Part 2. petrologic application. Can. J. Earth Sci., 4, 71-103.

Irvine, T.N., 1970. Crystallization sequences in the Muskox intrusion and other layered intrusions, I. olivine-pyroxene-plagioclase relations. Geol. Soc. S. Africa, Spec. Publ.,1, 441-476.

Irvine, T.N., 1975. Primary precipitation of concentrated deposits of magmatic ores. Geol. Surv. Can., paper 75-1, Part B, 73-79.

Irvine, T.N., 1977. Origin of chromitite layers in the Muskox intrusion and other stratiform intrusions: a new interpretation. Geology, 5, 273-277.

Irvine, T.N., 1979. Rocks whose composition is determined by crystal accumulation and sorting. in The Evolution of the Igneous Rocks, H.S. Yoder (ed.), Princeton University Press, 245-306.

Irvine, T.N., and Smith, C.H., 1967. The ultramafic rocks of the Muskox intrusion, Northwest Territories, Canada. in, Ultramafic and Related Rocks, P.J. Wyllie (ed.), 38-49.

Irvine, T.N., and Smith, C.H., 1969. Primary oxide minerals in the layered series of the Muskox intrusion. in Magmatic Ore Deposits, H.D.B. Wilson (ed.), Econ. Geol. Mono., 4, 76-94.

Irvine, T.N., and Findlay, T.C., 1972. Alpine-type peridotite with particular reference to the Bay of Islands igneous complex. Pub. Earth Phys. Branch, Dept. Energy, Mines and Res., Canada, 42, 97-128.

Jackson, E.D., 1961. Primary textures and mineral associations in the ultramafic zone of the Stillwater Complex, Montana. U.S. Geol. Survey Prof. Paper 358, 106p.

Jackson, E.D., 1969. Chemical variation in coexisting chromite and olivine in chromitite zones of the Stillwater Complex. in Magmatic Ore Deposits, H.D.B. Wilson (ed.), Econ. Geol. Mono., 4, 41-75.

Jackson, E.D., 1970. The cyclic unit in layered intrusions-a comparison of the repetitive stratigraphy in the ultramafic parts of the Stillwater, Muskox, Great Dyke and Bushveld Complexes. Geol. Soc. S. Africa, Spec. Publ., 1, 391-424.

Jamieson, B.G., 1966. Evidence on the evolution of basaltic magma at elevated pressures. Nature, 212, 243-246.

Jamieson, R.A., 1977. A suite of alkali basalts and gabbros associated with the Hare Bay Allochthon of western Newfoundland. Can. J. Earth Sci., 14, 346-356.

Jamieson, R.A., 1979. The St. Anthony Complex, northwestern Newfoundland: a petrological study of the relationship between a peridotite sheet and its dynamothermal aureole. Unpub. Ph.D. thesis, Memorial University of Newfoundland.

Jamieson, R.A., 1980a. Formation of metamorphic aureoles beneath ophiolites-evidence from the St. Anthony Complex, Newfoundland. Geology, 8, 150-154.

Jamieson, R.A., 1980b. Ophiolite emplacement as recorded in the dynamothermal aureole of the St. Anthony Complex, northwestern Newfoundland. Proc. Internat. Ophiolite Symp. Cyprus, 1979, 620-628.

Jamieson, R.A., and Talkington, R.W., 1980. A jacupirangite-syenite assemblage beneath the White Hills Peridotite, northwestern Newfoundland. Am. J. Sci., 280, 459-477.

Jaques, A.L., and Green, D.H., 1980. Anhydrous melting of peridotite at 0-15 kb pressure and the genesis of tholeiitic basalts. Contr. Mineral. Petrol., 73, 287-310.

Johnson, H., 1941. Paleozoic lowlands of western Newfoundland. Trans. N.Y. Acad. Sci., series 2, 3, 141-145.

Juteau, T., A. Nicolas, J. Dubessy, J.C. Fruchard, J.L. Bouchez, 1977. Structural relationships in the Antalya ophiolite complex, Turkey: possible model for an oceanic ridge. Bull. Geol. Soc. Amer., 88, 1740-1748.

Katsura, T., and Muan, A., 1964. Experimental study of equilibria in the system FeO-MgO-Cr_2O_3 at 1300°C. Trans. Met. Soc. AIME, 230, 77-84.

Kay, M., 1945. Paleogeographic and palinspastic maps. Am. Assoc. Petrol. Geol., 29, 426-450.

Kay, R.W., and Senechal, R.G., 1976. The rare earth geochemistry of the Troodos Ophiolite Complex. J. Geophys. Res., 81, 964-970.

Keith, M.L., 1954. The system MgO-Cr_2O_3-SiO_2. J. Am. Ceramic Soc., 37, 490-496.

Kurat, G., H. Palme, B. Spettel, H. Baddenhausen, H. Hofmeister, C. Palme, H. Wänke, 1980. Geochemistry of ultramafic xenoliths from Kapfenstein, Austria: evidence for a variety of upper mantle processes. Geochim. Cosmochim. Acta, 44, 45-60.

Kushiro, I., 1968. Compositions of magmas formed by partial zone melting of the earth's upper mantle. J. Geophys. Res., 73, 619-634.

Kushiro, I., and Yoder, H.S.,Jr., 1966. Anorthite-forsterite and anorthite-enstatite reactions and their bearing on the basalt-eclogite transformation. J. Petrol., 7, 337-362.

Kwestroo, W., 1959. Spinel phase in the system MgO-Fe_2O_3-Al_2O_3. J. Inorg. Nucl. Chem., 9, 65-70.

Langmuir, C.H., J.F. Bender, A.E. Bence, G.N. Hanson, S.R. Taylor, 1977. Petrogenesis of basalts from the FAMOUS area, Mid-Atlantic Ridge. Earth Planet. Sci. Lett., 36, 133-156.

Laurent, R., R. Hebert, Y. Herbert, 1979. Tectonic setting and petrological features of the Quebec Appalachian Ophiolites. in Ophiolites of the Canadian Appalachians and Soviet Urals, J. Malpas and R.W. Talkington (eds.), Memorial University of Newfoundland, Dept. of Geology, Rept. 8, I.G.C.P. Proj. 39, 53-77.

LeBas, M.J., 1962. The role of aluminum in igneous clinopyroxenes with relation to their parentage. Am. J. Sci., 260, 4, 267-288.

LeBlanc, M., 1980. Chromite growth, dissolution and deformation from a morphological view point: SEM investigations. Mineral. Deposita, 15, 201-210.

Lindsley, D.H., 1976. Experimental studies of oxide minerals. in Oxide Minerals, D. Rumble III, (ed.), Min. Soc. Amer., 3, L61-L88.

Loney, R.A., G.R. Himmelberg, R.G. Coleman, 1971. Structure and petrology of the alpine-type peridotite at Burro Mountain, California, U.S.A. J. Petrol., 12, 245-309.

Loubet, M., M. Bougault, N. Shimizu, C.J. Allègre, 1976. Geochemical study (REE, Ba and partially major and transition elements analysis) of pyroxenolite layers in lherzolite type alpine massives (abstr.), Trans. Am. Geophys. Union, 57, 1025.

Lovering, J.F., and White, A.J.R., 1969. Granulitic and eclogitic inclusions from basic pipes at Delegate, Australia. Contr. Mineral. Petrol., 21, 9-52.

Ludden, J.N., and Thompson, G., 1979. An evaluation of the behavior of the rare earth elements during the weathering of sea-floor basalts. Earth Planet. Sci. Lett., 43, 85-92.

Lynas, C.M.T., and Calon, T.J., 1980. Northwestward-directed thrusting related to closing of the Iapetus Ocean in the Hare Bay Allochthon, Newfoundland, (abstr.). Bull. Geol. Soc. Amer., 12, 2, 71.

Maaloe, S., and Aoki, K., 1977. The major element composition of the upper mantle estimated from the composition of lherzolites. Contr. Mineral. Petrol., 63, 161-173.

MacGregor, I.D., 1965. Stability fields of spinel and garnet peridotite in the synthetic system MgO-CaO-Al_2O_3-SiO_2. Carnegie Inst. Wash. Yb., 64, 126-134.

MacGregor, I.D., 1974. The system MgO-Al_2O_3-SiO_2: solubility of Al_2O_3 in enstatite for spinel and garnet peridotite compositions. Am. Mineral. 59, 110-119.

Malpas, J.G., 1976. The petrology and petrogenesis of the Bay of Islands ophiolite suite, western Newfoundland. unpubl. Ph.D. thesis, Memorial University of Newfoundland.

Malpas, J., 1978. Magma generation in the upper mantle, field evidence from ophiolite suites, and application to the generation of oceanic lithosphere. Phil. Trans. R. Soc. London, A. 288, 527-546.

Malpas, J., 1979. The dynamothermal aureole of the Bay of Islands ophiolite suite. Can. J. Earth Sci., 16, 2086-2101.

Malpas, J., and Strong, D.F., 1975. A comparison of chrome-spinels in ophiolites and mantle diapirs of Newfoundland. Geochim. Cosmochim. Acta, 39, 1045-1060.

Malpas, J., and Stevens, R.K., 1977. The origin and emplacement of the ophiolite suite with examples from western Newfoundland. Geotectonics, 11, 453-466.

Medaris, L.G., 1972. High-pressure peridotites in southwestern Oregon. Bull. Geol. Soc. Amer., 83, 41-58.

Medaris, L.G., 1975. Co-existing spinel and silicates in alpine peridotites of the granulite facies. Geochim. Cosmochim. Acta, 39, 947-958.

Menzies, M., 1975. Spinel compositional variation in the crustal and mantle lithologies of the Othris Ophiolite. Contr. Mineral. Petrol., 51, 303-309.

Menzies, M., 1976. Rare earth geochemistry of fused ophiolitic and alpine lherzolites-I. Othris, Lanzo and Troodos. Geochim. Cosmochim. Acta, 40, 645-656.

Menzies, M., and Allen, C., 1974. Plagioclase-lherzolite-residual mantle relationships within two eastern Mediterranean ophiolites. Contr. Mineral. Petrol., 45, 197-213.

Menzies, M., D. Blanchard, J. Brannon, R. Korotev, 1977. Rare earth and trace element geochemistry of a fragment of Jurassic seafloor, Point Sal, California. Geochim. Cosmochim. Acta, 41, 1419-1430.

Mercier, J-C.C., 1980. Single-pyroxene thermobarometry. Tectonophysics, 70, 1-37.

Mercier, J-C.C., and Nicolas, A., 1975. Textures and fabrics of upper-mantle peridotites as illustrated by xenoliths from basalts. J. Petrol., 16, 454-487.

Miyashiro, A., 1973. The Troodos ophiolitic complex was probably formed in an island arc. Earth Planet. Sci. Lett., 19, 218-224.

Montigny, R., H. Bougault, Y. Bottinga, C.J. Allègre, 1973. Trace element geochemistry and genesis of the Pindos Ophiolite suite. Geochim. Cosmochim. Acta, 37, 2135-2147.

Morse, S.A., 1973. BPD-1. Basalts and phase diagrams (Part 1). University of Massachusetts Press, 158p.

Morse, S.A., 1976. The lever rule with fractional crystallization and fusion. Am. J. Sci., 276, 330-346.

Muan, A., J. Hauck, T. Löfall, 1972. Equilibrium studies with a bearing on lunar rocks. Proc. Third Lunar Sci. Conf., 185-196.

Mysen, B.O., 1976. Experimental determination of some geochemical parameters relating to conditions of equilibration of peridotite in the upper mantle. Am. Mineral., 61, 677-683.

Mysen, B.O., and Holloway, J.R., 1977. Experimental determination of rare earth fractionation patterns in partial melts from peridotite in the upper mantle. Earth Planet. Sci. Lett., 34, 231-237.

Mysen, B.O., and Kushiro, I., 1977. Compositional variations of coexisting phases with degree of melting of peridotite in the upper mantle. Am. Mineral., 62, 843-865.

Nicholls, G.D., 1967. Geochemical studies in the ocean as evidence for the composition of the mantle. in Mantles of the Earth and Terrestrial Planets, S.K. Runcorn (ed.), Wiley-Interscience, New York.

Nicolas, A., 1976. Flow in upper-mantle rocks: some geophysical and geodynamic consequences. Tectonophysics, 32, 93-106.

Nicolas, A., F. Boudier, A.M. Boullier, 1973. Mechanisms of flow in naturally and experimentally deformed peridotites. Am. J. Sci., 273, 853-876.

Nicolas, A., F. Boudier, J.L. Bouchez, 1980. Interpretation of peridotite structures from ophiolitic and oceanic environment. E.D. Jackson Volume, Am. J. Sci., 280-A, pt. 1, 192-210.

Obata, M., 1976. The solubility of Al_2O_3 in orthopyroxenes in spinel and plagioclase peridotites and spinel pyroxenite. Am. Mineral., 61, 804-816.

Obata, M., 1977. Petrology and petrogenesis of a high-temperature peridotite intrusion: Serrania de la Ronda, southern Spain. unpublished Ph.D. thesis, Massachusetts Institute of Technology.

Obata, M., S. Banno, T. Mori, 1974. The iron-magnesium partitioning between naturally occurring coexisting olivine and Ca-rich clinopyroxene: an application of the simple mixture model to olivine solid solution. Bull. Soc. Fr. Mineral. Cristallogr., 97, 101-107.

Obata, M., and Dickey, J.S., Jr., 1976. Phase relations of mafic layers in the Ronda Peridotite. Carnegie Inst. Wash. Yb., 75, 562-566.

O'Hara, M.J., 1967. Mineral parageneses in ultrabasic rocks. in Ultramafic and Related Rocks, P.J. Wyllie, (ed.), Willey and Son's, New York, 393-402.

O'Hara, M.J., 1968. The bearing of phase equilibria studies in synthetic and natural systems on the origin and evolution of basic and ultrabasic rocks. Earth Sci. Rev., 4, 69-133.

Panayiotou, A., 1978. The mineralogy and chemistry of the podiform chromite deposits in the serpentinites of the Limassol Forest, Cyprus. Mineral. Deposita, 13, 259-274.

Pike, J.E.N., and Schwarzman, E.C., 1977. Classification of textures in ultramafic xenoliths. J. Geology, 85, 49-61.

Presnall, D.C., S.A. Dixon, J.R. Dixon, T.H. O'Donnell, N.L. Brenner, R.L. Schrock, D.W. Dycus, 1978. Liquidus phase relations on the join diopside-forsterite-anorthite from 1 atm to 20 kbar: their bearing on the generation and crystallization of basaltic magma. Contr. Mineral. Petrol., 66, 203-220.

Pringle, I.R., J.A. Miller, D.M. Warrell, 1971. Radiometric age determinations from the Long Range Mountains, Newfoundland. Can. J. Earth Sci., 8, 1325-1330.

Raleigh, C.B., 1965. Structure and petrology of an Alpine Peridotite on Cypress Island, Washington, U.S.A. Beit. Mineral. Petrog., 11, 719-741.

Reid, J.B., Jr., and Woods, G.A., 1977. A comparison of partial melting processes beneath Hawaii and the Southern Rio Grande Rift. in Magma Genesis, H.J.B. Dick (ed.), Oregon Department of Geology and Mineral Industries, Bull., 96, 307.

Reid, J.B., Jr., and Woods, G.A., 1978. Oceanic mantle beneath the southern Rio Grande Rift. Earth Planet. Sci. Lett., 41, 303-316.

Riccio, L., 1976. Stratigraphy and petrology of the peridotite-gabbro component of the western Newfoundland ophiolites. unpubl. Ph.D. thesis, University of Western Ontario.

Ringwood, A.E., 1975. Composition and Petrology of the Earth's Mantle. McGraw-Hill, 618p.

Robin, P-Y.,F., 1979. Theory of metamorphic segregation and related processes. Geochim. Cosmochim. Acta, 43, 1587-1600.

Rodgers, J., 1965. Long Point and Clam Bank Formations, western Newfoundland. Proc. Geol. Assoc. Canada, 16, 83-94.

Rodgers, J., and Neale, E.R.W., 1963. Possible taconic klippen in western Newfoundland. Am. J. Sci., 261, 713-730.

Roeder, P.L., and Emslie, R.F., 1970. Olivine-liquid equilibrium. Contr. Mineral. Petrol., 29, 275-289.

Roeder, P.L., I.H. Campbell, H.E. Jamieson, 1979. A re-evaluation of the olivine-spinel geothermometer. Contr. Mineral. Petrol., 68, 325-334.

Rose, H.J., I. Adler, F.J. Flanagan, 1962. Use of La_2O_3 as a heavy absorber in the x-ray fluorescence analysis of silicate rocks. U.S. Geol. Surv. Prof. Pap. 450-B, 80, B80-B82.

Scarfe, C.M., B.O. Mysen, C.S. Rai, 1979. Invariant melting behavior of mantle material: partial melting of two lherzolite nodules. Carnegie Inst. Wash. Yb.,78, 498-501.

Shepperd, N., 1962a. Report on the western White Hills, Hare Bay Area, Newfoundland. Newfoundland Dept. Mines and Energy Report, M.B. #2M/5 (24), 3p.

Shepperd, N., 1962b. Geological report on the Mt. Mer Area, Hare Bay, Newfoundland. Newfoundland Dept. Mines and Energy Report, M.B. #2M/5 (23), 2p.

Shepperd, N., 1962c. Geological and geophysical report on the western White Hills area, Hare Bay, Newfoundland. Newfoundland Dept. Mines and Energy Report, M.B. #2M/5 (22), 3p.

Shervais, J.W., 1979. Thermal emplacement model for the alpine lherzolite massif at Balmuccia, Italy. J. Petrol., 20, 795-820.

Shih, Chi-yu, and Gast, P.W., 1971. Rare earths in abyssal tholeiites, gabbros and their mineral separates from Mid-Atlantic Ridge near 24°N. (abstr.). EOS Trans. Am. Geophys. Union, 52, 376.

Sigurdsson, H., and Schilling, J.-G., 1976. Spinels in Mid-Atlantic Ridge basalts: chemistry and occurrence. Earth Planet. Sci. Lett., 29, 7-20.

Sinton, J.M., 1977. Equilibration history of the basal alpine-type peridotite, Red Mountain, New Zealand. J. Petrol., 18, 216-246.

Sleep, N.H., 1974. Segregation of magma from a mostly crystalline mush. Bull. Geol. Soc. Amer., 85, 1225-1232.

Smewing, J.D., K.O. Simonian, I.G. Gass, 1975. Metabasalts from the Troodos Massif, Cyprus: genetic implication deduced from petrography and rare earth element geochemistry. Contr. Mineral. Petrol., 51, 49-64.

Smewing, J.D., and Potts, P.J., 1976. Rare-earth abundances in basalts and metabasalts from the Troodos Massif, Cyprus. Contr. Mineral. Petrol., 57, 245-258.

Smith, C.H., 1958. Bay of Islands Igneous Complex, western Newfoundland. Geol. Survey, Can., Mem., 290, 132p.

Smith, D., and Levy, S., 1976. Petrology of the green knob diatreme and implications for the upper mantle below the Colorado plateau. Earth Planet. Sci. Lett., 29, 107-125.

Smyth, W.R., 1971. Stratigraphy and structure of part of the Hare Bay Allochthon, Newfoundland. Proc. Geol. Assoc. Can., 24, 47-51.

Smyth, W.R., 1973. The stratigraphy and structure of the southern part of the Hare Bay Allochthon, north-western Newfoundland. unpub. Ph.D. thesis, Memorial University of Newfoundland.

Snelgrove, A.K., 1934. Chromite deposits of Newfoundland. Newfoundland Dept. Nat. Res. Geol. Sec. Bull., I.

Snelgrove, A.K., F.W. Roebling, III., J.L.J. Kaminara, 1934. The blow me down intrusive complex. Am. Mineral., 19, 21-23.

Snethlage, R., and Klemm, D.D., 1978. Intrinsic oxygen fugacity measurements on chromites from the Bushveld Complex and their petrogenetic significance. Contr. Mineral. Petrol., 67, 127-138.

Speidel, D.H., 1967. Phase equilibria in the system MgO-FeO-Fe_2O_3: the 1300° isothermal section and extrapolations to other temperatures. J. Amer. Ceram. Soc., 50, 243-248.

Spry, A. 1969. Metamorphic Texures. Pergamon Press, 350p.

Stancioff, A., and Hill, P.A., 1979. Satellite image analysis in mineral exploration in complicated structural terranes, Great Northern Peninsula, Newfoundland. Bull. Amer. Assoc. Petrol. Geol., 63, 951-966.

Stevens, R.E., 1944. Composition of some chromites of the Western Hemisphere. Am. Mineral., 29, 1-34.

Stevens, R.K., 1970. Cambro-Ordovician flysch sedimentation and tectonics in west Newfoundland and their possible bearing on a Proto-Atlantic Ocean. Geol. Assoc. Can. Spec. Paper 7, 165-177.

Streckeisen, A., 1976. To each plutonic rock its proper name. Earth Sci. Rev., 12, 1-33.

Strong, D.F., and Williams, H., 1972. Early Paleozoic flood basalts of northwest Newfoundland: their petrologic and tectonic significance. Proc. Geol. Assoc. Can., 24, 43-54.

Strong, D.F., W.L. Dickson, C.F. O'Driscoll, B.F. Kean, R.K. Stevens, 1974. Geochemical evidence for an east-dipping Appalachian subduction zone in Newfoundland. Nature, 248, 37-39.

Strong, D.F., and Dostal, J., 1980. Dynamic melting of a Proterozoic upper mantle: evidence from rare earth elements in oceanic crust of Eastern Newfoundland. Contr. Mineral. Petrol., 72, 165-173.

Stukas, V., and Reynolds, P.H., 1974. $^{40}Ar/^{39}Ar$ dating of the Long Range dikes, Newfoundland. Earth Planet. Sci. Lett., 22, 256-266.

Suen, C-Y.J., 1978. Geochemistry of peridotites and associated mafic rocks, Ronda ultramafic complex, Spain. unpubl. D.Sc. thesis, Massachusetts Institute of Technology, 283p.

Suen, C.J., and Frey, F.A., 1979. Geochemical characteristics of the Bay of Islands ophiolite suite with emphasis on rare earth element geochemistry (abstr.). Geol. Assoc. Can., 4, 81.

Suen, C.J., F.A. Frey, J. Malpas, 1979. Bay of Islands ophiolite suite, Newfoundland: petrologic and geochemical characteristics with emphasis on rare earth element geochemistry. Earth Planet. Sci. Lett., 45, 337-348.

Talbot, J.C., B.E. Hobbs, H.G. Wilshire, T.R. Sweatman, 1963. Xenoliths and xenocrysts from lavas of the Kergullen Archipelago. Am. Mineral., 48, 159-179.

Talkington, R.W., 1979. An unusual occurrence of gabbro veins in a west Newfoundland ophiolite: White Hills Peridotite, St. Anthony Complex (abstr.). Geol. Assoc. Can., 4, 82.

Talkington, R.W., and Jamieson, R.A., 1979. The geology of the St. Anthony Complex, northwestern Newfoundland-a note. in Ophiolites of the Canadian Appalachians and Soviet Urals. J. Malpas and R.W. Talkington (eds.), Memorial Univeristy of Newfoundland, Dept. of Geology, Rept. 8, I.G.C.P. Proj. 39, 43-53.

Talkington, R., and Malpas, J., 1980a. Spinel phases of the White Hills Peridotite, St. Anthony Complex, Newfoundland: Part I occurrence and chemistry. in Proceedings Inter. Ophiolite Symp., Cyprus, 1979, 607-619.

Talkington, R., and Malpas, J., 1980b. Compositional variation of spinels in the White Hills Peridotite, Newfoundland: a consequence of upper mantle partial fusion processes? (abstr.). Bull. Geol. Soc. Amer., 12, 2, 86.

Talkington, R., and Malpas, J., 1980c. A layered ophiolite mantle peridotite section from Newfoundland: the White Hills Peridotite. (abstr.). Bull. Geol. Soc. Amer., 12, 2, 86.

Talkington, R.W., and Malpas, J., 1980d. Genesis of spinels and chromite deposits in the White Hills Peridotite, St. Anthony Complex, northwestern Newfoundland. Symposium on Metallogeny of Mafic and Ultramafic Complexes, Athens, Greece, 124-125.

Taylor, S.R., 1965. The application of trace element data to problems in petrology. Phys. Chem. Earth, 6, 133-213.

Thayer, T.P., 1946. Preliminary chemical correlation of chromite with the containing rocks. Econ. Geol., 41, 202-217.

Thayer, T.P., 1964. Principal features and origin of podiform chromite deposits and some observations on the Guleman-Soridag District, Turkey. Econ. Geol., 59, 1497-1524.

Thayer, T.P., 1969. Gravity differentiation and magmatic reemplacement of podiform chromite deposits. in Magmatic Ore Deposits, H.D.B. Wilson (ed.), Econ. Geol., Mono., 4, 132-146.

Thayer, T.P., 1970. Chromite segregations as petrogenetic indicators. Geol. Soc. S. Africa, Spec. Publ., 1, 380-390.

Thompson, G., 1973. Trace element distributions in fractionated oceanic rocks, 2. gabbros and related rocks. Chem. Geol., 12, 99-111.

Thompson, R.N., 1974. Some high-pressure pyroxenes. Mineral. Mag., 39, 768-787.

Thompson, R.N., I.L. Gibson, G.F. Marriner, D.P. Matley, M. Ann Morrison, 1980. Trace element evidence of multistage mantle fusion and polybaric fractional crystallization in the Palaeocene lavas of Skye, NW Scotland. J. Petrol., 21, 265-293.

Tiezzi, L.J., 1977. Petrology of a dredged cumulate-textured gabbroic complex from the Mid-Atlantic Ridge, Lat. 26°N. MSc. thesis, Texas A&M University.

Tuke, M.F., 1966. Lower Paleozoic rocks and klippen in the Pistolet Bay area, northern Newfoundland. unpubl. Ph.D. thesis, University of Ottawa.

Tuke, M.F., 1968. Autochthonous and allochthonous rocks in the Pistolet Bay area in northernmost Newfoundland. Can. J. Earth Sci., 5, 501-513.

Turnock, A.C., and Eugster, H.P., 1962. Fe-Al oxides: phase relations below 1000°C. J. Petrol., 3, 533-565.

Ulmer, G.C., 1969. Experimental investigations of chromite spinels. in Magmatic Ore Deposits, H.D.B. Wilson (ed.), Econ. Geol., Mono., 4, 114-131.

Ulmer, G.C., 1970. Chromite spinel. in High Temperature Oxides, Pt. 1, Magnesia, Lime and Chrome Refractories. A.M. Alper (ed.), Refractory Materials, 5, 251-314.

Ulmer, G.C., and Smothers, W.J., 1968. The stystem MgO-Cr_2O_3-Fe_2O_3 at 1300°C in air. J. Amer. Ceram. Soc., 51, 315-319.

Varne, R., 1977. On the origin of spinel lherzolite inclusions in basaltic rocks from Tasmania and elsewhere. J. Petrol., 18, 1-23.

Vernon, R.H., 1970. Comparative grain boundary studies of some basic and ultrabasic granulites, nodules and cumulates. Scott. J. Geol., 6, 337-351.

Wager, L.R., G.M. Brown, W.J. Wadsworth, 1960. Types of igneous cumulates. J. Petrol., 1, 73-85.

Wager, L.R., and Brown, G.M., 1968. Layered Igneous Rocks. Oliver and Boyd, 588p.

Wass, S.Y., 1973. Plagioclase-spinel intergrowths in alkali basaltic rocks from the Southern Highlands, N.S.W. Contr. Mineral. Petrol., 38, 167-175.

Wells, P.R.A., 1977. Pyroxene thermometry in simple and complex systems. Contr. Mineral. Petrol., 62, 129-139.

White, R.W., 1966. Ultramafic inclusions in basaltic rocks from Hawaii. Contr. Mineral. Petrol., 12, 245-314.

Whitney, P.R., 1972. Spinel inclusions in plagioclase of metagabbros from the Adirondack Highlands. Am. Mineral., 57, 1429-1436.

Wilkinson, J.F.G., 1975. An Al-spinel ultramafic-mafic inclusion suite and high pressure megacrysts in an analcimite and their bearing on basaltic magma fractionation at elevated pressures. Contr. Mineral. Petrol., 53, 71-104.

Williams, H., 1964. The Appalachians in northeastern Newfoundland-a two-sided symmetrical system. Am. J. Sci., 262, 1137-1158.

Williams, H., 1971. Mafic-ultramafic complexes in west Newfoundland Appalachians and the evidence for their transportation: a review and interim report. in A Newfoundland Decade, Geol. Assoc. Can. Proc. 24, 9-25.

Williams, H., 1973. Bay of Islands Map-Area, Newfoundland. Geol. Surv. Can. Pap. 72-34, 7p.

Williams, H., 1975. Structural succession, nomenclature, and interpretation of transported rocks in western Newfoundland. Can. J. Earth Sci., 12, 1874-1894.

Williams, H., 1976. Tectonic stratigraphic subdivision of the Appalachian Orogen (abstr.). Bull. Geol. Soc. America, 8, 2, 300.

Williams, H., 1978a. Tectonic-lithofacies map of the Appalachian Orogen. Memorial University of Newfoundland, Map No. 1.

Williams, H., 1978b. Geological development of the northern Appalachians: its bearing on the evolution of the British Isles. in Crustal Evolution in the Northwestern Britain and Adjacent Regions, D.R. Bowes and B.E. Leake (eds.), Seal House Press, Liverpool, 1-22.

Williams, H., 1979. Appalachian Orogen in Canada. Can. J. Earth Sci., 16, 792-807.

Williams, H., M.J. Kennedy, E.R.W. Neale, 1972. The Appalachian structural province. Geol. Assoc. Can. Spec. Paper 11, 181-261.

Williams, H., and Smyth, W.R., 1973. Metamorphic aureoles beneath ophiolite suites and alpine peridotites: tectonic implications with west Newfoundland examples. Am. J. Sci., 273, 594-621.

Williams, H., W.R. Smyth, R.K. Stevens, 1973. Hare Bay Allochthon, northern Newfoundland. Geol. Surv. Can., Paper 73-1, 8-14.

Williams, H., and Stevens, R.K., 1974. The ancient continental margin of eastern North America. in The Geology of Continental Margins, C.A. Burk and C.L. Drake, (eds.), Springer-Verlag, 781-796.

Williams, H., M.J. Kennedy, E.R.W. Neale, 1974. The northeastward termination of the Appalachian Orogen. in The Ocean Basins and Margins, v. 2, A.E.M. Nairn and F.G. Stehli(eds.),Plenum, 79-123.

Williams, H., and Talkington, R.W., 1977. Distribution and tectonic setting of ophiolites and ophiolitic melanges in the Appalachian Orogen. in North American Ophiolites, R.G. Coleman and W.P. Irwin (eds.), Oregon Department of Geology and Mineral Industries, Bull. 95, 1-11.

Williams, H., and Smyth, W.R., in press. The Hare Bay Allochthon, northern Newfoundland. Geol. Surv. Canada. Bull.

Wilshire, H.G., and Jackson, E.D., 1975. Problems in determining mantle geotherms from pyroxene compositions of ultramafic rocks. J. Geology, 83, 313-329.

Wilshire, H.G., and Pike, J.E.N., 1975. Upper-mantle diapirism: evidence from analogous features in alpine peridotite and ultramafic inclusions in basalt. Geology, 3, 467-470.

Wilshire, H.G., and Shervais, J.W., 1975. Al-augite and Cr-diopside ultramafic xenoliths in basaltic rocks from western United States. Phys. Chem. Earth, 9, 257-272.

Wilson, J.T., 1966. Did the Atlantic close and then re-open? Nature, 211, 676-681.

Wood, B.J., 1975. The application of thermodynamics to some subsolidus equilibria involving solid solutions. Fortschr. Mineral., 52, 21-45.

Wood, B.J., and Banno, S., 1973. Garnet-orthopyroxene and orthopyroxene-clinopyroxene relationships in simple and complex systems. Contr. Mineral. Petrol., 42, 109-124.

Wood, B.J., and Fraser, D.G., 1976. Elementary Thermodynamics for Geologists. Oxford University Press, 303p.

Wyckoff, R.W.G., 1965. Crystal Structures, 2nd. ed., Wiley-Interscience, New York, Volume 3.

Wyllie, P.J., 1970. Ultramafic rocks and the upper mantle. Mineral. Soc. Amer. Spec. Pap. 3, 1-32.

Wyllie, P.J., 1971. The Dynamic Earth, Wiley-Interscience, New York, 416p.

Yoder, H.S., Jr., 1976. Generation of Basaltic Magma. National Academy of Sciences. 265p.

APPENDICES

APPENDIX I

(a) Mineral Element Analysis

Mineral analyses have been determined by a JOEL JX50A electron microprobe equipped with an automated system (KRIESEL) designed by Finger and Hadidiacos (1972) using a PDP11/20 minicomputer. Data have been reduced on-line using the Geolab program of Finger and Hadidiacos (1972).

Instrument operating conditions are 15Kv filament voltage, a beam current of 300μA, a beam diameter of approximately 2 microns (a defocused beam of approximately 30-50 microns has been used on some plagioclase grains), and counting time of 30 seconds (or 30,000 counts) per element.

The following natural and synthetic standards have been used:

1. Olivine:
   - Mg - SWOL;MOL;P140
   - Al - ENAL-5; WCPX
   - Si - SWOL; P140
   - CA - Di2Ti
   - Ti - Di2Ti; WCPX
   - Cr - SPIN-B; JOPX
   - Mn - HEDEN; JOPX
   - Fe - SWOL; P140
   - Ni - NiOl; P140

2. Orthopyroxene:
   - Mg - JOPX; ENAL-10
   - Al - ENAL-5
   - Si - JOPX; Di2Ti
   - Ca - Di2Ti, JOPX; WCPX
   - Ti - Di2Ti; WCPX
   - Cr - SPIN-B; JOPX
   - Mn - HEDEN; JOPX
   - Fe - JOPX; WCPX
   - Ni - NiOL; P140

3. Clinopyroxene:
   - Na - JADI; JOPX
   - Mg - A-CPX; HEDEN
   - Al - A-CPX; WCPX
   - Si - A-CPX; Di2Ti

	Ca	- Di2Ti; WCPX
	Ti	- Di2Ti; WCPX
	Cr	- SPIN-B; JOPX
	Mn	- HEDEN; JOPX
	Fe	- A-CPX; HEDEN; WCPX
	Ni	- NiOl; P140
4. Feldspar:	Na	- ANOR
	Al	- ANOR
	Si	- ANOR
	K	- Or-1
	Ca	- LC-PLAG
	Fe	- Vg-2
5. Hornblende:	Na	- K-HB
	Mg	- K-HB
	Al	- K-HB
	Si	- K-HB
	K	- K-HB
	Ca	- K-HB
	Ti	- K-HB
	Mn	- HEDEN
	Fe	- K-HB
6. Spinel:	Mg	- K-HB
	Al	- SPIN-B
	Ti	- 53IN8
	V	- 53IN8
	Cr	- 53IN8
	Mn	- 53IN8
	Fe	- SCHB
	Ni	- NiOL

Instrumental error for all elements is less than 1.5 percent, except for Na, K and Ti which is less than 5 percent.

b. Major Element Analysis

Major element analyses have been determined by x-ray fluorescence on fused powder pellets and atomic absorption spectrophotometry. The powder fusion technique is used on samples containing spinel which are insoluble in aqua regia. Conventional chemical analyses have been performed on samples that completely went into solution.

The fusion technique is similar to the procedure of Rose et al (1962) and uses $Li_2B_4O_7$ as a flux and La_2O_3 as a heavy element absorber. Approximately 4.0 grams of lithium tetraborate are mixed with approximately 0.5 grams of sample powder. Added to this mixture is lanthanum oxide of exactly the same weight as sample powder. Fusions are made in platinum crucibles. The samples are fused at about 1000°C for 5-10 minutes in a automated 6 sample Claisse fluxer. For this technique, the samples are first heated until all powders are fused; then, automatically stirred to homogenize the melt. The melt is poured into stainless steel dishes and is cooled to room temperature to form glass pellets.

A correction factor ({E-A}/{C-B})* is applied to the raw data (straight line linear calibration curve) to obtain oxide concentration (D. Press, pers. comm., 1980).

Analytical precision has been determined on sample 782-II (spinel lherzolite) for 11 batch runs on the XRF. The results are given in Table AI.1.

**For atomic absorption analysis, exactly 0.2000 grams of sample powder is weighed in a plastic cap and placed in

* A= weight of empty Pt-crucible; B= weight of Li2B4O7; C= weight of sample powder; D= weight of La2O3 (equal to (C-B)+C); E= weight of Pt-crucible plus all contents after fusion. All weights are made on dry materials. To insure all ingredients are dry for weighing the sample powders and Li2B4O7 are dried overnight at 100°C; La2O3 is dried overnight at about 850°C. All powders are cooled and stored in a dessicator.

** From Malpas (1976)

Table AI.1. Precision determination for major elements determined by XRF

	Mean	S.D.	Variance	95% C.I.
SiO_2	40.17	0.31	.086	40.17± .18
Al_2O_3	2.15	0.04	.001	2.15± .02
Fe_2O_3	9.70	0.07	.004	9.70± .04 (4.07)
(FeO*)	--	--	--	5.08 --
MgO	38.33	0.83	.622	38.33± .49
CaO	2.60	0.01	.000	2.60± .005
K_2O	0.02	0.00	.000	0.02± .00
TiO_2	0.11	0.00	.000	0.11± .00
P_2O_5	0.10	0.01	.000	0.10± .005
MnO	0.15	0.13	.016	0.15± .08
(LOI)	--	--	--	7.60 --
TOTAL	100.38	0.89	0.728	100.38± .53

* - FeO determined gravimetrically.

Sample 782-II
N = 11

Rh - Tube for X-ray source.

a polycarbonate digestion bottle with 5 c.c. of hydrofluoric acid. The bottles are heated on a steam bath for about 1 hour. After cooling, 50 c.c. of saturated boric acid is added to each bottle in order to complex undissolved fluorides. The samples are again heated to insure complete dissolution, cooled and diluted with 145 c.c. of distilled deionized water to yield 200 c.c. of 1000 ppm solution. Standards are prepared in a similar manner.

Loss on ignition (L.O.I.) for H_2O, CO_2, SO_2, is determined by weighing an amount of sample powder in porcelein crucibles, heating to 1050°C for two to three hours, cooling in a dessicator, and weighing to determine the percent loss of volatiles.

(c) Trace Element Analysis

Determination of trace elements has been carried out by x-ray fluoresence on pressed powder pellets. Pellets are prepared by weighing and combining 10.0 grams of sample powder with 1.0 gram of binder. The mixture is homogenized by an automatic shaker for 10-15 minutes. After homogenization, powders are cooled to room temperature, then poured into a steel anvil press. a twelve ton force is used to press the pellets. The pressed pellets are placed in a 200°C oven for 5-10 minutes to activate the binder. Standards are prepared in a similar manner. Precision and accuracy results of trace element analyses are listed in Tables AI.2., and AI.3.

Table AI.2. Precision determination for trace elements (ppm) determined by XRF

	Mean	S.D.	Variance	95% C.I.
Nb	1.74	1.15	1.17	1.74± .75
Th	1.28	1.60	2.26	1.28± 1.1
Zr	4.61	0.55	0.27	4.61± .36
Y	3.16	0.91	0.73	3.16± .59
Sr	0.70	0.54	0.26	0.70± .35
Rb	0.12	0.36	0.12	0.12± .24
Pb	0.42	0.75	0.50	0.42± .49
Cr	2745	22.9	465.5	2745±14.9
V	61.8	2.45	5.35	61.8± 1.60
Ga	2.68	0.90	0.73	2.68± .59
Zn	40.9	1.53	2.09	40.9± 1.0
Cu	9.98	2.59	5.98	9.98± 1.69
Ni	2194	34.2	1036.8	2194±22.34

N = 9

Sample 77WH40SL

Rh-Tube for X-ray source.

Table AI.3. Accuracy determination for trace elements (ppm) determined by XRF

	GSP-1		AGV-1		W-1	
	(1)	(2)	(1)	(2)	(1)	(2)
Nb	32	29	18	15	8	9.5
Th	105	104	8	6.41	2	2.42
Zr	475	500	233	225	91	105
Y	17	30.4	20	21.3	24	25
Sr	235	233	670	657	190	190
Rb	258	254	68	67	22	21
Pb	54	51.3	35	35.1	6	7.8
Cr	21	12.5	22	12.2	117	114
V	43	52.9	120	125	256	264
Ga	21	22	22	20.5	18	16
Zn	99	98	82	84	86	86
Cu	29	33.3	59	59.7	109	110
Ni	23	12.5	20	18.5	79	76

(1) XRF, Rh-tube for X-ray source, M.U.N., runs = 2.

(2) Flanagan (1976), Table 107, p. 171-172.

(d) Rare Earth Elements

(1) Sample Preparation:

Into previously weighed polyethelene containers approximately 0.50 grams of sample powder are added. The containers are sealed then reweighed to determine the exact weight of sample. Containers are scratched for identification. To the marked container a length of Fe-wire, approximately equal to the circumference of the container and weighing approximately 0.03 grams, is wrapped around its midsection and secured in place by cellophane tape.

(2) Standards: MIT internal standards S-4, NB9 and NB11 have been prepared for use by Steve Roy.

(3) Irradiation: Prior to irradiation, the polyethelene sample containers are put into an additional polyethelene container by MIT reactor personnel. Irradiation time is 8 hours at a thermal neutron flux of approximately 7×10^{12} n cm^{-2} rec^{-1} (Suen, 1978).

(4) Counting Procedure: The samples are allowed to cool for 5 days. The outer containers are cut away, Fe-wire removed and placed in a labelled envelope and stored for counting (to correct for non-homogeneous distribution of the thermal flux during irradiation). The inner container is placed in a plastic capsule and made ready for counting. The count schedule and Gamma-ray energies of photopeaks used for unknown and standard samples are:

Nuclide	KeV	Half-life	Cooling time, detector, Counts
Ho 166	80.6	26.9H	1
Nd 147	91.1	266.4H	3
Sm 153	103.2	47.1H	1
Eu 152	121.8	12.2Y	4
Ce 141	145.4	780 H	3
Lu 177	208.4	161 H	2
Yb 175	282.6	100.8H	2
Tb 160	298.6	72 D	4
La 140	1596.2	40.27H	2

1 - 5 days; LEPS; 10K
2 - 8 days; Ge(Li); 20K
3 - 15 days; LEPS; 10K
4 - 30 days; Ge(Li); 20K

Raw data are reduced at MIT using a computer program developed at that facility (S. Roy, pers. comm., 1978).

Precision and accuracy are probably better than 10% for all elements by this method (S. Roy. pers. comm., 1978).

(5) Absolute Abundances of REE in White Hills Peridotite Samples (ppm)

	A	B	C	D
La	0.75	0.24	0.45	0.33
Ce	2.42	1.00	1.76	4.71
Nd	2.49	1.28	1.92	3.74
Sm	1.17	0.60	0.83	1.16
Eu	0.67	0.30	0.47	0.47
Tb	0.23	--	--	0.25
Ho	0.37	0.25	0.25	0.42
Yb	1.04	0.62	0.86	0.70
Lu	0.11	0.12	0.15	0.12
ΣREE	9.25	4.41	6.69	11.90
La/Yb	0.72	0.39	0.52	0.47

A: Recrystallized, equigranular gabbro vein; sample 77WH60; location 193.
B: Fine-grained gabbro vein; sample 77WH89; location 243.
C: Coarse-grained gabbro vein; sample 77WH90; location 243.
D: Clinopyroxenite vein; sample 77WH70; location 208.

APPENDIX II

Mineral Analyses of the White Hills Peridotite Lithologies.

TABLE AII.1.Olivine compositions from rocks of the White Hills Peridotite

Spinel lherzolite

	77WH1-3	77WH76-1	77WH94-2	7862-2	77WH5
SiO_2	40.70	39.78	41.82	41.42	39.75
TiO_2	n.d.	n.d.	0.02	n.d.	n.d.
Al_2O_3	0.02	n.d.	0.04	n.d.	n.d.
Cr_2O_3	n.d.	n.d.	n.d.	n.d.	0.01
FeO*	8.05	8.64	8.70	9.62	9.31
MnO	0.14	0.13	0.14	0.11	0.11
MgO	49.80	50.36	49.03	48.14	49.39
NiO	0.24	0.21	0.27	0.24	0.35
TOTAL	98.95	99.12	100.02	99.53	98.92
Si	1.001	0.981	1.017	1.017	0.986
Ti	--	--	--	--	--
Al	0.001	--	0.001	--	--
Cr	--	--	--	--	--
Fe	0.166	0.178	0.177	0.198	0.193
Mn	0.003	0.003	0.003	0.002	0.002
Mg	1.825	1.825	1.778	1.762	1.826
Ni	0.005	0.004	0.005	0.005	0.007
Fo(mole %)	91.6	91.1	90.8	89.8	90.4

* - Total iron as FeO.
n.d. - not detected
-- - not determined

77WH1-3 - recrystallized olivine.
77WH76-1 - recrystallized olivine.
77WH94-2 - recrystallized olivine.
7862-2 - recrystallized olivine.
77WH5 - recrystallized olivine, CaO = 0.01.

n - average value

TABLE AII.1. (Continued)

	77WH5-1	78105	78105-1	77WH12	7822
SiO_2	41.21	40.76	41.15	41.11	41.17
TiO_2	0.02	0.01	n.d.	n.d.	n.d.
Al_2O_3	n.d.	0.02	n.d.	n.d.	0.06
Cr_2O_3	0.01	0.03	n.d.	n.d.	n.d.
FeO*	9.10	9.62	9.85	9.69	9.73
MnO	0.11	0.08	0.11	0.14	0.09
MgO	49.73	49.41	49.13	49.63	49.55
NiO	0.36	0.40	0.30	0.29	0.28
TOTAL	100.54	100.33	100.54	100.86	100.88
Si	1.001	0.996	1.003	0.999	1.000
Ti	--	--	--	--	--
Al	--	0.001	--	--	0.002
Cr	--	0.001	--	--	--
Fe	0.185	0.197	0.201	0.197	0.198
Mn	0.002	0.002	0.002	0.003	0.002
Mg	1.801	1.799	1.785	1.797	1.793
Ni	0.007	0.008	0.006	0.006	0.005
Fo(mole %)	90.6	90.1	89.8	90.0	90.0

77WH5-1 recrystallized olivine, CaO = 0.02.
78105 recrystallized olivine, CaO = 0.04.
78105-1 recrystallized olivine, olivine apophysis in primary orthopyroxene.
77WH12 primary olivine, CaO = 0.02.
7822 primary olivine, CaO = 0.01.

TABLE AII.1. (Continued)

	795	795-2	7815	7815-1	78151
SiO_2	40.63	39.91	40.30	40.58	40.20
TiO_2	n.d.	0.01	n.d.	0.02	n.d.
Al_2O_3	n.d.	n.d.	n.d.	n.d.	n.d.
Cr_2O_3	n.d.	n.d.	n.d.	0.02	n.d.
FeO*	10.07	10.13	9.60	9.39	9.87
MnO	0.14	0.11	0.11	0.11	0.11
MgO	49.39	49.62	50.59	49.82	49.50
NiO	0.40	0.40	0.26	0.45	0.42
TOTAL	100.63	100.18	100.86	100.39	100.10
Si	0.993	0.981	0.981	0.991	0.987
Ti	--	--	--	--	--
Al	--	--	--	--	--
Cr	--	--	--	--	--
Fe	0.206	0.208	0.195	0.192	0.203
Mn	0.003	0.002	0.002	0.002	0.002
Mg	1.798	1.819	1.835	1.814	1.812
Ni	0.008	0.008	0.005	0.009	0.008
Fo(mole%)	89.6	89.7	90.3	90.4	89.9

795 primary olivine.
795-2 subhedral olivine in primary orthopyroxene.
7815 primary olivine.
7815-1 primary olivine.
78151 recrystallized olivine.

TABLE AII.1. (Continued)

	77WH11	77WH15A	77WH9	77WH16	796
SiO_2	39.21	39.83	40.39	40.44	39.27
TiO_2	0.03	n.d.	n.d.	n.d.	0.01
Al_2O_3	n.d.	n.d.	--	--	n.d.
Cr_2O_3	n.d.	0.02	0.04	n.d.	n.d.
FeO*	10.17	8.83	9.98	9.52	10.24
MnO	0.13	0.13	0.16	0.13	0.10
MgO	49.23	49.63	49.50	49.39	49.21
NiO	0.30	0.25	0.41	0.41	0.32
TOTAL	99.08	98.69	100.48	99.89	99.15
Si	0.976	0.987	0.988	0.993	0.977
Ti	0.001	--	--	--	--
Al	--	--	--	--	--
Cr	--	--	0.001	--	--
Fe	0.212	0.183	0.204	0.196	0.213
Mn	0.003	0.003	0.003	0.003	0.002
Mg	1.826	1.834	1.806	1.808	1.824
Ni	0.006	0.005	0.008	0.008	0.006
Fo(mole %)	89.5	90.8	89.7	90.2	89.5

77WH11 recrystallized olivine.
77WH15A recrystallized olivine.
77WH9 recrystallized olivine, Na_2O = 0.03.
77WH16 recrystallized olivine.
796 olivine enclosing clinopyroxene megacryst.

TABLE AII.1. (Continued) Harzburgites

	788	77WH56-2	7910	7914
SiO_2	40.13	41.94	40.54	40.04
TiO_2	0.01	0.02	n.d.	n.d.
Al_2O_3	n.d.	n.d.	n.d.	n.d.
Cr_2O_3	n.d.	0.03	n.d.	0.11
FeO*	9.57	8.65	8.97	9.31
MnO	0.10	0.13	0.11	0.14
MgO	49.36	49.36	50.36	49.89
NiO	0.45	0.28	0.36	0.44
TOTAL	99.62	100.41	100.34	99.93
Si	0.989	1.016	0.989	0.984
Ti	--	--	--	--
Al	--	--	--	--
Cr	--	0.001	--	--
Fe	0.197	0.175	0.183	0.191
Mn	0.002	0.003	0.002	0.003
Mg	1.813	1.783	1.830	1.828
Ni	0.009	0.005	0.007	0.009
Fo(mole %)	90.1	90.5	90.8	90.4

788 recrystallized olivine.

77WH56-2 recrystallized olivine.
7910 primary(?) olivine.
7914 deformed primary olivine.

TABLE AII.1. (Continued)

	Dunite				
	7818	797	797-1	799	7914
SiO_2	40.19	40.55	39.66	39.85	40.62
TiO_2	n.d.	n.d.	0.01	0.01	n.d.
Al_2O_3	n.d.	n.d.	n.d.	n.d.	n.d.
Cr_2O_3	0.01	n.d.	0.02	0.01	0.04
FeO*	8.57	9.30	9.28	10.10	9.55
MnO	0.07	0.11	0.10	0.10	0.09
MgO	50.66	50.39	50.79	50.07	50.70
NiO	0.39	0.21	0.45	0.46	0.42
TOTAL	99.89	100.56	100.31	100.60	101.42
Si	0.984	0.988	0.972	0.973	0.983
Ti	--	--	--	--	--
Al	--	--	--	--	--
Cr	--	--	--	--	0.001
Fe	0.175	0.189	0.190	0.208	0.193
Mn	0.001	0.002	0.002	0.002	0.002
Mg	1.848	1.829	1.855	1.835	1.829
Ni	0.008	0.004	0.009	0.009	0.008
Fo(mole %)	91.3	90.5	90.7	89.8	90.4

7818 - primary olivine.

797 - primary olivine; dunite dike cutting harzburgite.
797-1 - primary olivine; dunite dike cutting harzburgite.
799 - deformed primary olivine; dunite dike cutting harzburgite(7910).
7914 - deformed primary olivine; dunite layer interlayered with harzburgite(7914).

TABLE A.II.1. (Continued)

	78114	78152	7883	77WH55-1	77WH80-1
SiO_2	40.20	39.88	40.56	40.77	40.97
TiO_2	n.d.	0.02	n.d.	n.d.	0.01
Al_2O_3	n.d.	n.d.	n.d.	0.04	0.02
Gr_2O_3	n.d.	0.05	n.d.	0.04	n.d.
FeO*	9.28	10.47	9.46	8.64	8.26
MnO	0.11	0.09	0.08	0.12	0.13
MgO	50.42	49.29	49.07	50.88	51.14
NiO	0.54	0.36	0.39	0.32	0.31
TOTAL	100.55	100.16	99.56	100.81	100.84
Si	0.981	0.982	0.998	0.988	0.990
Ti	--	--	--	--	--
Al	--	--	--	0.001	0.001
Cr	--	0.001	--	0.001	--
Fe	0.190	0.216	0.195	0.175	0.167
Mn	0.002	0.002	0.002	0.002	0.003
Mg	1.835	1.809	1.800	1.838	1.842
Ni	0.011	0.007	0.008	0.006	0.006
Fo(mole %)	90.6	89.3	90.2	91.2	91.6

78114 recrystallized olivine; dunite megalens.
78152 deformed primary(?) olivine; dunite dike cutting spinel lherzolite(78151).
7883 recrystallized olivine; dunite dike cutting harzburgite(7882).
77WH55-1 recrystallized olivine; dunite layer interlayered with harzburgite(77WH56).
77WH80-1 recrystallized olivine; dunite layer interlayered with harzburgite(77WH81).

TABLE AII.1. (Continued)

	77WH93-1	78147-2	78141	77WH77	7841
SiO_2	40.15	39.43	39.63	41.39	41.38
TiO_2	n.d.	n.d.	0.01	n.d.	--
Al_2O_3	0.02	n.d.	n.d.	n.d.	--
Cr_2O_3	0.05	0.02	0.02	n.d.	--
FeO*	8.21	8.67	10.11	9.05	9.40
MnO	0.12	0.14	0.17	0.18	--
MgO	51.06	51.59	48.88	50.69	49.41
NiO	0.24	0.19	0.34	0.21	--
TOTAL	99.85	100.04	99.16	101.52	100.19
Si	0.981	0.966	0.984	0.996	1.008
Ti	--	--	--	--	--
Al	0.001	--	--	--	--
Cr	0.001	--	--	--	--
Fe	0.168	0.178	0.210	0.182	0.191
Mn	0.002	0.003	0.004	0.004	--
Mg	1.860	1.884	1.810	1.818	1.793
Ni	0.005	0.004	0.007	0.004	--
Fo(mole %)	91.6	91.3	89.5	90.7	90.4

77WH93-1 recrystallized olivine; dunite layer interlayered with spinel lherzolite(77WH94).
78147-2 recrystallized olivine; dunite layer interlayered with harzburgite(78146).
78141 deformed primary olivine; dunite dike.
77WH77 dunite layer interlayered with spinel lherzolite(77WH76).
7841 recrystallized olivine; dunite approximately 5 m above basalt thrust fault.

TABLE AII.1. (Continued)

	78117	77WH37	794
SiO_2	41.72	40.94	40.18
TiO_2	--	n.d.	n.d.
Al_2O_3	--	n.d.	n.d.
Cr_2O_3	--	0.04	n.d.
FeO*	9.11	8.48	10.88
MnO	--	0.18	0.11
MgO	47.94	50.10	48.81
NiO	--	0.25	0.34
TOTAL	98.77	99.99	100.32
Si	1.027	0.998	0.988
Ti	--	--	--
Al	--	--	--
Cr	--	0.001	--
Fe	0.188	0.173	0.224
Mn	--	0.004	0.002
Mg	1.759	1.821	1.789
Ni	--	0.005	0.007
Fo(mole %)	90.4	91.2	88.8

78117 recrystallized olivine; dunite megalens.
77WH37 deformed primary olivine.
794 recrystallized olivine; dunite layer interlayered with spinel lherzolite(795); CaO = 0.06.

TABLE AII.2. Olivine compositions from pyroxenite veins of the White Hills Peridotite

	Orthopyroxenite		
	7821	7850	7857
SiO_2	40.16	38.07	40.46
TiO_2	n.d.	n.d.	n.d.
Al_2O_3	0.01	0.01	n.d.
Cr_2O_3	n.d.	n.d.	n.d.
FeO*	9.59	16.79	8.61
MnO	0.07	0.22	0.07
MgO	49.75	43.81	49.35
NiO	0.31	n.d.	0.32
TOTAL	99.89	98.90	98.81
Si	0.987	0.978	0.999
Al	--	--	--
Ti	--	--	--
Cr	--	--	--
Fe^{2+}	0.197	0.361	0.178
Mg	1.822	1.678	1.816
Mn	0.001	0.005	0.001
Ni	0.006	--	0.006
Fo (mole %)	90.2	82.1	91.0

* - Total iron as FeO.
n.d. - not detected.
-- - not determined.

7821 - intercumulus olivine; sulphide-bearing pod; n = 3.
7850 - intercumulus olivine; orthopyroxenite boudin.
7857 - intercumulus-cumulus olivine; orthopyroxenite vein parallel to foliation; CaO = 0.01.

TABLE AII.2. (Continued)

	Websterite			
	77WH2	77WH7	783	78155
SiO_2	40.65	39.84	40.29	40.64
TiO_2	0.01	0.01	0.01	n.d.
Al_2O_3	--	0.01	n.d.	0.03
Cr_2O_3	n.d.	n.d.	0.01	n.d.
FeO*	6.64	11.19	9.27	8.82
MnO	0.12	0.11	0.13	0.07
MgO	51.97	48.75	50.40	49.86
NiO	0.37	0.33	0.32	0.36
TOTAL	99.76	100.24	100.43	99.78
Si	0.987	0.983	0.984	0.995
Al	--	--	--	0.001
Ti	--	--	--	--
Cr	--	--	--	--
Fe^{2+}	0.135	0.231	0.189	0.181
Mg	1.881	1.793	1.834	1.819
Mn	0.002	0.002	0.003	0.001
Ni	0.007	0.007	0.006	0.007
Fo (mole %)	93.2	88.6	90.6	90.9

77WH2 - recrystallized olivine; n = 3.
77WH7 - recrystallized olivine; websterite dike(?) approximately 8 cm wide; n = 3.
783 - recrystallized olivine; n = 2.
78155 - intercumulus olivine; websterite pod approximately 1/2 m x 1/3 m parallel to foliation; CaO = 0.02.

TABLE AII.2. (Continued)

Clinopyroxenite

	77WH70	77WH74	77WH79	78110	78118
SiO_2	40.23	39.41	40.47	39.80	39.69
TiO_2	0.04	n.d.	n.d.	n.d.	n.d.
Al_2O_3	n.d.	n.d.	0.01	n.d.	n.d.
Cr_2O_3	0.05	n.d.	n.d.	0.05	0.02
FeO*	11.58	13.77	11.78	14.59	14.57
MnO	0.21	0.14	0.20	0.14	0.14
MgO	46.69	46.84	47.34	45.73	45.93
NiO	0.20	0.27	0.21	0.27	0.27
TOTAL	99.00	100.43	100.01	100.58	100.62
Si	1.005	0.980	1.001	0.993	0.990
Al	--	--	--	--	--
Ti	0.001	--	--	--	--
Cr	0.001	--	--	0.001	--
Fe^{2+}	0.242	0.287	0.244	0.304	0.304
Mg	1.738	1.740	1.745	1.700	1.707
Mn	0.004	0.003	0.004	0.003	0.003
Ni	0.004	0.005	0.004	0.005	0.005
Fo (mole %)	87.6	85.8	87.6	84.7	84.8

77WH70 - recrystallized olivine.
77WH74 - recrystallized olivine; clinopyroxenite vein parallel to foliation; n = 3; no orthopyroxene; CaO = 0.01.
77WH79 - recrystallized olivine; n = 2.
78110 - recrystallized olivine; clinopyroxenite vein oblique to foliation.
78118 - recrystallized olivine; clinopyroxenite vein cutting dunite megalens; n = 2.

TABLE AII.2.(Continued)

	78128	78144	78159	798	7917
SiO_2	39.36	39.29	38.96	40.48	39.22
TiO_2	n.d.	n.d.	0.04	0.04	n.d.
Al_2O_3	--	n.d.	--	n.d.	--
Cr_2O_3	n.d.	n.d.	n.d.	0.02	n.d.
FeO*	15.07	13.86	13.79	11.21	14.18
MnO	0.20	0.13	0.23	0.13	0.14
MgO	45.71	46.87	46.93	48.40	46.12
NiO	0.23	0.19	0.18	0.36	0.21
TOTAL	100.57	100.34	100.13	100.64	99.87
Si	0.985	0.980	0.975	0.994	0.985
Al	--	--	--	--	--
Ti	--	--	0.001	0.001	--
Cr	--	--	--	--	--
Fe^{2+}	0.315	0.289	0.289	0.230	0.298
Mg	1.705	1.743	1.751	1.771	1.726
Mn	0.004	0.003	0.005	0.003	0.003
Ni	0.005	0.004	0.004	0.007	--
Fo (mole %)	84.3	85.7	85.7	88.4	85.2

78128 - deformed primary olivine; clinopyroxenite pod.
78144 - recrystallized olivine; clinopyroxenite vein cutting dunite (compare with 78118); n = 3; CaO = 0.01.
78159 - deformed primary olivine.
798 - recrystallized olivine; clinopyroxenite vein cutting dunite dike.
7917 - deformed primary olivine; n = 4.

TABLE AII.2. (Continued)

	Wehrlite
	78142
SiO_2	39.64
TiO_2	n.d.
Al_2O_3	n.d.
Cr_2O_3	0.02
FeO*	12.47
MnO	0.18
MgO	47.21
NiO	0.23
TOTAL	99.75
Si	0.998
Al	--
Ti	--
Cr	--
Fe^{2+}	0.260
Mg	1.754
Mn	0.004
Ni	0.005
Fo (mole %)	87.0

78142 - deformed primary olivine; wehrlite layer(?) parallel to foliation.

TABLE AII.3. Olivine compositions from gabbros of the White Hills Peridotite

	77WH60	77WH62	77WH89	77WH90	78111
SiO_2	38.60	38.88	39.27	38.16	38.93
TiO_2	n.d.	0.01	n.d.	0.02	0.01
Al_2O_3	0.37	n.d.	n.d.	0.04	n.d.
Cr_2O_3	n.d.	0.02	n.d.	n.d.	n.d.
FeO*	20.11	19.60	15.86	17.88	16.58
MnO	0.30	0.27	0.24	0.16	0.14
MgO	39.87	42.25	44.80	43.19	44.79
NiO	0.10	0.13	0.17	0.19	0.14
TOTAL	99.35	101.16	100.34	99.64	100.59
Si	1.000	0.987	0.988	0.978	0.981
Al	0.011	--	--	0.001	--
Ti	--	--	--	--	--
Cr	--	--	--	--	--
Fe^{2+}	0.436	0.416	0.334	0.383	0.349
Mg	1.539	1.599	1.681	1.650	1.682
Mn	0.007	0.006	0.005	0.003	0.003
Ni	0.002	0.003	0.003	0.004	0.003
Fo(mole %)	77.7	79.1	83.2	81.0	82.7

* - Total iron as FeO.
n.d. - not detected.
-- - not determined.

77WH60 - recrystallized olivine; gabbro vein within fault zone; n = 2.
77WH62 - recrystallized olivine; gabbro vein within fault zone.
77WH89 - deformed primary olivine; fine-grained gabbro vein.
77WH90 - deformed primary olivine; coarse-grained gabbro vein adjacent to 77WH89; n = 3; CaO = 0.01.
78111 - recrystallized olivine; gabbro vein; n = 3; CaO = 0.04.

TABLE AII.3. (Continued)

	78128	78129	78134	78135	78136
SiO_2	38.54	39.53	37.46	38.07	38.89
TiO_2	n.d.	n.d.	n.d.	0.02	n.d.
Al_2O_3	0.01	n.d.	n.d.	0.04	0.02
Cr_2O_3	n.d.	n.d.	n.d.	n.d.	0.01
FeO*	15.99	15.25	20.00	18.32	18.16
MnO	0.14	0.25	0.27	0.16	0.18
MgO	45.46	43.69	42.75	43.50	43.54
NiO	0.24	0.20	0.24	0.19	0.19
TOTAL	100.38	98.92	100.72	100.30	100.99
Si	0.972	1.005	0.962	0.972	0.983
Al	—	—	—	0.001	0.001
Ti	—	—	—	—	—
Cr	—	—	—	—	—
Fe^{2+}	0.337	0.324	0.430	0.391	0.384
Mg	1.709	1.656	1.636	1.655	1.641
Mn	0.003	0.005	0.006	0.003	0.004
Ni	0.005	0.004	0.005	0.004	0.004
Fo(mole %)	83.4	83.4	79.0	80.8	80.9

78128 - deformed primary olivine; gabbro vein cutting clinopyroxenite pod; n = 3; CaO = 0.02.
78129 - deformed primary olivine; gabbro vein approximately 18 cm wide; n = 2.
78134 - deformed primary olivine; fine-grained foliated gabbro vein.
78135 - deformed primary olivine; medium to coarse-grained gabbro vein; n = 3.
78136 - recrystallized(?) olivine; medium to coarse-grained gabbro vein; n = 3.

TABLE AII.3. (Continued)

	78150
SiO_2	38.81
TiO_2	0.01
Al_2O_3	n.d.
Cr_2O_3	n.d.
FeO*	16.97
MnO	0.14
MgO	44.57
NiO	0.28
TOTAL	100.78
Si	9.979
Al	—
Ti	--
Cr	--
Fe^{2+}	0.358
Mg	1.675
Mn	0.003
Ni	0.006
Fo(mole %)	82.3

78150 - recrystallized olivine; gabbro vein; n = 3.

TABLE AII.4: Olivine compositions from rocks associated with chromite from the White Hills Peridotite.

	77WH19	77WH30	7898	784	7897
SiO_2	40.98	41.85	40.79	40.68	39.75
TiO_2	n.d.	n.d.	0.01	n.d.	n.d.
Al_2O_3	0.02	0.02	n.d.	n.d.	0.03
Cr_2O_3	0.01	0.02	0.01	n.d.	n.d.
FeO*	7.15	6.79	7.77	6.94	7.56
MnO	0.12	0.07	0.11	0.05	0.04
MgO	50.92	50.13	51.17	51.80	51.43
NiO	0.42	0.74	0.44	0.62	0.32
TOTAL	99.62	99.62	100.30	100.09	99.13
Si	0.998	1.016	0.990	0.987	0.977
Al	0.001	0.001	--	--	0.001
Ti	--	--	--	--	--
Cr	--	--	--	--	--
Fe	0.146	0.138	0.158	0.141	0.155
Mg	1.848	1.813	1.851	1.873	1.883
Mn	0.002	0.001	0.002	0.001	0.001
Ni	0.008	0.014	0.009	0.012	0.006
Fo (mole %)	92.6	92.9	92.1	93.0	92.4

* - Total iron as FeO.
n.d. - not detected.
-- - not determined.

77WH19 - recrystallized olivine; orthopyroxenite vein associated with a seam of chromitite; n = 3.
77WH30 - intercumulus olivine; orthopyroxenite vein associated with a seam of chromite.
7898 - intercumulus olivine; orthopyroxenite vein associated with disseminated chromite; n = 5.
784 - intercumulus olivine; n = 4.
7897 - intercumulus olivine; fine-grained orthopyroxenite vein.

TABLE AII.5. Orthopyroxene compositions from rocks of the White Hills Peridotite

Spinel lherzolite

	77WH1-4	77WH-1	77WH16	77WH76-2	77WH94-1
SiO_2	53.84	53.48	54.03	53.19	54.55
TiO_2	0.04	0.05	0.05	0.05	0.03
Al_2O_3	5.57	6.14	5.14	4.90	4.38
Cr_2O_3	0.77	0.95	0.64	0.56	0.59
FeO*	5.50	6.63	6.08	6.24	6.15
MnO	0.13	0.16	0.11	0.19	0.10
MgO	33.10	31.83	31.77	34.25	33.75
CaO	1.48	0.68	1.21	0.32	0.95
Na_2O	0.05	n.d.	0.07	0.01	0.03
K_2O	n.d.	--	n.d.	--	--
NiO	0.07	0.05	0.08	0.09	0.02
TOTAL	100.55	99.97	99.18	99.80	100.55
Si	1.854	1.856	1.885	1.849	1.879
Al^{IV}	0.146	0.144	0.115	0.151	0.121
Al^{VI}	0.080	0.107	0.097	0.049	0.057
Ti	0.001	0.001	0.001	0.001	0.001
Cr	0.021	0.026	0.018	0.015	0.016
Fe	0.158	0.192	0.177	0.181	0.177
Mg	1.699	1.646	1.652	1.774	1.733
Mn	0.004	0.005	0.003	0.006	0.003
Ni	0.002	0.001	0.002	0.003	0.001
Ca	0.055	0.025	0.045	0.012	0.035
Na	0.003	--	0.005	0.001	0.002
K	--	--	--	--	--

TABLE AII.5. (Continued)

	77WH1-4	77WH-1	77WH16	77WH76-2	77WH94-1
Ca	2.85	1.35	2.41	0.60	1.80
Mg	88.69	88.11	87.89	89.93	88.96
Fe_T	8.46	10.54	9.60	9.47	9.24

* - Total iron as FeO.
n.d. - not detected.
-- - not determined.

77WH1-4 - primary orthopyroxene.
77WH-1 - primary orthopyroxene.
77WH16 - deformed primary orthopyroxene.
77WH76-2 - deformed primary orthopyroxene.
77WH94-1 - primary orthopyroxene.

TABLE AII.5. (Continued)

	795	796	7815	7862	78151
SiO_2	51.68	53.41	53.91	54.32	53.90
TiO_2	0.17	0.15	0.07	0.05	0.11
Al_2O_3	7.19	5.31	4.77	5.31	4.79
Cr_2O_3	0.55	0.50	0.74	0.56	0.56
FeO*	6.42	6.40	5.95	6.16	5.89
MnO	0.11	0.11	0.13	0.10	0.13
MgO	32.55	32.27	32.02	32.95	32.65
CaO	0.58	0.65	1.96	0.50	1.14
Na_2O	0.09	0.06	0.01	n.d.	0.05
K_2O	--	--	--	--	--
NiO	0.04	0.05	0.13	0.14	0.12
TOTAL	99.38	98.91	99.69	100.09	99.34
Si	1.806	1.870	1.878	1.879	1.879
Al^{IV}	0.194	0.130	0.122	0.121	0.121
Al^{VI}	0.102	0.089	0.074	0.095	0.076
Ti	0.004	0.004	0.002	0.001	0.003
Cr	0.015	0.014	0.020	0.015	0.015
Fe	0.188	0.187	0.173	0.178	0.172
Mg	1.695	1.684	1.662	1.688	1.695
Mn	0.003	0.003	0.004	0.003	0.004
Ni	0.001	0.001	0.004	0.004	0.003
Ca	0.022	0.024	0.073	0.019	0.043
Na	0.006	0.004	0.001	--	0.003
K	--	--	--	--	--

TABLE AII.5. (Continued)

	795	796	7815	7862	78151
Ca	1.14	1.28	3.82	0.98	2.23
Mg	88.86	88.68	86.94	89.45	88.62
Fe_T	10.00	10.04	9.24	9.57	9.15

* - Total iron as FeO.
n.d. - not detected.
-- - not determined.

795 - primary orthopyroxene
796 - orthopyroxene in spinel lherzolite enclosing clinopyroxene megacryst.
7815 - primary orthopyroxene.
7862 - slightly deformed primary orthopyroxene.
78151 - primary orthopyroxene.

TABLE A1.5. (Continued)

	77WH12	77WH5	7822	788	788-1
SiO_2	55.42	55.04	56.25	54.13	54.12
TiO_2	0.06	0.09	0.07	0.11	0.14
Al_2O_3	3.83	5.00	3.89	5.88	5.55
Cr_2O_3	0.49	0.58	0.45	0.59	0.46
FeO*	6.04	6.00	6.45	6.17	5.94
MnO	0.11	0.11	0.13	0.07	0.08
MgO	33.20	32.82	32.68	32.18	32.50
CaO	0.64	0.71	0.65	1.19	0.86
Na_2O	--	--	--	0.10	0.05
K_2O	--	--	--	--	--
NiO	0.06	0.15	0.09	0.11	0.02
TOTAL	99.85	100.50	100.66	100.53	99.72
Si	1.915	1.891	1.929	1.865	1.874
Al^{IV}	0.085	0.109	0.071	0.135	0.126
Al^{VI}	0.071	0.093	0.086	0.104	0.101
Ti	0.002	0.002	0.002	0.003	0.004
Cr	0.013	0.016	0.012	0.016	0.013
Fe	0.175	0.172	0.185	0.178	0.172
Mg	1.710	1.681	1.670	1.652	1.677
Mn	0.003	0.003	0.004	0.002	0.002
Ni	0.002	0.004	0.002	0.003	0.001
Ca	0.024	0.026	0.024	0.044	0.032
Na	—	—	—	0.007	0.003
K	--	--	--	—	--

TABLE AII.5. (Continued)

	77WH12	77WH5	7822	788	788-1
Ca	1.24	1.39	1.27	2.34	1.69
Mg	89.47	89.31	88.72	88.09	89.05
Fe_T	9.29	9.30	10.01	9.57	9.26

77WH12 - primary orthopyroxene.
77WH5 - primary orthopyroxene.
7822 - primary orthopyroxene.
788 - deformed primary orthopyroxene.
788-1 - deformed primary orthopyroxene.

TABLE AII.5. (Continued)

	77WH11	77WH15A	78105	78105-1	78105-2
SiO_2	53.34	55.56	54.18	54.02	54.98
TiO_2	0.18	0.07	0.07	0.11	0.07
Al_2O_3	6.32	3.40	5.63	6.53	4.01
Cr_2O_3	0.45	0.27	0.68	0.74	0.35
FeO*	5.38	5.95	6.47	6.13	6.72
MnO	0.11	0.11	0.11	0.10	0.11
MgO	31.51	33.56	31.89	31.29	33.24
CaO	1.90	0.59	0.67	1.64	0.32
Na_2O	0.18	0.02	--	--	--
K_2O	--	--	--	--	--
NiO	0.14	0.09	0.09	0.09	0.15
TOTAL	99.51	99.62	99.79	100.65	99.95
Si	1.855	1.923	1.878	1.859	1.904
Al^{IV}	0.145	0.077	0.122	0.141	0.096
Al^{VI}	0.114	0.062	0.109	0.124	0.067
Ti	0.005	0.002	0.002	0.003	0.002
Cr	0.012	0.007	0.019	0.020	0.010
Fe	0.156	0.172	0.188	0.176	0.195
Mg	1.633	1.731	1.648	1.605	1.715
Mn	0.003	0.003	0.003	0.003	0.003
Ni	0.004	0.003	0.003	0.002	0.004
Ca	0.071	0.022	0.025	0.060	0.012
Na	0.012	0.001	--	--	--
K	--	--	--	--	--

TABLE A.II.5. (Continued)

	77WH11	77WH15A	78105	78105-1	78105-2
Ca	3.79	1.13	1.33	3.27	0.62
Mg	87.66	89.78	88.44	87.02	89.13
Fe_T	8.55	9.09	10.23	9.71	10.25

77WH11 - primary orthopyroxene.
77WH15A - primary orthopyroxene.
78105 - rim of primary orthopyroxene adjacent to primary clinopyroxene.
78105-1 - core of primary orthopyroxene adjacent to primary clinopyroxene.
78105-2 - primary orthopyroxene adjacent to olivine(analysis 78105-1, see Table A.II.1.).

TABLE AII.5. (Continued)

	Harzburgite				
	77WH56-1	7910	7914	7818	78104
SiO_2	56.37	55.92	56.31	55.63	55.97
TiO_2	0.04	0.06	0.09	n.d.	0.07
Al_2O_3	2.00	2.56	2.71	2.10	4.02
Cr_2O_3	0.45	0.41	0.64	0.46	0.44
FeO*	6.04	5.65	5.90	5.67	6.26
MnO	0.15	0.09	0.14	0.12	0.14
MgO	34.78	34.66	33.91	34.89	33.35
CaO	0.31	0.74	0.81	0.91	0.75
Na_2O	n.d.	0.04	n.d.	n.d.	--
K_2O	--	--	--	--	--
NiO	0.05	0.12	0.07	0.01	0.04
TOTAL	100.19	100.25	100.58	99.79	101.04
Si	1.941	1.925	1.933	1.925	1.913
Al^{IV}	0.059	0.075	0.067	0.075	0.087
Al^{VI}	0.022	0.028	0.042	0.011	0.075
Ti	0.001	0.002	0.002	--	0.002
Cr	0.012	0.011	0.017	0.013	0.012
Fe	0.174	0.163	0.169	0.164	0.179
Mg	1.785	1.778	1.735	1.800	1.699
Mn	0.004	0.003	0.004	0.004	0.004
Ni	0.001	0.003	0.002	--	0.001
Ca	0.011	0.027	0.030	0.034	0.027
Na	--	0.003	--	--	--
K	--	--	--	--	--

TABLE AII.5. (Continued)

	77WH56-1	7910	7914	7818	78104
Ca	0.58	1.38	1.54	1.69	1.44
Mg	90.40	90.24	89.52	89.94	88.98
Fe_T	9.02	8.38	8.94	8.37	9.58

77WH56-1 - primary orthopyroxene.
7910 - primary orthopyroxene.
7914 - primary orthopyroxene.
7818 - primary orthopyroxene.
78104 - primary orthopyroxene.

TABLE AII-6. Orthopyroxene compositions from pyroxenites of the White Hills Peridotite

	Orthopyroxenite		
	7821	7850	7857
SiO_2	52.99	53.55	53.84
TiO_2	0.08	0.12	0.04
Al_2O_3	5.43	4.45	4.85
Cr_2O_3	0.47	0.35	0.64
FeO^*	6.08	6.42	6.09
MnO	0.10	0.12	0.11
MgO	32.42	32.83	32.96
CaO	1.08	0.68	0.52
Na_2O	--	--	--
K_2O	--	--	--
NiO	0.07	0.16	0.11
TOTAL	98.72	98.68	99.16
Si	1.860	1.881	1.878
Al^{IV}	0.140	0.119	0.172
Al^{VI}	0.084	0.065	0.077
Ti	0.002	0.003	0.001
Cr	0.013	0.010	0.018
Fe	0.178	0.189	0.178
Mg	1.696	1.719	1.713
Mn	0.003	0.004	0.003
Ni	0.002	0.005	0.003
Ca	0.041	0.026	0.019
Na	--	--	--
K	--	--	--

TABLE AII.6. (Continued)

	7821	7850	7857
Ca	2.12	1.32	1.01
Mg	88.43	88.78	89.55
Fe_T	9.45	9.90	9.44

* - Total iron as FeO.
n.d. - not detected.
-- - not determined

7821 - cumulus orthopyroxene; sulphide-bearing pod; n = 4.
7850 - cumulus orthopyroxene; orthopyroxenite boudin; n = 3.
7857 - cumulus orthopyroxene; orthopyroxenite boudin parallel to foliation; n = 3.

TABLE AII.6. (Continued)

	Websterite			
	77WH2	77WH7	783	7854
SiO_2	54.28	53.09	53.80	53.58
TiO_2	0.04	0.05	0.09	0.08
Al_2O_3	5.24	5.59	6.95	4.99
Cr_2O_3	0.22	0.29	0.42	0.24
FeO*	5.38	7.11	5.99	8.28
MnO	0.15	0.13	0.12	0.14
MgO	34.12	31.82	31.89	31.66
CaO	0.57	0.99	1.22	0.44
Na_2O	0.01	--	0.04	n.d.
K_2O	--	--	n.d.	--
NiO	0.07	0.11	0.05	0.07
TOTAL	100.08	99.18	100.57	99.48
Si	1.868	1.860	1.849	1.878
Al^{IV}	0.132	0.139	0.151	0.122
Al^{VI}	0.081	0.093	0.131	0.085
Ti	0.001	0.001	0.002	0.002
Cr	0.006	0.008	0.011	0.007
Fe	0.155	0.209	0.172	0.243
Mg	1.751	1.663	1.634	1.654
Mn	0.004	0.004	0.003	0.004
Ni	0.002	0.003	0.001	0.002
Ca	0.021	0.037	0.045	0.017
Na	0.001	—	0.003	--
K	--	—	—	--

TABLE AII.6. (Continued)

	77WH2	77WH7	783	7854
Ca	1.09	1.94	2.42	0.86
Mg	90.67	86.97	88.11	86.28
Fe_T	8.24	11.09	9.47	12.86

77WH2 - deformed primary orthopyroxene; n = 3.
77WH7 - deformed primary orthopyroxene; websterite dike(?) approximately 8 cm wide; n = 3.
783 - deformed primary orthopyroxene; n = 2.
7854 - recrystallized orthopyroxene; websterite boudin approximately 2 cm above basal fault; no olivine, spinel.

TABLE AII.6. (Continued)

Clinopyroxenite

	77WH79	78110	78118	78159	798
SiO_2	54.38	54.48	54.48	52.09	53.48
TiO_2	0.10	0.11	0.11	0.13	0.19
Al_2O_3	4.37	3.71	3.71	5.81	5.49
Cr_2O_3	0.48	0.18	0.18	0.61	0.33
FeO*	7.59	9.62	9.02	9.35	6.65
MnO	0.21	0.18	0.18	0.24	0.13
MgO	32.73	31.87	31.87	31.17	31.67
CaO	0.44	0.52	0.52	0.63	1.54
Na_2O	0.03	0.01	0.01	0.03	0.05
K_2O	n.d.	n.d.	--	--	--
NiO	0.06	0.03	0.03	0.04	0.08
TOTAL	100.39	100.71	100.11	100.10	99.58
Si	1.885	1.898	1.904	1.832	1.866
Al^{IV}	0.115	0.102	0.096	0.168	0.134
Al^{VI}	0.064	0.051	0.057	0.073	0.092
Ti	0.003	0.003	0.003	0.003	0.005
Cr	0.013	0.005	0.005	0.017	0.009
Fe	0.220	0.280	0.264	0.275	0.194
Mg	1.691	1.655	1.660	1.634	1.647
Mn	0.006	0.005	0.005	0.007	0.004
Ni	0.002	0.001	0.001	0.001	0.002
Ca	0.016	0.019	0.019	0.024	0.058
Na	0.002	0.001	0.001	0.002	0.003
K	--	--	--	--	--

TABLE A11.5. (Continued)

	77WH79	78110	78118	78159	798
Ca	0.84	0.99	1.00	1.22	3.02
Mg	87.47	84.44	85.20	84.24	86.59
Fe_T	11.69	14.57	13.80	14.54	10.39

77WH79 - recrystallized orthopyroxene.
78110 - recrystallized orthopyroxene; clinopyroxenite vein oblique to foliation.
78118 - recrystallized orthopyroxene; clinopyroxenite vein cutting dunite megalens.
78159 - deformed primary orthopyroxene; n = 7.
798 - recrystallized orthopyroxene; clinopyroxenite vein cutting dunite dike; n = 2.

TABLE AII.6. (Continued)

	7917
SiO_2	53.88
TiO_2	0.24
Al_2O_3	4.55
Cr_2O_3	0.20
FeO*	8.96
MnO	0.15
MgO	30.71
CaO	0.62
Na_2O	0.04
K_2O	--
NiO	0.02
TOTAL	99.37
Si	1.896
Al^{IV}	0.104
Al^{VI}	0.085
Ti	0.006
Cr	0.006
Fe	0.264
Mg	1.611
Mn	0.004
Ni	0.001
Ca	0.023
Na	0.003
K	—

TABLE AII.6. (Continued)

	7917
Ca	1.23
Mg	84.68
Fe_T	14.09

7917 - deformed primary orthopyroxene.

TABLE AII.7. Orthopyroxene compositions from gabbros of the White Hills Peridotite

	77WH60	77WH86	78134	78136
SiO_2	52.95	53.59	54.09	54.25
TiO_2	0.21	0.20	0.13	0.09
Al_2O_3	4.31	5.20	3.95	3.64
Cr_2O_3	0.06	0.13	0.01	0.01
FeO*	12.83	11.30	12.43	9.97
MnO	0.29	0.24	0.24	0.27
MgO	28.71	29.02	29.67	31.96
CaO	0.69	0.90	0.46	0.59
Na_2O	0.02	0.02	0.04	0.01
K_2O	--	n.d.	n.d.	n.d.
NiO	0.03	0.04	n.d.	0.04
TOTAL	100.10	100.64	101.02	100.83
Si	1.886	1.883	1.901	1.893
Al^{IV}	0.114	0.117	0.099	0.107
Al^{VI}	0.067	0.098	0.065	0.043
Ti	0.006	0.005	0.003	0.002
Cr	0.002	0.004	--	--
Fe^{2+}	0.382	0.332	0.365	0.291
Mg	1.524	1.520	1.554	1.662
Mn	0.009	0.007	0.007	0.008
Ni	0.001	0.001	--	0.001
Ca	0.026	0.034	0.017	0.022
Na	0.001	0.001	0.003	0.001
K	--	--	--	--

TABLE AII.7. (Continued)

	77WH60	77WH86	78134	78136
Ca	1.36	1.79	0.89	1.11
Mg	78.51	80.30	79.95	83.82
Fe_T	20.13	17.91	19.16	15.07

* - Total iron as FeO.
n.d. - not detected.
-- - not determined.

77WH60 - recrystallized orthopyroxene; gabbro vein within fault zone; n = 2.
77WH86 - recrystallized orthopyroxene; gabbro vein within fault zone.
78134 - recrystallized(?) orthopyroxene; fine-grained foliated gabbro vein.
78136 - recrystallized(?) orthopyroxene; medium to coarse-grained gabbro vein.

TABLE AII.8. Orthopyroxene compositions from rocks associated with chromite from the White Hills Peridotite

	77WH19	77WH30	7898	7898t	78119
SiO_2	57.85	56.36	55.42	55.68	58.20
TiO_2	0.03	0.03	0.01	n.d.	0.05
Al_2O_3	0.68	0.90	1.68	1.02	1.43
Cr_2O_3	0.37	0.55	0.70	0.48	0.50
FeO*	4.97	4.48	5.33	5.64	5.23
MnO	0.15	0.10	0.15	0.15	0.09
MgO	35.89	36.28	36.24	36.70	34.64
CaO	0.56	0.68	0.94	0.49	0.59
Na_2O	n.d.	0.04	0.01	0.01	0.02
K_2O	n.d.	n.d.	n.d.	n.d.	n.d.
NiO	0.14	0.16	0.13	0.12	0.16
TOTAL	100.64	99.58	100.61	100.29	100.91
Si	1.974	1.946	1.907	1.921	1.979
Al^{IV}	0.026	0.037	0.068	0.041	0.021
Al^{VI}	0.001	--	--	--	0.036
Ti	0.001	0.001	--	--	0.001
Cr	0.010	0.015	0.019	0.013	0.013
Fe	0.142	0.129	0.153	0.163	0.149
Mg	1.825	1.867	1.859	1.887	1.756
Mn	0.004	0.003	0.004	0.004	0.003
Ni	0.004	0.004	0.004	0.003	0.004
Ca	0.020	0.025	0.035	0.018	0.021
Na	--	0.003	0.001	0.001	0.001
K	--	--	--	--	--

TABLE AII.8. (Continued)

	77WH19	77WH30	7898	7898t	78119
Ca	1.03	1.24	1.69	0.87	1.11
Mg	91.65	92.24	90.63	91.08	91.06
Fe_T	3.32	6.52	7.68	8.05	7.83

* - Total iron as FeO.
n.d. - not detected.
-- - not determined.

77WH19 - cumulus orthopyroxene; orthopyroxenite vein associated with a seam of chromitite; n = 3.
77WH30 - cumulus orthopyroxene; orthopyroxenite vein associated with a seam of chromitite; n = 2.
7898 - cumulus orthopyroxene; orthopyroxenite vein associated with disseminated chromite; n = 3.
7898t - recrystallized orthopyroxene adjacent to cumulus orthopyroxene; orthopyroxenite vein associated with disseminated chromite.
78119 - cumulus orthopyroxene; orthopyroxenite vein with core of chromitite (~1cm wide).

TABLE AII.8. (Continued)

	78122X	78123X	784	7897
SiO_2	56.44	56.55	59.16	57.41
TiO_2	0.02	0.02	0.02	0.01
Al_2O_3	2.28	1.32	1.23	1.31
Cr_2O_3	0.78	0.46	0.48	0.38
FeO*	5.31	6.00	4.47	5.09
MnO	0.14	0.10	0.07	0.10
MgO	34.81	34.25	35.24	34.28
CaO	0.77	0.59	0.84	0.96
Na_2O	0.01	n.d.	--	--
K_2O	n.d.	n.d.	--	--
NiO	0.13	0.24	0.15	0.12
TOTAL	100.69	99.53	101.66	99.66
Si	1.932	1.961	1.989	1.978
Al^{IV}	0.068	0.039	0.011	0.022
Al^{VI}	0.024	0.039	0.038	0.031
Ti	0.001	0.015	0.001	--
Cr	0.021	0.013	0.013	0.010
Fe	0.152	0.174	0.126	0.147
Mg	1.776	1.771	1.766	1.760
Mn	0.004	0.003	0.002	0.003
Ni	0.004	0.003	0.004	0.003
Ca	0.028	0.022	0.030	0.035
Na	0.001	--	--	--
K	--	--	--	--

TABLE AII.8.(Continued)

	78122X	78123X	784	7898
Ca	1.44	1.11	1.57	1.82
Mg	90.61	89.93	91.81	90.50
Fe_T	7.95	8.96	6.62	7.68

78122X - cumulus orthopyroxene; "websterite" assemblage associated with chromitite.
78123X - cumulus orthopyroxene; "websterite" assemblage associated with chromitite.
784 - cumulus orthopyroxene; n = 3.
7897 - cumulus orthopyroxene; fine-grained orthopyroxenite vein; n = 3.

TABLE AII.9. Clinopyroxene compositions from rocks of the White Hills Peridotite

Spinel lherzolite

	77WH1-2	77WH76-4	77WH94-3	7862-1	795
SiO_2	51.91	50.76	52.46	48.92	51.01
TiO_2	0.12	0.23	0.20	0.16	0.63
Al_2O_3	6.07	5.43	4.89	6.19	8.46
Cr_2O_3	1.20	1.14	1.08	0.98	0.77
FeO^*	2.07	2.63	2.46	2.35	2.88
MnO	0.10	0.05	0.09	0.05	0.07
MgO	15.84	16.53	17.94	15.84	14.46
CaO	22.88	23.77	20.54	23.34	20.16
Na_2O	0.70	0.68	0.69	0.86	1.70
K_2O	n.d.	--	--	--	--
NiO	0.02	n.d.	0.11	0.05	0.06
TOTAL	100.91	101.22	100.46	98.74	100.20
Si	1.864	1.837	1.879	1.815	1.838
Al^{IV}	0.136	0.163	0.121	0.185	0.162
Al^{VI}	0.120	0.068	0.090	0.086	0.197
Ti	0.003	0.006	0.005	0.004	0.017
Cr	0.034	0.033	0.031	0.029	0.022
Fe^{3+}	0.024	--	0.037	--	0.028
Fe^{2+}	0.038	0.080	0.036	0.073	0.059
Mg	0.848	0.891	0.958	0.876	0.776
Mn	0.003	0.002	0.003	0.002	0.002
Ni	0.001	—	0.003	0.001	0.002
Ca	0.880	0.922	0.789	0.928	0.778
Na	0.049	0.048	0.048	0.062	0.119
K	—	—	--	--	—

TABLE AII.9. (Continued)

	77WH1-2	77WH76-4	77WH94-3	7862-1	795
Ca	49.08	48.66	43.18	49.36	47.30
Mg	47.29	47.06	52.63	46.67	47.29
Fe_T	3.64	4.28	4.19	3.96	5.40

* - Total iron as FeO.
n.d. - not detected.
-- - not determined.

77WH1-2 - primary clinopyroxene.
77WH76-4 - recrystallized clinopyroxene.
77WH94-3 - deformed primary clinopyroxene.
7862-1 - primary clinopyroxene.
795 - primary clinopyroxene.

TABLE AII.9. (Continued)

	7815	78151	77WH11	77WH11-exs	77WH5
SiO_2	51.96	52.01	51.12	50.06	52.61
TiO_2	0.10	0.22	0.57	0.82	0.33
Al_2O_3	5.18	5.59	7.33	7.56	5.73
Cr_2O_3	1.16	1.07	0.71	0.86	0.88
FeO*	2.22	2.17	2.55	2.12	2.32
MnO	0.05	0.05	0.04	0.04	0.05
MgO	15.62	15.41	14.80	14.62	15.65
CaO	23.35	22.57	20.98	21.32	22.18
Na_2O	0.20	0.69	1.29	1.59	--
K_2O	--	--	--	--	--
NiO	0.12	0.04	0.09	0.02	0.08
TOTAL	99.96	99.82	99.48	99.01	99.83
Si	1.888	1.889	1.858	1.834	1.901
Al^{IV}	0.112	0.111	0.142	0.166	0.099
Al^{VI}	0.110	0.128	0.172	0.161	0.145
Ti	0.003	0.006	0.016	0.023	0.009
Cr	0.033	0.031	0.020	0.025	0.025
Fe^{3+}	--	--	0.009	--	--
Fe^{2+}	0.067	0.066	0.069	0.065	0.070
Mg	0.846	0.834	0.802	0.798	0.843
Mn	0.002	0.002	0.001	0.001	0.002
Ni	0.004	0.001	0.003	0.001	0.002
Ca	0.909	0.878	0.817	0.837	0.859
Na	0.014	0.049	0.091	0.113	--
K	--	--	--	--	--

TABLE AII.9. (Continued)

	7815	78151	77WH11	77WH11-exs	77WH5
Ca	49.95	49.32	48.06	49.17	48.37
Mg	46.48	46.90	47.31	46.94	47.60
Fe_T	3.78	3.79	4.36	3.89	4.03

7815 - primary clinopyroxene.
78151 - primary clinopyroxene.
77WH11 - recrystallized clinopyroxene.
77WH11-exs - clinopyroxene exsolution in primary orthopyroxene.
77WH5 - recrystallized clinopyroxene.

TABLE AII.9. (Continued)

	77WH5-1	78105	78105-r	77WH12	7822
SiO_2	51.38	50.86	52.55	52.54	51.83
TiO_2	0.39	0.30	0.25	0.11	0.19
Al_2O_3	6.34	6.44	4.21	4.55	6.09
Cr_2O_3	1.08	0.95	0.47	1.02	0.97
FeO*	2.25	2.32	2.48	2.54	1.97
MnO	0.07	0.06	0.05	0.06	0.05
MgO	14.98	15.49	16.57	16.10	15.57
CaO	22.49	22.76	22.74	23.50	23.14
Na_2O	--	--	--	--	--
K_2O	--	--	--	--	--
NiO	0.07	0.03	0.05	0.04	0.06
TOTAL	99.05	99.21	99.37	100.46	99.87
Si	1.877	1.859	1.914	1.900	1.878
Al^{IV}	0.123	0.141	0.086	0.100	0.122
Al^{VI}	0.150	0.136	0.095	0.094	0.138
Ti	0.011	0.008	0.007	0.003	0.005
Cr	0.031	0.027	0.014	0.029	0.028
Fe^{3+}	--	--	--	--	--
Fe^{2+}	0.069	0.071	0.076	0.077	0.060
Mg	0.816	0.844	0.900	0.868	0.841
Mn	0.002	0.002	0.002	0.002	0.002
Ni	0.002	0.001	0.001	0.001	0.002
Ca	0.880	0.891	0.888	0.911	0.898
Na	--	--	--	--	--
K	--	--	--	--	--

TABLE AII.9.4 (Continued)

	77WH5-1	78105	78105-r	77WH12	7822
Ca	49.77	49.28	47.57	49.01	49.85
Mg	46.22	46.70	48.29	46.76	46.75
Fe_T	4.01	4.02	4.14	4.23	3.40

77WH5-1 - recrystallized clinopyroxene.
78105 - primary clinopyroxene.
78105-r - recrystallized clinopyroxene adjacent to primary clinopyroxene.
77WH12 - primary clinopyroxene.
7822 - primary clinopyroxene.

TABLE AII.9.(Continued)

	Harzburgite			
	796	77WH56-3	78104	78104-1
SiO_2	51.44	51.80	51.33	51.13
TiO_2	0.49	0.20	0.21	0.26
Al_2O_3	6.72	3.76	5.94	6.01
Cr_2O_3	0.74	1.38	0.88	0.85
FeO^*	2.80	1.71	2.66	2.60
MnO	0.09	0.07	0.07	0.05
MgO	15.17	16.62	16.27	15.94
CaO	20.70	24.01	21.85	22.49
Na_2O	1.76	0.63	--	--
K_2O	--	--	--	--
NiO	0.08	0.06	0.04	0.04
TOTAL	99.99	100.24	99.25	99.37
Si	1.854	1.886	1.872	1.866
Al^{IV}	0.146	0.114	0.128	0.134
Al^{VI}	0.139	0.047	0.128	0.125
Ti	0.013	0.005	0.006	0.007
Cr	0.021	0.040	0.025	0.024
Fe^{3+}	0.082	--	--	--
Fe^{2+}	0.002	0.052	0.081	0.079
Mg	0.815	0.902	0.884	0.867
Mn	0.003	0.002	0.002	0.002
Ni	0.002	0.002	0.001	0.001
Ca	0.799	0.937	0.854	0.880
Na	0.123	0.044	--	--
K	--	--	--	--

TABLE AII.9. (Continued)

		Harzburgite		
	796	77WH56-3	78104	78104-1
Ca	46.92	49.44	46.85	48.10
Mg	47.46	47.70	48.58	47.48
Fe_T	5.12	2.86	4.57	4.42

796 - clinopyroxene megacryst.

77WH56-3 - primary clinopyroxene.
78104 - primary clinopyroxene.
78104-1 - exsolved clinopyroxene in primary orthopyroxene.

TABLE AII.10. Clinopyroxene compositions from pyroxenites of the White Hill Peridotite

	Orthopyroxenite		Websterite	
	7850	7857	77WH2	77WH7
SiO_2	52.05	53.82	49.99	51.71
TiO_2	0.48	0.15	0.16	0.19
Al_2O_3	6.37	5.13	6.68	6.10
Cr_2O_3	0.66	0.94	0.44	0.57
FeO*	2.76	2.29	2.19	3.71
MnO	0.06	0.05	0.13	0.08
MgO	14.44	15.82	15.94	15.63
CaO	21.32	21.77	23.48	20.72
Na_2O	1.26	0.54	0.46	0.54
K_2O	--	--	--	--
NiO	0.03	0.01	0.02	0.02
TOTAL	99.43	99.72	99.49	99.27
Si	1.895	1.918	1.830	1.887
Al^{IV}	0.105	0.082	0.170	0.113
Al^{VI}	0.168	0.137	0.119	0.150
Ti	0.013	0.004	0.004	0.005
Cr	0.019	0.027	0.013	0.016
Fe^{3+}	--	--	--	--
Fe^{2+}	0.084	0.069	0.067	0.113
Mg	0.783	0.853	0.870	0.850
Mn	0.002	0.002	0.004	0.002
Ni	0.001	--	0.001	0.001
Ca	0.832	0.844	0.921	0.810

TABLE AII.10. (Continued)

	7850	7857	77WH2	77WH7
Na	0.089	0.038	0.003	0.038
K	--	--	--	--
Ca	48.87	47.73	49.45	45.61
Mg	46.09	48.26	46.73	47.88
Fe_T	5.04	4.01	3.82	6.51

* - Total iron as FeO.
n.d. - not detected.
-- - not determined.

7850 - intercumulus clinopyroxene; orthopyroxenite boudin; n = 2.
7857 - intercumulus clinopyroxene; orthopyroxenite vein parallel to foliation.

77WH2 - recrystallized clinopyroxene; n = 2.
77WH7 - recrystallized clinopyroxene; websterite dike(?) approximately 8 cm wide; n = 2.

TABLE AII.10. (Continued)

	783	7853	7854	78155
SiO_2	49.90	54.71	51.45	53.01
TiO_2	0.28	0.20	0.31	0.28
Al_2O_3	7.20	3.75	6.38	4.79
Cr_2O_3	0.65	0.69	0.42	1.00
FeO^*	2.47	3.23	3.49	2.39
MnO	0.08	0.09	0.07	0.04
MgO	15.16	16.12	15.15	15.51
CaO	23.12	20.56	21.63	21.75
Na_2O	0.49	1.19	0.54	0.80
K_2O	n.d.	--	n.d.	n.d.
NiO	0.02	0.08	0.07	0.02
TOTAL	99.37	100.62	99.51	99.59
Si	1.821	1.963	1.877	1.924
Al^{IV}	0.179	0.037	0.173	0.076
Al^{VI}	0.131	0.122	0.151	0.129
Ti	0.008	0.005	0.009	0.008
Cr	0.019	0.020	0.012	0.029
Fe^{3+}	0.048	--	--	--
Fe^{2+}	0.028	0.097	0.106	0.073
Mg	0.825	0.862	0.824	0.839
Mn	0.002	0.003	0.002	0.001
Ni	0.001	0.002	0.002	0.001
Ca	0.904	0.791	0.846	0.846
Na	0.035	0.083	0.038	0.056
K	--	--	--	--

TABLE AII.10. (Continued)

	783	7853	7854	78155
Ca	50.03	45.05	47.50	48.08
Mg	45.66	49.26	46.39	47.72
Fe_T	4.31	5.69	6.11	4.20

783 - deformed primary clinopyroxene; n = 2.
7853 - recrystallized clinopyroxene; fine-grained vein 2 - 3 cm wide; no olivine, spinel; n = 2.
7854 - recrystallized clinopyroxene; websterite boudin approximately 2 m above basal fault; no olivine, spinel; n = 2.
78155 - intercumulus clinopyroxene; websterite pod approximately 1/2 m x 1/3 m parallel to foliation; n = 2.

TABLE AII.10. (Continued)

Clinopyroxenite

	77WH70	77WH74	77WH79	78110	78118
SiO_2	49.44	51.66	50.13	51.35	51.14
TiO_2	0.39	0.33	0.52	0.54	0.59
Al_2O_3	4.39	5.19	6.71	6.28	6.13
Cr_2O_3	0.39	0.80	0.87	0.51	0.50
FeO^*	3.09	3.68	3.00	3.37	3.17
MnO	0.10	0.10	0.13	0.09	0.10
MgO	17.09	15.65	15.70	15.41	15.41
CaO	23.99	21.57	22.66	21.64	21.84
Na_2O	0.55	0.70	0.65	0.73	0.70
K_2O	n.d.	--	n.d.	n.d.	--
NiO	n.d.	0.08	n.d.	0.06	0.05
TOTAL	99.43	99.76	100.37	99.98	99.63
Si	1.830	1.884	1.812	1.866	1.864
Al^{IV}	0.170	0.116	0.188	0.134	0.136
Al^{VI}	0.022	0.107	0.098	0.135	0.128
Ti	0.011	0.009	0.014	0.015	0.016
Cr	0.011	0.023	0.025	0.015	0.014
Fe^{3+}	--	0.017	0.083	0.006	0.010
Fe^{2+}	0.096	0.095	0.008	0.096	0.086
Mg	0.943	0.851	0.846	0.835	0.837
Mn	0.003	0.003	0.004	0.003	0.003
Ni	—	0.002	—	0.002	0.001
Ca	0.952	0.843	0.878	0.843	0.853

TABLE AII.10. (Continued)

	77WH70	77WH74	77WH79	78110	78118
Na	0.039	0.050	0.046	0.051	0.049
K	--	--	--	--	--
Ca	47.74	46.54	48.27	47.22	47.62
Mg	47.30	47.09	46.52	46.88	46.81
Fe_T	4.96	6.37	5.21	5.90	5.57

77WH70 - deformed primary clinopyroxene.
77WH74 - deformed primary clinopyroxene; clinopyroxenite vein parallel to foliation.
77WH79 - deformed primary clinopyroxene.
78110 - deformed primary clinopyroxene; clinopyroxenite vein oblique to foliation; n = 2.
78118 - deformed primary clinopyroxene; clinopyroxenite vein cutting dunite megalens; n = 6.

TABLE AII.10. (Continued)

	78128	78144	78159	798	7917
SiO_2	50.44	50.90	49.40	50.92	52.36
TiO_2	0.69	0.47	0.58	0.70	0.78
Al_2O_3	6.07	6.46	6.36	7.00	4.30
Cr_2O_3	0.66	0.78	0.83	0.63	0.26
FeO*	3.98	3.52	3.52	2.39	3.26
MnO	0.11	0.09	0.13	0.08	0.09
MgO	14.42	14.72	15.30	14.84	15.83
CaO	21.50	21.69	22.96	22.10	23.05
Na_2O	1.09	0.78	0.84	0.93	0.68
K_2O	--	--	--	--	--
NiO	0.05	0.05	0.04	0.05	0.04
TOTAL	99.01	99.46	99.96	99.64	100.65
Si	1.855	1.864	1.816	1.854	1.892
Al^{IV}	0.145	0.136	0.184	0.146	0.108
Al^{VI}	0.119	0.143	0.092	0.154	0.076
Ti	0.019	0.013	0.016	0.019	0.021
Cr	0.019	0.023	0.024	0.018	0.007
Fe^{3+}	0.046	--	--	--	0.030
Fe^{2+}	0.076	0.108	0.108	0.073	0.069
Mg	0.791	0.803	0.838	0.805	0.853
Mn	0.003	0.003	0.004	0.002	0.003
Ni	0.001	0.001	0.001	0.001	0.001
Ca	0.847	0.851	0.905	0.862	0.893
Na	0.078	0.055	0.060	0.066	0.048
K	—	--	—	—	--

TABLE AII.10. (Continued)

	78128	78144	78159	798	7917
Ca	48.00	48.18	48.73	49.43	48.31
Mg	44.87	45.56	45.23	46.25	46.21
Fe_T	7.13	6.26	6.04	4.32	5.48

78128 - deformed primary clinopyroxene; clinopyroxenite pod; n = 2.
78144 - deformed primary clinopyroxene; clinopyroxenite vein cutting dunite; n = 2.
78159 - deformed primary clinopyroxene; n = 5.
798 - recrystallized clinopyroxene; clinopyroxenite vein cutting dunite dike; n = 2.
7917 - deformed primary clinopyroxene.

TABLE AII.10. (Continued)

	Wehrlite
	78142
SiO_2	50.18
TiO_2	0.59
Al_2O_3	6.10
Cr_2O_3	0.54
FeO^*	3.40
MnO	0.10
MgO	15.46
CaO	22.26
Na_2O	0.56
K_2O	--
NiO	0.06
TOTAL	99.25
Si	1.838
Al^{IV}	0.162
Al^{VI}	0.102
Ti	0.016
Cr	0.016
Fe^{3+}	0.052
Fe^{2+}	0.052
Mg	0.844
Mn	0.003
Ni	0.002
Ca	0.874
Na	0.040
K	—

TABLE AII.10. (Continued)

	78142
Ca	47.83
Mg	46.30
Fe_T	5.87

78142 - deformed primary clinopyroxene; wehrlite layer(?) parallel to foliation; n = 2.

TABLE AII.11. Clinopyroxene compositions from gabbros of the White Hills Peridotite

	77WH60	77WH62	77WH86	77WH89	77WH90
SiO_2	49.63	49.90	51.33	51.74	50.82
TiO_2	1.25	1.08	0.77	0.81	0.75
Al_2O_3	7.23	6.84	6.46	6.82	7.23
Cr_2O_3	0.22	0.18	0.19	0.49	0.42
FeO^*	5.36	6.32	4.41	4.21	5.41
MnO	0.13	0.14	0.12	0.08	0.11
MgO	14.19	14.00	14.35	14.89	13.90
CaO	21.38	19.32	21.61	20.85	20.08
Na_2O	1.21	1.18	0.96	1.25	1.07
K_2O	--	n.d.	n.d.	--	n.d.
NiO	--	0.01	0.04	n.d.	0.02
TOTAL	100.60	98.97	100.24	101.14	99.81
Si	1.800	1.912	1.868	1.859	1.860
Al^{IV}	0.200	0.088	0.132	0.141	0.140
Al^{VI}	0.110	0.221	0.145	0.148	0.172
Ti	0.034	0.031	0.021	0.022	0.021
Cr	0.006	0.005	0.005	0.014	0.012
Fe^{3+}	0.100	--	0.007	0.023	--
Fe^{2+}	0.062	0.203	0.128	0.104	0.166
Mg	0.767	0.801	0.778	0.797	0.758
Mn	0.004	0.005	0.004	0.002	0.003
Ni	--	--	0.001	--	0.001
Ca	0.831	0.589	0.843	0.803	0.787
Na	0.085	0.088	0.068	0.087	0.076
K	--	--	--	--	--

TABLE AII.11. (Continued)

	77WH60	77WH62	77WH86	77WH89	77WH90
Ca	47.09	36.87	47.88	46.43	45.91
Mg	43.47	50.15	44.29	46.12	44.24
Fe_T	9.44	12.98	7.83	7.45	9.85

* - Total iron as FeO.
n.d. - not detected.
-- - not determined.

77WH60 - recrystallized clinopyroxene; gabbro vein within fault zone; n = 3.
77WH62 - recrystallized clinopyroxene; gabbro vein within fault zone.
77WH86 - deformed primary(?) clinopyroxene; gabbro vein within fault zone.
77WH89 - deformed primary clinopyroxene; fine-grained gabbro vein.
77WH90 - deformed primary clinopyroxene; coarse-grained gabbro vein adjacent to 77WH89; n = 2.

TABLE AII.11. (Continued

	78111	78128	78129	78134	78135
SiO_2	49.93	49.57	50.30	52.42	48.96
TiO_2	0.93	0.73	0.80	0.75	0.71
Al_2O_3	7.01	7.53	7.38	7.13	7.83
Cr_2O_3	0.22	0.65	0.52	0.07	0.59
FeO*	4.30	4.17	4.13	4.97	4.43
MnO	0.11	0.14	0.16	0.17	0.14
MgO	14.48	14.10	14.44	14.96	13.87
CaO	22.00	22.22	21.43	20.14	22.24
Na_2O	1.09	1.12	1.08	0.94	1.05
K_2O	n.d.	n.d.	n.d.	n.d.	n.d.
NiO	0.05	0.02	0.02	n.d.	0.02
TOTAL	100.12	100.25	100.26	101.55	99.84
Si	1.815	1.800	1.826	1.875	1.787
Al^{IV}	0.185	0.200	0.174	0.125	0.213
Al^{VI}	0.115	0.123	0.142	0.176	0.124
Ti	0.025	0.020	0.022	0.020	0.019
Cr	0.006	0.019	0.015	0.002	0.017
Fe^{3+}	0.090	0.097	0.050	--	0.106
Fe^{2+}	0.041	0.030	0.075	0.149	0.029
Mg	0.784	0.763	0.781	0.798	0.755
Mn	0.003	0.004	0.005	0.005	0.004
Ni	0.001	0.001	0.001	—	0.001
Ca	0.857	0.865	0.834	0.772	0.870
Na	0.077	0.079	0.076	0.065	0.074
K	—	—	--	--	—

TABLE AII.11. (Continued)

	78111	78128	78129	78134	78135
Ca	48.22	49.15	47.75	44.79	49.30
Mg	44.23	43.41	44.79	46.28	42.79
Fe_T	7.55	7.44	7.46	8.93	7.91

78111 - recrystallized clinopyroxene; gabbro vein.
78128 - deformed primary clinopyroxene; gabbro vein cutting clinopyroxenite pod.
78129 - deformed primary clinopyroxene; gabbro vein approximately 18 cm wide.
78134 - recrystallized (?) clinopyroxene; fine-grained foliated gabbro.
78135 - deformed primary clinopyroxene; medium to coarse-grained gabbro vein.

TABLE AII.11. (Continued)

	78136	78150
SiO_2	50.91	51.11
TiO_2	0.70	0.77
Al_2O_3	7.41	7.55
Cr_2O_3	0.23	0.57
FeO*	3.87	4.66
MnO	0.14	0.14
MgO	14.11	15.23
CaO	21.46	19.62
Na_2O	1.04	1.07
K_2O	n.d.	n.d.
NiO	0.04	0.11
TOTAL	99.91	100.83
Si	1.855	1.843
Al^{IV}	0.145	0.157
Al^{VI}	0.173	0.164
Ti	0.019	0.021
Cr	0.007	0.016
Fe^{3+}	--	0.001
Fe^{2+}	0.118	0.130
Mg	0.766	0.818
Mn	0.004	0.004
Ni	0.001	0.003
Ca	0.838	0.758
Na	0.074	0.075
K	--	--

TABLE AII.11. (Continued)

	78136	78150
Ca	48.50	43.96
Mg	44.42	47.64
Fe_T	7.08	8.40

78136 - deformed primary clinopyroxene; medium to coarse-grained gabbro vein.
78150 - recrystallized clinopyroxene; gabbro.

TABLE AII.12. Clinopyroxene compositions from rocks associated with chromite from the White Hills Peridotite

	7898	78122X	78123X	78123XR
SiO_2	53.59	53.36	54.10	54.01
TiO_2	0.02	0.05	0.08	0.07
Al_2O_3	1.82	1.93	2.24	1.96
Cr_2O_3	0.78	1.23	1.00	0.96
FeO*	1.56	1.67	2.07	2.21
MnO	0.06	0.04	0.04	0.04
MgO	18.06	18.15	16.78	17.33
CaO	24.18	24.36	23.51	23.15
Na_2O	0.12	0.48	0.39	0.54
K_2O	n.d.	--	n.d.	n.d.
NiO	0.02	0.14	0.11	0.13
TOTAL	100.21	101.41	100.32	100.40
Si	1.941	1.919	1.959	1.950
Al^{IV}	0.059	0.081	0.043	0.050
Al^{VI}	0.019	0.001	0.052	0.033
Ti	0.001	0.001	0.002	0.002
Cr	0.022	0.035	0.029	0.027
Fe^{3+}	--	--	--	0.024
Fe^{2+}	0.047	0.050	0.063	0.043
Mg	0.975	0.973	0.905	0.932
Mn	0.002	0.001	0.001	0.001
Ni	0.001	0.004	0.001	0.001
Ca	0.938	0.939	0.911	0.896
Na	0.008	0.033	0.027	0.038
K	--	--	--	--

TABLE AII.12. (Continued)

	7898	78122X	78123X	78123XR
Ca	47.81	47.72	48.40	47.14
Mg	49.69	49.66	48.21	49.28
Fe_T	2.50	2.62	3.39	3.58

* - Total iron as FeO.
n.d. - not detected.
-- - not determined.

7898 - intercumulus clinopyroxene; orthopyroxenite vein associated with disseminated chromite.
78122X - intercumulus clinopyroxene; "websterite" assemblage associated with chromitite.
78123X - colorless, cumulus clinopyroxene; "websterite" assemblage associated with chromitite.
78123XR - green, pleochroic recrystallized(?) clinopyroxene; "websterite" assemblage associated with chromitite; n = 5.

TABLE AII.13. Plagioclase compositions from gabbros of the White Hills Peridotite

	77WH60	77WH62	77WH89	78128	78129
SiO_2	54.00	56.22	54.01	54.75	53.32
TiO_2	n.d.	0.03	n.d.	n.d.	0.01
Al_2O_3	28.59	29.68	29.65	29.71	31.34
Cr_2O_3	--	n.d.	--	n.d.	n.d.
FeO*	0.04	0.07	0.36	0.14	0.05
MnO	--	n.d.	0.01	n.d.	n.d.
MgO	--	n.d.	--	--	--
CaO	12.05	8.61	8.91	10.77	13.40
Na_2O	5.05	4.07	6.50	4.98	3.76
K_2O	0.13	0.04	0.04	0.04	0.03
NiO	--	0.01	0.06	0.01	0.07
TOTAL	99.86	98.73	99.54	100.40	101.97
Si	9.791	10.093	9.781	9.811	9.468
Al	6.112	6.283	6.331	6.278	6.562
Ti	--	0.004	--	--	0.001
Cr	--	--	--	--	--
Fe	0.006	0.011	0.055	0.021	0.007
Mg	--	--	--	--	--
Mn	--	--	0.002	--	--
Ni	--	0.001	0.009	0.001	0.010
Ca	2.341	1.657	1.729	2.068	2.550
Na	1.776	1.417	2.283	1.731	1.295
K	0.030	0.009	0.009	0.009	0.007
An	42.8	53.7	43.0	54.3	66.2

TABLE AII.13. (Continued)

* - Total iron as FeO.
n.d. - not detected.
-- - not determined.

77WH60 - recrystallized plagioclase; gabbro vein within fault zone; n = 2.
77WH62 - recrystallized plagioclase; gabbro vein within fault zone.
77WH89 - recrystallized plagioclase; fine-grained gabbro vein.
78128 - recrystallized plagioclase; gabbro vein cutting clinopyroxenite pod.
78129 - deformed primary plagioclase; gabbro vein approximately 18 cm wide.

TABLE AII.13. (Continued)

	78131	78134	78135	78136	78150
SiO_2	53.03	52.94	52.80	48.88	54.08
TiO_2	0.04	n.d.	n.d.	n.d.	n.d.
Al_2O_3	30.42	30.52	30.17	31.74	29.64
Cr_2O_3	0.03	n.d.	0.02	n.d.	n.d.
FeO*	0.05	0.15	0.14	0.12	0.04
MnO	0.00	n.d.	n.d.	n.d.	0.01
MgO	--	--	--	--	--
CaO	13.67	12.42	11.93	15.03	12.18
Na_2O	3.55	4.18	3.96	3.52	4.12
K_2O	0.11	0.06	0.04	0.08	0.01
NiO	n.d.	0.05	0.02	n.d.	n.d.
TOTAL	100.90	100.32	99.08	99.37	100.08
Si	9.525	9.548	9.613	9.012	9.740
Al	6.442	6.490	6.476	6.900	6.294
Ti	0.005	--	--	--	--
Cr	0.004	--	0.003	--	--
Fe	0.008	0.023	0.021	0.019	0.006
Mg	--	--	--	--	--
Mn	--	--	--	--	0.010
Ni	--	0.007	0.003	--	--
Ca	2.631	2.401	2.328	2.970	2.351
Na	1.236	1.462	1.398	1.258	1.439
K	0.025	0.014	0.009	0.019	0.002
An	67.6	61.9	62.3	69.9	62.0

TABLE AII.13. (Continued)

78131 - recrystallized plagioclase; anorthositic vein cutting other gabbro veins.
78134 - recrystallized plagioclase; fine-grained foliated gabbro vein.
78135 - recrystallized plagioclase; medium to coarse-grained gabbro vein.
78136 - deformed primary plagioclase; medium to coarse-grained gabbro vein.
78150 - recrystallized plagioclase; gabbro vein.

TABLE AII.14, Spinel compositions from rocks of the White Hills Peridotite.

Spinel lherzolite

	77WH1	77WH1-1	77WH15A	77WH15A-1	77WH76
TiO_2	0.04	0.07	0.07	0.06	0.03
Al_2O_3	53.36	52.51	52.27	50.34	52.39
Cr_2O_3	14.83	15.39	16.11	17.42	15.12
Fe_2O_3[1]	0.38	1.04	1.72	1.49	1.83
FeO	11.41	11.30	11.83	14.26	11.98
MnO	0.04	0.04	0.10	0.18	0.04
MgO	18.74	18.81	18.75	16.73	18.47
NiO	--	--	--	0.23	--
V_2O_3	--	--	--	--	--
TOTAL	98.80	99.16	100.85	100.71	99.86
Fe_2TiO_4	0.08	0.14	0.14	0.12	0.06
$FeCr_2O_4$	15.61	16.21	16.79	18.50	15.89
$MgCr_2O_4$	--	--	--	--	--
$MgAl_2O_4$	74.52	74.82	73.79	67.71	73.29
$FeAl_2O_4$	9.41	7.79	7.57	12.26	8.94
$MgFe_2O_4$	--	--	--	--	--
$FeFe_2O_4$	0.38	1.04	1.71	1.50	1.83

77WH1 - anhedral porphyroclast; surrounded by magnetite rim.
77WH1-1 - anhedral porphyroclast; surrounded by magnetite rim.
77WH15A - anhedral porphyroclast.
77WH15A-1 - anhedral porphyroclast.
77WH76 - anhedral porphyroclast, light brown region, compare to 77WH76-1.

1 - Fe^{2+} - Fe^{3+} determined from stoichiometry.

TABLE AII.14. (Continued)

	77WH76-1	77WH94	7862	78151	78105
TiO_2	0.10	0.10	0.09	0.05	0.07
Al_2O_3	51.77	51.50	54.28	52.54	52.91
Cr_2O_3	15.97	16.28	14.91	15.41	13.45
Fe_2O_3	0.62	2.10	1.21	0.80	2.44
FeO	13.35	12.68	11.07	14.26	11.62
MnO	0.10	0.10	0.09	0.04	0.08
MgO	17.41	18.14	19.55	17.09	18.43
NiO	--	--	--	--	0.33
V_2O_3	--	--	--	--	0.12
TOTAL	99.32	100.90	101.20	100.19	99.45
Fe_2TiO_4	0.20	0.20	0.18	0.10	0.14
$FeCr_2O_4$	16.98	17.06	15.32	16.26	14.17
$MgCr_2O_4$	--	--	--	--	--
$MgAl_2O_4$	69.89	71.81	75.88	68.12	74.02
$FeAl_2O_4$	12.31	8.83	7.45	14.71	9.23
$MgFe_2O_4$	--	--	--	--	--
$FeFe_2O_4$	0.62	2.10	1.18	0.80	2.44

77WH76-1 - anhedral porphyroclast, dark brown region, compare to 77WH76.
77WH94 - anhedral interstitial spinel associated with orthopyroxene and olivine.
7862 - anhedral porphyroclast with rim of chlorite and serpentine.
78151 - subhedral spinel in primary olivine within primary orthopyroxene
78105 - exsolved spinel associated with recrystallized clinopyroxene, orthopyroxene and olivine.

TABLE AII.14. (Continued)

	77WH11	7815	7815-1	796	795
TiO_2	0.08	0.04	0.03	0.10	0.07
Al_2O_3	57.63	48.43	50.35	58.15	60.09
Cr_2O_3	8.98	18.91	17.91	9.25	7.79
Fe_2O_3	2.30	1.47	1.99	1.85	0.58
FeO	10.19	13.30	11.87	11.13	11.34
MnO	0.11	0.11	0.13	0.16	0.10
MgO	19.88	16.89	18.28	19.50	19.42
NiO	0.32	0.29	0.32	0.33	0.38
V_2O_3	--	--	--	--	--
TOTAL	99.49	99.44	100.88	100.47	99.77
Fe_2TiO_4	0.16	0.08	0.06	0.19	0.14
$FeCr_2O_4$	9.22	20.39	18.84	9.43	7.93
$MgCr_2O_4$	--	--	--	--	--
$MgAl_2O_4$	77.75	69.43	73.30	75.79	75.45
$FeAl_2O_4$	10.63	8.59	5.81	12.79	15.93
$MgFe_2O_4$	--	--	--	--	--
$FeFe_2O_4$	2.24	1.50	1.99	1.79	0.56

77WH11 - anhedral porphyroclast.
7815 - exsolved spinel associated with primary orthopyroxene and primary olivine (see Plate 10.A.).
7815-1 - exsolved spinel associated with primary orthopyroxene and primary olivine.
796 - anhedral porphyroclast (~ 7mm long).
795 - interstitial spinel with scalloped grain boundaries.

TABLE AII.14. (Continued)

Harzburgite

	77WH56	78104	78104-1	7818	7910
TiO_2	0.17	0.13	0.10	0.05	0.07
Al_2O_3	36.88	49.38	49.54	27.34	34.46
Cr_2O_3	31.04	17.41	17.43	38.89	30.52
Fe_2O_3	2.25	2.62	3.12	3.30	3.21
FeO	15.06	10.96	10.77	15.75	15.41
MnO	0.18	0.11	0.11	0.25	0.28
MgO	14.99	18.56	18.86	12.95	13.66
NiO	--	0.29	0.24	0.12	0.23
V_2O_3	--	0.14	0.16	--	--
TOTAL	100.57	99.60	100.33	98.65	97.84
Fe_2TiO_4	0.37	0.26	0.20	0.12	0.16
$FeCr_2O_4$	35.03	18.54	18.43	40.64	35.83
$MgCr_2O_4$	--	--	--	6.23	--
$MgAl_2O_4$	62.18	75.27	75.82	49.22	60.43
$FeAl_2O_4$	--	3.28	2.42	--	--
$MgFe_2O_4$	1.72	--	--	3.79	0.68
$FeFe_2O_4$	0.70	2.65	3.14	--	2.91

77WH56 - anhedral porphyroclast in recrystallized groundmass of olivine and orthopyroxene.
78104 - anhedral porphyroclast adjacent to primary orthopyroxene.
78104-1 - exsolved(?) subhedral spinel in primary orthopyroxene. Spinel is, in part, surrounded by clinopyroxene(exsolution lamellae).
7818 - pull-apart texture spinel associated with olivine.
7910 - anhedral interstitial spinel associated with olivine and orthopyroxene.

TABLE AII.14. (Continued)

Dunite

	77WH55L	77WH37	77WH77	77WH80	77WH93SL
TiO_2	0.72	0.04	0.39	0.47	0.11
Al_2O_3	30.97	42.73	39.21	35.18	50.29
Cr_2O_3	29.17	21.92	22.39	26.34	15.49
Fe_2O_3	9.43	6.15	8.76	9.08	3.30
FeO	16.59	12.52	16.94	15.64	11.74
MnO	0.18	0.13	0.13	0.16	0.06
MgO	13.67	17.20	14.46	14.79	18.31
NiO	--	--	--	--	--
V_2O_3	--	--	--	--	--
TOTAL	100.73	100.69	102.28	101.66	99.30
Fe_2TiO_4	1.60	0.08	0.83	1.01	0.22
$FeCr_2O_4$	34.00	23.91	24.86	29.78	16.49
$MgCr_2O_4$	--	--	--	--	--
$MgAl_2O_4$	53.92	19.62	60.65	59.42	73.60
$FeAl_2O_4$	--	--	4.40	--	6.35
$MgFe_2O_4$	6.26	1.23	--	3.74	--
$FeFe_2O_4$	4.22	5.16	9.27	6.05	3.34

77WH55L – anhedral, interstitial spinel; interlayered with harzburgite (77WH56) (From Talkington and Malpas, 1980a).
77WH37 – subhedral to anhedral spinel; dunite layer(?).
77WH77 – dunite layer interlayered with spinel lherzolite (77WH78).
77WH80– – anhedral spinel, opaque; dunite layer interlayered with harzburgite.
77WH93SL – subhedral to anhedral spinel; dunite layer interlayered with spinel lherzolite(77WH94) (From Talkington and Malpas, 1980a).

TABLE AII.14. (Continued)

	78114	78117	78117-1	78117-2	78117ML
TiO_2	0.79	0.23	0.24	0.18	0.66
Al_2O_3	35.83	46.11	46.60	46.85	34.68
Cr_2O_3	28.93	18.07	17.99	18.11	31.01
Fe_2O_3	5.03	4.50	4.00	3.91	4.43
FeO	14.34	15.01	15.03	14.77	14.34
MnO	0.18	0.06	0.06	0.06	0.20
MgO	15.75	15.93	15.98	16.17	15.55
NiO	--	--	--	--	--
V_2O_3	--	--	--	--	--
TOTAL	100.85	99.91	99.90	100.09	100.87
Fe_2TiO_4	1.70	0.48	0.50	0.37	1.43
$FeCr_2O_4$	31.28	19.71	19.58	19.65	32.06
$MgCr_2O_4$	1.32	--	--	--	3.06
$MgAl_2O_4$	60.31	65.63	65.69	66.26	58.67
$FeAl_2O_4$	--	9.51	10.08	9.67	--
$MgFe_2O_4$	5.40	--	--	--	4.78
$FeFe_2O_4$	--	4.67	4.15	4.04	--

78114 - subhedral to anhedral spinel, dunite megalens.
78117 - subhedral, zoned cumulus spinel; dunite megalens.
78117-1 - subhedral, zoned cumulus spinel; dunite megalens.
78117-2 - subhedral, zoned cumulus spinel; dunite megalens.
78117ML - anhedral spinel; dunite megalens(From Talkington and Malpas,1980a).

TABLE AII.14. (Continued)

	78147	78152D	7841	797	78141
TiO_2	0.61	0.41	0.05	0.90	0.15
Al_2O_3	35.31	38.98	51.83	29.35	44.26
Cr_2O_3	28.63	23.75	13.84	31.20	18.77
Fe_2O_3	6.23	6.13	4.31	6.92	5.78
FeO	15.08	17.02	11.37	16.57	14.49
MnO	0.18	0.08	0.14	0.26	0.15
MgO	15.17	14.07	18.64	12.96	15.77
NiO	--	--	0.38	0.22	0.19
V_2O_3	--	--	--	--	--
TOTAL	101.21	100.44	100.56	98.38	99.56
Fe_2TiO_4	1.31	0.88	0.10	2.06	0.32
$FeCr_2O_4$	32.36	26.81	14.50	37.43	20.70
$MgCr_2O_4$	--	--	--	--	--
$MgAl_2O_4$	59.62	59.97	74.55	52.60	66.11
$FeAl_2O_4$	--	5.75	6.55	--	6.80
$MgFe_2O_4$	5.14	--	--	6.66	--
$FeFe_2O_4$	1.57	6.59	4.31	1.26	6.08

78147 - subhedral-anhedral spinel; dunite layer interlayered with spinel lherzolite (78146).
78152D - anhedral spinel; dunite dike cutting spinel lherzolite (78151) (From Talkington and Malpas, 1980a).
7841 - euhedral, green, disseminated spinel; within 5 m of basal thrust fault.
797 - anhedral, elongate disseminated spinel; dunite dike cutting harzburgite.
78141 - anhedral disseminated spinel; dunite dike.

TABLE AII.14. (Continued)

	798
TiO_2	0.31
Al_2O_3	41.08
Cr_2O_3	22.00
Fe_2O_3	7.22
FeO	16.61
MnO	0.18
MgO	14.66
NiO	0.23
V_2O_3	--
TOTAL	102.29
Fe_2TiO_4	0.65
$FeCr_2O_4$	24.22
$MgCr_2O_4$	--
$MgAl_2O_4$	61.47
$FeAl_2O_4$	6.09
$MgFe_2O_4$	--
$FeFe_2O_4$	7.58

798 - anhedral disseminated spinel; dunite dike.

TABLE AII.15. Spinel compositions from rocks associated with chromite from the White Hills Peridotite

	77WH19	77WH30	7898	78122Y	78122Y
TiO_2	0.31	0.15	0.08	0.26	0.28
Cr_2O_3	9.56	10.45	20.94	18.52	14.55
Al_2O_3	57.21	60.10	45.17	48.30	51.63
Fe_2O_3[1]	4.69	2.54	4.61	4.85	5.68
FeO	18.65	14.24	16.47	13.31	14.53
MnO	0.11	0.11	0.09	0.31	0.33
MgO	9.96	12.79	12.19	13.87	12.70
NiO	--	--	--	0.16	0.19
V_2O_3	--	--	--	0.19	0.13
TOTAL	100.49	100.38	99.55	99.77	100.02
Fe_2TiO_4	0.77	0.36	0.18	0.61	0.67
$FeCr_2O_4$	50.14	38.03	42.97	34.38	38.36
$MgCr_2O_4$	24.50	38.60	12.79	25.19	26.73
$MgAl_2O_4$	18.63	19.90	38.62	34.12	27.40
$FeAl_2O_4$	--	--	--	--	--
$MgFe_2O_4$	5.94	3.08	5.42	5.70	6.83
$FeFe_2O_4$	--	--	--	--	--

n.d. - not detected.
-- - not determined.
1 - Fe^{2+} - Fe^{3+} determined from stoichiometry.

77WH19 - massive sheared chromite; orthopyroxenite vein associated with a seam of chromite; n = 2.
77WH30 - cumulus spinel; orthopyroxentie vein associated with a seam of chromite; n = 2.
7898 - - cumulus spinel; orthopyroxenite vein associated with disseminated spinel; n = 2.
78122Y - massive spinel; massive chromite associated with bastite pseudomorph orthopyroxene.
78122Y - resorbed spinel in bastite pseudomorph; massive chromite associated with bastite pseudomorph orthopyroxene; n = 5.

TABLE AII.15. (Continued)

	78122Y	78123X	78123XC
TiO_2	0.21	0.25	0.19
Al_2O_3	17.91	19.68	19.29
Cr_2O_3	49.79	46.79	47.47
Fe_2O_3	4.91	5.63	4.25
FeO	12.53	13.44	15.28
MnO	0.32	0.30	0.30
MgO	14.38	13.95	12.57
NiO	0.23	0.34	0.27
V_2O_3	0.17	0.16	0.14
TOTAL	100.45	100.54	99.76
Fe_2TiO_4	0.49	0.58	0.45
$FeCr_2O_4$	32.40	34.35	40.04
$MgCr_2O_4$	28.60	22.69	18.78
$MgAl_2O_4$	32.78	35.84	35.71
$FeAl_2O_4$	--	--	--
$MgFe_2O_4$	5.73	6.54	5.02
$FeFe_2O_4$	--	--	--

78122Y - Spinel at margin of bastite and clinoamphibole rim; massive chromite associated with bastite pseudomorph orthopyroxene.
78123X - massive chromite; "websterite" assemblage associated with chromite; n = 2.
78123XC - spinel euhedral associated with green pleochroic clinopyroxene; "websterite" assemblage associated with chromite; n = 6.

TABLE AII.16. Spinel compositions from pyroxenites of the White Hills peridotite

	Websterite			Clinopyroxenite
	77WH2	783	783a	77WH70
TiO_2	n.d.	0.04	0.62	0.07
Al_2O_3	63.28	60.07	63.56	59.03
Cr_2O_3	4.83	6.46	4.30	7.02
Fe_2O_3[1]	0.80	2.55	0.94	1.91
FeO	7.80	8.94	10.69	14.02
MnO	0.04	0.12	0.13	0.04
MgO	22.11	20.86	20.78	17.87
NiO	—	0.39	0.52	—
TOTAL	98.86	99.43	101.54	99.96
Fe_2TiO_4	—	0.08	1.17	0.14
$FeCr_2O_4$	4.82	6.55	4.25	7.23
$MgCr_2O_4$	—	—	—	—
$MgAl_2O_4$	83.41	80.63	78.53	69.47
$FeAl_2O_4$	11.01	10.29	15.21	21.30
$MgFe_2O_4$	—	—	—	—
$FeFe_2O_4$	0.76	2.46	0.85	1.87

n.d. - not detected.
— - not determined.
1 - Fe^{2+} - Fe^{3+} determined from stoichiometry.

77WH2 - anhedral spinel; n = 3.
783 - anhedral porphyroclast spinel.
783a - anhedral spinel (< 0.3 mm).

77WH70 - anhedral interstitial spinel; n = 2.

TABLE AII.16. (Continued)

	77WH79	78118	78159	798	798a
TiO_2	0.05	0.07	0.10	0.07	0.31
Al_2O_3	57.01	57.80	54.83	55.93	41.08
Cr_2O_3	9.88	8.51	10.70	10.70	22.00
Fe_2O_3	1.50	1.09	2.14	0.82	7.22
FeO	14.31	14.77	15.81	12.56	16.61
MnO	0.06	0.15	0.05	0.13	0.18
MgO	17.53	16.98	16.26	17.91	14.66
NiO	--	0.20	--	0.37	0.23
TOTAL	100.34	99.57	99.89	98.49	102.29
Fe_2TiO_4	0.10	0.14	0.20	0.14	0.65
$FeCr_2O_4$	10.23	8.86	11.28	11.25	24.22
$MgCr_2O_4$	--	--	--	--	--
$MgAl_2O_4$	68.56	67.21	64.76	71.88	61.47
$FeAl_2O_4$	19.63	22.71	21.61	15.93	6.09
$MgFe_2O_4$	--	--	--	--	--
$FeFe_2O_4$	1.48	1.08	2.14	0.81	7.58

77WH79 - anhedral interstitial spinel; n = 3.
78118 - anhedral interstitial spinel; clinopyroxenite vein cutting dunite megalens.
78159 - anhedral interstitial spinel; n = 5.
798 - exsolved spinel in clinopyroxene; clinopyroxenite vein cutting dunite dike.
798a - anhedral interstitial spinel; clinopyroxenite vein cutting dunite dike.

TABLE ATI.16. (Continued)

	Wehrlite	
	7917	78142
TiO_2	0.11	0.16
Al_2O_3	57.66	56.83
Cr_2O_3	7.43	9.11
Fe_2O_3	3.95	1.86
FeO	15.64	14.20
MnO	0.15	0.06
MgO	16.84	17.52
NiO	0.33	n.d.
TOTAL	102.11	99.74
Fe_2TiO_4	0.22	0.32
$FeCr_2O_4$	7.62	9.48
$MgCr_2O_4$	--	--
$MgAl_2O_4$	65.90	68.87
$FeAl_2O_4$	22.41	19.49
$MgFe_2O_4$	--	--
$FeFe_2O_4$	3.85	1.84

7917 - anhedral interstitial spinel associated with clinopyroxene.

78142 - anhedral interstitial spinel; wehrlite layer(?) parallel to foliation; n = 3.

TABLE AII.17. Spinel compositions from gabbros of the White Hills Peridotite

	77WH60	77WH89	77WH90	78129	78136
TiO_2	0.08	0.03	0.06	0.03	0.03
Al_2O_3	62.20	60.67	63.61	63.32	63.79
Cr_2O_3	2.36	3.22	1.44	1.54	2.37
Fe_2O_3[1]	2.53	4.52	2.77	2.96	1.33
FeO	19.30	11.03	15.51	14.20	15.57
MnO	0.01	0.11	0.01	--	0.01
MgO	15.11	19.63	17.59	18.26	17.48
NiO	--	0.25	n.d.	n.d.	--
TOTAL	101.59	99.46	100.99	100.31	100.58
Fe_2TiO_4	0.16	0.06	0.12	0.06	0.06
$FeCr_2O_4$	2.41	3.28	1.45	1.56	2.39
$MgCr_2O_4$	--	--	--	--	--
$MgAl_2O_4$	58.33	76.01	66.96	69.66	66.70
$FeAl_2O_4$	36.84	16.27	28.82	25.88	29.57
$MgFe_2O_4$	--	--	--	--	--
$FeFe_2O_4$	2.47	4.38	2.66	2.85	1.28

n.d. - not detected.
-- - not determined.
1 - Fe^{2+} - Fe^{3+} determined from stoichiometry.

77WH60 - anhedral interstitial spinel; gabbro vein within fault zone.
77WH89 - anhedral interstitial spinel; fine-grained gabbro vein.
77WH90 - anhedral interstitial spinel; coarse-grained gabbro vein adjacent to 77WH89; n = 2.
78129 - anhedral interstitial spinel; gabbro vein approximately 18 cm wide; n = 2.
78136 - anhedral interstitial spinel; medium to coarse-grained gabbro vein; n = 3.

APPENDIX III

Bulk rock analyses and CIPW norms of the White Hills Peridotite lithologies and associated lithologies of the St. Anthony Complex.

SPINEL LHERZOLITE

SAMPLE	77WH1	77WH9	77WH11	77WH16	77WH29	77WH45	77WH73
SIO2	38.98	42.60	43.45	43.78	41.07	43.68	39.62
TIO2	0.07	0.13	0.16	0.12	0.10	0.15	0.11
AL203	1.88	2.85	3.58	2.46	1.75	2.91	1.97
FE203	3.52	2.99	2.82	1.52	3.08	2.28	4.02
FEO	4.66	5.90	5.93	6.37	4.90	5.82	3.68
MNO	0.11	0.12	0.12	0.12	0.12	0.13	0.11
MGO	40.38	39.58	38.56	40.93	40.16	38.08	38.45
CAO	1.93	2.40	3.32	2.36	2.18	2.80	1.81
NA2O	0.03	0.04	0.23	0.04	0.03	0.07	0.04
K2O	0.0	0.02	0.0	0.02	0.02	0.03	0.02
P2O5	0.0	0.05	0.0	0.06	0.07	0.05	0.06
LOI	6.69	4.68	2.20	3.00	7.42	4.60	9.95
TOTAL	98.25	101.36	100.37	100.78	100.90	100.60	99.84
ZR	5	4	7	5	5	0	5
SR	4	3	10	1	4	0	9
RB	0	0	0	0	0	0	0
ZN	36	42	47	45	41	0	41
CU	14	15	28	24	18	0	20
BA	4	1	47	0	32	0	28
GA	1	2	6	3	2	0	4
TH	0	0	0	2	4	0	2
NB	2	2	2	2	4	0	1
U	0	0	0	0	0	0	0
PB	0	0	0	0	2	0	1
NI	2008	2017	1880	2071	2050	0	1987
CR	2599	2792	2692	2925	2715	0	2570
V	52	64	78	64	61	0	53
Y	3	4	4	4	4	0	4
Q	0.0	0.0	0.0	0.0	0.0	0.0	0.0
OR	0.0	0.12	0.0	0.12	0.13	0.18	0.13
AB	0.28	0.35	1.97	0.34	0.27	0.62	0.37
AN	5.43	7.76	8.86	6.59	4.88	7.85	5.69
NE	0.0	0.0	0.0	0.0	0.0	0.0	0.0
LE	0.0	0.0	0.0	0.0	0.0	0.0	0.0
COR	0.0	0.0	0.0	0.0	0.0	0.0	0.0
WO	2.07	1.74	3.28	2.06	2.57	2.62	1.60
EN	1.72	1.42	2.66	1.66	2.13	2.12	1.35
FER	0.09	0.11	0.23	0.16	0.13	0.20	0.04
EN	13.43	20.80	16.70	20.00	19.20	24.61	23.87
FER	0.72	1.68	1.41	1.97	1.17	2.28	0.78
WO	0.0	0.0	0.0	0.0	0.0	0.0	0.0
FO	66.02	55.56	54.69	57.54	59.69	50.49	56.66
FA	3.91	4.95	5.10	6.25	4.02	5.16	2.04
LAR	0.0	0.0	0.0	0.0	0.0	0.0	0.0
MAG	5.55	4.46	4.15	2.24	4.76	3.44	6.46
IL	0.14	0.25	0.31	0.23	0.20	0.30	0.23
HEM	0.0	0.0	0.0	0.0	0.0	0.0	0.0
CHR	0.61	0.62	0.59	0.64	0.62	0.0	0.61
AP	0.0	0.12	0.0	0.14	0.17	0.12	0.15

77WH1 LOCATION 117 SPINEL LHERZOLITE
77WH9 LOCATION 124 SPINEL LHERZOLITE
77WH11 LOCATION 126 SPINEL LHERZOLITE
77WH16 LOCATION 133 SPINEL LHERZOLITE
77WH29 LOCATION 143 SPINEL LHERZOLITE
77WH45 LOCATION 173 SPINEL LHERZOLITE
77WH73 LOCATION 212 SPINEL LHERZOLITE

SPINEL LHERZOLITE

SAMPLE	77WH78	77WH81	77WH94	77WH95	77WH97	782	785
SIO2	40.69	43.58	41.51	43.99	41.54	39.11	41.35
TIO2	0.15	0.13	0.09	0.16	0.12	0.06	0.13
AL203	2.05	2.58	1.84	3.25	2.42	1.95	2.24
FE203	3.01	2.74	3.68	2.82	2.94	4.41	2.68
FEO	5.50	5.52	4.88	6.59	5.03	5.08	4.70
MNO	0.12	0.12	0.11	0.12	0.12	0.12	0.11
MGO	39.78	39.23	41.49	39.09	38.82	39.22	38.34
CAO	3.39	2.57	2.00	3.35	2.37	2.53	2.35
NA20	0.04	0.05	0.03	0.22	0.04	0.04	0.25
K20	0.02	0.02	0.0	0.0	0.02	0.0	0.02
P205	0.06	0.06	0.0	0.0	0.07	0.0	0.06
LOI	6.13	4.65	5.09	0.40	6.54	7.05	7.12
TOTAL	100.94	101.25	100.72	99.99	100.03	99.57	99.35
ZR	5	5	5	7	5	5	5
SR	5	3	1	5	1	2	2
RB	0	0	0	0	0	0	0
ZN	45	46	40	48	40	41	39
CU	53	23	11	45	25	17	16
BA	7	8	0	3	0	10	0
GA	4	3	3	4	4	3	2
TH	1	1	4	0	4	2	5
NB	0	0	3	2	3	2	3
U	0	0	0	0	0	0	0
PB	0	0	1	0	1	1	0
NI	1965	2018	1974	1924	2013	1949	2059
CR	3277	2499	2262	2581	2240	2572	3037
V	73	71	50	86	57	64	52
Y	3	4	5	5	4	3	5
Q	0.0	0.0	0.0	0.0	0.0	0.0	0.0
OR	0.12	0.12	0.0	0.0	0.13	0.0	0.13
AB	0.36	0.44	0.26	1.86	0.36	0.36	2.28
AN	5.62	6.97	5.09	7.88	6.78	5.53	5.32
NE	0.0	0.0	0.0	0.0	0.0	0.0	0.0
LE	0.0	0.0	0.0	0.0	0.0	0.0	0.0
COR	0.0	0.0	0.0	0.0	0.0	0.0	0.0
WO	4.85	2.41	2.18	3.64	2.20	3.32	2.86
EN	3.98	1.97	1.81	2.93	1.81	2.76	2.36
FER	0.29	0.15	0.10	0.28	0.12	0.15	0.15
EN	10.65	24.29	18.00	16.22	21.89	13.06	19.59
FER	0.77	1.89	0.99	1.57	1.48	0.73	1.24
WO	0.0	0.0	0.0	0.0	0.0	0.0	0.0
FO	62.60	52.06	61.57	54.81	55.60	62.59	56.81
FA	4.99	4.44	3.74	5.83	4.15	3.87	3.95
LAR	0.0	0.0	0.0	0.0	0.0	0.0	0.0
MAG	4.58	4.10	5.56	4.09	4.54	6.88	4.19
IL	0.30	0.25	0.18	0.30	0.24	0.12	0.27
HEM	0.0	0.0	0.0	0.0	0.0	0.0	0.0
CHR	0.74	0.55	0.51	0.56	0.51	0.60	0.71
AP	0.15	0.14	0.0	0.0	0.17	0.0	0.15

77WH78 LOCATION 214 SPINEL LHERZOLITE
77WH81 LOCATION 231 SPINEL LHERZOLITE
77WH94 LOCATION 266 SPINEL LHERZOLITE
77WH95 LOCATION 270 SPINEL LHERZOLITE
77WH97 LOCATION 281 SPINEL LHERZOLITE
782 LOCATION 310 SPINEL LHERZOLITE
785 LOCATION 314 SPINEL LHERZOLITE

SPINEL LHERZOLITE

SAMPLE	787	788	7815	7822	7824	7826	7830
SIO2	41.55	43.88	38.72	42.03	43.02	42.15	42.49
TIO2	0.13	0.17	0.07	0.11	0.12	0.11	0.13
AL203	2.38	3.10	1.86	2.38	2.44	2.42	2.55
FE203	2.71	0.84	2.28	2.20	1.49	1.03	2.03
FEO	5.19	7.45	5.11	5.46	6.52	6.71	5.93
MNO	0.12	0.11	0.10	0.12	0.12	0.12	0.11
MGO	37.05	40.08	36.21	38.37	39.01	38.99	39.53
CAO	2.33	3.00	2.64	2.20	2.61	2.31	2.72
NA20	0.04	0.11	0.03	0.03	0.04	0.04	0.05
K20	0.02	0.02	0.0	0.02	0.03	0.02	0.02
P205	0.05	0.06	0.0	0.06	0.07	0.06	0.05
LOI	7.17	1.58	11.11	6.67	4.50	6.13	3.36
TOTAL	98.74	100.40	98.13	99.65	99.97	100.09	98.97
ZR	5	6	14	5	4	4	4
SR	3	3	89	53	13	2	2
RB	0	0	2	0	0	0	0
ZN	45	53	46	45	44	0	46
CU	24	30	23	21	33	15	13
BA	8	11	51	82	25	0	0
GA	3	3	8	2	4	2	3
TH	2	2	0	0	2	1	0
NB	1	1	5	0	1	1	0
U	0	0	0	0	0	0	0
PB	0	0	0	1	0	0	3
NI	2065	2146	1798	2032	2088	2048	2172
CR	2604	2727	2687	2872	1787	2621	2765
V	68	81	62	70	71	63	59
Y	5	5	5	4	4	3	5
Q	0.0	0.0	0.0	0.0	0.0	0.0	0.0
OR	0.13	0.12	0.0	0.13	0.19	0.13	0.12
AB	0.37	0.94	0.29	0.27	0.35	0.36	0.44
AN	6.80	7.97	5.65	6.74	6.67	6.75	6.95
NE	0.0	0.0	0.0	0.0	0.0	0.0	0.0
LE	0.0	0.0	0.0	0.0	0.0	0.0	0.0
COR	0.0	0.0	0.0	0.0	0.0	0.0	0.0
WO	2.26	2.77	3.91	1.90	2.67	2.08	2.83
EN	1.85	2.19	3.19	1.55	2.13	1.66	2.29
FER	0.14	0.28	0.26	0.13	0.23	0.19	0.21
EN	26.57	15.03	18.47	24.55	20.84	19.43	18.45
FER	2.00	1.89	1.48	2.02	2.26	2.24	1.66
WO	0.0	0.0	0.0	0.0	0.0	0.0	0.0
FO	50.39	58.42	57.10	53.39	55.02	57.34	57.32
FA	4.19	8.09	5.05	4.85	6.58	7.28	5.68
LAR	0.0	0.0	0.0	0.0	0.0	0.0	0.0
MAG	4.27	1.23	3.78	3.41	2.26	1.58	3.07
IL	0.27	0.33	0.15	0.22	0.24	0.22	0.26
HEM	0.0	0.0	0.0	0.0	0.0	0.0	0.0
CHR	0.61	0.59	0.66	0.66	0.40	0.60	0.62
AP	0.13	0.14	0.0	0.15	0.17	0.15	0.12

787 LOCATION 315 SPINEL LHERZOLITE
788 LOCATION 317 SPINEL LHERZOLITE
7815 LOCATION 328 SPINEL LHERZOLITE
7822 LOCATION 338 SPINEL LHERZOLITE
7824 LOCATION 341 SPINEL LHERZOLITE
7826 LOCATION 342 SPINEL LHERZOLITE
7830 LOCATION 353 SPINEL LHERZOLITE

SPINEL LHERZOLITE

SAMPLE	7832	7840	7846	7849	7851	7856	7858
SIO2	40.18	43.98	42.98	42.00	42.27	42.64	43.19
TIO2	0.06	0.16	0.15	0.12	0.11	0.11	0.11
AL203	1.93	2.92	3.00	2.73	2.24	2.77	2.19
FE203	3.76	2.19	1.60	2.05	1.86	1.45	2.63
FEO	4.94	6.00	6.29	5.97	5.96	6.37	5.58
MNO	0.11	0.11	0.11	0.11	0.11	0.11	0.12
MGO	39.03	39.55	38.00	39.14	40.69	39.40	39.92
CAO	2.23	2.93	2.80	2.51	2.09	2.43	2.12
NA20	0.03	0.09	0.08	0.05	0.05	0.05	0.02
K20	0.0	0.02	0.03	0.02	0.03	0.02	0.02
P205	0.0	0.08	0.06	0.07	0.06	0.05	0.06
LOI	5.05	3.26	3.15	4.72	4.78	3.13	5.45
TOTAL	97.32	101.29	98.25	99.49	100.25	98.53	101.41
ZR	5	5	5	4	4	4	4
SR	3	3	4	0	0	0	0
RB	0	0	0	0	0	0	0
ZN	37	49	48	47	43	45	44
CU	12	37	26	26	20	8	17
BA	0	0	6	3	0	4	6
GA	1	3	4	4	3	3	3
TH	5	1	0	0	0	2	0
NB	2	1	0	1	0	2	0
U	0	0	0	0	0	0	0
PB	0	3	0	0	0	1	0
NI	2021	2080	2090	2187	2203	2140	2194
CR	2880	2707	2836	2645	2648	2782	2531
V	65	65	76	63	54	57	66
Y	4	5	4	3	4	4	3
Q	0.0	0.0	0.0	0.0	0.0	0.0	0.0
OR	0.0	0.12	0.19	0.12	0.18	0.12	0.12
AB	0.27	0.77	0.71	0.44	0.44	0.44	0.18
AN	5.54	7.62	8.10	7.53	6.05	7.59	6.05
NE	0.0	0.0	0.0	0.0	0.0	0.0	0.0
LE	0.0	0.0	0.0	0.0	0.0	0.0	0.0
COR	0.0	0.0	0.0	0.0	0.0	0.0	0.0
WO	2.66	2.76	2.52	2.12	1.82	1.94	1.87
EN	2.20	2.24	2.02	1.71	1.47	1.56	1.52
FER	0.13	0.20	0.21	0.16	0.13	0.16	0.12
EN	18.95	20.83	21.53	18.95	18.33	19.45	24.77
FER	1.11	1.86	2.23	1.74	1.64	2.01	1.94
WO	0.0	0.0	0.0	0.0	0.0	0.0	0.0
FO	58.66	53.96	52.92	57.30	60.20	57.04	53.89
FA	3.79	5.32	6.05	5.78	5.95	6.51	4.65
LAR	0.0	0.0	0.0	0.0	0.0	0.0	0.0
MAG	5.88	3.23	2.43	3.12	2.81	2.19	3.96
IL	0.12	0.31	0.30	0.24	0.22	0.22	0.22
HEM	0.0	0.0	0.0	0.0	0.0	0.0	0.0
CHR	0.67	0.59	0.64	0.60	0.59	0.62	0.57
AP	0.0	0.19	0.15	0.17	0.15	0.12	0.14

7832 LOCATION 357 SPINEL LHERZOLITE
7840 LOCATION 378 SPINEL LHERZOLITE
7846 LOCATION 397 SPINEL LHERZOLITE
7849 LOCATION 399 SPINEL LHERZOLITE
7851 LOCATION 403 SPINEL LHERZOLITE
7856 LOCATION 424 SPINEL LHERZOLITE
7858 LOCATION 426 SPINEL LHERZOLITE

SPINEL LHERZOLITE

SAMPLE	7859	7860	7862	7864	7865	7891	7893
SIO2	43.60	43.48	43.93	42.76	43.90	41.88	42.46
TIO2	0.15	0.18	0.12	0.13	0.12	0.11	0.11
AL2O3	2.87	3.38	2.15	2.53	3.36	1.93	2.18
FE2O3	1.02	1.44	2.15	1.90	2.72	2.64	1.75
FEO	6.93	6.49	5.74	6.31	4.87	5.02	6.01
MNO	0.12	0.11	0.12	0.13	0.13	0.12	0.12
MGO	40.05	38.66	38.08	39.26	36.46	37.94	40.48
CAO	2.85	2.88	2.80	2.56	3.18	2.13	1.98
NA2O	0.14	0.23	0.10	0.05	0.08	0.01	0.17
K2O	0.02	0.03	0.02	0.04	0.07	0.02	0.03
P2O5	0.06	0.07	0.06	0.06	0.07	0.05	0.07
LOI	2.68	4.05	4.63	4.50	3.38	6.42	5.38
TOTAL	100.49	101.00	99.90	100.23	98.34	98.27	100.74
ZR	6	7	4	4	5	4	4
SR	9	18	6	0	1	0	0
RB	0	0	0	0	1	0	0
ZN	42	50	44	0	45	42	45
CU	26	45	21	25	11	19	20
BA	3	19	0	3	0	0	5
GA	3	5	3	3	6	1	4
TH	2	2	0	1	2	3	0
NB	2	1	0	1	0	0	1
U	0	0	0	0	0	0	0
PB	0	3	0	0	3	2	0
NI	2081	2019	1955	2056	1856	2107	2164
CR	2514	2095	2949	2695	3322	2605	2734
V	69	75	69	72	65	52	62
Y	6	6	4	5	5	4	3
Q	0.0	0.0	0.0	0.0	0.0	0.0	0.0
OR	0.12	0.18	0.12	0.25	0.43	0.13	0.19
AB	1.21	2.00	0.88	0.44	0.71	0.09	1.50
AN	7.28	8.33	5.60	6.83	9.01	5.60	5.32
NE	0.0	0.0	0.0	0.0	0.0	0.0	0.0
LE	0.0	0.0	0.0	0.0	0.0	0.0	0.0
COR	0.0	0.0	0.0	0.0	0.0	0.0	0.0
WO	2.81	2.47	3.55	2.50	2.94	2.30	1.86
EN	2.23	1.97	2.88	2.01	2.41	1.89	1.51
FER	0.26	0.21	0.26	0.20	0.17	0.13	0.14
EN	15.67	17.47	26.25	19.89	28.82	27.70	17.92
FER	1.81	1.88	2.33	1.97	2.01	1.98	1.65
WO	0.0	0.0	0.0	0.0	0.0	0.0	0.0
FO	58.64	55.74	49.02	55.93	44.78	51.05	60.16
FA	7.48	6.61	4.79	6.12	3.43	4.02	6.10
LAR	0.0	0.0	0.0	0.0	0.0	0.0	0.0
MAG	1.51	2.15	3.26	2.87	4.13	4.15	2.65
IL	0.29	0.35	0.24	0.26	0.24	0.23	0.22
HEM	0.0	0.0	0.0	0.0	0.0	0.0	0.0
CHR	0.55	0.46	0.66	0.60	0.75	0.61	0.61
AP	0.14	0.17	0.15	0.15	0.17	0.13	0.17

7859 LOCATION 428 SPINEL LHERZOLITE
7860 LOCATION 432 SPINEL LHERZOLITE
7862 LOCATION 436 SPINEL LHERZOLITE
7864 LOCATION 443 SPINEL LHERZOLITE
7865 LOCATION 445 SPINEL LHERZOLITE
7891 LOCATION 481 SPINEL LHERZOLITE
7893 LOCATION 487 SPINEL LHERZOLITE

NA2O<0.01

A100

SPINEL LHERZOLITE

SAMPLE	7894	78133	78146	78151	791	795
SIO2	42.32	37.56	40.64	40.24	44.12	42.10
TIO2	0.10	0.08	0.08	0.07	0.15	0.19
AL203	1.73	2.13	2.01	1.94	3.44	3.90
FE203	2.94	5.09	4.36	3.29	1.15	1.63
FEO	4.41	3.48	3.96	5.52	6.81	6.26
MNO	0.11	0.12	0.10	0.12	0.11	0.10
MGO	40.37	38.39	39.47	40.02	39.68	38.77
CAO	1.56	1.74	2.06	2.10	2.93	3.49
NA2O	0.01	0.04	0.02	0.04	0.76	0.24
K2O	0.02	0.0	0.0	0.0	0.02	0.02
P2O5	0.07	0.0	0.0	0.0	0.06	0.07
LOI	7.71	9.33	7.89	5.05	1.68	3.30
TOTAL	101.35	97.96	100.59	98.39	100.91	100.07
ZR	5	7	5	5	6	10
SR	1	4	2	2	5	9
RB	0	0	0	0	0	0
ZN	39	42	41	42	47	45
CU	16	16	19	24	33	31
BA	2	0	0	0	0	0
GA	12	2	3	2	4	5
TH	2	5	3	3	1	4
NB	2	3	3	1	0	2
U	0	0	0	0	0	0
PB	0	2	0	0	3	5
NI	2186	2007	2094	2093	2102	1994
CR	2888	2600	2661	2554	2804	2392
V	43	58	55	66	66	73
Y	3	7	5	3	5	8
Q	0.0	0.0	0.0	0.0	0.0	0.0
OR	0.13	0.0	0.0	0.0	0.12	0.12
AB	0.09	0.38	0.18	0.36	6.45	2.09
AN	4.91	6.33	5.80	5.46	5.94	9.79
NE	0.0	0.0	0.0	0.0	0.0	0.0
LE	0.0	0.0	0.0	0.0	0.0	0.0
COR	0.0	0.0	0.0	0.0	0.0	0.0
WO	1.19	1.40	2.16	2.36	3.45	3.16
EN	0.98	1.19	1.82	1.93	2.75	2.54
FER	0.05	0.02	0.06	0.14	0.31	0.26
EN	27.41	18.03	22.57	15.63	7.08	9.70
FER	1.46	0.37	0.78	1.13	0.80	0.98
WO	0.0	0.0	0.0	0.0	0.0	0.0
FO	55.00	61.80	56.90	62.22	62.61	61.09
FA	3.22	1.39	2.16	4.95	7.79	6.78
LAR	0.0	0.0	0.0	0.0	0.0	0.0
MAG	4.53	8.29	6.79	5.09	1.67	2.43
IL	0.20	0.17	0.16	0.14	0.29	0.37
HEM	0.0	0.0	0.0	0.0	0.0	0.0
CHR	0.66	0.63	0.62	0.59	0.61	0.53
AP	0.17	0.0	0.0	0.0	0.14	0.17

7894 LOCATION 489 SPINEL LHERZOLITE NA2C<0.01
78133 LOCATION 529 SPINEL LHERZOLITE
78146 LOCATION 544 SPINEL LHERZOLITE
78151 LOCATION 556 SPINEL LHERZOLITE
791 LOCATION 600 SPINEL LHERZOLITE
795 LOCATION 608 SPINEL LHERZOLITE

A101

HARZBURGITE

SAMPLE	77WH8	77WH13	77WH14	77WH32	77WH38	77WH46	77WH56
SIO2	41.96	39.48	41.08	37.68	37.37	42.22	42.24
TIO2	0.11	0.08	0.10	0.09	0.08	0.15	0.11
AL203	1.53	1.18	0.89	0.75	0.90	1.44	1.12
FE203	1.74	3.78	2.09	5.26	4.85	1.26	1.24
FEO	5.38	3.85	4.86	2.14	2.73	6.91	7.28
MNO	0.12	0.08	0.11	0.11	0.10	0.12	0.12
MGO	41.64	44.21	44.12	39.82	38.74	40.83	42.61
CAO	1.22	0.56	0.57	1.04	1.02	1.05	0.98
NA2O	0.02	0.04	0.05	0.01	0.01	0.03	0.02
K2O	0.02	0.0	0.02	0.02	0.03	0.03	0.04
P2O5	0.05	0.0	0.05	0.06	0.06	0.05	0.05
LOI	5.61	7.78	7.04	13.52	13.61	4.88	4.54
TOTAL	99.40	101.04	100.98	100.50	99.50	98.97	100.35
ZR	5	5	4	5	5	4	5
SR	11	1	1	18	16	3	2
RB	0	0	0	0	0	0	0
ZN	37	37	35	34	32	51	44
CU	11	10	6	6	6	9	11
BA	27	6	11	18	19	6	10
GA	3	13	1	3	3	4	4
TH	1	1	1	2	3	3	3
NB	0	2	1	1	0	3	2
U	0	0	0	0	0	0	0
PB	0	0	0	0	0	1	0
NI	2195	2298	2242	2052	2104	2151	2237
CR	2565	2344	2470	1920	1990	2572	2875
V	33	29	25	33	38	51	36
Y	2	2	2	11	3	4	4
Q	0.0	0.0	0.0	0.0	0.0	0.0	0.0
OR	0.13	0.0	0.13	0.14	0.21	0.19	0.25
AB	0.18	0.36	0.45	0.10	0.10	0.27	0.18
AN	4.28	2.96	2.27	2.23	2.69	3.92	2.96
NE	0.0	0.0	0.0	0.0	0.0	0.0	0.0
LE	0.0	0.0	0.0	0.0	0.0	0.0	0.0
COR	0.0	0.11	0.0	0.0	0.0	0.0	0.0
WO	0.76	0.0	0.16	1.36	1.14	0.52	0.73
EN	0.62	0.0	0.13	1.17	0.98	0.42	0.58
FER	0.05	0.0	0.01	0.0	0.01	0.05	0.07
EN	22.06	14.89	17.65	23.42	24.58	22.68	18.24
FER	1.73	0.49	1.11	0.0	0.20	2.52	2.06
WO	0.0	0.0	0.0	0.0	0.0	0.0	0.0
FO	61.27	71.99	69.18	62.40	60.53	59.24	64.08
FA	5.31	2.64	4.80	0.0	0.55	7.25	7.99
LAR	0.0	0.0	0.0	0.0	0.0	0.0	0.0
MAG	2.68	5.85	3.21	7.51	8.16	1.93	1.87
IL	0.22	0.16	0.20	0.20	0.18	0.30	0.22
HEM	0.0	0.0	0.0	0.85	0.0	0.0	0.0
CHR	0.59	0.54	0.56	0.47	0.50	0.59	0.64
AP	0.12	0.0	0.12	0.16	0.16	0.12	0.12

77WH8 LOCATION 123 HARZBURGITE
77WH13 LOCATION 129 HARZBURGITE
77WH14 LOCATION 130 HARZBURGITE
77WH32 LOCATION 145 HARZBURGITE NA2O<0.01
77WH38 LOCATION 164 HARZBURGITE NA2O<0.01
77WH46 LOCATION 174 HARZBURGITE
77WH56 LOCATION 189 HARZBURGITE

HARZBURGITE

SAMPLE	792	7910	7818	7827	7834	7847	7848
SIO2	41.28	40.19	39.53	39.15	40.78	41.29	41.36
TIO2	0.09	0.08	0.04	0.11	0.11	0.10	0.13
AL2O3	1.19	1.22	0.74	1.35	1.61	2.09	2.22
FE2O3	1.59	3.09	3.46	3.56	3.07	1.82	1.90
FEO	5.51	4.42	4.46	4.23	5.47	5.60	5.60
MNO	0.10	0.39	0.10	0.11	0.11	0.11	0.11
MGO	45.36	42.35	41.82	41.15	40.98	40.72	40.24
CAO	0.85	0.82	0.77	0.87	1.30	1.66	1.93
NA2O	0.03	0.03	0.01	0.03	0.04	0.05	0.07
K2O	0.02	0.02	0.0	0.02	0.02	0.02	0.02
P2O5	0.04	0.05	0.0	0.05	0.06	0.05	0.06
LOI	4.71	8.09	9.11	10.62	6.30	5.71	5.79
TOTAL	100.77	100.75	100.04	101.25	99.85	99.22	99.43
ZR	4	3	4	4	4	5	0
SR	0	1	32	5	2	2	0
RB	0	0	0	0	0	0	0
ZN	40	43	36	40	54	41	0
CU	9	7	10	12	38	16	0
BA	0	0	64	10	0	10	0
GA	2	2	1	2	3	3	0
TH	0	0	0	-1	0	4	0
NB	0	0	0	1	0	2	0
U	0	0	0	0	0	0	0
PB	0	0	0	0	2	0	0
NI	2356	2166	2262	2204	2317	2252	0
CR	2491	2331	2840	2242	2096	2855	0
V	15	24	38	34	37	47	0
Y	2	2	2	2	3	4	0
Q	0.0	0.0	0.0	0.0	0.0	0.0	0.0
OR	0.12	0.13	0.0	0.13	0.13	0.13	0.13
AB	0.26	0.27	0.09	0.28	0.36	0.45	0.63
AN	3.17	3.37	2.16	3.84	4.43	5.77	6.07
NE	0.0	0.0	0.0	0.0	0.0	0.0	0.0
LE	0.0	0.0	0.0	0.0	0.0	0.0	0.0
COR	0.0	0.0	0.0	0.0	0.0	0.0	0.0
WO	0.39	0.27	0.85	0.23	0.85	1.11	1.56
EN	0.32	0.23	0.71	0.19	0.70	0.90	1.27
FER	0.02	0.01	0.03	0.01	0.05	0.08	0.11
EN	12.04	18.94	20.09	19.64	19.82	18.43	17.81
FER	0.91	1.05	0.98	0.87	1.41	1.53	1.55
WO	0.0	0.0	0.0	0.0	0.0	0.0	0.0
FO	73.43	66.03	65.31	65.05	61.82	62.11	61.63
FA	6.11	4.04	3.51	3.19	4.85	5.70	5.90
LAR	0.0	0.0	0.0	0.0	0.0	0.0	0.0
MAG	2.39	4.82	5.49	5.67	4.74	2.81	2.94
IL	0.18	0.16	0.08	0.23	0.22	0.20	0.26
HEM	0.0	0.0	0.0	0.0	0.0	0.0	0.0
CHR	0.56	0.54	0.67	0.53	0.48	0.65	0.0
AP	0.10	0.12	0.0	0.13	0.15	0.12	0.15

792 LOCATION 601 HARZBURGITE
7910 LOCATION 619 HARZBURGITE
7818 LOCATION 330 HARZBURGITE
7827 LOCATION 349 HARZBURGITE
7834 LOCATION 358 HARZBURGITE
7847 LOCATION 398 HARZBURGITE
7848 LOCATION 399 HARZBURGITE

NA2O<0.01

A103

HARZBURGITE

SAMPLE	7852	7867	7888	7889	7895	78116	78153
SIO2	40.45	40.59	40.85	41.83	40.09	39.51	38.38
TIO2	0.10	0.10	0.11	0.10	0.06	0.09	0.10
AL203	1.89	1.00	1.49	1.87	1.40	1.23	1.27
FE203	1.42	2.72	2.99	3.05	3.97	4.36	3.40
FEO	6.06	4.32	4.74	4.86	3.65	4.77	4.36
MNO	0.11	0.03	0.11	0.12	0.10	0.12	0.12
MGO	41.10	42.30	41.72	39.68	41.72	42.11	40.74
CAO	1.58	0.65	1.41	1.75	1.44	0.93	0.77
NA20	0.04	0.03	0.03	0.03	0.02	0.02	0.03
K20	0.03	0.02	0.02	0.02	0.0	0.0	0.02
P205	0.06	0.04	0.07	0.04	0.0	0.0	0.04
LOI	6.10	7.65	6.66	6.62	7.85	7.12	8.43
TOTAL	98.94	99.45	100.20	99.97	100.30	100.26	97.66
ZR	4	6	4	4	4	5	4
SR	1	0	0	0	0	0	0
RB	0	0	0	0	0	0	0
ZN	42	36	42	44	38	41	42
CU	10	7	20	18	21	28	10
BA	0	0	0	0	11	7	4
GA	2	2	2	4	3	4	2
TH	3	0	0	0	0	0	0
NB	1	0	1	1	0	0	0
U	0	0	0	0	0	0	0
PB	0	0	1	0	0	0	0
NI	2247	2293	2344	2068	2155	1967	2273
CR	2485	2477	2506	2629	3140	2509	2117
V	55	8	23	45	41	42	33
Y	4	2	3	3	2	2	2
Q	0.0	0.0	0.0	0.0	0.0	0.0	0.0
OR	0.19	0.13	0.13	0.13	0.0	0.0	0.13
AB	0.36	0.28	0.27	0.27	0.18	0.18	0.28
AN	5.25	2.75	4.12	5.24	4.01	3.49	3.65
NE	0.0	0.0	0.0	0.0	0.0	0.0	0.0
LE	0.0	0.0	0.0	0.0	0.0	0.0	0.0
COR	0.0	0.0	0.0	0.0	0.0	0.0	0.0
WO	1.15	0.20	1.19	1.57	1.53	0.60	0.14
EN	0.93	0.16	0.98	1.29	1.29	0.50	0.11
FER	0.09	0.01	0.06	0.08	0.04	0.02	0.01
EN	14.49	22.31	19.17	25.04	19.23	17.44	18.45
FER	1.32	1.11	1.10	1.55	0.57	0.82	0.91
WO	0.0	0.0	0.0	0.0	0.0	0.0	0.0
FO	66.15	64.35	63.41	55.42	63.98	66.02	66.39
FA	6.89	3.54	3.99	3.79	2.11	3.40	3.59
LAR	0.0	0.0	0.0	0.0	0.0	0.0	0.0
MAG	2.21	4.28	4.62	4.72	6.20	6.76	5.51
IL	0.20	0.21	0.22	0.20	0.12	0.18	0.21
HEM	0.0	0.0	0.0	0.0	0.0	0.0	0.0
CHR	0.57	0.58	0.57	0.60	0.73	0.58	0.51
AP	0.15	0.10	0.17	0.10	0.0	0.0	0.10

7852 LOCATION 404 HARZBURGITE
7867 LOCATION 447 HARZBURGITE
7888 LOCATION 478 HARZBURGITE
7889 LOCATION 480 HARZBURGITE
7895 LOCATION 493 HARZBURGITE
78116 LOCATION 516 HARZBURGITE
78153 LOCATION 559 HARZBURGITE

DUNITE

SAMPLE	77WH36	77WH41	77WH55	77WH77	77WH80	77WH93	794
SIO2	38.71	38.82	37.84	36.66	34.47	35.56	38.37
TIO2	0.09	0.10	0.07	0.13	0.05	0.06	0.10
AL203	0.50	0.92	0.71	1.15	1.20	2.16	0.93
FE203	7.04	8.77	2.62	3.62	5.88	5.15	2.94
FEO	2.29	4.11	7.59	6.71	4.23	5.16	7.08
MNO	0.12	0.12	0.12	0.12	0.12	0.12	0.12
MGO	45.43	43.03	47.05	43.57	42.02	45.31	43.69
CAO	0.25	0.42	0.32	0.26	0.29	0.34	0.39
NA2O	0.03	0.02	0.02	0.02	0.01	0.01	0.48
K2O	0.02	0.02	0.0	0.02	0.0	0.0	0.03
P2O5	0.08	0.08	0.0	0.05	0.0	0.0	0.05
LOI	6.23	10.83	3.88	7.55	11.19	6.79	6.82
TOTAL	100.79	108.24	100.22	99.86	99.46	100.66	101.00
ZR	4	5	4	4	4	5	5
SR	3	0	1	0	1	1	6
RB	0	0	0	0	0	0	0
ZN	43	37	49	47	42	58	57
CU	9	7	6	115	29	6	14
BA	17	17	17	13	24	17	0
GA	2	2	3	2	4	3	3
TH	1	1	2	0	0	4	3
NB	0	2	0	0	0	2	1
U	0	0	0	0	0	0	0
PB	0	0	0	1	0	1	6
NI	2458	2357	2552	2265	2354	2440	2436
CR	618	3625	2721	4297	4211	3643	2299
V	19	15	21	26	25	29	8
Y	2	3	2	2	2	3	4
Q	0.0	0.0	0.0	0.0	0.0	0.0	0.0
OR	0.12	0.12	0.0	0.13	0.0	0.0	0.19
AB	0.27	0.18	0.0	0.18	0.10	0.0	4.29
AN	0.77	1.65	1.63	1.04	1.60	1.77	0.31
NE	0.0	0.0	0.09	0.0	0.0	0.05	0.0
LE	0.0	0.0	-2.12	0.0	0.0	-0.21	0.0
COR	0.17	0.31	0.10	0.80	0.74	1.65	0.0
WO	0.0	0.0	0.0	0.0	0.0	0.0	0.58
EN	0.0	0.0	0.0	0.0	0.0	0.0	0.47
FER	0.0	0.0	0.0	0.0	0.0	0.0	0.04
EN	15.15	13.67	0.0	8.35	7.07	0.0	0.0
FER	0.0	0.0	0.0	0.43	0.17	0.0	0.0
WO	0.0	0.0	0.0	0.0	0.0	0.0	0.0
FO	73.14	69.51	84.87	78.06	77.54	83.75	80.34
FA	0.0	0.0	9.20	6.97	2.05	3.98	8.41
LAR	0.0	0.0	0.0	0.0	0.0	0.0	0.0
MAG	7.77	13.19	3.93	5.65	9.59	7.91	4.51
IL	0.18	0.20	0.14	0.27	0.11	0.12	0.20
HEM	2.07	0.14	0.0	0.0	0.0	0.0	0.0
CHR	0.14	0.82	0.61	1.00	1.02	0.83	0.52
AP	0.20	0.20	0.0	0.13	0.0	0.0	0.12

77WH36 LOCATION 153 DUNITE

77WH41 LOCATION 169 DUNITE LAYERS

77WH55 LOCATION 189 DUNITE LAYERS + 1.54 KALIOPHYLITE

77WH77 LOCATION 214 DUNITE LAYERS

77WH80 LOCATION 231 DUNITE LAYER

77WH93 LOCATION 266 DUNITE LAYER WITH SPINEL LHERZOLITE

794 LOCATION 608 DUNITE LAYER

DUNITE

SAMPLE	797	799	7823	7841	7890	7896	78112
SIO2	36.90	36.18	38.14	33.74	37.59	33.58	40.34
TIO2	0.09	0.08	0.06	0.10	0.09	0.04	0.12
AL203	0.78	0.58	0.46	3.71	0.57	0.23	1.34
FE203	3.57	4.06	4.28	4.47	3.54	5.03	2.77
FEO	5.04	5.05	4.20	4.55	5.53	3.31	5.50
MNO	0.10	0.10	0.11	0.11	0.12	0.10	0.13
MGO	45.01	44.48	42.83	41.34	44.17	43.32	42.48
CAO	0.36	0.35	0.40	0.35	0.46	0.18	0.86
NA2O	0.02	0.01	0.01	0.01	0.01	0.01	0.02
K2O	0.02	0.02	0.0	0.02	0.02	0.0	0.02
P2O5	0.05	0.06	0.0	0.05	0.04	0.0	0.04
LOI	9.03	8.73	8.47	10.96	7.78	11.00	6.68
TOTAL	100.97	99.70	98.96	99.41	99.92	96.80	100.30
ZR	4	4	6	4	4	4	4
SR	0	1	6	6	0	0	1
RB	0	0	0	0	0	0	0
ZN	49	48	36	64	47	37	42
CU	8	18	7	7	7	8	23
BA	0	0	26	0	0	19	0
GA	2	2	2	5	2	2	1
TH	1	0	3	0	1	1	1
NB	0	0	1	0	0	1	0
U	0	0	0	0	0	0	0
PB	1	0	1	0	1	0	0
NI	2525	2471	2413	2383	2553	2593	2227
CR	2890	2089	2785	6944	769	2601	2623
V	5	7	21	28	8	9	23
Y	2	3	2	2	2	1	3
Q	0.0	0.0	0.0	0.0	0.0	0.0	0.0
OR	0.13	0.13	0.0	0.13	0.13	0.0	0.13
AB	0.18	0.09	0.09	0.09	0.09	0.10	0.18
AN	1.58	1.48	1.33	1.58	1.57	0.68	3.73
NE	0.0	0.0	0.0	0.0	0.0	0.0	0.0
LE	0.0	0.0	0.0	0.0	0.0	0.0	0.0
COR	0.21	0.05	0.0	3.52	0.0	0.0	0.0
WO	0.0	0.0	0.35	0.0	0.26	0.15	0.22
EN	0.0	0.0	0.30	0.0	0.21	0.13	0.18
FER	0.0	0.0	0.01	0.0	0.01	0.0	0.01
EN	4.08	3.59	16.10	4.79	7.20	1.92	17.21
FER	0.22	0.18	0.59	0.18	0.47	0.03	1.22
WO	0.0	0.0	0.0	0.0	0.0	0.0	0.0
FO	82.18	82.53	70.73	77.28	78.36	86.28	66.67
FA	4.83	4.69	2.87	3.16	5.66	1.61	5.22
LAR	0.0	0.0	0.0	0.0	0.0	0.0	0.0
MAG	5.60	6.45	6.83	7.24	5.56	3.46	4.27
IL	0.19	0.17	0.13	0.21	0.19	0.09	0.24
HEM	0.0	0.0	0.0	0.0	0.0	0.0	0.0
CHR	0.67	0.49	0.66	1.67	0.18	0.65	0.60
AP	0.13	0.15	0.0	0.13	0.10	0.0	0.10

797	LOCATION 613	DUNITE DIKE	
799	LOCATION 619	DUNITE LAYER	NA2<0.01
7823	LOCATION 341	DUNITE LAYER	NA2<0.01
7841	LOCATION 381	DUNITE RUBBLE	NA2<0.01
7890	LOCATION 481	DUNITE LAYER	NA2<0.01
7896	LOCATION 493	DUNITE UNKNOWN	NA2<0.01
78112	LOCATION 516	DUNITE MEGALENS	

DUNITE

SAMPLE	78113	78114	78115	78117	78138	78141	78145
SIO2	36.87	35.75	35.99	37.32	36.33	36.21	35.21
TIO2	0.11	0.05	0.11	0.11	0.11	0.13	0.06
AL203	0.96	0.58	1.07	1.36	0.93	1.49	0.71
FE203	3.61	4.72	2.16	3.60	4.27	3.81	5.33
FEO	5.38	5.44	6.39	6.16	5.43	5.73	4.30
MNO	0.13	0.12	0.13	0.13	0.13	0.13	0.12
MGO	43.45	45.77	43.60	43.39	40.50	39.80	43.41
CAO	0.43	0.32	0.46	0.45	0.68	0.96	0.28
NA2O	0.01	0.01	0.01	0.01	0.02	0.01	0.01
K2O	0.02	0.0	0.03	0.02	0.02	0.02	0.0
P2O5	0.04	0.0	0.05	0.06	0.06	0.05	0.0
LOI	8.45	6.44	8.91	7.92	10.81	10.35	10.45
TOTAL	99.46	99.20	98.91	100.53	99.29	98.69	99.88
ZR	3	4	4	4	4	4	5
SR	1	1	0	0	3	2	2
RB	0	0	0	0	0	0	0
ZN	45	49	48	54	44	52	48
CU	168	5	22	10	41	16	11
BA	0	17	0	0	0	0	0
GA	3	0	2	4	4	5	2
TH	0	1	0	0	0	0	2
NB	0	1	1	0	1	0	2
U	0	0	0	0	0	0	0
PB	0	0	1	0	0	0	0
NI	2551	2528	2415	2537	2272	2315	2506
CR	4647	2740	2372	6117	2627	3001	2809
V	10	17	9	16	17	27	24
Y	2	3	3	2	3	2	3
Q	0.0	0.0	0.0	0.0	0.0	0.0	0.0
OR	0.13	0.0	0.20	0.13	0.13	0.13	0.0
AB	0.09	0.0	0.09	0.09	0.19	0.10	0.09
AN	2.04	1.65	2.17	1.97	2.69	4.46	1.53
NE	0.0	0.05	0.0	0.0	0.0	0.0	0.0
LE	0.0	-1.49	0.0	0.0	0.0	0.0	0.0
COR	0.26	0.0	0.34	0.69	0.0	0.0	0.21
WO	0.0	0.0	0.0	0.0	0.28	0.22	0.0
EN	0.0	0.0	0.0	0.0	0.23	0.18	0.0
FER	0.0	0.0	0.0	0.0	0.01	0.01	0.0
EN	7.32	0.0	0.94	7.87	11.96	10.55	5.34
FER	0.43	0.0	0.08	0.56	0.73	0.75	0.16
WO	0.0	0.0	0.0	0.0	0.0	0.0	0.0
FO	77.57	85.74	83.56	75.47	70.99	70.71	80.58
FA	5.03	4.87	8.23	5.87	4.79	5.52	2.67
LAR	0.0	0.01	0.0	0.0	0.0	0.0	0.0
MAG	5.71	7.35	3.47	5.58	6.97	6.22	8.60
IL	0.23	0.10	0.23	0.22	0.24	0.28	0.13
HEM	0.0	0.0	0.0	0.0	0.0	0.0	0.0
CHR	1.09	0.63	0.57	1.41	0.64	0.73	0.67
AP	0.10	0.0	0.13	0.15	0.16	0.13	0.0

78113 LOCATION 516 DUNITE MEGALENS NA2<0.01
78114 LOCATION 516 DUNITE MEGALENS NA2<0.01
78115 LOCATION 516 DUNITE MEGALENS NA2<0.01
78117 LOCATION 516 DUNITE MEGALENS NA2<0.01
78138 LOCATION 531 DUNITE DIKE OR LAYER
78141 LOCATION 534 DUNITE LAYER NA2<0.01
78145 LOCATION 544 DUNITE LAYER FROM H-D CONTACT NA2<0.01

DUNITE

SAMPLE	78147	78152	78157	78158	78160
SIO2	33.26	36.07	36.13	35.04	37.52
TIO2	0.07	0.06	0.09	0.09	0.05
AL203	2.15	0.71	1.03	0.81	0.51
FE203	6.42	5.75	4.72	4.31	5.63
FEO	3.44	5.25	5.02	4.22	5.34
MNO	0.12	0.13	0.12	0.11	0.22
MGO	41.93	43.20	42.31	42.59	39.54
CAO	0.26	0.49	0.37	0.40	2.27
NA2O	0.01	0.01	0.01	0.01	0.12
K2O	0.0	0.0	0.02	0.02	0.0
P2O5	0.0	0.0	0.04	0.05	0.0
LOI	11.14	8.00	10.81	11.85	7.85
TOTAL	98.80	99.67	100.67	99.50	99.05
ZR	5	4	4	4	5
SR	2	0	1	1	51
RB	0	0	0	0	0
ZN	61	51	50	46	96
CU	11	59	25	22	8
BA	13	11	0	18	13
GA	4	3	3	3	1
TH	1	0	3	1	0
NB	0	0	1	1	1
U	0	0	0	0	0
PB	1	0	1	1	0
NI	2418	2201	2398	2483	2289
CR	9999	2312	3040	2973	2411
V	37	27	12	15	55
Y	3	1	3	3	4
Q	0.0	0.0	0.0	0.0	0.0
OR	0.0	0.0	0.13	0.13	0.0
AB	0.09	0.09	0.09	0.10	1.11
AN	1.43	2.06	1.75	1.89	0.93
NE	0.0	0.0	0.0	0.0	0.0
LE	0.0	0.0	0.0	0.0	0.0
COR	1.87	0.0	0.46	0.18	0.0
WO	0.0	0.24	0.0	0.0	4.75
EN	0.0	0.20	0.0	0.0	3.95
FER	0.0	0.01	0.0	0.0	0.21
EN	5.27	6.17	9.45	5.80	8.56
FER	0.0	0.27	0.45	0.21	0.45
WO	0.0	0.0	0.0	0.0	0.0
FO	78.41	77.47	75.14	80.31	66.60
FA	0.0	3.76	3.94	3.22	3.85
LAR	0.0	0.0	0.0	0.0	0.0
MAG	10.14	9.06	7.58	7.09	8.92
IL	0.15	0.12	0.19	0.19	0.10
HEM	0.21	0.0	0.0	0.0	0.0
CHR	2.41	0.54	0.72	0.73	0.57
AP	0.0	0.0	0.10	0.13	0.0

78147 LOCATION 544 DUNITE LAYER WITH HARZBURGITE NA2<0.01
78152 LOCATION 556 DUNITE DIKE NA2<0.01
78157 LOCATION 564 DUNITE LAYER NA2<0.01
78158 LOCATION 564 DUNITE LAYER NA2<0.01
78160 LOCATION 567 DUNITE LAYER

ORTHOPYROXENITE

SAMPLE	77WH25	784	7825	7850	7857	7897	7898
SIO2	48.07	48.75	47.90	50.80	50.34	51.45	49.27
TIO2	0.18	0.10	0.13	0.02	0.13	0.11	0.06
AL203	4.72	1.53	3.29	4.59	4.21	1.39	1.75
FE203	5.41	0.68	0.69	0.74	0.94	1.01	1.62
FEO	0.0	4.18	7.05	5.21	4.65	4.67	4.85
MNO	0.12	0.12	0.12	0.11	0.12	0.11	0.10
MGO	30.30	37.18	35.90	30.33	31.28	35.37	35.01
CAO	5.27	1.79	3.54	2.47	3.86	1.13	1.42
NA20	0.14	0.10	0.10	0.23	0.0	0.04	0.85
K20	0.07	0.04	0.03	0.24	0.19	0.06	0.0
P205	0.08	0.04	0.08	0.06	0.06	0.04	0.0
LOI	4.82	4.83	1.58	4.57	3.66	5.26	3.66
TOTAL	99.18	99.34	100.41	99.37	99.44	100.64	98.59
ZR	9	6	0	6	5	4	4
SR	202	73	0	3	1	2	2
RB	3	0	0	20	12	1	2
ZN	30	26	0	36	33	32	35
CU	36	4	0	92	4	8	1
BA	188	31	0	18	13	7	3
GA	4	2	0	7	5	2	1
TH	0	2	0	2	3	2	3
NB	2	2	0	2	2	2	2
U	0	0	0	0	0	0	0
PB	0	0	0	0	0	3	0
NI	1960	2214	0	1123	1026	1166	1252
CR	4357	3407	0	2895	4215	3673	6323
V	94	18	0	106	125	49	71
Y	5	3	0	3	3	3	3
Q	0.0	0.0	0.0	0.0	0.0	0.0	0.0
OR	0.44	0.25	0.18	1.49	1.16	0.37	0.0
AB	1.25	0.89	0.86	2.04	0.0	0.35	7.50
AN	12.68	3.80	8.54	11.32	11.33	3.58	1.00
NE	0.0	0.0	0.0	0.0	0.0	0.0	0.0
LE	0.0	0.0	0.0	0.0	0.0	0.0	0.0
COR	0.0	0.0	0.0	0.0	0.0	0.0	0.0
WO	5.43	2.22	3.64	0.48	3.40	0.83	2.64
EN	4.70	1.82	2.84	0.38	2.74	0.68	2.15
FER	0.0	0.13	0.39	0.04	0.25	0.06	0.17
EN	52.46	51.93	34.26	61.07	56.33	68.40	47.04
FER	0.0	3.78	4.75	7.08	5.23	5.66	3.70
WO	0.0	0.0	0.0	0.0	0.0	0.0	0.0
FO	15.60	30.62	37.39	12.52	15.23	15.94	29.27
FA	0.0	2.46	5.71	1.60	1.56	1.45	2.53
LAR	0.0	0.0	0.0	0.0	0.0	0.0	0.0
MAG	0.0	1.04	1.01	1.13	1.41	1.53	2.45
IL	-0.40	0.20	0.25	0.04	0.26	0.22	0.12
HEM	5.69	0.0	0.0	0.0	0.0	0.0	0.0
CHR	0.99	0.77	0.0	0.65	0.94	0.82	1.42
AP	0.20	0.10	0.19	0.15	0.14	0.10	0.0

77WH25	LOCATION 142	OPXITE
784	LOCATION 313	OPXITE, low alumina
7825	LOCATION 342	OPXITE NO TRACES
7850	LOCATION 399	OPXITE
7857	LOCATION 426	OPXITE NA20 NOT DETERMINED
7897	LOCATION 493	ORTHOPYROXENITE, low alumina
7898	LOCATION 493	OPXITE, low alumina

WEBSTERITE

SAMPLE	77WH2	77WH7	7853	7854	78155
SIO2	47.00	44.11	53.88	48.84	52.66
TIO2	0.09	0.16	0.22	0.25	0.22
AL2O3	8.86	7.21	3.01	5.42	4.30
FE2O3	1.69	2.06	0.57	0.60	0.20
FEO	3.41	4.08	4.98	5.79	4.90
MNO	0.11	0.11	0.12	0.12	0.12
MGO	29.23	26.09	23.83	24.33	27.91
CAO	7.16	10.58	10.70	10.33	7.89
NA2O	0.08	0.24	0.58	0.30	0.20
K2O	0.0	0.0	0.09	0.07	0.02
P2O5	0.0	0.0	0.14	0.10	0.09
LOI	1.34	4.78	1.85	3.20	1.09
TOTAL	98.97	99.42	99.97	99.35	99.60
ZR	6	8	6	7	7
SR	30	81	10	63	4
RB	1	1	3	2	0
ZN	33	37	25	29	27
CU	2	42	9	32	59
BA	30	49	5	42	0
GA	7	5	4	7	4
TH	4	1	1	3	3
NB	4	2	2	2	3
U	0	0	0	0	0
PB	0	0	0	1	2
NI	959	933	852	820	1190
CR	3255	2832	3188	2107	5787
V	153	140	107	201	137
Y	5	9	6	10	10
Q	0.0	0.0	0.0	0.0	0.0
OR	0.0	0.0	0.54	0.43	0.12
AB	0.69	2.14	4.98	2.63	1.70
AN	4.28	19.56	5.42	13.72	10.85
NE	0.0	0.0	0.0	0.0	0.0
LE	0.0	0.0	0.0	0.0	0.0
COR	0.0	0.0	0.0	0.0	0.0
WO	4.98	14.89	19.84	16.19	11.68
EN	4.11	12.11	15.53	12.47	9.28
FER	0.25	1.00	2.13	1.99	1.06
EN	31.39	10.02	40.12	26.75	46.88
FER	1.94	0.83	5.50	4.27	5.37
WO	0.0	0.0	0.0	0.0	0.0
FO	27.12	32.38	3.18	16.53	9.66
FA	1.85	2.95	0.48	2.91	1.22
LAR	0.0	0.0	0.0	0.0	0.0
MAG	2.50	3.14	0.84	0.90	0.29
IL	0.17	0.32	0.42	0.49	0.42
HEM	0.0	0.0	0.0	0.0	0.0
CHR	0.71	0.64	0.70	0.47	1.25
AP	0.0	0.0	0.33	0.24	0.21

77WH2 LOCATION 117 WEBSTERITE
77WH7 LOCATION 123 WEBSTERITE
7853 LOCATION 408 WEBSTERITE
7854 LOCATION 413 WEBSTERITE
78155 LOCATION 560 WEBSTERITE

WEHRLITE

SAMPLE	78142
SIO2	38.29
TIO2	0.19
AL2O3	3.43
FE2O3	5.74
FEO	5.22
MNO	0.14
MGO	35.49
CAO	4.23
NA2O	0.05
K2O	0.0
P2O5	0.0
LOI	6.78
TOTAL	99.56
ZR	8
SR	3
RB	0
ZN	61
CU	138
BA	1
GA	6
TH	3
NB	2
U	0
PB	1
NI	1729
CR	3304
V	119
Y	10
Q	0.0
OR	0.0
AB	0.45
AN	9.79
NE	0.0
LE	0.0
COR	0.0
WO	5.30
EN	4.41
FER	0.22
EN	9.59
FER	0.47
WO	0.0
FO	56.59
FA	3.08
LAR	0.0
MAG	8.92
IL	0.39
HEM	0.0
CHR	0.76
AP	0.0

78142 LOCATION 535 WEHRLITE

CLINOPYROXENITE

SAMPLE	77WH70	77WH74	77WH79	78118	78128	78143	78144
SIO2	47.84	50.30	48.39	42.00	48.22	43.56	47.20
TIO2	0.41	0.41	0.32	0.40	0.54	0.42	0.43
AL203	5.35	5.78	5.39	5.65	5.64	5.00	4.85
FE203	1.74	0.86	1.88	1.31	2.31	1.24	1.43
FEO	4.44	4.28	4.07	7.05	5.64	5.82	5.27
MNO	0.12	0.12	0.11	0.13	0.14	0.12	0.13
MGO	22.12	19.59	22.14	26.83	22.42	23.40	22.93
CAO	15.58	16.24	15.46	12.85	13.62	15.49	14.70
NA20	0.38	0.51	0.40	0.38	0.59	0.46	0.45
K20	0.0	0.07	0.0	0.04	0.04	0.07	0.03
P205	0.01	0.16	0.0	0.11	0.14	0.18	0.16
LOI	0.52	1.11	1.43	1.25	0.95	3.27	2.96
TOTAL	98.51	99.43	99.59	98.00	100.25	99.03	100.54
ZR	13	11	30	14	19	14	15
SR	19	18	37	13	15	19	16
RB	0	0	23	1	0	1	1
ZN	24	19	22	44	36	30	0
CU	199	282	264	217	228	226	0
BA	0	11	7	0	0	2	13
GA	7	6	5	7	6	7	0
TH	1	0	64	3	1	0	2
NB	2	2	32	2	1	0	1
U	0	0	0	0	0	0	0
PB	1	0	54	0	0	1	1
NI	882	926	1006	1218	927	955	0
CR	2345	4347	3365	3598	2201	2641	3721
V	226	206	204	207	229	217	213
Y	16	15	46	15	16	16	15
Q	0.0	0.0	0.0	0.0	0.0	0.0	0.0
OR	0.0	0.42	0.0	0.0	0.24	0.0	0.18
AB	3.27	4.36	3.43	0.0	5.01	0.0	3.88
AN	13.11	13.42	13.09	14.31	12.67	12.07	11.34
NE	0.0	0.0	0.0	1.83	0.0	2.24	0.0
LE	0.0	0.0	0.0	0.20	0.0	0.34	0.0
COR	0.0	0.0	0.0	0.0	0.0	0.0	0.0
WO	27.32	27.96	27.00	15.17	22.65	22.94	25.86
EN	21.82	22.05	21.78	11.66	17.75	17.77	20.31
FER	2.36	2.78	2.04	1.92	2.40	2.70	2.69
EN	4.32	11.91	6.79	0.0	9.89	0.0	3.60
FER	0.47	1.50	0.64	0.0	1.33	0.0	0.48
WO	0.0	0.0	0.0	0.0	0.0	0.0	0.0
FO	20.94	10.74	19.15	41.13	19.90	30.89	24.02
FA	2.50	1.49	1.98	7.46	2.96	5.18	3.50
LAR	0.0	0.0	0.0	2.43	0.0	2.06	0.0
MAG	2.57	1.26	2.76	2.00	3.36	1.91	2.11
IL	0.79	0.79	0.62	0.80	1.03	0.85	0.83
HEM	0.0	0.0	0.0	0.0	0.0	0.0	0.0
CHR	0.51	0.95	0.73	0.82	0.48	0.60	0.82
AP	0.02	0.38	0.0	0.27	0.33	0.44	0.38

77WH70 LOCATION 208 CLINOPYROXENITES
77WH74 LOCATION 212 CLINOPYROXENITES
77WH79 LOCATION 214 CLINOPYROXENITES
78118 LOCATION 516 CLINOPYROXENITES
78128 LOCATION 519 CLINOPYROXENITES pod MATERIAL
78143 LOCATION 537 CLINOPYROXENITES ZONED CLINOPYROXENITES
78144 LOCATION 547 CLINOPYROXENITES MAJORS BY A.A. VEIN CUTTING DUNITE

CLINOPYROXENITE

SAMPLE	78159
SIO2	43.26
TIO2	0.37
AL203	6.55
FE203	2.80
FEO	5.50
MNO	0.13
MGO	23.89
CAO	12.06
NA20	0.52
K20	0.0
P205	0.0
LOI	1.63
TOTAL	96.71
ZR	12
SR	13
RB	0
ZN	51
CU	231
BA	7
GA	8
TH	1
NB	1
U	0
PB	0
NI	1161
CR	4678
V	224
Y	16
Q	0.0
OR	0.0
AB	4.18
AN	16.23
NE	0.22
LE	0.0
COR	0.0
WO	19.31
EN	15.35
FER^	1.76
EN	0.0
FER	0.0
WO	0.0
FO	32.78
FA	4.14
LAR	0.0
MAG	4.24
IL	0.73
HEM	0.0
CHR	1.05
AP	0.0

78159 LOCATION 567 CLINOPYROXENITE

GABBRO

SAMPLE	77WH62	77WH86	77WH89	77WH90	78111	78129	78130
SIO2	45.70	49.20	43.40	46.80	38.20	46.94	47.67
TIO2	0.51	0.30	0.24	0.30	0.33	0.29	0.29
AL203	13.58	15.90	5.90	20.10	11.70	14.60	16.50
FE203	2.15	0.79	11.24	0.88	2.93	0.93	0.88
FEO	6.31	3.64	0.0	2.63	4.15	4.98	3.60
MNO	0.12	0.09	0.17	0.06	0.12	0.09	0.06
MGO	17.00	12.96	29.00	9.08	19.54	15.82	12.97
CAO	10.53	12.76	7.53	12.00	15.88	11.75	13.03
NA2O	2.03	2.29	0.66	3.60	0.07	1.85	2.30
K2O	0.04	0.30	0.03	0.32	0.0	0.04	0.08
P2O5	0.0	0.02	0.0	0.0	0.0	0.0	0.0
LOI	1.15	2.00	1.46	3.19	7.06	1.18	1.64
TOTAL	99.12	100.25	99.63	98.96	99.98	98.47	99.02
ZR	22	17	12	20	17	14	14
SR	165	269	87	367	42	193	233
RB	0	3	0	1	0	0	1
ZN	40	21	56	29	34	31	19
CU	112	84	90	96	105	113	80
BA	23	8	2	66	1	6	17
GA	12	10	6	11	6	10	10
TH	0	0	0	0	2	0	1
NB	1	1	2	0	1	3	1
U	0	0	0	0	0	0	0
PB	0	0	0	0	1	0	1
NI	589	410	1119	604	685	642	541
CR	962	755	1263	1409	953	992	775
V	149	120	118	146	132	126	128
Y	16	9	16	12	14	11	9
Q	0.0	0.0	0.0	0.0	0.0	0.0	0.0
OR	0.24	1.80	0.18	1.97	0.0	0.24	0.48
AB	15.42	19.30	5.68	17.33	0.0	16.06	16.38
AN	28.36	32.75	13.27	39.31	35.76	32.24	35.34
NE	1.13	0.21	0.0	7.80	0.36	0.0	1.94
LE	0.0	0.0	0.0	0.0	0.0	0.0	0.0
COR	0.0	0.0	0.0	0.0	0.0	0.0	0.0
WO	10.41	13.17	10.11	9.53	8.03	11.54	12.95
EN	7.73	10.06	8.74	7.36	6.46	8.65	9.93
FER	1.66	1.75	0.0	1.15	0.63	1.74	1.66
EN	0.0	0.0	14.86	0.0	0.0	0.40	0.0
FER	0.0	0.0	0.0	0.0	0.0	0.08	0.0
WO	0.0	0.0	0.0	0.0	0.0	0.0	0.0
FO	24.81	15.94	34.91	11.35	34.05	21.99	16.26
FA	5.86	3.05	0.0	1.96	3.67	4.88	3.01
LAR	0.0	0.0	0.0	0.0	5.28	0.0	0.0
MAG	3.18	1.16	0.0	4.33	4.81	1.38	1.31
IL	0.99	0.58	0.18	0.59	0.71	0.57	0.56
HEM	0.0	0.0	11.43	0.0	0.0	0.0	0.0
CHR	0.21	0.17	0.28	0.32	0.23	0.22	0.17
AP	0.0	0.05	0.0	0.0	0.0	0.0	0.0

77WH62 LOCATION 193 GABBRO VEIN
77WH86 LOCATION 237 GABBRO VEIN
77WH89 LOCATION 243 FINE GRAINED GABBRO VEIN
77WH90 LOCATION 243 GABBRO VEIN COARSE GRAINED
78111 LOCATION 514 GABBRO VEIN CUTTING FOLIATION
78129 LOCATION 519 GABBRO VEIN FROM WIDE LAYER APP. 18 CM ADJ TO CPX pod
78130 LOCATION 519 GABBRO VEIN FROM 3 CM WIDE VEIN

GABBRO

SAMPLE	78131	78132	78134	78135	78136	78150	78156
SIO2	46.00	47.10	47.24	47.28	46.84	46.40	43.40
TIO2	0.22	0.42	0.29	0.43	0.31	0.36	0.23
AL203	18.10	14.80	17.28	10.21	13.92	12.98	17.30
FE203	0.70	0.99	5.58	7.87	1.16	1.35	0.80
FEO	2.06	3.21	0.0	0.0	4.74	4.69	1.90
MNO	0.05	0.09	0.09	0.14	0.11	0.11	0.04
MGO	13.28	14.60	12.23	17.80	16.81	18.14	15.88
CAO	11.64	12.79	12.51	13.26	12.10	12.08	9.61
NA2O	2.74	2.03	2.37	1.17	1.67	1.47	2.19
K2O	0.12	0.13	0.06	0.11	0.04	0.03	0.07
P2O5	0.02	0.0	0.04	0.01	0.0	0.0	0.0
LOI	4.43	2.88	1.51	0.96	0.93	1.77	7.39
TOTAL	99.36	99.04	99.20	99.24	98.63	99.38	98.81
ZR	18	18	25	15	15	13	17
SR	430	269	287	122	158	192	380
RB	0	0	0	2	0	0	0
ZN	15	24	27	35	35	39	20
CU	80	85	79	145	127	128	101
BA	22	2	0	0	7	5	28
GA	12	12	11	9	11	12	8
TH	0	2	0	0	5	0	4
NB	0	1	2	2	1	1	0
U	0	0	0	0	0	0	0
PB	0	0	1	3	0	0	0
NI	718	604	390	594	638	853	1186
CR	584	908	552	1660	1097	1510	1260
V	95	149	117	200	145	162	61
Y	8	12	11	14	11	12	8
Q	0.0	0.0	0.0	0.0	0.0	0.0	0.0
OR	0.75	0.80	0.36	0.66	0.24	0.18	0.45
AB	16.07	15.54	20.51	10.05	14.44	12.71	16.72
AN	38.65	32.07	37.16	22.62	31.03	29.36	40.56
NE	4.51	1.24	0.0	0.0	0.0	0.0	1.90
LE	0.0	0.0	0.0	0.0	0.0	0.0	0.0
COR	0.0	0.0	0.0	0.0	0.0	0.0	0.0
WO	9.24	14.15	10.57	17.83	12.67	13.34	4.84
EN	7.49	11.19	9.14	15.41	9.67	10.32	4.00
FER	0.65	1.37	0.0	0.0	1.69	1.58	0.24
EN	0.0	0.0	0.76	10.96	0.14	0.33	0.0
FER	0.0	0.0	0.0	0.0	0.02	0.05	0.0
WO	0.0	0.0	0.0	0.0	0.0	0.0	0.0
FO	19.14	18.61	14.89	13.05	23.10	24.89	27.44
FA	1.82	2.50	0.0	0.0	4.44	4.20	1.81
LAR	0.0	0.0	0.0	0.0	0.0	0.0	0.0
MAG	1.07	1.49	0.0	0.0	1.72	2.00	1.27
IL	0.44	0.83	0.11	0.06	0.60	0.70	0.48
HEM	0.0	0.0	5.71	7.99	0.0	0.0	0.0
CHR	0.13	0.20	0.12	0.36	0.24	0.33	0.30
AP	0.05	0.0	0.10	0.02	0.0	0.0	0.0

78131 LOCATION 529 GABBRO VEIN ANORTHOSITIC CUTTING OTHER GABBRO VEINS
78132 LOCATION 529 GABBRO VEIN ZONED VEIN
78134 LOCATION 529 GABBRO VEIN FINED GRAINED FOLIATED GABBRO
78135 LOCATION 529 GABBRO VEIN
78136 LOCATION 529 GABBRO VEIN MED-C.G.
78150 LOCATION 551 GABBRO VEIN APP. PAR TO FOL.
78156 LOCATION 560 GABBRO VEIN CUTS FOL. ASSOC WITH 78155 WEB.

GABBRO

SAMPLE	78167
SIO2	47.40
TIO2	0.26
AL2O3	11.90
FE2O3	1.27
FEO	4.77
MNO	0.12
MGO	18.92
CAO	13.13
NA2O	1.07
K2O	0.03
P2O5	0.0
LOI	1.26
TOTAL	100.13
ZR	12
SR	135
RB	0
ZN	38
CU	131
BA	0
GA	13
TH	21
NB	0
U	0
PB	9
NI	716
CR	2125
V	205
Y	13
Q	0.0
OR	0.18
AB	9.13
AN	27.81
NE	0.0
LE	0.0
COR	0.0
WO	15.82
EN	12.25
FER	1.88
EN	3.69
FER	0.57
WO	0.0
FO	22.12
FA	3.74
LAR	0.0
MAG	1.86
IL	0.50
HEM	0.0
CHR	0.46
AP	0.0

78167 LOCATION 578 GABBRO VEIN

STRAT SECT 98

SAMPLE	77WH98-0	77WH98-2	77WH98-10	77WH98-20	77WH98-30	77WH98-40	77WH98-50
SIO2	35.71	39.91	43.72	43.17	44.47	44.52	44.47
TIO2	0.88	0.14	0.18	0.14	0.13	0.12	0.12
AL203	12.03	1.08	3.73	2.45	2.61	2.17	2.53
FE203	6.45	4.52	2.60	1.22	0.66	2.33	1.27
FEO	10.62	3.08	6.28	7.25	7.37	5.73	6.84
MNO	0.11	0.11	0.12	0.13	0.12	0.12	0.12
MGO	12.62	41.10	38.06	40.91	41.66	39.62	41.43
CAO	8.14	0.87	3.49	2.62	2.42	1.86	2.05
NA20	2.01	0.03	0.34	0.09	0.04	0.05	0.03
K20	1.32	0.03	0.0	0.04	0.02	0.03	0.03
P205	0.09	0.06	0.0	0.05	0.06	0.07	0.06
LOI	3.02	9.83	0.36	2.96	1.01	4.09	2.14
TOTAL	98.00	100.76	98.88	101.03	100.47	100.71	100.79
ZR	75	7	12	5	5	4	5
SR	264	9	16	10	1	4	1
RB	14	0	0	0	0	0	0
ZN	84	38	49	54	47	44	46
CU	128	6	30	21	22	14	20
BA	68	4	11	0	2	0	0
GA	24	0	6	3	4	3	3
TH	0	3	0	5	1	1	3
NB	35	3	1	3	1	2	2
U	0	0	0	0	0	0	0
PB	0	0	0	3	0	0	0
NI	84	2233	1984	2134	2220	2222	2283
CR	11	2551	2581	2918	2816	2890	2901
V	605	31	87	72	64	53	54
Y	7	5	6	7	5	5	3
Q	0.0	0.0	0.0	0.0	0.0	0.0	0.0
OR	5.26	0.19	0.0	0.24	0.12	0.18	0.18
AB	0.0	0.28	2.91	0.77	0.34	0.44	0.26
AN	22.12	2.98	8.75	6.26	6.89	5.78	6.74
NE	10.24	0.0	0.0	0.0	0.0	0.0	0.0
LE	2.67	0.0	0.0	0.0	0.0	0.0	0.0
COR	0.0	0.0	0.0	0.0	0.0	0.0	0.0
WO	9.28	0.55	3.66	2.76	1.98	1.36	1.31
EN	6.11	0.47	2.95	2.19	1.57	1.11	1.05
FER	2.51	0.01	0.28	0.26	0.19	0.09	0.11
EN	0.0	25.62	15.14	14.07	17.78	29.99	21.90
FER	0.0	0.38	1.43	1.65	2.17	2.51	2.25
WO	0.0	0.0	0.0	0.0	0.0	0.0	0.0
FO	20.19	60.06	54.47	61.09	59.07	49.46	56.90
FA	9.15	0.99	5.56	7.89	7.95	4.56	6.45
LAR	0.0	0.0	0.0	0.0	0.0	0.0	0.0
MAG	10.39	7.18	3.81	1.80	0.96	3.48	1.86
IL	1.86	0.29	0.35	0.27	0.25	0.23	0.23
HEM	0.0	0.0	0.0	0.0	0.0	0.0	0.0
CHR	0.0	0.60	0.56	0.64	0.61	0.64	0.63
AP	0.23	0.15	0.0	0.12	0.14	0.18	0.14

77WH98-0 LOCATION 282 STRAT SECT 98
77WH98-2 LOCATION 282 STRAT SECT 98
77WH98-10 LOCATION 282 STRAT SECT 98 PLAGICCLASE BEARING
77WH98-20 LOCATION 282 STRAT SECT 98
77WH98-30 LOCATION 282 STRAT SECT 98
77WH98-40 LOCATION 282 STRAT SECT 98
77WH98-50 LOCATION 282 STRAT SECT 98

STRAT SECT 98

SAMPLE	77WH98-60	77WH98-70	77WH98-80	77WH98-90	77WH98-200
SIO2	43.78	40.24	42.66	38.21	35.27
TIO2	0.11	0.11	0.11	0.10	0.10
AL2O3	2.11	2.08	2.31	0.77	0.46
FE2O3	1.36	3.09	2.86	3.46	6.74
FEO	6.42	5.45	4.98	6.15	6.54
MNO	0.11	0.12	0.12	0.12	0.14
MGO	40.34	39.43	39.20	43.56	40.21
CAO	1.90	1.65	1.75	0.21	0.13
NA2O	0.03	0.03	0.02	0.01	0.01
K2O	0.02	0.03	0.03	0.02	0.02
P2O5	0.07	0.06	0.05	0.05	0.05
LOI	2.97	5.92	6.73	6.96	9.23
TOTAL	99.22	98.21	100.82	99.62	98.90
ZR	4	5	4	5	5
SR	2	2	2	0	1
RB	0	0	0	0	0
ZN	42	44	40	48	106
CU	17	20	17	28	5
BA	0	0	1	0	0
GA	3	3	2	1	1
TH	4	4	2	3	3
NB	2	3	3	2	2
U	0	0	0	0	0
PB	0	0	0	2	1
NI	2264	2215	2123	2426	2557
CR	2847	2872	2855	2260	2407
V	53	57	60	15	11
Y	5	5	4	4	2
Q	0.0	0.0	0.0	0.0	0.0
OR	0.12	0.19	0.19	0.13	0.13
AB	0.26	0.27	0.18	0.09	0.09
AN	5.76	5.88	6.48	0.77	0.36
NE	0.0	0.0	0.0	0.0	0.0
LE	0.0	0.0	0.0	0.0	0.0
COR	0.0	0.0	0.0	0.50	0.34
WO	1.47	1.06	0.99	0.0	0.0
EN	1.17	0.87	0.81	0.0	0.0
FER	0.12	0.06	0.05	0.0	0.0
EN	24.40	19.91	28.20	11.68	12.81
FER	2.51	1.45	1.87	0.88	0.80
WO	0.0	0.0	0.0	0.0	0.0
FO	54.90	59.66	52.05	73.56	68.97
FA	6.22	4.78	3.80	6.13	4.73
LAR	0.0	0.0	0.0	0.0	0.0
MAG	2.04	4.83	4.39	5.39	10.86
IL	0.22	0.23	0.22	0.20	0.21
HEM	0.0	0.0	0.0	0.0	0.0
CHR	0.63	0.67	0.65	0.52	0.58
AP	0.17	0.15	0.12	0.12	0.13

77WH98-60 LOCATION 282 STRAT SECT 98
77WH98-70 LOCATION 282 STRAT SECT 98
77WH98-80 LOCATION 282 STRAT SECT 98
77WH98-90 LOCATION 282 STRAT SECT 98 NA2O<.01
77WH98-200 LOCATION 282 STRAT SECT 98 NA2O<.01

STRAT SECT 100

SAMPLE	77WH100-0	77WH100-10	77WH100-20	77WH100-30	77WH100-40	77WH100-50	77WH100-60
SIO2	43.04	43.99	43.71	41.85	43.35	42.55	43.03
TIO2	0.19	0.23	0.20	0.21	0.21	0.17	0.19
AL203	2.35	3.73	3.36	3.17	3.58	2.73	3.58
FE203	8.95	1.21	0.31	2.02	5.22	1.88	1.61
FEO	1.80	7.00	7.32	6.29	3.30	6.04	6.61
MNO	0.12	0.12	0.11	0.12	0.12	0.11	0.12
MGO	39.29	38.36	37.44	38.33	38.21	39.18	37.09
CAO	2.52	3.23	3.36	2.89	3.13	2.41	3.17
NA2O	0.10	0.20	1.63	0.13	0.17	0.12	0.17
K2O	0.03	0.04	0.02	0.02	0.03	0.04	0.04
P2O5	0.07	0.09	0.07	0.06	0.07	0.06	0.06
LOI	1.76	2.00	3.22	4.03	2.83	3.64	3.09
TOTAL	100.22	100.20	100.75	99.12	100.22	98.93	98.76
ZR	7	11	9	10	10	7	7
SR	7	14	10	9	10	9	7
RB	0	0	0	1	0	0	0
ZN	63	48	49	50	49	47	49
CU	48	31	29	29	31	27	32
BA	0	0	0	0	0	0	0
GA	6	4	5	4	6	4	5
TH	0	0	2	2	2	0	2
NB	1	1	0	1	1	1	1
U	0	0	0	0	0	0	0
PB	2	2	1	1	1	0	2
NI	2197	1936	1989	2013	1902	2091	1966
CR	1768	2556	2734	2548	2637	2666	2563
V	66	70	69	65	73	55	76
Y	4	7	5	5	5	5	6
Q	0.0	0.0	0.0	0.0	0.0	0.0	0.0
OR	0.18	0.24	0.12	0.12	0.18	0.25	0.25
AB	0.86	1.72	9.43	1.15	1.47	1.06	1.50
AN	5.95	9.29	1.83	8.39	9.12	7.10	9.25
NE	0.0	0.0	2.52	0.0	0.0	0.0	0.0
LE	0.0	0.0	0.0	0.0	0.0	0.0	0.0
COR	0.0	0.0	0.0	0.0	0.0	0.0	0.0
WO	2.61	2.66	6.15	2.60	2.63	2.09	2.81
EN	2.26	2.11	4.82	2.09	2.25	1.68	2.23
FER	0.0	0.25	0.66	0.21	0.03	0.16	0.25
EN	28.87	17.11	0.0	16.02	25.82	19.38	19.08
FER	0.0	2.04	0.0	1.58	0.35	1.81	2.15
WO	0.0	0.0	0.0	0.0	0.0	0.0	0.0
FC	47.64	54.44	63.34	57.37	48.53	56.70	52.45
FA	0.0	7.14	9.52	6.25	0.72	5.84	6.50
LAR	0.0	0.0	0.0	0.0	0.0	0.0	0.0
MAG	5.32	1.78	0.46	3.07	7.74	2.85	2.43
IL	0.37	0.44	0.39	0.42	0.41	0.34	0.38
HEM	5.40	0.0	0.0	0.0	0.0	0.0	0.0
CHR	0.39	0.56	0.60	0.57	0.58	0.60	0.57
AP	0.16	0.21	0.17	0.15	0.17	0.15	0.15

77WH100-0 LOCATION 283
77WH100-10 LOCATION 283
77WH100-20 LOCATION 283
77WH100-30 LOCATION 283
77WH100-40 LOCATION 283
77WH100-50 LOCATION 283 GABBRO
77WH100-60 LOCATION 283

STRAT SECT 100

SAMPLE	77WH100-70	77WH100-80	77WH100-100	77WH100-150	77WH100-180D	77WH100-180H
SIO2	44.12	43.83	43.85	43.19	34.59	43.36
TIO2	0.15	0.18	0.14	0.12	0.11	0.14
AL2O3	2.74	3.16	2.76	2.26	2.30	2.13
FE2O3	1.59	2.44	0.91	1.70	4.23	1.89
FEO	6.33	6.43	6.71	6.43	5.62	5.98
MNO	0.12	0.13	0.13	0.13	0.13	0.13
MGO	39.56	37.08	39.96	40.44	43.60	38.69
CAO	2.35	2.82	2.23	2.30	0.19	2.84
NA2O	0.10	0.79	0.04	0.03	0.01	0.03
K2O	0.02	0.04	0.02	0.02	0.02	0.02
P2O5	0.07	0.08	0.04	0.05	0.05	0.09
LOI	2.27	3.35	1.79	1.91	7.55	3.66
TOTAL	99.42	100.33	98.56	98.58	98.40	98.96
ZR	6	6	5	4	4	5
SR	3	4	1	2	0	2
RB	0	0	0	0	0	0
ZN	46	47	45	46	61	45
CU	23	31	23	34	459	53
BA	0	0	0	0	0	0
GA	4	5	3	3	4	3
TH	0	1	2	0	0	3
NB	0	0	0	1	0	1
U	0	0	0	0	0	0
PB	0	1	0	3	1	0
NI	2161	1994	2224	2151	2741	2037
CR	2795	2661	2703	2797	6575	2910
V	52	70	51	57	22	58
Y	3	5	5	4	3	5
Q	0.0	0.0	0.0	0.0	0.0	0.0
OR	0.12	0.24	0.12	0.12	0.13	0.12
AB	0.87	6.87	0.35	0.26	0.09	0.27
AN	7.14	5.09	7.50	6.15	0.67	5.87
NE	0.0	0.0	0.0	0.0	0.0	0.0
LE	0.0	0.0	0.0	0.0	0.0	0.0
COR	0.0	0.0	0.0	0.0	0.0	0.0
WO	1.81	3.65	1.51	2.20	0.0	3.44
EN	1.46	2.93	1.20	1.77	0.0	2.78
FER	0.15	0.30	0.14	0.18	0.0	0.26
EN	23.35	14.05	21.90	20.05	1.12	23.56
FER	2.35	1.43	2.47	2.01	0.06	2.22
WO	0.0	0.0	0.0	0.0	0.0	0.0
FO	53.38	54.56	55.56	57.41	82.09	52.08
FA	5.93	6.12	6.91	6.34	5.04	5.40
LAR	0.0	0.0	0.0	0.0	0.0	0.0
MAG	2.36	3.63	3.36	2.54	0.23	2.86
IL	0.29	0.35	0.27	0.23	0.0	0.28
HEM	0.0	0.0	0.0	0.0	1.54	0.0
CHR	0.62	0.59	0.60	0.62	0.0	0.65
AP	0.17	0.19	0.10	0.12	0.13	0.22

77WH100-70 LOCATION 283
77WH100-80 LOCATION 283
77WH100-100 LOCATION 283
77WH100-150 LOCATION 283
77WH100-180D LOCATION 283
77WH100-180H LOCATION 283

METAMORPHICS

SAMPLE	77WH10	77WH31	77WH31A	7836	7837	7844	7845
SIO2	47.49	46.56	45.69	47.19	47.73	47.03	49.28
TIO2	1.52	0.30	2.20	0.39	1.38	1.54	1.19
AL203	13.55	17.11	13.19	16.73	13.81	15.43	14.09
FE203	1.96	0.61	2.78	0.54	1.62	2.18	4.93
FEO	9.79	5.04	12.28	5.38	9.51	9.76	4.91
MNO	0.12	0.11	0.14	0.12	0.54	0.16	0.14
MGO	7.99	10.47	7.74	9.97	7.68	7.90	6.19
CAO	9.53	13.87	9.17	13.20	8.64	10.73	11.75
NA20	3.47	1.86	4.56	2.07	3.66	3.24	3.75
K20	0.37	1.06	0.12	0.49	0.93	0.33	0.38
P205	0.23	0.14	0.29	0.14	0.21	0.23	0.16
LOI	3.14	4.03	3.80	4.06	3.82	3.01	2.71
TOTAL	99.16	101.16	101.96	100.28	99.53	101.54	99.48
ZR	90	7	106	11	52	82	71
SR	318	141	109	224	339	380	299
RB	7	31	1	12	23	13	6
ZN	80	28	120	38	155	110	77
CU	40	111	151	46	64	79	35
BA	355	132	6	383	154	206	0
GA	18	13	17	14	21	16	17
TH	0	0	0	0	1	2	0
NB	5	0	11	0	6	10	1
U	0	0	0	0	0	0	0
PB	0	1	2	1	2	2	3
NI	70	185	60	138	75	83	88
CR	116	751	48	569	168	134	295
V	354	153	475	166	380	385	260
Y	39	9	52	11	34	40	30
Q	0.0	0.0	0.0	0.0	0.0	0.0	0.0
OR	2.28	6.44	0.72	3.01	5.74	1.98	2.32
AB	29.77	7.55	24.44	16.07	28.44	23.80	32.49
AN	21.13	36.20	15.45	36.24	19.32	26.97	21.16
NE	0.43	4.68	8.05	1.14	2.11	2.17	0.15
LE	0.0	0.0	0.0	0.0	0.0	0.0	0.0
COR	0.0	0.0	0.0	0.0	0.0	0.0	0.0
WO	11.15	14.07	12.11	12.92	10.09	10.72	15.89
EN	6.27	9.77	6.28	8.77	5.48	6.03	11.86
FER	4.43	3.14	5.50	3.16	4.25	4.25	2.46
EN	0.0	0.0	0.0	0.0	0.0	0.0	0.0
FER	0.0	0.0	0.0	0.0	0.0	0.0	0.0
WO	0.0	0.0	0.0	0.0	0.0	0.0	0.0
FO	10.12	11.94	9.35	11.92	10.15	9.76	2.84
FA	7.88	4.22	9.02	4.73	8.67	7.57	0.65
LAR	0.0	0.0	0.0	0.0	0.0	0.0	0.0
MAG	2.96	0.91	4.11	0.81	2.45	3.21	7.38
IL	3.00	0.59	4.26	0.77	2.74	2.97	2.33
HEM	0.0	0.0	0.0	0.0	0.0	0.0	0.0
CHR	0.03	0.17	0.01	0.13	0.04	0.03	0.07
AP	0.56	0.33	0.69	0.34	0.51	0.54	0.38

77WH10 LOCATION 125 META GREEN RIDGE
77WH31 LOCATION 144 META GREEN RIDGE
77WH31A LOCATION 144A META GREEN RIDGE
7836 LOCATION 363 META GREEN RIDGE
7837 LOCATION 366 META GREEN RIDGE
7844 LOCATION 387 META GREEN RIDGE
7845 LOCATION 391 META GREEN RIDGE

SAMPLE	7911
SIO2	48.88
TIO2	0.55
AL203	14.71
FE203	1.54
FEO	5.40
MNO	0.39
MGO	9.90
CAC	10.56
NA20	2.68
K20	0.44
P205	0.14
LOI	3.55
TOTAL	98.74
ZR	27
SR	250
RB	8
ZN	50
CU	82
BA	220
GA	13
TH	0
NB	1
U	0
PB	1
NI	116
CR	396
V	267
Y	16
Q	0.0
OR	2.73
AB	23.80
AN	28.14
NE	0.0
LE	0.0
COR	0.0
WO	10.87
EN	7.46
FER	2.54
EN	7.52
FER	2.56
WO	0.0
FO	7.64
FA	2.87
LAR	0.0
MAG	2.34
IL	1.10
HEM	0.0
CHR	0.09
AP	0.34

7911 LOCATION 623 META GREEN RIDGE

BASAL ZONE RX

SAMPLE	77WH51	77WH52	77WH53	77WH54	77WH82	77WH91	7813
SIO2	52.91	42.52	40.05	31.40	45.30	33.60	40.69
TIO2	1.25	2.36	0.16	5.20	1.86	5.00	0.87
AL2O3	23.48	7.51	3.46	8.30	7.52	7.68	5.73
FE2O3	2.25	2.01	3.46	8.97	3.36	3.70	1.80
FEO	4.01	14.18	4.76	13.81	6.29	14.65	8.05
MNO	0.13	0.17	0.11	0.35	0.21	0.29	0.12
MGO	1.27	5.68	38.92	7.63	10.47	7.19	29.49
CAO	4.05	18.55	1.98	16.25	21.05	17.90	5.92
NA2O	6.65	1.89	0.0	1.22	1.23	1.32	0.70
K2O	2.23	0.04	0.04	0.53	0.06	0.33	0.10
P2O5	0.44	0.89	0.07	3.60	0.0	3.25	0.12
LOI	2.08	3.05	8.47	1.66	1.49	3.71	6.08
TOTAL	100.75	98.85	101.48	98.95	98.84	98.62	99.67
ZR	140	198	13	213	164	193	31
SR	1987	1879	38	1331	793	534	70
RB	29	0	0	4	0	6	3
ZN	75	139	45	192	68	156	71
CU	18	65	14	62	6	46	49
BA	1490	0	0	323	64	69	3
GA	16	17	3	20	12	17	10
TH	0	0	0	0	0	0	3
NB	62	0	5	58	2	29	7
U	0	0	0	0	0	0	0
PB	0	0	0	0	0	0	1
NI	13	39	2148	53	136	26	1358
CR	12	9	2629	43	151	12	1717
V	23	122	45	220	177	237	183
Y	22	36	4	38	32	27	10
Q	0.0	0.0	0.0	0.0	0.0	0.0	0.0
OR	13.33	0.25	0.25	0.0	0.0	0.0	0.63
AB	48.22	0.71	0.0	0.0	0.0	0.0	6.31
AN	18.38	12.39	9.98	16.18	15.43	15.06	13.00
NE	4.71	8.64	0.0	5.77	5.87	6.48	0.0
LE	0.0	0.0	0.0	2.53	0.29	1.64	0.0
COR	3.50	0.0	0.0	0.0	0.0	0.0	0.0
WO	0.0	32.63	0.03	16.75	35.17	19.22	7.30
EN	0.0	13.32	0.02	10.35	25.84	9.86	5.62
FER	0.0	19.56	0.0	5.42	5.99	8.87	0.91
EN	0.0	0.0	19.21	0.0	0.0	0.0	3.08
FER	0.0	0.0	1.09	0.0	0.0	0.0	0.50
WO	0.0	0.0	0.0	0.0	0.0	0.0	0.0
FO	2.24	1.00	59.25	6.48	0.91	6.53	48.74
FA	2.85	1.61	3.70	3.74	0.23	6.47	8.68
LAR	0.0	0.0	0.0	0.52	1.44	1.81	0.0
MAG	3.30	3.04	5.37	13.41	5.07	5.75	2.78
IL	2.40	4.67	0.33	10.18	3.68	10.17	1.76
HEM	0.0	0.0	0.0	0.0	0.0	0.0	0.0
CHR	0.0	0.0	0.61	0.01	0.0	0.0	0.39
AP	1.03	2.16	0.17	8.63	0.0	8.09	0.30

77WH51 LOCATION 188 SYENITIC MYLONITE @ CONTACT
77WH52 LOCATION 188 ALK. PYROXENITE @ CONTACT
77WH53 LOCATION 188 UM 10 M ABOVE CONTACT NA2O NOT DETERMINED
77WH54 LOCATION 188 JACUPIRANGITE 3 M BELOW CONT FROM JAT TABLE 3
77WH82 LOCATION 232 ALK. PXITE FROM JAT TABLE 3
77WH91 LOCATION 245 JACUPIRANGITE FROM JAT TABLE 3
7813 LOCATION 326 BANDED PXITE AT BASE

BASAL ZONE RX

SAMPLE	78161
SIO2	42.38
TIO2	0.22
AL203	3.77
FE203	0.58
FEO	7.69
MNO	0.11
MGO	38.40
CAO	3.37
NA2O	1.22
K2O	0.03
P2O5	0.06
LOI	1.22
TOTAL	99.05
ZR	11
SR	18
RB	0
ZN	51
CU	33
BA	0
GA	4
TH	0
NB	1
U	0
PB	3
NI	1970
CR	2521
V	80
Y	6
Q	0.0
OR	0.18
AB	5.52
AN	4.81
NE	2.70
LE	0.0
COR	0.0
WO	4.94
EN	3.86
FER	0.53
EN	0.0
FER	0.0
WO	0.0
FO	65.53
FA	9.94
LAR	0.0
MAG	0.86
IL	0.43
HEM	0.0
CHR	0.55
AP	0.14

78161 LOCATION 574 SPINEL LHERZOLITE @ CONT WITH UM PLAG EXSOL FROM OPX

PRECISION

SAMPLE	77WH40
SIO2	40.96
TIO2	0.10
AL203	1.79
FE203	2.28
FEO	5.37
MNO	0.11
MGO	40.72
CAO	1.51
NA20	0.02
K20	0.03
P205	0.05
LOI	7.56
TOTAL	100.50
ZR	4
SR	1
RB	0
ZN	42
CU	14
BA	0
GA	4
TH	1
NB	1
U	0
PB	0
NI	2226
CR	2768
V	60
Y	2
Q	0.0
OR	0.19
AB	0.18
AN	5.04
NE	0.0
LE	0.0
COR	0.0
WO	1.10
EN	0.90
FER	0.07
EN	19.71
FER	1.48
WO	0.0
FO	61.67
FA	5.10
LAR	0.0
MAG	3.54
IL	0.20
HEM	0.0
CHR	0.64
AP	0.12

77WH40 LOCATION 169 HARZBURGITE-SPINEL LHERZOLITE

APPENDIX IV

Mineral and additional bulk rock analyses from associated rock types of the St. Anthony Complex.

TABLE AIV.1. Olivine analyses from associated rock types of the St. Anthony Complex

	77WH98-10e	7922c	7813	77WH67b
SiO_2	39.34	38.89	39.32	39.33
TiO_2	0.01	n.d.	n.d.	0.03
Al_2O_3	n.d.	n.d.	n.d.	0.33
Cr_2O_3	n.d.	n.d.	0.01	n.d.
FeO*	10.81	8.86	14.75	12.59
MnO	0.13	0.12	0.18	0.13
MgO	48.73	50.90	45.78	47.52
NiO	0.45	0.40	0.35	0.36
TOTAL	99.4	99.17	100.39	100.
Si	0.978	0.963	0.985	0.977
Al	--	--	--	0.010
Ti	--	--	--	0.001
Cr	--	--	--	--
Fe	0.225	0.184	0.309	0.262
Mg	1.806	1.879	1.710	1.759
Mn	0.003	0.003	0.004	0.003
Ni	0.009	0.008	0.007	0.007
Fo(mole %)	88.9	91.0	84.6	87.0

77WH98-10e - recrystallized olivine; basal zone rock ~3m above basal thrust.
7922c - primary olivine; spinel lherzolite from Milan Arm Melange?
7813c - recrystallized olivine; ultramafic basal zone rock, White Hills Peridotite.
77WH67b - recrystallized olivine; peridotite sliver in hornblendite; within basal thrust zone; CaO = 0.01.

TABLE AIV.2. Orthopyroxene analyses from associated rock types of the St. Anthony Complex.

	77WH98-10c	77WH98-10d	7922b	77WH67a	7813b
SiO_2	53.40	54.36	55.77	54.89	54.93
TiO_2	0.18	0.17	0.04	0.05	0.09
Al_2O_3	4.29	4.80	3.82	2.80	4.54
Cr_2O_3	0.35	0.46	0.48	0.40	0.33
FeO*	7.05	6.84	5.64	8.44	8.72
MnO	0.14	0.16	0.11	0.14	0.11
MgO	32.80	33.43	33.82	32.59	31.71
CaO	0.72	0.62	0.60	0.50	0.43
Na_2O	0.05	0.04	0.02	--	0.03
K_2O	n.d.	n.d.	n.d.	--	n.d.
NiO	0.18	0.13	0.08	0.05	0.23
TOTAL	99.16	101.01	100.38	99.86	101.12
Si	1.874	1.869	1.914	1.919	1.897
Al^{IV}	0.126	0.131	0.086	0.081	0.103
Al^{VI}	0.052	0.064	0.068	0.035	0.082
Ti	0.005	0.004	0.001	0.001	0.002
Cr	0.010	0.012	0.013	0.011	0.009
Fe	0.207	0.197	0.162	0.247	0.252
Mg	1.716	1.713	1.730	1.698	1.632
Mn	0.004	0.005	0.003	0.004	0.003
Ni	0.005	0.004	0.002	0.001	0.006
Ca	0.027	0.023	0.022	0.019	0.016
Na	0.003	0.003	0.001	--	0.002
K	--	--	--	--	--

TABLE AIV.2. (Continued)

	77WH98-10c	77WH98-10d	7922b	77WH67a	7813b
Ca	1.38	1.18	1.15	0.95	0.83
Mg	87.84	88.45	90.25	86.31	85.81
Fe_T	10.78	10.37	8.60	12.74	13.36

* - Total iron as FeO.
n.d. - not detected.
-- - not determined.

77WH98-10c - primary orthopyroxene; basal zone rock ~3m above basal thrust fault.
77WH98-10d - primary orthopyroxene; basal zone rock ~3m above basal thrust fault.
7922b - primary orthopyroxene; spinel lherzolite from Milan Arm Melange.
77WH67a - recrystallized orthopyroxene; peridotite sliver in hornblendite.
7813b - primary orthopyroxene; ultramafic basal zone rock.

TABLE AIV.3.Clinopyroxene analyses from associated rock types of the St. Anthony Complex

	77WH98-10a	77WH98-10b	7813a	7922a	7922-1
SiO_2	51.10	52.02	52.66	53.03	52.45
TiO_2	0.72	0.71	0.23	0.10	0.11
Al_2O_3	5.98	6.24	5.53	4.62	5.91
Cr_2O_3	0.55	0.69	0.64	0.98	1.20
FeO*	2.59	2.88	3.79	2.30	2.34
MnO	0.08	0.07	0.07	0.06	0.08
MgO	15.52	15.12	15.78	15.93	15.78
CaO	21.22	21.66	20.00	22.07	21.72
Na_2O	1.28	1.34	1.18	1.01	1.07
K_2O	n.d.	n.d.	n.d.	n.d.	n.d.
NiO	0.04	0.04	0.12	0.05	0.08
TOTAL	99.08	100.77	100.00	100.15	100.74
Si	1.862	1.869	1.908	1.916	1.883
Al^{IV}	0.138	0.131	0.092	0.084	0.117
Al^{VI}	0.119	0.134	0.144	0.113	0.133
Ti	0.020	0.019	0.006	0.003	0.003
Cr	0.016	0.020	0.018	0.028	0.034
Fe^{3+}	0.053	0.032	--	0.008	0.018
Fe^{2+}	0.026	0.054	0.115	0.061	0.052
Mg	0.843	0.810	0.852	0.858	0.844
Mn	0.002	0.002	0.002	0.002	0.002
Ni	0.001	0.001	0.003	0.001	0.002
Ca	0.829	0.834	0.776	0.855	0.836
Na	0.090	0.093	0.083	0.071	0.074
K	--	--	--	--	--

TABLE AIV.3. (Continued)

	77WH98-10a	77WH98-10b	7813a	7922a	7922-1
Ca	47.24	48.11	44.39	47.87	47.61
Mg	48.12	46.78	48.92	48.13	48.24
Fe_T	4.64	5.11	6.69	4.00	4.15

* - Total iron as FeO.
n.d. - not detected.
-- - not determined.

77WH98-10a - recrystallized clinopyroxene; basal zone rock ~3 m above basal thrust fault.
77WH98-10b - recrystallized clinopyroxene; basal zone rock ~3 m above basal thrust fault.
7813a - recrystallized clinopyroxene; ultramafic basal zone rock.
7922a - primary clinopyroxene; spinel lherzolite from Milan Arm Melange.
7922-1 - primary clinopyroxene; spinel lherzolite from Milan Arm Melange.

TABLE AIV.4. Amphibole and biotite analyses from associated rock types of the St. Anthony Complex

	77WH67c	77WH67d	7812b	7844	7912c
SiO_2	42.34	42.24	43.05	43.27	37.05
TiO_2	4.24	3.65	1.21	2.07	3.19
Al_2O_3	14.38	15.16	10.98	11.05	15.70
FeO*	5.56	5.36	15.82	16.17	17.98
MnO	0.07	0.05	0.49	0.26	0.12
MgO	16.11	16.99	11.77	11.51	12.27
CaO	11.67	11.85	11.29	10.66	0.02
Na_2O	3.07	2.95	1.73	2.20	0.17
K_2O	0.83	0.83	0.85	0.09	8.91
TOTAL	98.27	99.08	97.19	97.28	95.41
Si	6.040	5.970	6.478	6.474	5.584
Al^{IV}	1.960	2.030	1.522	1.526	2.416
Al^{VI}	0.459	0.497	0.426	0.424	0.374
Ti	0.455	0.388	0.137	0.233	0.362
Fe	0.663	0.634	1.991	2.024	2.267
Mg	3.426	3.579	2.640	2.567	2.756
Mn	0.008	0.006	0.062	0.033	0.015
Ca	1.784	1.795	1.821	1.709	0.003
Mg	0.849	0.809	0.505	0.638	0.050
Fe_T	0.151	0.150	0.163	0.017	0.1714

* - Total iron as FeO.

77WH67c - amphibole porphyroblast; hornblendite, <1m below basal thrust fault.
77WH67d - recrystallized amphibole; hornblendite, <1m below basal thrust fault.
7912b - amphibole; Green Ridge Amphibolite, ~100m(?) below the basal thrust fault.
7844 - amphibole; Green Ridge Amphibolite, ~3m below basal thrust fault.
7912c - biotite; Green Ridge Amphibolite, ~100m(?) below basal thrust

TABLE AIV.5. Plagioclase analyses from associated rock types of the St. Anthony Complex

	78161c	78161d	78161e	78161f	77WH98-10f
SiO_2	55.85	55.57	56.73	55.17	57.94
TiO_2	n.d.	n.d.	n.d.	n.d.	n.d.
Al_2O_3	27.41	27.27	26.80	27.88	27.04
Cr_2O_3	n.d.	n.d.	n.d.	n.d.	n.d.
FeO*	0.16	0.11	0.19	n.d.	0.12
MnO	n.d.	n.d.	n.d.	n.d.	0.01
MgO	--	--	--	--	--
CaO	9.49	9.37	8.68	9.95	9.00
Na_2O	6.41	6.95	7.24	6.64	6.22
K_2O	n.d.	n.d.	n.d.	0.01	0.09
NiO	n.d.	n.d.	n.d.	n.d.	0.02
TOTAL	99.32	99.27	99.64	99.65	100.44
Si	10.114	10.090	10.237	9.998	10.326
Al^{IV}	5.853	5.838	5.702	5.951	5.682
Ti	--	--	--	--	--
Cr	--	--	--	--	--
Fe^{3+}	--	--	--	--	--
Fe^{2+}	0.024	0.017	0.029	--	0.018
Mg	--	--	--	--	--
Mn	--	--	--	--	0.002
Ni	--	--	--	--	0.003
Ca	1.842	1.823	1.678	1.930	1.719
Na	2.251	2.447	2.533	2.331	2.150
K	--	--	--	0.002	0.020
An	45.0	42.7	39.9	45.3	44.2

TABLE AIV.5. (Continued)

* - Total iron as FeO.
n.d. - not detected.
-- - not determined.

78161c	- secondary plagioclase exsolved from primary orthopyroxene; basal zone rock, White Hills Peridotite.
78161d	- secondary plagioclase in groundmass adjacent to primary orthopyroxene; basal zone rock, White Hills Peridotite.
78161e	- secondary plagioclase in groundmass adjacent to primary orthopyroxene; basal zone rock, White Hills Peridotite.
78161f	- secondary plagioclase in groundmass adjacent to primary orthopyroxene; basal zone rock, White Hills Peridotite.
77WH98-10f	- secondary plagioclase exsolved from primary orthopyroxene; basal zone rock, White Hills Peridotite.

TABLE AIV.5. (Continued)

	78161a	78161b	77WH10	7912a
SiO_2	55.50	55.55	69.57	59.42
TiO_2	n.d.	n.d.	n.d.	n.d.
Al_2O_3	27.91	28.02	20.63	24.65
Cr_2O_3	n.d.	n.d.	n.d.	n.d.
FeO*	0.17	0.10	0.04	0.24
MnO	n.d.	n.d.	n.d.	n.d.
MgO	--	--	--	--
CaO	9.62	8.83	0.05	5.93
Na_2O	6.82	6.51	11.99	8.63
K_2O	n.d.	0.01	0.02	0.23
NiO	n.d.	n.d.	n.d.	n.d.
TOTAL	100.02	99.07	102.30	99.10
Si	10.010	10.070	11.883	10.712
Al^{IV}	5.935	5.989	4.155	5.240
Ti	--	--	--	--
Cr	--	--	--	--
Fe^{3+}	--	--	--	--
Fe^{2+}	0.026	0.015	0.006	0.036
Mg	--	--	--	--
Mn	--	--	--	--
Ni	--	--	--	--
Ca	1.859	1.715	0.009	1.146
Na	2.385	2.289	3.971	3.017
K	--	--	--	--
An	43.8	42.8	0.2	27.2

TABLE AIV.5. (Continue-)

78161a - secondary plagioclase exsolved from primary orthopyroxene; basal zone rock, White Hills Peridotite.
78161b - twinned plagioclase exsolved from primary orthopyroxene; basal zone rock, White Hills Peridotite.
77WH10 - plagioclase; Green Ridge Amphibolite, 4 m below basal thrust fault.
7912a - plagioclase; Green Ridge Amphibolite, ~100 m(?) below basal thrust fault.

TABLE AIV.6. Spinel analyses from basal zone rocks of the White Hills Peridotite

	78161	77WH98-10	7813
TiO_2	0.11	n.d.	0.05
Al_2O_3	55.25	56.50	51.93
Cr_2O_3	11.18	11.17	12.43
Fe_2O_3	2.59	1.31	3.77
FeO	10.49	11.28	17.15
MnO	0.06	0.14	0.14
MgO	19.46	19.11	14.97
NiO	0.37	0.21	0.29
V_2O_3	0.10	--	--
TOTAL	99.61	99.72	100.73
Fe_2TiO_4	0.22	--	0.10
$FeCr_2O_4$	11.60	11.54	13.27
$MgCr_2O_4$	--	--	--
$MgAl_2O_4$	77.03	74.99	60.98
$FeAl_2O_4$	8.59	12.19	21.82
$MgFe_2O_4$	--	--	--
$FeFe_2O_4$	2.56	1.28	3.83

78161 - anhedral porphyroclast; basal zone rock.
77WH98-10 - anbedral porphyroclast; basal zone rock (~3m from basal thrust).
7813 - anhedral porphyroclast; basal zone rock.

TABLE AIV.7. Hydrous phase compositions from rocks associated with chromite from the White Hills Peridotite

	77WH19	78122Y	78122Yi	78123X	78122Y
SiO_2	48.23	56.58	58.14	48.04	39.46
TiO_2	0.36	0.13	0.11	0.61	n.d.
Al_2O_3	9.38	3.23	2.07	10.55	8.12
Cr_2O_3	2.08	--	--	1.97	--
FeO*	3.04	1.41	0.69	2,41	4.53
MnO	0.07	0.04	0.02	0.01	0.02
MgO	20.93	23.42	23.54	19.39	33.73
CaO	12.52	12.89	13.44	12.57	0.08
Na_2O	1.61	0.54	0.39	n.d.	n.d.
K_2O	n.d.	0.07	0.04	n.d.	0.02
NiO	0.09	--	--	0.31	--
TOTAL	98.31	98.32	98.44	95.86	85.96
Si	7.019	7.677	7.839	6.794	--
Al^{IV}	0.981	0.323	0.161	1.206	--
Al^{VI}	0.629	0.189	0.168	0.553	--
Ti	0.039	0.013	0.011	0.065	--
Cr	0.239	--	--	0.220	--
Fe	0.370	0.160	0.078	0.285	--
Mg	4.540	1.160	4.731	4.087	--
Mn	0.009	0.005	0.002	0.001	--
Ni	0.011	--	--	0.035	--
Ca	1.953	1.874	1.942	1.905	--
Na	--	0.142	0.102	--	--
K	--	0.012	0.007	--	--

TABLE AIV.7. (Continued)

* - Total iron as FeO.
n.d. - not detected.
-- - not determined.

77WH19	- alteration product of orthopyroxene(?); orthopyroxenite vein associated with a seam of chromite.
78122Y	- clinoamphibole from amphibole rim around bastite pseudomorph; massive chromite associated with bastite pseudomorph orthopyroxene.
78122Yi	- interstitial amphibole in massive chromite; massive chromite associated with bastite pseudomorph orthopyroxene.
78123X	- interstitial amphibole in massive chromite; "websterite" assemblage associated with chromite.
78122Y	- bastite pseudomorph; massive chromite associated with bastite pseudomorph orthopyroxene.

Table AIV.8. Bulk rock analyses of rock types associated with the St. Anthony Complex.

	789G	7810
SiO_2	42.64	48.41
TiO_2	2.17	2.23
Al_2O_3	14.62	15.42
Fe_2O_3	2.58	10.66
FeO	7.72	2.01
MnO	0.12	0.12
MgO	5.85	1.59
CaO	12.68	4.35
Na_2O	6.26	6.16
K_2O	0.43	2.45
P_2O_5	0.31	0.45
LOI	5.01	4.32
TOTAL	100.39	98.17
Zr(ppm)	124	172
Sr	951	181
Rb	7	50
Zn	99	76
Cu	104	33
Ba	137	364
Ga	21	21
Th	0	0
Nb	32	23
U	0	0
Pb	0	0

Table AIV.8. (Continued)

	789G	7810
Ni	106	65
Cr	133	26
V	252	171
Y	21	46

789G - gabbro, Maiden Point Formation, unit 3b; Howe Harbour area.

7810 - rhyolite(?), Maiden Point Formation, unit 3b; Howe Harbour area.

APPENDIX V

Publications relevant to this thesis.

STATE OF OREGON
DEPARTMENT OF GEOLOGY AND MINERAL INDUSTRIES
1069 State Office Building, Portland, Oregon 97201

BULLETIN 95

NORTH AMERICAN OPHIOLITES

Edited by
R. G. Coleman and W. P. Irwin
U. S. Geological Survey

The preparation of this report was sponsored by the International Geological Program (IGCP) as part of the North American meeting of the IGCP working group: "Ophiolites of continents and comparable oceanic rocks."



GOVERNING BOARD
Leeanne MacColl Portland
Robert W. Doty Talent
John L. Schwabe Portland

STATE GEOLOGIST
Ralph S. Mason
1977

NORTH AMERICAN OPHIOLITES

DISTRIBUTION AND TECTONIC SETTING OF OPHIOLITES AND OPHIOLITIC MELANGES IN THE APPALACHIAN OROGEN

Harold Williams and R.W. Talkington

Department of Geology
Memorial University of Newfoundland
St. John's, Newfoundland, Canada

ABSTRACT

Ophiolites of highly allochthonous character and associated ophiolitic melange occur along the western margin of the Appalachian Orogen, i.e. the ancient continental margin of eastern North America (Humber Zone). The Bay of Islands Complex is a typical example of a transported ophiolite, and ophiolitic melanges such as the Milan Arm, Second Pond and Coachman's Melanges are all interpreted as related to ophiolite obduction. The melanges vary in structural style from undeformed thin sheets in the west to polydeformed and metamorphosed in the east.

Small mafic-ultramafic bodies in eastern parts of the Humber Zone occur along the entire length of the orogen. Some of these are blocks in ophiolitic melange and others are sited at major structural contacts. They are affected by the full range of deformations and metamorphism related to the destruction of the ancient continental margin of eastern North America. Most are probably dismembered parts of ophiolite suites, and their occurrence from Newfoundland to Alabama implies a similar structural history for western parts of the system.

In central parts of the Appalachian Orogen, ophiolites that represent vestiges of an ancient Iapetus Ocean (Dunnage Zone) occur along the Baie Verte-Brompton Line and they form the basement to island arc sequences farther east. Mafic-ultramafic complexes along eastern parts of the Dunnage Zone in the north may be blocks in melange, and some may represent diapiric intrusions.

Relationships in the northern Appalachians imply a major suture within the exposed parts of the southern Appalachians, either at the Brevard Zone or somewhere between the Brevard Zone and the Carolina Slate Belt.

Appalachian ophiolites are Late Cambrian and Early Ordovician in age, where dated, and they were emplaced and deformed during the Ordovician Taconic Orogeny. Silurian or younger ophiolites are unknown and the stratigraphic record for this period indicates largely terrestrial conditions without the presence of important continental margins or major oceans.

INTRODUCTION

The interpretation of the on-land ophiolite suits of rock units as oceanic crust and mantle has brought new and considerable interest to the study of ophiolitic rocks in orogenic belts. Because the ophiolite suite of rock units relate in a total way to their place and mode of generation, their presence provides an important adjunct to the interpretation of the regional geology of the orogen in which they are found. In ancient orogenic belts, ophiolite suites occur as highly allochthonous structural slices transported across former continental margins, e.g. western Newfoundland, Oman, Zagros, Himalayas, or as imbricated and deformed slices in central parts of orogens, e.g. northeastern Newfoundland, Ballantrae, Indus Suture, and Pindus Zone. Ophiolitic melanges (Gansser, 1974), or chaotic rocks that contain blocks derived from the ophiolite suite of rock units are associated with allochthonous ophiolites (obduction) or they are related to the destruction of oceanic crust by its descent at oceanic trenches (subduction). The distribution and structural setting of ophiolitic melanges in orogenic belts are in most cases therefore as important to tectonic syntheses as the presence of the ophiolite suite itself.

The common occurrence of mafic-ultramafic rocks in the Appalachian Orogen was first pointed out by Hess (1939; 1955), and since then there have been numerous attempts to explain their origin. Most occurrences are interpreted now as ancient oceanic crust and mantle (Moores, 1970; Stevens, 1970; Church and Stevens, 1971; Dewey and Bird, 1971). Some are part of well-preserved ophiolite suites, e.g. Bay of Islands Complex, others are dismembered ophiolites, e.g. Advocate Complex, and still others form blocks in ophiolitic melange, e.g. Coachman's Melange. In a few cases, local examples are interpreted as intrusions (Chidester and Cady, 1972; Kennedy and Phillips, 1971) or mantle diapirs situated above subduction zones (Stevens and others 1974; Kean, 1974).

Although Hess suggested that there were two ultramafic belts in the Appalachian Orogen, new data require a revision of this view and indicate a wide spectrum of occurrences in a variety of different tectonic settings. Recent geologic syntheses of the Appalachian Orogen are based upon the recognition of contrasting tectonic-stratigraphic zones across the system. Nine zones are defined in the Canadian Appalachians (Williams and others 1972; 1974) and these have been amalgamated for purposes of broad correlation into five zones that are extrapolated along the full length of the system from Newfoundland to Alabama (Williams, 1976). From west to east these zones are given local names in the northern Appalachians, viz: Humber, Dunnage, Gander, Avalon, Meguma (plate 1). Ophiolitic rocks are restricted almost entirely to the Humber and Dunnage Zones.

The model for the development of the Appalachian Orogen follows the suggestion of Wilson (1966) and involves the generation and destruction of a late Precambrian - early Paleozoic Iapetus Ocean (Dewey, 1969, Bird and Dewey, 1970; Stevens, 1970; McKerrow and Cocks, 1977; etc.). The Humber Zone records the development and destruction of an Atlantic type

continental margin of eastern North America (Williams and Stevens, 1974). It contains the best examples of transported complete ophiolite suites (e.g. Bay of Islands Complex; Williams, 1973) as well as a variety of ophiolitic melanges in various states of structural complexity. The Dunnage Zone represents the former site of the Iapetus Ocean. In places it exhibits well-developed ophiolite suites (e.g. Betts Cove Complex, Upadhyay and others 1971; Thetford Mines ophiolites, Laurent, 1975), commonly overlain by thick island arc volcanic sequences. As well, it contains melanges that possibly relate to subduction (e.g. Dunnage Melange, Kay, 1976; Fournier Complex, N. Rast, pers. comm. 1975), and in the northeast a belt of mafic-ultramafic complexes that are either blocks in melange or mantle diapirs. The Gander and Avalon Zones developed upon continental crust and lay to the east and southeast of the Iapetus Ocean. Neither contains well-preserved examples of a complete ophiolite. The Meguma Zone may represent the eastern continental margin of an ancient ocean that lay to the east of the Avalon Zone (Schenk, 1971). Like the Gander and Avalon Zones, it too is devoid of ophiolite suites.

In the Canadian Appalachians, the boundary between the Humber and Dunnage Zones is marked by the occurrence of ophiolites in a steep structural belt. These ophiolites can be traced as discontinuous bodies from Baie Verte, Newfoundland, to Brompton Lake, Quebec. Accordingly, the steep ophiolite zone has been termed the Baie Verte-Brompton Line (St. Julien and others 1976). It is an important structural junction in the Northern Appalachians and its ophiolites are host to the asbestos deposits that make this zone the world's richest asbestos belt. In places where the ophiolitic rocks are absent, the Humber-Dunnage boundary is marked by faults that separate Humber Zone metamorphosed clastics (west) and Dunnage Zone less metamorphosed volcanic rocks (east). In other places, the boundary is hidden by Silurian and younger cover rocks, e.g. Gaspé Peninsula (plate 1).

South of the Canada-United States border, the projection of the Baie Verte-Brompton Line is marked by a zone of small isolated ultramafic bodies in Vermont that extends all the way southward to Staten Island, New York. Farther South, the Baltimore Gabbro Complex (Crowley, 1969) of Maryland lies at or near the continuation of the same structural zone, and the zone may be marked by local occurrences of ophiolitic melange in the James River Synclinorium (Brown, 1976). From there, it projects between the Grenvillian basement rocks of the Blue Ridge and Sauratown Mountains, and appears to continue farther south along the Brevard Zone (Hatcher, 1972). In the northern Appalachians, the Baie Verte-Brompton Line marks an ancient continent-ocean interface and it is the most westerly possible root zone for allochthonous ophiolites found farther west. If this same structural zone continues southward, as proposed, the Brevard Zone of the southern Appalachians is an important suture marking the site of the former Iapetus Ocean.

The distrubution and tectonic setting of ophiolitic rocks in the Humber and Dunnage Zones form the basis of the discussion that follows. No attempt is made to describe each individual ophiolite occurrence. Instead, a description of the regional geology and extrapolations along the length of the system for each kind of ophiolite occurrence is followed by a description of a type example. Most examples are taken from the northern Appalachians because of a greater familiarity to the authors and because southerly examples are treated by other contributions to this volume (see papers by Laurent and Morgan).

OPHIOLITES AND OPHIOLITIC MELANGES OF THE HUMBER ZONE

The Humber Zone consists of a crystalline Grenvillian basement overlain by a thick clastic sequence with associated volcanic rocks, and a prominent Cambro-Ordovician carbonate sequence. Ophiolites of highly allochthonous nature occur in western parts of the zone where they overlie relatively undeformed parts of the autochthonous carbonate sequence. These ophiolites are associated with transported sedimentary rocks and collectively they constitute allochthons emplaced during Middle Ordovician.

The carbonate sequence of the Humber Zone and correlative coarse limestone breccias in overlying structural slices are interpreted as bank and bank foot deposits, respectively, formed at the ancient continental margin of eastern North America (Rodgers, 1968). Underlying clastics that rest on Grenvillian gneisses formed a rise prism at the margin (Williams and Stevens, 1974), and transported ophiolites represent oceanic crust and mantle that lay farther east (Church and Stevens, 1971).

Examples of allochthonous ophiolites in westerly parts of the Humber Zone include the White Hills Peridotite of the Hare Bay Allochthon, the Bay of Islands Complex of the Humber Arm Allochthon, and the Mount Albert ophiolite of the Shick Shock Mountains (Williams, 1975). The Baltimore Gabbro Complex of Maryland occurs in a similar structural position but lies nearer the east boundary of the zone.

Ophiolitic melanges occur across the Humber Zone and they are particularly well-developed in western Newfoundland. Their formation is attributed to the transport of ophiolites from their root zone at the Baie Verte-Brompton Line, across the rise prism and carbonate bank successions, to their present positions. The best exposed and most extensive melanges form integral parts of the Humber Arm and Hare Bay Allochthons, e.g. Companion and Milan Arm Melanges (Williams, 1975), and comparable examples, though lacking ophiolitic blocks in most places, are associated with transported sedimentary rocks in Taconic klippen all the way southward to Harrisburg, Pennsylvania. These melanges are mainly thin subhorizontal sheets between other transported rocks that collectively lie above the carbonate sequence. Ophiolitic melanges occur also at the east margin of the carbonate terrane in Maryland and in western White Bay, Newfoundland, e.g. Second Pond Melange (Williams, 1977a). Farther east, ophiolitic melanges are associated with clastics of the rise prism at the eastern margin of the Humber Zone (e.g. Coachman's Melange, Williams, 1972b).

Deformation and metamorphism increase from west to east across the Humber Zone. Melanges associated with Taconic-type allochthons above the carbonate terrane have been little deformed since formation. These near the present easternmost exposures of the carbonate sequence vary from polydeformed and metamorphosed in Maryland to locally deformed and mildly metamorphosed in Newfoundland. Ophiolitic melanges at the eastern margin of the Humber Zone are everywhere polydeformed and metamorphosed and now bear little resemblance to occurrences farther west.

Small mafic-ultramafic bodies are common throughout the full length of the Appalachian Orogen in the belt of deformed clastic rocks at the eastern margin

of the Humber Zone. Although locally interpreted as intrusions, some are clearly blocks in ophiolitic melange and other isolated bodies occur at structural contacts. All are affected by the full range of deformation and metamorphism that accompanied the destruction of the ancient continental margin of eastern North America. Examples in easterly parts of the Fleur de Lys Supergroup in Newfoundland are thought to occur at structural discontinuities (Williams and others, 1977), the Pennington Dike and nearby ultramafic bodies of the Eastern Townships of Quebec are sited at structural contacts (Pierre St. Julien, pers. comm. 1975), the continuous string of small ultramafic occurrences from Vermont to Staten Island marks a zone of nappes and imbricate slices (Barry Doolan, pers. comm. 1976), and many of the small ultramafic bodies of the eastern Blue Ridge from Virginia to Alabama may owe their presence to structural emplacement.

If these small mafic-ultramafic occurrences are intrusions, there is no apparent mechanism or obvious reason for their emplacement into an undeformed rise prism of clastic sediments. More likely, they represent blocks in melange and dismembered ophiolite at structural contacts. Their widespread occurrence within the deformed and metamorphosed clastic terrane at the eastern margin of the Humber Zone implies a similar early tectonic history for the full length of the western part of the Appalachian System.

The distinction between the Humber and Dunnage Zones is subtle in places where deformed ophiolitic melanges, which are incorporated structurally within the Humber Zone clastics, are juxtaposed with ophiolite suites along the Baie Verte-Brompton Line. The latter are a natural part of the Dunnage Zone, but the melanges are grouped in places with the Humber Zone clastic rocks and considered a natural part of local stratigraphic successions. This situation exists at the Baie Verte-Brompton Line in Newfoundland and it may be a common circumstance elsewhere. Stratigraphic studies in metamorphic terranes that include ophiolitic melanges or small ultramafic bodies of possible ophiolitic parentage should be made with extreme caution, as experience has shown that major structural disruptions have gone unnoticed in the polydeformed and metamorphosed rocks immeidately west of the Baie Verte-Brompton Line (Williams and others 1977; Williams, 1977b; Pierre St. Julien, pers. comm. 1976; Barry Doolan, pers. comm. 1976).

Allochthonous complete ophiolite suites: The Bay of Islands Complex

The Bay of Islands Complex affords an excellent example of an allochthonous complete ophiolite suite that forms the highest structural slice of a composite allochthon in the western part of the Humber Zone. It is represented in four separate massifs, which from south to north are Lewis Hills, Blow Me Down, North Arm Mountain, and Table Mountain (pl. 1). All lie in the same structural position and either represent separate transported bodies or erosional remnants of a once continuous slice. Two of the massifs (Blow Me Down and North Arm Mountain) display a completely developed ophiolite stratigraphy, but all four include the basal ultramafic unit.

The sequences of ophiolite units in the three northernmost massifs are disposed in synclines with northeast-trending subhorizontal axes and moderately to steeply dipping limbs. The present tectonic base of each massif is subhorizontal so that the ophiolite

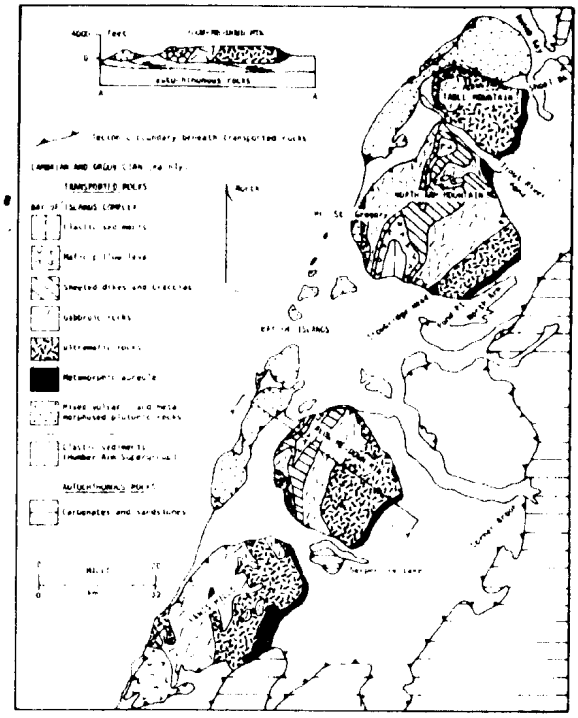

Figure 1: Geologic setting of the Bay of Islands Complex, Western Newfoundland (after Williams and Smyth, 1973).

units are structurally truncated at depth in much the same way as they are truncated at their top by the present erosional surface (see cross-section AA, fig. 1). A contact between the stratigraphic base of the ophiolite sequence and a dynamo-thermal aureole of supracrustal rocks, now frozen into the folded ophiolite slices, is interpreted to represent the actual zone of obduction where the hot oceanic plate moved across the continental margin. The contacts of latest emplacement of the structural slices are marked now by thin zones of shale melange with sedimentary, volcanic, and sparse gabbro and serpentinite blocks. These are the result of mass wastage and tectonic mixing that accompanied gravity sliding.

Trondhjemite from the Bay of Islands Complex has been dated isotopically at 504 m.y. ± 10 (Mattinson, 1976) and amphiboles from its dynamo-thermal aureole at 460 to 470 m.y. (Dallmeyer and Williams, 1975; Archibald and Farrar, 1976). The former gives the time of generation of the ophiolite suite as Late Cambrian. The latter indicates an Early Ordovician age for initial displacement and agrees with the sedimentologic evidence of ophiolite detritus in Lower Ordovician sedimentary rocks deposited during ophiolite transport (Stevens, 1970). An upper limit to the time of final emplacement is given by the Middle Ordovician age of the [illegible] allochthonous Long Point Formation (Bergström and others 1974). For more detailed descriptions the reader is referred to Smith (1958) and Malpas (this volume).

Ophiolitic melanges of the Humber Zone

The Milan Arm Melange (Williams, 1975) of northern Newfoundland is the clearest example of an ophiolitic melange that forms an integral part of a Taconic-type allochthon above the Humber Zone carbonate sequence. It structurally overlies autochthonous rocks in some places and intervening transported clastics of the rise prism (Maiden Point Formation) in other places. It is in turn structurally overlain by the ophiolitic White Hills Peridotite. The melange is similar in most respects to all of the shale melanges that separate structural slices of the west Newfoundland allochthons, however, it has a much wider variety of exotic blocks; some up to a kilometer or more across and resembling the largest slices that make up the west Newfoundland allochthons.

Its commonest blocks are serpentinized peridotite, mafic volcanic rocks, amphibolites, foliated gabbro, greywacke, diorite, and exceptionally coarse grained pyroxenite and hornblendite associated with tonalite and hornblende-biotite schist. Nephrite blocks are also known locally (R.K. Stevens, pers. comm. 1976). Most of these rock types can be matched directly with rocks in nearby structural slices, but a few are of unknown origin.

Many of the amphibolite, gabbro, and diorite blocks are encased in a relatively thin, hard rind of light grey calc-silicate alteration products (rodingite). The tough and resistant alteration halos form coastal wave-washed outcrop surfaces where the matrix shales are eroded. In some examples the rodingite alteration halos are surrounded in turn by a thinner serpentinite coating, implying that the rodingite represents an alteration zone between mafic rocks and serpentinite. These blocks appear therefore to have been once immersed in serpentinite or serpentinite melange, so that they are recycled where they now occur in a shale matrix.

Local serpentinite and gabbro blocks in melanges at the base of the west Newfoundland allochthons imply that the sequences of transported slices were emplaced as already-assembled allochthons (Stevens and Williams, 1973).

The recently recognized Coachman's Melange (Williams, 1977b) is an example of a polydeformed and metamorphosed ophiolitic melange that occurs at the eastern margin of the Newfoundland Humber Zone. It is closely associated with psammitic schists of the rise prism (Fleur de Lys Supergroup) and it has been affected by the full range of deformations recognized in nearby rocks. The melange occurs in a multitude of narrow zones that rarely exceed more than 50 m in structural thickness. If all occurrences represent a complexly folded single unit, exceedingly tight isoclines of more than 3 km amplitude affected easternmost local exposures of the rise prism.

The Coachman's Melange has a black pelitic matrix with conspicuous deformed and recrystallized ultramafic blocks now represented by bright green actinolite-fuchsite schist. Sedimentary blocks with ill-defined outlines are common everywhere, and in some places large serpentinized ultramafic blocks, foliated gabbro blocks, and marble are also known.

Actinolite-fuchsite schist occurs in lenses from 10 cm to 3 m in length and rarely more than 1 m in width. They exhibit minor folds and folded schistosities identical to structures in the surrounding schistose matrix and nearby psammitic schists. Pale green actinolite crystals are locally 2-4 cm in length, set in a fine-grained fuchsite-carbonate matrix. An ultramafic origin for these rocks is indicated by their mineralogy and because larger nearby ultramafic blocks are recrystallized to similar mineral assemblages at their margins. Interior parts of large ultramafic blocks are in places brecciated, and this feature predates both serpentinization and incorporation into the melange.

Recognition of the Coachman's Melange and an appreciation of its complex structural history bears upon one of the major problems of northern Appalachian geology, i.e. the timing of deformation and metamorphism within the rise prism in relation to the time of generation of nearby ophiolite suites and the time of their transport across an ancient continental margin. As is the case with other worldwide examples of ophiolitic melanges, the Coachman's Melange implies transport of oceanic crust across the rise prism represented by the local Fleur de Lys Supergroup. This transport is equated most reasonably with the emplacement of highly allochthonous ophiolites in western parts of the Humber Zone from an initial position to the east of the Baie Verte-Brompton Line. Similar structural histories for both the Coachman's Melange and nearby parts of the Fleur de Lys Supergroup indicate that the rise prism was undeformed at the time of melange formation and initial ophiolite displacement. This conclusion leads to a simple model for the place of origin and time of transport of ophiolitic complexes in western Newfoundland compared to the time of deformation and metamorphism in the intervening Fleur de Lys terrane (fig. 2). As well, it explains the marked structural contrasts between the Fleur de Lys Supergroup and nearby ophiolite suites, while implying a mechanism for deformation and metamorphism through ophiolite transport and structural loading at the ancient continental margin.

Ophiolitic melanges comparable to those at Coachman's Harbour, Newfoundland are unknown elsewhere in the Appalachian Humber Zone. Other occurrences are predicted because of structural similarities along the length of the system.

OPHIOLITES AND OPHIOLITIC MELANGES OF THE DUNNAGE ZONE

Ophiolites and ophiolitic melanges are represented in the Dunnage Zone from Newfoundland to Virginia. Farther south, rocks typical of the Dunnage Zone are absent and the Humber Zone is bordered eastward by crystalline rocks of the Inner Piedmont (Hatcher, 1972). Relationships in the northern Appalachians predict a major suture in the southern Appalachians, either at the Brevard Zone or somewhere between this zone and Avalon Zone equivalents of the Carolina Slate Belt.

The most prominent ophiolite occurrences in the Dunnage Zone are found at its western margin along the Baie Verte-Brompton Line. In Newfoundland, examples can be traced from Baie Verte of the Burlington Peninsula, e.g. Advocate and Point Rousse Complexes (Williams and others 1977) to Glover Island of Grand Lake. From there, the Baie Verte-Brompton Line is ill-defined, but it is probably coincident with the Cape Ray Suture (Brown, 1973) farther south, and transported ophiolites at Cape Ray presumably root in this zone. In mainland Canada, volcanic rocks and deformed mafic-ultramafic rocks of the Fournier Complex, New Brunswick may lie at or near the Baie Verte-Brompton Line Farther west, the line is

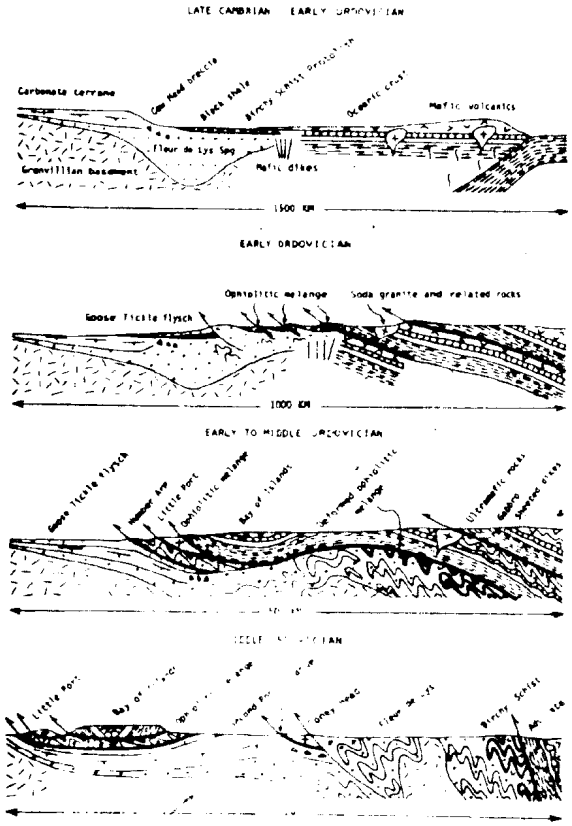

Figure 2: Model for the development of ophiolitic melange and the transport of ophiolites across the Humber Zone (after Williams, 1977b).

covered by Upper Ordovician rocks of the Metapedia Belt and Silurian rocks of the Gaspé Synclinorium. Where the Baie Verte-Brompton Line reappears in the Eastern Townships of Quebec, it is marked by major ophiolite occurrences along most of its length.

The Baie Verte-Brompton Line is a zone of intense deformation and ophiolites along its length are in most places thrust-imbricated and penetratively deformed. The ophiolite suites are mainly steeply-dipping to overturned, but their stratigraphic sections face eastwards. In Newfoundland, the Baie Verte-Brompton Line is a zone of marked gravity gradient with negative anomalies on its western continental side, and positive anomalies across oceanic rocks to the east (Miller and Deutsch, 1976).

East of the Baie Verte-Brompton Line, separate ophiolite occurrences are common throughout central parts of the Dunnage Zone. These form the basement to thick volcanic arc sequences that are locally dated as Lower Ordovician, thus defining an upper age limit for the underlying ophiolite suites. In Newfoundland, the Betts Cove Complex is probably the best known example, but sheeted dikes occur throughout the central volcanic terrane (Strong, 1972) and gabbros and ultramafic rocks occur locally at South Pond, Brighton and Gull Island of Cape St. John. In Maine, mafic-ultramafic rocks along the southern margin of the Chain Lakes massif are interpreted as ophiolites (G.M. Boone, pers. comm. 1975). Their occurrence and relationships to nearby crystalline rocks are still poorly understood.

Olistostromes that contain ophiolitic blocks occur along the east margin of the Thetford Mines ophiolite belt, e.g. St. Daniel Formation (St. Julien and Hubert, 1975), and megaconglomerates with outcrop size gabbro and penetratively deformed and altered ultramafic blocks occur along the east margin of the Advocate Complex in Newfoundland. The significance and time of deposition of these rocks is still poorly understood, but in Newfoundland, deposition post-dates earliest deformations in nearby ophiolites and predates Silurian volcanism. Farther south in the New England Appalachians, small metamorphosed ultramafic bodies in sulphidic schists of the Partridge Formation may represent blocks in olistostrome rather than small intrusions.

The Dunnage Melange (Kay, 1976), which lies to the east of the central Newfoundland island arc terrane, is not itself ophiolitic but a similar melange, 20 km eastward at Carmanville, contains sparse ultramafic blocks. The Carmanville melange may represent a subsurface continuation of the Dunnage. The Dunnage Melange has been interpreted as an oceanic trench fill (Dewey and Bird, 1971; Williams and Hibbard, 1976; Kay, 1976). If so, then ophiolitic melange would be expected in this position.

A prominent belt of mafic-ultramafic complexes along the eastern margin of the Dunnage Zone in Newfoundland, and east of the Dunnage Melange, remains poorly understood in present models for the development of the Appalachian Orogen. Some occurrences contain ultramafic rocks, gabbros and volcanic rocks that collectively are reminiscent of an ophiolite suite, e.g. Pipestone Pond (Kean, 1974). Others are mainly clinopyroxenite bodies in structural contact with surrounding dark shales, e.g. Gander River Belt, and still others may represent differentiated intrusions of mantle derivation, e.g. Great Bend of Gander River (Stevens and others 1974). At one locality on the north shore of Gander Lake, penetratively deformed ultramafic rocks are unconformably overlain by conglomerates of probable Caradocian age, thus defining an upper age limit for some of these occurrences.

Transported ophiolites of the Humber Zone, ophiolites at the Baie Verte-Brompton Line, and ophiolites that form the basement to island arc sequences across the Dunnage Zone may all relate to a single cycle of ophiolite generation (as summarized in Figure 2). This simple view is contrasted with an earlier interpretation that relates each ophiolite belt to an equal number of small ocean basins that formed, at least in part, after deformation and metamorphism of the Humber Zone continental rise prism (Dewey and Bird, 1971; Kennedy, 1975; Kidd, in press).

Ophiolites at the Baie Verte-Brompton Line

Ophiolites along the Baie Verte-Brompton Line are bounded to the west by polydeformed and metamorphosed clastic rocks of the Humber Zone, and they are bounded to the east by olistostromes and volcanic sequences. Several occurrences in Newfoundland and Quebec are overlain by thick volcanic sequences, which are similar to volcanic arc sequences found above ophiolites farther east. The Advocate and Point Rousse Complexes along the Baie Verte-Brompton Line

POOR COPY
COPIE DE QUALITEE INFERIEURE

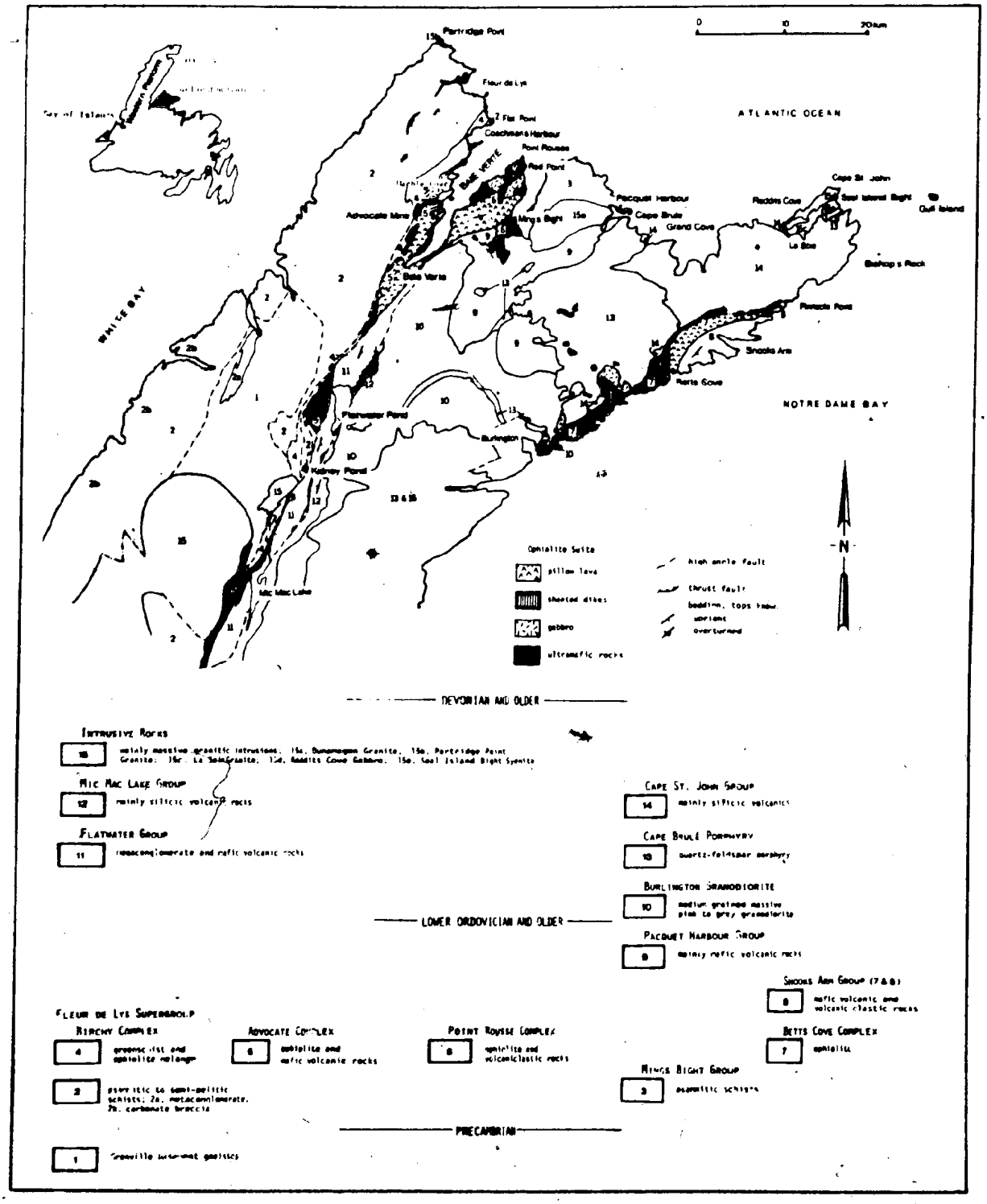

Figure 5: Distribution of ophiolites at and near the Baie Verte-Brompton Line, Burlington Peninsula, Newfoundland (After Williams and others, 1977).

POOR COPY
COPIE DE QUALITÉE INFÉRIEURE

in northern Newfoundland are taken as a type example and their distribution and relationships to nearby groups are summarized in Figure 3.

The Advocate Complex can be traced from Baie Verte 60 km southward beyond Mic Mac Lake. It has a steep northeast-trending foliation in most places and it is cut by numerous steep northeast-trending shear zones that repeat its rock units. A large ultramafic body at its northwest margin near Baie Verte consists of intensely foliated and fractured serpentinites that are host to the Advocate asbestos deposit. Its gabbros vary from massive to intensely foliated and some are distinctive white-altered rocks with green fuchsitic smears, e.g. those at Marble Cove. Sheeted dikes are best exposed 1 km northeast of Baie Verte and well-preserved pillow lavas occur nearby.

Black and green slates, black pebbly slates and chaotic black slaty melange are also present in the Advocate Complex. Some of these rocks occur at tectonic contacts so that they are structurally comingled with the segmented ophiolite. Their chaotic character results, in part, from tectonic processes that accompanied imbrication of the ophiolite suites. Others may be depositional breccias. Some of these chaotic shale zones in the Advocate Complex resemble nearby chaotic rocks and black schists of the Coachman's Melange, so that all appear to mark significant structural dislocations.

The Point Rousse Complex is made up of several distinct structural blocks with their tectonic boundaries marked by foliated serpentinite or foliated carbonate-talc-fuchsite alterations of ultramafic rocks (Norman and Strong, 1975). Three separate blocks on Point Rousse Peninsula contain southeast-facing, overturned sections of gabbro, sheeted dikes and pillow lava. The most complete section occurs south of Red Point where a northwest-dipping, southeast-facing sequence of gabbro, sheeted dikes and pillow lava is followed by local chert beds and a thick section of volcaniclastic rocks, all southeast-facing. Locally, on the western side of the Point Rousse Peninsula, pillow lavas of the complex are intensely deformed and converted to greenschists. Southward thrusting of gabbros above the greenschists postdates the development of a steep foliation in the mafic volcanic rocks.

The Point Rousse Complex is less altered and deformed than the Advocate Complex, except in local zones of intense deformation. Farther east, the Betts Cove Complex is even less deformed. The regional distribution of ophiolite complexes across the Burlington Peninsula and the pattern of their deformation suggest westward imbrication of east facing ophiolitic suites with pervasive intense deformation in lower levels (Coachman's Melange, Advocate Complex) and less intense deformation and fewer deformed zones higher in the structural pile (Point Rousse Complex, Betts Cove Complex).

Ophiolites beneath volcanic arc sequences

The Betts Cove Complex (fig. 4) is the clearest example of an ophiolite suite that forms the basement to a volcanic arc sequence. It consists of a basal ultramafic member overlain transitionally by a poorly developed gabbroic member, in turn overlain by a sheeted dike complex that consists of practically 100% mafic dikes (Upadhyay and others 1971). The sheeted dike complex is faulted against nearby mafic volcanic rocks, but locally the contact is gradational

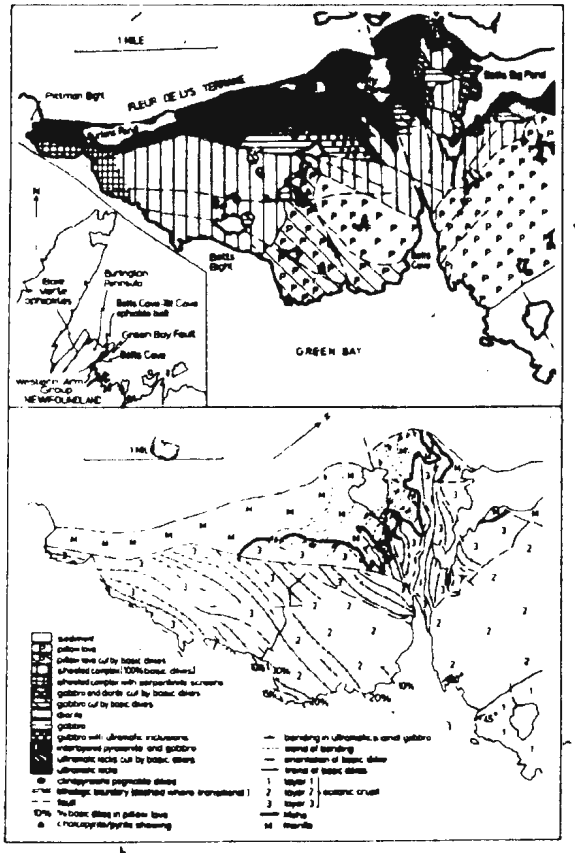

Figure 4: Geology of the Betts Cove Complex and its comparison to models of oceanic crust and mantle (after Upadhyay and others 1971).

across a narrow zone that shows a large decrease in the percentage of dikes over a short distance. Overlying Lower Ordovician rocks of the Snooks Arm Group are nearly 4 km thick and comprise a conformable sequence of pillow lavas, cherts, argillites, andesitic pyroclastic rocks and immature volcanic sediments. A lowermost pillow lava unit constitutes the upper part of the Betts Cove Complex so that a completely conformable transition exists from the ultramafic member of the ophiolite complex to the top of the thick overlying mainly volcanic succession.

Nearby correlatives of the Snooks Arm Group show a lithological evolution from lowermost pillow lavas upward through marine cherts and turbidites into pyroclastic rocks and volcaniclastic sedimentary rocks capped by limestone and subareal tuffs. The overall deep to shallow water lithic change is accompanied by geochemical changes in the volcanic stratigraphy from low potassium tholeiites at the base to calc-alkaline low-silica andesites toward the top that show progressive enrichment in Al_2O_3 and K_2O and a decrease in CaO and MgO (Kean and Strong, 1975). Accordingly, the Dunnage Zone volcanic sequences are interpreted as analogues to modern island arcs and the relationships at Betts Cove leave little doubt that volcanic rocks of the Dunnage Zone, at least in westerly exposures, directly overlie oceanic crust.

POOR COPY
COPIE DE QUALITEE INFERIEURE

The prominent island arc volcanism of the Dunnage Zone continued into the Middle Ordovician, indicating that island arcs were evolving in the Dunnage Zone during the emplacement of allochthonous ophiolites across the Humber Zone. A cessation to Ordovician volcanism and the deposition of Caradocian black shales across the entire Dunnage Zone coincides exactly with the time of final emplacement of allochthonous ophiolites such as the Bay of Islands Complex in the Humber Zone.

Melanges, olistostromes and megaconglomerates of the Dunnage Zone

The Dunnage Melange, though devoid of ophiolitic components, is included in this analysis because of its similarity and possible subsurface continuity with melange at Carmanville that locally contains ultramafic and gabbroic blocks. As well, it is a prominent feature of the Dunnage Zone and its interpretation as an oceanic trench deposit bears heavily upon models proposed for the development of the northern Appalachians.

The melange is a strikingly heterogeneous deposit composed of blocks of mainly clastic sedimentary and mafic volcanic rocks enveloped in a dark scaly shale matrix. It is well-exposed along the rugged coast and clusters of islands of the Bay of Exploits, where it extends for 40 km along strike with a maximum outcrop width of 10 km (fig. 5). Its clasts vary in size from granules and cobbles to boulders and huge blocks up to a kilometre in diameter, thus producing a chaotic mosaic that contrasts sharply with nearby stratified volcanic and sedimentary rocks. Most blocks are indigeneous to nearby volcanic arc sequences and they can be matched with formations of the Exploits and Summerford Groups (Williams and Hibbard, 1976). Shale is much more important in the melange than in nearby terranes.

The Dunnage Melange overlies and interdigitates with the New Bay Formation of the Exploits Group in the southwest, and it has an apparent ghost stratigraphy comparable to that of the Exploits Group. Its matrix is Tremadocian (Hibbard and others 1977) and the melange is overlain by Caradocian black shales toward the northwest. These are succeeded by greywackes and Silurian conglomerates that are coarser and of shallower water deposition higher in the stratigraphic section. The sequence of units above the melange can be viewed therefore as representing the gradual sedimentary infilling of a marine trough, or an upward shoaling sequence built upon a melange basement.

A variety of small intrusions that are localized within the melange terrane are rare or absent in surrounding country rocks. These are mainly quartz-feldspar porphyries and related rocks, which in places contain numerous small mafic and ultramafic inclusions. Dated isotopically as Early to Middle Ordovician and exhibiting relationships suggesting contemporaneity with melange formation (Williams and Hibbard, 1976), the intrusions imply a direct magmatic linkage with deeper parts of the crust. Mafic and ultramafic inclusions in the porphyries indicate that the melange is underlain by a mafic-ultramafic substrate.

West of the Dunnage Melange, the main volcanic sequences of Notre Dame Bay are interpreted as island arc accumulations built upon oceanic crust. These are bordered to the southeast by mixed sedimentary and volcanic rocks of the Exploits Group, that interdigitate farther southeastward with the Dunnage Melange. The melange is interpreted therefore to occupy a fore arc area, based on the geographical distribution of these ancient elements and their similarity to that outlined for modern volcanic arcs (Dickinson, 1974; Karig, 1974). There is no evidence that the Dunnage Melange was ever buried in an actual subduction zone. It is most reasonably considered therefore as a trench-slope deposit that overlies an accretionary prism, analogous to the positioning of some modern melanges with respect to the arc and oceanic trench (Seely and others 1974; Karig and Sharman, 1975).

A zone of megaconglomerates and olistostromal melange with local ophiolitic blocks occurs along the east margin of the Thetford Mines ophiolite belt of Quebec. These rocks are known as the St. Daniel Formation and they rest conformably on basic volcanic rocks of the ophiolite suite. The unsorted rocks contain fragments of greywacke, quartz arenite, shale, siltstone, volcanic rocks, and outsize serpentinite blocks, all set in a dark grey to red and green shale matrix. The age of the St. Daniel Formation is unknown, more than that it is overlain by the Middle Ordovician Beauceville Formation.

The St. Daniel shale-melange facies has been interpreted as an offshore oceanic deposit equivalent to clastics of the Humber Zone rise prism, i.e. Rosaire and Caldwell Groups of Quebec (St. Julien and Hubert, 1975). It has been interpreted also as a subduction related melange (Laurent, 1975).

In Newfoundland, unsorted shale matrix megaconglomerates occupy a similar position to the St. Daniel Formation where they lie to the east of the Advocate Complex (included in Flatwater Group of Figure 3). These locally contain gabbro blocks up to tens of metres in diameter, a variety of sedimentary and volcanic clasts, granodiorite pebbles, altered and deformed ultramafic blocks, and rare semipelitic schist blocks. Deposition of the Newfoundland examples followed deformation in nearby ophiolites and deformation in sedimentary rocks of the rise prism to the west, i.e. Fleur de Lys Supergroup. These examples are interpreted therefore as coarse slump conglomerates derived mainly from deformed ophiolitic rocks at a destroyed continental margin. They are therefore not thought to be correlative with sediments of the rise prism or connected with subduction, as has been suggested for the Quebec examples.

Dismembered ophiolites or mantle diapirs at the eastern margin of the Dunnage Zone

Mafic-ultramafic bodies along the east side of the Dunnage Zone in Newfoundland (Gander River Belt) have been interpreted as blocks in melange or as mantle diapirs related to subduction and intruded into the country rocks. One occurrence on the north shore of Gander Lake is overlain by conglomerate of presumed Middle Ordovician age, indicating an upper time limit for the age of some of these bodies.

The largest body at Pipestone Pond is approximately 16 km long and 5 km wide, and it is composed mainly of pyroxenite, gabbro, diorite and serpentinized equivalents. It is faulted against metasediments to the east and it is followed westward by volcanic rocks that may be an integral part of the plutonic complex.

A nearby occurrence at Great Bend of Gander

POOR COPY
COPIE DE QUALITÉE INFERIEURE

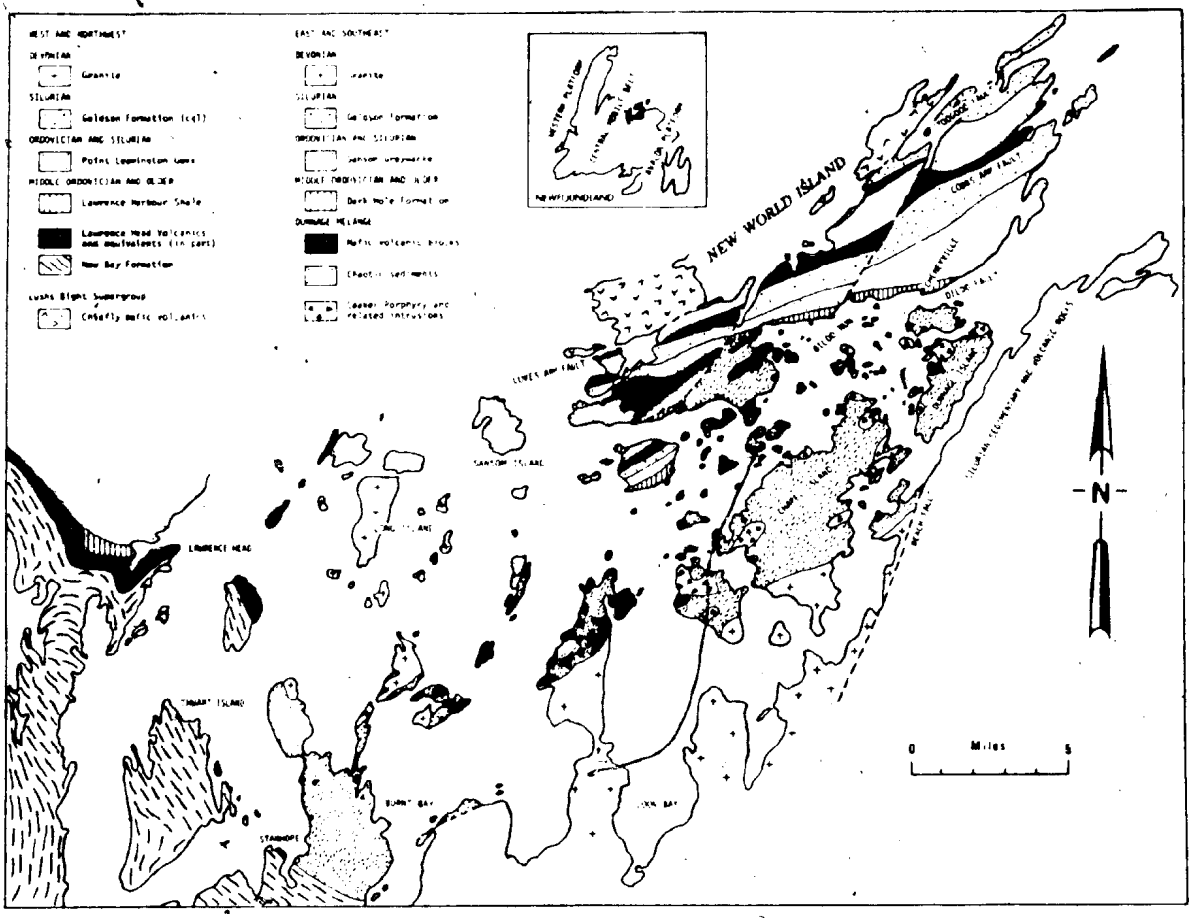

Figure 5: Internal characteristics and regional setting of the Dunnage Melange (after Williams and Hibbard, 1976).

River is composed of dunite and peridotite with an outer zone of gabbro, anorthosite and minor serpentinite. It is circular in shape and surrounded by hornfels of probable Silurian age. This body is most likely an intrusion (Kean, 1974).

Numerous circular, oval and elongate ultramafic bodies occur along the shores of Gander Lake and extend northward along the east side of Gander River. These range in size from a kilometre to less than a metre in diameter and extend over a distance of 60 km. They are mainly pyroxenites and gabbros with minor amounts of peridotite. Although described as intrusions, most contacts are tectonic.

MAFIC-ULTRAMAFIC ROCKS OF THE SOUTHERN APPALACHIANS

In the Southern Appalachians (plate I), the greatest concentration of small mafic-ultramafic bodies lies to the west of the Brevard Zone. These occurrences are equated with similar occurrences farther north throughout the eastern parts of the Humber Zone. East of the Brevard Zone, small ultramafic bodies within the crystalline terrane of the Inner Piedmont are of unknown significance and have no northern counterparts, except perhaps for occurrences in metamorphosed easterly parts of the Dunnage Zone in Newfoundland. Farther east, in metamorphosed parts of the Carolina Slate Belt, small ultramafic bodies occur near the Georgia-South Carolina state line and in the Raleigh Belt of eastern North Carolina. All of these occurrences are of unknown significance and many of them may represent metamorphosed small intrusions rather than oceanic ophiolites.

APPALACHIAN OPHIOLITES AND THE AGE OF IAPETUS

Stratigraphic analysis of the Humber Zone (Williams and Stevens, 1974) indicates rifting and the development of an ancient continental margin of Eastern North America in the late Precambrian with a stable margin existing well into the Ordovician. Destruction of this margin began in the Lower Ordovician and it was completed by Middle Ordovician. Ophiolite suites of the Appalachian Orogen are all of Late Cambrian to Early Ordovician age, where dated. Whether or not the preserved ophiolites represent the crust of a wide Iapetus Ocean, or a sampling of the floor of a related small ocean basin, remains debatable.

The Silurian and later development of the Appalachian Orogen presents a picture entirely different from that which prevailed during its

POOR COPY
COPIE DE QUALITEE INFERIEURE

Cambrian and Ordovician development. Ophiolites of Silurian or younger age are unknown in the Appalachian Orogen and it is impossible to restore the stratigraphy of possible oceans and margins for the Silurian and later periods. An unconformity beneath Silurian rocks across the Humber Zone and westerly parts of the Dunnage Zone indicates the destruction of an earlier Ordovician continental margin and ocean basin. Elsewhere in central areas of the Dunnage Zone, where the stratigraphic record is complete, marine Ordovician shales pass upward into Silurian conglomerates and continental volcanics and red beds.

The common view that a Silurian or Devonian Iapetus Ocean closed in the Devonian to produce the Acadian orogeny (Dewey, 1969; McKerrow and Ziegler, 1971; Schenk, 1971; McKerrow and Cox, 1977) is based more on the premise that orogeny is the result of moving plates and closing oceans, rather than on the stratigraphic record.

ACKNOWLEDGEMENTS

We wish to thank W.R. Church, J.F. Dewey, B. Doolan, R.D. Hatcher, J. Malpas, R.K. Stevens, P. St. Julien and D.F. Strong who through discussions helped extrapolate zones of mafic-ultramafic occurrences along the Appalachian System. The first author also wishes to acknowledge financial support of his field work on ophiolites in the Northern Appalachians through the National Research Council of Canada, the Canadian Department of Energy, Mines and Resources, and an Izaak Walton Killam Special Senior Research Scholarship. The second author wishes to acknowledge financial support of his studies through a Memorial University of Newfoundland Fellowship.

REFERENCES CITED

Archibald, D.A., and Farrar, E., 1976, K-Ar ages of amphiboles from the Bay of Islands ophiolite and the Little Port Complex, Western Newfoundland, and their geological implications: Can. Jour. Earth Sci., v. 13, p. 993-996.

Bergström, S.M., Riva, John, and Kay, Marshall, 1974, Significance of conodonts, graptolites, and shelly faunas from the Ordovician of western and north-central Newfoundland: Can. Jour. Earth Sci., v. 11, p. 1625-1660.

Bird, J.M. and Dewey, J.F., 1970, Lithosphere plate-continental margin tectonics and the evolution of the Appalachian Orogen: Geol. Soc. America Bull., v. 81, p. 1031-1060.

Brown, P.A., 1973, Possible cryptic suture in southwest Newfoundland: Nature, Phys. Sci., v. 245, p. 9-10.

Brown, W.R., 1976, Tectonic melange in the Arvonia Slate District of Virginia (abs.): Geol. Soc. America Abs. with Programs, v. 8, no. 2, p. 142.

Chidester, A.H., and Cady, W.M., 1972, Origin and emplacement of Alpine-type ultramafic rocks: Nature Phys. Sci., v. 240, p. 27-31.

Church, W.R., and Stevens, R.K., 1971, Early Paleozoic ophiolite complexes of Newfoundland Appalachians as mantle-ocean crust sequences: Jour. Geo-Phys. Research, v. 76, p. 1460-1466.

Crowley, W.P., 1969, Stratigraphic evidence for a volcanic origin of part of the Bel Air belt of Baltimore Gabbro Complex in Baltimore County, Maryland (abs.): Geol. Soc. America, pt. 1, p. 30.

Dallmeyer, R.D., and Williams, Harold, 1975, $^{40}Ar/^{39}Ar$ release spectra of hornblende from the Bay of Islands metamorphic aureole, western Newfoundland: their bearing on the timing of ophiolite obduction at the Ordovician continental margin of eastern North America: Can. Jour. Earth Sci., v. 12, p. 1685-1690.

Dewey, J.F., 1969, The evolution of the Appalachian/Caledonian Orogen: Nature, v. 222, p. 124-129.

Dewey, J.F., and Bird, J.M., 1971, Origin and emplacement of the ophiolite suite: Appalachian ophiolites in Newfoundland: Jour. Geophys. Research, v. 76, p. 3179-3207.

Dickinson, W.R., 1974, Plate tectonics and sedimentation: Society Econ. Paleont. and Miner. Special Pub. no. 22, p. 1-27.

Gansser, A., 1974, The ophiolitic melange, a world wide problem on Tethyan examples: Eclogae Geologicae Helvetiae, v. 67, p. 479-507.

Hatcher, R.D., Jr., 1972, Developmental model for the Southern Appalachians: Geol. Soc. America Bull., v. 83, p. 2735-2760.

Hess, H.H., 1939, Island arcs, gravity anomalies and serpentinite intrusions: Internat. Geol. Cong. 17th, Moscow 1937, Rept. 17, v. 2, p. 763-783.

Hess, H.H., 1955, Serpentinites, orogeny and epeirogeny: Geol. Soc. America Spec. Paper 62, p. 391-408.

Hibbard, J.P., Stouge, S., and Skevington, D., 1977, Fossils from the Dunnage Melange, north central Newfoundland: Can. Jour. Earth Sci., v. 14, p. 1176-1178.

Karig, D.E., 1974, Evolution of arc systems in the Western Pacific: Ann. Rev. Earth and Plan. Sci., v. 2, p. 51-75.

Karig, D.E., and Sharman, G.F., 1975, Subduction and accretion in trenches: Geol. Soc. America Bull., v. 86, p. 337-389.

Kay, Marshall, 1976, Dunnage Melange and subduction of the Protacadic Ocean, Northeast Newfoundland: Geol. Soc. America, Spec. Paper 175, 49p.

Kean, B.F., 1974, Notes on the Geology of the Great Bend and Pipestone Pond ultramafic bodies: Newfoundland Department of Mines and Energy, Min. Dev. Div., Report of Activities, p. 33-42.

Kean, B.F., and Strong, D.F., 1975, Geochemical evolution of an Ordovician island arc of the central Newfoundland Appalachians: Am. Jour. Sci., v. 275, p. 97-118.

Kennedy, M.J., 1975, Repetitive orogeny in the northeastern Appalachians - new plate models based upon Appalachians examples: Tectonophysics, v. 28, p. 39-87.

Kennedy, M.J., and Phillips, W.E.A., 1971, Ultramafic rocks of Burlington Peninsula, Newfoundland, in A Newfoundland Decade. Proc. Geol. Assoc. Canada, v. 24, p. 35-46.

Kidd, W.S.F., (in press), The Baie Verte Lineament, Newfoundland: ophiolite complex floor and mafic volcanic fill of a small Ordovician marginal basin: Maurice Ewing Volume.

Laurent, Roger, 1975, Occurrences and origin of the ophiolites of Southern Quebec, Northern Appalachians: Can. Jour. Earth Sci., v. 12, p. 443-455.

Mattinson, J.M., 1976, Ages of zircons from the Bay of Islands ophiolite complex, Western Newfoundland: Geology, v. 4, p. 393-394.

McKerrow, W.S., and Cocks, L.R.M., 1977, The location of the Iapetus Ocean suture in Newfoundland: Can. Jour. Earth Sci., v. 14, p. 488-495.

McKerrow, W.S., and Ziegler, A.M., 1971, The Lower Silurian paleogeography of New Brunswick and adjacent areas: Jour. Geology, v. 79, p. 635-646.

Miller, H.G., and Deutsch, E.R., 1976, New gravitational evidence for the subsurface extent of oceanic crust in north-central Newfoundland: Can. Jour. Earth Sci., v. 13, p. 459-469.

Moores, E., 1970, Ultramafics and orogeny, with models of the U.S. Cordillera and the Tethys: Nature, v. 228, p. 837-842.

Norman, R.E. and Strong, D.F., 1975, The geology and geochemistry of ophiolitic rocks exposed at Ming's Bight, Newfoundland: Can. Jour. Earth Sci., v. 12, p. 777-797.

Rodgers, John, 1968, The eastern edge of the North American continent during the Cambrian and Early Ordovician, in Zen, E-an, White, W.S., Hadley, T. B. and Thompson, J.B., Jr. (eds.), Studies of Appalachian Geology: northern and martime: Wiley-Interscience, New York, p. 141-149.

Schenk, P.E., 1971, Southeastern Atlantic Canada, Northwestern Africa and continental drift: Can. Jour. Earth Sci., v. 10, p. 1218-1251.

Seely, D.R., Vail, P.R., and Walton, G.G., 1974, Trench slope model, in Burk, C.A. and Drake, C.L. (eds.), The Geology of Continental Margins: Springer-Verlag, New York, p. 249-260.

Smith C.H., 1958, Bay of Islands Igneous Complex, western Newfoundland: Geol. Survey Canada, Memoir 290, 132p.

Stevens, R.K., 1970, Cambro-Ordovician flysch sedimentation and tectonics in West Newfoundland and their possible bearing on a proto-Atlantic ocean, in Lajoie, J. (ed.), Flysch sedimentology in North America: Geol. Assoc. Canada Spec. Paper No. 7, p. 165-177.

Stevens, R.K., Strong, D.F., and Kean, B.F., 1974, Do some Eastern Appalachian ultramafic rocks represent mantle diapirs produced above a subduction zone? Geology, v. 2, p. 175-178.

Stevens, R.K., and Williams, Harold, 1973, The emplacement of the Humber Arm Allochthon, Western Newfoundland (abs.): Geol. Soc. America, Northeast Section Annual Meeting Program, Allentown, Pennsylvanic, v. 4, No. 2, p. 222.

Strong, D.F., 1972, Sheeted diabases of Central Newfoundland: new evidence for Ordovician seafloor spreading: Nature, v. 235, p. 102-104.

St. Julien, P., and Hubert, C., 1975, Evolution of the Taconian orogen in the Quebec Appalachians. Am. Jour. Sci., v. 275A, p. 337-362.

St. Julien, Pierre, Hubert, C., and Williams, Harold, 1976, The Baie Verte-Brompton Line and its possible tectonic significance in the Northern Appalachians (abs.): Geol. Soc. America Abs. with Programs, v. 8, p. 259-260.

Upadhyay, H.D., Dewey, J.F., and Neale, E.R.W., 1971, The Betts Cove ophiolite complex, Newfoundland: Appalachian oceanic crust and mantle, in A Newfoundland Decade: Proc. Geol. Assoc. Canada, v. 24, p. 27-34.

Williams, Harold, 1973, Bay of Islands Map-Area, Newfoundland, Geol. Survey Canada Paper 72-34, 7p.

Williams, Harold, 1975, Structural succession, nomenclature and interpretation of transported rocks in Western Newfoundland: Can. Jour. Earth Sci., v. 12, p. 1874-1894.

Williams, Harold, 1976, Tectonic-stratigraphic subdivision of the Appalachian orogen (abs.): Geol. Soc. America Abs. with Programs, v. 8, no. 2, p. 300.

Williams, Harold, 1977a, The Coney Head Complex. Another Taconic allochthon in west Newfoundland: Am. Jour. Sci. (in press).

Williams, Harold, 1977b, Ophiolitic melange and its significance in the Fleur de Lys Supergroup, northern Appalachians: Can. Jour. Earth Sci., v. 14, p. 987-1003.

Williams, Harold and Hibbard, J.P., 1976, The Dunnage Melange, Newfoundland: Geol. Survey Canada, Paper 76-1A, p. 183-185.

Williams, Harold, Hibbard, J.P., and Bursnall, J.T., 1977, Geologic setting of asbestos-bearing ultramafic rocks along the Baie Verte Lineament, Newfoundland: Geol. Survey Canada, Paper 77-1, pt. A, p. 351-360.

Williams, Harold, Kennedy, M.J., and Neale, E.R.W., 1972, The Appalachian structural province, in Price, R.A. and Douglas, R.J.W. (eds.), Variations in tectonic styles in Canada: Geol. Assoc. Canada Spec. Paper 11, p. 181-261.

Williams, Harold, Kennedy, M.J., and Neale, E.R.W., 1974, The northeastward termination of the Appalachian orogen, in Nairn, A.E.M. and Stehli, F.G. (eds.), The Ocean Basins and Margins, v. 2, the North Atlantic: Plenum, New York, p. 79-123.

Williams, Harold, and Smyth, W.R., 1973, Metamorphic aureoles beneath ophiolite suites and Alpine peridotites: Tectonic implications with west Newfoundland examples: Am. Jour. Sci., v. 273, p. 594-621.

Williams, Harold, and Stevens, R.K., 1974, The ancient continental margin of Eastern North America, in Burk, C.A. and Drake, C.L. (eds.), the geology of continental margins: Springer-Verlag, New York, N.Y., p. 781-796.

Wilson, J.T., 1966, Did the Atlantic close and then reopen? Nature, v. 211, p. 696-681.

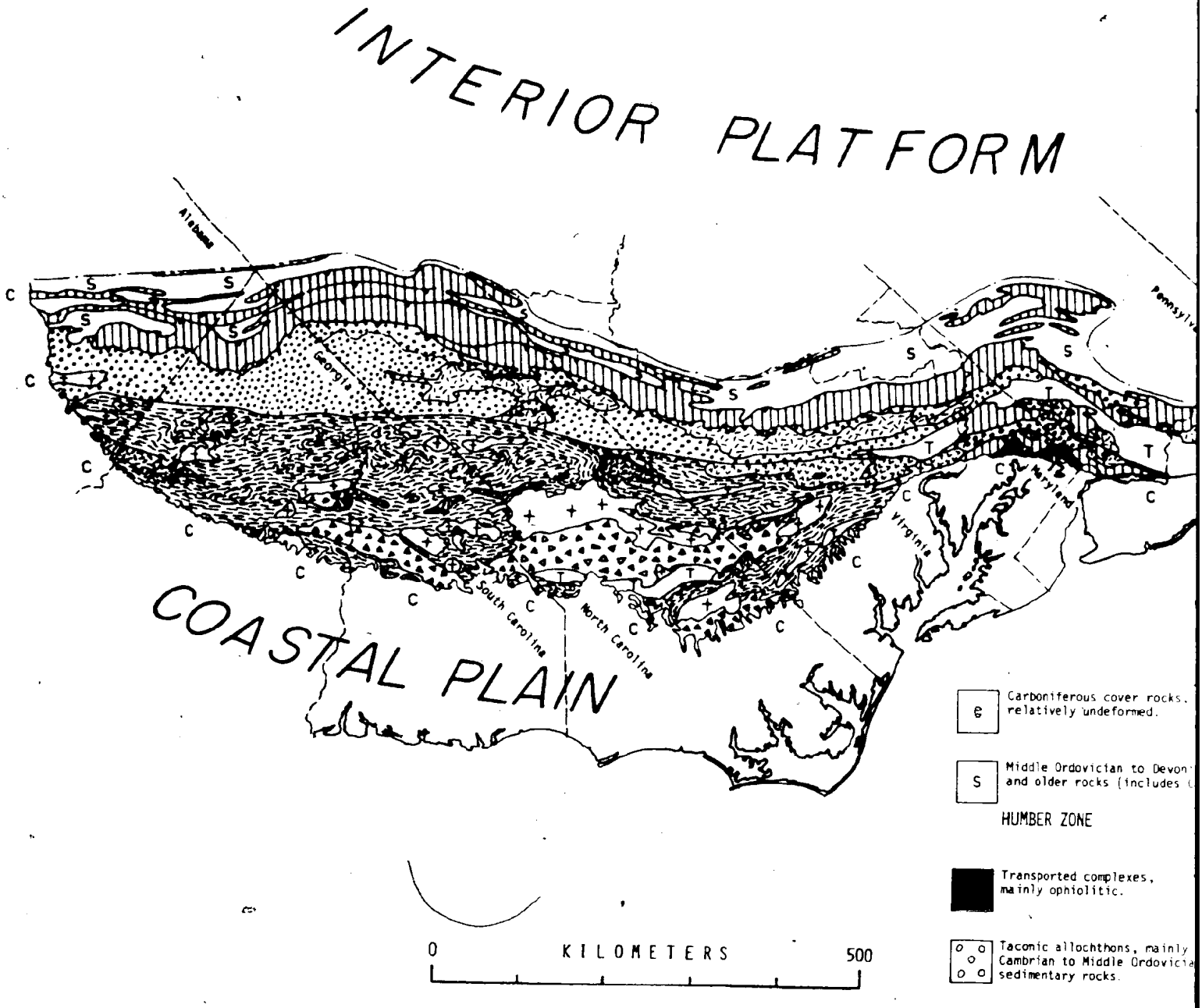
INTERIOR PLATFORM
COASTAL PLAIN
Alabama
Georgia
South Carolina
North Carolina
Virginia
Maryland
Pennsylv
C
S
T
0
KILOMETERS
500
Carboniferous cover rocks, relatively undeformed.
Middle Ordovician to Devon and older rocks (includes
HUMBER ZONE
Transported complexes, mainly ophiolitic.
Taconic allochthons, mainly Cambrian to Middle Ordovicia sedimentary rocks.
Cambrian to Middle Ordovicia carbonate sequence and overlying southeasterly-deri clastic sedimentary rocks.
Late Precambrian to Cambrian mainly clastic sedimentary rocks and associated rift-facies volcanic rocks, mostl in amphibolite facies.
Grenvillian inliers, commonl retrograded and deformed by Paleozoic orogenesis.

7

1 of

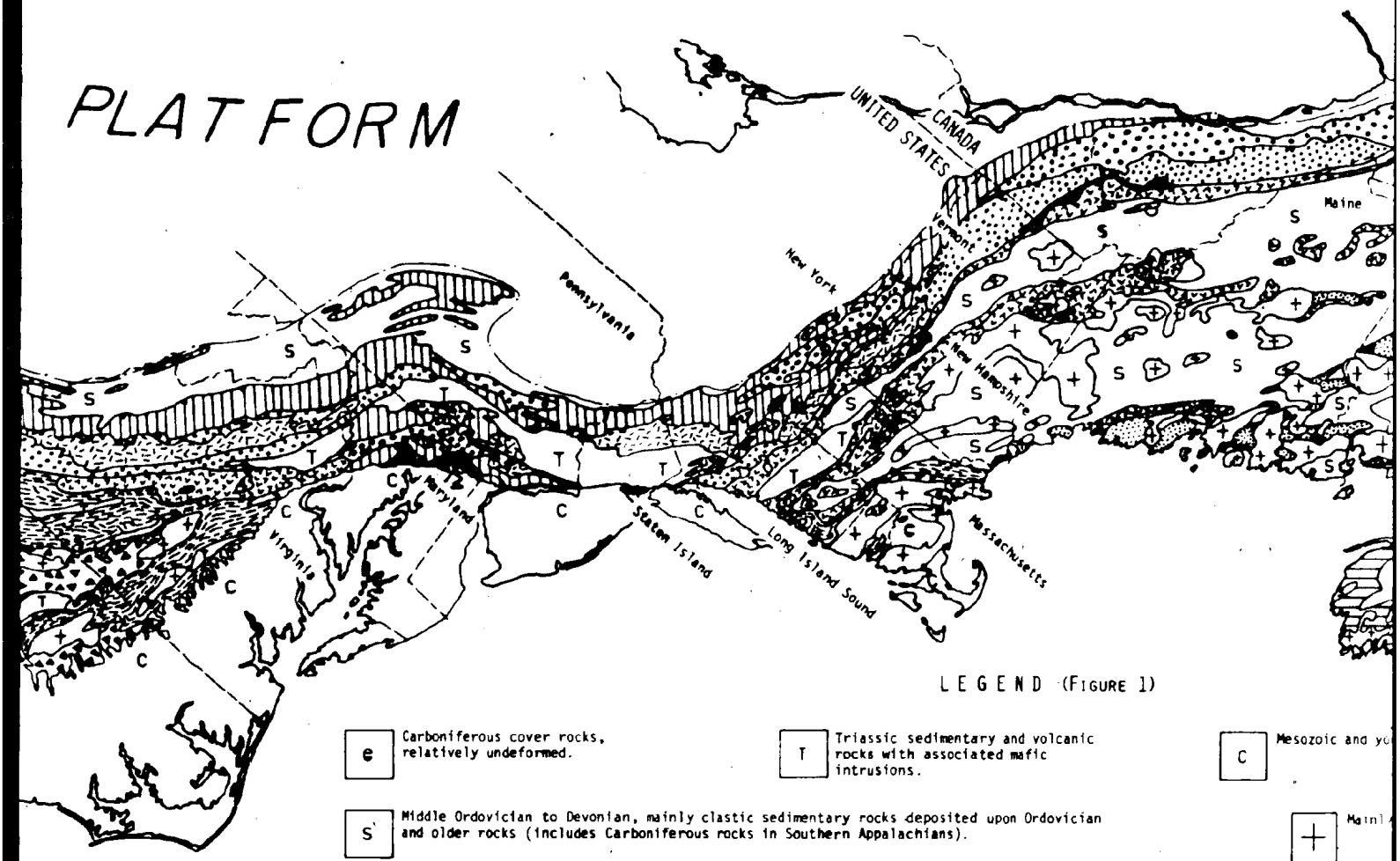

LEGEND (FIGURE 1)

e — Carboniferous cover rocks, relatively undeformed.

T — Triassic sedimentary and volcanic rocks with associated mafic intrusions.

C — Mesozoic and yo

S — Middle Ordovician to Devonian, mainly clastic sedimentary rocks deposited upon Ordovician and older rocks (includes Carboniferous rocks in Southern Appalachians).

+ — Mainl

HUMBER ZONE | DUNNAGE ZONE | GANDER ZONE | AVALO

Transported complexes, mainly ophiolitic.

TERS 500

Taconic allochthons, mainly Cambrian to Middle Ordovician sedimentary rocks.

Cambrian to Middle Ordovician marine facies volcanic rocks, slates, cherts, greywackes and mélange.

Cambria shales trilob

Cambrian to Middle Ordovician carbonate sequence and overlying southeasterly-derived clastic sedimentary rocks.

Mainly ophiolite complexes.

Lower Ordovician and older clastic sedimentary rocks.

Late Precambrian to Cambrian. mainly clastic sedimentary rocks and associated rift-facies volcanic rocks, mostly in amphibolite facies.

Amphibolite facies metamorphic rocks, mainly of unknown age and affinity.

Mainly cambria and vo

Grenvillian inliers, commonly retrograded and deformed by Paleozoic orogenesis.

Gneisses and mig dated at ~ 100 overlying marble

(24)



LEGEND (FIGURE 1)

imentary and volcanic
ssociated mafic

osited upon Ordovician
ans).

C — Mesozoic and younger cover rocks.

Mainly granitic intrusions

GANDER ZONE

AVALON ZONE

MEGUMA ZONE

dle Ordovician
olcanic rocks,
greywackes

Cambrian to Ordovician shales with Atlantic trilobite faunas

Lower Ordovician and older grey-wackes and slates

Lower Ordovician and older clastic sedimentary rocks.

Amphibolite facies metamorphic rocks, mainly of unknown age and affinity.

Mainly Late Pre-cambrian sedimentary and volcanic rocks.

Gneisses and migmatites, locally dated at ~ 1000 m.y. includes overlying marbles and quartzites.

1 3 of

PLATE I

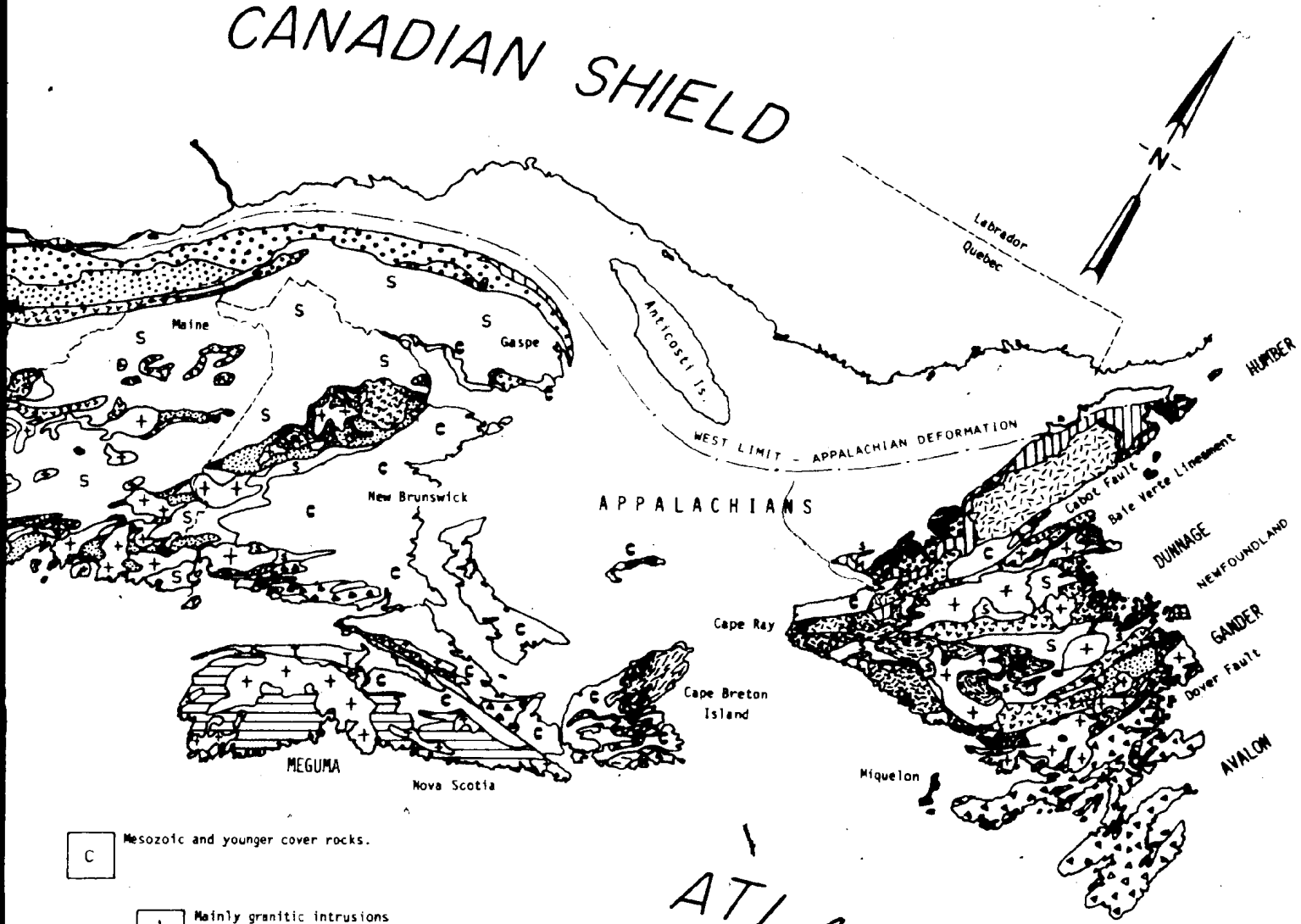

C — Mesozoic and younger cover rocks.

Mainly granitic intrusions

AVALON ZONE

MEGUMA ZONE

Cambrian to Ordovician shales with Atlantic trilobite faunas

Lower Ordovician and older grey-wackes and slates

Mainly Late Pre-cambrian sedimentary and volcanic rocks.

Gneisses and migmatites, locally dated at ~ 1000 m.y. includes overlying marbles and quartzites.

PLATE I

4 of 4



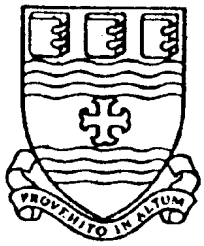

THE GEOLOGY OF THE ST. ANTHONY COMPLEX, NORTHWESTERN NEWFOUNDLAND — A NOTE

R.W. Talkington[1] and R.A. Jamieson[2]
[1]Department of Geology
Memorial University of Newfoundland
St. John's, Newfoundland, Canada
A1B 3X5

[2]Department of Geology
Dalhousie University
Halifax, Nova Scotia, Canada
B3H 3J5

Memorial University of Newfoundland
Department of Geology
Report No. 8
Contribution to I.G.C.P. Project 39

1979

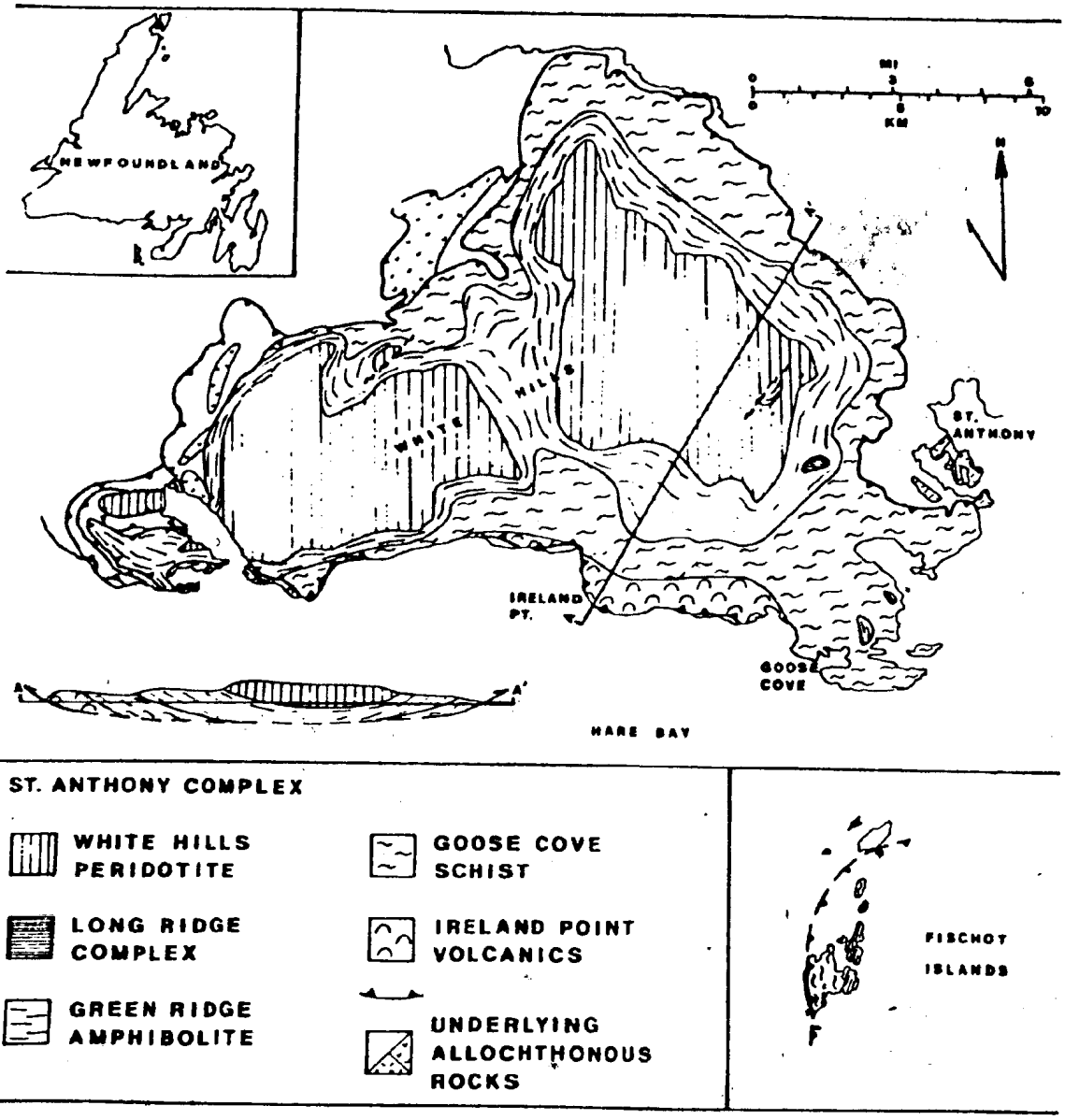

Figure 1 Generalized geological map of the St. Anthony Complex.

INTRODUCTION

The St. Anthony Complex, unlike the more extensively studied Bay of Islands Ophiolite Complex, has only recently become an ophiolite complex of intense geological study. As in the Humber Arm Allochthon, most early geological investigations of the Hare Bay Allochthon were concentrated on the sedimentary and volcanic sequences underlying the main ophiolite slices. Quite naturally, because of their relative proximity to one another, direct comparisons have been made between the rock associations of the two allochthons (Cooper, 1937; Tuke, 1968; Stevens, 1970; Smyth, 1971, 1973; Williams, 1975; Williams and Smyth, in press).

Since 1974, detailed studies of the upper slices of the allochthonous sequences, specifically the metamorphic aureole and the ultramafic massifs (White Hills Peridotite) have been carried out. Structural and microstructural studies of the peridotite, metamorphic aureole and structurally lower allochthonous slices are still ongoing. This work has shown that the St. Anthony Complex (Fig. 1) and specifically the White Hills Peridotite has features which readily distinguish it from the Bay of Islands ophiolite: I. only the ultramafic section of the ophiolite is preserved; II. harzburgite interlayered with spinel lherzolite forms about 85% of the peridotite; III. dunite occurs as layers, lenses and dikes throughout the peridotite; IV. olivine gabbro veins, found in the eastern massif, cut all rock types, and lie oblique to the tectonite fabric; V. there are rare occurrences of plagioclase lherzolite; VI. alkali pyroxenites are found between the peridotite and a well developed metamorphic aureole.

The purpose of this communication is to present in a synthesized form current results from the studies of the peridotite, metamorphic aureole and their relationships. Detailed descriptions of the peridotite and metamorphic aureole have been presented elsewhere (Riccio, 1976; Jamieson, 1979; Talkington, 1979; Jamieson and Talkington, in press; Talkington and Malpas, in press).

GENERAL FEATURES OF THE ST. ANTHONY COMPLEX

The St. Anthony Complex forms the structurally highest slice of the Hare Bay Allochthon (Williams and Smyth, in press). It includes from top to bottom, the White Hills Peridotite, the Long Ridge Metagabbro, the Green Ridge Amphibolite, the Goose Cove Schist and the Ireland Point Volcanics (Williams, 1975; Jamieson, 1979; Williams and Smyth, in press). The base of the Complex is defined by the Hare Bay thrust fault (Cooper, 1937) which cuts all the units and is post-metamorphic. Post-thrusting (Middle Ordovician) disturbances have caused mild upright folding and high angle faulting, affecting most rocks.

WHITE HILLS PERIDOTITE

The White Hills Peridotite is structurally the highest unit of the St. Anthony Complex. The peridotite crops out in two large massifs and a smaller outlier totaling approximately 150 Km^2. The minimum stratigraphic thickness of the peridotite is approximately 2 Km. Faulting and folding within the massifs makes an accurate estimate for the actual stratigraphic thickness impossible. Additionally, no satisfactory 'idealized' stratigraphic section, either lithological or chemical, may be constructed due to the complexity and density of faults and folds.

(a) Rock Types

Harzburgite and spinel lherzolite are the dominant rock types making up approximately 85% of the peridotite. Complex interlayering with dunite, with either sharp or diffuse contacts, difficulty in discerning clinopyroxene in the rocks and folding and faulting make it difficult to ascertain definite amounts of each rock type. The harzburgite and spinel lherzolite occur in layers which range in thickness from less than 1 mm to ½ m. Their lateral extent is highly variable ranging from a few metres to hundreds of metres. Units may pinch out, end abruptly or pass gradually into another

lithology. A 'homogeneous' primary rhythmic banding is commonly developed in these layers. The banding (here termed the foliation) is caused by variations in the olivine/orthopyroxene ratio. Contacts between bands are gradational and although bands of uniform thickness (< 2 cm) have been traced laterally for distances up to 300 m it is noticeable that when the dunite component increases, the persistence of the banding decreases. Locally, bands may thus be only a few metres long before they pinch out, pass into another lithology or are disrupted and occur as rafts in a dunite matrix.

Dunite, more common in the eastern massif (Fig. 1), occurs in several forms as layers, lenses, and dikes. Dunite layers range in thickness from less than 1 mm to tens of metres, though commonly averaging 1 to 10 cm. Layers are always parallel to the tectonite foliation and to layers of harzburgite and spinel lherzolite. Dunite layers may be continuous for centimetres or a few tens of metres, and only rarely can be traced for longer distances. Contacts with adjacent lithologies are sharp. The dunite is almost pure olivine except for 1-3% disseminated spinel. Spinel occurs rarely as seams in the dunite layers, generally not exceeding 3 to 4 mm in thickness and flattening of spinel parallel to foliation is common. The percentage of dunite as layers in any one locale and region is variable, ranging from less than 1% to 20%. Where higher percentages occur the other dunite types commonly are more abundant.

Sequences of layers are commonly found including: a) spinel lherzolite — dunite — spinel lherzolite — harzburgite; b) harzburgite - dunite — harzburgite; c) spinel lherzolite — dunite — spinel lherzolite; d) dunite — harzburgite; e) dunite — spinel lherzolite. Mineral chemistry of spinel from adjacent layers indicates that the spinel from the dunite reequilibrated to a chemistry similar to the spinel of the adjacent harzburgite or spinel lherzolite (Talkington and Malpas, in press).

Lenses of dunite range in size from small centimetre size pockets to bodies 50 m x 400 m. Lenses are always oblique to the tectonite foliation. Contacts with the country rock are sharp for both small and large pockets, but in the latter are more irregular. Xenoliths of harzburgite or spinel lherzolite are occasionally present close to the contact and apophyses of dunite from the enses extend a few metres into the country rock. Spinel occurs as disseminated crystals (1-4%) or as narrow discontinuous stringers in the lenses. Any sedimentological features that may have been defined by spinel (e.g. trough scours, graded beds, etc.) are no longer visible in the lenses.

Dunite dikes range in size from a few centimetres to approximately ½ m in width. Laterally they can never be traced for more than a few tens of metres, when they either end abruptly or taper out. No source region for the dunite dikes can be directly traced, but in regions where dunite lenses are common, dunite dikes are present in greater abundance. The anastomosing veinlets common to the larger dunite lenses are not included here with dunite dikes and the relationship between the two, if any, remains to be proven. The dikes are always oblique to the tectonite foliation and contacts between dunite dikes and country rocks are sharp. Spinel is disseminated throughout the dikes and in the longer dikes may occur concentrated as narrow (<4 mm) seams in the core region. Any flattening of spinels is parallel to the dike margins.

Pyroxenite veins can be divided into 3 types: clinopyroxenite (± secondary spinel); websterite (+ secondary spinel); orthopyroxenite (+ olivine; + spinel). Each type occurs in varying proportions throughout the peridotite. Collectively, the veins range in size from 1 mm to 15 cm in width and can be traced for hundreds of metres. They may either parallel the tectonite foliation or cut across it. Folded veins of pyroxenite (cpxite and opxite) occur throughout the peridotite sequence and appear to post-date the development of the tectonite foliation. Websterite veins are on average the widest and increase in abundance locally as dunite becomes more common. Chromite concentrations are associated with orthopyroxenite veins.

Gabbro veins (± olivine) crop out only on the eastern massif where they are restricted to a 200-300 m wide zone of the central and eastern part. The veins occur within the harzburgite — spinel lherzolite, and only rarely do they cut

dunite. They range in size from less than 1 mm to 40 cm in thickness and single veins have been traced laterally for approximately 20 m.

On the eastern part of the massif small olivine clinopyroxenite bodies can be mapped. Their size is not readily discernable since the outcrop is essentially felsenmeer, but they appear to be about 15 m long and 1-2 m wide. Numerous gabbro dikes are found in the area, and are presumed to be connected with those bodies although there is no clear evidence to prove this, though in one location gabbro dikes are found cutting the pyroxenite bodies (Talkington, 1979). Close to the bodies of pyroxenite, the density of gabbro dikes makes up as much as 40% of the rocks. This decreases to about 1% at a distance of 40 m. Thickness of dikes likewise decreases with distance from the bodies, but there is no apparent change in dike chemistry along their lengths. In some places rare zoned dikes, with plagioclase-rich margins and pyroxene- and olivine-rich cores, are observed. Although the exact shape of the pyroxenite bodies are not known, their long axes appears to parallel the tectonite fabric in surrounding rocks.

(b) Structural Features of the Peridotite

Two major planar fabrics are developed in the peridotite: 1) the tectonite fabric, persistent throughout the peridotite and 2) an emplacement foliation which locally overprints the tectonite fabric in the basal thrust zone and is restricted to the lower 25 m of the peridotite shoot. Three generations of folding are recognized in the peridotite. The earliest appears to be a mantle deformation and is reflected in isoclinal folds with thickened fold hinges. These are most easily seen where they fold pyroxenite veins within the peridotite. The second phase of folding produced recumbent folds in the lower parts of the peridotite and are thought to relate to emplacement. The last deformation is preserved as symmetrical folds with vertical axial planes, wavelengths average 30 m, but amplitudes may be as great as the total thickness of the complex. They are essentially late syn- or post-tectonic. All folds have northeast — southwest striking axial planes which plunge either northeast or southwest.

THE METAMORPHIC AUREOLE

The White Hills Peridotite is underlain by a metamorphic aureole up to 700 m thick, which ranges from upper amphibolite to lower greenschist facies rocks. It is exposed in the hills surrounding the peridotite, in the barrens between St. Anthony and Goose Cove, along the coast, and on the Fischot Islands, 11 km south of Goose Cove (Fig. 1).

The upper part of the aureole, referred to as the Green Ridge Amphibolite (Williams, 1975), comprises amphibolite facies metabasic rocks with minor marble bands. Near Brimstone Pond in the western White Hills, two-pyroxene amphibolite occurs in contact with the peridotite. Clinopyroxene-bearing amphibolite occurs in the eastern White Hills, while on the Fischot Islands the unit consists mainly of partially melted amphibolite. The amphibolites have a strong foliation trending nearly parallel to the contacts of the unit; in the White Hills it is parallel to the base of the peridotite. The typical mineral assemblage of the Green Ridge Amphibolite is hornblende + plagioclase (andesine) + quartz + sphene or ilmenite ± pyroxene. Metamorphic temperature estimates for a pressure of 3-5 kb range from 860°C at the contact to 680°C near the base of the unit (Jamieson, 1979).

The lower part of the aureole, referred to as the Goose Cove Schist (Smyth, 1973; Williams, 1975), comprises epidote amphibolite and greenschist facies metavolcanic and metasedimentary rocks. It is characterized by a strong schistosity which is complexly folded by at least two fold generations, the second also affecting the Green Ridge Amphibolite. The epidote amphibolites are characterized by the assemblage hornblende + plagioclase (albite-oligoclase — andesine) sphene + epidote + quartz, which grade into the overlying amphibolites with the loss of epidote from the assemblage. The greenschist contains actinolite + plagioclase (albite-oligoclase) + epidote + chlorite grading into epidote amphibolite with the loss of chlorite from the assemblage. Actinolite is always much more abundant than chlorite. Psammites and pelites are restricted to the lower part of the Goose Cove Schist, occurring mainly on the Goose Cove Peninsula

and the Fischot Islands where garnetiferous metachert is locally present. The most common assemblage is muscovite + chlorite + quartz + feldspar (albite and/or potassium feldspar) ± garnet, with biotite replacing chlorite at higher grades. Metamorphic temperature estimates, based on the phase assemblages in the metabasic rocks, are 550°C to 650°C for the epidote amphibolites and 350°C to 550°C for the greenschists, at pressures of 2 to 4 kb (Jamieson, 1979).

The Green Ridge Amphibolite is separated from the Goose Cove Schist by a biotite-rich mylonite zone 40 to 100 m thick. It is interpreted to have formed by potash metasomatism from the surrounding amphibolites late in the metamorphic episode which produced the aureole. The mylonite is localized near the epidote-out isograd, and trends approximately parallel to the surrounding metamorphic units.

The aureole also includes an enigmatic assemblage of gabbro, dunite, and anorthosite, inhomogeneously deformed and metamorphosed under amphibolite facies conditions, referred to as the Long Ridge Metagabbro (Jamieson, 1979). It occurs structurally above the Green Ridge Amphibolite, from which it may grade with increasing deformation, but its relationship to the White Hills Peridotite is not known. Spinel and clinopyroxene-bearing coronas around olivine in the least deformed metagabbros indicate reactions in the temperature range 850-910°C at pressures of 7-10 kb.

The lowest unit in the St. Anthony Complex is the Ireland Point Volcanics, a suite of undeformed pillow lavas and pyroclastic rocks which passes into the Goose Cove Schist with increasing deformation and metamorphic grade. Primary plagioclase, titanaugite, and olivine in these alkali basalts are extensively replaced by albite and chlorite, but actinolite does not occur below the transition to the Goose Cove Schist.

The Goose Cove Schist is interpreted to have formed by the deformation and metamorphism of the Ireland Point Volcanics and the Maiden Point Formation on the basis of lithological similarities and the observed gradational relationships. Primary features are obliterated from the Green Ridge Amphibolite except for local relict phase layering in the metagabbroic rocks and rare marble horizons. The rocks geochemically are tholeiitic to transitional. The composition and lithology of the Long Ridge Metagabbro resemble those of the Critical Zone (Malpas, 1976) assemblages in the Bay of Islands and other ophiolites, suggesting an origin near the base of the oceanic crust.

SUMMARY

The St. Anthony Complex is made up of an overlying peridotite sheet and an underlying metamorphic aureole. The peridotite though significantly resembling the ultramafic section found in other ophiolites, has features that readily distinguish it from most. Notable is the high percentage of spinel lherzolite. For example, in the Bay of Islands Complex spinel lherzolite occurs at the base of the harzburgite sequence and is only approximately 200 m thick, whereas the minimum stratigraphic thickness for the White Hills Peridotite is 2 Km. Lenses of dunite are found throughout the peridotites as are gabbro veins and mafic 'chambers'. No gabbro veins are found in the Bay of Islands harzburgite-spinel lherzolite units. Gabbro veins and 'pegmatitic' gabbro veins have, however, been reported from the Lanzo Massif (Boudier, 1976), the Oman (Smewing, pers. comm.), and Ronda Massif (Dickey, *et al.*, 1977; Obata, 1977).

The origin of the White Hills Peridotite is suggested to be similar to that for all ophiolite ultramafic sections. Ophiolite ultramafic sections that contain harzburgite as the dominant rock type have undergone approximately 20-25% partial fusion of 'primitive' mantle material (Malpas, 1976). The high proportion of spinel lherzolite in the White Hills Peridotite suggests a lower percentage of partial fusion (15-20%, Talkington, unpublished data) of the primitive mantle material; leaving a layered spinel lherzolite — harzburgite — dunite sequence, with localized regions of high — pressure gabbro crystallization (Talkington, 1979). Additionally, the common occurrence of dunite layers and lenses throughout the peridotite may define regions where partial fusion products of the spinel lherzolite were unable to rise through the ultramafic pile. High

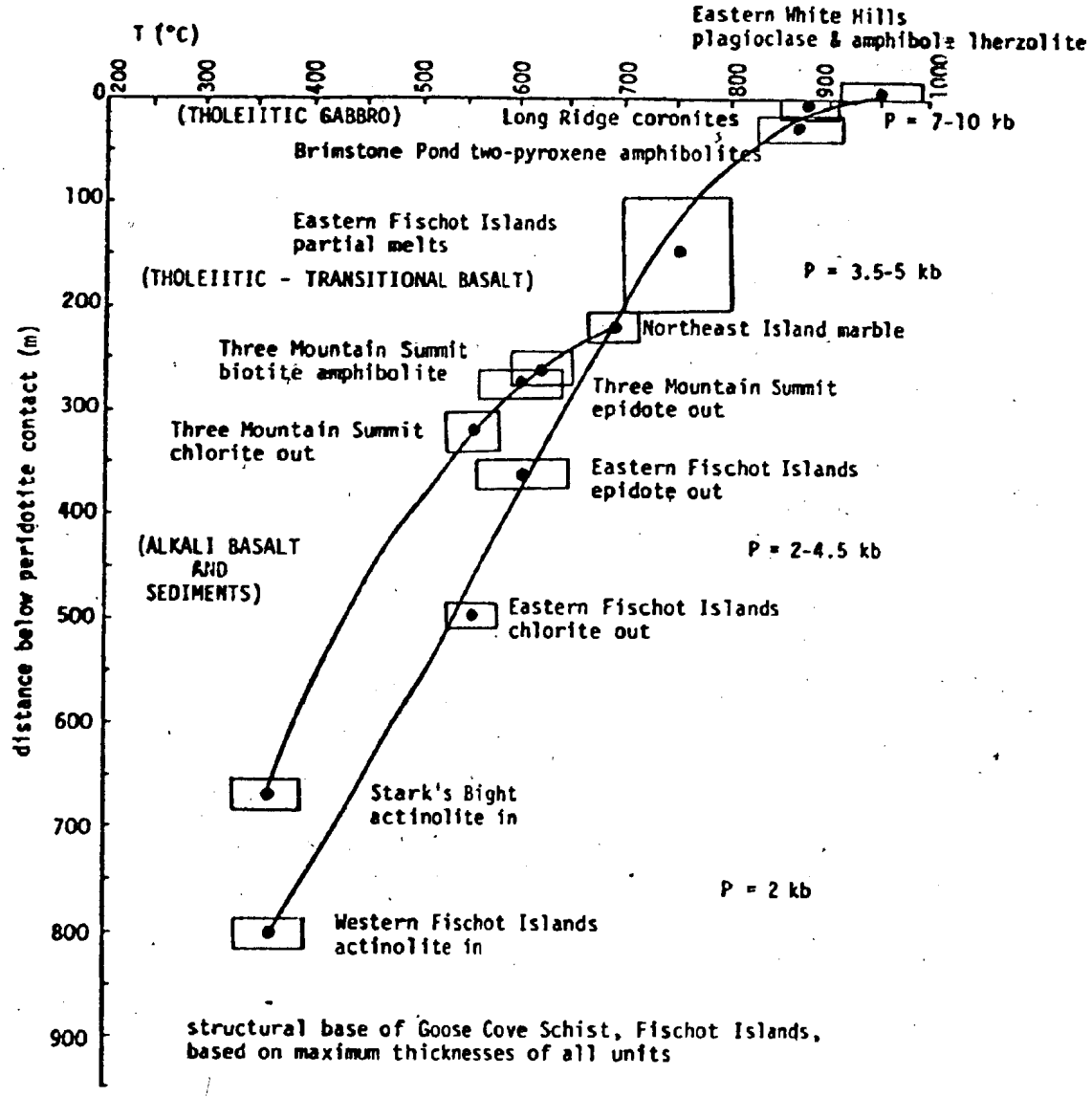

Figure 2 Composite metamorphic profile through the St. Anthony Complex aureole, showing the pressures and temperatures of metamorphism and protoliths of the metamorphic rocks in parentheses.

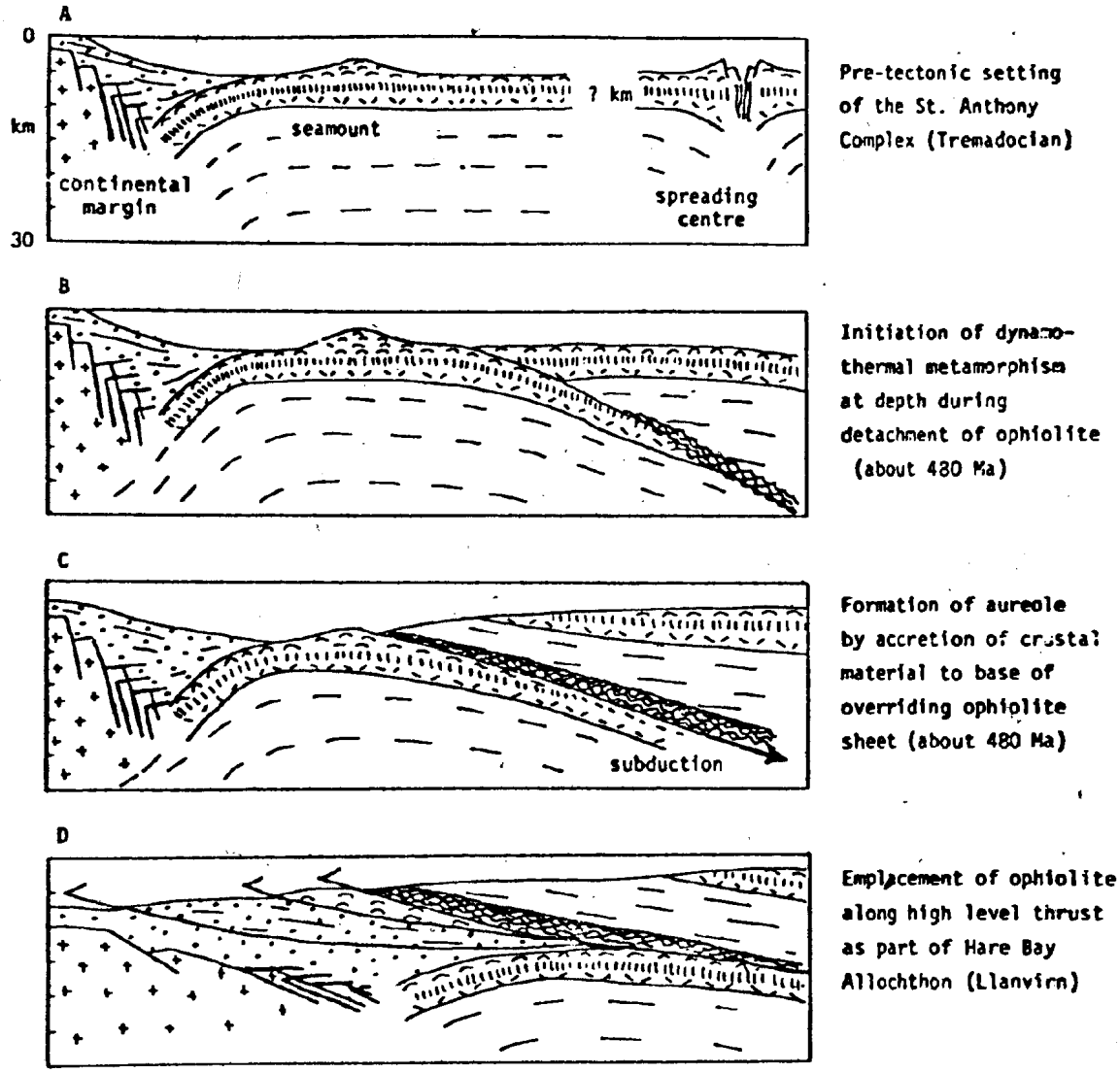

Figure 3 Model for the formation and emplacement of the St. Anthony Complex, based on regional geology and detailed study of the metamorphic aureole.

pressure crystallization of these liquids produced only olivine and spinel and possibly some pyroxenite vein material instead of lower pressure rocks of basaltic mineralogy. It is quite probable that the gabbro veins represent the crystallization product of this magma, formed at lower pressures.

A definite lithological zonation is preserved within the aureole beneath the White Hills Peridotite. Tholeiitic metagabbros (Long Ridge Metagabbro and part of the Green Ridge Amphibolite) occur immediately below the peridotite, along with a small amount of alkaline plutonic material. The amphibolites and epidote amphibolites beneath the metagabbros (most of the Green Ridge Amphibolite and part of the Goose Cove Schist) were derived from compositionally homogeneous tholeiitic to transitional basaltic rocks. Below this are greenschists (Goose Cove Schist) derived from the upper part of the Ireland Point Volcanics and from psammitic and pelitic sediments of the Maiden Point Formation. The regional geology suggests that the Ireland Point Volcanics were Tremadocian alkali basalts formed close to the continental margin where the Maiden Point Formation turbidites were deposited. Thus the aureole is a lithologically composite feature.

Estimates of the metamorphic conditions through the aureole indicate a gradient in terms of both pressure and temperature (Fig. 2). The highest pressure (7-10 kb) and temperature (850-950°C) assemblages occur at the peridotite — aureole contact, grading down into relatively low pressure (less than 2 Kb) and temperature (about 350°C) assemblages at the transition from the Goose Cove Schist to the Ireland Point Volcanics.

The aforementioned evidence supports the following model for the formation of the St. Anthony Complex (Fig. 3):

1) Generation of the White Hills peridotite at a spreading centre.
2) Peridotite and its cover were detached at depth (between 20 and 30 Km) along an incipient thrust probably related to the initiation of a subduction zone.
3) As this ophiolite sheet overrode the adjacent oceanic crust, fragments of the rocks which it encountered en route to the surface — gabbros, volcanics, and sediments — attached to its base as the locus of displacement moved downwards away from the contact (cf. Malpas, 1976). The aureole thus grew downward by the accretion of rocks of progressively shallower provenance which were deformed and metamorphosed during the transport of the ophiolite sheet.
4) Final emplacement of the peridotite and its aureole was accomplished along high level thrust faults, and may have been facilitated by isostatic rebound of a partially subducted continental margin.

This model is consistent with the two-stage ophiolite emplacement hypothesis discussed for western Newfoundland by Malpas and Stevens (this volume).

[AMERICAN JOURNAL OF SCIENCE, VOL. 280, MAY, 1980, P. 459-477]

A JACUPIRANGITE–SYENITE ASSEMBLAGE BENEATH THE WHITE HILLS PERIDOTITE, NORTHWESTERN NEWFOUNDLAND

R. A. JAMIESON* and R. W. TALKINGTON

Department of Geology, Memorial University,
St. John's, Newfoundland, Canada A1B 3X5

ABSTRACT. An assemblage of alkaline rocks, including jacupirangite, alkaline pyroxenite, hornblende gneiss, and syenitic mylonite, occurs between the White Hills Peridotite and its metamorphic aureole. Undeformed jacupirangite and alkaline pyroxenite (titanaugite + kaersutite + ilmenite + apatite) at the top of the sequence grade downward into hornblende gneiss (titaniferous amphibole + sodic plagioclase) and syenitic mylonite (albite + augite + hornblende + magnetite) at the base of the sequence. The ultramafic alkaline rocks have high concentrations of FeO, CaO, TiO_2, and P_2O_5, whereas the felsic rocks have high concentrations of Na_2O and Al_2O_3. Their mineralogy and geochemistry are consistent with an origin as a single igneous suite which differentiated either by crystal fractionation or liquid immiscibility. The geological setting of the jacupirangite–syenite assemblage suggests that it may have formed part of an oceanic island that was overridden by the White Hills Peridotite thrust sheet during its Taconic emplacement.

INTRODUCTION

An assemblage of undersaturated alkaline rocks, ranging from jacupirangite to syenite, occurs within the St. Anthony Complex of northwestern Newfoundland. The rocks are sandwiched between the White Hills Peridotite, the ultramafic remnant of an ophiolite, and a dynamothermal aureole formed during its emplacement (Williams and Smyth, 1973; Jamieson, ms). Although alkali basalts commonly occur beneath ophiolite suites (for example, Strong, 1974; LaPierre and Rocci, 1976; Jamieson, 1977), to the authors' knowledge this association of alkaline ultramafic rocks with transported oceanic rocks is unique.

The alkaline assemblage includes jacupirangite, alkaline pyroxenite, hornblende gneiss, and syenitic mylonite. It was previously mapped as part of the amphibolite unit underlying the peridotite (Williams and Smyth, in press) but was recognized by the authors during detailed work on the St. Anthony Complex. In this paper, the geology, mineralogy, petrology, and possible origin of these rocks are discussed in the context of their geological setting within the St. Anthony Complex.

GEOLOGICAL SETTING

The St. Anthony Complex comprises the White Hills Peridotite, a harzburgite–lherzolite tectonite, and an underlying aureole of upper amphibolite facies to lower greenschist facies rocks which grade into undeformed alkali basalts (Williams and Smyth, 1973; Jamieson, ms) (fig. 1). The sequence is roughly horizontal, with peridotite on the top and pillow lavas at the base, and has been virtually undisturbed since its emplacement during the Taconic orogeny. The protoliths of the metamorphic rocks included gabbros and basalts of tholeiitic to transitional

* Present address: Department of Geology, Dalhousie University, Halifax, Nova Scotia B3H 3J5 Canada

affinities, alkaline basaltic rocks, graywacke, and minor marble and chert. The entire complex probably originated as part of an ocean basin and an adjacent continental margin.

The jacupirangite–syenite assemblage is restricted to the northeastern part of the White Hills, where it outcrops in three streambeds and at one lakeshore locality (fig. 1, A to D). Its upper contact with the peridotite is locally visible, but its lower contact is not exposed. Since none of the sections is complete, a composite sequence is described below.

Mylonitic peridotite, locally containing thin layers of pargasite, directly overlies the alkaline rocks. It is typical of the basal zone of the White Hills Peridotite and shows no sign of having been intruded or altered by the alkaline rocks beneath it. Where exposed, the contact is sharp and planar. At each locality somewhat different lithologies occur adjacent to the peridotite: at A it is alkaline pyroxenite, at B, jacupirangite, at C, amphibole-rich jacupirangite, and at D, hornblende gneiss. Only at D are the alkaline rocks at the peridotite contact strongly deformed.

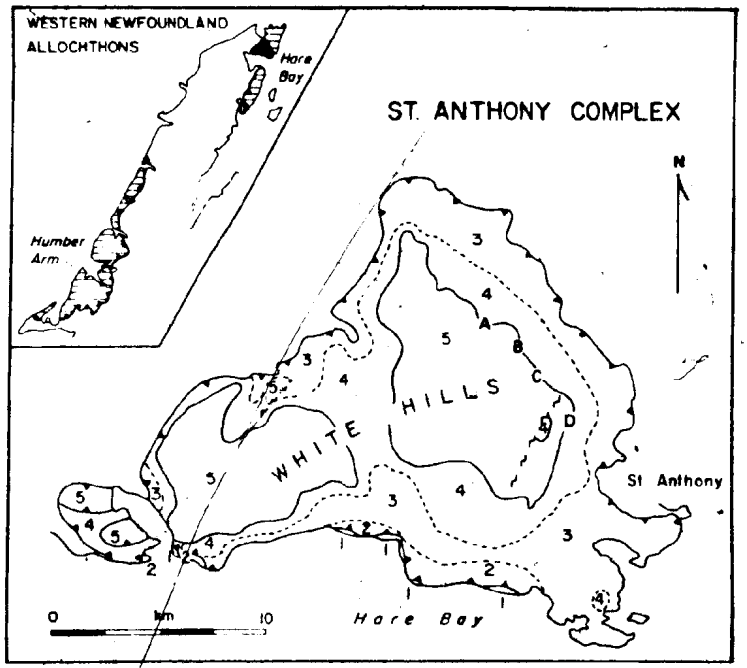

Fig. 1. Location map with insert showing position of the St. Anthony Complex (black) within the Hare Bay Allochthon. (1) Maiden Point Formation (underlying allochthonous flysch); (2) Ireland Point Volcanics (alkali basalt); (3) Goose Cove Schist (greenschist); (4) Green Ridge Amphibolite (amphibolite); (5) White Hills Peridotite (harzburgite–lherzolite with minor dunite, pyroxenite, gabbro); (A,B,C,D) outcrops of the jacupirangite–syenite assemblage.

The jacupirangite and alkaline pyroxenite are dense, equigranular, purple-black rocks, consisting mainly of clinopyroxene with variable amounts of amphibole, mica, ilmenite, and apatite. Except for locally common diffuse green veins, the ultramafic rocks are fresh. This massive, pyroxene-rich zone may be up to 5 m thick.

Hornblende gneiss underlies the jacupirangite–alkaline pyroxenite unit. It is distinguished by a marked increase in the proportion of amphibole to pyroxene, by the appearance of feldspar, and by the development of a gneissic fabric trending parallel to the base of the White Hills Peridotite. The result is a 1 to 4 m thick zone of banded black and white gneiss, containing augen of amphibole surrounded by fine-grained plagioclase. At locality A, instead of gneiss, there is a 3 to 4 m thick unit of black, friable hornblendite containing thin, laterally continuous, monomineralic layers of fine-grained plagioclase. A lens of massive alkaline pyroxenite occurs in the middle of this zone, with the hornblendite and feldspar bands deflected around it (pl. 1-A). Locally, hornblende crystals over 10 cm long can be found.

The lowest unit of the jacupirangite–syenite assemblage consists of fine-grained, gray to white syenitic mylonite, containing thin bands of mafic minerals and rare zircon porphyroclasts in a plagioclase matrix. The mafic layers define both a strong foliation parallel to the base of the White Hills Peridotite and a northwest-southeast trending lineation.

The contact of the jacupirangite–syenite assemblage with the underlying rocks is not exposed. It probably abuts structurally concordant amphibolites of the metamorphic aureole, which also have foliations parallel to the base of the peridotite, but the presence of intervening lithologies or a major structural break cannot be ruled out.

MINERALOGY

The changes in the overall appearance of the rocks in the field correspond to changes in their mineralogy and microstructure. The transition from massive jacupirangite through hornblende gneiss to syenitic mylonite can be traced in thin section as amphibole and feldspar increase at the expense of clinopyroxene and as the grain size decreases with the increasing intensity of deformation (fig. 2). Modal analyses are listed in table 1, and representative microprobe analyses are given in table 2.

The jacupirangite contains equigranular, purple-brown, slightly pleochroic, subhedral titanaugite. Interstitial deep red-brown titaniferous biotite and kaersutite are common, kaersutite locally mantling titanaugite. These silicates form 70 to 80 percent of the jacupirangite; ilmenite, apatite, and small amounts of carbonate account for the rest (pl. 1-B). The apatite has the purple cathodoluminescence characteristic of that from alkaline rocks (Smith and Stenstrom, 1965). Locally the ilmenite forms bulbous embayments into the clinopyroxene. Equigranular carbonate forms 20 percent of one sample (table 1, 241); as the carbonate is not associated with veins or secondary minerals, has sharp boundaries

PLATE 1



A. Lens of massive alkaline pyroxenite, 50 cm across, within zone of interlayered syenite (white) and hornblendite (black), locality A, figure 1.

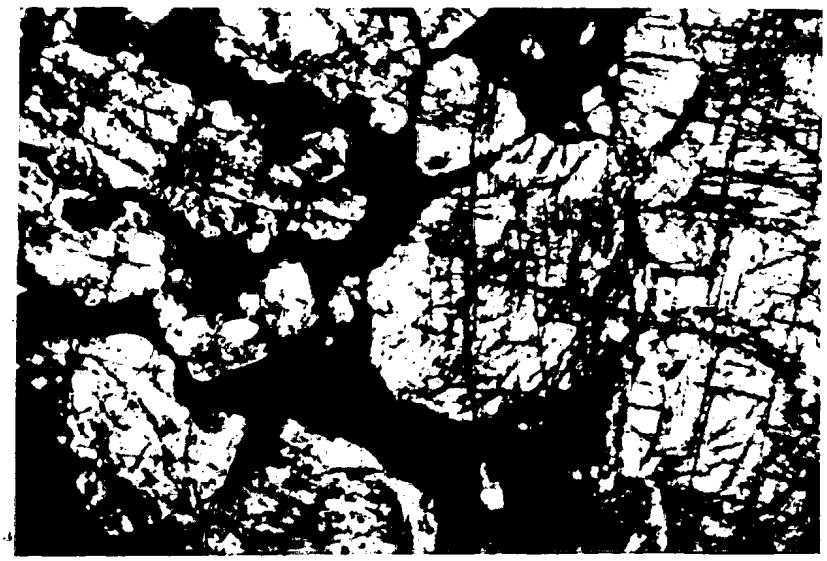

B. Jacupirangite (RJ76-492) showing titanaugite (gray) in matrix of ilmenite (black) and apatite (white). Plane polarized light; width of field about 2.5 mm.

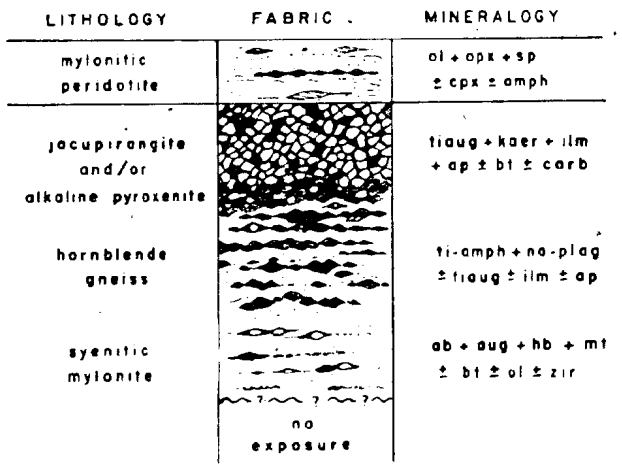

Fig. 2. Schematic section through the jacupirangite–syenite assemblage showing changes in lithology, fabric, and mineralogy and relative structural positions of the units. Diagram not to scale, but the relative proportions of the units (except peridotite) are approximately as shown.

TABLE 1

Modal analyses (volume percent) of jacupirangites, alkaline pyroxenites, hornblende gneisses, and syenitic mylonites

	Jacupirangites				Alkaline pyroxenites	
	RJ76-492	RJ76-491	RJ76-490	RS-71-241	77WH82	RJ76-489
Clinopyroxene	48.4	61.1	32.3	13.7	60.6	22.5
Amphibole	24.4	13.3	47.4	24.1	1.6	63.3
Biotite	1.0	7.3	0.2	5.1		
Oxides	17.4	11.2	12.1	15.9	0.1	0.9
Apatite	8.4	5.7	7.5	3.8		1.3
Calcite	0.3	1.4	0.5	20.7	1.3	
Secondary*					36.4	8.3
Feldspar						3.5
Olivine						
Zircon						

	Hornblende gneisses			Syenitic mylonites		
	RJ76-488	RJ76-487	RJ76-486	RJ76-496	RJ76-497	RJ77-651
Clinopyroxene	1.1		0.5	3.0	4.4	1.0
Amphibole	51.2	32.1	47.0	5.5	3.4	1.1
Biotite	0.6			7.9	4.3	1.5
Oxides	3.4	0.8	1.2	2.9	3.5	5.2
Apatite	3.1	1.3	2.3	2.6	0.8	
Secondary*						
Feldspar	40.6	65.9	49.0	78.2	83.6	85.9
Olivine						4.4
Zircon					0.1	0.9

* "Secondary" refers to the augite–green hornblende assemblage which replaces titanaugite in some samples.

TABLE 2
Representative microprobe analyses from the

(A) Clinopyroxene			(B) Amphibole		
	491-3-7[a]	651-3-1[b]	491-2-2[c]		486-1-1[d]
SiO_2	46.25	52.41	37.54		37.00
TiO_2	1.87	0.48	4.75		3.55
Al_2O_3	7.69	2.15	14.74		14.95
Cr_2O_3		0.01			
Fe_2O_3*	5.02	2.27	0.20		2.17
FeO	8.83	11.82	19.88		17.34
MnO	0.39	0.19	0.31		0.41
MgO	7.47	10.79	5.98		6.66
CaO	22.03	17.81	11.37		10.77
Na_2O	1.35	1.94	1.67		2.80
K_2O			1.97		1.12
NiO					
TOTAL	100.90	99.85	98.41		96.77
Si	1.755	1.978	5.780		5.751
Al^{IV}	0.247	0.022	2.220		2.249
Al^{VI}	0.096	0.073	0.456		0.491
Ti	0.053	0.014	0.550		0.415
Cr					
Fe^{3+}	0.143	0.064	0.024		0.254
Fe^{2+}	0.280	0.373	2.560		2.254
Mg	0.422	0.608	1.372		1.543
Mn	0.013	0.006	0.040		0.054
Ca	0.895	0.720	1.876		1.794
Na	0.099	0.142	Na^{M4}	0.124	0.206
			Na^{A}	0.375	0.638
			K	0.387	0.222

* Ferric iron calculated stoichiometrically: for clinopyroxene, assuming 4 cations and 6 oxygens; for amphiboles, assuming 23 oxygens and no Fe^{2+} or Mn in the M4 site (maximum ferric iron)

[a] Titanaugite from jacupirangite
[b] Augite from syenitic mylonite
[c] Ferroan kaersutite from jacupirangite
[d] Titaniferous ferroan pargasite from hornblende gneiss

against subhedral silicates, and occurs in an otherwise undeformed and unaltered rock, it is considered a primary phase. Two samples that contain over 80 percent titanaugite ± kaersutite with little ilmenite or apatite are referred to here as alkaline pyroxenites. A penetrative fabric is not developed in these ultramafic rocks, although large, homogeneous titanaugite crystals are locally recrystallized into polygonal aggregates.

The degree of replacement of titanaugite along grain boundaries and cleavages by titaniferous amphibole (ranging from kaersutite to titaniferous ferropargasite in composition according to the classification of Leake, 1978) increases toward the base of the jacupirangite unit, until amphibole is the most abundant mafic silicate. At the base of the ultramafic zone, bands of sodic plagioclase (albite to oligoclase) appear, coinciding with the development of a strong foliation; amphibole-rich jacupirangite is transformed over a distance of less than 1 m to a "hornblende" gneiss (the field name is retained for simplicity, since the amphiboles have a range of compositions and a correspondingly variable precise nomenclature).

jacupirangite–syenite assemblage

(C) Feldspar			(D) Biotite	(E) Olivine
	488-1-1[a]	651-1-1[b]	491-1-1[c]	651-2-1[d]
SiO_2	64.02	66.24	33.41	33.09
TiO_2			8.37	
Al_2O_3	22.25	21.09	16.00	
Cr_2O_3				0.04
Fe_2O_3*	0.06			
FeO*			22.72	51.49
MnO			0.20	0.45
MgO			6.51	15.25
CaO	2.61	0.68		
Na_2O	10.25	11.42	0.35	
K_2O	0.04	0.04	7.98	
SrO	0.48	0.25		NiO 0.07
TOTAL	99.71	99.72	95.54	100.39
Si	2.838	2.915	5.175	1.000
Al	1.162	1.095	2.922	
Ti			0.975	
Cr				0.001
Fe	0.002		2.943	1.300
Mg			1.506	0.686
Mn			0.026	0.010
Ca	0.124	0.032		
Na	0.881	0.975	0.105	
K	0.002	0.002	1.577	
Sr	0.012	0.007		Ni 0.001

* For feldspars, total iron = ferric iron; for biotite and olivine, total iron = ferrous iron

[a] Sodic oligoclase, hornblende gneiss
[b] Albite, syenitic mylonite
[c] Titaniferous biotite, jacupirangite
[d] Fayalitic olivine, syenitic mylonite

The hornblende gneiss consists of augen of titaniferous pargasite 2 to 5 mm across, locally containing inclusions of ilmenite, apatite, and titanaugite, in a matrix of fine-grained sodic plagioclase and amphibole of the same composition. The plagioclase is invariably anhedral with serrated grain boundaries; larger grains show kinked polysynthetic twinning and extensive subgrain development.

The syenitic mylonites that underlie the hornblende gneiss contain up to 85 percent alkali feldspar (with albite much more abundant than potassium feldspar), with variable amounts of augite, fayalitic olivine, zircon, hornblende, biotite, and magnetite. The mafic minerals occur in granular layers within the mylonitic albite-rich matrix. Green, sodium-rich augite occurs as clusters of isolated grains elongated parallel to the foliation or as augen with pressure shadows of magnetite and biotite. Pale yellow, iron-rich olivine and magnetite form thin networks of granular crystals. Rare zircon porphyroclasts up to 10 mm across contain euhedral biotite inclusions. The strong foliation and lineation and augened porphyroclasts in an extremely fine-grained matrix serve to classify these rocks as mylonites according to the definition of Bell and Etheridge (1973).

Two types of secondary mineral assemblages are present. One consists of diffuse veins and patches of green salite, green hornblende, plagioclase, and carbonate in massive alkaline pyroxenite. The salite forms bleached zones in the titanaugite surrounding irregular aggregates of the other secondary minerals. Trails of tiny inclusions, independent of existing grain boundaries, cleavages, or fractures, cross the pyroxenite between the areas of altered clinopyroxene; similar inclusion trails are locally associated with the replacement of titanaugite by kaersutite. The secondary pyroxene and hornblende are poorer in Ti, Al, Na, Fe, and Ca than the primary minerals that they replace.

A post-kinematic greenschist facies alteration produced thin veins of chlorite and epidote, and small, irregular patches of epidote, chlorite, and sericite in all lithologies. Blue-green hastingsite replaces kaersutite adjacent to these veins. Clinopyroxene is locally replaced by fibrous actinolite, while in the syenitic mylonites, sodic amphibole forms fibrous rims on augite and magnetite.

GEOCHEMISTRY

Fourteen samples, representing all the lithologies from jacupirangite to syenite, have been analyzed for major and trace elements (table 3). The entire suite is undersaturated with the exception of the two most siliceous syenites, which contain small amounts of normative hypersthene.

The geochemical data must be interpreted with caution, in the absence of quantitative data on the behavior of the mobile components in these rocks during the intense deformation that affects the base of the sequence. One essentially unaltered jacupirangite (table 3, RJ76-491) can be used as a reliable guide to the original composition of the ultramafic rocks, but there is no pristine equivalent of the syenitic mylonites. Comparison of sample 491 with the adjacent amphibole-rich jacupirangites (490, 492) shows considerable depletion of Rb and Ba in the altered samples, suggesting that the hydration was accompanied by chemical changes even in undeformed rocks. The syenitic mylonites show no evidence of pervasive metasomatic alteration (apart from local post-kinematic sericitization), but the intense deformation may have obscured replacement textures.

Within the limitations of the geochemical data, some features of the bulk rock compositions are remarkable. The jacupirangites have very high concentrations of TiO_2, P_2O_5, and total FeO, whereas the syenitic mylonites have low concentrations of these components and very high Al_2O_3 and Na_2O. The hornblende gneisses have intermediate compositions. High CaO and low TiO_2 and P_2O_5 in the alkaline pyroxenites reflect their mineralogy and suggest a cumulate origin for these rocks. The ultramafic rocks have high concentrations of Ba, Nb, Sr, Rb, and Zr, whereas the syenites are relatively poor in these elements with the exception of Zr in two zircon-bearing samples. This overall geochemical pattern is common in alkaline mafic-ultramafic complexes, sometimes associated with carbonatite, such as Magnet Cove, Arkansas (Erickson and Blade, 1963) and Mount Yamaska, Quebec (Ghandi, 1970).

Both alkaline pyroxenite analyses show anomalously high concentrations of MgO, Cr, and Ni and low concentrations of Ba, Sr, Al_2O_3, and Na_2O, even when their mineralogy is taken into account. Both samples contain secondary salite–hornblende–plagioclase–carbonate assemblages, suggesting that metasomatism associated with this alteration may have affected their bulk compositions.

PETROGENESIS

A complete petrological description of the jacupirangite–syenite assemblage should account for the relationships among the various lithologies, the distribution of major and trace elements, and the relationship of the entire sequence to the rest of the St. Anthony Complex. Unfortunately, some critical pieces of evidence are missing. Deformation has disrupted the sequence, possibly removing large parts of it, and obliterated the original contact relationships and primary textures in the gneisses and mylonites. The possible redistribution of mobile elements has already been noted. For these reasons, the petrogenesis of the alkaline rocks can only be dealt with in terms of the relative merits of alternative hypotheses.

The jacupirangite and alkaline pyroxenite are the only parts of the sequence preserving an igneous paragenesis and texture. Titanaugite crystallized first, kaersutite and biotite later. Titanaugite was partly replaced by kaersutite, probably in response to an increase in the volatile and alkali concentration in the interstitial melt with advancing crystallization. The non-silicate matrix phases apparently formed contemporaneously with the clinopyroxene, since the titanaugite contains ilmenite and apatite inclusions, and the ilmenite contains titanaugite inclusions. The presence of small amounts of carbonate in the jacupirangite suggests that the alkaline ultramafic rocks crystallized from a CO_2-rich melt. The mineralogy and composition of the alkaline pyroxenites suggests that they are titanaugite cumulates from this melt (fig. 3).

Recent work on the effect of CO_2 on the melting and crystallization behavior of peridotite has shown that CO_2-saturated melts are more alkaline and silica-undersaturated than H_2O-rich melts at similar temperatures and pressures (for example, Mysen and Boettcher, 1975; Koster van Groos, 1975; Boettcher, Mysen, and Modreski, 1975; Wyllie, 1977; Eggler, 1976). Mysen and Boettcher (1975) found that nepheline-normative melts were produced by partial melting of natural peridotite for vapor compositions with a mole fraction of $CO \geqslant 0.5$. Similar results have been obtained on synthetic systems (Boettcher, Mysen, and Modreski, 1975; Eggler, 1975, 1976); apparently, the high activity of CO_2 raises the liquidus temperature. With increasing pressure at constant temperature and mole fraction of CO_2, Mysen and Boettcher (1975) found an increase in the FeO/MgO ratio of the melt. It is conceivable that the iron-rich jacupirangite and alkaline pyroxenite crystallized from a melt derived directly by high-pressure anatexis of peridotite in the presence of a CO_2-rich vapor. However, olivine is generally a liquidus

TABLE 3

Major and trace element compositions and CIPW norms of jacupirangites, alkaline pyroxenites, hornblende gneisses, and syenitic mylonites

	Jacupirangites				Alkaline Pyroxenites			Hornblende Gneisses				Syenitic Mylonites		
	RJ76-492*	RJ76-491*	RJ76-490*	77MH91**	77MH54**	77MH82**	RJ76-489*	RJ76-488*	RJ76-487*	RJ76-486*	RJ76-496*	RJ76-497*	RJ77-651**	RJ77-654**
SiO_2	34.46	36.18	34.08	33.60	31.40	45.30	43.35	43.87	46.23	46.09	54.63	57.47	63.80	65.70
TiO_2	5.14	4.40	5.45	5.00	5.20	1.86	2.63	2.83	2.79	2.26	1.04	0.98	0.27	0.10
Al_2O_3	6.58	10.28	8.97	7.68	8.33	7.52	11.03	16.20	16.52	16.86	17.53	18.42	18.80	19.50
Fe_2O_3	6.85	2.12	2.35	3.70	8.97	3.36	2.81	2.23	2.22	2.12	1.89	1.59	n.d.	n.d.
FeO	13.65	17.01	17.13	14.65	13.81	6.29	9.54	9.32	8.80	8.95	3.23	3.06	2.16	0.60
MnO	0.31	0.38	0.36	0.29	0.35	0.21	0.22	0.17	0.26	0.24	0.13	0.11	0.03	0.01
MgO	6.67	6.71	5.30	7.19	7.63	10.47	9.32	3.44	2.79	3.11	3.94	1.76	0.93	0.30
CaO	17.92	13.63	15.59	17.90	16.25	21.05	14.84	10.55	8.86	9.07	3.89	3.97	1.19	0.82
Na_2O	1.26	0.97	1.80	1.32	1.22	1.23	2.20	4.45	5.16	5.31	6.56	7.20	9.20	10.55
K_2O	0.18	1.81	1.03	0.33	0.53	0.06	0.93	1.16	1.12	1.14	1.48	2.32	1.30	0.16
P_2O_5	2.16	0.68	1.78	3.25	3.60	--	0.15	1.60	1.16	1.29	0.34	0.29	--	--
L.O.I.	2.43	3.67	3.76	3.71	1.66	1.49	2.42	2.08	2.18	2.09	3.21	1.70	0.74	0.49
TOTAL	97.61	97.85	97.60	98.47	98.61	98.84	99.44	97.90	98.09	98.53	97.84	98.87	98.42	98.23
							Trace Elements (ppm)							
Zr	238	275	295	196	216	175	143	118	127	154	151	489	744	105
Sr	949	1461	1653	532	1339	786	661	2854	2651	2446	1645	1992	869	1140
Rb	1	48	5	5	6	4	12	9	10	10	33	23	20	1
Zn	163	193	201	148	175	73	94	91	117	98	63	63	29	18
Cu	44	23	63	59	75	13	57	23	33	18	13	13	11	12
Ba	140	2250	539	124	397	77	752	1386	1752	950	1485	1653	416	273
Nb	24	102	142	22	36	4	23	17	85	34	18	19	7	3
Pb	1	5	2	--	14	9	--	--	2	1	6	1	--	--
Ni	10	30	11	21	39	132	163	10	10	7	6	2	12	9
Cr	1	54	--	14	27	134	390	6	--	5	--	10	9	12

V	362	250	270	338	342	184	286	165	136	124	47	44	12	--
Ga	22	29	23	22	20	17	18	20	19	16	18	16	23	20
							CIPW Norms (wt. %)							
qz														0.92
or							5.66	7.13	6.88	6.97	9.22	14.08	7.86	0.97
ab							1.08	21.61	30.24	27.76	58.28	56.87	76.94	91.26
an	12.51	19.94	14.63	15.06	16.18	15.43	17.99	21.65	19.35	19.45	14.78	11.39	6.31	4.59
ne	6.14	4.83	9.04	6.48	5.77	5.87	9.80	9.52	8.21	10.14	0.13	3.09		
lc	0.89	9.12	5.23	1.64	2.53	0.29								
cor														0.34
(di)	(48.40)	(27.73)	(32.77)	(37.94)	(32.48)	(67.00)	(46.25)	(19.42)	(16.60)	(16.32)	(3.29)	(6.45)	(0.09)	
wo	24.72	13.84	16.27	19.21	16.73	35.17	23.87	9.72	8.27	8.13	1.72	3.30	0.04	
en	13.99	5.86	6.33	9.85	10.32	25.82	15.08	4.27	3.37	3.31	1.21	1.90	0.02	
fs	9.68	8.03	10.16	8.87	5.44	6.02	7.30	5.44	4.95	4.88	0.36	1.25	0.03	
(hy)													(4.43)	(1.74)
en													1.74	0.76
fs													2.69	0.97
(ol)	(5.80)	(24.23)	(18.74)	(14.86)	(10.80)	(2.63)	(9.47)	(7.83)	(7.06)	(8.63)	(8.48)	(3.15)	(1.16)	
fo	2.56	8.62	5.69	6.54	6.50	0.94	6.17	3.26	2.70	3.29	6.40	1.82	0.43	
fa	1.96	13.03	10.07	6.49	3.77	0.24	3.29	4.57	4.37	5.34	2.08	1.33	0.73	
la	1.28	2.57	2.97	1.82	0.53	1.45								
mt	10.56	3.34	3.73	5.75	13.41	5.07	4.19	3.36	3.35	3.18	2.89	2.37		
il	10.38	9.08	11.34	10.18	10.19	3.68	5.14	5.59	5.51	4.44	2.08	1.91	0.52	0.19
ap	5.34	1.72	4.53	8.09	8.63		0.36	3.87	2.80	3.10	0.83	0.69		

-- not detectable n.d. not determined

Trace element analyses by XRF on powder pellets

* Major element analyses by XRF on fused pellets. Analyst: R. A. Jamieson. RJ76-492 to 486: loc. B, numbers increasing toward peridotite; RJ76-496, 497: loc. C.

** Major element analyses by atomic absorption. Analyst: G. Andrews. 77WH91: loc. B; 77WH54: loc. C; 77WH82, RJ77-651, 652: loc. A.

phase in basic and ultrabasic undersaturated alkaline systems (Edgar, 1974), and olivine is common in alkaline pyroxenites and the rocks associated with them (Upton, 1967). The absence of olivine and the very low concentrations of Cr, Ni, and MgO suggest that olivine fractionation played a role in the development of the iron-rich magmas from which the jacupirangite and alkaline pyroxenite crystallized.

A major problem centers on the origin of the leucocratic rocks now represented by syenitic mylonites. Possible relationships between the ultramafic and felsic rocks include the following:

1. the two lithologies are unrelated and were juxtaposed as the result of deformation;

2. the syenites were produced by fenitization associated with the emplacement of the alkaline ultramafic rocks;

3. the syenites were produced by partial melting during metamorphism;

4. the syenites and jacupirangites were part of the same igneous suite and were related by (i) crystal fractionation or (ii) liquid immiscibility.

The first two possibilities can be quickly dismissed. Tectonic interleaving of originally discrete rock units on the scale displayed by the hornblende gneisses and the banded hornblende–syenite unit (pl. 1-A) is highly unlikely on mechanical grounds. The mineralogical similarity of the syenitic mylonites to fenites is superficial, as no aegirine or acmite occurs, and the sodic amphibole is clearly post-kinematic. Fenitization generally involves desilication, even where basic rocks are affected (Ver-

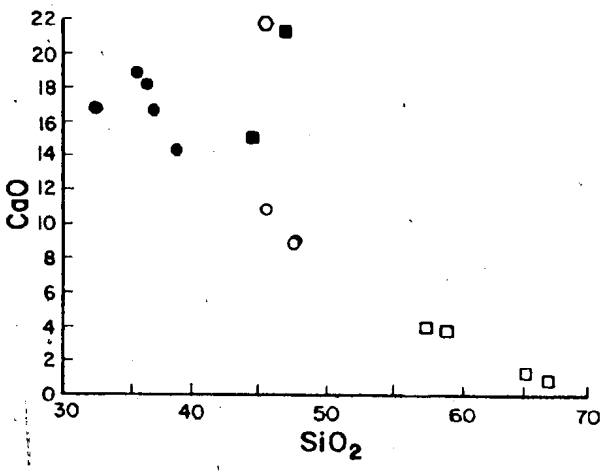

Fig. 3. CaO versus SiO_2 (wt percent, anhydrous), showing compositions of jacupirangite (closed circles), alkaline pyroxenite (closed squares), hornblende gneiss (open circles), syenitic mylonite (open squares), and average titanaugite (open hexagon).

woerd, 1966), whereas considerable SiO_2 must be added to produce syenite from the basic and ultrabasic material surrounding the alkaline rocks.

Upper amphibolite facies conditions caused partial melting in some parts of the aureole beneath the White Hills Peridotite (Jamieson, ms). The correlation between deformation and the occurrence of syenitic rocks suggests that they could have formed as a result of the metamorphism. However, as a unit, the syenites are characterized by decreasing concentrations of most trace elements, including Rb and Ba, with increasing SiO_2 (table 3, last four analyses), independent of the degree of deformation or structural position of the samples within the syenite unit. This pattern is not consistent with a simple partial melting model, which would predict the concentration of incompatible elements in the earliest, most silica-rich melts (for example, Carmichael, Turner, and Verhoogen, 1974, p. 632). The coincidence of the felsic material with the zone of most intense deformation can be accounted for by the relative ease of recrystallization of plagioclase compared to amphibole and pyroxene, and the partial melting hypothesis is therefore considered unlikely.

The remaining possibility is that the syenitic mylonites and jacupirangites were originally part of a single igneous suite which evolved through either crystal fractionation or liquid immiscibility. Alkaline pyroxenites, jacupirangites, and syenites commonly form parts of strongly differentiated alkaline complexes, although gabbro and olivine-rich rocks are generally present (for example, Upton, 1967; Perrault, 1970; Grapes, 1975).

In the first case, the various lithologies would represent either liquids or cumulates formed during the differentiation of an alkaline basic or ultrabasic magma. Figure 3 shows CaO plotted against SiO_2 as an example of the major element distributions in the sequence. The diagram shows the clustering of the jacupirangite, hornblende gneiss, and syenite compositions and illustrates that the accumulation of titanaugite accounts for the alkaline pyroxenites. Accumulation of titanaugite–kaersutite–ilmenite–apatite rocks, corresponding to the jacupirangites, from a basic melt, possibly similar in composition to the hornblende gneisses, could produce a differentiation trend towards the syenites. The scarcity of rocks of gabbroic composition is puzzling, and the clustering of compositions would not be expected if the rocks formed part of a continuous evolutionary sequence, but the assemblage is probably incomplete owing to deformation. The high Zr and Nb contents of the ultramafic rocks are unusual if they are cumulates, since they apparently lack Zr and Nb-concentrating phases like zircon, perovskite, or anatase.

Liquid immiscibility is an alternative differentiation mechanism that could explain the relationships between the rocks. According to this hypothesis, the ultramafic and felsic rocks would represent the two liquid compositions, with the hornblende gneiss the mixed zone in which separation occurred. Recent experimental work on the origin of ocellar alkaline ultramafic rocks and lunar basalts has shown that many synthetic and natural systems have fields of liquid immiscibility (for example,

Roedder and Wieblen, 1971; Hess and others, 1975; Naslund, 1976; Philpotts, 1976; Hess, 1977; Roedder, 1978). Generally, one of the immiscible liquids is enriched in FeO, MgO, and CaO, and the other in SiO_2, Al_2O_3, Na_2O, and K_2O. Partitioning of minor and trace elements like TiO_2, P_2O_5, MnO, Zr, Cr, Sr, Ba, and the rare earth elements into the mafic melt is favored, with particularly high partition coefficients for TiO_2 and P_2O_5 (Watson, 1976). Figure 4 shows TiO_2 and P_2O_5 plotted against $(Na_2O + K_2O + Al_2O_3)/(FeO_T + MgO + MnO + CaO)$ to emphasize the extent of their concentration in the mafic phase. This extreme enrichment is compatible with the immiscibility hypothesis (but also with ilmenite and apatite accumulation). The distribution of trace elements is also generally compatible with this model, although Zr is locally concentrated

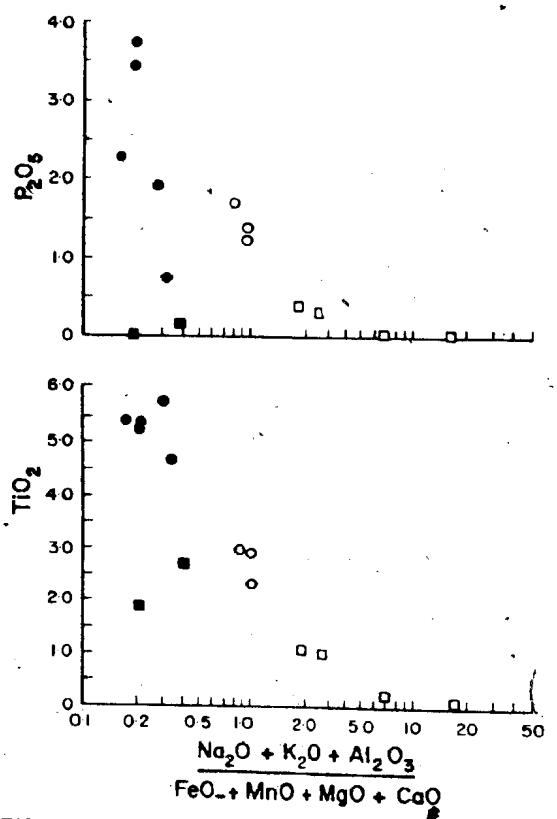

Fig. 4. TiO_2 and P_2O_5 (wt percent, anhydrous) versus $(Na_2O + K_2O + Al_2O_3)/(FeO + MnO + MgO + CaO)$, showing extent of partition of minor components into the ultramafic rocks. Note logarithmic scale on abscissa. Symbols as for figure 3.

in zircon-bearing syenites, and Sr and Ba are irregularly distributed, possibly as the result of later alteration. On an AFM diagram (fig. 5) the jacupirangites and syenites plot on opposite sides of the miscibility gap outlined by Philpotts (1976) for natural rocks; the jacupirangites plot near the composition at which fractionated lunar KREEP basalts split into two liquid phases (Hess and others, 1975). The overall pattern, however, is not radically different from that observed for many alkaline suites (Barker, 1978). The liquid immiscibility model has the advantage of not requiring the removal of large amounts of basic material during the deformation. However, pyroxenes of different composition occur in the ultramafic and felsic rocks (table 2); this is not strictly compatible with immiscibility, although it may reflect chemical evolution subsequent to liquid separation. (for example, Philpotts, 1977). The textural evidence required to test the immiscibility hypothesis further has been obliterated by the deformation.

Given the fragmentary nature of the alkaline sequence, it is concluded that although the rocks probably formed part of a single igneous suite, an unambiguous choice between crystal fractionation and liquid immiscibility cannot be made.

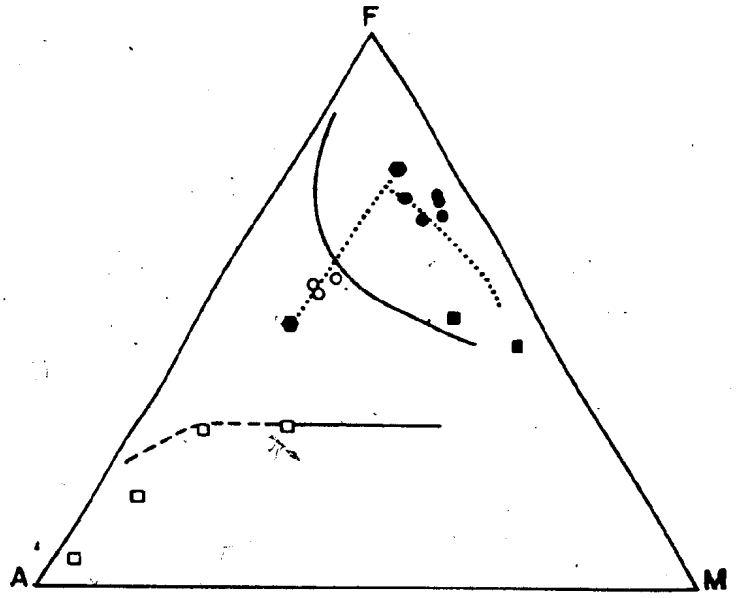

Fig. 5. AFM diagram (wt percent) showing compositions of alkaline rocks with respect to the fields of immiscibility shown by Philpotts (1976) (solid line-dashed line). Closed hexagons indicate the compositions of coexisting mafic and felsic liquids described by Hess and others (1975) following fractionation of lunar KREEP basalt along path shown by dotted line.

DISCUSSION

From the preceding sections, the following features bearing on the origin of the alkaline assemblage are evident:

1. the jacupirangite–syenite assemblage occurs between a transported peridotite and its metamorphic aureole; no intrusive contacts are preserved, nor has any petrological relationship of the alkaline rocks to any others in the St. Anthony Complex been discovered in thorough studies of both the peridotite and the aureole;

2. ultramafic rocks form the structural top of the alkaline assemblage, mafic rocks the middle, and felsic rocks the base; this parallels an increase in deformation downward away from the peridotite contact (fig. 2);

3. the mineralogy and geochemistry of the assemblage are consistent with its evolution as a single alkaline suite through either crystal fractionation or liquid immiscibility, subsequently modified by metamorphism (particularly the replacement of clinopyroxene by amphibole).

Apart from detailed petrogenetic arguments, the origin of the jacupirangite–syenite assemblage would pose no problem were it not for its geological setting. Clearly, an iron-rich alkaline magma, generated in the upper mantle by melting in the presence of a CO_2-rich fluid and probably modified by olivine fractionation, underwent differentiation to form a suite ranging from jacupirangite to syenite. However, the overwhelming majority of similar alkaline rock suites has been described from continental environments where they are generally associated with rifting (for example, Gittins, 1966). It is difficult to explain the present setting of these rocks within a sequence derived from an ocean basin and contiguous continental slope and rise deposits. No continental shelf or cratonic rocks have been recognized in the St. Anthony Complex or in any of the underlying thrust sheets (Jamieson, ms; Williams and Smyth, in press).

The emplacement relationships of the jacupirangite–syenite assemblage, as constrained by the geology, are puzzling. Peridotite, with a mylonitic fabric clearly related to its emplacement, abuts undeformed jacupirangite. No intrusive contact is preserved. The alkaline rocks are strongly deformed at their base where they are presumably in tectonic contact with the amphibolites of the aureole underlying the White Hills Peridotite. As only gentle post-emplacement folding has affected the St. Anthony Complex, the deformation of the alkaline rocks must post-date the formation of the mylonite in the peridotite, and pre-date the final emplacement of the St. Anthony Complex (Llanvirn).

The alkaline rocks occur at the base of the steep slope of the eastern White Hills massif, a topographic feature that elsewhere coincides with the base of the peridotite. In terms of their fabric and location, they form the base of the White Hills Peridotite structural unit. In terms of their time of deformation, however, they should form part of the metamorphic aureole, which gives a $^{40}Ar/^{39}Ar$ age of 480 Ma (Dallmeyer, 1977). The most likely explanation is that the alkaline rocks were over-

ridden by the peridotite during its tectonic displacement from the mantle, subsequently becoming attached to the base of the ophiolite thrust sheet and deformed with it. This is consistent with the model proposed for the formation of the St. Anthony Complex (Jamieson, this), which appears to have been built up by the progressive accretion of oceanic material to the base of an overriding ophiolite sheet. This has resulted in the inversion of a pseudo-stratigraphic sequence through structural imbrication, with metamorphism obscuring the dislocations between the units, and could account for the upside-down nature of the alkaline assemblage, where dense jacupirangite occurs at the top and light syenite occurs at the base.

There are two types of alkaline rocks in the St. Anthony-Strait of Belle Isle region to which the jacupirangite–syenite assemblage might have been related. A suite of alkaline to transitional basalts, possibly once part of a seamount located near a continental margin, forms the base of the St. Anthony Complex (Jamieson, 1977 and ms). Although there are some mineralogical similarities, no direct connection can be shown between the two rock suites. It is possible that the jacupirangite–syenite assemblage formed part of a plutonic complex associated with a seamount. Alkaline complexes occur in the cores of some islands such as Tahiti (McBirney and Aoki, 1968) and the Canaries (Gastesi, 1969; Borley, Suddaby, and Scott, 1971; Dillon and Sougy, 1974) and may be more common in oceanic environments than is generally believed simply because they are small, deep-seated bodies that are difficult to sample.

A geographically more remote possibility is a connection with the alkaline intrusions of the St. Lawrence rift valley, part of a system several thousand kilometers long which has been the site of alkaline magmatism since the late Precambrian (Doig, 1970; Philpotts, 1978). At Mutton Bay on the Strait of Belle Isle a syenitic complex was emplaced at 568 Ma (Doig and Barton, 1968), while Ordovician alkalic rocks occur in eastern Quebec. The possible time-space relationships of the jacupirangite–syenite assemblage to the St. Lawrence rift system are extremely vague, as the only constraint on its age is that it predate the 480 Ma emplacement of the St. Anthony Complex and as it has been transported a considerable distance as part of the Hare Bay Allochthon. However, since some modern continental fracture systems are continuous with oceanic transform faults or seamount chains (for example, Charlie Fracture Zone, Haworth, 1977; Newfoundland Seamounts, Sullivan, ms), it is conceivable that both the alkali basalts and the jacupirangite–syenite assemblage were associated with an oceanic fracture zone related to the St. Lawrence rift valley system.

ACKNOWLEDGMENTS

The authors thank D. Press and G. Andrews for assistance with the chemical analyses, A. Thompson for assistance with the microprobe analyses, and G. Campbell for help with the drafting. C. A. Gallagher and N. Noel provided excellent assistance in the field. Special thanks go to

D. F. Strong and T. J. Calon for helpful comments during the preparation of the manuscript and W. R. Smyth, who provided the original thin sections and sample locations. Referees comments were very useful in the final revision of the manuscript, although the reviewers do not necessarily agree with the conclusions. R. A. Jamieson acknowledges the National Research Council of Canada for financial support through a 1967 Science Scholarship and operating grants awarded to D. F. Strong in 1976 and 1977. R. W. Talkington was supported by a Memorial University Fellowship and an NRC operating grant held by J. G. Malpas.

References

Barker, D. S., 1978, Magmatic trends on alkali–iron–magnesium diagrams: Am. Mineralogist, v. 63, p. 531-534.

Bell, T. H., and Etheridge, M. A., 1973, Microstructure of mylonites and their descriptive terminology: Lithos, v. 6, p. 337-348.

Boettcher, A. L., Mysen, B. O., and Modreski, P. J., 1975, Melting in the mantle: Phase relationships in natural and synthetic peridotite–H_2O and peridotite–H_2O–CO_2 systems at high pressures: Physics Chemistry Earth, v. 9, p. 855-867.

Borley, G. D., Suddaby, P., and Scott, P., 1971, Some xenoliths from the alkalic rocks of Teneriffe, Canary Islands: Contr. Mineralogy Petrology, v. 31, p. 102-114.

Carmichael, I. S. E., Turner, F. J., and Verhoogen, J., 1974, Igneous Petrology: New York, McGraw-Hill, 739 p.

Dallmeyer, R. D., 1977, Diachronous ophiolite obduction in western Newfoundland: evidence from $^{40}Ar/^{39}Ar$ ages of the Hare Bay metamorphic aureole: Am. Jour. Sci., v. 277, p. 61-72.

Dillon, W. P., and Sougy, J. M. A., 1974, Geology of west Africa and the Canary and Cape Verde Islands, *in* Nairn, A. E. M., and Stehli, F. G., eds, The Ocean Basins and Margins: New York, Plenum Press, p. 315-390.

Doig, R., 1970, An alkaline rock province linking Europe and North America: Canadian Jour. Earth Sci., v. 7, p. 22-28.

Doig, R., and Barton, J. M., 1968, Ages of carbonatites and other alkaline rocks in Quebec: Canadian Jour. Earth Sci., v. 5, p. 1401-1407.

Edgar, A. D., 1974, Experimental studies, *in* Sørenson, H., ed, The Alkaline Rocks: New York, John Wiley & Sons, p. 355-389.

Eggler, D. H., 1975, CO_2 as a volatile component of the mantle: the system Mg_2SiO_4–SiO_2–H_2O–CO_2: Physics Chemistry Earth, v. 9, p. 869-881.

———— 1976, Composition of the partial melt of carbonated peridotite in the system CaO–MgO–SiO_2–CO_2: Carnegie Inst. Washington Yearbook 75, p. 623-626.

Erickson, R. L., and Blade, L. V., 1963, Geochemistry and petrology of the alkalic igneous complex at Magnet Cove, Arkansas: U.S. Geol. Survey Prof. Paper 426, 95 p.

Gastesi, P., 1969, Petrology of the ultramafic and basic rocks of Betancuria Massif, Fuerteventura Island (Canarian Archipelago): Bull. volcanol., v. 33, p. 1008-1038.

Ghandi, S. S., 1970, Petrology of the Monteregian intrusions of Mount Yamaska, Quebec: Canadian Mineralogist, v. 10, p. 452-484.

Gittins, J. 1966, Summaries and bibliographies of carbonatite complexes, *in* Tuttle, O. J., and Gittins, J., eds., Carbonatites: New York, Intersci. Publishers, p. 417-541.

Grapes, R. H., 1975, Petrology of the Blue Mountain Complex, Marlborough, New Zealand: Jour. Petrology, v. 16, p. 371-428.

Haworth, R. T., 1977, The continental crust northeast of Newfoundland and its ancestral relationship to the Charlie Fracture Zone: Nature, v. 266, p. 246-249.

Hess, P. C., 1977, Structure of silicate melts: Canadian Mineralogist, v. 15, p. 162-178.

Hess, P. C., Rutherford, M. J., Guillemette, R. N., Ryerson, F. J., and Tuchfield, H. A., 1975, Residual products of fractional crystallization of lunar magmas: an experimental study: Sixth Lunar Sci. Conf. Proc., v. 1, p. 895-909.

Jamieson, R. A., 1977, A suite of alkali basalts and gabbros associated with the Hare Bay Allochthon of western Newfoundland: Canadian Jour. Earth Sci., v. 14, p. 546-556.

———— ms, 1979, The St. Anthony Complex, northwestern Newfoundland: A petrological study of the relationship between a peridotite sheet and its dynamothermal aureole: Ph.D. thesis, Memorial Univ., Newfoundland.

Koster Van Groos, A. F., 1975, The effect of high CO_2 pressures on alkalic rocks and its bearing on the formation of alkalic ultrabasic rocks and the associated carbonatites: Am. Jour. Sci., v. 275, p. 163-185.

Lapierre, H. and Rocci, G., 1976, Le volcanisme alcalin du Sud-Ouest de Chypre et le probleme de l'ouverture des regions tethysiennes au Trias: Tectonophysics, v. 30, p. 299-313.

McBirney, A. R., and Aoki, K., 1968, Petrology of the island of Tahiti: Geol. Soc. America Mem. 116, p. 523-556.

Mysen, B. O., and Boettcher, A. L., 1975, Melting of a hydrous mantle: II. Geochemistry of crystals and liquids formed by anatexis of a mantle peridotite at high pressures and high temperatures as a function of controlled activities of H_2O, H_2, and CO_2: Jour. Petrology, v. 16, p. 549-593.

Naslund, H. R., 1976, Liquid immiscibility in the system $KAlSi_2O_6$–$NaAlSi_2O_6$–FeO–Fe_2O_3–SiO_2 and its applications to natural magmas: Carnegie Inst. Washington Yearbook 75, p. 592-597.

Perrault, G., ed., 1970, Alkaline rocks: the Monteregian Hills: Canadian Mineralogist, v. 10, p. 295-598.

Philpotts, A. R., 1976, Silicate liquid immiscibility: its probable extent and petrogenetic significance: Am. Jour. Sci., v. 276, p. 1147-1177.

———— 1977, Archean variolites — quenched immiscible liquids: Discussion: Canadian Jour. Earth Sci., v. 14, p. 139-144.

———— 1978, Rift-associated igneous activity in eastern North America, *in* Neumann, E.-R., and Ramberg, I. B., eds., Petrology and Geochemistry of Continental Rifts: Dordrecht, D. Reidel, p. 133-154.

Roedder, E., 1978, Silicate liquid immiscibility in magmas and in the system K_2O–FeO–Al_2O_3–SiO_2: an example of serendipity: Geochim. et Cosmochim. Acta, v. 42, p. 1597-1617.

Roedder, E., and Weiblen, P. W., 1971, Petrology of silicate melt inclusions, Apollo 11 and Apollo 12 and terrestrial equivalents, *in* Proc. Second Lunar Science Conference: Geochim. et Cosmochim. Acta, Suppl. 2, v. 1, p. 507-528.

Smith, J. V., and Stenstrom, R. C., 1965, Electron-excited luminescence as a petrological tool: Jour. Geology, v. 73, p. 627-635.

Strong, D. F., 1974, An "off-axis" alkali volcanic suite associated with the Bay of Islands ophiolite, Newfoundland: Earth Planetary Sci. Letters, v. 21, p. 301-309.

Sullivan, K. D., ms, 1978, Structure and evolution of the Newfoundland Basin, offshore eastern Canada: Ph.D. thesis, Dalhousie Univ.

Upton, B. G. J., 1967, Alkaline pyroxenites, *in* Wyllie, P. J., ed., Ultramafic and Related Rocks: New York, John Wiley & Sons, p. 281-288.

Verwoerd, W. J., 1966, Fenitization of basic igneous rocks, *in* Tuttle, O. J., and Gittins, J., eds., Carbonatites: New York, Interaci. Publishers, p. 295-308.

Watson, B. E., 1976, Two-liquid partition coefficients: experimental data and geochemical implications: Contr. Mineralogy Petrology, v. 56, p. 119-134.

Williams, H., and Smyth, W. R., 1973, Metamorphic aureoles beneath ophiolite suites and alpine peridotites: tectonic implications with west Newfoundland examples: Am. Jour. Sci., v. 273, p. 594-621.

Williams, H., and Smyth, W. R., in press, The geology of the Hare Bay Allochthon: Canada Geol. Survey Bull.

Wyllie, P. J., 1977, Effects of H_2O and CO_2 on magma generation in the crust and mantle: Geol. Soc. London Jour., v. 134, p. 215-234.

Ophiolites

Proceedings International Ophiolite Symposium Cyprus 1979

The Symposium was organized and sponsored by the Government of the Republic of Cyprus and the International Association of Volcanology and Chemistry of the Earth's Interior and co-sponsored by the International Geological Correlation Programme, Project 39 "Ophiolites", and the Hellenic Mining Company Limited. It was held in Nicosia from 1 to 8 April, 1979.

Edited by A. Panayiotou



Republic of Cyprus

Ministry of Agriculture and Natural Resources
Geological Survey Department
1980

Spinel phases of the White Hills peridotite, St. Anthony Complex, Newfoundland: Part 1 occurrence and chemistry

R. Talkington and J. Malpas

Memorial University of Newfoundland, Department of Geology, St. John's, Newfoundland
Canada A1B 3X5

Abstract

The White Hills peridotite is composed of an interlayered sequence of spinel lherzolite and harzburgite. Subordinate dunite occurs as layers parallel to spinel lherzolite and harzburgite and "dykes" and lenses that lie oblique to the tectonite fabric. Crosscutting and occasionally parallel to the tectonite fabric are pyroxenite dykes (e.g. orthopyroxenite, websterite, clinopyroxenite and wehrlite) and gabbroic dykes. Chromitite lenses or seams are associated with orthopyroxenite.

Spinel is an accessory phase in all these rocks. In the ultramafic rocks and chromitite, spinel spans a range in Cr/Cr+Al ratio from 150 to 800 and lies within the alpine-type peridotite field. Spinel in clinopyroxenite, websterite, wehrlite and gabbro has low Cr/Cr+Al values and does not lie within the alpine-type peridotite field.

A variety of rock textures are preserved in these rocks. Coarse-granular texture (Basu, 1977) is recognized as the most "primitive" and is present in spinel lherzolite and harzburgite. Porphyroclastic texture (Mercier and Nicolas, 1975; Basu, 1977; Pike and Schwarzman, 1977) is the most common in the peridotite, but it occurs in all rock types. Allotriomorphic-granular texture (Pike and Schwarzman, 1977) is present in dunite lithologies and is interpreted as a "relict" cumulate texture in this suite. True cumulate texture is preserved in orthopyroxenite veins. Granoblastic texture, equigranular and elongate, is preserved in dunite and gabbro lithologies. Mortar texture is preserved in lithologies near the basal thrust zone of the peridotite.

Particular spinel-forms are characteristic for each rock texture. In the most "primitive" coarse-granular texture, spinel forms vermicules exsolved in orthopyroxene. Progressive deformation and change in rock texture, coarse-granular to porphyroclastic to mortar, results in a decrease in silicate grain size and an increase and change in spinel grain size and form. The progressive spinel-form sequence is, in general, vermicules, interstitial, cluster and porphyroclast, but variations and combinations are not uncommon.

Therefore, there seems to be temporal significance between texture and spinel-form. Additionally, the chemistry of the spinel phase seems to more clearly reflect the Cr/Al ratio of the bulk rock and mineral phases than the Mg/ Fe^{2+} ratio.

Introduction

Spinel Group minerals are a common accessory phase in the ultramafic and mafic portions of ophiolites. As an early — or late — forming phase (subsolidus) of these rocks, the chemistry and texture of the spinel must indicate genetic links between either the liquid phase or solid phase from which they formed provided the system operated under equilibrium, "closed" chemical conditions. Textural and chemical relationships of the spinel phases to their host rock in the ophiolite suite have not been tabulated in any single publication. Recent work on "ophiolitic" rocks and ultramafic xenoliths (Loney et al., 1971; Malpas and Strong, 1975; Menzies, 1975; Basu, 1977; Sinton, 1977) has only provided a partial compilation of spinel-silicate textural and compositional relationships.

Spinel Group minerals are present in all rock types of the White Hills Peridotite (i.e. spinel lherzolite, plagioclase lherzolite, harzburgite, dunite, pyroxenites, gabbro and chromitites); and as such provide a good opportunity to determine the relationships between spinels and silicates.

The purpose of this paper is to present spinel-silicate relationships and to discuss the changes in character of the spinel-form with changing rock texture and chemistry in the ultramafic section of the west Newfoundland ophiolites.

Location and general geology

The White Hills Peridotite is located at the northernmost tip of the Great Northern Peninsula of Newfoundland (Fig. 1).

The geology of the St. Anthony area has been summarized by Williams (1971, 1975), Williams and Smyth (in press), and Jamieson (1979). The St. Anthony Complex is the highest structural slice of the Hare Bay Allochthon (Stevens, 1970, Williams, 1975). It consists of the White Hills Peridotite and its dynamothermal aureole (Williams and Smyth, 1973; Jamieson, 1979, this volume) (Fig. 1).

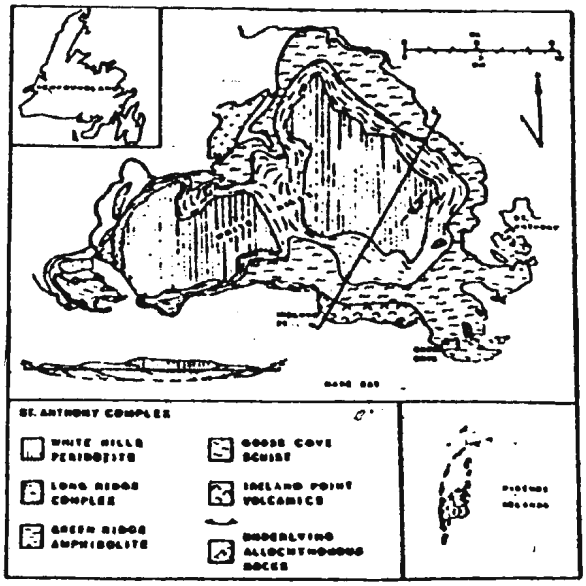

Fig. 1 *Location map and general geology of the St. Anthony Complex (from Jamieson, 1979).*

The peridotite crops out as two massifs which are recognized as dissected remnants of a once possibly complete ophiolite complex emplaced onto the continental margin of eastern North America as the Iapetus Ocean closed during the Ordovician. The minimum stratigraphic thickness of the peridotite is approximately two kilometres. Faulting and folding within the massifs makes an accurate estimate for the actual stratigraphic thickness impossible.

Harzburgite interlayered with spinel lherzolite forms about 85% of the massifs. Dunite occurs in two forms making up about 10% of the massifs; as layers parallel to the tectonic fabric in the harzburgite and spinel lherzolite and as lenses and "dykes" oblique to the tectonite fabric. Pyroxenite (e.g. orthopyroxenite, websterite and clinopyroxenite) and wehrlite veins and lenses are found as minor constituents throughout the White Hills massifs; wehrlite veins crop out only in the eastern massif, and are parallel or oblique to the tectonite fabric. Gabbroic veins have been found only in the eastern massif and generally lie oblique to the tectonic fabric (Talkington, 1979). Chromitites occur more commonly in the eastern massif, but they are also found in the western massif. The chromitites occur as seams and lenses associated with orthopyroxenite and dunite and either parallel or lie oblique to the tectonite fabric.

Textural relationships

The textural relationships betweeen spinels and silicates are discussed on a rock-type basis, and each rock type is subdivided on the basis of microscopic texture. The nomenclature for rock textures proposed by Mercier and Nicolas (1975), Basu (1977) and Pike and Schwarzman (1977) is adopted and rock terminology is after Streckeisen (1976). A summary of the textural variations of the spinel phases from the White Hills Peridotite is presented in Table 1 based on data collected from about 300 thin sections. We have tried to avoid using rock texture terms which may imply specific deformational processes.

Spinel lherzolite

Two rock textures coarse-granular (Basu, 1977) and porphyroclastic (Mercier and Nicolas, 1975; Basu, 1977, Pike and Schwarzman, 1977) are identified for spinel lherzolite.

Coarse-granular texture is considered to be the most "primitive" texture in rocks from the White Hills Peridotite and is characterized by coarse-grained (~3mm) orthopyroxene, clinopyroxene and olivine. These minerals show few signs of deformation (e.g. subgrain structure, development of KBB*, recrystallization) other than undulose extinction. Grain shapes are regular and mostly interlocking.

In the most "primitive" samples, spinel occurs only as exsolved vermicules in orthopyroxene (Fig. 2). The vermicules characteristically occur at the margins of the orthopyroxenes. In slightly more deformed rocks, still classed as coarse granular but where recrystallization and decrease in grain size are observed, spinel has accumulated into either irregularly shaped, interstitial clusters or porphyroclasts (Fig. 3). A gradational development of rock texture-type and spinel textures is observed in thin section.

Coarse-granular texture is almost exlusively found in rocks of the western massif (Fig. 1). The reason for this distribution is not known at present.

* KBB is the notation for Kink band boundaries



Fig. 2 *Exsolved vermicular spinel in orthopyroxene in coarse-granular texture spinel lherzolite. Sample 7815. Scale bar 0.5 mm.*

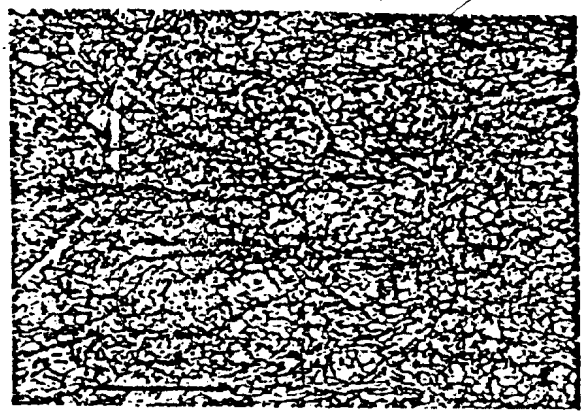

Fig. 3 *Porphyroclast spinel-form with spinel "trail" in porphyroclastic texture spinel lherzolite. Sample 7830. Scale bar 0.5 mm.*

Porphyroclastic texture is the most common texture of the spinel lherzolite. Grain size of the silicates is variable (.01mm to 4mm) and undulose extinction is present in porphyroclasts and neoblasts. Subgrain structures are developed in olivine. KBB (recrystallized and non-recrystallized) elongate-forms with aspect ratios of 7:1 (maximum 17:1), and retorted, non-recrystallized turning fork like kink bands (Basu, 1977) are developed in orthopyroxene. Clinopyroxene is bent and occasionally KBB are developed. Recrystallized and non-recrystallized grain shapes are irregular and polygonization of neoblasts is in various stages of development.

Spinel forms in the porphyroclastic spinel lherzolite are considered a result of increasing rock deformation (Mercier and Nicolas, 1975, Pike and Schwarzman, 1977).

Although a spinel phase is present in all spinel lherzolite samples, we are unable to distinguish "primary" and "residual" forms. Essentialy the form of the spinel is related to the development of less "primitive", or more deformed rock textures, at least in this suite of rocks.

Plagioclase lherzolite

We have found plagioclase lherzolite to outcrop only in one location on the eastern massif where it occurs within 3 metres of the basal thrust zone of the peridotite.

POOR COPY
COPIE DE QUALITEE INFERIEURE

Within the basal thrust zone, from the thrust plane to about 30-60 metres into the peridotite sheet, mortar texture is dominant. The spinel forms of this texture are "Holly-Leaf" or porphyroclastic or gradations of one form into the other. Both forms are orientated parallel to foliation.

Harzburgite

As in spinel lherzolite, two rock textures are developed in harzburgite, coarse-granular and porphyroclastic. The distribution of these textures in the massifs and descriptions of the silicate minerals are identical to spinel lherzolite. The spinel forms (Figs. 2-4) are believed to have formed in a manner similar to that in spinel lherzolite. Porphyroclast spinel-forms (Fig. 4), which may contain occluded silicates, commonly olivine, occur in both coarse-granular and porphyroclastic textures. We have not yet determined if a compositional variation exists between spinels of the various forms. The presence of porphyroclasts in "primitive" coarse-granular texture suggests they may be residual spinels which are commonly found in harzburgites of the Alpine-type (e.g. Dickey and Yoder, 1972; Malpas and Strong, 1975).



Fig. 4 *"Tadpole" porphyroclast spinel-form with occluded olivine in porphyroclastic texture harzburgite. Sample 78116. Scale bar 1.0 mm.*

Dunite

Two rock textures are recongized in dunite, an allotriomorphic-granular (Pike and Schwarzman, 1977) and equigranular or elongate granoblastic.

In the allotriomorphic-granular texture (Pike and Schwarzman, 1977) olivine grain size is large (average 6mm, maximum 1.4 cm) and recrystallization is negligible. Olivine grain boundaries are smooth and rounded and the grains appear to be elongate parallel to the foliation plane, but the degree of deformation and subgrain structure development suffered by olivine is minimal (T. Calon, per. comm.). Spinel forms are euhedral to anhedral and commonly show pull apart texture (Fig. 5). Severely corroded (due to resorption?) spinel forms "Holly-Leaf"-like forms. Spinel occurs at grain boundaries, occluded in olivine, and may define a lineation.

The character of spinel, its shapes and lack of consistent and pervasive deformational characteristics with respect to olivine and an appearance similar to cumulate spinel-forms of stratiform intrusions (Jackson, 1961, Fig. 59, p. 55) suggests this texture was of cumulate origin and suffered minor deformation. However, the possibility that this texture may represent the end product of complete annealing of a deformed dunite cannot be disregarded as yet.



Fig. 5 *Pull apart texture in allotriomorphic-granular texture dunite. Sample 7841. Scale bar 1.0 mm.*

The granoblastic textures are developed in dunites which are close to the basal thrust zone (70 m).

Grain size is greatly reduced to approximately .2mm for both types of texture. Undulose extinction is ubiquitous and subgrain structures are present in olivine. However, recrystallization is not observed. Polygonal grains with well-developed 120° triple-point junctions are everywhere present. Spinel is xenoblastic interstitial, and dominantly altered to magnetite (Table 2, analysis 78152D; Fig. 6). It is generally aligned parallel to the foliation.

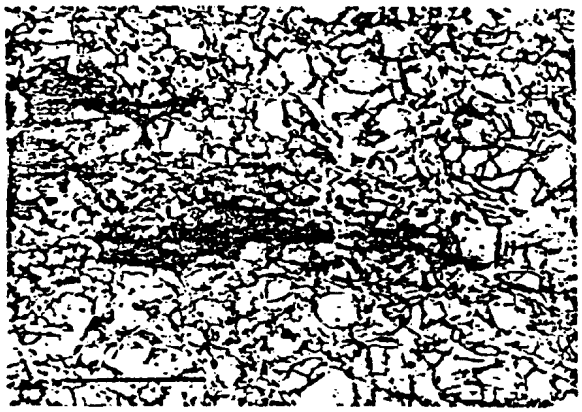

Fig. 6 *Corroded "Holly-Leaf" form in granoblastic texture dunite. Sample 78152. Scale bar 0.5 mm.*

Gabbro

Porphyroclastic (Mercier and Nicolas, 1975; Basu, 1977; and Pike and Schwarzman, 1977) and granoblastic textures occur in gabbro and are gradational into each other. Porphyroclasts of olivine, clinopyroxene, plagioclase and minor orthopyroxene are about .5mm in size. Neoblasts are commonly less than .05mm. Undulose extinction is ubitquitous and subgrain structures are developed in olivine. Clinopyroxene porphyroclasts are sometimes bent and both clinopyroxene and plagioclase show grain

POOR COPY
COPIE DE QUALITEE INFERIEURE

POOR COPY
COPIE DE QUALITEE INFERIEURE

Table 1 *Summary of the textural variations of the spinel phases in the rocks of the White Hills Peridotite.*

Rock Type	Microscopic Rock Texture	Colour[1]	Grain Shapes and Sizes[2]	Grain Boundary	Orientation
Spinel lherzolite:	a. coarse-granular[3]	straw-yellow to light red-brown	porphyroclasts (.6mm x .3mm); irregular interstitial to opx, cpx, ol (.2mm); vermicular, wormlike exsolution from opx (.1mm x .02mm); exsolved droplets from cpx (.01mm)	irregular to curvilinear for porphyroclasts and exsolution forms; smooth and rounded for droplet form	random
	b. porphyroclastic[4]	bronze to light red-brown[5]	'Holly-Leaf' (.8mm); porphyroclasts with spinel trails (.1mm); exsolved droplets along ENE in opx and cpx (.1mm); exsolved droplets in opx and cpx (.1mm)	scalloped to irregular for 'Holly-Leaf' and porphyroclast forms; rounded to subidioblastic for droplet form	'Holly-Leaf' and porphyroclast forms parallel to foliation; random for droplets
Plagioclase lherzolite:	mortar	bronze to brown-green	'Holly-Leaf' (.4mm); porphyroclasts (.3mm)	scalloped to irregular for 'Holly-Leaf' and porphyroclast forms	'Holly-Leaf' and porphyroclast forms parallel foliation
Harzburgite:	a. coarse-granular[3]	various shades of red-brown	porphyroclasts (ovoid shaped) (.3mm); vermicular exsolution in opx (.2mm); exsolved droplets in opx (.1mm)	scalloped to serrate for porphyroclast form; smooth, curvilinear for vermicular form; round to subidioblastic for droplets	porphyroclasts either random or parallel to foliation; random for vermicular and droplet forms
	b. porphyroclastic[4]	various shades of red-brown	'Holly-Leaf' (2mm x .3mm); porphyroclast (ovoid and tadpole forms with ol and opx, some porphyroclasts show pull-apart texture)(1mm)	scalloped to irregular for 'Holly-Leaf' and porphyroclast forms	all forms parallel to foliation plane; random or defining a lineation
Dunite[6]:	a. allotriomorphic-granular[7]	green-brown to red-brown	porphyroclasts (ovoid, showing pull-apart texture; severely corroded to produce 'Holly-Leaf' like structure) (.5mm, range .2mm to 4mm)	regular, scalloped and curvilinear	random or parallel to foliation
	b. equigranular and elongate granoblastic[8]	deep red-brown or black[9]	xenoblastic interstitial (various size ranges, .01mm to .2mm)	irregular	random
Chromite:	porphyroclastic[4] and equigranular granoblastic (foliated and non-foliated)	green(translucent)	'Holly-Leaf' (.2mm); cluster interstitial (.15mm); vermicular in opx, cpx, pl (.1mm) and exsolved droplets in opx, cpx, pl (.01mm)	scalloped to irregular for 'Holly-Leaf' and cluster forms; rounded for droplets in primary and recrystallized pl; commonly irregular for droplets in cpx and opx	random
Pyroxenite: i. orthopyroxenite (opx)	a. cumulate	red-brown	subedral to euhedral interstitial and occluded within opx (.3mm); rarely elongate parallel and subparallel to (010) opx (.1mm)	irregular to rounded	'Holly-Leaf' defines a lineation; for other forms random
ii. websterite (cpx)	b. porphyroclastic[4]	various shades of green-brown	'Holly-Leaf' (1.3mm); clusters interstitial (.4mm); exsolved droplets in opx (.1mm)	scalloped to irregular for 'Holly-Leaf' and cluster forms; rounded for droplet form	random
iii. clinopyroxenite (cpx)	c. porphyroclastic[4]	various shades of	clusters interstitial to cpx,	scalloped to irregular for cluster	

		green-brown	cpx, ol (.15mm); exsolved droplets along KSB cpx (<.1mm)	form; irregular to curvilinear for droplet form	
iv. wehrlite	d. porphyroclastic[4]	green-brown	clusters (.1mm)	scalloped to irregular	random
Chromitites	cumulus-massive	red-brown	euhedral to anhedral cumulus (.2mm to massive); anhedral to rounded when granulated due to deformation (<.02mm)	regular to rounded	random

1. colour as seen in transmitted light
2. size - average grain size
3. coarse - granular texture as defined by Bass (1977)
4. porphyroclastic texture as defined by Mercier and Nicolas (1975), Bass (1977), and Pike and Schwarzman (1977)
5. bronze colour for higher modal amounts of cpx
6. the disposition of spinel grains with respect to olivine is such to suggest a 'cumulus' origin, and therefore a primary crystallization phase
7. allotriomorphic texture as defined by Pike and Schwarzman (1977)
8. the development of this texture results in only a trace of spinel, less than 1 modal per cent, left in dunite
9. when a black colour, the spinel has altered to magnetite

POOR COPY
COPIE DE QUALITÉE INFÉRIEURE

POOR COPY
COPIE DE QUALITEE INFERIEURE

Table 2 *Representative spinel compositions from the White Hills Peridote.*

	Lherzolite			Harzburgite		Dunite			Gabbro		Pyroxenite			Chromitite	
	77N11	77N194	78151	77N156	77N155L	77N193SL	78117ML	78152D	78136	7898o	77N42W	77N479C	78142WE	77N119o	77N130D
TiO_2	0.04	0.10	0.05	0.17	0.72	0.11	0.66	0.41	0.02	0.09	--	0.07	0.14	0.31	0.13
Al_2O_3	53.36	51.50	52.54	36.88	30.97	50.29	34.68	38.98	64.12	21.36	60.87	57.29	55.97	9.75	10.45
Cr_2O_3	14.83	16.28	15.41	31.04	29.17	15.49	31.01	23.75	1.44	44.67	7.16	9.75	9.68	57.21	60.63
Fe_2O_3	0.38	2.10	0.80	2.25	9.43	3.30	4.43	6.13	1.22	4.55	0.74	1.54	0.98	4.46	2.11
FeO	11.41	12.68	14.20	15.06	16.59	11.74	14.34	17.02	15.76	16.18	8.29	14.30	15.28	17.22	14.01
MnO	0.04	0.10	0.04	0.18	0.18	0.06	0.29	0.08	0.01	0.08	0.04	0.06	0.06	0.12	0.10
MgO	18.75	18.14	17.09	14.99	13.67	18.31	15.55	14.07	17.22	12.39	21.28	17.64	16.48	10.73	12.93
Total	98.81	100.90	100.19	100.57	100.73	99.30	100.87	99.82	100.36	99.32	98.58	100.65	98.59	99.82	100.36
Usp	0.08	0.20	0.10	0.37	1.60	0.22	1.43	0.88	0.04	0.21	--	0.14	0.28	0.82	0.31
Chr	15.61	17.06	16.26	35.03	34.00	16.49	32.06	26.81	1.47	42.08	7.25	10.06	10.25	46.31	37.47
MgChr	--	--	--	--	--	--	3.06	--	--	13.02	--	--	--	28.33	39.77
Sp	74.52	71.81	68.12	62.18	53.92	73.60	58.67	59.97	66.08	39.35	82.12	68.73	65.87	19.00	19.89
Her	9.41	8.83	14.71	--	--	6.35	--	5.75	31.24	--	9.92	19.56	22.62	--	--
Mgf	--	--	--	1.72	6.26	--	4.78	--	--	5.34	--	--	--	5.54	2.59
Mt	0.38	2.10	0.80	0.70	4.22	3.34	--	6.59	1.17	--	0.71	1.51	0.98	--	--

Fe^{2+} - Fe^{3+} calculated from total Fe by assuming spinel stoichiometry
Usp = ulvospinel; Chr = chromite; MgChr = magnesiochromite; Sp = spinel; Her = hercynite; Mgf = magnesioferrite; Mt = magnetite. End members calculated according to the method of Irvine (1965).

boundary recrystallization. Grain boundaries vary from irregular to regular-polygonal.

In the granoblastic textures, all silicates phases are about .2mm and show similar deformation and grain boundary features to the porphyroclastic texture.

Spinel-forms are "Holly-Leaf", cluster (Fig. 7), vermicular (Figs. 8 and 9), and as exsolved droplets in clinopyroxene, orthopyroxene and plagioclase (Fig. 10). These spinel-forms have been described by many authors (e.g. Mason, 1967; Gardner and Robins, 1974; Sapountzis, 1975; Talkington and Gaudette, in preparation; and others) and commonly occur in metagabbroic rocks.



Fig. 7 *Spinel clusters in gabbro. Porphyroclastic texture. Sample 78136. Scale bar 0.5 mm.*



Fig. 8 *Vermicular spinel in clinopyroxene (?). Porphyroclastic texture. Sample 77WH90. Scale bar 0.05 mm.*

Pyroxenite

Orthopyroxenite veins have textures that resemble cumulate textures of stratiform-type intrusions. Orthopyroxene is euhedral to subhedral with grain size about 3.5mm. Undulatory extinction and minor kink band development are observed. The orthopyroxene grain boundaries are regular and interlocking, suggesting adcumulate growth (see Jackson, 1961, p. 56, Fig. 62), olivine and clinopyroxene are anhedral, intercumulate phases. Orthopyroxene, clinopyroxene and olivine are compositionally distinct from those of the other rock types (Tables 3 and 4; olivine in orthopyroxenite has NiO = 0.4 wt%).



Fig. 9 *Plagioclase-clinopyroxene (?) -spinel-olivine symplectite. Porphyroclastic texture. Sample 78136. Scale bar 0.1 mm.*



Fig. 10 *Exsolved spinel droplets in clinopyroxene and plagioclase. Porphyroclastic texture. Sample 77WH60. Scale bar 0.5 mm.*

Spinel in the orthopyroxenite is euhedral to anhedral and interstitial or occluded in orthopyroxene; rarely spinel is elongate parallel or subparallel to (100) opx (Fig. 11).



Fig. 11 *Cumulate texture in orthopyroxenite. Note interlocking (adcumulate) grain boundaries. Spinel is subhedral to anhedral. Sample 7898. Scale bar 1.0 mm.*

POOR COPY
COPIE DE QUALITEE INFERIEURE

Table 3 *Representative orthopyroxene analyses from the White Hills Peridotite.*

	Lherzolite		Harzburgite	Gabbro		Pyroxenite		Chromitite	
	77WH1	77WH94	77WH56	77WH60	7898o	77WH2W	77WH79C	77WH19o	77WH30D
SiO_2	53.84	54.55	56.37	52.55	55.68	55.52	54.38	57.15	55.66
TiO_2	0.04	0.03	0.04	0.14	--	0.03	0.10	0.05	0.02
Al_2O_3	5.57	4.38	2.00	3.85	1.02	4.53	4.37	0.89	1.01
Cr_2O_3	0.77	0.59	0.45	0.05	0.48	0.24	0.48	0.44	0.59
FeO_T	5.50	6.15	6.04	12.70	5.64	5.50	7.59	5.00	4.57
MnO	0.13	0.10	0.15	0.31	0.15	0.16	0.21	0.15	0.10
MgO	33.10	33.75	34.78	29.32	36.70	33.94	32.73	35.27	36.74
CaO	1.48	0.95	0.31	0.51	0.49	0.60	0.44	0.78	0.80
Na_2O	0.05	0.03	--	0.02	0.01	--	0.03	--	0.07
NiO	0.07	0.02	0.05	0.04	0.12	0.04	0.06	0.14	0.18
Total	100.55	100.55	100.19	99.50	100.29	100.56	100.39	99.87	99.74

Table 4 *Representative clinopyroxene analyses from the White Hills Peridotite.*

	Lherzolite		Harzburgite	Gabbro	Pyroxenite		
	77WH1	77WH94	77WH56	78129	7898o	77WH2W	77WH79C
SiO_2	51.91	52.46	51.80	50.37	53.59	50.59	50.13
TiO_2	0.12	0.20	0.20	0.80	0.02	0.16	0.52
Al_2O_3	6.07	4.99	3.76	7.38	1.82	6.38	6.71
Cr_2O_3	1.20	1.08	1.38	0.52	0.78	0.41	0.87
FeO_T	2.07	2.46	1.71	4.13	1.56	2.35	3.00
MnO	0.10	0.09	0.07	0.16	0.06	0.13	0.13
MgO	15.84	17.94	16.62	14.44	18.06	16.36	15.70
CaO	22.88	20.54	24.01	21.43	24.18	23.39	22.66
Na_2O	0.70	0.69	0.63	1.08	0.12	0.42	0.65
NiO	0.02	0.11	0.06	0.02	0.02	0.01	--
Total	100.91	100.56	100.24	100.32	100.21	100.20	100.37

POOR COPY
COPIE DE QUALITÉE INFÉRIEURE

Websterite, Clinopyroxenite, Wehrlite

Porphyroclastic texture is developed in websterite, clinopyroxenite and wehrlite. Grain size is variable, ranging from .4mm to 1.5mm for porphyroclasts to about .2mm for neoblasts. Undulose extinction is ubiquitous. Grain shapes are irregular for porphyroclasts, but neoblasts show varying stages of polygonization. Clinopyroxene porphyroclasts are bent and may show recrystallized KBB, olivine shows limited development of subgrain structures and orthopyroxene is commonly bent and KBB are not recrystallized.

The spinel phases of these rocks have similar forms. "Holly-Leaf", clusters and droplets (Fig. 12). These spinels probably developed during subsolidus re-equilibration during deformation.



Fig. 12 *Exsolved droplets in clinopyroxene and spinel interstitial to silicates. Porphyroclastic texture. Sample 78159, websterite. Scale bar 0.5 mm.*

Chromitite

Spinel of chromite occurrences have cumulate textures. Spinel grains are euhedral to anhedral, although in shear zones, spinel is commonly "granulated" and reduced in size (Fig. 13). Spinels with high Cr/Cr+Al ratios tend to retain a "sphericity" during deformation, whereas spinels with low Cr/Cr+Al ratios tend to flatten and develop "trails" (Basu, 1977) (Fig. 3).



Fig. 13 *Chromitite in orthopyroxenite lense. Note small "granulated" spinel grains in shear zone. Dark area is massive spinel. Sample 77WH19. Scale bar 1.0 mm.*

Spinel compositions

Spinel compositions are listed in Table 2 and are diagrammatically represented in figures 14 and 15. Compositions of the spinels and silicate phases were determined by electron microprobe. All Fe was determined as FeO. Fe^{2+} and Fe^{3+} for spinel were determined assuming ideal spinel stoichiometry. Complete descriptions of spinel phases are included in Table 1.

Spinel lherzolite

The compositions of the bronze to straw yellow spinels in spinel lherzolite cluster in a small field (Fig. 14). Fe^{3+} content is almost zero for all rock types (Fig. 15). No compositional variation exists between the vermicular spinel in orthopyroxene porphyroclasts (Fig. 2) of the coarse-

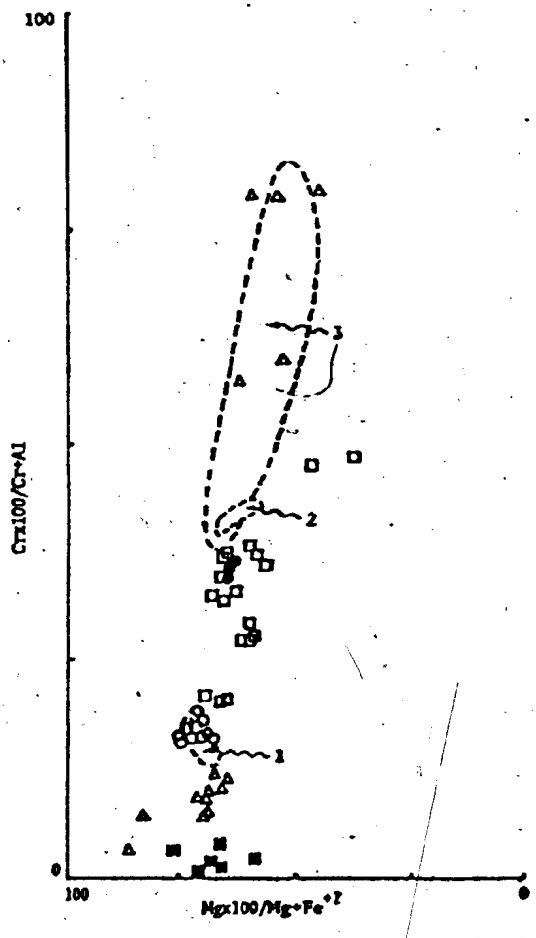

Fig. 14 *Plot of White Hills Peridotite spinel analyses. Symbols: open circle-spinel lherzolite; solid circle-harzburgite; open square -dunite; solid square -gabbro; open triangle -pyroxenites. Outlined fields from Bay of Islands (Malpas and Strong, 1975); 1-spinel lherzolite; 2-dunite; 3-harzburgite.*

POOR COPY
COPIE DE QUALITEE INFERIEURE

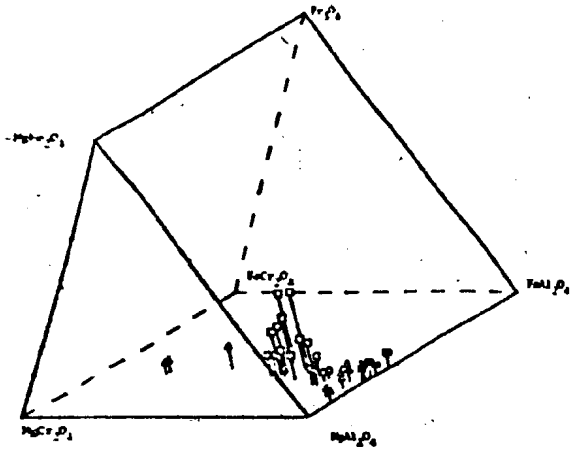

Fig. 15 *Plot of White Hills Peridotite spinel analyses in spinel prism by the method of Irvine (1965). Symbols as in Fig. 14.*

granular texture. Spinels with high Al/Cr ratio tend to develop "trails" (Fig. 3) (Basu, 1977). The spinel composition field for spinel lherzolite of the Bay of Islands ophiolites (Malpas and Strong, 1975) overlap the White Hills data (Fig. 14, field 1).

No spinel data are available for plagioclase lherzolite, but on the basis of colour, a composition similar to those of spinel lherzolites and dunite sample 77WH93SL (Table 2) is assumed.

Harzburgite

The red-brown spinel in harzburgite is compositionally distinct from spinel in spinel lherzolite (Figs. 14 and 15). This appears as an increase in the Cr/Cr+Al ratio and a slight decrease in $Mg/Mg+Fe^{2+}$. Comparison with analyses from the Bay of Islands ophiolite (Fig. 14, field 3) shows no overlap of the two fields. More spinel analyses for both areas may extend the respective fields. Comparison of the ultramafic sections of the two ophiolites in fact show that the spinels from the White Hills may, because of the layered and more "residual" nature of the ultramafics, contain spinel phases with higher Al/Cr ratios, but similar $Mg/Mg+Fe^{2+}$ ratios to non-layered ultramafic sections. No compositional differences between spinels of the different textural types are recorded.

Harzburgite spinels are easily distinguished from lherzolite spinels in thin section by colour in transmitted light. Bronze to straw-yellow colours dominate in spinel lherzolite, whereas various shades of red-brown are common for harzburgite. Colour variation between the two groups appears to be dependent on the modal amount of clinopyroxene in the rock, i.e. modal amounts greater than 5-7% results in bronze-straw-yellow colours; less than this amount the spinel is varying colours of red-brown.

Dunite

Spinel in dunite is divided into four groups based on chemistry:

1. disseminated spinel in dunite layers intercalated with harzburgite;
2. disseminated spinel in dunite intercalated with spinel lherzolite;
3. disseminated spinel in dunite "dykes";
4. disseminated spinel in dunite "lenses".

Spinel in dunite layers intercalated with harzburgite is a red-brown colour, often euhedral to subhedral with pull-apart texture (Fig. 5). This variety has the highest Cr/Cr+Al ratio (Fig. 14) of the dunite types. The compositional field for this group contains the harzburgite spinel field.

Spinel in dunite intercalated with spinel lherzolite is a green-brown colour, often euhedral to subhedral and shows pull-apart texture. This type has the lowest Cr/Cr+Al ratio of the dunite types (Fig. 14). The spinel composition for this group is coincident with the spinel lherzolite field (Figs. 14 and 15).

Spinel in dunite "dykes" is dark red-brown to black in colour and anhedral. The Cr/Cr+Al ratios are intermediate within the dunite group (Fig. 14).

Spinel in dunite "lenses" is a deep red-brown to black colour, euhedral to anhedral and shows pull-apart texture. The Cr/Cr+Al ratio is about 0.200.

Spinel in dunite, therefore, shows a range in Cr/Cr+Al ratio from 0.200 to 0.400. The Bay of Islands dunite field (Malpas and Strong, 1975) (Fig. 14, field 2) has a higher and more restricted range for Cr/Cr+Al ratios. Spinel in dunite of the Burro Mountain ophiolite (Loney et al., 1971, Table 8, p. 292) shows a large range in Cr/Cr+Al ratios (.30 to .75) correlated with dunite occurrence (lense, dyke, sill). Loney et al. (1971) suggest this is a consequence of variations in original bulk rock chemistry.

Gabbro

Spinel in gabbro is translucent green and xenoblastic. The Cr/Cr+Al ratio is approximately 0.010. The $Mg/Mg+Fe^{2+}$ ratio shows more spread than spinel of the other rock types. The composition of the spinel does not vary with mineral association (i.e. vermicular (Fig. 8), cluster, "Holly-Leaf" droplet).

Pyroxenite

A. *Orthopyroxenite.* Disseminated spinel has been found in only a few orthopyroxenite veins. Massive spinel (chromitite) occurring with orthopyroxenite and dunite is common, and is described in a later section. In orthopyroxenite spinel is red-brown and euhedral to anhedral (Fig. 11). The Cr/Cr+Al ratio is 0.583. A Cr/Cr+Al ratio of 0.630 is reported by Loney et al. (1971, Table 8, p. 292) for Burro Mountain.

B. *Websterite.* Spinel in websterite is commonly interstitial to the silicates and is green-brown (Fig. 12). The Cr/Cr+Al ratio is approximately 0.100.

C. *Clinopyroxenite.* Spinel in clinopyroxenite is commonly interstitial to the silicates and green-brown. The Cr/Cr+Al ratio is approximately 0.100, identical to websterite. The $Mg/Mg+Fe^{2+}$ ratio for clinopyroxenite is less than in websterite (Fig. 14).

D. *Wehrlite.* Spinel in wehrlite occurs as clusters interstitial to silicates and is green-brown. The Cr/Cr+Al ratio is similar to clinopyroxenite and websterite (Fig. 14). The $Mg/Mg+Fe^{2+}$ ratio is similar to clinopyroxenite (Fig. 14).

Chromitites

Spinel accumulations in seam or lens form are termed chromitites. Spinel of this association is a deep red-brown colour and euhedral to subhedral (Fig. 13). Two compositional varieties are recognized on the basis of varying

POOR COPY
COPIE DE QUALITEE INFERIEURE

Cr/Cr+Al ratios; a high-Cr/Cr+Al ratio spinel and a low-Cr/Cr+Al ratio spinel.

The high-Cr/Cr+Al ratio spinel is associated with spinel seams (~1 cm wide) in the core of orthopyroxenite veins and lenses (Table 2, sample 77WH19c; Fig. 14, pyroxenite symbol with the highest Cr/Cr+Al ratio), and in lenses (less than 4m x 3m) associated with disseminated, kinked euhedral orthopyroxene crystals (8cm x 4cm). The Cr/Cr+Al and Mg/Mg+Fe^{2+} ratios are similar to those for podiform chromites of alpine-type peridotites (Irvine, 1967; Thayer, 1970, Dickey, 1975; Greenbaum, 1977; and Panayiotou, 1978).

The low-Cr/Cr+Al ratio spinel occurs as seams (3cm wide) in dunite (Fig. 14, dunite symbol showing the highest Cr/Cr+Al ratio and the lowest Mg/Mg+Fe^{2+} ratio). The low Mg/Mg+Fe^{2+} ratio (Figs. 14 and 15) is a result of enrichment in iron and oxidation during serpentization (Dickey, 1975).

Interpretation

For the rocks of the White Hills Peridotite we are able to relate spinel-form to a specific rock texture and place temporal significance on both spinel form and rock texture. This is only possible because we have a well-developed, progressively deformed suite of rock textures and spinel forms. The transition from one texture form to another is not instantaneous but gradational and, as such, a strict classification scheme is not feasible. We have outlined the general, yet complete, characteristics and have tried to do so using non-genetic terms where we were unsure of the operative processes.

The transition from coarse-granular textures (most "primitive") to porphyroclastic is recognized by a change from exsolved vermicular spinel in orthopyroxene porphyroclasts to irregular shaped spinel interstitial to slightly deformed silicates, then into porphyroclasts which flatten, elongate parallel to the foliation and develop "trails". Where this gradation is observable for a single rock-type, it appears possible to distinguish between a "primary" spinel and one exsolved from pyroxene. We have not determined any compositional differences between these two types from a single rock type, but Menzies (1975) has shown that for harzburgite which contains a groundmass spinel and a spinel exsolved from pyroxene, the groundmass spinel is enriched in Al^{3+} relative to the exsolved spinel*.

Spinel phases in websterite, clinopyroxenite, wehrlite, and gabbro are all green in colour and show relationships to silicates that are similar to those in porphyroclastic texture spinel lherzolite and harzburgite. They thus appear secondary. Cr/Cr+Al values for these spinels are low and do not lie within the alpine-type peridotite field as outlined by Irvine and Findlay (1972).

Spinel and rock textures in dunite, orthopyroxenite and chromitite suggest a cumulate origin. We, therefore, consider these rock types a result of early high-pressure fractionation of picritic primary melts from the mantle (Malpas, 1978).

The Cr/Cr+Al ratio of the analysed spinels is the most notable chemical variation (Fig. 14). All spinel analyses, except gabbro, clinopyroxenite, websterite, and wehrlite, lie within the alpine-type peridotite field (cf. Irvine and Findlay, 1972). Comparison of spinel compositions from the Bay of Islands with the White Hills trend shows good agreement with the spinel lherzolite field, but not with the harzburgite or dunite fields.

The ultramafic zone of Bay of Islands contains a thin (~200m) unit of spinel lherzolite overlain by a homogeneous harzburgite unit (~3km) and a cumulate dunite zone (~300m), respectively (Malpas, 1976). In the White Hills, however, spinel lherzolite and harzburgite are interlayered with varying amounts of dunite. The spinel lherzolite represents the "primary" mantle from which the harzburgite residiuum and dunite fraction are partial fusion and subsequent crystallization products. Chrome spinels may either represent fractional crystallization products or a residual phase after partial melting (Dickey and Yoder, 1972; Dickey, 1975). We suggest that the partial fusion process has progressed further for the Bay of Islands than the White Hills fractions. Lower degrees of partial fusion of the White Hills rocks has resulted in bulk rock analyses with higher alumina and lower Cr/Al ratio for harzburgite and dunite spinels.

The different Cr/Cr+Al ratios for dunite and harzburgite spinels of the Bay of Islands is anticipated for an evolved alpine-type peridotite magma sequence. The Cr^{3+} is concentrated in the residual phase, harzburgite after partial fusion as chromium results from the incongruent melting of diopside of the lherzolite (Dickey and Yoder, 1972). The lherzolite clinopyroxenes of the Bay of Islands are, on average, enriched in the kosmochlor molecule relative to harzburgite, which is expected if the lherzolite is the parent material. The amount of partial fusion of the spinel lherzolite of the White Hills has not allowed incongruent melting of clinopyroxene (Table 4) to advance to the Bay of Islands conditions.

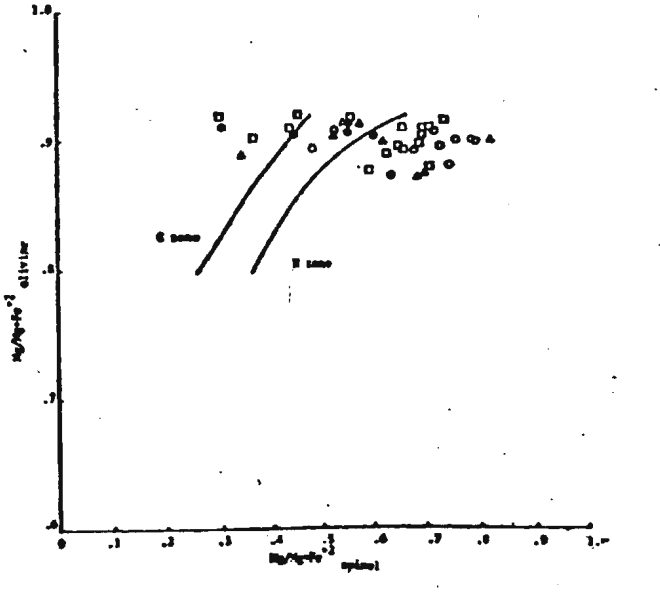

Fig. 16 *Mg-Fe^{2+} partitioning between spinel and olivine from ophiolitic ultramafic rocks. Solid lines-G zone and H zone (Jackson, 1969) from Stillwater complex. Data from Burro Mountain, Loney et al. (1977); Troodos, Allen (1975); Bay of Islands, Malpas (1976); S.W. Oregon, Medaris (1975); Red Mountain, Sinton (1977); Oman, Smewing (unpub. data); White Hills, Talkington (unpub. data). Symbols as in Fig. 14.*

* After submitting this manuscript, analyses were made on the spinel exsolved from orthopyroxene (see Fig. 2). The following microprobe analysis is representative of this spinel type (sample 7815): TiO_2= 0.04; Al_2O_3=48.43; Cr_2O_3=18.91; Fe_2O_3=1.47; FeO=13.25; MnO=0.11; MgO=16.89; NiO=0.29; Total=99.43. As Menzies (1975) showed, and is consistent with these data, the groundmass spinel has a lower Cr/Al ratio than the exsolved phase (compare the above analyses with those of Table 2 for lherzolite).

POOR COPY / /
COPIE DE QUALITEE INFERIEURE

Bulk rock and co-existing silicate chemistries have been suggested by some authors to control spinel composition (e.g. Irvine, 1965; Loney et al., 1971; Sinton, 1977). Unlike spinels from stratiform intrusions, spinel compositions of alpine-type peridotites do not show a dependence on $Mg/Mg+Fe^{2+}$ ratio of olivine (Fig. 16), which Roeder and Emslie (1970) note as an accurate measure of liquid $Mg/Mg+Fe^{2+}$ ratio. The Cr/Al ratios for spinels, however, closely approaches that of the bulk rock for the White Hills peridotite. In addition, variations of Al_2O_3 in orthopyroxene and clinopyroxene are duplicated by spinel in peridotitic rocks. Therefore, the compositional variability of spinels of alpine-type peridotites appear to reflect differing P-T conditions and are more sensitive to Cr/Al variations (Fig. 17) than $Mg/Mg+Fe^{2+}$ variations of the bulk rock (Irvine, 1967; Allen, 1975; Sinton, 1977).

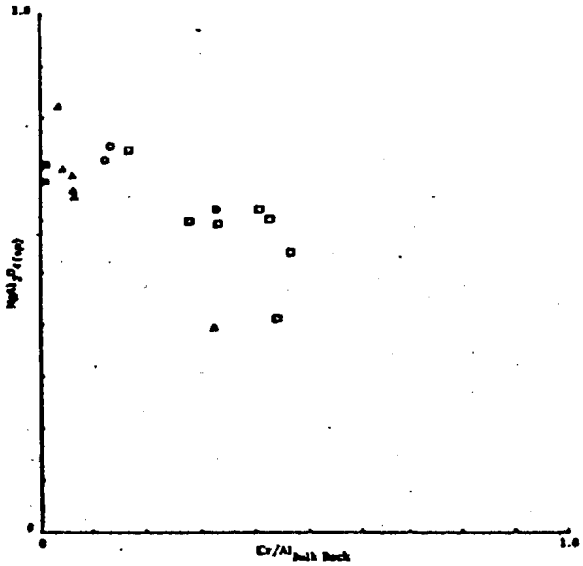

Fig. 17 *Cr/Al ratios of spinel phases and bulk rocks from White Hills Peridotite sheet (Symbols as in Fig. 14).*

Acknowledgements

We thank T. Calon and D. Strong for comments during the preparation of this manuscript. We are grateful to J. Smewing for the use of unpublished spinel data from the ultramafic zone of the Oman ophiolite. The study was financially supported by a National Research Council of Canada Grant to J. Malpas.

References

Allen, C.R., 1975, The petrology of a portion of the Troodos plutonic complex, Cyprus. *Unpubl. Ph. D. thesis, Cambridge University.*

Basu, A.R., 1977, Textures, microstructures and deformation of ultramafic xenoliths from San Quintin, Baja, California. *Tectonophysics*, 43, 212-246.

Dickey, J.S., 1975, A hypothesis of origin for podiform chromite deposits. *Geochim. Cosmochim. Acta*, 39.

Dickey, J.S. and Yoder, H.S., 1972, Partitioning of chromium and aluminum between clinopyroxene and spinel. *Carnegie Inst. Washington Yb.* 71, 384-392.

Gardner, P.M. and Robins, B., 1974, The olivine-plagioclase reaction: geological evidence from the Seiland petrographic province, Northern Norway. *Contr. Miner. Petr.*, 44, 149-156.

Greenbaum, D., 1977, The chromitiferous rocks of the Troodos Ophiolite Complex, Cyprus. *Econ. Geol.*, 72, 1175-1194.

Irvine, T.N., 1965 Chromian spinel as a petrogenetic indicator, Part 1: Theory. *Can. J. Earth Sci.*, 2, 648-672.

Irvine, T.N., 1967, Chromian spinel as a petrogenetic indicator, Part 2: Petrologic applications. *Can. J. Earth Sci.*, 4, 71-103.

Irvine, T.N. and Findlay, T.C., 1972, Alpine-type peridotite with particular reference to the Bay of Islands Igneous Complex. *Publ. Earth Phys. Branch, Dept. Energy, Mines Resour., Canada*, 42, 97-140.

Jackson, E.D., 1961, Primary textures and mineral associations in the ultramafic zone of the Stillwater Complex, Montana. *U.S. Geol. Surv. Prof. Paper*, 358, 106p.

Jackson, E.D., 1969, Chemical variation in co-existing chromite and olivine in chromitite zones of the Stillwater Complex. In *Magmatic Ore Deposits*. Ed. Wilson, H.D.B. Econ. Geol. Mono. 4, 41-71.

Jamieson, R.A., 1979, The St. Anthony Complex, Northwestern Newfoundland: A petrological study of the relationship between a peridotite sheet and its dynamothermal aureole. *Ph. D. thesis, Memorial University.*

Loney, R.A., Himmelberg G.R. and Coleman, R.G., 1971, Structure and petrology of the alpine-type peridotite at Burro Mountain, California, U.S.A.. *J. Petrol.*, 12, 2, 245-309.

Malpas, J., 1976, The petrology and petrogenesis of the Bay of Islands ophiolite suite, western Newfoundland. *Unpubl. Ph.D. thesis, Memorial University.*

Malpas, J., 1978, Magma generation in the upper Mantle, field evidence from ophiolite suites, and application to the generation of oceanic lithosphere. *Roy. Soc. London Phil. Trans.* A., 288, 527-546.

Malpas, J. and Strong, D.F., 1975, A comparison of chrome-spinels in ophiolites and mantle diapirs of Newfoundland. *Geochim. Cosmochim. Acta*, 39, 1045-1060.

Mason, R., 1967, Electron-probe microanalysis of coronas in a Troctolite from Sulitjelma, Norway. *Mineral. Mag.*, 36, 504-514.

Medaris, L.G., 1975, Co-existing spinel and silicates in alpine peridotites of the granulite facies. *Geochim. Cosmochim. Acta*, 39, 947-958.

Menzies, M., 1975, Spinel compositional variation in the crustal and mantle lithologies of the Othris ophiolite. *Contr. Miner. Petr.*, 51, 303-309.

Mercier, J-C.C. and Nicolas, A., 1975, Textures and fabrics of upper mantle peridotites as illustrated by xenoliths from basalts. *J. Petrol.*, 16, 454-487.

Panayiotou, A., 1978, The mineralogy and chemistry of the podiform chromite deposits in the serpentinites of the Limassol Forest, Cyprus. *Mineral. Deposita*, 13, 259-274.

Pike, J.E. Nielson and Schwarzman, E.C., 1977, Classification of textures in ultramafic xenoliths. *J. Geol.*, 85, 49-61.

Roeder, P.L. and Emslie, R.F., 1970, Olivine-liquid equilibrium. *Cont. Miner. Petr.*, 29, 275-289.

Sapountzis, E.S., 1975, Coronas from the Thessaloniki gabbros (North Greece). *Contr. Miner. Petr.*, 51, 197-203.

Sinton, J.M., 1977, Equilibration history of the basal alpine-type peridotite, Red Mountain, New Zealand. *J. Petrol.*, 18, 2, 216-248.

Stevens, R.R., 1970, Cambro-Ordovician flysch sedimentation and tectonics in West Newfoundland and their possible bearing on a Proto-Atlantic Ocean. *Geol. Assoc. Canada Spec. Paper*, 7, 165-177.

Streckeisen, A., 1976, To each plutonic rock its proper name. *Earth Sci. Rev.*, 12, 1-33.

Talkington, R.W., 1979, An unusual occurrence of gabbro veins in a west Newfoundland ophiolite: White Hills Peridotite, St. Anthony Complex (abs.). *Geol. Assoc. Canada*, 4, 82.

Talkington, R.W. and Gaudette, H.E., Corona structures from the Harriman peridotite, Maine: Their chemistry and origin. *Can. J. Earth Sci.* (submitted ms.).

Thayer, T.P., 1970, Chromite segregations as petrogenetic indicators. *Geol. Soc. S. Africa, Spec. Publ.*, 1, 380-390.

Williams, H., 1971, Mafic-ultramafic complexes in West Newfoundland Appalachians and the evidence for their transportation: A review and interim report. In *A Newfoundland Decade*, Geol. Assoc. Canada, Proc. 24, 1, 9-25.

Williams, H. and Smyth, W.R., 1973, Metamorphic aureoles beneath ophiolite suites and alpine peridotites: tectonic implications with West Newfoundland examples. *Am. Journ. Sci.*, 273, 594-621.

Williams, H., 1975, Structural succession, nomenclature, and interpretation of transported rocks in western Newfoundland. *Can. J. Earth Sci.*, 12, 1874-1894.

Williams, H., and Smyth, W.R., (in press), The Hare Bay Allochthon, Northern Newfoundland. *Geol. Surv. Can. Bull.*

POOR COPY
COPIE DE QUALITEE INFERIEURE

Discussion

Dr. J.S. Pallister In Oman, preliminary data indicates a crude correlation between stratigraphic position of tectonite harzburgite and dunite and Cr/Cr+Al in their spinels. Do you find a similar relationship in the White Hills peridotite?

Dr. R.W. Talkington We have not found a variation in the Cr/Cr+Al ratio of spinels in tectonized peridotite or dunite with stratigraphic position for the White Hills peridotite; though, if we assume the White Hills peridotite is a deeper sample of upper mantle material than the Bay of Islands, and contiguous, then we do find a variation in Cr/Cr+Al ratio of the spinels of the tectonized peridotite and dunite. The change is a decrease in Cr/Cr+Al with depth.

Dr. O.D. Kleemn Your diagrams indicate only 2-valent iron within your spinel-phases. Probably the analyses are calculated, but could you not find any 3-valent iron in your analyses. It would be most unusual if no 3-valent iron would be present in your spinels especially within the chromites.

Dr. R.W. Talkington Yes, there is trivalent iron in the spinels. Spinel compositions were determined by electron microprobe. Recalculation of $R^{3+} - R^{3+}$ was done assuming spinel stoichiometry using the method of Irvine (1965).

Dr. S.E. Tischler Is deviation of plots Cr/Al+Cr vs. Fe/Mg+Fe trend line due to metamorphism or serpentinization?

Dr. R.W. Talkington We believe the increase in Fe^{3+} is the result of serpentinization.

POOR COPY
COPIE DE QUALITEE INFERIEURE



A panorama, looking northwest, of the northern section of the eastern massif showing a region of interlayered spinel lherzolite and harzburgite (dark brown) and dunite (tan). The coast of Labrador is visible in the background and the Cape Onion Peninsula to the left center of the photo.

ENDPIECE